Open International Conference on Modeling and Simulation - OICMS 2005

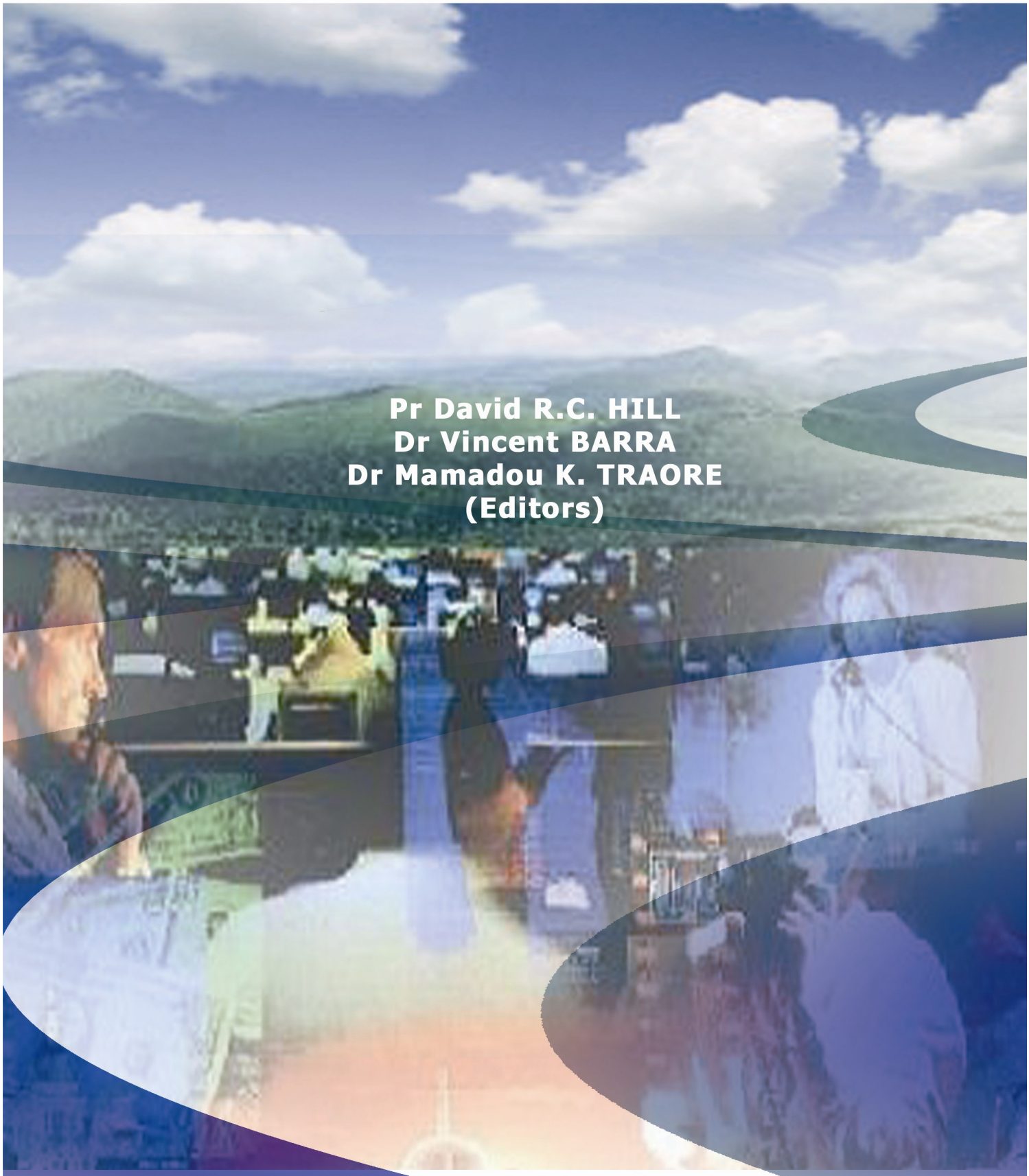

Pr David R.C. HILL
Dr Vincent BARRA
Dr Mamadou K. TRAORE
(Editors)

Blaise Pascal University, France

Open International Conference on Modeling and Simulation - OICMS 2005

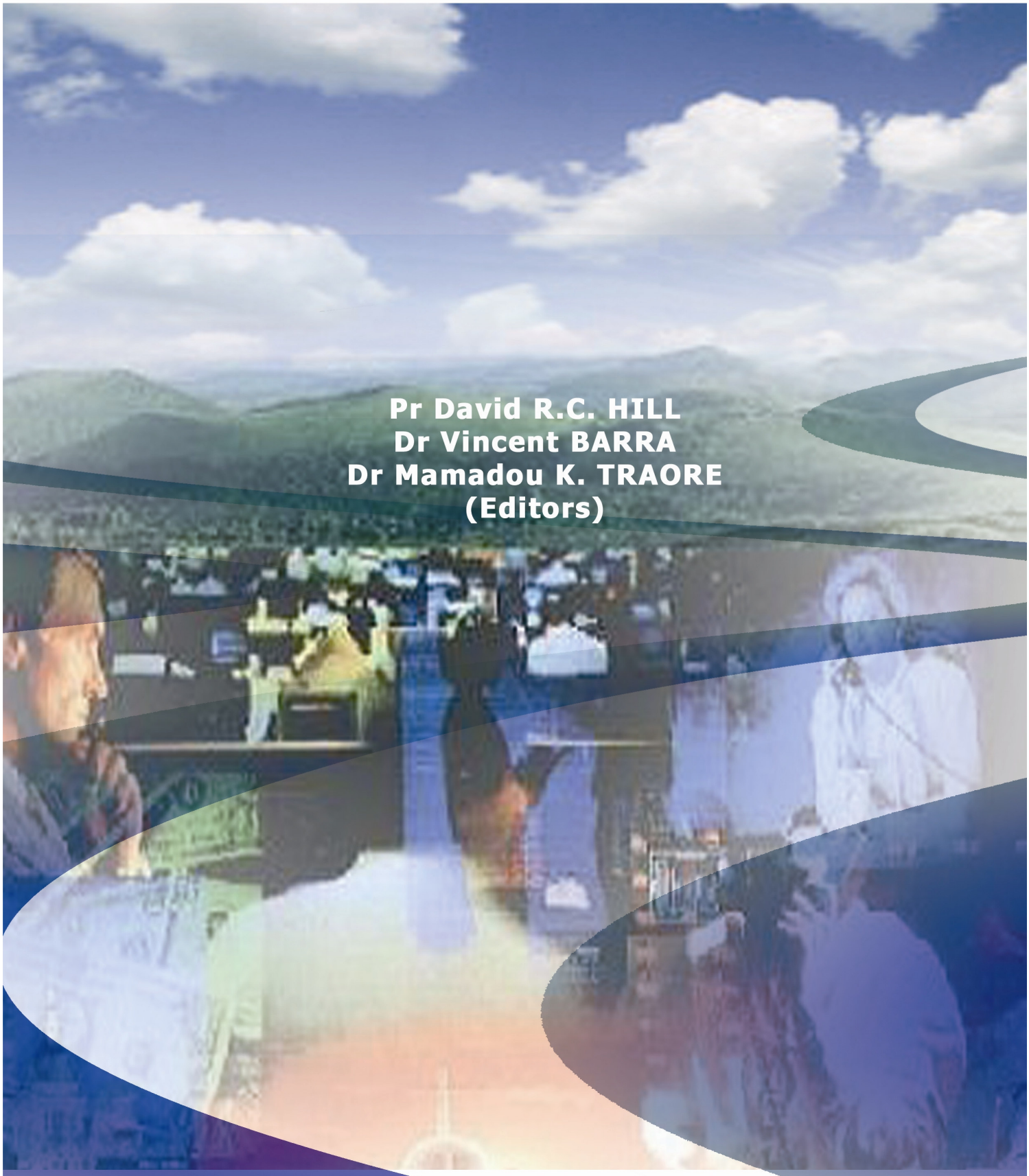

Pr David R.C. HILL
Dr Vincent BARRA
Dr Mamadou K. TRAORE
(Editors)

Blaise Pascal University, France

Preface

Welcome to the first Open International Conference on Modeling and Simulation. The main goal of this multi-disciplinary conference is to strengthen the connections between the fields of Computer Science and Life Sciences. The purpose is to give a focus on the computer science and simulation side of modeling applications in Environmental and Health sciences. Modeling methodology has not been forgotten and we have dedicated a track to deal with more theoretical aspects. Interdisciplinary research is the place where new concepts can be discovered and it is also a place where new methodologies can express their power. However, many academic scientists are currently concerned both by the quality of reviews and by the price increase in conference registrations. OICMS aims at launching a type of conference that wants to free scientists as much as possible from the business and financial aspect of symposiums. The International Program Committee focus was to raise the quality of papers more than the registration price and number of participants. We have retained the registration costs for authors of selected papers as low as possible within university standards. This also implies less comfort in accommodation, transports and a decrease in the quality of the proceedings cover page but with less limits in page size for original research articles. After rigorous reviewing by the Program Committee, and as in some IEEE conferences we wanted to retain a maximum of 40 papers (our rejection rate has been between 20% and 50% for the most severe track). We have also invited 2 papers associated to keynote speeches and reporting on cutting-edge research in all 2 areas of Life Science simulation. In addition we have also welcome 4 invited speeches, 2 from industry and 2 from an academic background (but also dealing with concrete applications).

We would like to thank authors for their contributions, but also the scientific committee which did a very good job (most papers had more than 2 extended reviews and rejected papers were given constructive advices). Authors of top papers will be contacted to submit their contribution in refereed journals.

General chair : Hill David
General co-chair : Barra Vincent
Program chair : Traore Mamadou

Scientific Program Committee

Amblard Frédéric, University of Toulouse, France.
Axtell Rob, The Brookings Institute, Washington DC, USA.
Barros Fernando, University of Coimbra, Portugal.
Bernardi Fabrice, Universita di Corti, Corsica – France.
Bousquet François, CIRAD/IRRI, Thailand.
Breckling Broder, University of Bremen, Germany.
Breton Vincent, LPC – IN2P3, France.
Bunus Peter, Linköping University, Sweden.
Campos Andre, Federal University of Natal, Brazil.
Cheon Saehoon, University of Arizona, USA.
Coquillard Patrick, University of Nice, France.
Craigen Dan, ORA, Canada.
Crane Lawrence, Trinity College Dublin, Ireland.
Crane Martin, Dublin City University, Ireland.
Deissenberg Christophe, University of Aix-en-Provence, France.
Dos Santos Carlos Luiz N., Federal University of Rio de Janeiro, Brazil.
Duboz Raphaël, IRD, France.
Dumont Bertrand, INRA, France.
Felez Mindan Jesus, Universidad Politécnica de Madrid, Spain.
Filippi Batti, University of Tokyo, Japan.
Fishwick Paul, University of Florida, USA.
Frederic Amblard, University of Toulouse, France.
Fritzson Peter, Linköping University, Sweden.
Fukiharu Toshitaka, Faculty of Economics, Hiroshima University, Japan.
Gignoux Jacques, ENS, France.
Gotts Nick, The Macaulay Land Research Institute, Aberdeen, UK.
Groot Jeroen, Wageningen UR - Plant Sciences Group, The Netherlands.

Local Organizing Committee

PRINTED IN FRANCE

Imprimerie de l'université Blaise Pascal

Contents

Session 2 - METHODOLOGY

Session 3 – LIFE SCIENCES

KEYNOTE - INVITED PAPERS

A Powerful Factorization Method to Compute Plant Growth and Architecture, Applications in Agronomy and Computer Graphics

Philippe de Reffye
CIRAD, AMAP
& INRIA, DigiPlante
BP105, 78153 Le Chesnay
France
+33 141 131 289
philippe.de_reffye@inria.fr

Paul-Henry Cournède
Laboratoire MAS, DigiPlante
Ecole Centrale Paris
92295, Châtenay Malabry
France
+33 139 635 774
cournede@ecp.fr

ABSTRACT
Numerical simulation of plant growth has been facing a bottleneck due to the cumbersome computation implied by the complex plant topological structure. In this paper, we present a new mathematical model for plant growth, GreenLab, overcoming these difficulties. GreenLab is based on a powerful factorization of the plant structure. Fast simulation algorithms are derived for deterministic and stochastic trees. The computation time no longer depends on the number of organs and grows linearly with the age of the plant. This factorization finds applications in the context of Geometric Models, to build trees very efficiently, and in the context of Functional Structural Models, to compute biomass production and partitioning, as well as secondary growth.

KEYWORDS
Plant Growth, Geometric Models, Functional Structural Models, Substructures, Deterministic and Stochastic Automatas

1. Introduction

Virtual plants are more and more used for different applications, mainly in computer graphics, (urbanism and landscaping) and environmental sciences (agronomy). Different plant growth models (see for example [Aono *et al.* 84], [Viennot *et al.* 1989], [Deussen 2005]) handled by good designers produce nice plant shapes without introducing much botanical or physiological knowledge. If it works quite well for little plants (at least from a visual point of view), limitations occur when it comes to tree representation.

Botanical knowledge and computer resources are crucial factors for tree growth simulation. Trees contain a lot of items to compute and assemble, which requires a fast CPU and a large amount of memory. A big tree can gather more than one million organs that have to be generated and positioned in the 3D space. The problem increases dramatically for grove or stand simulations. The cost of computation is related to three main problems: the construction of the plant topological structure, the functioning of the plant and eventually its rendering. Sievanen [Sievänen *et al.* 2000] distinguishes two kinds of models for virtual plants, Geometrical Models (GM) [Reffye *et al.* 1988], [Lindenmayer Prusinkiewicz 1990] and Functional Structural Models (FSM) [Perttunen *et al.* 1996], [Reffye *et al.* 1996], [Jallas *et al.* 1999]. The former only use organogenesis and geometrical rules for the plant construction. The shape of organs and their expansions are directly controlled by their sizes. In that case, Sievanen observed empirically that the computational time is proportional to the square of the number of items. The latter are more devoted to agronomy. Source and sink processes, biomass production and biomass partitioning are modeled. Biomass partition gives volumes of organs by density and allometry rules. It is necessary to explore several times the topological structure in order to partition biomass. Light interception, water transportation or tree mechanics will also increase heavily the computational time (up to 8 times, see [Sievänen *et al.* 2000]). Therefore, appropriate simplifications are needed.

The main problem relies in the concept of parallel simulation which is generally used to build topological structure, by mimicking the simultaneous bud functioning, see for example [Lindenmayer Prusinkiewicz 1990] and other related works based on L-systems or automata. If parallel simulation is natural from the point of view of computer sciences, it is not relevant mathematically. Likewise, most programs are obliged to build the plant completely in order to compute its production. But a total topological representation of the plant is very heavy for computer memory. The role of mathematical modeling is to find powerful algorithms that bypass the simple and natural way of counting. It is necessary to introduce extra biological knowledge and take one step back from the complex simulation techniques previously developed. Besides improving simulation efficiency, mathematical equations of growth are necessary to use differentiation techniques that open

virtual plants to analytic optimization and control, and thus to applications. Without this formalism, solving optimization problems becomes far more tedious. Heuristic methods like genetic algorithms or simulated annealing have to be used and the growth process is run thousands of times.

In this paper we will show the advantages of reconsidering completely the way to simulate virtual plants using algorithms based on a mathematical model rather than complex simulation techniques. We will present a powerful factorization of the plant structures and how to use this factorization for functional, graphical or stochastic applications. A real breakthrough is achieved as the bottleneck linked to the cumbersome tree architecture is suppressed. The case of AMAP model and its evolution to GreenLab model will serve as a typical example of comparison. This paper is a review of former results about the gain obtained on virtual tree computation.

2. Basic Concepts for Plant Growth Simulation

In this section, we describe the interdisciplinary knowledge used in AMAP. It covers botany, ecophysiology and numerical simulation techniques.

2.1. Botanical Concepts

The plant description is based on its hierarchical organization using the botanical notion of Physiological Age (PA) [Barthélémy *et al.* 1997], and described in a recurrent form. The P.A. represents the differentiation of organs based on an endogenous program. The PA concerns not only organs (leaves, flowers, internodes, roots), but also the types of axis and branch organization. For instance, on a coffee tree, there are two types: orthotropic trunk and plagiotropic branches. Usually, we need less than 6 PA to describe the typology of branches in a tree. The oldest PA is the ultimate state of differentiation for an axis, it is usually short and not branched. Organs, such as leaves, flowers, internodes, are sub differentiations, linked to the main PA of the metamer.

- The metamer is a set composed of organs (internode (pith + rings), buds, leaves). All the necessary information for a given PA is stored at this level. It concerns the number of organs, their shapes and their functioning.
- The Growth Unit (GU) is a set of metamers built by a bud during a growth cycle (GC). These metamers can be of different kinds and ordered according to botanical rules, like acrotony.
- The bearing axis (BA) is a set of GU of the same kind that gives birth to the main axis of a branch.

These concepts were first gathered in the architectural model named Reference Axis, based on an automaton and described in Figure 1, see [Barczi *et al.* 1997].

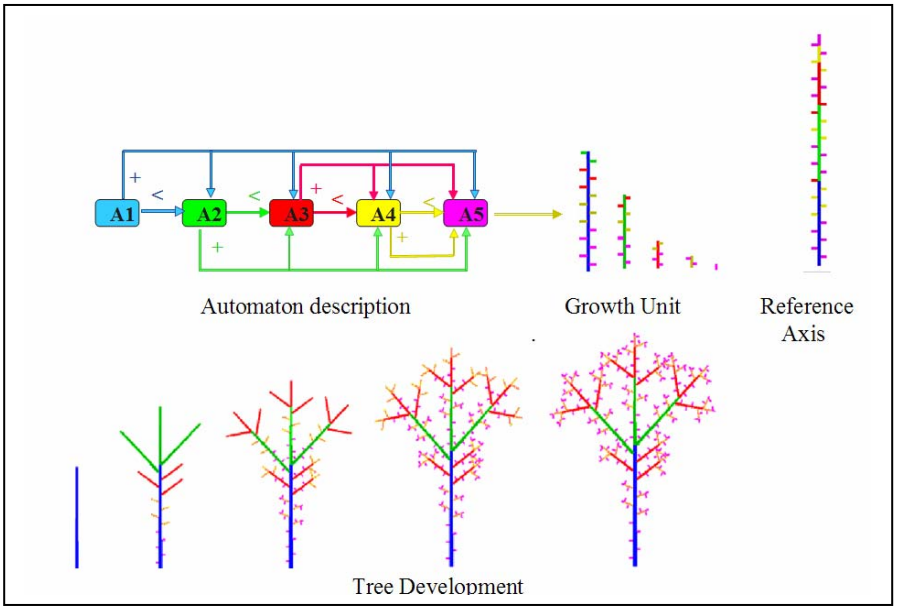

Figure 1: Tree organogenesis simulated by an automaton based on the concept of Physiological Age

To simulate the functioning of buds, it is necessary to integrate the notion of physiological age that describes the level of

differentiation of the tissues. Buds stay in the same state or change states according to repetition and transition laws. For example, the bud of a sunflower will produce about 40 times the same metamer before transforming into a flower. There are clearly two steps here. The first one corresponds to a vegetative state (internode +leaf) and it is repeated 40 times, the second one is the flowering state, reached after a transition when the first state is over.

On figure 2, we can see the flowchart of the parallel simulation based on bud functioning [Blaise *et al.* 1998]. A scheduler gives at each step of growth all the events to realize. An automaton controls the bud differentiation and parallelism controls the bud productions at each cycle. A topological structure is generated and if no biomass partitioning is needed, some geometric features can be used to obtain a geometrical model. The computational time is a quadratic function of the number of organs created.

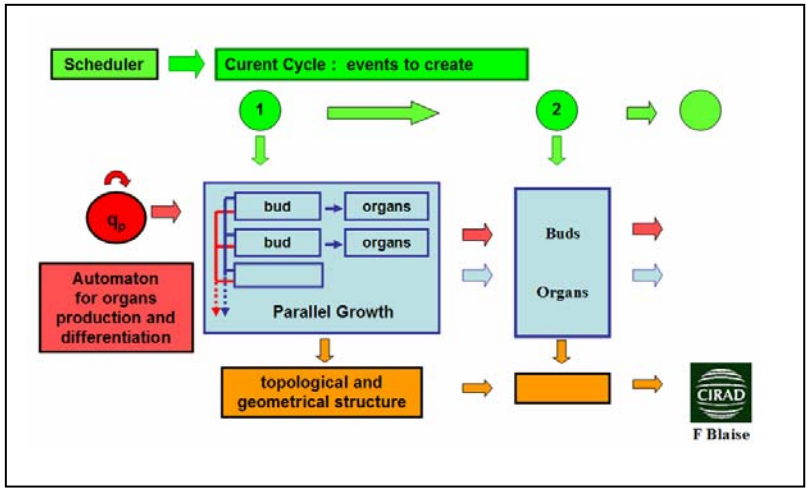

Figure 2: Parallel simulation of bud functioning

2.2. Ecophysiological Concepts

2.2.1 A time unit for plant development

The time unit for organogenesis and photosynthesis must be consistent, insuring a good synchronization between the two processes [Reffye Houllier 1997]. In the plant structure, primary growth of leafy axis consists in adding new metamers rhythmically at their top. The time needed between the creation of two growth units ranges from several days (herbaceous, shrubs) to one year (temperate trees). For a given plant, it varies with the environmental conditions. However, it becomes quite stable if we define a thermal time. The number of organs set in place by a bud is proportional to the sum of daily temperatures received by the plant and so called "the Law of the Sum of Temperatures" (LST) in Agronomy. We define the growth cycle (GC) as the thermal time unit necessary to increase the plant organogenesis of one step. The plant age in GC is called the Chronological Age (CA). During the GC, all the working buds may produce new metamers according to their PA and CA.

On the other hand, on long periods the plant biomass acquisition is approximately proportional to the plant transpiration. This phenomenon is known as Water Use Efficiency (WUE). WUE is generally considered constant over a sufficient period. We suppose as well that at the level of the GC, the fluctuations of WUE are reasonable. WUE(*n*) represents the average value at GC *n*. Thus, we will rely on the laws of LST and WUE to monitor simultaneously the plant production of both organs and biomass.

2.2.2 Biomass Acquisition and Partitioning

The biomass computed from the water transpiration is the fresh biomass used to build the organs. Each leaf will have a transpiration depending on its surface area. The biomass produced by each leaf is added and stored in a common pool of reserve and redistributed to all the organs according to their sink strengths. The initial seed and the leaves are sources. Leaves, internodes, fruits and rings are sinks during the number of growth cycles equal to their expansion times. The sink values are not necessarily constant. The root system is not described but is considered as a big sink that runs from the first cycle of growth to the current plant age. The flowchart of the plant simulation is given in Figure 3.

At GC *n*, the available biomass for an organ is the total amount of biomass reserves denoted *Q(n)*, multiplied by the organ sink value and divided by the demand at cycle *n* denoted *D(n)*. *D(n)* is defined as the sum of all the sinks in the topological structure at GC *n*. The biomass partitioning is the final result of the step by step diffusion process between neighbouring GU of the biomass produced by the leaf photosynthesis. As the time period of a GC is long enough, we do not need to compute

this diffusion process. The biomass allocation in the plant architecture according to the sink values can be considered as immediate. Therefore, the organ sizes are the result of several steps of biomass allocation during their expansion time. At a given plant age, all the organs of the same CA and PA, have the same sizes.

The secondary growth is the process controlling the increase of the branch diameters. The ring volume of a branch at a given spot in the plant architecture is proportional to the number of leaves seen above. For this computation, we need to run through the complete plant topological structure at least once. It adds to the computational time.

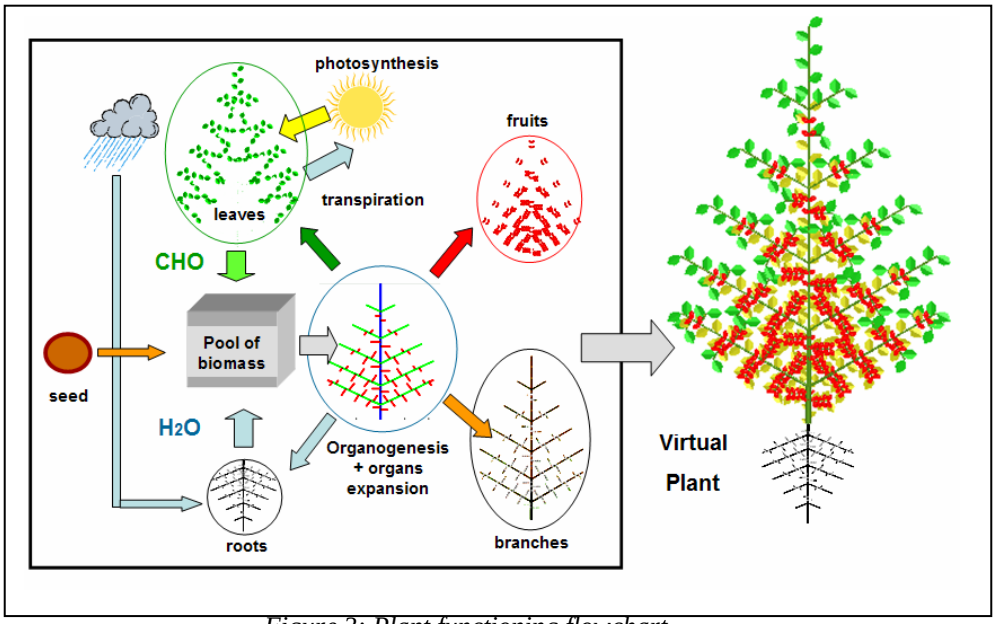

Figure 3: Plant functioning flowchart

Thus, computing the biomass production, the demand of organs and the biomass partitioning requires using and exploring heavy topological structures for big trees, and can lead to unreasonable computing times.

3. Former Results on Plant Growth Simulation with AMAP Software Programs

3.1. AMAPSim as a GM Virtual Plant Maker

Most complex tree architectures according based on botanical concepts can be simulated by the AMAPSim software developed at CIRAD [Barczi *et al.* 1997]. The elm tree and the oil palm tree with its root systems are certainly some of the most complex plants ever simulated by computers.

Figure 4: Complex architectures simulated by AMAPsim
(a) Japanese elm tree [Reffye et al. 1990] (b) Oil palm tree with roots [Jourdan Rey 1997]

Of course, to compute such virtual plants, we need high computational time and memory (several hours). For this reason, GM

virtual trees are necessarily difficult to handle. It mainly results from the parallel growth process used for the topological structure construction.

3.2. AMAPHydro as a FSM Virtual Plant Maker

Introducing plant functioning implies that source and sink relationships, biomass partitioning and secondary growth have to be computed at each step of the growth. For this purpose, the topological structure is explored one or several times. Even the geometry is more complex than for GM as organs expands on several GC and their shapes are obtained from the allometric rules and the density.

It adds approximately three times the computational time used to build the topological structure. This ratio is the minimum one between GM and FSM models, see [Sievänen *et al.* 2000]. Such complex simulations realized with AMAPHydro are presented in [Reffye *et al.* 1996]. The photosynthesis is given by an empirical formula, using LAI for instance. But introducing light interception by the tree geometrical structure will still increase dramatically the computing time. This computation was realized by Soler *et al*., see [Soler *et al.* 2003]. The results obtained can be useful for the calibration of simpler empirical models of photosynthesis.

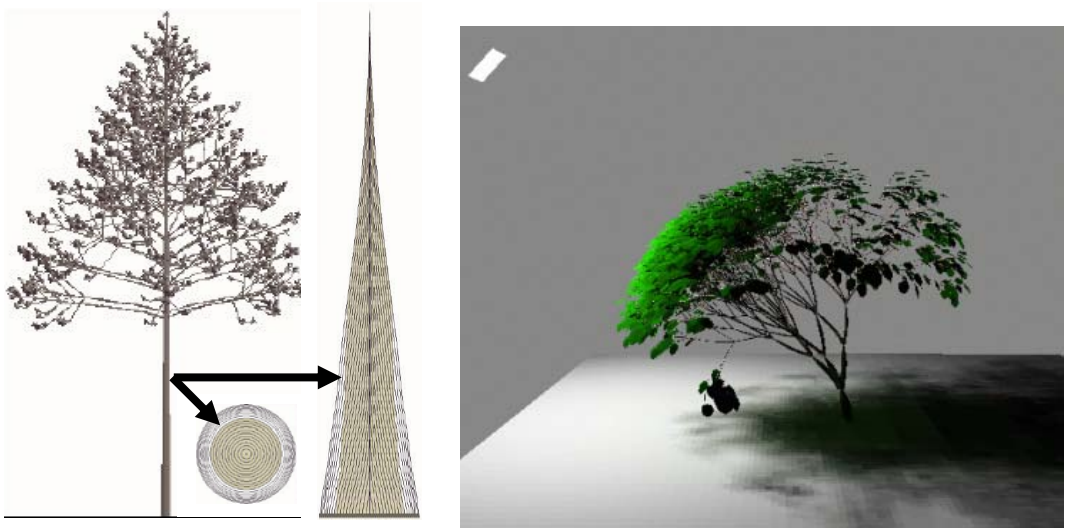

Figure 5: (a) Simulation of biomass partitioning with secondary growth on a pine tree [Reffye et al. 1996]; (b) Simulation of photosynthesis with radiosity [Soler et al. 2003]

3.3. Conclusion on Classical Virtual Plant Simulations

It is possible to simulate tree development and tree growth thanks to computer simulation techniques that imitate closely the process of plant functioning, i.e. the parallelism of bud growth (all organs must be created one by one). The creation and the circulation of the fresh biomass use the paths of the topological and geometrical structures (all the organs have to be reached) in the tree architecture. But this method leads to cumbersome computations. Moreover, the lack of mathematical models prevents from studying the system behaviour, which makes bug proof very difficult.

4. Towards a Dynamical Approach of Plant Growth: GreenLab Model

4.1. Preliminary Remarks

Our approach to develop the mathematical model of plant growth strongly relies on the plant organization described by botany. This leads to relevant choices in order to obtain an efficient method of factorization based on plant instantiations. Plant development purely concerns organogenesis, i.e. the number of organs. Growth depends on photosynthesis that insures organ creation and expansion. We consider here the case without interactions between organogenesis and photosynthesis. On the common assumption of the existence of a global pool of reserves, it is not necessary to consider local conditions and we can distinguish 3 steps to control plant development and growth.

1. Computing the organogenesis. This step can be performed independently on the photosynthesis. It provides the number of organs produced by the buds.
2. Computing photosynthesis. This step needs the organogenesis results that provide the total plant demand i.e. the sum of sinks. The number and sizes of leaves can be computed and the resulting biomass production can be shared

between the different organs according to their sinks to insure their expansion. The yield is thus computed according to the sizes and the weights of the different organs produced.

3. Building the plant architecture for visualization or to study plant interaction with the environment. This last step needs the results of the two previous ones. It needs numerous geometrical operations.

For most applications in agronomy only the first two steps are necessary, and no geometry is required.

4.2. Botanical Instantiations in GreenLab Model

4.2.1 At Metamer Level:

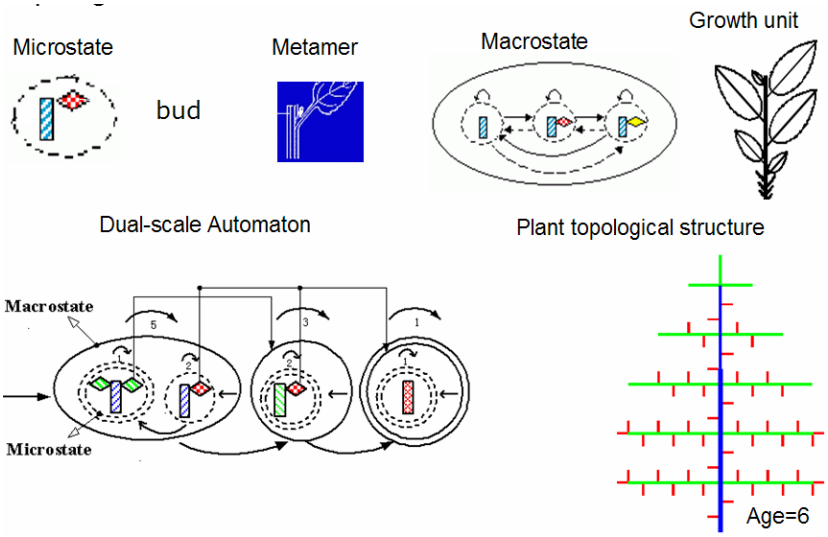

Figure 6 : Dual scale Automaton for Plant Organogenesis

In most cases, a dual scale automaton [Hu *et al.* 2003] is sufficient to describe the full organogenesis. The number of physiological ages is very small (less than 6). The Plant is organized in metamers (microstates) and growth unit (macrostates). Each metamer is a set of organs (internode, leaf, fruits and axillary buds). It is more efficient to create metamers than organs one by one because it gives directly the organ production and speeds up the computing of organogenesis. Each growth unit is a set of metamers and the repetition of GU gives birth to an axis so called Bearing Axis (BA).

4.2.2 At Substructure Level

The terminal bud with a given PA produces different kinds of metamers bearing axillary buds of various PA. These buds give birth to axillary branches. Even the PA of the main bud can change by mutation. This phenomenon is represented in the automaton as a transition between macro-states.

These processes create substructures. A substructure is characterized by its physiological age PA and its chronological age CA. All the substructures with the same PA and CA are identical if they have been set in place at the same moment in the tree architecture. Let us consider the example of a particular 100 year old tree. Its trunk is of PA 1, main branches of PA 2 and live about 15 years, twigs of PA 3, 4, 5 and respectively live less than 7, 5, 2 years. Here, the total number of substructures with different PA and CA is about 30. It is very small, even if the total number of organs is high. These substructures will be repeated a lot of times in the tree architecture, but they need to be computed only once for each kind. The tree production will be obtained by stacking the substructures in the right way.

5. A New Way to Build Tree Architecture

From this description of the botanical plant organization using metamers, substructures and PA, we set up a powerful recurrent algorithm for tree construction, see [Yan 2003].

5.1. Deterministic trees

We present in this section the recurrent algorithm for a deterministic tree of CA = T with a number of PA = m.

The algorithm is initialized with the last substructures of PA m. They are easy to compute as they are not branched. Now

suppose that all the substructures of $1 \le CA \le T$ and $K < PA \le m$ are built. Then, to compute the substructure of CA=*T* and PA=*K* (for $1 \le K \le m$ **)** is easy. We build the bearing axis of PA=*K* according to the macrostates and the microstates generated by the dual scale automaton, up to CA=*T*. Then, each macrostate bears substructures of CA<*T* and of PA >K given by the automaton. But these substructures are already built (recurrence hypothesis). Thus, the construction of all the substructures of CA=*T* is achieved. The substructure of PA 1 gives the full tree.

Each kind of substructure is built only once. This method is no longer natural but relies on the tree botanical composition. The algorithm performance is high. The time to compute the number of items in a GreenLab tree is proportional to the number of PA multiplied by the CA and thus no longer proportional to the number of organs. As a consequence, the principal problem of tree construction is solved. A binary tree with 2^T organs at CA *T* will be computed at the same speed than a linear tree with T organs.

This can be illustrated by the following example shown by Figure 7. We choose a theoretical plant built by a dual scale automaton with 4 PA. At the CA 18, the architecture is completed: all the buds have reached their ultimate step of differentiation. On this example the multi-scale organization is quite clear. The GU of PA=1 bears substructures of PA 2,3,4, the GU of PA=2 bears substructures of PA 3, 4, the GU of PA=3 bears substructure of PA 4, and those are not branched.

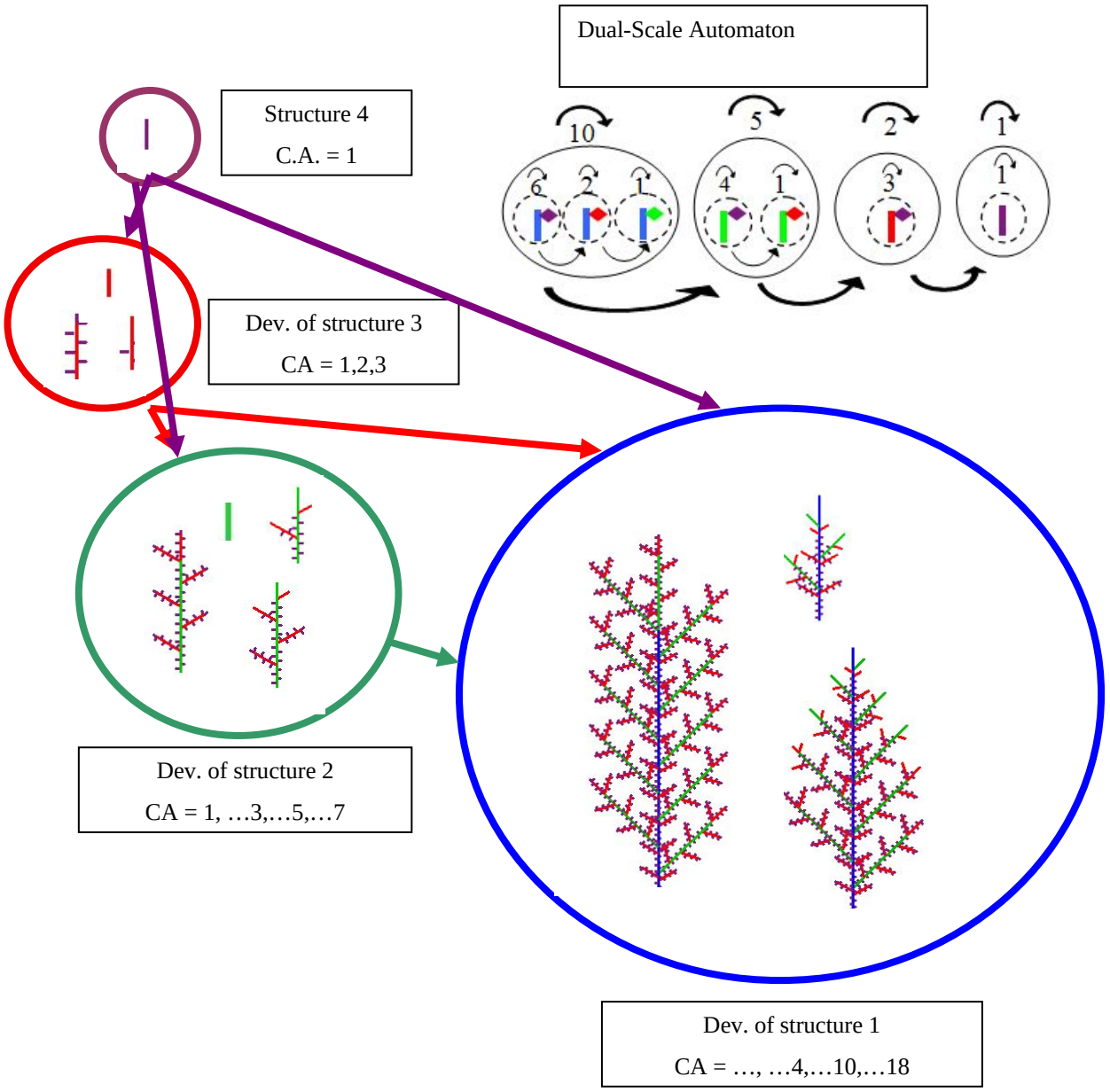

Figure 7: A combinatorial algorithm to insure plant development by stacking substructures according to their chronological and physiological ages

5.2. Stochastic trees

The method can be easily extended to stochastic trees, assuming that the dual scale-automaton integrates probabilities that control growth, branching and death processes, see [Kang *et al.* 2003]. For the deterministic growth, for given chronological and physiological ages, we build only one substructure. For the stochastic growth, we take several samples of substructures that are realizations of the same stochastic distribution.

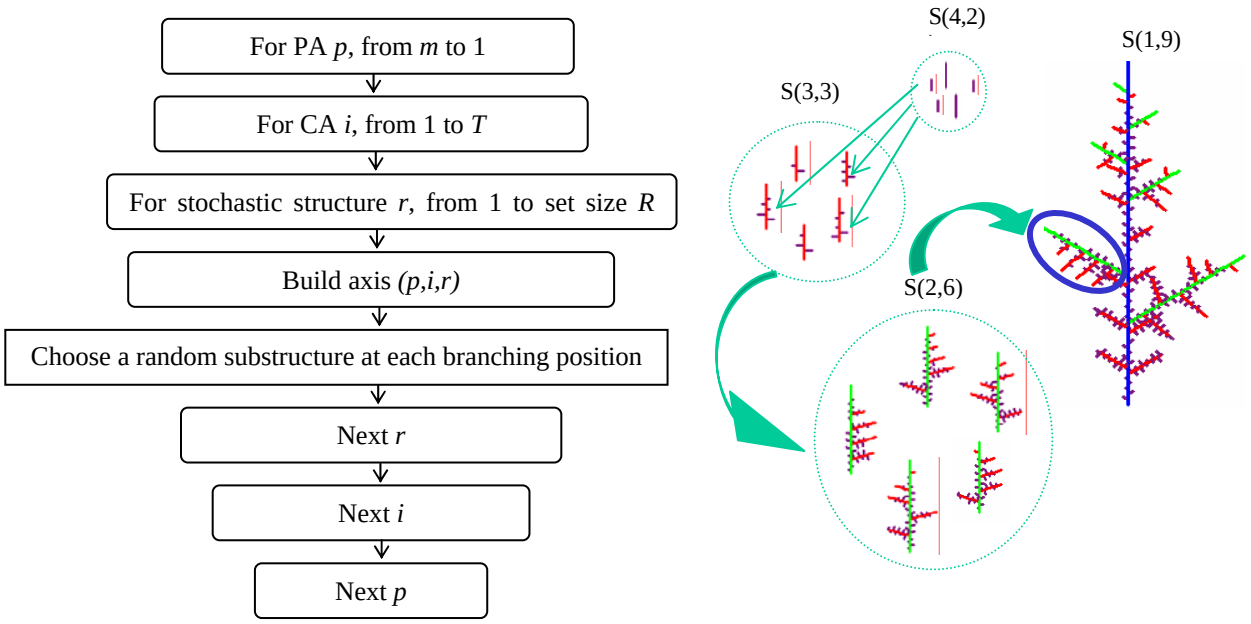

Figure 10: Description of the stochastic algorithm for stochastic trees
(a) Simulation Flowchart - (b) Visualization [Kang et al. 2003]

Each sample of substructure in a given set (for given PA and CA) is obtained by first building a random axis, realization of the stochastic automaton and then by branching substructures of higher PA and smaller CA. These are randomly chosen in the corresponding set of samples (for the right PA and CA). The same recurrence as in the deterministic case is used, which insures that these sets have already been built. Figure 10 shows a concise flowchart of the simulation. The size of the substructure sets *R* can vary for each PA and CA. Of course, the accuracy will increase with *R*.

This method to simulate stochastic trees is very efficient. Once again, it does not depend on the number of organs to create. It is important to note that the algorithm is even more interesting to build stochastic forests, as the sets of substructures built for the first stochastic tree can be used to build other trees of the same kind that are realizations of the same stochastic distribution. The time necessary to build the first tree is proportional to $m \times T \times R$ but only to $m \times T$ for the others in the stand.

6. Applications of the Substructure Decomposition

From this construction process, we can deduce the equations of recurrence controlling organogenesis. Several applications taking advantage of this factorization are also presented.

6.1. Computing Organogenesis

In the case of parallel simulation, counting the number of organs is a typical bottleneck; the computing time can be tremendous for big trees and forests. To overcome this difficulty, GreenLab model takes advantages of the plant architecture organized thanks to the concept of PA. Similar substructures (of same PA and CA) are found in the main architecture many times.

Suppose a tree with *m* PA and finite growth for the axes: the repetition of macrostates (i.e. the number of GU) of PA=*k* is equal to N_K. Beyond this limit, the terminal bud can undergo a mutation and change PA (say *k+1*), or die if *k=m*. So there are *m* kinds of substructures here that are represented by arrays whose fields contain the cumulated number of metamers

according to their PA. A structure S_k^t is defined by its chronological age *CA*= *t* and its physiological age PA = *k*. It contains all the cumulated numbers of metamers produced from its birth until GC *t*.

$$\left[S_1^t\right]=\left[s_{1,1} \quad s_{1,2},\ldots \quad s_{1,m}\right]^t ,\left[S_2^t\right]=\left[0 \quad s_{2,2},\ldots \quad s_{2,m}\right]^t , \ldots ,\left[S_m^t\right]=\left[0 \quad 0,\ldots \quad s_{m,m}\right]^t$$

All the items $s_{i,j}$ with $j < i$ are null because of the production rules. Structure S_1^t sums up all the metamers produced at GC *t*, for the whole plant.

Let u_k be the number of metamers per GU for a given PA *k* and $n_{i,j}$ be the number of substructures of PA *j* branched on the *i*th GU of the bearing axis of PA *k*. We have to stick the lateral and terminal substructures directly on the bearing axis of PA *k*, according to their positions as follows:

$$\left[S_k^t\right]=t\cdot\left[u_k\right]+\sum_{i=1}^{t-1}\sum_{j=k+1}^{m}\left(n_{k,j}\cdot\left[S_j^i\right]\right) \qquad (t \le N_k) \qquad (1)$$

If $t>N_k$, and along the trunk, an apical terminal substructure of physiological age $k+1$ is born, so we have:

$$\left[S_k^t\right]=N_k.\left[u_k\right]+\sum_{i=t-N_k}^{t-1}\sum_{j=k+1}^{m}\left(n_{k,j}.\left[S_j^i\right]\right)+\left[S_{k+1}^{t-N_k}\right] \qquad (t > N_k \ , \ t < m) \qquad (2)$$

This plant construction algorithm is very fast. Obviously, the computation time depends only on *t*m* and not on the number of organs produced. The substructures are constructed by a double loop, *i.e.*, bottom up from the youngest CA=1 to the final CA=*t* and top down from the oldest PA=*m* to PA=1. A library of substructures is created for each PA and CA and will be used to build substructures of older CA and younger PA.

As the number of organs per metamer is botanically known, GreenLab provides a mathematical tool that enables to compute the organ production of a virtual plant very quickly and thus suppresses the drawback of counting the number of organs one by one by simulation.

6.2. Building GM trees

If we add geometrical rules (internode lengths, branching angles, phyllotaxy) to the construction algorithm, we will obtain the 3D architecture of a geometrical tree, see [Reffye *et al.* 2003]. We can extend the role of substructures to be a set of polygons that stores the geometric shape of the substructures into a library. They become meta-organs, and positioning a substructure in the plant architecture needs the same operations as for a simple 3D organ. They can also be displayed separately, which can be useful.

The tree of Figure 11 built by AMAPsim software [Barczi *et al.* 1997] can be computed either with the classical parallel way or with GreenLab substructure factorization. Resulting computational times are compared: more than one hour for the parallel simulation, less than one second with substructure factorization! The mathematical algorithm proposed totally suppresses the computation cost of tree simulation.

Figure 11a: Tree built by AMAPsim sofware.

Plant age	Substructures	Parallel- simulation
5 years	0.1	3.3 (seconds)
10 years	0.3	437.2
15 years	0.7	4743.0

Figure 11b: Comparison of computing times between substructure method and bud-by-bud simulation [Yan et al. 2003a].

6.3. Computing the Biomass Production

It is not necessary to build the tree structure to compute biomass production and partitioning at a given chronological age. We only have to compute organ production, plant demand and photosynthesis [Yan *et al.* 2004]. All these data can be immediately derived from formula (1) and (2) giving the number of metamers in the plant as we know the number of organs per metamer and their durations.

6.3.1 Biomass acquisition

Every leaf produces biomass that will fill the pool of reserves according to an empirical nonlinear function depending on its surface *A*, on parameters *r1*, *r2*, and on water use efficiency at GC *k: E(k).* We suppose that the size of a leaf depends on its cycle of apparition (because of expansion). Let N_K^L be the number of leaves produced at GC *k*, known from Equation (1), the plant biomass production is:

$$Q_t = \sum_{k=1}^{t} N_k^L . f(A_k, r_1, r_2, E(k)) \qquad (3)$$

The empirical function chosen for the leaf functioning in GreenLab is:

$$f(A_k, r_1, r_2, E) = \frac{E}{r_1 / A_k + r_2} \quad (4)$$

This function can be easily changed according to modellers' choices.

6.3.2 Biomass partitioning

Each organ has a potential biomass attraction value that we name sink or organ demand. This sink $p_k(i)$ depends on the organ PA *k* and on its CA *i* (because of expansion). The shape chosen for *p* is up to the user, but it should be able to fit properly any kind of numerical variations of the sinks according to the organ CA, it must be flexible enough to give bell shapes, *c* or *s* shapes, *etc*.

We define the plant demand at GC *n* as the total biomass attraction of all organs (leaves, internodes, fruits, layers, roots…):

$$D_n = \sum_{o=L,I,F} \sum_{i=1}^{t} N_{t-i+1}^o \; p_o(i) \qquad (5)$$

The N_k^o are given by Equation (1). It gives instantaneously the biomass $\Delta q_{i,t}^o$ allocated to an organ of type *o* created at GC $t-i+1$ and its total cumulated biomass $q_{i,n}^o$:

$$\Delta q_{i,t}^o = \frac{p_o(i)}{D_t} Q_{t-1} \quad , \quad q_{i,t}^o = \sum_{j=i}^{t} \Delta q_{i,j}^o \qquad (6)$$

Eventually, the organ volume depends on its apparent density and its dimensions on allometric rules. All this features can be measured directly from the organ shape.

6.3.3 General recurrent formula in GreenLab

We suppose here that the leaf thickness *e* is constant. Then the leaf surface is deduced simply from (6) by dividing the leaf volume by *e*. Then Equation (3) can be rewritten in the following form:

$$Q_n = E \cdot \sum_{i=1}^{t_B} \frac{N^L_{t-i+1} \cdot \sum_{j=1}^{i} \frac{p_L(j) \cdot Q_{t-(i-j)-1}}{D_{t-(i-j)}}}{\alpha + \beta \cdot \sum_{j=1}^{i} \frac{p_L(j) \cdot Q_{t-(i-j)-1}}{D_{t-(i-j)}}} \quad , \qquad (7)$$

where: $\alpha = r_1.e$; $\beta = r_2$; t_B is the number of GC for which the leaf functions.

Equation (7) is a generic recurrent relation that monitors the plant development corresponding to any given architecture coming from the dual scale automaton [Reffye *et al.* 2003]. It gives the total biomass produced by the plant architecture at each GC. The computing time of this equation depends only on the number of PA and CA of the plant, so it is very fast. The asymptotic behaviour of (7) is studied in [Yan *et al.* 2003b]. For numerous applications, this equation can bypass the full code of plant simulation.

6.3.4 Calibration of the model on real Plants

Some parameters of the model can not be directly measured on real plants, we call them hidden parameters. Heuristic methods have to be carried out. The number of organs and their weights are targets to fit and the generalized least square method can be used [Zhan *et al.* 2003]. This numerical method implies computation of the system partial derivatives. This can be done formally using equations (1) to (7) see [Lin 2005], or numerically. Once again, numerical derivation is made possible thanks to the substructure factorization allowing a fast computation of plant growth. About ten parameters have to be assessed and the convergence is very fast (less than ten iterations).

6.4. Building FSM Trees

The applications presented so far do not necessitate building the tree. The number and volume of each kind of organs are known and it is sufficient to get the yield quality and quantity. It is of course possible to get the tree structure running the same procedure as for the GM trees. The resulting set of polygons can be used at each step to compute light interception and to assess photosynthesis. But this heavy procedure should be bypassed by formula (3).

6.4.1 Computing the Secondary Growth on deterministic trees.

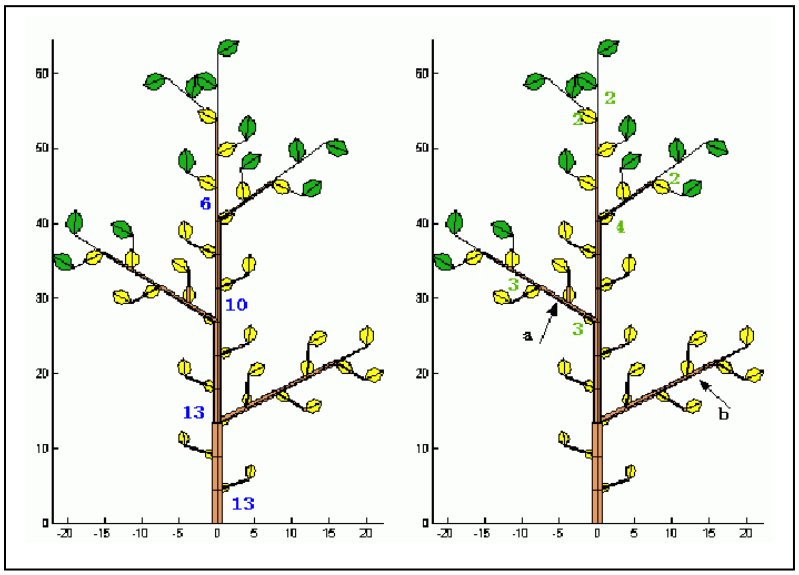

Figure 12: Counting functioning leaves inside substructure [Kang et al. 2002]

An important feature of tree growth is the permanent increase of branch diameters called secondary growth. Each year, a new ring of biomass is added. The branch profile is made of a stack of rings. At a given level, the number of rings gives the branch CA.

It is assumed that the ring thickness at a given spot in the tree architecture is proportional to the leaf surface seen upward [Reffye *et al.* 1997]. It is also proportional to the number of leaves, considering the average single leaf surface. A simple

operation on substructures gives this number for all bearing axis in the main architecture, see Figure 12. If the amount of biomass allocated to the rings is known, it is easy and fast to propagate the algorithm on the whole tree structure and finally compute the biomass allocated to all metamers for their secondary growth [Kang *et al.* 2002]. With the classical parallel simulation this procedure is very long (proportional to the size of the topological structure) as for every leaf, it is necessary to run through the tree architecture (from the leaf position to the roots) and allocate biomass all along the way.

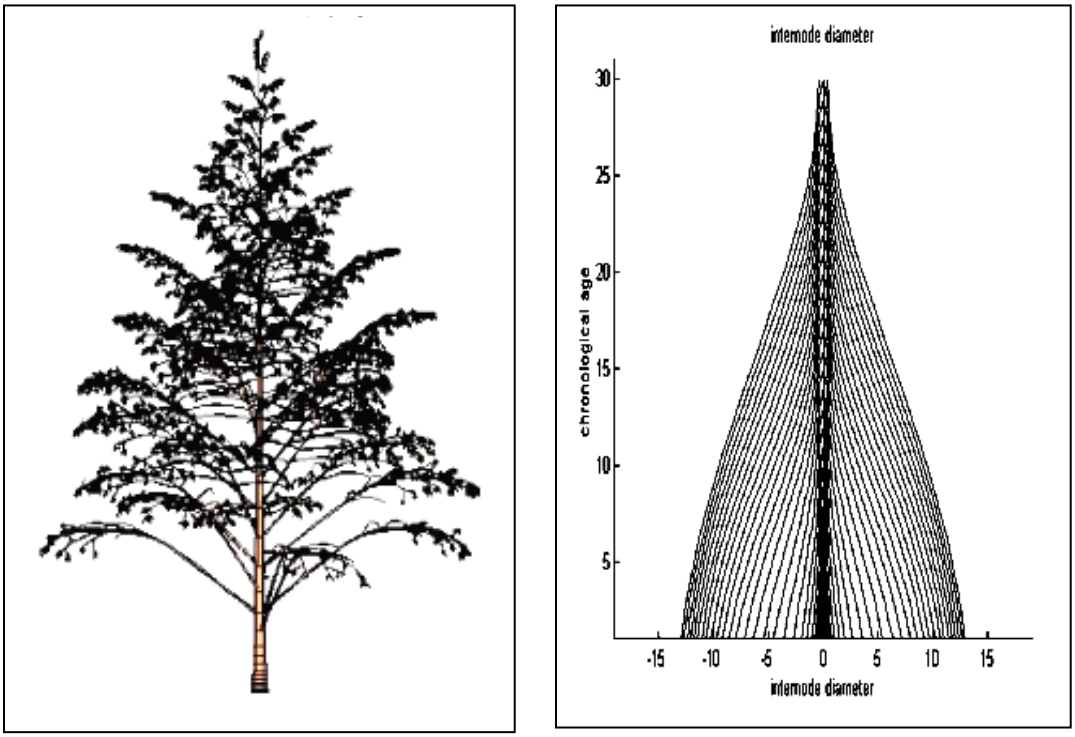

Figure 13: Secondary growth with GreenLab - Tree Architecture and structure of the trunk [Kang et al. 2002]

The tree on Figure 13 is computed with GreenLab model. It is quite comparable in terms of complexity and biological assumptions to the tree on Figure 5 produced by Amaphydro. But the latter was computed in more than one hour and the former in a few seconds. In fact, introducing functioning in GreenLab model does not load so much the computing time and certainly less than a factor 2.

6.5. Computing Organs and Biomass Distributions on Stochastic Trees.

There are two problems to solve: to compute the stochastic distribution of the number of metamers and that of biomass. As the metamer distribution comes from a parallel stochastic process, it is very close to a normal distribution. So the mean and variance are sufficient to obtain the distribution shape with accuracy.

Equations (1) and (2) can be extended to compute means and variances of the organs production. Using compound law formulas, it is possible to compute the theoretical mean, variance and covariances of the number of metamers in a plant generated by the stochastic automaton. The theoretical formulas avoid heavy Monte-Carlo simulations to get the distribution shape as it was done before with several days of computation! It is also possible to get a very good approximation of the mean and variance of the biomass produced using differential statistics applied to equation (7).

The detailed calculations and formulas can be found in [Kang *et al.* 2004], but we show on Figure 14 comparisons between the theoretical distributions in blue and the numerical distributions obtained by Monte-Carlo simulation, for organ and biomass productions in a stochastic plant with probabilities for bud branching, growing and dying. These results are synthetic and do not need plant reconstruction. For many experiments they can be quite sufficient to assess the means and variance of the yield.

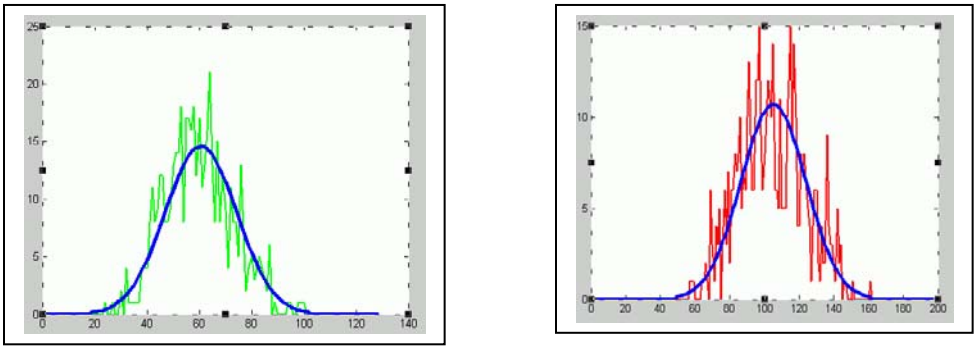

Figure 14: Comparison between theoretical distributions and Monte-Carlo simulation (250 samples); (a) Number of organs (b) Biomass [Kang et al. 2004]

7. Conclusion

Virtual plants are new tools for agronomical and environmental applications, not only as visualization tools, but also to simulate or to assess the effects of environmental factors such as hydric stresses, densities etc… There are several possible scales of observation. Remote sensing on satellite or aerial images provides information at the landscape or plantation scale. At the level of fields or greenhouses, process based models compute the biomass production from environmental data using organ compartments (leaves, internodes, fruits, roots…) to assess the global yield. Functional structural models try to integrate biomass production and partitioning in the plant structure. It leads to cumbersome computing procedures. In this paper, we have described a new mathematical model for plant construction, GreenLab, based on a factorization of the plant structure. The algorithms derived from the mathematical model avoid the main drawbacks currently encountered by most usual plant simulation programs. Heavy computation times are no longer necessary to solve simulation or optimization problems. The GreenLab model allows simulating a virtual forest stand more quickly than the previous Amaphydro model could simulate a single tree (on the same biological assumptions)!

GreenLab also remains consistent when changing scales. The complete model can be simplified without major drawbacks. Instead of creating compartments like process based models, we transform branches into meta-organs (*i.e.* a substructure) being at the same time sources and sinks, whose values depend on the cumulative actions of the underlying organs. The ultimate transformation is to consider the tree as a single structure that is source and sink. The changing of scales relies on the equations of the full model and can be properly written.

We hope that this new numerical tools will contribute to arouse interest in virtual plants. The final objective is to obtain relevant simulations and predictions of plant yields, interacting with the environment and to introduce efficient tools for optimization and control.

REFERENCES

[Aono *et al.* 84] Aono, M., Kunii, T.L. Botanical tree image generation. IEEE Computer Graphics and Applications, Vol.4(5), pp 10-33, 1984.

[Barczi *et al.* 1997] Barczi J.F., de Reffye P., Caraglio Y. « Essai sur l'identification et la mise en oeuvre des paramètres nécessaires à la simulation d'une architecture végétale: le logiciel AMAPsim. » In: Modélisation et Simulation de l'Architecture des Végétaux : Science Update, INRA Editions : 205-254, 1997.

[Barthélémy *et al.* 1997] Barthélémy D., Caraglio Y., Costes E., Architecture, gradients morphogénétiques et âge physiologique chez les végétaux, in: Bouchon J., de Reffye Ph., Barthélémy D. (Eds.), Modélisation et simulation de l'architecture des végétaux, INRA Éditions, Versailles, France, pp. 89-136, 1997.

[Blaise *et al.* 1998] Blaise F., Barczi J.F., Jaeger M., Dinouard P. , Reffye (de) P. Simulation of the. Growth of Plants – Modeling of Metamorphosis and Spatial Interactions in the Architecture and Development of Plants. In Cyberworlds 6. 81-109. Eds T.L. Kuni, A. Luciani, Springer Verlag Tokyo, 1998.

[Deussen 2005] Deussen O. Digital Design of Nature - computer generated plants and organics, Bernd Lintermann Springer Verlag New York, 2005.

[Hu *et al.* 2003] Hu B.-G., de Reffye P., Zhao X., Yan H.-P., Kang M.-Z. GreenLab: A New Methodology towards Plant Functional-Structural Model — Structural Aspect, In: (PMA'03). Beijing, China: Tsinghua University Press and Springer, 2003.

[Jallas *et al.* 1999] Jallas E., Sequeira R., Martin P., Cretenet M., Turner S., and McKinion J., "Virtual cottons, the firstborn of the next generation of simulation model", in Beltwide Cotton Conferences, Orlando, Florida, pp. 393-395, 1999.

[Jourdan Rey 1997] Jourdan C., Rey H. « Architecture and development of the oil-palm (Elaeis guineensis Jacq.) root system. » Plant and Soil, 189 : 33-48, 1997.

[Kang *et al.* 2002] Kang M.-Z., Yan H.-P., de Reffye P., Jaeger M., Hu B.-G. and Houllier F.. A fast algorithm for calculating stem and branch radial growth in a tree. *IUFRO colloque*, Vancouver, Sept. 2002.

[Kang *et al.* 2003] Kang, MZ , de Reffye P, Barczi JF, Hu BG. *Fast Algorithm for Stochastic 3D Tree Computation and Forest Simulation.* WSCG'2003 - the 11-th International Conference in Central Europe on Computer Graphics, Visualization and Computer Vision'2003 in co-operation with EUROGRAPHICS, 2003.

[Kang *et al.* 2004] Kang M.Z., Cournède P.H., Le Roux J., de Reffye P., Hu B.G., Theoretical Study and Numerical Simulation of a Stochastic Model for Plant Growth, in CARI'04, Hammamet, Tunisia, 2004.

[Lindenmayer Prusinkiewicz 1990] Lindenmayer A., Prusinkiewicz P. The Algorithmic Beauty of Plants, Springer-Verlag, Berlin, 1990.

[Perttunen *et al.* 1996] Perttunen J., Sievänen R., Nikinmaa E., Salminen H., Saarenmaa H., Väkevä J. LIGNUM: a tree model based on simple structural units, Annals of Botany 77. 87-98, 1996.

[Reffye *et al.* 1988] de Reffye P., Edelin C., Françon J., Jaeger M., Puech C. Plant models faithful to botanical structure and development. Proceedings of SIGGRAPH 88, in: Computer Graphics, 22 (4), 151-158, 1988.

[Reffye *et al.* 1990] de Reffye P. Dinouard P., Jaeger M. Basic concepts of computer plant growth simulation. In: Computer Graphics: "Where do we go now that we've arrived?, NICOGRAPH' 90, Tokyo (JPN), Nov. 1990, pp. 219-234, 1990.

[Reffye *et al.* 1996] de Reffye P, Fourcaud T, Blaise F., Barthélémy D., Houllier F. An Ecophysiological Model for Tree Growth and Tree Architecture, in: Silva Fennica eds., Workshop on Functional Structural Tree Models, Helsinki, 1996.

[Reffye Houllier 1997] de Reffye P., Houllier F. Modelling plant growth and architecture: some recent advances and applications to agronomy and forestery, Curr.Sci. 73, 984-992, 1997.

[Reffye *et al.* 1997] Reffye P. de, Houllier F., Blaise F., Fourcaud T. « Essai sur les relations entre l'architecture d'un arbre et la grosseur de ses axes végétatifs. » *In* : *Modélisation et Simulation de l'Architecture des Végétaux*, Bouchon J., de Reffye P., Barthélémy D. Eds.; Paris (FRA) : Science Update, INRA Editions : 255-423, 1997.

[Reffye *et al.* 2003] de Reffye P., Goursat M., Quadrat J.P., Hu B.-G., 2003. The Dynamic equations of the tree morphogenesis GreenLab model. In: *PMA'03*, Beijing, China: Tsinghua University Press and Springer

[Sievänen *et al.* 2000] Sievänen R., Nikinmaa E., Nygren P., Ozier-Lafontaine H., Perttunen J., Hakula H. Components of a functional-structural tree model, Ann. For. Sci. 57, 399-412, 2000.

[Soler *et al.* 2003] Soler C,. Sillion F., Blaise F., de Reffye P., An Efficient Instantiation Algorithm for Simulating Radiant Energy Transfer in Plant Models ACM Transactions On Graphics number 2 volume 22, April 2003

[Viennot *et al.* 1989] Viennot, X., Eyrolles, G., Janay, N., Arques, D. Combinatorial Analysis of Ramified Patterns and Computer Imagery of Trees. Computer Graphics, Vol.23(3), pp.31-40, 1989.

[Yan *et al.* 2003a] Yan H.P., de Reffye P., Pan C.H., Hu B.G. "Fast construction of plant architectural models based on substructure decomposition". Journal of Computer Science and Technology 18:780-787, 2003.

[Yan *et al.* 2003b] Yan H.-P., de Reffye P., Leroux J., Hu B.-G. : Study on Plant Growth Behaviors Simulated by the Functional-structural Plant Model GreenLab. In: *PMA'03*, Beijing, China: Tsinghua University Press and Springer, 2003.

[Yan *et al.* 2004] Yan H.P., Kang M.Z., De Reffye P., Dingkuhn M. "A dynamic, architectural plant model simulating resource-dependent growth". Annals of Botany 93:591-602, 2004.

[Wu 2005] Wu L., "Variational Methods Applied to Plant Functional Structural Dynamics: Parameter Identification, Control and Data Assimilation", Thèse de Doctorat de l'Université Grenoble I, 2005.

[Zhan *et al.* 2003] Zhan Z.-G., de Reffye P., Houllier F., Hu B.-G. "Fitting a Structural-Functional Model with Plant Architectural Data", In: PMA'03, Beijing, China: Tsinghua University Press and Springer.

Darwin and Computational Ecology: How Simple Models of Evolution Help our Search for Better Models of Ecological Systems

James P. Hoffmann
University of Vermont
Department of Botany
109 Carrigan Drive
Burlington, VT 05405 USA
+1 802 656 0429
James.Hoffmann@uvm.edu

ABSTRACT
The addition to computational ecology of two emerging technologies (evolutionary computation and ecoinformatics) offers an opportunity to advance our ability to build better ecological models and thus deepen our understanding of the mechanistic complexity of ecological systems. This paper describes one feasible approach toward this goal – the combining of inductive and deductive modeling techniques with the optimizing power of simple algorithms of Darwinian evolution that include information-theoretic model selection methods. Specifically, I show a way to extend classic genetic algorithms beyond typical parameter fitting of a single, previously chosen model, to a more flexible technique that can work with a suite of possible models. Inclusion of the Akaike information-theoretic model selection method within an evolutionary algorithm makes it possible to accomplish simultaneous parameter fitting and parsimonious model selection. Experiments with synthetic data show the feasibility of this approach, and experiments with time-series field data of the Zebra mussel invasion of Lake Champlain (USA) result in a model of the invasion dynamics that is consistent with the known hydrodynamic features of the lake, and a life-history stage of this invasive species. I also describe a way to extend this approach with a modified genetic-programming algorithm.

KEYWORDS
Computational ecology, ecological models, evolutionary computation, information theory, model selection, genetic algorithms, genetic programming, Zebra mussels

1. Introduction

Modeling ecological systems is important for many reasons. Models aid our attempts to predict future changes and can be invaluable for management purposes, and models can help us to understand better the inner workings of these systems and make our management decisions better informed and more effective. A modeler has many modeling techniques and approaches to choose from in building ecological models. Two fundamentally different ways to begin the modeling process are with deductive and inductive reasoning. The deductive method requires expert knowledge to build a mechanistic-based model, and is based on a first-principles understanding of the mechanisms acting within the ecological system. In contrast, the inductive method only needs the information contained in the available empirical data of the ecological system to construct a predictive model. Both methods have their strengths and weaknesses. The deductive approach can be more robust since its basis is the important operating mechanisms; however, this approach can be difficult because we often have an incomplete understanding of cause and effect in these systems. The inductive approach can produce models that are very precise in describing the empirical data, but they may not generalize or scale well, and it can be difficult to extract causality from these models.

These different modeling approaches can produce models of diverse forms (structures), and the quality and consistency of predictions can be dependent on the particular model chosen. At times, the predictions can even be contradictory among the different models. Attempts to model invasive species spread dynamics illustrate this point. Efforts to model mathematically the spatial spread of invasive species have been ongoing for nearly fifty years (for a summary see [Shigesada Kawasaki 1997]). Several invasive species model types have been developed, including both deterministic and stochastic models, and various combinations of these approaches. Some of these models are parameter-sparse and others are not. Models based on partial differential equations (PDE), integrodifference and integrodifferential equations, metapopulations, cellular automata, neural nets, and discrete-event simulation techniques have been used to predict spatial spread [Hastings 1996, Higgins Richardson 1996, Kot *et al.* 1996, Hill *et al.* 1997, Wang *et al.* 2002]. Although some robust predictions have been produced

(i.e. the asymptotic spread rate of invasive species appears to be linear in time), other predictions seem to be entirely dependent on the particular model chosen.

The model we choose invariably includes our biases and implicit assumptions, which can lead to mis-specification of the model structure (by mis-specification I mean omission of relevant explanatory mechanisms or variables, or inclusion of irrelevant ones, or the adoption of wrong functional forms). Some of the problems with mis-specified models are that they can be difficult to fit, and the quality of the model predictions can suffer from super-sensitivity to small changes in model structure [Wood Thomas 1999]. Conversely, if the model structure is correctly specified for the system of interest, then much can be learned via sensitivity tests of the model parameters, and a deeper insight can be obtained into the mechanisms that are operating to cause the observed system behavior. Furthermore, the model will likely be robust in its predictions. However, prior to model fitting and sensitivity tests the initial selection of a properly specified model structure must be made. Therefore, choosing a good model is more important than the subsequent fitting of model parameters. The critical question then is – ***Given a set of models to select from, how does one decide on the best model for a given problem?***

The rapidly growing field of ecoinformatics is providing us with new tools for managing and analyzing increasing amounts of spatially and temporally diverse ecological data, thus aiding our efforts for data-driven inductive modeling. At the same time, the use of model-selection methods based on information theory is becoming increasingly popular among ecologists [Johnson Omland 2004]. Evolutionary computation (EC) when combined with information-theoretic model selection, can serve as a bridge linking deductive knowledge-driven modeling to inductive data-driven modeling. This paper shows two ways to integrate these two modeling approaches; with a model selection genetic algorithm that uses variable-length genomes, and with a potentially more powerful genetic programming algorithm that incorporates domain-specific knowledge to evolve model structure. I first provide some background by describing the essentials of evolutionary computation and model selection, and then I describe the modified genetic algorithm that incorporates variable-length genomes and the information-theoretic Akaike model selection method. Following that, I will present some results of experiments that used noisy synthetic data, and some promising preliminary results with real field data. Finally, I will briefly describe a way to extend this approach by using a genetic programming algorithm instead of a genetic algorithm, and end with some suggestions for future work and thoughts of the challenges that lie ahead.

2. Essentials of Evolutionary Computation

Evolutionary computation uses algorithms that emulate the basic principles of biological evolution. There are several types of evolutionary algorithms (EA); the three most common are Genetic Algorithms (GA), Evolutionary Strategies (ES), and Genetic Programming (GP). These algorithms are a class of non-deterministic (derivative-free), stochastic, iterative search techniques that emulate some of the principles of Darwinian evolution (precisely, selection and reproduction of the fittest individuals, with some introduced variation during the reproduction step). They resemble random search methods (i.e. a Monte Carlo approach), but with an important difference - through a selection procedure, an evolution of increasingly better solutions results in a directed search that eventually converges to an optimal solution. These algorithms are robust and are capable of solving a variety of combinatorial and numerical function global optimization problems. They are often the method of choice for difficult model fitting/optimization problems where there is a single model structure to fit, particularly when optimizing models that exhibit multimodality [Bäck *et al.* 2000, Eiben Smith 2003]. The following description is based on a simple GA; however, the principles apply to all EA.

The essential components are:

- population of individual solutions
- fitness function to evaluate the quality of each solution (a.k.a. an objective or payoff function, or a figure of merit).
- selection mechanism for choosing some individuals to reproduce
- operators for rearranging and changing the information content of those individuals chosen to reproduce
- termination criterion.

Figure 1 shows an EA with these essential components in the order they are typically used.

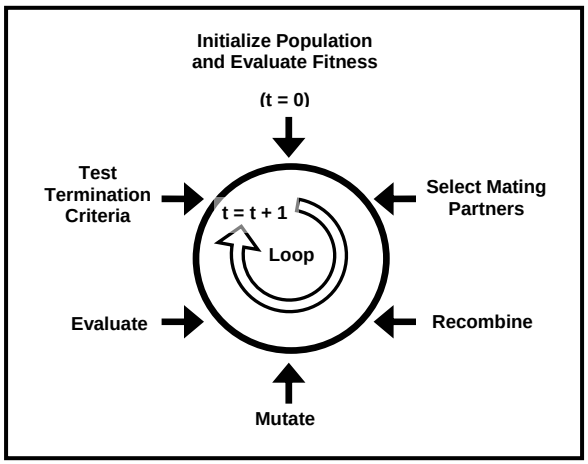

Individual solutions are randomly generated one-dimensional arrays that encode the parameter values of a previously chosen model structure. These linear arrays equate to chromosomes, the parameter values to genes (often binary, integer, character or real values), and their information content to the genotype. Fitness evaluation consists of decoding the genotype to express the phenotype. This is done by running the chosen model with the individual's parameter values and comparing the model predictions to known data. Fitness often consists of some measure of total error between model prediction and observed data. This measure is the scalar fitness score that maps directly to the quality of the predictions of that individual and is essential in the selection procedure. Selection of mating partners is either deterministic or probabilistic and typically favors individuals for reproduction with higher fitness values. This is how an EA achieves a directed search as opposed to simply a random walk.

Figure 1. The basic iterative loop of an evolutionary algorithm. Modified from [Schwefel Kursawe 1998].

Parameter values (genes) change during the search via recombination and mutation operators. Recombination, also known as crossover, mixes genes from two parent chromosomes to produce two offspring chromosomes each of which has some genes from both parents. Mutation introduces random modifications to the genes, thus allowing the exploration of new areas in the search space, which in theory guarantees that every point in the search space is possible to reach. Mutation is the ultimate source of new genetic information for evolution, since crossover only recombines existing information. Note that mutation alone, without selection or crossover, amounts to a random walk through the search space, whereas mutation with selection, but without crossover, creates a parallel, noise-tolerant, hill-climbing algorithm. Over many iterations of the algorithm, optimal parameter values evolve. Therefore, the typical EA does model fitting but not model selection.

3. Model Selection Background

Our hypothetico-deductive method of science when applied to modeling consists of four basic steps that start with creating a plausible set of hypotheses based on our knowledge and assumptions of the system we are observing. We have long recognized that considering multiple working hypotheses helps us to minimize our human biases and tendency toward adopting a favorite hypothesis [Chamberlain 1990], which can hinder efficient progress in our understanding [Platt 1964]. Each hypothesis is in effect a model that needs to be expressed mathematically, and then confronted with data to fit the parameters. Finally, either a "best" or a best set of models is chosen. These are the four essential steps of model selection that provide the researcher with the ability to weigh the evidence for the various hypotheses, and hopefully to infer the processes most likely to have operated in generating the observed patterns in the data.

The formalization of the model selection step has a rich history, starting with the famous postulate of William of Occam - the simplest model that adequately describes the empirical data is usually the correct one (Occam's razor). There are many techniques to select the "best" model and Occam's emphasis on simplicity (parsimony) provides the philosophical basis of the quantitative model-selection methods we use today. Some of these specific methods include: the classical null-hypothesis approach via likelihood-ratio tests, best-subset regression, cross-validation, bootstrapping, Akaike Information Criterion (AIC), Bayesian Information Criterion (BIC), Minimum Descriptive Length (MDL), Mallow's C_p Statistic, (all based on asymptotic methods), and lately non-asymptotic methods using concentration inequalities such as the Talagrand inequality (for an overview of these techniques see [Forster 2000]). Statistically, parsimony represents a tradeoff between bias and variance in the parameter estimators - the former decreases and the latter increases with more parameters in the model. Therefore, too few parameters cause underfitting and fail to include effects in the model supported by the data, while too many parameters cause overfitting and include effects in the model not supported by the data (i.e. fitting the noise in the data) resulting in poor model generalization. Both of these situations can result in mis-specified models, and parsimonious model-selection methods seek to minimize both underfitting and overfitting by finding an optimal balance between the bias and variance of the parameter estimators.

Hirotugu Akaike introduced a model-selection method in 1973 [Akaike 1973] known as the AIC (see [deLeeuw 1992] for a comprehensive description of this method). The AIC method is attractive for several reasons. It is widely regarded as a breakthrough in the theory of mathematical statistics because it formalized a robust relationship between the expected, relative Kullback-Leibler distance (a dominant paradigm in information theory) and Fisher's maximum likelihood theory. It

is relatively easy to calculate and use for selecting the "best" model, and it is easy to understand qualitatively what the AIC means – a measure of the lack of model fit (negative log of maximum likelihood) corrected for bias (the number of model parameters). In addition, unlike the null-hypothesis likelihood-ratio tests that require nested models and do not quantify the relative support for the various models, AIC does not require nested models and allows weighing the relative support for each model. Akaike saw his method as extending the maximum likelihood method, an extension that makes model selection and parameter fitting a joint optimization problem [Burnham Anderson 2002]. Since EC is a proven optimization technique, it is reasonable to expect that including AIC within an EA might enhance our abilities to choose and fit good models of ecological systems.

4. Incorporating Model Selection Criteria into Evolutionary Algorithms

Including a model selection criterion in the fitness function of an EA is known as complexity-based fitness evaluation [Iba 2000]. This approach to modeling is largely unexplored. Most experience with this method has been with GP (a type of EA that is based on parse trees) to control decision-tree growth. Results are promising ([Iba 2000] and references cited therein). However, few studies have used complexity-based fitness evaluation in GA. Konagaya and Konoto in 1993 (cited in [Iba 2000]) used MDL for their fitness evaluation of a bioinformatics classification problem to minimize overlearning due to noise. Model identification and parameter estimation of linear ARMA models was attempted with an EA that combined GA and ES operators [Rolf *et al.* 1997]. They tried different statistical criteria in their fitness function, and although estimation of the error series by the EA was successful, correct model identification was achieved only 20% of the time. In contrast, some success was reported with using MDL in a simplex GA for selection of regressors in linear AR models and in nonlinear polynomial models [Vesin Grüter 1999]. They accurately identified the correct operating models, and demonstrated fast convergence rates compared to exhaustive search techniques. Therefore, EA with the inclusion of model selection criterion, such as AIC, offers the potential of an automated, efficient search technique for good candidate models. In effect, the EA orchestrates a competition among a community of candidate models while simultaneously optimizing parameter fit to the observed data. Furthermore, by inserting expert knowledge into the set of candidate models the EA can incorporate deductive modeling into the optimization process. Thus, evolutionary computation when combined with information-theoretic model selection, can serve as a bridge linking deductive knowledge-driven modeling to inductive data-driven modeling. Figure 2 gives an overview of this combined approach. The key element that is required to implement this approach is variable-length genomes in the EA. Variable-length genomes are necessary in order to incorporate knowledge in the form of multiple model structures in the community of candidate models. Next, I describe one way to implement effective variable-length genomes in a GA.

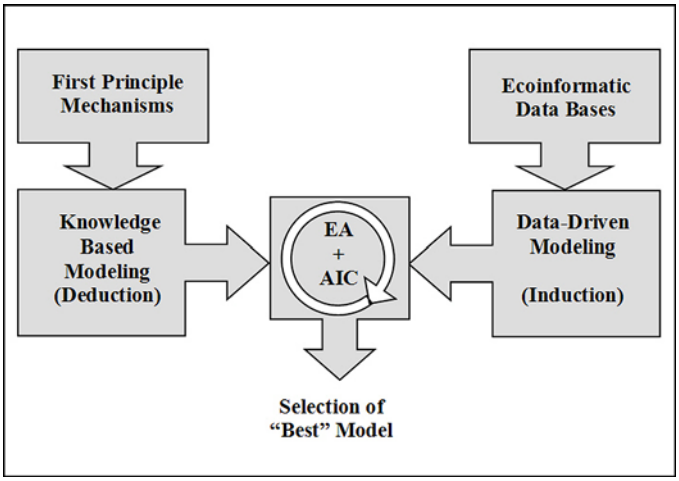

Figure 2. Conceptual view of the combining of deductive and inductive modeling via a complexity-based EA.

4.1. Variable-Length Genomes in GA

Variable-length genomes are implemented by mapping an evolvable switch to each gene of the chromosome, and consequently the modified GA can activate/inactivate each model parameter in each individual. Therefore, each individual has a complete genome and can potentially represent the most complex (global) model of a nested set (i.e. parameters for all models are contained in each individual). This is conceptually equivalent to totipotency in biological chromosomes. The switches are evolvable in the same way as are the values of the model parameters. Thus, virtual variable-length individuals are created that effectively represent all the model variations of the set, depending on which model parameters are switched

on. In the GA, the mutation operator randomly turns on and off these switches, and selective pressure ultimately evolves a best model structure. Figure 3 provides an overview of how the variable-length genome GA can conduct model selection.

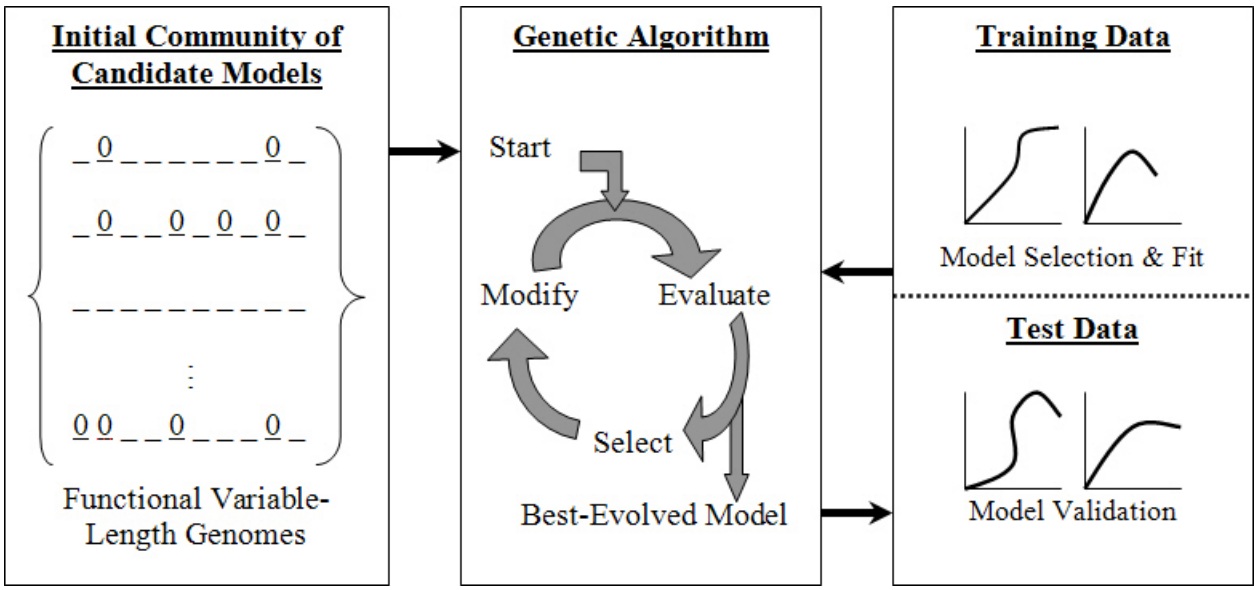

Figure 3. GA model selection and fitting procedure. The community of candidate models is randomly initialized. Some parameters are effectively turned off (0 indicates an inactive parameter), depending on the state of the internal switch at initialization. Therefore, although all models have the same fixed genome length, their structure when evaluated by the fitness function is functionally variable. The observations are divided into two data subsets; a training set used by the fitness function for evolving the best models, and a test set for independently validating the best-evolved models.

Specifically, the modulo remainder function creates the evolvable switch that turns the genes on and off. One of the less-significant digits of the gene value itself determines whether a gene is active or not. This modulo approach utilizing internal gene switches has a parallel in real organisms, where in some ribosomal RNA and tRNA genes, part of their coding sequence has a double function and serves as a regulatory switch for the gene. A binary switch is created by using modulus 2 on the integer-transformed gene value. Thus,

$$\left[Int\left(a_i \times 10^k\right)\right] (\mathrm{mod}\, 2) = 0 \tag{1}$$

or

$$\left[Int\left(a_i \times 10^k\right)\right] (\mathrm{mod}\, 2) = 1 \tag{2}$$

for any i, where a_i refers to the gene value at position i on the chromosome and k is of sufficient magnitude to shift a less-significant digit to the unit position of the resulting integer. Therefore, the integer value in the unit position of the transformed gene determines whether the gene is active or not. The number of active genes is counted by the fitness function and is used in the calculation of the bias correction term of the AIC. These internal evolvable switches, created by overloading the gene variables, are the essence of the model-selection GA method (hereafter referred to as MSGA).

4.2. Experimental Tests of the MSGA – Synthetic Data

Initial testing of this method used synthetic training data generated by a known model that was included among the set of candidate models available to the MSGA (for specific details of these tests see [Hoffmann *et al.* 2004]). Note that in each test, the GA is conducting a "blind" evolutionary search for the best model – no prior information is available to the algorithm about the correct data-generating model. Both noisy (Gaussian) and noise-free data were used in these tests. Three types of models (general polynomial equations, stock and flow system dynamic models (process models), and diffusive-reaction PDE models) were tested. The GA software package used for these tests is a public domain, parallel genetic algorithm function library written in ANSI C, known as PGAPack [Levine 1996], and it is available from the United States DOE Argonne National Laboratory (ftp://ftp.mcs.anl.gov/pub/pgapack). The fitness functions and models are coded in C,

optimized, and parallelized for SMP (Symmetrical Multiple Processors) and the numerical PDE solvers are licensed from NAG (The Numerical Algorithms Group, Inc., Downers Grove, IL, USA), and optimized in FORTRAN for SMP.

4.2.1 Polynomial Models

The general polynomial for these tests was

$$y(x) = a_n x^n + a_{n-1} x^{n-1} + \ldots + a_1 x + a_0 \tag{3}$$

where $a_0, a_1, \ldots, a_{n-1}, a_n$ are real-valued model parameters. In these experiments, n values of five and nine were used. Initialization by the GA created the community of competing models comprised of the complete fifth or ninth-order polynomials and their associated subset models. In the fifth-order polynomial experiments, the maximum number of competing candidate models was 64, and for the ninth order, it was 1024. Each individual genome represented the coefficients of the various model structures. The 'correct' model used for generating the 'true' data for these experiments was a specific fourth-order model $y(x) = -20x^4 + 20x^2 + 14$ over the domain {-1.0, -0.9, -0.8,..., 1.0}. Noise was added as "true" data + z*("true" data), where z is a random deviate from a Gaussian distribution ($\mu = 0$, $\sigma = 0.05$).

Model fitness is expressed as total error, calculated as the log residual sum of squares (RSS)

$$e = \log \sum_{j=1}^{m} \left(y_j - \hat{y}_j \right)^2 \tag{4}$$

where m is the number of data points, y_j is the true value of the correct operating model at point j and $\hat{y}_j$ is the predicted value of a candidate model at point j. The $\hat{y}_j$ value is calculated as

$$\hat{y}_j = \sum_{i=0}^{n} \left\{ \left[Int\left(a_i \times 10^8 \right) \right] (\mathrm{mod}\ 2) \right\} a_i x_j^i \tag{5}$$

where n is the order of the complete polynomial model, and a_i refers to the gene (coefficient) value at position i on the chromosome. This estimated RSS is then transformed to the maximized log-likelihood (Burnham and Anderson 2002), and the AIC bias correction term added. Therefore, the fitness of each candidate polynomial model is the true AIC.

4.2.2 Dynamic-System Models of Leaf Photosynthesis

These models are useful to evaluate the ability of the MSGA to choose the correct model structure when presented with data produced from models considerably more complex than the polynomial test models. The system dynamic models for these tests simulated the physiological ecology of a leaf undergoing photosynthesis. Several sub-models simulated the leaf's response to variation of different environmental factors. The leaf-photosynthesis model simulated the dynamics of the carbon, water and heat budgets of the leaf over time. Soil water potential, herbivory, and ozone effects were also included in the model. The model comprised six ordinary-differential equations that describe the state variables and fluxes. External forcing functions accounted for the influence of light intensity and duration, temperature, humidity and wind velocity, and feedback loops linked the various model subcomponents together. The nonlinearities and interdependencies in the model produced complex behaviors in leaf temperature, heat content, and water and carbon content. Each individual in the GA contained thirteen genes that represented the model parameters associated with the state variables and fluxes of the carbon, water and heat budgets, and effects of ozone and herbivory. The 'true' model output data were generated from a subset model whose genes for ozone and herbivore effects were turned off. These data comprised a parallel time series of ten metrics (photosynthetic rate, leaf carbon...) observed at 15-minute intervals over a 24-hour period. For each candidate simulation model, a sum of the relative error of each metric at each time point was calculated, and a penalty for the number of active parameters in the model was added to this sum. Therefore, fitness is similar to a common analog of AIC [Hongzhi 1989].

4.2.3 Diffusion-Reaction Models

The final tests with synthetic data used diffusion-reaction (DR) models of the basic form shown in equation 6.

$$\frac{\partial n}{\partial t} = D\left(\frac{\partial^2 n}{\partial x^2} + \frac{\partial^2 n}{\partial y^2} \right) + f(n)\, n \tag{6}$$

where D is the diffusion coefficient (a measure of how quickly the organisms move over a surface), n is the population density, and $f(n)$ is the per capita growth rate.

DR models are partial-differential equations, which incorporate dispersal terms and population dynamics associated with the spread dynamics of an invasive species. Specifically, they can represent species whose densities and dynamics change due to (i) movement and (ii) birth and death, and they have a continuous functional dependence on both space and time. However, they do not mechanistically describe most of the key ecological factors that influence the spread of invasions. Spatial effects such as habitat heterogeneity, mass transport via advection, linear or non-linear density-dependent growth, and long and short distance dispersal can play important roles in invasive species dynamics [Murray 1989, Hastings 1990, Cantrell Cosner 1991, Karieva 1991, Renshaw 1991, Holmes *et al* 1994, Shigesada *et al.* 1995, Cantrell Cosner 1998, Mendez *et al.* 2003]. It is possible to extend equation 6 to include some of these factors. Equation 7 was used in these tests and allows for a community of candidate models that incorporate one type of dispersal (simple diffusion), two types of population growth (exponential and logistic), and advection in the X and Y directions. The form of the complete model is

$$\frac{\partial n}{\partial t} = D\left(\frac{\partial^2 n}{\partial x^2} + \frac{\partial^2 n}{\partial y^2}\right) - w_x \frac{\partial n}{\partial x} - w_y \frac{\partial n}{\partial y} + \varepsilon\left(1 - \frac{\mu n}{\varepsilon}\right)n \tag{7}$$

where D is the diffusion coefficient, w_x and w_y are advection parameters, ε and μ are growth parameters relating to density dependence and per-capita growth. The genome length of the DR models is five and allows for a community of thirty-two candidate models. The "true" model output data were generated from a subset model with diffusion turned on, linear density-dependent growth, and advection in the Y direction turned off. Fitness for these experiments was the common analog of AIC [Hongzhi 1989]. The spatial domain was a square 21 x 21 grid, and the spread dynamics occurred over 10 time units.

4.3. Experimental Tests of the MSGA – Field Data

A final test of the MSGA used a field data set of the Zebra mussel invasion of Lake Champlain, USA. This data comprises a ten-year time series of the veliger larvae, juveniles, and adult forms of this invasive species. It is publicly available (http://www.anr.state.vt.us/dec/waterq/lakes/htm/lp_lczebramon.htm) and is the best whole-lake Zebra mussel data set in existence due to the consistency of the method used and the fact that the initial sampling occurred at the very beginning of the invasion in 1993. Zebra mussels were first discovered in the extreme southern portion of the lake and over the next ten years spread northward throughout the entire lake.

Lake Champlain occupies a north-south fault zone and is long (193 km) and narrow (19 km at its widest point). It is located at 44.50 latitude and -73.25 longitude, and is the sixth largest lake in the United States. The predominant flow is north into the Richelieu River in Quebec, Canada, and the mean hydrologic residence time is 3.3 years. Additional information on the lake is available at http://www.worldlakes.org/lakedetails.asp?lakeid=8518.

The "true" model is unknown when using field data, so for these tests it is necessary to use known facts of the life history stages of Zebra mussels, and the hydrodynamic features of Lake Champlain as criteria for judging whether the MSGA has evolved a "correct" model. The Zebra mussel data set includes a time series of veliger larvae densities. The larvae are released by the adults in large numbers (~10^6/adult) from late spring to early fall. This stage of their life history is planktonic for up to several weeks and it is expected that the large-scale hydrodynamic features of the lake (predominant northward flow) will dominate their spread dynamics at an annual time scale. Therefore, a "correct" DR model of their dynamics should include anisotopic advection in the northern direction, and the magnitude of the advection should approximate the known average annual northward flow rate of the lake. Furthermore, due to the extremely high fecundity of the mussels and large-scale mixing of the planktonic larvae, no Allee effect (positive density dependence over a limited range of density) is expected, however the data do suggest some negative density dependence. To see if this method would evolve a model structure consistent with these expectations, a gridded spatial domain of the lake was constructed whose cell size was approximately 1.6 km^2. The MSGA was then used with a genome encoding for a seven-parameter DR model whose complete form (equation 8) can describe dispersal as both simple diffusion and mass transport advection, linear and non-linear negative density-dependent growth, density-independent growth (exponential), and positive density-dependent growth (Allee effect).

$$\frac{\partial n}{\partial t} = D\left(\frac{\partial^2 n}{\partial x^2} + \frac{\partial^2 n}{\partial y^2}\right) - w_x \frac{\partial n}{\partial x} - w_y \frac{\partial n}{\partial y} + \frac{a}{b} n^{1-2b}\left(K^b - n^b\right)\left(n^b - q^b\right) \tag{8}$$

where D is the diffusion coefficient, w_x and w_y are advection parameters in the E-W and N-S directions respectively, a is a scaled intrinsic growth rate, b is a dimensionless constant, which describes the rate of growth and density dependence (shape parameter) of the population, n is density, K is the carrying capacity, and q is the Alee effect population density such that for $n < q$ population density declines and eventually becomes extinct, whereas for $n > q$ the population grows toward K.

The observed veliger larvae densities were supplemented with linearly interpolated values in grid cells without sampling data, and then locally averaged and smoothed to produce the training data. The data were scaled to annual time units for consistency with the known large-scale annual hydrodynamic features of the lake.

4.4. Test Results – Synthetic and Field Data

The initial testing with synthetic data showed that for all the model types the MSGA consistently evolved "correct" model structures even when the data were degraded with noise. When parsimonious model selection via AIC was not active all the evolved models were incorrect (with only one exception), and were over parameterized and over fit to the data (Table 1).

Table 1. Effect of Parsimony (AIC) and Noise (N) on the Success of the MSGA.

Treatment→ **Model ↓**	**- AIC** **- N**	**- AIC** **+ N**	**+ AIC** **- N**	**+ AIC** **+ N**
Polynomial (5^{th} order)	0/1000	0/1000	995/1000	983/1000
Polynomial (9^{th} order)	0/100	0/100	91/100	94/100
Photosynthesis	0/100	0/100	96/100	93/100
Diffusion-Reaction	0/50	1/50	40/50	38/50

Note: the numerator is the number of correct models evolved
and the denominator is the total number of replicates.

This is particularly evident in Figure 4 where all the replicates without AIC had a considerably better fit to the noisy data by using additional parameters to fit the noise. However, this was achieved with mis-specified, incorrect models. Whereas, greater than 90% of the runs with AIC evolved the correct model and produced accurate and precise estimates of the "true" parameters despite the noisy data. The "correct" polynomial models produced parameter estimates that were identical (to within 0.001) of those produced with a least- squares regression on the noisy data, after using the best-subset method with Mallow's Cp statistic for variable selection. Note, that the larger the negative fitness value the better the model fit to the data.

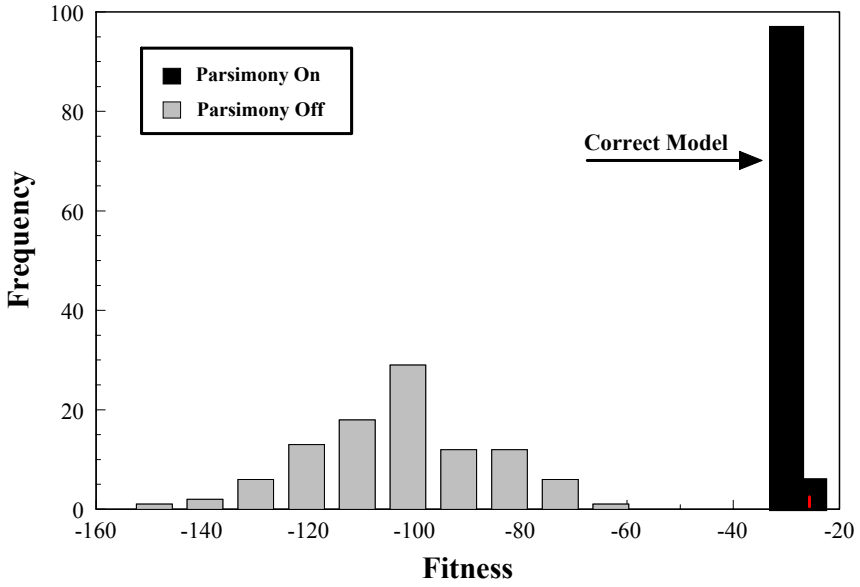

Figure 4. Success of the MSGA evolving the correct data-generating model. Frequency histogram of two experiments using the ninth-order Polynomial model with Gaussian noise ($\mu = 0$, $\sigma = 0.05$). Each experiment involved 100 replicates.

Twenty-nine of thirty-six MSGA experiments using the Lake Champlain veliger density data evolved the "correct" model structure. The average advection northward of the larvae was 62.9 km/yr (± 1.5 SD) which compares favorably to an estimated 60 km/yr calculated from the known hydrologic residence time and length of Lake Champlain. These results show that the MSGA approach is feasible, and that over fitting of models can be avoided with the incorporation of AIC, even with noisy data.

5. An Alternative Approach – Genetic Programming

GP is a variation of GA in which both the model structure and associated parameters are encoded into the individual genomes [Eiben Smith 2003]. Typically, the genome is represented as a tree that can increase or decrease in size via variation operators (mutation and recombination). Therefore, variable-length genomes are intrinsic to GP. This expands the search for a good model by allowing not only the parameter values, but also the model structure to evolve during the search. However, this also greatly increases the search space and makes the evolution of a good model computationally more difficult. Nevertheless, GP has the potential to address some of the disadvantages of the MSGA, while retaining its advantages.

5.1. Advantages and Disadvantages of the MSGA

In the MSGA the modeler explicitly creates the set of competing candidate models, which incurs some advantages; the specified model structures include the empirical knowledge and mechanistic understanding of experts of the ecological system being modeled. However, there are also disadvantages; the models invariably also include the modeler's biases and implicit assumptions, which can lead to mis-specification of the correct model structure. In addition, an adequately specified model must exist among the set of candidate models contained within the global model, and furthermore the set of competing models is closed, therefore the MSGA cannot generate, via the evolutionary process, any novel model structures. Thus our ability to discover novel models, with the ability to generate new understanding of internal mechanisms, is limited. These disadvantages are not unique to the MSGA, but are recognized as general limitations of model selection methods.

Several different approaches have been used to minimize these general limitations. One method to avoid bias and unintentional assumptions is to use partially specified models to improve the fitting of complex biological systems [Wood 2001]. In this approach the model structure includes only well understood elements whereas less well-known parts of the

biology are represented in a flexible non-parametric way. Although this approach does minimize model mis-specification problems, it does not allow for the discovery of new model structures. Another approach that has been pursued in the field of Artificial Intelligence is known as Automated Modeling (AM) [Keppens Shen 2001]. AM, specifically a type called Compositional Modeling, has been most successful when modeling physical systems. In AM the model is constructed automatically by using model-fragment libraries of varying complexity. Some researchers have attempted to use these techniques on biological systems [Keppens Shen 2000], especially ecological systems, but this effort is only in the initial stages. A related approach, known as Equation Discovery uses a context-free grammar, parse trees, and parsimony implemented via minimum description length [Todorovski *et al.* 2000, Dzeroski Todoroski 2002]. The Equation Discovery method has been successful in constructing models of ecological systems, but is limited by the exhaustive nature of its search method. A directed evolutionary search with GP may be a better way to address these limitations.

5.2. A Proposed GP Model Selection Procedure

GP can evolve a set of models from a construction set of model components (fragments) that can be assembled in various ways to represent a complex biological system. There would need to be a set of rules for their assembly (biologically impossible connections should be prevented). It would also be necessary to incorporate some measure of complexity to insure parsimonious model evolution. It may be possible to extend AIC to include the number of components and their interconnections, and another option would be to use MDL. The library of model components in the construction set would include stocks (state variables i.e. population density…), flows (fluxes i.e. growth or dispersal rates…), inputs (environmental factors i.e. temperature, currents…), and protected combinations of the previous three components that encapsulate expert knowledge. The latter component (known as model blocks, super-blocks, or fixed sub-models, depending on their complexity) would exist as pre-defined functions (PDF) in the construction set. Model structure would be comprised of two primary components: stocks and flows. Stocks are state variables that can be modified by flows. Flows are rates of change, and are determined by formulas. The operands of these formulas are combinations of external input data, previously calculated stock values (feedback), and mathematical constants. The operators are a basic set of mathematical functions (+, -, *,/,exp...). Figure 5 depicts this GP model selection procedure.

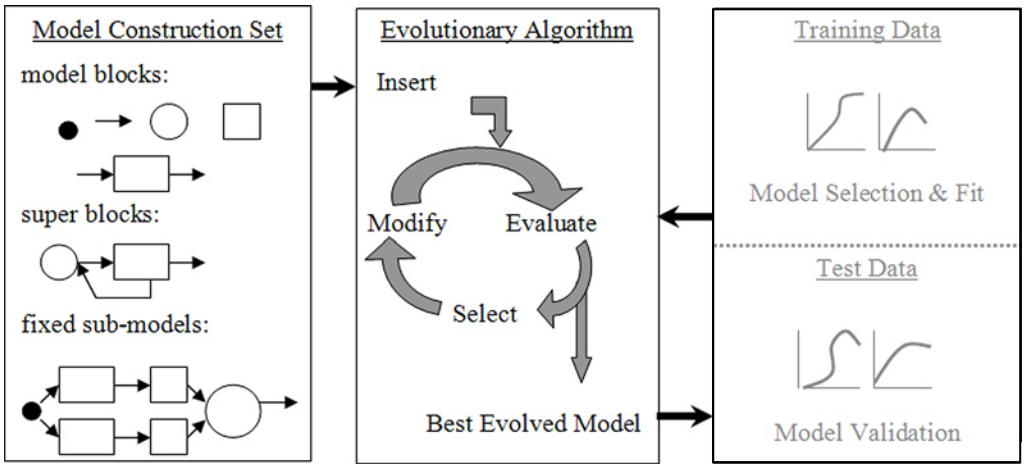

Figure 5. GP model selection and fitting procedure. The model construction set is initialized randomly but can also be 'seeded' with models drawn from the set used in the MSGA approach. State variables are represented as rectangles, fluxes as arrows, and inputs as circles. The observations are divided into two data subsets; a training set used by the fitness function for evolving the best models, and a test set for independently validating the best-evolved models.

This GP approach shares some similarity with AM, but differs in that it relies on Darwinian evolution to direct the search for good model structures. Model fitness would be evaluated by comparing model predictions to a subset of the measured data. Another subset of the data would be used for validation of the best-evolved model. This approach is similar to one adopted for modeling industrial processes [Brucherseifer *et al.* 2001, Hinchliffe Willis 2003]. Another group in New Zealand is using grammar-based GP to evolve models of water quality. Their approach differs from this method in that their grammar rules significantly bias the model search space to a limited set of structured equations; specifically single-equation time-series models [Whigham Recknagel 2001].

6. Summary and Conclusions

Evolution by natural selection is a superb optimizer of biological structure and function. Akaike's significant contribution to our understanding of mathematical statistics brought together model selection and model fitting under the theoretical framework of optimization. The behavior of ecological systems derives from the optimized biological structure, function, and interactive mechanisms of its component parts. Therefore, since we seek to understand the operating mechanisms of ecological systems through modeling, it is good sense to explore the potential of combining algorithms of simple evolution with model selection methods to develop better models of these systems.

The results reported here suggest that this approach has significant potential and warrants future exploration. Nevertheless, formidable challenges lie ahead, specifically in increasing the computational efficiency of these algorithms to explore adequately the very large search spaces. Faster computers, and clusters of computers, will help to alleviate this difficulty, but they will not eliminate this problem. Of the two methods outlined here, the MSGA is more tractable than GP because it constrains the search to the *a priori* specified closed set of candidate models; however, it is more likely to suffer from biases and incorrect assumptions. In theory GP does not suffer from these weaknesses and has the potential of discovering novel models, however because it attempts to search all model and parameter space simultaneously, it too must constrain the search by inserting expert knowledge and by the judicious choice of mathematical operators for model building.

ACKNOWLEDGMENTS

The progress reported here would not have been possible without the expert contributions of several colleagues. Drs. Daniel Bentil, and Bonsu Osei of the Mathematics Department at the University of Vermont are the force behind all of the PDE-based modeling, and Mr. Chris Ellingwood has singly managed to implement all the diverse code necessary to bring these ideas to reality. USDA Hatch and US DOE Computational Biology grants to the University of Vermont funded this work.

REFERENCES

[Akaike 1973] Akaike, H. Information theory and an extension of maximum likelihood principle, In: *Second International Symposium on Information Theory* (Petrov, B. N. & Csaki, F. Eds.) Budapest, Hungary Akademia Kiado: 267-281, 1973.

[Back *et al. 20*00] Bäck, T., Fogel, D.B., & Michalewicz, T. *Evolutionary Computation 1: Basic Algorithms and Operators*. Bristol, UK, Institute of Physics Publishing, Ltd, 2000.

[Brucherseifer *et al.* 2001] Brucherseifer, E., Bechtel, P., Freyer, S., & Marenbach, P An indirect block-oriented representation for Genetic Programming. Proceedings of the 4th EuroGP Conference, Springer, 268-279, 2001.

[Burnham Anderson 2002] Burnham, K.P. & Anderson, D.R. *Model Selection and Multimodel Inference: A Practical Information-Theoretic Approach*, Springer, New York, 2002.

[Cantrell Cosner 1991] Cantrell, R.S. & Cosner, C. The Effects of Spatial Heterogeneity in population Dynamics. *Journal of Mathematical Biology*, **29**:315-338, 1991.

[Cantrell Cosner 1998] Cantrell, R. S. & Cosner, C. On The Effects of Spatial Heterogeneity on Persistence of Interacting Species. *Journal of Mathematical Biology*, **37**:103-145, 1998.

[Chamberlain 1990] Chamberlain, T.C. The method of multiple working hypotheses. *Science* **15**:92-96, 1890.

[deLeeuw 1992] deLeeuw, J. Introduction to Akaike (1973) information theory and an extension of the maximum likelihood principle. In: *Breaakthroughs in Statistics*. (Kotz, S. & Johnson, N.L. Eds.), Springer-Verlag, London, **1**:599-609, 1992.

[Dzeroski Todoroski 2002] Dzeroski, S. & Todorovski, L. Encoding and using domain knowledge on population dynamics for equation discovery. In L. Magnani, N. J, Nersessian, and C. Pizzi, eds. *Logical and Computational Aspects of Model-Based Reasoning*, Kluwer, Dordrecht, 227-247, 2002.

[Eiben Smith 2003] Eiben, A.E. & Smith, J.E. *Introduction to Evolutionary Computing*. Springer, Berlin, 2003.

[Forster 2000] Foster, M.R. Key concepts in model selection: Performance and generalizability. *Journal of Mathematical Psychology* **44**-1:205-231, 2000.

[Hastings 1990] Hastings, A. Spatial heterogeneity and ecological models. *Ecology*, **71**: 426-428, 1990.

[Hastings 1996] Hastings, A. Models of spatial spread: A synthesis. *Biological Conservation* **78**:143-148, 1996.

[Higgins Richardson 1996] Higgins, S.J. & Richardson, D.M. A review of models of alien plant spread. *Ecological Modelling* **87**:249-265, 1996.

[Hill *et al.* 1997] Hill D., Coquillard P., & De Vaugelas J., Discrete-Event Simulation of Alga Expansion, *Simulation*, **68-**5: 269-277, 1997.

[Hinchliffe Willis 2003] Hinchliffe, M.P. & Willis, M.J. Dynamic systems modeling using genetic programming. *Computers & Chemical Engineering* **27**-12:1841-1854.

[Hoffmann *et al.* 2004] Hoffmann, J.P., Ellingwood, C.D., Bonsu, O.M. & Bentil, D.E. Ecological model selection via evolutionary computation and information theory. Special issue on biological applications of evolutionary computation in *Journal of Genetic Programming and Evolvable Machines* **5**-2: 229-241, 2004.

[Holmes *et al.* 1994] Holmes, E. E., Lewis, M. A., Banks, J. E., & Viet, R. R. Partial differential equations in ecology: Spatial interactions and population dynamics. *Ecology* **75**:17-29, 1994.

[Hongzhi 1989] Hongzhi, A. Fast stepwise procedures of selection of variables by using AIC and BIC criteria. *Acta Mathematicae Applicatae Sinica* **5**:60-67, 1989.

[Iba 2000] Iba, H. Complexity-based fitness evaluation. In: *Evolutionary Computation 2*, (Bäck, T., Fogel, D.B., & Michalewicz, T. Eds.), Bristol, UK, Institute of Physics Publishing, Ltd., 15-24, 2000.

[Johnson Omland 2004] Johnson, J. B., & K. S. Omland. Model selection in ecology and evolution. *Trends in Ecology & Evolution* **19**:101-108, 2004.

[Karieva 1991] Kareiva, P. Population dynamics in spatially complex environments: Theory and data. *Phil. Trans. Roy. Soc. Lond. B* **330**: 175-190, 1991.

[Keppens Shen 2000] Keppens, J. & Shen, Q. Towards compositional modeling of ecological systems via dynamic flexible constraint satisfaction. Proceedings of the 14th International Workshop on Qualitative Reasoning, 74-82, 2000.

[Keppens Shen 2001] Keppens, J. & Shen, Q. On Compositional Modelling. *The Knowledge Engineering Review* **16**:157-200, 2001.

[Kot *et al.*l996] Kot, M., Lewis, M., & van den Driessche, P. Dispersal data and the speed of invading organisms. *Ecology* **77**:2027-2042, 1996.

[Levine 1996] Levine, D. *Users Guide to the PGAPack Parallel Genetic Algorithm Library*, Argonne National Laboratory, Batavia, IL, USA, Technical Report ANL-95/18, ftp://ftp.mcs.anl.gov/pub/pgapack, 73 pp. 1996.

[Mendez *et al.* 2003] Mendez, V., Fort, J., Rotstein, H.G. & Fedotov, S. Speed of reaction-diffusion fronts in spatially heterogeneous media. *Physical Review E*, **68**:041105-1 - 041105-11, 2003.

[Murray 1989] Murray, J. D. *Mathematical Biology*. Springer-Verlag, Berlin, 1989.

[Platt 1964] Platt, J.R. Strong inference. *Science* **146**:347-353.

[Renshaw 1991] Renshaw, E. *Modelling Biological Populations in Space and Time*. Cambridge University Press, 1991.

[Rolf *et al.* 1997] Rolf, S., Sprave, J. & W. Urfer Model identification and parameter estimation of ARMA models by means of evolutionary algorithms. Proceedings, IEEE/IAFE Conference on Computational Intelligence for Financial Engineering, New York, IEEE Press, Piscataway, NJ, 237-243, 1997.

[Schwefel Kursawe 1998] Schwefel, H-P. & Kursawe, F. 1998. On natural life's tricks to survive and evolve. In Fogel, D.B., Schwefel, H-P., Bäck, T. & Yao, X. (Eds.), Proceedings of the Second IEEE World Congress on Computational Intelligence with the Fifth IEEE Conference on Evolutionary Computation, Anchorage Alaska, IEEE Press, Piscataway, NJ, **1**:1-8, May, 1998.

[Shigesada *et al.* 1995] Shigesada, N., Kawasaki, K. & Takeda, Y. Modeling stratified diffusion in biological invasions. *American Naturalist* **146**:229-251, 1995.

[Shigesada Kawasaki 1997] Shigesada, N. & Kawasaki, K. *Biological Invasions: Theory and Practice*. Oxford Series in Ecology and Evolution. [Eds.] R. May and P. Harvey. Oxford University Press, 1997.

[Todorovski *et al.*20 00] Todorovski, L., Dzeroski, S., Srinivasan, A., Whiteley, J. & Gavaghan. D. Discovering the structure of partial differential equations from example behavior. Proceedings of the 17th International Conference on Machine Learning. Morgan Kaufmann Pub., 991-998, 2000.

[Vesin Grüter 1999] Vesin, J-M. & Grüter R. Model selection using a simplex reproduction genetic algorithm. *Signal Processing* **78**:321-327, 1999.

[Wang *et al.* 2002] Wang, M.H., Kot, M., & Neubert, M.G. Integrodifference equations, Allee effects, and invasions. *Journal of Mathematical Biology* **44**:150-168, 2002.

[Whigham Recknagel 2001] Whigham, P.A. An inductive approach to ecological time series modeling by evolutionary computation. *Ecological Modeling* **146**:275-287. 2001.

[Wood 2001] Wood, S.N. Partially specified ecological models. *Ecological Monographs* **71**:1-25, 2001.

[Wood Thomas 1999] Wood, S.N. & Thomas, M.B. Super-sensitivity to structure in biological models. *Proc. Roy. Soc. (B)* **266**:565-570, 1999

.

Track 1

ENVIRONMENTAL & ECOLOGICAL MODELLING

The Interface Problem in Model Coupling: Examples from Atmospheric Science

Wilfried Winiwarter
ARC systems research
A-2444 Seibersdorf
Austria
Tel.: +43-50550-3868
wilfried.winiwarter@arcs.ac.at

ABSTRACT
Examples drawn from atmospheric sciences demonstrate that models focus on internal consistency. This optimization, while necessary, prevents a focus on interface adaptation. Model validation primarily assesses the internal model behavior, rather than the adaptation and usability of its interface to the output. With the development of solutions from computer science to overcome issues of data incompatibility, the conceptual issues of model interface coverage gain importance. Covering processes along interfaces may become the major challenge of modeling in the future. The interfaces should in part be regarded problems of communication between scientists, and thus be attributed a sociological approach. The "middle ground" could at the same time describe an ill-defined interface calling for better description, but also reflect a challenge to overcoming scientists' disciplinary divergence.

KEYWORDS
Interface, Atmospheric science, modeling, system boundaries

1. Introduction

Computer simulation models provide an incomplete reflection of systems within the physical world. Adding details and features to a model is the default way to deal with the incompleteness inherent in any modeling approach. Often these additions help to improve model behavior drastically and are fundamental for successful model validation. Still models describe only small sections of the real world, when it may be desirable to cover a larger part of it, or models require input information which is as such not available.

Modelers have resorted to apply results from other models in such cases. Information preprocessing usually has been a tedious task, requiring to obtain information on data formats, units, and detailed description of the background of the information delivered. Where data input had to be performed more frequently, data interfaces and model links have been developed. Data flow may be unidirectional as preprocessing of input information, but also bidirectional data transfer (2-way links) has been established allowing feedback of results from the receiving model.

Such solutions have been hampered by the technical difficulties associated with such data transfer. Not only formats and units, but also resolution and general scopes of models have to be reconciled. Model coupling therefore has become an important topic for theoretical considerations. Under terms like composability [Davis Anderson 2003] or meta-modeling and multi-paradigm modeling [Mosterman Vangheluwe 2004] concepts for bringing together different model components have been discussed. While not being blindfolded towards real-world issues, focus of these approaches obviously was directed towards general data interoperability, without specifically recognizing data information content.

Concepts for data integration in environmental information have been envisioned [Denzer 2002], and work has started at least in the context of environmental disaster management [ORCHESTRA 2005]. The aim of such endeavors is to facilitate information exchange across the boundaries of different platforms or models which are equipped with a predefined interface, allowing for direct model coupling. Such activities are supported by standardization efforts concerning the underlying information, e.g. harmonization of spatial data detrimental for many environmental applications [INSPIRE 2005].

As the technological advance will allow for increased data interoperability in the foreseeable future, it seems useful to consider the more practical implications of such improved data merging. This paper will discuss the opportunities and the limitations of intense coupling of models especially regarding atmospheric sciences. Consequences towards evaluation of

atmospheric model results and strategies to evade possible pitfalls caused by this increased potential of computing will be discussed.

2. Boundaries Between Real Systems and Their Representation in Models

One of the simplest ways to define systems is by way of its boundaries. Natural systems are enclosed by natural boundaries (e.g. set at the point of phase transition), economic systems by political boundaries and economic classification. The common point is that systems tend to be defined such that internal homogeneity prevails. Processes within such boundaries tend to be reasonably well understood. Models trying to emulate real systems take advantage of such definitions, as homogenous conditions favor modeling and support successful validation exercises.

As a consequence of this definition, boundaries of systems are along inhomogeneities. The inhomogeneity itself then is neither part of the system, nor part of the model emulating this system. Even if two systems are separated by such an inhomogeneity, models covering the respective systems can technically be linked to exchange data via an interface. Such a linkage may however often not be sufficient to describe the overall behavior of the coupled systems. Bridging the inhomogeneity, which is not included in any of the models, possibly will prove to be more challenging than the representation of any of the homogeneous systems alone.

A practical example may be taken from climate research. The global climate of the atmosphere is closely influenced by the heat and material transfer from the oceans. Both atmospheric and ocean circulation models exist, and it seems but logical to build a coupled ocean-atmosphere model. Still the processes which were sufficient to describe the transport within one media alone, ocean or atmosphere, did not seem sufficient to also cover the phase transfer. Specific modeling of wave behavior had to be added to better characterize the surface related processes [Hasselmann 1991].

In practice, more issues may appear than can be resolved by introducing an interface model. E.g., adequate treatment of transfer across the interface may require a different resolution (notably, a higher temporal resolution) than necessary for either of the homogeneous realms and thus pose additional data requirements. Interestingly, in the largely different field of defense modeling and simulation, such issues of information quality have been recognized as being part of the "composability" of a model [Davis Anderson 2003]. These authors describe the "science of the subjects being modeled" in clear contrast to the science of modeling and simulation.

3. Defining Boundaries in Atmospheric Sciences

The setting of system boundaries and defining homogeneities may also be a matter of perspective. In environmental science, systems to be considered may comprise physical environments as well as socio-economic issues. National statistics, which are basic ingredients to inventories of air pollutants [Winiwarter 2002], represent a unique and seemingly also homogeneous source of information, e.g. on a certain type of manufacturing process. In the physical world, the individual installations which run this process can be very far apart, contributing very differently and inhomogeneously to the physical atmosphere. What is a homogeneous area in the economic realm (and also in the economic model) is far from that in the physical reality (and physical model).

Still even such differences have to be reconciled and interfaces between diverse sets of information have to be sought. The symbolic language used in models may even be helpful in the reconciliation process [Winiwarter Schimak 2005]. In the following we will go into the details to explore a few examples of such interface problems.

3.1. Emissions of Air Pollutants from Natural Sources

In any political process on air pollution abatement, convening parties are to be considered responsible only for their own pollution. There is, however, a considerable rest which also affects the atmosphere. Such sources of air pollution are volcanoes, lightning, wild animals and natural vegetation [Simpson *et al.* 1999]. Statistics on the latter kind of material transfer into the atmosphere is difficult to obtain, if available at all, as not (or not directly) connected with human activities. Economically based models (and national emission inventories) tend to include the human-induced part of emissions only. If natural emissions are not considered specifically, an atmospheric model will receive only incomplete data on material input and therefore not be able to fully reflect the real situation.

Moreover, the exact definition of natural vs. anthropogenically caused flux of air pollutants is ambiguous [Winiwarter *et al.* 1999]. A strict separation and a full accounting of emissions (avoiding both double counting and neglecting specific sources) can not possibly be generalized. Only an individual negotiation of contents will fully reflect the situation and the degree to which sources are considered natural or human-induced, i.e. where boundaries are defined.

3.2. Release Point into the Atmosphere

Flux of material into the atmosphere through well-defined entrance points is termed point source emissions. Point sources provide a well-defined boundary. The major part of material flux derives from elsewhere, however. Pollutants arrive in the air in street canyons or in forest canopies (or even indoors). Such confined spaces are not covered in standard atmospheric models. The behavior of compounds is considerably different compared to the well-mixed atmosphere, as the strongly elevated concentrations enhance chemical transformation and the proximity to surfaces increases their deposition/removal. In order to adequately link material fluxes and atmospheric concentrations, coverage of the interface would require adding street canyon models or forest canopy models, respectively.

3.3. Scale Issues

Even in the undisturbed atmosphere large differences in concentrations occur. Depending on the spatial and temporal resolution, atmospheric models may be able to reflect these differences. Large point sources cause pollution plumes which do not immediately disperse. Again specific models, the plume-in-grid models, are required to close the gap between available models and their interfaces. Likewise, plumes from an agglomeration of sources (conurbations) are responsible for increased local concentrations, and a potentially different chemical regime with respect to the resolution of the atmospheric model. Such sub-grid effects have been studied in detail in the past [Neftel Spirig 2003, CityDelta 2004] and may under certain conditions also allow for parameterization instead of explicit coverage. Nevertheless they have to be addressed directly. These studies also confirm the obvious observation that resolution of all important input parameters needs to be improved in order to obtain results at a final detail. Applying averages instead of grid-specific data for only one of these inputs will lead to decreasing output resolution at the same time (and call for parameterization of sub-grid effects).

The very same issues that are valid for spatial scales apply to temporal scales. In the atmosphere, space and time relate over atmospheric mixing and the characteristic times of the respective atmospheric processes, which are *a priori* independent of the resolution. The dispersion of pollutants is governed by physical processes, specifically wind and eddy diffusion. Finer spatial scales will basically also require shorter timescales, but only until atmospheric mixing is faster than transformation and removal processes. As many processes are driven by the diurnal cycle, a minimum temporal resolution is a fraction of a day. Coinciding effects occur e.g. at atmospheric deposition, a removal process. High concentrations at high removal rates lead to considerably more material loss than when only averages were considered.

4. Methods to Adequately Cover Interfaces

During the difficult process of data manipulation to overcome data transfer between different sources, usually not only data format issues, but also the information content has been dealt with in some detail by the operators. As an implicit procedure, data conversion always prompted to check the quality of the data to be converted. This did however not follow a standardized or reproducible methodology. The loss of this quality check due to use of an automated conversion scheme opens the possibility to apply more adequate ways of quality assessment. The options presented below are not exclusive, i.e. more than one may be applied to the same interface problem.

4.1. Detailed Interface Description

The key issue in correctly coupling datasets is that it is fully clear which kind of data is actually contained. In a similar way as a complete (and machine-readable) description of the data format, a very detailed and comprehensive description of information content should be prepared. Based on such a description, an expert could decide if the information content fully reflects the requirements of this coupling. Data transfer could then be permitted immediately, or an additional treatment of the interface (e.g., by an interface model) could be recommended. One way to safeguard this option on a procedural level is to incorporate it as part of a quality assurance/quality control program. Such a program would then require prescribing the expert solicitation of model interfaces.

4.2. Comprehensive Models

Tacit knowledge plays a decisive part in information flow. If all interfaces between models or model components can be kept within a modeling team, such informal exchange of information which leads to tacit knowledge can be taken advantage of. A comprehensive model covering the full extent of information flow required would serve such a purpose. The only disadvantage of such an approach is that there is a limit to the number of experts that can work together and communicate closely, and therefore also a limit exists on the size such a comprehensive model could take. As soon as the informal communication is broken (e.g. by further increasing the team size), team members will be less clear on the implicit assumptions taken at a model boundary, and more formal ways will have to be implemented to attain the same level of understanding.

4.3. Interface Validation

Validation of models is a standard tool to check their applicability. As discussed above, there is a tendency that validated models cover areas that are better described and easier to model than the interstices. Thus it seems useful to develop validation tools which cover just the interfaces to connect the models. The only alternative, validation of the full model complex encompassing all interfaces, may be impractical. Not only can it be difficult to provide such a comprehensive validation, but also there is the risk that a successful validation just masks the fact that erroneous behavior of one model component or interface compensates that of one or more other.

Validation in general requires testing model results against independent information such as atmospheric measurements. Interface validation by measurements may include to challenge assumptions of homogeneous atmospheric concentrations, implicitly assumed when transferring concentration data from one model component to an other.

4.4. Integrated Assessment Models

One possibility to bring back the model of a very complex system into the hands of one modeling team is integrated assessment modeling. Comprehensive models of the partial systems are parameterized, and the parameterized versions of these partial models are linked. Integrated assessment models retain the complexity of the interfaces between the individual partial models. The respective partial model itself remains as a largely simplified version, which is still able to emulate the model's behavior. The quality of parameterization to actually reflect this behavior is key to a successful validation, and can be made subject to validation.

Examples for this procedure have been presented [Leimbach Jaeger 2005, Amann *et al.* 2001]. Integrated assessment models have been applied successfully for policy purposes due to their capability for scenario evaluation. Moreover, the approach allows covering complex systems and still leaving the control over the interface to a small modeling group that can relatively easily communicate and sort out potential discrepancies at the interfaces.

5. Discussion and Conclusions

Surface effects and heterogeneous processes in chemistry and physics are not only subject of intense study, but even form a sub-discipline of its own. Even for these disciplines that allow clear definitions of the interfaces, it can be shown that an important part of the overall chemical and physical transfer takes place in a very small part of the total volume available, very close to the surfaces.

In the systems of quite diverse origin considered here, including physical as well as economic systems, such a clear definition is not available and has to be derived case-specific. In a sociological context, Richard White describes such an ill-defined interface (in that case: the relations between two factions of humans, specifically Indians and American settlers) as the "Middle Ground" [White 1991]. Taking up this analogy, this middle ground not only is an area worth of intense study, but further to that allows for interfacing contents at a level beyond simple data transfer. Due to negotiations of the individual contents (and iterative improvement of communication) the information flow may easily exceed original expectations.

Understanding model interfaces as tools of a communication process – specifically between the scientists involved – allows to also adopt sociological concepts. Focusing on the middle ground, the extended model interfaces will be further required in model linkage. Technological advance of not having to deal with translation problems is extremely beneficial. Results of linked models will not be available "on-the-fly", however, as the interfaces in data content will require additional attention. Here the time and the resources gained can be much better invested than previously, when focusing on format issues, to provide decisive improvements in the overall model results assessment.

ACKNOWLEDGMENTS

This paper has been prepared in part as a contribution to the project NATAIR, an FW6 activity funded by the European Commission, contract no. 513669.

REFERENCES

[Amann *et al.* 2001] Amann M., M. Johansson, A. Lükewille, W. Schöpp, H. ApSimon, R. Warren, T. Gonzales, L. Tarrason, S. Tsyro. An integrated assessment model for fine particulate matter in Europe. *Water, Air and Soil Pollution* **130:** 223-228, 2001.

[CityDelta 2004] Web site of the City-Delta project. On-line at http://rea.ei.jrc.it/netshare/thunis/citydelta/

[Davis Anderson 2003] Davis, P.K., R. H. Anderson. Improving the composability of Department of Defense models and simulations. RAND Corporation, Santa Monica, CA, 2003. On-line at http://www.rand.org/publications/MG/MG101/

[Denzer 2002] Denzer, R. Generic Integration in Environmental Information and Decision Support Systems. In: A.E. Rizzoli and A.J. Jakeman (Eds.) Integrated Assessment and Decision Support. Proceedings of the 1st biennial meeting of the International Modelling and Software Society, Lugano, June 24-27, 2002, Vol. 3, 53-60. University of Lugano, Switzerland, 2002.

[Hasselmann 1991] Hasselmann K. Epilogue: waves, dreams and visions. In: R. Beal (Ed.), Directional ocean wave spectra, pp. 205-208, Appl. Phys. Lab., John Hopkins Univ., Laurel, MD, 1991, as cited by F. Ardhuin *et al., EOS Transactions, AGU*, **86-4**: 37, 25 Jan 2005.

[INSPIRE 2005] Web site of the European Commission's work programme of preparatory actions to support the future implementation of an EC proposal for a Directive aimed at establishing an Infrastructure for Spatial Information in Europe, INSPIRE. On-line at http://www.ec-gis.org/inspire/

[Leimbach Jaeger 2005] Leimbach M., C. Jaeger. A modular approach to Integrated Assessment modeling. *Environmental Modeling and Assessment* **9** (4): 207-220, 2005.

[Mosterman Vangheluwe 2004] Mosterman P.J., H. Vangheluwe Computer Automated Multi-Paradigm Modeling: An Introduction. *Simulation* **80**: 433-450, 2004.

[Neftel Spirig 2003] Neftel, A., C. Spirig, Eds. EUROTRAC - LOOP (Limitation Of Oxidant Production) Final Report. GSF, Munich, Germany, 2003. On-line at http://loop.web.psi.ch/Annual_Reports/LOOP_final.pdf

[ORCHESTRA 2005] Web site of the EU funded FP6 integrated project ORCHESTRA. On-line at http://www.eu-orchestra.org/

[Simpson *et al.* 1999] D. Simpson, W. Winiwarter, G. Börjesson, S. Cinderby, A. Ferreiro, A. Guenther, C.N. Hewitt, R. Janson, M.A.K. Khalil, S. Owen, T.E. Pierce, H. Puxbaum, M. Shearer, U. Skiba, R. Steinbrecher, L Tarrasón, and M.G. Öquist. Inventorying emissions from Nature in Europe. *J. Geophys. Res* **104**: 8113-8152, 1999.

[White 1991] White, R. The Middle Ground. Indians, Empires and Republics in the Great Lakes Region, 1650-1815. Cambridge Univ. Press, 1991.

[Winiwarter *et al.* 1999] Winiwarter W., H. Haberl, D. Simpson. On the boundary between man-made and natural emissions: Problems in defining European ecosystems. *J. Geophys. Res.* **104**: 8153-8159, 1999.

[Winiwarter 2002] Winiwarter W. Scientific Foundations for Atmospheric Emission Inventories. Habilitationsschrift, eingereicht bei der Fakultät für Technische Naturwissenschaften und Informatik, TU Wien. ARC Seibersdorf research report, ARC--S-0184, December 2002. On-line at http://www.arcs.ac.at/extranet/winiwarterw/papers/arcs0184.pdf

[Winiwarter Schimak 2005] Winiwarter, W., G. Schimak. Software Systems for Emission Inventories. *Environmental Modelling and Software*, in press

3Worlds: Design of a generic software Platform for Simulating Multi-scale Ecological Systems

Jacques Gignoux
Biogéochimie et écologie
des milieux continentaux
ENS, 46 rue d'Ulm
75230 Paris cedex 05, France
+33 1 44 32 37 06
gignoux@biologie.ens.fr

Ian D. Davies
Ecosystem Dynamics
RSBS / ANU
GPO Box 475
Canberra ACT 2601, Australia
+61 (02) 6125 5046
ian.davies@anu.edu.au

David R.C. Hill
ISIMA/LIMOS
Université Blaise Pascal
BP 10125
73173 Aubière cedex, France
+33 4 73 40 50 19
drch@isima.fr

ABSTRACT
We describe the rationale, specifications and architectural design of a new simulation software (3Worlds), devoted to the simulation of ecological systems at different scales from individuals to the world. We focus here on concepts, i.e. on the class design that enables such flexibility. 3Worlds relies on (1) a hierarchical description of ecological objects within an ecosystem, (2) a separation of geometric, physical and biological processes defined in different classes, (3) the ability to overlay different spatial representations of the same system in relation to the modelled ecological processes. Examples of the feasibility of these solutions in previous ecological software are given.

KEYWORDS
Ecosystem, Structure-function relationships, Scale, Hierarchy, Simulation

1. Introduction

This paper describes the rationale, specifications and architectural design of a new simulation software platform called 3Worlds (in reference to the Dutch artist M.C. Escher's litograph, see cover picture), devoted to the simulation of ecological systems at various scales from individuals to the world. We focus here on concepts, i.e. on the class design that enables such a flexibility. The coding of the software is just starting, and the design is still open to discussion for future improvement.

The issue addressed by this project is that of the relationship between structure and function in biological systems, an issue that arose independently in plant physiology [Le Dizès *et al.* 1997; Lemoine *et al.* 1999; Lacointe 2000], in ecosystem studies [Simioni *et al.* 2000, 2003], and landscape dynamics. Our analysis is restricted here to terrestrial ecosystems with a strong vegetation component, but the concepts developed in this framework might be extended to aquatic systems or animal-dominated systems (these two aspects being possible future extensions of the 3Worlds project).

1.1. The current practice of simulation in ecology

1.1.1. Structure-function relationships: simulation as an integration and synthesis tool

At the plant and ecosystem scale, the spatial organisation of a living system (its spatial structure or geometry) and its organisation into connected sub-units (its topology, or its biodiversity) may affect its biophysical functioning (matter and energy fluxes through the system, biological impact on its sub-units, feedback on the whole system).

At the plant scale, the objective of such research is to understand how a morphology (or architecture) determines water, carbon and nitrogen fluxes within the plant and how the species genetic program adapts this morphology during plant development in response to those fluxes. The ultimate goal is to model and predict the development of a plant in interaction with its physical and chemical environment while retaining its internal biological constraints (genetic development program, physiological limits). Architectural models [Barthélémy *et al.* 1995a,b; Caraglio 1996; Jay *et al.* 1995; Jourdan and Rey 1996, 1997] proposed a sound formal framework describing plant geometry and topology, and the evolution through time of such geometries/topologies based on plant estimated architectural parameters [Godin and Caraglio 1998]. Recent advances tend to couple this purely morphogenetic description with physiological knowledge [Le Dizès *et al.* 1997; Balandier *et al.* 2000; de Reffye *et al.* 1997], at the scale of the plant and of small communities. Whereas the geometry/physiology integration is relatively advanced, the spread of resources (in particular photosynthetically active radiation) within the space occupied by a plant with a complex architecture remains a difficult problem.

At the ecosystem scale, the objective of such researches is to understand (1) how the spatial structure and species diversity of an ecosystem influence the fluxes, and (2) how the ecosystem structure evolves in response to those fluxes, in the short and long term. The ultimate objective is to predict the temporal dynamics of ecosystems (species invasion/exclusion, change in matter fluxes, effects on renewable resources like drinking water or soil fertility), particularly its response to perturbations of its usual functioning, at the scale of a few seasonal cycles or at the century/millenium scale. The numerous existing models can be classified along two axes: (1) from spatial models (often individual based) to non spatial models, and (2) from physiology (short time scale, seconds to days) to demography (long time scale, months to years). Among these, one finds the large family of the gap models for forest dynamics, where spatial structure is reduced to a vertical structure but coupling physiological and demographic processes [Botkin *et al.* 1972; Bugmann 1994; Friend *et al.* 1993; Kellomäki and Väisänen 1991; Lauenroth *et al.* 1993; Noble *et al.* 1980; Pastor and Post 1985; Prentice *et al.* 1993]; spatialized individual-based models based either on demography [Gourlet-Fleury 1997; Moravie *et al.* 1997; Menaut *et al.* 1990], or on physiology [Simioni *et al.* 2000; Korzukhin and Ter-Mikaelian 1995], which rarely integrate both aspects [Coquillard *et al.* 2000a,b; Gignoux *et al.* 1998; Pacala *et al.* 1993]; 'cellular automata' models, generally with a restricted meaning in ecology (discrete space automata with only one individual per cell, and where the state of a cell depends on neighbouring cells [Hochberg *et al.* 1994; Colasanti and Grime 1993; Franc 1996; Jeltsch *et al.* 1996; Lett *et al.* 1999; Prado 1991; Thiéry *et al.* 1997; Wiegand and Milton 1996]); non spatial Markov-chain models used for example to simulate vegetation succession [Moore and Noble 1993; Noble and Slatyer 1980]. The MUSE model was an attempt to synthesize these tools [Gignoux *et al.* 1998].

Common concepts between these two scales are the need to consider the geometry, the diversity of sub-units (growth

units of trees or individual plants), the relations between those sub-units (topology of connections between growth units, competition for resources required by survival, development, reproduction), and their interactions with physical and biological laws. The goal of a modelling approach, in both cases, is to:

1. yield a synthesis of current knowledge on a particular biological object (plant, ecosystem, landscape) through the coupling of different 'views' (geometric, physical, biological) of the object to understand its functioning as a system composed of numerous interacting sub-systems. Building such a simulation model is perceived as a constraining synthesis exercise ('it has to run'), hence more formal than a purely verbal or heuristic synthesis of the processes demonstrated through the classical analytical approach;

2. provide a tool for conducting virtual ecological experiments giving researchers long-term access to a tool where, for example, fluxes between all components of a simulated system could be measured. A major benefit of running simulations is to perform experiments impossible to conduct in the real world.

1.1.2. Effects of global change on living systems: simulation as a forecasting and/or management tool

Climate and land-use changes have important impacts on living systems. The scientific objective is invariably to predict the response of this complex system to perturbations of its usual functioning.

The complexity of interactions between physical, biological and socio-economic processes has lead to many different approaches at many different scales. These approaches are often specific to the field leading the modelling study. To deal with such complexity, we believe it is important to first tackle the issue of structure and function in ecological systems.

Models developed in this context span scales from the ecosystem to the globe:

1. at the landscape scale (~100 km²), cellular automata models are used, where each cell represents a landscape piece not limited to a single individual, allowing the coupling of biological and physical processes (or disturbances) at the same or coarser resolutions, such as water runoff, fire spread or land-use heterogeneity. Theoretical exploration tools on the role of propagule dispersal in heterogeneous landscapes [Lavorel *et al.* 1994] as well as prediction tools for environment studies [Scanlan 1992; Coughenour 1994] sometimes including trophic web sub-models [Coughenour 1994] are found in this class of models; water catchment hydrological models make up a family of models mainly based on physical processes (interaction with vegetation is rarely considered). These last models present an interesting feature: they require a geometry/topology appearing at scales larger than the ecosystem.

2. at the regional (sub-continent) or global scale, simulation models use a physical approach, even if the biosphere is more and more present in the models [Schimel *et al.* 1997; Steffen *et al.* 1994; Martin 1992; Leemans *et al.* 1996; Keane *et al.* 1996; Beerling *et al.* 1997]. Only at this scale can feedbacks from the vegetation to the climate be modelled. Even if physics is and must remain the dominant scientific field for these models, biology is or at least should be parameterized in those models in a summarized way.

In this context, simulation is used not only as a synthesis and virtual experimentation tool, but also as a forecasting tool. Another interesting approach called holistic simulation can be used when enough computing power is available. This holistic simulation is explored on the Earth Simulator. In contrast to existing nonlinear simulations of individual phenomena, what we is called Holistic Simulation explores a complex interdependence between micro and macro scale processes [Sato 2003].

1.2. Expected gains from a generic simulation platform for ecological systems

Simulation models are used as tools for the synthesis of knowledge acquired in the study of complex biological systems, and as exploratory or even predictive tools for the behaviour of such systems. The general framework of structure-function relationships in the context of global change constitutes a federative concept for various fields, from the plant to the landscape (or to the globe).

We think that a synthesis of the knowledge gained in those fields as a generic simulation platform could constitue a major scientific gain for the following reasons:

1. **a better use of computer science**: the general objective of simulation models is always the same: answering particular questions for complex coupled systems. This complexity usually makes simple modelling techniques (e.g. differential equation systems) inadequate. Many components of simulation models are very similar among different models: most models use discrete space grids, discrete time (sometime discrete event) simulation driving, very similar physiological process sub-models (photosynthesis, respiration, carbon allocation, stomatal regulation, organic matter decomposition models, etc...) or similar demographic processes (fecundity/survival tradeoff, propagule dispersal). For example, the photosynthesis model used in almost all models is that of [Farquhar 1980] and there are only a few stomatal conductance models (while the process in itself is not fully understood - cf [Jarvis 1976]). But because of the lack of a common computer science formalism, models obtained by assembling similar or identical sub-models usually have a different behaviour, and differ in the coding of the same sub-models. This leads to large amounts of time wasted on code maintenance, particularly in the area of geometric representation which can be very complex. It

seems clear that a platform flexible enough to encompass all the cases described above would optimize the use of computer science resources in ecological modelling.

2. **a standardized method for conducting simulation experiments**: many model comparison workshops have been conducted in the recent past, in various fields such as global dynamic vegetation modelling [VEMAP 1995], soil organic matter decomposition models [Smith *et al.* 1998], or tree-grass system functioning [House *et al.* 2001]. A common observation in such workshops is the difficulty in identifying exactly what aspect of two models causes them to produce different outputs: As the models differ on many points, it is usually impossible to relate a behaviour difference to a particular submodel or ecological process. A common platform based on common concepts would be a major step forward in dealing with model comparisons. Our objective is not to solve the (formal) computer science problem of model or program comparison, but to enable sound comparisons between simulations, imitating the classical experimental approach. For example, in a model such as LAMOS [Lavorel *et al.* 2000; Davies *et al.* 2001], it is possible to compare two models differing by only one sub-model, and hence to identify which process is responsible for changes in model behaviour. The goal is simply to provide a tool for virtual experiments (including experiment designing facilities), analogous to real experiment tools, by manipulating parts of a virtual system.

This project deals with transferring technology from computer science to fields with a strong biological component (even if physics plays a significant role in ecology, ecology is before all a biological science). More than this, it has a methodological goal; to provide an approach for comparing ecological models across all scales. Simulation is an invaluable tool for ecological science, because it allows experiments to be performed which cannot be done in the real world: Simulation gives access to large spatial scales (cf. in climatology the success of the global circulation models), long time scales (e.g. forest dynamics, ecosystem stability), and to immeasurable variables (e.g. fluxes impossible to measure like net primary production, theoretically meaningful parameters such as intensity of competition) through properly designed virtual experiments.

2. The specific problems of simulating ecological systems

The following problems are constantly met in ecological simulation:

2.1. Diversity of scientific fields

2.1.1. No general agreement in process representation

Ecology is the science of diversity, not only in species, but also in system representations. In contrast to physics, there is no agreement among ecologists on any ecological process occurring in an ecosystem. Hence the great diversity of models, even for comparable scales, and the impossibility of making statistically valid model comparisons. This diversity might well be due to the imperfectness of measurement techniques in relation to the complexity of ecological systems, and to the implicit observational scale in any given model.

2.1.2. Physics and biology have different laws

Ecological systems are classically analyzed either as biological systems built upon evolutionary theory, or as physico-chemical systems based on thermodynamics. While physics deals with fluxes described by state variables with a continuous evolution in time, biology is characterized by death and reproduction, which introduce large discontinuities in fluxes over time. Hence biology is more often modelled through probabilities, bifurcations and random numbers. The mathematical formalisms adapted to both fields differ, and may explain the lack of models that truly couple physiology (from the 'physics' world) and demography (from the 'biology' world).

2.1.3. The overwhelming importance of space

Space is important in ecological modelling for two reasons: (1) the coupling between parts of an ecosystem is often only understood and modelled through their relative positions in space, and (2) many environment management problems require a spatial solution, i.e. where to act to induce a response of the system. Many models include space in a more or less crude or implicit way, sometimes explicitly, but without any well-established methodology for doing so. Ecological modellers often do not have the time to code the complex algorithms that deal with space description of individual-based models (IBMs).

2.2. The multiscale nature of ecological systems

2.2.1. Multiple organization scales

Although ecological simulation models span a large range of scales from individuals to the world, they rarely deal with more than 2 scales of organization. Almost all simulation models in ecology deal with 2 scales, since they are based on the population-individual relation. This is explicit in IBMs, but it is also present implicitly in 'cellular automata' where individual cells may have a complex internal dynamics which, through interactions with the other cells, produces the emerging property of the whole system. Very few models deal with 3 scales (e.g. [Soler *et al.* 2003] [Sato 2003]), from leaf to group of individual trees).

2.2.2. Multiple time and spatial scales

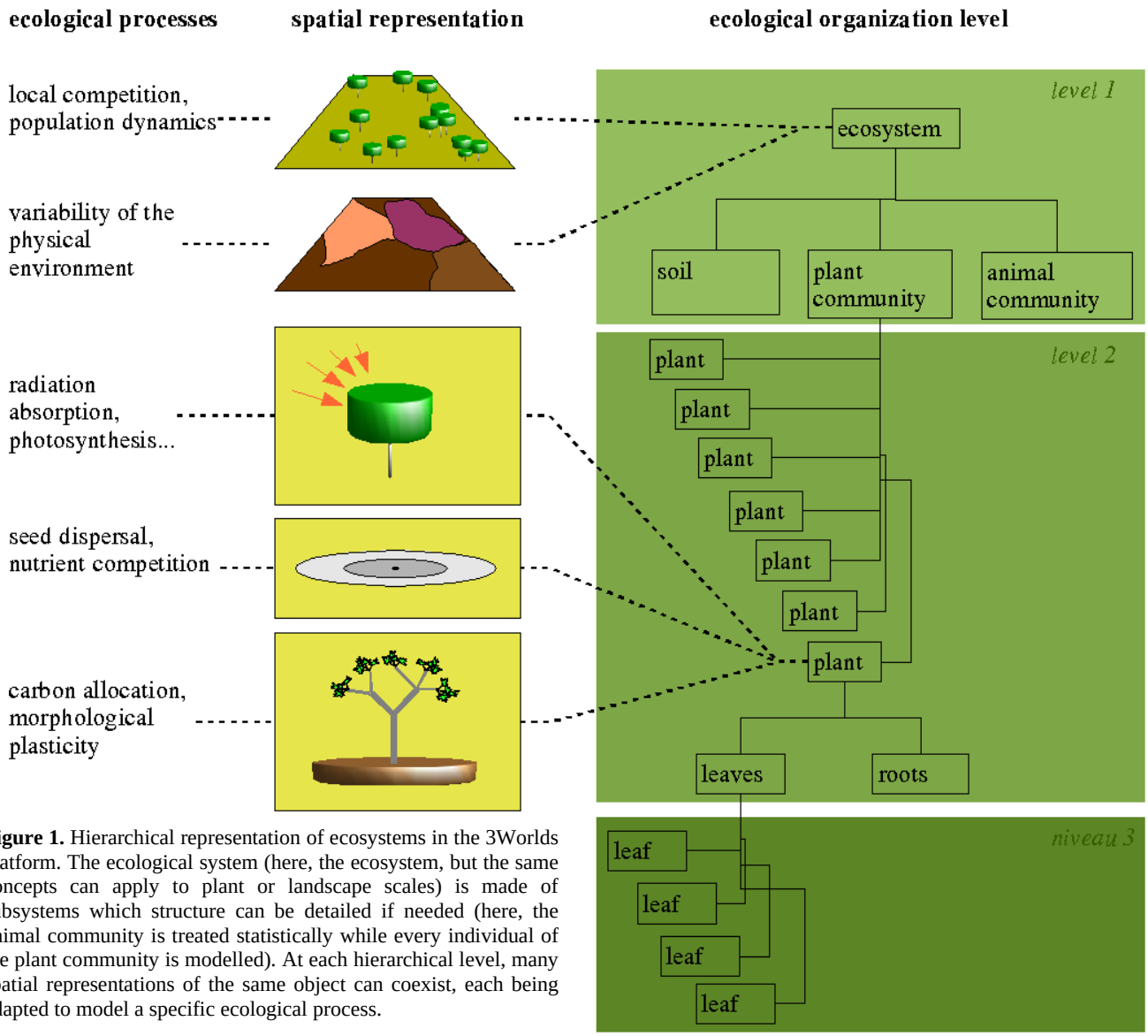

Figure 1. Hierarchical representation of ecosystems in the 3Worlds platform. The ecological system (here, the ecosystem, but the same concepts can apply to plant or landscape scales) is made of subsystems which structure can be detailed if needed (here, the animal community is treated statistically while every individual of the plant community is modelled). At each hierarchical level, many spatial representations of the same object can coexist, each being adapted to model a specific ecological process.

The individual plant or animal is often a useful organization scale to deal with in ecological modelling (for example in IBMs). However, the spatial and temporal scales associated with individuals vary over orders of magnitude, which makes the computation extremely difficult to optimize. For example, in a savanna, if trees and grasses are both represented as individuals, the simulator will spend almost all its time computing grass dynamics, having an overly well described population of grasses, and a poorly described population of trees with only a few individuals. Handling the interactions between such populations is difficult since one is required to describe them at different levels of abstraction. This multiplicity of time and spatial scales makes ecological simulation difficult when dealing with ecosystems with a high biodiversity.

2.2.3. The observation scale

Implicit in all models is a scale of observation. For example, a photosynthesis model does not have the same meaning in a global vegetation model and in a plant architecture model where it applies to single leaves. However, surprisingly, parameterizations may be very similar. The consequences of such practices are rarely examined.

3. Solutions for a general software architecture for ecological simulators

3.1. A unique conceptual framework

We have developed conceptual solutions to the issues raised in the previous section [Roche 2002].

3.1.1. Handling the interaction between space representation, physics and biology: the multiple 'view' paradigm

The key idea is to overlay and let interact in the same model three different 'views' of the ecosystem: a strictly geometric / topologic view (exchange surfaces, volumes, connections between those items), a strictly biological view (species, physiological and demographic processes), and a strictly physico-chemical view (matter and energy fluxes within a complex geometry system). These views will determine families of classes sharing privilegied relations (the three 'worlds'). Some ecological processes will belong to one world (e.g., photosynthesis belongs to biology, where it can have various formalizations), others are by nature spanning two different worlds (e.g. carbon allocation, depending on biology, determines the future geometry of the system; energy absorption by plants and soil depend on physics and geometry). The view concept is important here, since the same world could be seen in different ways by the others (e.g., the geometry adapted to treat plant morphogenesis may not be the best to compute radiation transfers). In this framework, it is possible to integrate tools as apparently different as plant architecture models like AMAP, spatial individual-based models like MUSE or cellular automata at any scale (Fig. 1).

3.1.2. The hierarchical representation of ecological systems

A way to approach this multiscale problem is to observe that there exist discontinuities when one moves from very small scales (e.g. the biological cell) to very large ones (the world). Considering just spatial scale alone, the relevance of particular physical laws changes suddenly at the scale of cells, individuals, topography, and finally the whole world:

- cells organize chemical reactions in space through their membrans;
- individuals modify fluxes to the soil, the atmosphere and the hydrosphere and constitute the unit of population dynamics;
- topography determines large scale fluxes of water, genes and 'disturbances' like fires and diseases;
- the whole world is the relevant scale for understanding the even short-term dynamics of the atmosphere.

It is well known that averaging as a modelling strategy starts to break down when approaching these scales too closely: hydrological models cannot represent rivers too coarsely if they are to make sensible predictions of water fluxes; ecosystem or population models must represent every individual when they are strongly spatially structured or when individuals have locally determined behaviours. At these spatial scales (which are also scales of organisation or system complexity), models must shift from a statistically averaged representation of smaller units to a representation of all units, where the statistical average emerges from the interaction of the units (a 'multi-agent' strategy). Where models must change scale, most scale up by aggregation without changing their physical or biological representation of ecosystems. In such models it is rare to work at the individual level. IBMs on the other hand are often system-specific and do not easily scale up.

Hence the two major problems for a general representation of ecological systems in a simulation model are (1) to have *coexistence* of different representations of the same system, i.e. we not only need different representation of the same system (e.g physical and biological, or individual-based and statistical), but they must coexist and interact; and (2) to account for the existence of discontinuities in ecosystem structure and organisation when scaling up in space.

3.1.3. Overall architecture for the 3Worlds simulator [Roche 2002]

Figure 2. shows the UML class diagram we propose to implement the 'view' system and the hiearchy of ecological objects.

The `Hierarchy` sub-package - `SimulItem` is the main class of the model kernel. It represents a relevant ecological organization level (leaf, root, plant, landscape unit...). Its main attribute is its hierarchical level within a scale going from the cell to the whole world. Through the use of `SimulItemContainer`, which contains a population of `SimulItem` of the same type, any hiearchy can be built: `SimulItem` can contain any number of `SimulItemContainer`, each representing a population of different `SimulItem` sub-components. `SimulItem` instances own `Process` objects, used to represent physical or biological processes. Each `SimulItem` object uses a `SecondaryView`, computed from a main view, to represent its spatial properties (shape, location, extent...). In this way, relationships between physics, biology and geometry within an ecological object are clearly defined.

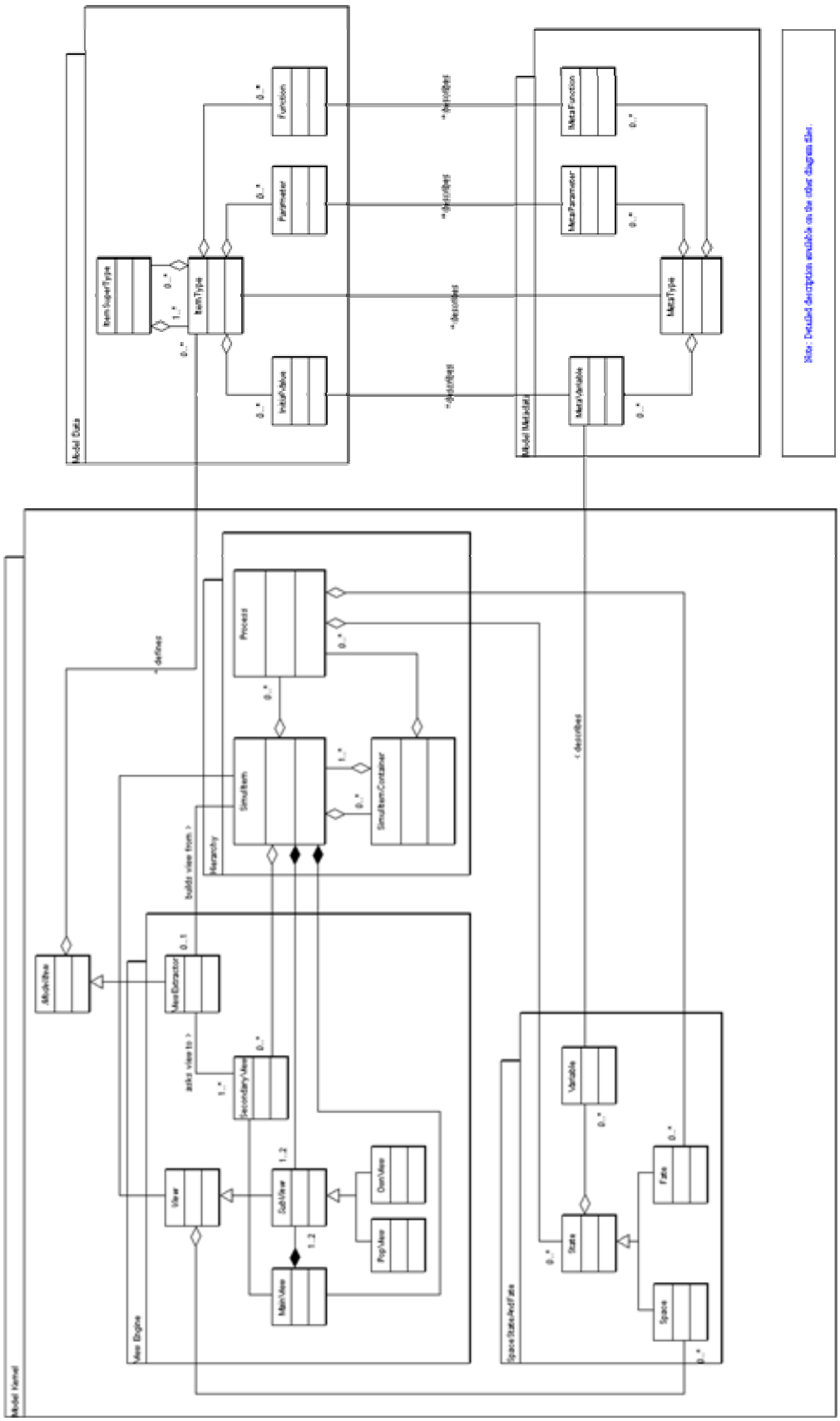

The `View` sub-package - `View` classes are used to represent geometric objects (connected groups of volumes, surfaces or lines) and methods for their spatial interactions (e.g. volume intersection, overlay, projection to a surface, geometric transformations...) and their visualization/display. A `MainView` is constructed from one or two `SubView`: one `OwnView`, which is an intrinsic geometric representation of an object (its 'basic shape', independent of any ecological

process applied to this object), and one `PopView`, which is a composite object holding a collection of the views of the sub-components of the `SimulItem`, together with the information (methods and topology/connexion scheme) needed to reconstruct their relations in space at the current hierarchical level. For example, the `OwnView` of an ecosystem might contain the topography of the site, while its `PopView` might contain the location of all individual plants currently present on that site. `ViewExtractor` enables `SimulItem` objects to construct `SecondaryViews` needed by each particular `Process`. `ViewExtractor` is placed at the top of the hierarchy of `SimulItems`, i.e. it has the visibility over the whole View and `SimulItem` hierarchies.

The `Space-State-Fate` sub-package -The `Process` class is used to implement the biological and physical processes through the `Fate` and `State` components, respectively. `State` contains all state variables describing a group of physical processes that can use the same geometry, while `Fate` implements all decision-making processes (birth, death, reproduction). The basic blocks of `State` and `Fate` are `Variable` objects, which contain a state variable's current value, but also its current variation, characteristic time step, and time since last update (which enables to handle multiple time steps by facilitating interpolation). `Space` is a specialization of `State` implementing geometric variables and methods used by the `Views`.

The `Data` and `MetaData` packages - Model data and metadata are grouped in these packages, which propose classes enabling to define specific ecosystem models simply by deriving their main classes from the `MetaData` package. This abstracts the interfacing mechanism between a (derived) user-code and the main code of 3Worlds. This enables a great flexibility in model specification, through the overloading of all model-specific physical and biological functions.

Some of these solutions derive from our previous experience in ecological simulation (cf. Section 4), and hence have been tested to some extent in real implementations.

3.2. Other constraints of the 3Worlds simulator

3Worlds accounts for the following constraints:

1. it provides a unique conceptual framework for the coupling of geometry / topology, physics / chemistry, and biology for models spanning scales from the plant to the ecosystem, and to the landscape or continent (multi-model for ecological objects at different spatio-temporal scales and different abstraction levels).
2. it provides a tool for (1) developing new models for specialized applications in various scientific areas, (2) validating models by comparing their results to field data, (3) analysing important datasets of simulation results, (4) conducting sound simulation experiments. The goal is to make accessible to the widest community methods that currently exist but are difficult to use.
3. it is easy to use for researchers specialists of a given field, either for teaching or doing research.

3.2.1. Targeted users

Users targeted by this project are researchers, teachers and land-use managers. The simulation platform must be easy to use by a wide range of people from non-scientist land managers to specialist researchers who may develop new models.

Platform developers (computer scientists and modellers in ecology) make up another group of actors, who will maintain and develop the platform into directions compatible with its assumptions and architecture.

3.2.2. A tool for conducting virtual experiments

The design and running of simulation (or virtual) experiments is an emerging area of science. We wish to provide with the 3Worlds platform, a toolbox making this easier and affordable for non modeller researchers.

The problems of virtual experimentation are: building sound experimental designs, evaluating their computation time cost, validating models and managing large datasets. These problems can be solved by classical statistical techniques, but it is important to make these statistical techniques more accessible by (1) developing a user-friendly interface, (2) developing a statistical toolbox for use with the generic simulation platform. For this last point, the experience of MUSE and LAMOS can be used: the MUSE model was completed by a series of SAS procedures helping to standardize the treatment of large datasets resulting from simulations, either for graphic production or for the systematic comparison to real datasets. LAMOS defines, through its scripting language, an interface for designing simple or complex simulation experiments. These tools will be included into the 3Worlds platform, with improvement as required. At the landscape scale and beyond, an interface with Geographic Information Systems should be planned.

3.2.3. A user-friendly interface

In a complex simulation model, a graphical interface is not only an advertising tool or pure aesthetics, it is required to quickly evaluate the quality of a model, to test model components as they are being built, and to compare simulations supposed to be identical. 3Worlds will benefit from the gains of MUSE and LAMOS (access to all model variables and dynamic graphs), to which a 3D map of the site will be added. This interface will make 3Worlds an easy-to-use tool for teaching, where various modelling strategies of ecological systems could be presented.

The design allows for the rapid development of user interfaces specifically tailored to the needs of a particular user – from complex to simply, from targeted to general.

4. Examples from past experience

4.1. The MUSE modelling shell [Gignoux *et al.* 1998, Gignoux and Davies 1996]

The ecological problem - MUSE (MUltistrata Spatially Explicit model) is a spatialized simulation model representing vegetation dynamics and functioning. It has been co-developed by the ENS and the RSBS with the objective of providing a tool designed to simulate vegetation systems with a strong spatial structure, such as savannas, fallows, oldfields, ecotones and more generally transition systems.

Spatial structure plays a major role in the functioning of those systems because of the limited range of interaction between plants: for example, tree/grass systems are subject to completely different growth and disturbance processes. Savannas present a particularly complex simulation problem which must account for spatial pattern and variously structured life forms represented by processes that may have nothing in common.

Studies based on MUSE enabled us to demonstrate for the first time a significant effect of the spatial structure of vegetation on carbon and water fluxes and a relationship between tree fire resistance and spatial pattern [Simioni *et al.* 2003].

The computing solution - To solve the spatial structure issue, a spatial IBM was required, where all trees and the associated parts of the grass layer influenced by the tree were represented. The behaviour of a savanna plot was then deduced from the simulation of many trees on a ~ 1 ha plot. To solve the life form issue, a great flexibility in the choice of ecological process representation for a group of species of the same life form was required, because of the great diversity of process modelling solutions. To solve the disturbance issue, a general enough code to represent very different regimes and effects on vegetation was required.

MUSE was developed in Object-Pascal. Given the heavy coding investment required by a savanna-compliant model, we tried to build up a reusable software architecture able to manage as many different ecosystems as possible: if a software is able to simulate individual plants of different life forms in a spatial framework, it should be able to handle simpler models. MUSE has therefore been implemented with a modular architecture where four main sub-models were identified: geometry, biology, resource and disturbance. Each sub-model defines interface variables for interaction with the other sub-models, which allows for some polymorphism of sub-models.

The basic assumptions of MUSE essentially deal with the geometric description of plants. For example, interactions between plants are local, hence only depend on the overlap between the volumes representing neighbouring plants. The geometry sub-model manages this representation (plant shape, volume overlap). A library of plant shapes enables to test different spatial representations of the same ecosystem. The biology sub-model manages all physiological and demographic processes of a particular life form. In the same model, plants with different biology sub-models can coexist. For such groups to interact, the resource sub-model implements a 'common currency', i.e. quantities all plant types are susceptible to compete for. Finally, the disturbance sub-model enables us to manage external agents interacting with the vegetation system through biomass removal, over-mortality, sudden variation of plant resources. This sub-model organization empirically arose during model implementation as the most practical approach. All sub-models implement ancestor types whose descendants constitute elementary blocks of many different ecosystems. It is therefore possible, within the MUSE framework, to model very different systems with a variety of spatial representations. These representations are based on different abstraction levels. MUSE thus enables the coexistence, in the same model, of groups of plants described with different abstraction levels (a constraint arising from the need to model savannas). MUSE is a typical multi-model [Coquillard and Hill 1997].

As a demonstration of the generality of the concepts used in the architecture of MUSE, ~15 models of the ecological literature have been recoded and run within the MUSE environment. All modelling students of our group at the ENS later used MUSE for their simulation work [Leriche 1997; Simioni 1998; Boulain 2000]. Significant effort has been placed on the user interface to ensure that every variable of the model can be tracked in real time on the screen through a virtual data acquisition system mimicking the real field data acquisition procedure. Thanks to object polymorphism and a simple coding interface (limited to a source file + a parameter file), new models can be quickly added to the platform.

Pros - The main strengths of MUSE are its flexibility and its user interface. Many published models, from gap models to spatial IBMs could be recoded within MUSE through a moderate coding effort. Implementing new ecosystem models is much easier (one week can be enough to build up a spatially explicit ecosystem model within MUSE).

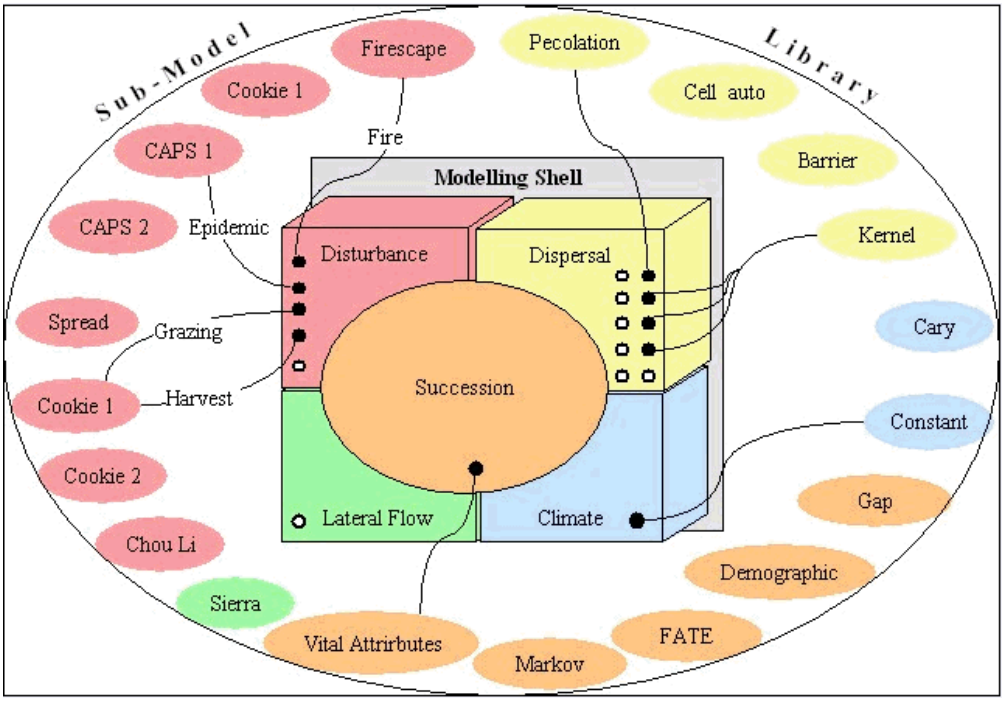

Figure 3. LAMOS. Sub-models are selected from the library to produce a particular landscape model configuration. Each plant functional type has one dispersal sub-model. There must be one and only one succession model. All the rest are optional. There can be any number of disturbance models and any number of plant functional types.

Cons -During the development of MUSE, some weakpoints of its architecture appeared:

- The resource concept enables us to simulate inter-individual competition well but is not adapted to the treatment of the resources' own dynamics (e.g. water has its own dynamics, linked to soil topography and soil properties). A fifth sub-model managing the dynamics of physical resources outside the neighbourhood of plants would have been needed.
- The neighbourhood concept introduced in MUSE to handle local resource competition is not a plant property, but depends on the type of resource (e.g., the interaction distance for competition for nutrients may not be the same as for competition for water). The current architecture (two neighbourhood radii, one for the aboveground part and one for the belowground part) limits model flexibility.
- Sub-model interchangeability is not always possible, since users can define ad libitum interface variables for their biology, resource and disturbance sub-models.
- The user interface does not scale well for large complex experimental designs.

4.2. The LAMOS modelling shell [Lavorel *et al.* 2000]

The ecological problem - LAMOS (LAndscape MOdelling Shell) is a landscape simulation model developed by the CEFE and the RSBS. It was developed as a generic tool for landscape modelling. Its goal was to study the dynamic interaction of spatial pattern and process. Some physical and biological processes only express at this scale, and not at the plot scale. Five processes (seed/propagule dispersal, vegetation succession, disturbance regime, climate, lateral matter flows) have been identified as the main drivers of landscape dynamics. The plant functional type concept [Noble and Gitay 1996, Smith *et al.* 1993] is used to deal with high biodiversity.

The computing solution - The five main ecological processes have been coded as five sub-models whose interactions are managed by LAMOS within a strict framework (Fig. 3): For example, interactions between the sucession and disturbance sub-models rely on a biomass interface variable, which must be present in all descendant sub-models. A library of sub-models is included, enabling the assembling of composite models. Thanks to object oriented programming, this library can be extended through the implementation of new descendants of the ancestor sub-models with a relatively small programming effort, in particular no input/output code is needed nor definition of complex data structures.

All LAMOS sub-models are descendants of a single ancestor analogous to a table of a relational database, which implements an interface enabling to access all variables of any combination of tables in a standard way, either through a graphical user interface or through a simple command-line scripting language. This language can be used for experimental designs.

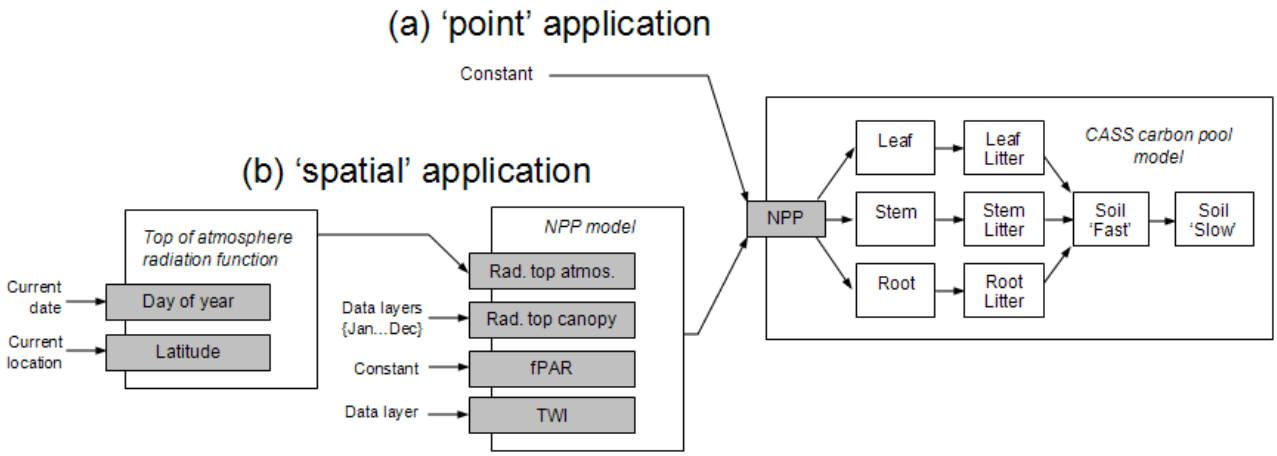

Figure 4. COINS drivers and model coupling. A driver function `top of the atmosphere radiation' performs its calculations over a monthly time step. The output is fed to an NPP driver model whose output can be fed to any number of point models.

Pros - LAMOS imposes a single spatial representation for landscapes, and so can be called a model aggregate rather than a multimodel. Compared to MUSE, LAMOS is a step forward towards a generic computing architecture for ecosystems, with (1) a guaranteed interchange-ability of sub-models; (2) the explicit integration of relational database approach, which considerably simplified the user interface coding; (3) the scripting language which enables an easy management of repeated tasks.

Cons - To simplify coupling between sub-models, LAMOS enforces a simple top level view of the ecological system with, amongst other things, a three strata system containing biomass on a resizable raster grid. This does not limit the complexity of models that can be implemented in LAMOS as it already contains IBMs such as a gap model, but it limits the complexity of their interaction. For example, the disturbance model cannot know if the succession model has detailed tree geometry or not, it just knows the total biomass in each of three strata. In a sense each model can have as complex a 'view' as required but the 'view' seen by LAMOS and used to couple the sub-models together is a fixed and simple one. The other major limitation is that scaling up is given by simple aggregation. Succession models are essentially point models in a raster grid, only interacting through disturbance propagation, seed dispersal and water flow. A stand in one pixel cannot be said to shade a stand in a neighbouring pixel.

4.3. COINS [Davies and Roxburgh 2003]

Ecological problem - The COINS (COmparison and INtegration Shell) modelling shell was developed by the Cooperative Research Centre for Carbon Accounting at the Australian National University. It was designed to analyse models of terrestrial carbon dynamics. The goal was to create a software environment within which new models could be developed and existing models modified. More importantly, there was a need for end users to take existing models, combine them for analysis and perform model inter-comparison and scenario exploration.

The project showed that models in this domain are less susceptible to factoring into component parts or processes than those addressed by MUSE and LAMOS. However, all had a common dependence on forcing variables, i.e. continuous streams of climate input data at various temporal scales, and all spanned a wide range of spatial scales from continental to 1 hectare plot and as non-spatial point models.

Computing solution- COINS was built on the same relational database system employed by LAMOS. The models housed within it are largely self-contained. Each model however, declares its requirements for forcing data to the COINS shell. This allows COINS to supply the data in a consistent, efficient, co-ordinated and flexible manner to any number of models running in parallel. The same climate scenario can therefore be fed to any number of models at the same time, deploy-ed in overlapping or partitioned spatial domains at mixed temporal grains (Fig. 4).

Pros - An important goal of COINS was to drive multiple model simulations with identical climate and management scenarios.

It shares with MUSE and LAMOS the -benefits of rapid model development in an environment which takes care of all input and output management.

The forcing driver system also allows a degree of model coupling, for example a model that produces NPP can be used to drive a carbon pools model.

It has flexibility in spatial deployment of models.

Cons - COINS does not provide any support for geometric constructs within models or biological functions such as those

addressed by MUSE. It focuses more on physics, i.e. state variables such as climate data, water balance and carbon/ nutrient cycling. It does not support interaction between models such as LAMOS. Such coupling as there is, is achieved by chaining functions together, with the single output of each function providing an input parameter to another function or model.

4.4. SimExplorer [Amblard *et al.* 2003]

Since the beginning of computer simulation, experimental design has been an active research field for efficiently testing and analyzing the behaviour of computer models, and it still remains a valuable technology in the decision-making context [Zeigler 1976, 2000] [Balci and Sargent 1981] [Kleijnen 1987] [Hill 1996] [Sarjoughian and Cellier 2001]. In order to conduct efficiently and rigorously simulation experiments, we have proposed a Platform Independent Model (PIM) and its implementation prototype, named SimExplorer [Amblard *et al.* 2003]. This software is currently able to distribute experiments on clusters and can be applied to handle both deterministic and random simulation. The case of stochastic distributed simulation was particularly targeted. Research results concerning the parallelization of pseudo-random number generators for stochastic simulation have been considered [Fujimoto 1990] [Traore and Hill 2001]. The MDA (Model Driven Architecture) has been retained for developing Simexplorer, it helped to focus first on the functionality and behavior of our distributed application which will handle experimental frameworks for sequential or parallel simulators, without the common distortions that are often implied by the technologies in which it will be implemented. Our current design solution, exposed in a PSM (Platform Specific Model), is using XMI (XML Metadata Interchange) and SOAP (Simple Object Access Protocol) for the communication between Java software components ; however with the choice of MDA, the functionality and behavior of SimExplorer is modeled once and for all even if we will move to other technologies.

Following Balci's arguments [Balci *et al*. 2000], the accreditation of simulation models passes through rigorous standard verification and validation processes of the model. During these processes, one needs to conduce a considerable number of simulation experiments aiming at exploring the model's behaviors. Moreover, in some cases, conducing simulation experiments is the only way to analyze and understand the behavior of a complex model. This is the case for instance of many individual based models, including social or ecological dynamics, and for which the cumulative effect of interactions can lead to unexpected effects, generally impossible to formalize analytically [Deffuant *et al.* 2002]. Thereafter, it was a need to automate both the run of a huge number of simulation experiments and to manage the corresponding experimental designs, i.e. the organization of the simulation experiments, in a more evolved and valuable fashion than a simple batch process implementation. This concern includes both an ergonomic interface for the specification of the experimental designs and the distribution of computations to launch the corresponding simulation experiments on parallel machines when possible. In addition, a true independency from targets simulation programs is almost impossible. This implies imposing a minimal set of non rigid guidelines, that a simulation software will follow in order to be able to adapt the same procedures to each concrete experimentation with an implemented model. Basically, with our approach the simulation executable model is considered as a simple program with a parametric structure containing a set of input and output variables. Thus the minimum requirements are:

- The initialization of a single file containing the simulation input parameters (this file could then hierarchically refer to other data files that can be exploited by the simulation program).
- The ability to launch the execution of the corresponding simulation program as another process.
- The description of an exploration zone. Instead of giving a single value to each parameter, the user specifies a set of values.
- The definition of an exploration method on an exploration zone by the choice of an experimental design.
- The definition of the outputs of the simulations: the user can select particular variables or combinations of variables, at particular time steps, to be analysed.
- The execution of the simulations corresponding to a set of parameters and a chosen experimental design [Kleijnen and Groenendaal 1992].
- The visualization of the simulation results in a post-processed and synthetic way to interpret them. It could correspond to the visualization of the simulation trace for a single simulation or to more evolved visualization to synthesize an exploration over a large number of simulation experiments.

From this set of minimum requirements, it can be deduced that Visual Interactive Simulators are not directly manageable. Indeed, explorations done with interactive environments are obviously not feasible in such an automatic "Explorer" software. However, scientific simulation tools with interactive visualization outputs, often propose a batch version with synthetic trace files to run many experiments, particularly when they deal with stochastic models. SimExplorer, can manage the exploration and the execution of simulation experiments by means of experimental designs on several simulation models and on several computers; it is perfectly adapted to cluster and grid computing.

5. Conclusion

We have proposed a survey of simulation platforms mainly in terrestrial ecology. The intent of this survey was to point out the essence of ecological modelling and to extract interesting ways of doing model coupling and comparison. This analysis enabled us to design 3world a software platform for multiscale simulation of ecological systems. Compared to other existing platforms in ecological modelling (AMAP for plant architecture modelling, CAPSIS for forest dynamics modelling), 3Worlds is characterized by:

1. its intended use for research and teaching rather than prediction or management, even if this use can arise in the future.
2. its multi-scale approach (from plant to landscape), which will rely on identifying common concepts between these scales rather than juxtaposing models at different scales.
3. its general application to all living systems. The starting point is the modelling of terrestrial vegetation systems because of the experience accumulated in this field, but this modelling should be open to any living system where the interaction between geometry, biology and physics can be described with 3Worlds concepts and object structures. This openness is the first constraint of 3Worlds's specifications.

The design of the 3Worlds platform is aimed to produce an interdisciplinary tool, bringing together three very different aspects of living systems across all spatial scales at which they operate. These are the geometric/structural, biological, and physico-chemical views. Based on our past experiences, we believe the raise of these 3 aspects is an original contribution to research. The next step will be to provide a full implementation of the 3world platform which is currently under development. A special focus will be given to formalize model coupling and comparison. To deal with this, the use of Zeigler's DEVS [Zeigler 2000] and of a scale transfer methodology such as what has been proposed by [Duboz 2004] is under consideration.

REFERENCES

[Amblard *et al.* 2003] Amblard F., Hill, D., Bernard S., Truffot J. Deffuant G. "MDA compliant Design of SimExplorer, A Software to handle simulation experimental frameworks" in Proceedings of the 2003 Summer Simulation Conference, pp.279-284, Montréal, July 20-24, 2003.

[Armstrong 1993] Armstrong, R., 1993 A comparison of index-based and pixel-based neighborhood simulations of forest growth. Ecology, 74(6):1707-1712, 1993.

[Balandier *et al.* 2000] Balandier P, Lacointe A, Le Roux X, Sinoquet H, Cruiziat P, Le Dizès S, 2000. SIMWAL: a structural-functional model simulating single walnut tree growth in response to climate and pruning. Annals of Forest Science, 57, 571-586.

[Balci and Sargent 1981] Balci O, Sargent R., 1981, "A Methodology for Cost-Risk Analysis in the Statistical Validation of Simulation Models ", Communication of the ACM, Vol, 24, N°4, pp. 15-29.

[Balci *et al.* 2000] Balci, O., Ormsby, W.F., Carr, J.T. and Saadi, S.D., 2000. “Planning for verification, validation and accreditation of modeling and simulation applications.” In Proceedings of the 2000 Winter Simulation Conference, J.A. Joines, R.R. Barton, K. Kang and P.A. Fishwick (eds), pp. 829-839.

[Barthélémy *et al.* 1995a] Barthélémy, D., Blaise, F., Fourcaud, T., Nicolini, E., 1995. Modélisation et simulation de l'architecture des arbres : bilan et perspectives. Revue Forestière Française, 47(n° sp.): 71-96.

[Barthélémy *et al.* 1995b] Barthélémy, D., Sabatier, S., Pascal, O., 1995. Le développement architectural du noyer commun Juglans regia L. (Juglandaceae). Forêt Entreprise, 103: 61-68.

[Baveco and Smeulders 1994] Baveco, J. and A. Smeulders, 1994. Objects for simulation: Smalltalk and ecology. Simulation, 58:42-56.

[Beerling *et al*. 1997] Beerling, D., F. Woodward, M. Lomas and A. Jenkins, 1997. Testing the responses of a dynamic global vegetation model to environmental change: a comparison of observations and predictions. Global Ecology and Biogeography Letters, 6:439-450.

[Botkin *et al*. 1972] Botkin, D., J. Janak and J. Wallis., 1972. Some ecological consequences of a computer model of forest growth. Journal of Ecology, 60:849-871.

[Bouchon *et al.* 1997] Bouchon, J., P. de Reffye and D. Barthélémy, 1997. Modélisation et simulation de l'architecture des végétaux, Paris, 1997, page 435. INRA éditions, Paris.

[Boulain 2000] Boulain, N., 2000. Modélisation de l'interaction végétation-hydrologie de surface en zone Sahélienne : effets du régimpe des précipitations et de l'occupation des sols. Mémoire de DEA Paris 6, ENS, INAPG.

[Boussoualine 1997] Boussoualine, H, 1997. Amélioration d'INCA, outil de simulation de la croissance de l'arbre. Mémoire de fin d'études, Université Blaise Pascal, Clermont-Ferrand.

[Bugmann 1994] Bugmann, H. 1994. Simulated forest dynamics along an altitudinal graident in the European Alps. The application of forest stand models to evaluate global change issues. thèse de doctorat, Institut fédéral de Zürich, 1994.

[Caraglio 1996] Caraglio, Y., 1996. Le développement architectural du merisier. Forêt Entreprise, 107: 72-80.

[Colasanti *et al.* 1993] Colasanti, R. and J. Grime. Resource dynamics and vegetation processes: a deterministic model using two-dimensional cellular automata. Functional Ecology, 7:169-176, 1993.

[Coquillard and Hill 1997] Coquillard P., Hill D., 1997. Modélisation et Simulation des Ecosystèmes, Masson. 273 p.

[Coquillard *et al.* 2000a] Coquillard P., B. Prévosto & D. R. C. Hill, 2000. Simulation of natural afforestation by Pinus sylvestris at mid-elevation after grazing abandonment. Part two: Refined model. Journal of Applied Ecology (soumis).

[Coquillard *et al.* 2000b] Coquillard P., B. Prévosto & D. R. C. Hill. 2000. Simulation of natural afforestation by Pinus sylvestris at mid-elevation after grazing abandonment. Part one: Concepts and general model. Journal of Applied Ecology (soumis).

[Coughenour 1994] Coughenour, M., 1994. Savanna - Landscape and regional ecosystem model. Documentation, 1994. Colorado State University.

[Davies and Roxburgh 2003] Davies, I., Roxburgh, S., 2003. COINS - an integrative modelling tool for greenhouse accounting and natural resource management. Poster presented at the Integrated research on coupled human environmental systems land open science conference, December 1-5, Morelia, Mexico.

[Davies *et al.* 2001] Davies, I., Gignoux, J., Lavorel, S., Noble, I.R., Roxburh, S., & Desanker P.V., 2001. Rapid model development. Challenges of a changing Earth, a global change open science conference, Amsterdam, 10-13 July 2001.

[de Reffye *et al.* 1997] de Reffye, P., Fourcaud, T., Blaise, F., Barthélémy, D., Houllier, F., 1997. A functional model of tree growth and tree architecture. Silva Fennica, 31(3): 297-311.

[Deffuant *et al.* 2002] Deffuant, G., Huet, S., Bousset, J.P., Henriot, J., Amon, G., Weisbuch, G. - 2002. "Agent based simulation of organic farming conversion in Allier département". in Complexity and Ecosystem Management. M.A. Janssen editor. Edward Elgar Publishers, pp 158-189.

[Duboz 2004] Duboz R. "Intégration de modèles hétérogènes pour la modélisation et la simulation de systèmes complexes", Ph.D. Thesis. Université du Littoral.

[Farquhar 1980] Farquhar, G.D., von Caemmerer S., Berry J.A., 1980. A biochemical model of photosynthetic CO2 assimilation in leaves of C3 species. Planta, 149:78-80.

[Franc 1996] Franc, A. Croissance des peuplements forestiers hétérogènes : modélisation par des réseaux d'automates cellulaires. Tendances nouvelles en modélisation pour l'environnement:86-92, 1996.

[Friend *et al.* 1993] Friend, A., H. Shugart and S. Running., 1993. A physiology-based gap model of forest dynamics. Ecology, 74(3):792-797.

[Fujimoto 1990] Fujimoto R., 1990, “Parallel Discrete-Event Simulation”, Communication of the ACM, Vol 33, N°10, pp.31-53.

[Gignoux and Davies 1996] Gignoux, J. & Davies, I.D., 1996. The MUSE vegetation modelling shell - Reference and user's manual. ANU, 76 pp.

[Gignoux *et al.* 1998] Gignoux, J., J. Menaut, I. Noble and I. Davies, 1998. A spatial model of savanna function and dynamics: model description and preliminary results, volume 37 of Annual symposium of the BES, Cambridge, 1998, pages 361-383. Blackwell scientific publications, Cambridge.

[Godin and Caraglio 1998] Godin, C., Caraglio, Y., 1998. A multiscale model of plant topological structures. Journal of Theoretical Biology, 191: 1-46.

[Gourlet-Fleury 1997] Gourlet-Fleury, S., 1997. Modélisation individuelle spatialement explicite de la dynamique d'un peuplement de forêt dense tropicale humide (dispositif de Paracou, Guyane Française), thèse de doctorat, Université Claude Bernard-Lyon I, Lyon.

[Hill 1996] Hill D., 1996, "Object-Oriented Analysis and Simulation", Addison-Wesley.

[Hochberg *et al.* 1994] Hochberg, M., J. Menaut and J. Gignoux, 1994. The influences of tree biology and fire in the spatial structure of the West African savanna. Journal of Ecology, 82(2):217-226.

[House *et al.* 2001] House, J., Coughenour, M., Gignoux, J., Le Roux, X., McKeon, G., Parton, W.J., Scholes, R. & Simioni, G. 2001. Modelling tree-grass ecosystems : testing and comparing the approach of four savanna models. in prep.

[Jarvis 1976] Jarvis, P., 1976. The interpretation of the variations in leaf water potential and stomatal conductance found in canopies in the field. Phil. Trans. Roy. Soc. Lond. B 273:593-610.

[Jay *et al.* 1995] Jay, M., Lichou, J., Costes, E., Audubert, A., 1995. Architecture de l'abricotier. Première Partie : Organisation naturelle de la ramification. Infos CTIFL(115): 32-37.

[Jeltsch *et al.* 1996] Jeltsch, F., S. Milton, W. Dean and N. Van Rooyen, 1996. Tree spacing and coexistence in semiarid savannas. Journal of Ecology, 84:583-595.

[Jourdan and Rey 1996] Jourdan, C., Rey, H., 1996. Architecture racinaire du palmier à huile. Modélisation et simulation. Plantations, 3(5): 313-327.

[Jourdan and Rey 1997] Jourdan, C., Rey, H., 1997. Architecture and development of the oil-palm (Elaeis guineensis Jacq.) root system. Plant and Soil, 189: 33-48.

[Keane *et al*. 1996] Keane, R., D. Long, J. Menakis, W. Hann and C. Bevins, 1996. Simulating coarse-scale vegetation dynamics using the Columbia River basin succession model-CRBSUM, 1996. USDA.

[Kellomäki and Väsäinen 1991] Kellomäki, S. and H. Väisänen 1991. Application of a gap model for the simulation of forest ground vegetation in boreal conditions. Forest Ecology and Management, 42:35-47.

[Kleijnen 1987] Kleijnen J.P.C., 1987, "Statistical Tools for simulation practitioners", Dekker New-York.

[Kleijnen and Groenendaal 1992] Kleijnen J., Van Groenendaal W., 1992, "Simulation: A Statistical Perspective", John Wiley, Chichester.

[Kleijnen and Groenendaal 1992] Kleijnen, J., and Groenendaal, 1992. Simulation, a statistical perspective. Wiley.

[Korzukhin and Ter-Mikaelian, 1995] Korzukhin, M. and M. Ter-Mikaelian, 1995. An individual tree-based model of competition for light. Ecological Modelling, 79:221-229.

[Lacointe 2000] Lacointe A, 2000. Carbon allocation among tree organs: a review of basic processes and representation in functional-structural tree models. Annals of Forest Science, 57, 521-533.

[Lauenroth *et al*. 1993] Lauenroth, W., D. Urban, D. Coffin, W. Parton, H. Shugart, T. Kirchner and T. Smith., 1993. Modelling vegetation structure-ecosystem process interactions across sites and ecosystems. Ecological Modelling, 67:49-80.

[Lavorel *et al*. 1994] Lavorel, S., V. O'Neill and R. Gardner, 1994. Spatio-temporal dispersal strategies and annual plant species coexistence in a structured landscape. Oikos, 71:75-88.

[Lavorel *et al*. 2000] Lavorel S, Davies ID, Noble IR, 2000 LAMOS: a LAndscape MOdelling Shell. In: B.C. Hawkes and M.D. Flannigan, editors, Landscape fire modeling - challenges and opportunities. Northern Forestry Centre Information Report NOR-X-371, Canadian Forest Service: 25-28.

[Lavorel *et al*. 2001] Lavorel S, Davies ID, Noble IR (2001) GCTE News, mars 2001.

[Le Dizès *et al.* 1997] Le Dizès, S., P. Cruiziat, A. Lacointe, H. Sinoquet, X. Le Roux, P. Balandier and P. Jacquet., 1997. A model for simulating structure-function relationships in walnut tree growth processes. Silva Fennica, 31(3):313-328.

[Leemans *et al*. 1996] Leemans, R., W. Cramer and J. van Minnen, 1996. Prediction of global biome distribution using bioclimatic equilibrium models, Chichester, 1996, pages 413-450. John Wiley and sons, Chichester.

[Lemoine *et al*. 1999] Lemoine D, Granier A, Cochard H, 1999. Mechanism of freeze-induced embolism in fagus sylvatica L. Trees: Structure and Function, 13, 206-210.

[Leriche 1997] Leriche H., 1997. Etude théorique de la production primaire d'un écosystème de savane humide en réponse à l'herbivorie. Mémoire de DEA Paris 6 et 11-INAPG.

[Lett *et al*. 1999] Lett, C., C. Silber and N. Barret, 1999. Comparison of a cellular automata network and an individual-based model for the simulation of forest dynamics. submitted.

[Martin 1992] Martin, P., 1992. EXE: a climatically sensitive model to study climate change and CO2 enhancement effects on forests. Australian Journal of Botany, 40:717-735.

[Menaut *et al*. 1990] Menaut, J., J. Gignoux, C. Prado and J. Clobert, 1990. Tree community dynamics in a humid savanna of the Côte d'Ivoire : modelling the effects of fire and competition with grass and neighbours. Journal of Biogeography, 17:471-481.

[Moore and Noble 1993] Moore, A. and I. Noble, 1993. Automatic model simplification: the generation of replacement sequences and their use in vegetation modelling. Ecological Modelling, 70:137-157.

[Moravie *et al*. 1997] Moravie, M., J. Pascal and P. Auger, 1997. Investigating canopy regeneration processes through individual-based spatial models: application to a tropical rain forest. Ecological Modelling, 104:241-260.

[Müller and Gaertner 2000] Müller, P.A. & Gaertner, N., 2000. Modélisation objet avec UML. Eyrolles, Paris.

[Noble and Gitay 1996] Noble, I. and H. Gitay. A functional classification for predicting the dynamics of landscapes, 1996. Journal of Vegetation Science, 7(3):329-336.

[Noble and Slatyer 1980] Noble, I. and R. Slatyer, 1980. The use of vital attributes to predict successional changes in plant communities subject to recurrent disturbances. Vegetatio, 43:5-21.

[Noble *et al*. 1980] Noble, I., H. Shugart and J. Schauer, 1980. A description of BRIND, a computer model of succession and fire response of the high altitude Eucalyptus forests of the Brindabella range, Australian Capital Territory, 1980. Oak Ridge National Laboratory.

[Pacala *et al*. 1993] Pacala, S., C. Canham and J. Silander, 1993. Forest models defined by field measurements: I. The design of a Northeastern forest simulator. Canadian Journal of Forest Research, 23:1980-1988.

[Pastor and Post 1985] Pastor, J. and W. Post, 1985. Development of a linked forest productivity-soil process model, 1985. US Dept of Energy, Environmental sciences division.

[Prado 1991] Prado, C., 1991 Plant community dynamics and species growth rules : a simulation study based on a cellular automata formalism, pages 75-87. ALEAS, Paris.

[Prentice *et al*. 1993] Prentice, I., M. Sykes and W. Cramer, 1993. A simulation model for the transient effects of climate change on forest landscapes. Ecological Modelling, 65:51-70.

[Roche 2002] Roche, A., 2002. Techniques de simulation et simulateurs d'écosystèmes. M.Sci. thesis, ISIMA.

[Sarjoughian and Cellier 2001] Sarjoughian, H.S. and Cellier, F.E., 2001. "Towards a Unified Foundation Simulation-Based Acquisition" in Discrete Event Modeling and Simulation Technologies: A Tapestry of Systems and AI-Based Theories and Methodologies, H.S. Sarjoughian and F.E. Cellier (eds.), Springer-Verlag, pp. 1-14.

[Sato 2003] The Earth Simulator - Holistic Simulation and Science Evolution, Vol. 58, No. 2, p79-85, 2003.

[Scanlan 1992] Scanlan, J., 1992. A model of woody-herbaceous biomass relationships in eucalypt and mesquite communities. Journal of Range Management, 45:75-80.

[Schimel *et al*. 1997] Schimel, D., W. Emanuel, B. Rizzo, T. Smith, F. Woodward, H. Fisher, T. Kittel, R. McKeown, T. Painter, N. Rosenbloom, D. Ojima, W. Parton, D. Kicklighter, A. McGuire, J. Melillo, Y. Pan, A. Haxeltine, C. Prentice, S. Sitch, K. Hibbard, R. Nemani, L. Pierce, S. Running, J. Borchers, J. Chaney, R. Neilson and B. Braswell, 1997. Continental scale variability in ecosystem processes: Models, data, and the role of disturbance. Ecological Monographs, 67(2):251-271.

[Simioni 1998] Simioni, G., 1998. Effet de la répartition spatiale et de la densité des ligneux sur le bilan hydrique et la production primaire en savane : application d'un modèle spatialement explicite, mémoire de DEA Paris 6 et 11-INAPG, Paris.

[Simioni *et al*. 2000] Simioni G, Le Roux X, Gignoux J, Sinoquet H, 2000. TREEGRASS: A 3D, process-based model for simulating plant interactions in tree-grass ecosystems. Ecological Modelling, 131, 47-63.

[Simioni *et al*. 2003] Simioni, G., Gignoux, J., & Le Roux, X., 2003. Tree layer spatial structure can affect savanna production and water budget: Results of a 3-D modelling approach. Ecology, 84(7):1879-1894.

[Smith *et al*. 1993] Smith, T., H. Shugart, F. Woodward and P. Burton, 1993. Plant functional types, pages 272-292. Chapman and Hall, New York.

[Smith *et al*. 1998] Smith, P., J. Smith, D. Powlson, W. McGill, J. Arah, O. Chertov, K. Coleman, U. Franko, S. Frolking, D. Jenkinson, L. Jensen, R. Kelly, H. Klein-Gunnewiek, A. Komarov, J. Molina, T. Mueller, W. Parton, J. Thornley and A. Whitmore, 1997. A comparison of the performance of nine soil organic matter models using datasets from seven long-term experiments. Geoderma, 81:153-225.

[Soler *et al*. 2003] Soler, C., Sillion, F.X., Blaise, F. et de Reffye, P., 2003. An efficient instantiation algorithm for simulating radiant energy transfer in plant models. ACM Transactions on Graphics, 22(2): 204-233.

[Steffen *et al*. 1994] Steffen, W., W. Cramer, M. Plöchl and H. Bugmann, 1994. Global vegetation models: incorporating transient changes to structure and composition, 1994. PIK.

[Thiéry *et al*. 1997] Thiéry, J., J. d'Herbès, M. Ehrmann, S. Galle, C. Peugeot, J. Seghieri and C. Valentin. Modèles de paysage et modèles de ruissellement pour une brousse tigrée nigérienne. Journées PIREVS - Les temps de l'environnement:557-563, 1997.

[Traore and Hill 2001] Traore M., Hill D., "The use of random number generation for stochastic distributed simulation: application to ecological modeling". 13th European Simulation Symposium, Marseille, October 18th-20th, 2001, pp. 555-559.

[VEMAP 1995] VEMAP members, 1995. Vegetation/ecosystem modeling and analysis project: comparing biogeography and biogeochemistry models in a continental-scale study of terrestrial ecosystem responses to climate change and CO2 doubling. Global Biogeochemical Cycles, 9(4):407-437.

[Wiegand and Milton 1994] Wiegand, T. and S. Milton, 1994. A simulation model for shrubland ecosystem dynamics in arid Karoo, South Africa. USDA, Forest service.

[Zeigler 1976] Zeigler B.P., 1976, " Theory of Modeling and Simulation", Wiley Interscience, New York.

[Zeigler 2000] Zeigler B.P., Praehofer H., Kim T.G., 2000, "Theory of Modeling and Simulation – Integrating Discrete Event and Continuous Complex Dynamic Systems", Augmented 2nd Edition. Wiley Interscience, Academic Press.

Small world properties in a DSDEVS model of ecosystem

Raphaël Duboz

Institut de Recherche pour le Développement (IRD)
Centre de Recherche Halieutique Méditerranéenne et Tropicale
Avenue Jean Monnet - BP 171
34203 Sete Cedex
Tel : (+33) (0)4 99 57 32 15
duboz@ird.fr

Christophe Cambier

Institut de Recherche pour le Développement (IRD)
Centre de Hann
Rte des Peres Maristes,
BP 1386 Dakar, Senegal
Tel : (+221) 849 35 35
cambier@ird.sn

ABSTRACT
This paper deals with the general formalisation of an ecosystems model. We consider an ecosystem as a graph where nodes are species and edges are trophic relations. For the specification of such a system, we use the DSDEVS formalism. DSDEVS enables formally describing dynamic structure systems and thus dynamic graphs. A measure of graph topology complexity (small world properties) can be formally defined through DSDEVS models. Small world properties are usually considered in a static configuration of graph. Here, we introduce a dynamic and a spatial view of these properties. We hope that this work will be useful for ecosystems management by providing an indicator of ecosystem resistance to perturbations. Indeed, small world properties are significant of the resistance of graph to the addition or deletion of nodes (i.e. species in our case).

KEYWORDS
Ecological networks, Dynamical Structures, System Specification, Theoretical Ecology.

1. Introduction

The modelling and simulation of ecosystems is known as a fundamental activity to understand ecological complexity [Coquillard Hill 1997]. Developing tools for sustainable development policy requires models that incorporate this complexity. The models that we use for decision making must have a theoretical and formal basis so that verification, communication and reproduction of model behaviours is possible. This paper takes place in such an activity by considering a measure of natural complexity in a formal specification of an ecological model. Ultimately, we want to build a model of the evolution of communities' structure in West African estuaries. These aquatic ecosystems are under control of physical perturbations such as the evolution of salinity that modify species composition. In this paper, we do not deal with our particular study case. We want to present a general architecture for ecological models dealing with the design and quantification of ecosystem reactions under environmental stress. Thus, the goal of this preliminary study is to use a formal basis for the modelling and simulation of food web as dynamical graphs and to identify the link between this formal specification and a measure of graph complexity.

It is well known that a food web can be defined as a graph $G(N,E)$ consisting in a finite set of nodes N and a finite set of edges E [Montaya Solé 2002]. Theoretical approaches consider the study of natural graph complexity as a mean to characterise food web reactions to perturbations (i.e. the addition or deletion of species in the food web). The limit of those studies lies in considering a static graph topology. Indeed, if we want to consider the evolution of species assemblage (i.e. natural graph topology) in a particular ecosystem stressed by some environmental changes, we need a food web topology that change over time. For instance, specific composition and therefore trophic relations change in estuaries ecosystems under the influence of salinity gradients [Albaret 1999].

In the following, we first present a formalism which takes into account dynamical changes of graph topology. Then we introduce a measure of graph complexity based on topology. Then, we incorporate this measure in a general specification of ecosystems considered as graphs.

2. Background

In this section, we give the reader the essential notions to fully understand the proposition made in this article. To do that, we first introduce the formal notations for the specification of dynamical structures and then we provide the computation method of small world properties (the measure of graph complexity we have chosen).

2.1 Formalisation of the dynamic changes of structure

In 1985, G Klir was the first to introduce the concept of dynamic structure within a framework of modelling and simulation [Klir 1985]. Recently, formal approaches were proposed by A.M. Uhrmacher [Uhrmacher 2001]. F. Barros has introduced the Dynamic Structure Discrete Event specification System (DSDEVS) [Barros 1996] and gave the most satisfactory formalisation for the modelling of dynamic changes of structure. DSDEVS is an extension of the discrete events system specification proposed by Zeigler [Zeigler *et. al.* 2000]. Let us cite F Barros writing about dynamic systems in general: "[...] structural changes can better reflect dynamic of real systems we want to model in which drastic changes of structure and behaviours can be observed". This assertion is particularly relevant in the context of ecological models where the relations between species are likely to change dynamically. Thus, DSDEVS seems quite suitable for the formalisation of trophic web in the context of dynamical systems. In order to give the reader the useful formal notions and general concepts, we introduce here the DSDEVS formalism.

DSDEVS is based on systems mathematics. It defines atomic model as a structure and allows the construction of complex models by coupling atomic models in a modular and hierarchical manner. DSDEVS defines the set of connections of a coupled model as a state of the system. Thus, connections can change over time on the evaluation of functions which modify this state. In the same way, it is possible to add or delete coupled or atomic models. A DSDEVS model defines a network of models such as:

$$DSDEVN_{\Delta} =< X_{\Delta}, Y_{\Delta}, \chi, M_{\chi} >$$

where:

Δ is the name of the network of models the DSDEVS defined,

X_{Δ} is the set of input events on the network of models,

Y_{Δ} is the set output events on the network of models,

χ is the name of the network executive model,

M_{χ} is the model of χ. It defines the dynamic of the structure (i.e. topology and composition of the network).

M_{χ} is an atomic DEVS model with the following structure:

$$M_{\chi} =< X_{\chi}, Y_{\chi}, S_{\chi}, \delta_{ext_{\chi}}, \delta_{\mathrm{int}_{\chi}}, \lambda_{\chi}, ta_{\chi} >$$

S_{χ} is a particular tuple defining the set of states of the executive model. It is defined by:

$$S_{\chi} = \left(D^{\chi}, \left\{M_i^{\chi}\right\}, \left\{I_i^{\chi}\right\}, \left\{Z_{i,j}^{\chi}\right\}, V^{\chi}\right)$$

where:

D^{χ} is the set of the models' names composing the network,

M_i^{χ} is the set of models composing the network $\forall\, i \in D^{\chi}$,

I_i^{χ} is the influence of $i \forall i \in D^{\chi} \cup \{\chi, \Delta\}$, i.e. the set of models which can received events from model *i*, including the DSDEVS model itself,

$Z_{i,j}^{\chi}$ is the $i \to j$ output to input function $\forall j \in I_i^{\chi}$,

V^{χ} is the set of other state variables useful for the computation of transition functions.

The 4-tuple $\left(D^{\chi}, \{M_i^{\chi}\}, \{I_i^{\chi}\}, \{Z_{i,j}^{\chi}\}\right)$ is referred to as the network structure. Any change in one of these variables is called a change of structure. Changes in this set are dynamic.

The functions of the executive model are the same as for an atomic DEVS model. The function of time advance ta_{χ} defines the time a model remains in the state $s \in S_{\chi}$ if no external event occurs. It is defined by:

$$ta_{\chi}: S_{\chi} \rightarrow R^{+}$$

The set Q_{χ} of total states of the system is:

$Q_{\chi} = \{(s,e) | s \in S_{\chi}, 0 < e < ta(s)\}$ where e is the elapsed time in state s.

The concept of total state (s,e) enables the specification of a future state according to the time elapsed in the current state. It also makes possible to specify the external transition function. Indeed, DEVS proposes two transition functions in order to make the difference between the autonomous evolutions of a model from those due to external events. The external transition function is written as follows:

$$\delta_{ext_{\chi}}: Q_{\chi} \times X_{\chi} \rightarrow S_{\chi}$$

This function specifies the response of the system to input events.

The internal transition function (autonomous part of the model) is defined by:

$$\delta_{int_{\chi}}: S_{\chi} \rightarrow S_{\chi}$$

This function specifies the lifespan of a state s evaluating $ta(s)$ when entering in state s.

The output function is an application of the set of states S_{χ} into the set of output events Y_{χ}. It is defined by:

$$\lambda_{\chi}: S_{\chi} \rightarrow Y_{\chi}$$

This function is activated when the time elapsed in a given state is equal to its lifespan.

It exists abstract simulators for DSDEVS making this formalism an operational semantic. In other words, it exist algorithms that simulate the behaviour of a DSDEVS model. The interested reader can refer to the article introducing the formalism [Barros 1996].

We now introduce the small world computation and thereafter we present our DSDEVS specification of ecosystems in a general manner.

2.2 Computation of small world properties

Recently, new theoretical approaches to natural graph complexity have emerged. The two main results of these studies are the presence of small world pattern of some economical, sociological and biological networks and the scale free distribution of connections in some ecological networks [Watts Strogatz 1998, Watts 1999]. The latter defines the number of nodes with k links as following a power law distribution $p(k) = k^{-\gamma}$ where most units are weakly connected and a few are highly linked to other nodes. The small world pattern is detected from two basic statistical properties, the clustering coefficient C_v and the path length L [Montaya Solé 2002]. In the following, C_v and L are call the small world properties.

We consider the set of link $\varepsilon_{i,j}$ where i and $j \in \{1,...,S\}$ and where $S \in \aleph^{+}$ is the number of species. $\varepsilon_{i,j} = 1$ if a link exists

and zero otherwise. Then, the set of nearer neighbours for species *i* is defined by $\Gamma_i = \{s_j \mid \varepsilon_{i,j} = 1$. The clustering coefficient for this species is then written $c_v(i) = l_i / (CS(CS-1)/2)$ with *C* the community matrix connectance and l_i defined such as:

$$l_i = \sum_{j=1}^{S} \varepsilon_{i,j} \left\{ \sum_{k \in \Gamma_i} \varepsilon_{j,k} \right\} \qquad (1)$$

The average overall species defined the clustering coefficient for the ecological web under concern:

$$C_v = \frac{1}{S} \sum_{i=1}^{S} C_v(i) \qquad (2)$$

C_v measures the average fraction of pairs of neighbours of a node that are also neighbours of each other.

The path length between two species *i* and *j* is written $L_{\min}(i, j)$. The average path length *L* is defined as follow:

$$L = \frac{2}{S(S-1)} \sum_{i=1}^{S} \sum_{j=1}^{S} L_{\min}(i, j) \qquad (3)$$

To decide if a graph is a small world, we compare C_v and *L* of this graph with another graph having the same number of nodes and a random distribution of links. If $C_v > C_v^{rand}$ and $L > L^{rand}$ but close to it, then the graph is a small world.

In the following, we introduce the measurement of small world properties in the DSDEVS specification of an ecosystem.

3. Small world properties in a model of ecosystem with dynamic structure

Ecosystems are fundamentally structured in time and space. In addition to the variation in time of the number of individuals for one species, we can observe the variation of trophic relations and of the number of species, particularly in exploited ecosystems. In this work, we adopt a structural view of ecosystems considering species and trophic relations respectively as nodes and edges in a graph. In this perspective, we must be able to specify dynamic graph and, at the same time, the set of processes we want to consider (i.e. growth, mortality...). Furthermore, all processes are spatially distributed. Then, the formalization must explicit the representation of space. We address these issues in the following.

3.1 DSDEVS specification of an ecosystem

In the previous section, we have introduced the DSDEVS formalism. DSDEVS in particularly well adapted for the specification of our model. Indeed, it both embeds the notion of dynamic graph and dynamic behaviours of models. Time is managed by a discrete event representation. It is possible to consider discrete time behaviours in such a specification but it is not our purpose here. In the following, we deal with the two main entities in an ecosystem: spatial entities and biological entities.

We consider space in a discrete manner. Every spatial entity corresponds to a place where the environmental conditions (temperature, physical substrate and so on) are identical and homogeneously distributed. This is the classical ergodic hypothesis of physic. Every spatial entity is specified by a DSDEVS. The coupled model corresponds to the connection of all spatial entities and defines the topological space. Therefore, network of models represent a set of places connected each others. This specification is general enough to consider geometries from classical lattice to a very complex geometry of space. We specify a place as a DSDEVS network defined as follow:

$$DSDEVN_{place} = < X_{place}, Y_{place}, P, M_P >$$

Biological entities are localised within a place. For simplicity here, we assume that every biological entity is a DEVS model[1]. The state S_P of the executive model M_P of place $DSDEN_{place}$ defines the interaction network between biological entities.

The nature of biological entities depends on the model objectives. For the general specification here, we consider that biological entities are species. Therefore, we associate one DEVS model with one species. Then, within a place, the food web is explicitly modelled by the state of the executive. In other words, the trophic relations between species are specified within the set $Z_{i,j}^{P}$ of the executive model of a place. Connections in a DSDEVS network are not all trophic relations. Then, we can write Θ the set of trophic relations in a place as follow: $\Theta_{i,j}^{P} \subset Z_{i,j}^{p}$, with *i,j* the index of DEVS models of species. We assume that $\Theta_{i,j}^{P} : Y_i \to X_j$ specifies the predation of *j* onto *i*. The set $\Phi_i^P \subseteq I_i^P$ specifies the potential trophic relations for species *i*, i.e. its potential predators.

In the next section, we introduce the measure of small world propertied in the DSDEVS model of a place. Doing that, we specify a dynamic view of small world measurement.

3.2 Incorporating small world properties

We have presented the computation of small world properties in section 2.2. We now incorporate this computation considering the ecosystem as a DSDEVS model.

The clustering coefficient for species *i* is then written:

$$c_v(i) = l_i / \left(C \times card\left(M^P\right)\left(C \times card\left(M^P\right) - 1\right)/2\right)$$

Considering equation 1 we can write:

$$l_i = \sum_{j=1}^{card(M^P)} \Theta_{i,j}^{P} \left\{ \sum_{k \in \Gamma_i} \Theta_{i,j}^{P} \right\}$$

We can compute the global clustering coefficient within a place following equation 2:

$$C_v^P = \frac{1}{card(M^P)} \sum_{i=1}^{card(M^P)} C_v(i) \qquad (4)$$

The path length is basely defined following equation 3:

$$L^P = \frac{2}{card(M^P)(card(M^P)-1)} \sum_{i=1}^{card(M^P)} \sum_{j=1}^{card(M^P)} L_{\min}(i,j) \qquad (5)$$

We define C_v^P and L^P as state variable of the executive M_P, i.e. $C_v^P \wedge L^P \subset V^P$. Any change in structure of the executive model implies a change of values C_v^P and L^P following equation 4 and 5.

This specification enables to follow the dynamical evolution of small world pattern in the food web localised within a place. If we consider the set of places, we can then build a dynamic map of small world properties. This kind of map can be very useful for ecosystem management. We discuss this point in the following conclusion.

[1]Considering modularity, hierarchical decomposition and system specification, the model of biological entities can be a coupled DEVS, a DSDEVS or any formalism embedded in a DEVS architecture. See for instance [Zeigler *et. al.* 2000, Duboz 2004] for details.

4. Conclusion and perspectives

In this paper, we have used the DSDEVS formalism for the modelling and simulation of food web. This formalism specifies dynamical changes of graph structure. Then we have introduced the computation of small world properties into a DSDEVS model. Doing that, we have a dynamic view of the evolution of the small world properties.

The consequences of small world patterns are far from trivial and can be of great interest for the understanding of ecological process that build trophic relations between species [Montaya Solé 2002]. It as been shown that small world graph resist to perturbations in term of deletion or addition of nodes. In the context of ecosystems management, it can be very useful to know if a particular ecosystem is a small world. Indeed, this property can justify the exploitation or not of species within the ecosystem.

The main contribution of this work is the dynamical and spatialised view small world representation. We hope that such a representation can improve the use of small world properties as an indicator of ecosystem resistance to perturbations. As far as we know, the dynamical and spatial aspects of small world have never been used in ecology.

The modelling and simulation of ecosystems is not limited to the representation of trophic interactions. Several processes like growth and mortality, matter and energy flux for instance, must be considered in order to simulate the dynamics of the populations. Considering the definition of DSDEVS models, it is possible to specify several functions and state variables for this purpose. For clarity and shortness, we have not presented such a specification here.

The computational nature of DSDEVS model allows the simulation of such models. We are currently developing a model of estuaries following the specification given in this paper. We use the Virtual Laboratory Environment (VLE) platform [Quesnel et. al. 2004, Duboz et. al. 2004] to implement the model. VLE is a framework for multi-modelling and simulation and implements DSDEVS abstract simulators. In a close future, we will build estuary model and we will be able to test our general formal specification of the measurement of dynamic food web complexity.

ACKNOWLEDGMENTS

Authors want to tanks the French research institute for developing countries (IRD) for funding this work with a postdoctoral position.

REFERENCES

[Albaret 1999] J.J. Albaret. *Les poissons des eaux continentales africaines*, chapter Les peuplements des estuaires et des lagunes, pages 325–349. 1999.

[Barros 1996] F. Barros. Dynamic structure discret event system specification: Formalism, abstract simulators and applications. *Transaction of the Society for Computer Simulation*, 13(1):35–46, 1996.

[Coquillard Hill 1997] P. Coquillard. and D. R. C. Hill. *Modélisation et simulation d'écosystèmes : des modèles déterministes aux simulations à évènements discrets*. Masson, 1997.

[Duboz et. al. 2004] R. Duboz, E. Ramat, and G. Quesnel. Systèmes multi-agents et théorie de la modélisation et de la simulation : une analogie opérationnelle. In Olivier Boissier and Zahia Guessoum, editors, *Actes des douzièmes Journées Francophones sur les Systèmes Multi-Agents (JFSMA). Systèmes multi-agents défis scientifiques et nouveaux usages*, pages 49–68, Paris, France, november 2004.

[Duboz 2004] R. Duboz. *Intégration de modèles hétérogènes pour la modélisation et la simulation de systèmes complexes : application au transfert d'échelles en écologie marine*. PhD thesis, Université du Littoral Côte d'Opale, mars 2004.

[Klir 1985] G. Klir. *Architecture of Systems Problem Solving*. Plenum press, 1985.

[Montaya Solé 2002] J.M. Montoya and R.V. Solé. Small worlds patterns in food webs. *J. Theor. Biol.*, 214:405–412, 2002.

[Quesnel et. al. 2004] G. Quesnel, R. Duboz, and É. Ramat. Wrapping into devs simulator: A case study. In *proceddings of the Conference on Conceptual Modeling and Simulation*, Genoa, Italy, 28-30 Octobre 2004.

[Uhrmacher 2001] A.M. Uhrmacher. Dynamics structure in modeling and simulation - a reflective approach. *ACM Transaction on Modeling and Simulation*, 11(2):206–232, 2001.

[Watts 1999] D.J. Watts. *Small Worlds*. Princeton University press, 1999.

[Watts Strogatz 1998] D.J. Watts and S.H. Strogatz. Collective dynamics in 'small world' networks. *Nature(London)*, 393:440–442, 1998.

[Zeigler *et. al*. 2000] B. Zeigler, D. Kim, and H. Praehofer. *Theory of modeling and simulation: Integrating Discrete Event and Continuous Complex Dynamic Systems*. Academic Press, 2000.

The use of Air Quality Modelling Systems for Industrial Real-Time and Forecasting applications in Spain

R. San Jose
Environmental Software and Modelling Group, Computer Science School, Technical University of Madrid (UPM) Campus de Montegancedo, Boadilla del Monte, 28660 Madrid (Spain).
+34-91-3367465, roberto@fi.upm.es

Juan L. Pérez
Environmental Software and Modelling Group, Computer Science School, Technical University of Madrid (UPM) Campus de Montegancedo, Boadilla del Monte, 28660 Madrid (Spain).
+34-91-3367465, jlperez@fi.upm.es

Rosa M. González
Department of Meteorology and Geophysics, Faculty of Physics, Complutense University of Madrid (UCM), Ciudad Universitaria, 28040 Madrid (Spain).
+34-91-394-4513,
rgbarras@fis.ucm.es.

ABSTRACT
The advances in air quality modeling during the last decade have been spectacular because of the continuous improvement in the understanding of the physics and chemistry in the atmospheric dynamics. In parallel the continuous progress in computer capability and software simulation have contributed decisively to the actual capability to control the air quality impact of industrial sources. The use of complex air quality modeling systems such as MM5-CMAQ is illustrated in this contribution. We have mounted and applied the system for air quality impact assessment studies and also for real-time and forecasting information services with high performance and excellent results. In this contribution we will show the results of several examples of application of the system over cities and industrial plants in historical mode (impact assessment studies) and real-time and forecasting modes. Implementation of cluster computer platform is imperative due to the complexity of the systems and because of the required computer time. The system provide a full description of the air concentrations in time and space in the urban domain and in the surrounding areas of the industrial plants such as combined cycle power plants and incinerators.

KEYWORDS
Air pollution, operational system, industrial plants,

1. Introduction

The air quality impact of industrial plants is an essential issue in air quality assessment and modeling which is becoming more important due to the more strict EU legislation in air quality standards. The 2002/3/EC Directive of the European Parlament and of the Council of 12 February 2002 related to ozone in ambient air provides information related to shirt-term action plans at the appropriate administrative levels. In accordance with this legislation, industrial plants are being requested by environmental authorities to have appropriate control systems to provide in real-time and forecasting mode information related to the relative impact of their industrial plants in the forecasted pollution levels – in particular on the O3, SO2, NOx, CO and PM10 levels which are limited by different EU Directives -. The capability to reduce specific emissions in real-time according to a forecast for a specific area and period of time is actually a challenging issue. In the past years, this objective was limited due to the limited computer power and the cost of vector parallel computers. Nowadays, cluster system composed by PC processors (3,4 Ghz or 3,6 Ghz) provide an acceptable capability – once we have designed a proper architecture of the air quality modeling systems – to run this complex systems in real-time and forecasting mode.

The concept of real-time in our case is related to the fact of taking appropriate decisions in advance to avoid specific exceeds of the EU Directive limits. Following above Directive the responsibility to design of short-term action plans, including trigger levels for specific actions, is the responsibility of Member States. Depending of the individual case, the plans may provide for graduated, cost-effective measures to control and, where necessary, reduce or suspend certain activities, including motor vehicle traffic, which contribute to emissions which result in the alert threshold being exceeded. These may also include effective measures in relation to the use of industrial plants or products. In this application we focus on the possible reduction of industrial activities – in our case, a combined cycle power plant -.

Air pollution modeling systems have experimented a considerable advance during the last decade. During the 70's and 80's most of the air pollution models for all applications, but in particular where the so-called Gaussian models which means that the atmospheric transport equation (partial differential Navier-Stokes equations) is solved after a substantial simplification.

As a consequence, the solution is an exponential Gaussian form which provides concentrations of the emitted pollutants in time and space provided that a detailed meteorology is available. The Gaussian model is capable to run a seconds in modern computer platforms but the accuracy of the results and the difficulties to deal with chemical reactions make it inappropriate for our purposes. On the other hand the physics parameterization involved in most of this Gaussian models is limited adding more uncertainty to the results. During the 90's up to now, the so-called Eulerian models are being used. Intermediate models are the so-called Lagragian models which simulated the pollution concentrations by releasing a considerable amount of particles and tracking them over a mobile reference system. The Eulerian approach allows a full description of the complete atmospheric system with a fixed coordinate system. The Eulerian Air pollution models are classically divided into meteorological models and transport and chemistry models. In both cases the numerical methods are used to solve the Navier-Stokes equations with a limited number of approximations. Eulerian models require a considerable amount of computer power and for real-time and forecasting applications – as the one showed in this contribution -.

The complete tool designed for this application is called TEAP (a Tool to Evaluate the Air quality impact of industrial Plants) (San José et al., 1998, 2004). This tool is designed to be used by the environmental impact department at the industrial site. The tool provides a response to air quality impact to industrial emissions in the form of surface patterns and lineal time series for specific geographical locations into the model domain. The model domain is designed in a way that the industrial source point is located approximately in the center of the model domain. The model domain can be as large as wished but a specific nesting architecture should be designed for each case together with a balanced computer architecture.

The TEAP tool (an EUREKA-EU project) has the capability to incorporate different modeling systems. In a preliminary stage we have tested thee system with the so-called OPANA model (ETC/ACC03). OPANA model (San José et al, 1998) stands for Operational Atmospheric Numerical pollution model for urban and regional areas and was developed at the middle of the 90's by the Environmental Software and modeling Group at the Computer Science School of the Technical University of Madrid (UPM) based on the MEMO model (ETC/ACC03) developed in the University of Karlsruhe (Germany) in 1989 and updated on 1995, for non-hydrostatic three dimensional mesoscale meteorological modeling and SMVGEAR model for chemistry transformations based on the CBM-IV mechanism and the GEAR implicit numerical technique developed at University of Los Angeles (USA) in 1994. The OPANA model has been used (different versions) for simulating the atmospheric flow – and the pollutant concentrations – over cities and regions in different EU funded projects such as EMMA (1996-1998), EQUAL (1998 – 2001), APNEE (2000-2001). In these cases and others the model has become an operational tool for several cities such as Leicester (United Kingdom), Bilbao (Spain), Madrid (Spain), Asturias region (North of Spain) and Quito (Ecuador, BID, 2000). In all these cases the model continue to operate under daily basis and simulates the atmospheric flow in a three dimensional framework. The OPANA model, however, is a limited area model – which means that the model domain is limited by the earth curvature – and the cloud chemistry and particulate matter is not included (aerosol and aqueous chemistry).

The cluster approaches open new scenarios for many applications and particularly on the atmospheric dynamics simulations. The atmospheric models have also reached high sophisticated levels which include the simulation of the aerosol processes and cloud and aqueous chemistry. These models include sophisticated land use information and deposition /emission models [San Jose *et al*. 1997]. The atmospheric models include traditionally two important modules: a) meteorological modelling and b) transport/chemistry modules. These two modules work in a full complementary mode, so that, the meteorological module provides full 4D datasets (3D wind components, temperature and specific humidity) to the transport/chemistry modules. CPU time is mainly used for transport/chemistry (70 – 80 %). This modelling system require important initial and boundary data sets to simulate properly specific time periods and spatial domains, such as landuse data, digital elevation model data, global meteorological data sets, vertical chemical profiles and emission inventory data sets. In this experiment we have used AVN (NCEP/NOAA, USA) global meteorological information as input for the MM5 meteorological model. The emission inventory for the proper spatial domain and for the specific period of time (at high spatial and temporal resolution) is possibly the most delicate input data for the sophisticated meteorological/transport/chemistry models. The accuracy of emission data is much lower than the accuracy of the numerical methods used for solving the partial differential equation systems (Navier – Stokes equations) for meteorological models [Grell *et al.* 1994] and the ordinary differential equation system for the chemistry module [San Jose *et al.* 1994], [San Jose *et al.* 1996], [San Jose *et al.* 1997]. Typical uncertainty associated to emission data is 25 – 50 %. However, in our application it is more important to see the relative impact of the industrial emissions in the mesoscale domain – where the tested industrial plant is located – than to quantify and qualify the absolute pollutant concentrations in the atmosphere.

Examples of "state-of-the-art" meteorological models are: MM5 (PSU/NCAR, USA), RSM (NOAA, USA), ECMWF (Redding, U.K.), HIRLAM (Finnish Meteorological Institute, Finland), etc. Examples of "state-of-the-art" of transport/chemistry models – also called "third generation of air quality modelling systems" – are: EURAD (University of Cologne, Germany), [Stockwell *et al.* 1977], EUROS (RIVM, The Netherlands), [Lagner *et al.* 1998], EMEP Eulerian

(DNMI, Oslo, Norway), MATCH (SMHI, Norrkoping, Sweden), [Dervent Jenkin 1991], REM3 (Free University of Berlin, Germany), [Walcek 2000], CHIMERE (ISPL, Paris, France), [Schmidt *et al.* 2001], NILU-CTM (NILU, Kjeller, Norway), [Gardner *et al.* 1997], LOTOS (TNO, Apeldoorm, The Netherlands), [Roemer *et al.* 1996], DEM (NERI, Roskilde, Denmark), [Gery *et al.* 1989], STOCHEM (UK Met. Office, Bracknell, U.K.), [Collins *et al.* 1997]. In USA, CAMx Environ Inc., STEM-III (University of Iowa) and CMAQ (EPA, US) are the most up-to-date air quality dispersion chemical models. In this application we have used the CMAQ model (EPA, U.S.) which is one of the most complete models and includes aerosol, cloud and aerosol chemistry.

2. The MM5-CMAQ Modeling System

The CMAQ model (Community Multi-scale Air Quality Modeling System, EPA, US) is implemented in a consistent and balanced way with the MM5 model [12]. The CMAQ model is fixed "into" the MM5 model with the same grid resolution (6 MM5 grid cells are used at the boundaries for CMAQ boundary conditions). As an example a domain architecture is showed in Figure 1 for an application in a combined cycle power plant in the south area of Madrid Community . MM5 is linked to CMAQ by using the MCIP module which is providing the physical variables for running the dispersion/chemical module (CMAQ) such as boundary layer height, turbulent fluxes (momentum, latent and sensible heat), boundary layer turbulent stratification (Monin-Obukhov length), friction velocity, scale temperature, etc. We have run the modeling system (MM5-CMAQ) with USGS 1 km landuse data and GTOPO 30'' for the Digital Elevation Model (DEM) which can be substituted for any more accurate high spatial resolution landuse information in the implementation of the input data.

The system uses EMIMO model to produce every hour and every 1 km grid cell the emissions of total VOC's (including biogenic), SO2, NOx and CO. EMIMO is a emission model developed at our laboratory in 2001. This model uses global emission data from EMEP/CORINAIR European emission inventory (50 km spatial resolution) and EDGAR global emission inventory (RIVM, The Netherlands). In addition the EMIMO (EMIssion Model) model uses data from DCW (Digital Chart of the World) and USGS land-use data from AVHRR/NOAA 1 km satellite information. The EMIMO model includes a biogenic module (BIOEMI) developed also in our laboratory based on the algorithms for natural NOx, monoterpene and isoprene emissions in function of LAI (leaf Area Index) and PAR (photosynthetic active radiation). The emission inventory is a model which provides in time and space the amount of a pollutant emitted to the atmosphere. In our case we should quantify the emissions due to traffic, domestic sources, industrial and tertiary sector and also the biogenic emissions in the three model domains with 9 km, 3 km and 1 km spatial resolution mentioned above. The mathematical procedures to create an emission inventory are essentially two: a) Top-down and b) Bottom-up. In reality a nice combination of both approaches offers the best results. Because of the high non-linearity of the atmospheric system, due to the characteristics of the turbulent atmospheric flow, the only possibility to establish the impact of the part of the emissions (due to traffic or one specific industrial plant, for example) in air concentrations, is to run the system several times, each time with a different emission scenario.

In Figure 2 we see a scheme of the computer platform needed to simulate different emission reduction scenarios in case of exceeding the pollution levels stated at the legislative directives (L282/69, 26.10.2001).

Each emission scenario involves to run a complete version of the model which differs from others only on the tested emission reduction so that in the case of industrial plants, we have an OFF scenarios which represents to run the model with the complete emission set (provided by EMIMO) but "without" the emissions from the industrial plant and the so-called ON scenario represents to run the model with exactly the same emissions as in the OFF scenario but "with" the expected hourly emissions from the industrial plant. Obviously the differences between ON and OFF represent the impact of the industrial emissions in the pollutant concentrations. A similar approach can be applied for any emission source which we would like to analyze (traffic flow, domestic emissions, etc.).

In order to run these complex systems, a single PC seems to be quite limited because the required CPU time exceeds the available time for daily operational application. It is possible to use cluster platforms to reduce significantly the amount of computer time required for the different simulations. For running the MM5-CMAQ modeling system in the cluster platform, we use the cluster version of both modules. The only possible alternative is probably the cluster, with an acceptable cost/benefit relation to run such a complex systems. Particularly in the case shown in this contribution, where the modeling system should be run in ON and OFF scenario but additional scenarios (to be compared each other or with the base case, OFF) can be included but much more CPU time will be required. We are working under an architecture of daily operation so that the CPU limit time is formally 24 hours but in practice (because the CMAQ CPU time depends on the maximum wind speed – Courant Law-), 18-20 CPU hours is a realistic limit.

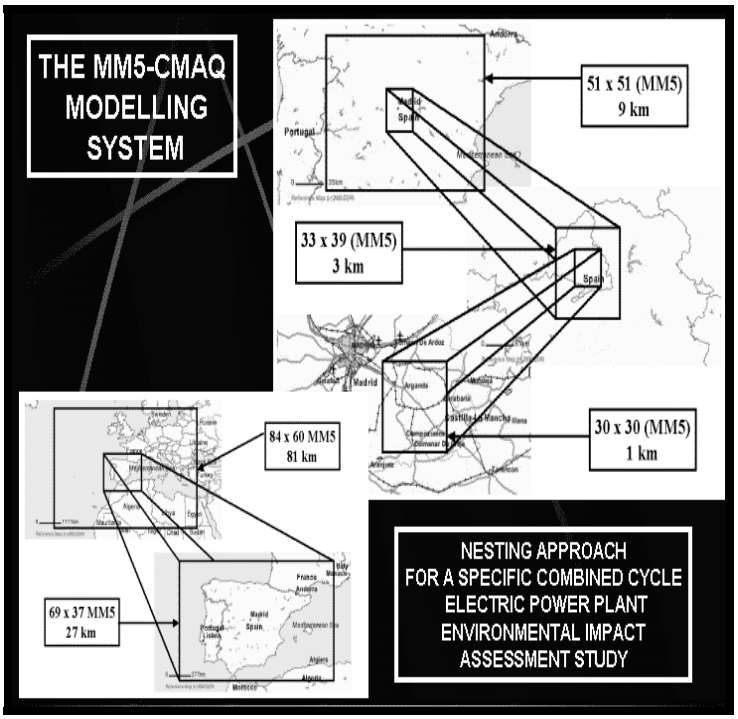

Fig. 1. MM5-CMAQ architecture for this experiment.

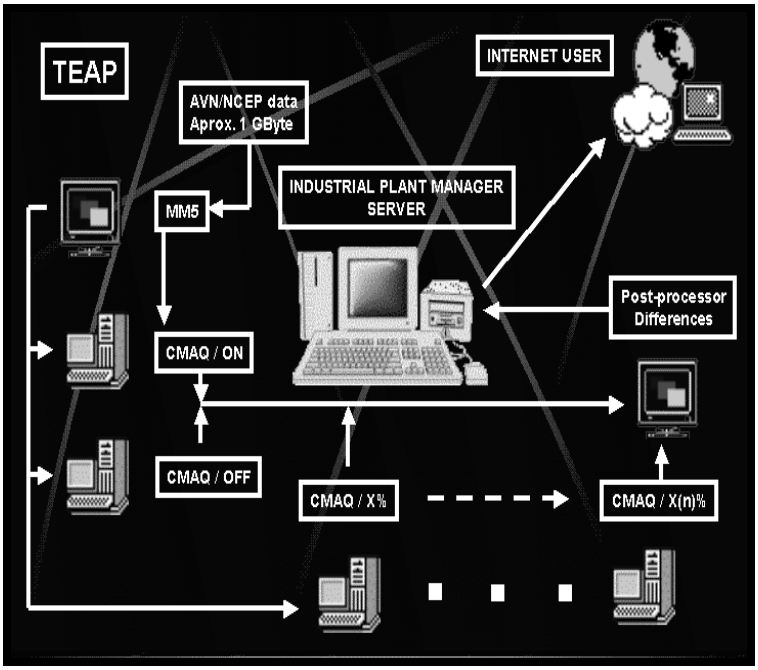

Fig. 2. TEAP Computer platform scheme.

The results over platforms of about 20 nodes provide increases of time of about 10- 11 times for both modules (meteorological and chemical/transport). This rate is highly satisfactory but it may probably be increased by using faster connection architectures between PC's. The MM5-CMAQ modeling system constitutes a reliable and robust software tool which allows a historic and on-line operational simulation over any domain at global scale with several different nesting capabilities and approaches. MM5 is used by several states in USA for weather forecasts and in Europe it is used by several meteorological Institutes as a research code and also for operational applications. In our lab, MM5 has been used (http://artico.lma.fi.upm.es) for operational weather forecasts – provided in the Internet – since year 2000 with reliable results.

3. Results

Different applications have been carried out over different domains and emission sources. In this contribution we will show particularly some examples over combined cycle power plants which required an air quality impact assessment before starting to operate and also the case of several incinerators in the Basque Country area in the north of Spain.

3.1. Combined Cycle Power Plant in Madrid domain

In this section we show results for an application of the MM5-CMAQ-EMIMO modeling system with the described input data (emissions – EMIMO -, landuse data – USGS -, topography – GTOPO -, etc.) over Madrid domain designed for a specific study of the impact of a future power plant construction. Several studies of this type have already been conducted at different areas in the Iberian Peninsula for different industrial type plants as mentioned above. In Figure 1 we showed the scheme designed for the study in the Madrid domain. Similar architecture has been used for different areas. Figure 3 shows the surface ozone concentration differences over a domain of 27 x 33 grid cells (3 km) centered at the planned power plant. The planned power plat emissions are incorporated to the system in ON scenario under the maximum impact mode i.e. the expected maximum hourly emissions produced by the power plant (worst scenario).

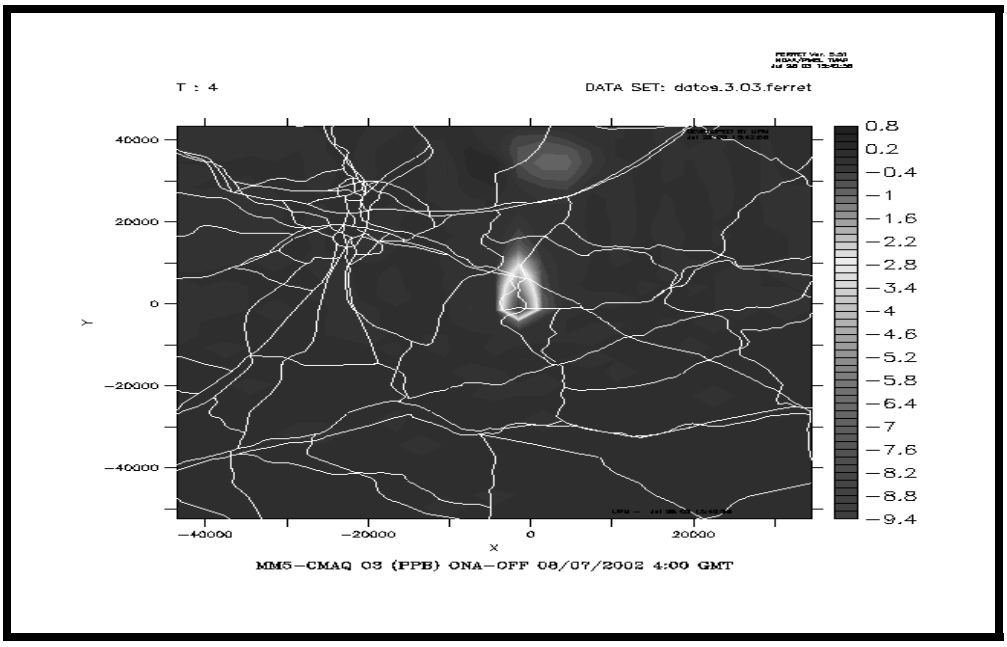

Fig. 3. Surface concentration differences over a domain of 27 x 33 grid cells (3 km) centered at the planned power plant. Differences between ozone concentrations (ppb) in OFF mode and with the planned power plant emissions at 4h00 (GMT) on July, 8, 2002.

These results show an excellent agreement between observations and modelling results in the calibration phase (before running the simulations adding the emissions from the planned industrial power plant). This agreement is essential for the reliability of the final results although the differences between the concentrations in ON and OFF modes are the most important relative results on these types of studies.

We should underline that the amount of information obtained for a typical air quality impact study of an industrial and power plant for 120 hours periods along 12 month a year and for five criteria pollutants, 3 different nesting levels (9 km, 3 km and 1 km) produces an amount of information (every hour analysis) of about 5 Gbytes and 400000 images (examples are shown in this contribution). The whole system should be controlled by the corresponding scripts running in automatic mode over several weeks in different PC platforms.

In real- time mode we should carefully design our architecture (generally over a cluster platform) and assure that the simulations of ON, OFF and all emission reduction scenarios (X %) run under daily basis for 120 hours period and obtain the differences between ON and X % runs with OFF mode to obtain the best performance emission reduction scenario for the next 48 – 72 hours. The X % emission reduction scenarios are simulated by applying this emission reduction over the last 48 – 72 hours. This operational architecture requires – as we said – cluster platforms. Our tests over a cluster with 20 nodes (2,4 Ghz.) and one main PC (with 2,4 Ghz) show an increase on the speed of about 10 –11 times. This test was performed at a cluster in the University of Iowa (USA). Currently the first real-time and forecasting system which is installed and operating under these characteristics is installed in a combined cycle power plant for two large electric power companies in Spain (Iberdrola S.A. and Unión Fenosa, S.A.) and it contains eight nodes, each node with one processor of P-IV-3,4Ghz, 1 Gbyte RAM each and running 5 different scenarios for four 400 MW groups.

3.2. Incinerator in Basque Country (North of Spain)

Another application has been carried out over an incinerator project in the Basque Country in Spain. In this case an special adaptation of the CMAQ modeling system (Hutzell W.T. 2002) is implemented. This adaptation allowed to obtain the impact of different metals (Cd, Ni, As), Polycyclic Aromatic Hydrocarbons such as B[A]P and dioxins and furans, PCDD/F. This implementation increased the CPU time in about 40 % respecting the “classical one” and the amount of information comprised about 20 Gbytes. Actually, a second application has been carried out for a larger incinerator located in the surrounding area of San Sebastián (Spain) and in this case a much more comprehensive study has been carried out since a number of large industrial source points already working in the area have been analyzed. This study included the relative impact of the most important highway (A8) located in the surrounding area of the potential location of the future incinerator plant. Figure 4 shows the percentage of reduction in ozone concentrations due to the expected emissions of the planned incinerator over the 1k spatial resolution model domain (24 x 24 km) at 17h00 GMT on July, 12, 2002.

The inclusion of up to six different industrial plants in the San Sebastian study required to use a large model domain for the highest spatial resolution domain (45 x 45 km with 1 km spatial resolution). Also, the inclusion of the dioxins and furans up to a total of 16 no only increased substantially the CPU time but also all the chemistry related to gas and particle forms induced changes in the results due to the chemical activity. Unfortunately there are not a lot of measured dioxins and furans but currently a network located in USA has been used to validate the results of the dioxins and furans version of the CMAQ model. The results offer a wide range of correlation for the different species but in general terms most of the accuracies – as it is the case in most applications of these complex air quality models – can be due to the uncertainties involved in the emission inventory. For the analysis of the relative (to the potential impact of the projected incinerator) impact of the A8 highway we used detailed vehicle counting data obtained from the highway and Basque Government databases.

4. Conclusions

In this contribution we have shown several applications and studies by using the sophisticated MM5-CMAQ modeling system. The system has been proved to be very robust and reliable. The results assure that it is possible to have in real-time and forecasting mode tools over the Internet which provides air quality impact forecasts for different industrial plants and urban areas and take emission reduction actions on time. Further work is currently under development to determine the best strategy to identify the best emission reduction strategies based on air quality forecasts. In the case of industrial plants the

complete switch off of the emissions for a period of 24-48 hours is the best possible solution assuming that the impact of the emissions of the industrial plant is the main cause of exceed of the EU legislative concentration limits (or any other world legislation). In the case of urban areas, the situation is much more complex since different emission sources and spatial locations should be studied and identify to take the optimal emission reduction strategy decision. This can only be accomplished by increasing the number of model runs by using massively the cluster approach. Further extensions and applications of this system can include the real-time analysis and impact of main highways and full traffic emission impact analysis from different districts and urban sectors according to the Municipality architecture.

The system is starting to operate in real time and forecasting mode in the south-west area of Madrid for a combined cycled power plant with four 400 MW groups and using a 8-node cluster platform under LINUX OS. The system has been proved to be reliable and suitable to identify the impact in space and time of different air pollutants in real-time and forecasting mode.

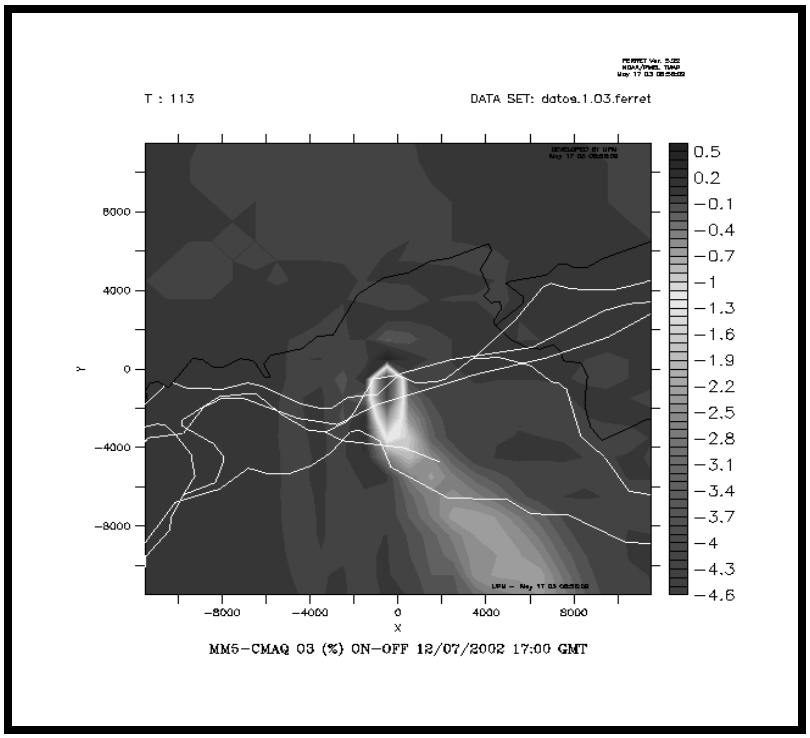

Fig. 4. Percentage of reduction in ozone concentrations due to the expected emissions (maximum mode) of the planned incinerator over the 1k spatial resolution model domain (24 x 24 km) at 17h00 GMT on July, 12, 2002.

ACKNOWLEDGEMENTS
We would like to thank PSU/NCAR and EPA (US) for the MM5 and CMAQ codes. Also the following companies and institutions for funding the corresponding studies and services: Txingudi, Soluziona, Electrabel and CDTI (Spanish Industrial Funding Agency, Ministry of Industry, Spain).

REFERENCES

[Collins *et al.* 1997] Collins W.J., Stevenson D.S., Johnson C.E. and Derwent R.G. (1997). Tropospheric ozone in a global scale3D Lagrangian model and its response to NOx emission controls. J. Atmos. Chem., 86, 223-274.

[Dervent Jenkin 1991] Derwent, R. and Jenkin M. (1991). Hydrocarbons and the long-range transport of ozone and PAN across Europe. Atmospheric Environment 8, 1661-1678.

[ETC/ACC 2003] European Topic Center on Air and Climate Change (http://air-climate.eionet.eu.int/databases/MDS/index_html) .

[Gardner *et al.* 1997] Gardner R.K., Adams K., Cook T., Deidewig F., Ernedal S., Falk R., Fleuti E., Herms E., Johnson C., Lecht M., Lee D., Leech M., Lister D., Masse B., Metcalfe M., Newton P., Schmidt A., Vandenberg C. and van Drimmelen R. (1997). The ANCAT/EC global inventory of NOx emissions from aircraft. Atmospheric Environment 31, 1751-1766.

[Gery *et al.* 1989] Gery M.W., Whitten G.Z., Killus J.P. and Dodge M.C (1989), A photochemical kinetics mechanism for urban and regional scale computer modelling, *Journal of Geophysical Research*, 94, D10, pp. 12925-12956.

[Grell *et al.* 1994] Grell G.A., Dudhia J. and Stauffer D.R. (1994). A description of the Fifth-Generation Penn State/NCAR Mesoscale Model (MM5). NCAR/TN- 398+ STR. NCAR Technical Note.

[Lagner *et al.* 1998] Langner J., Bergstrom R. and Pleijel K. (1998). European scale modeling of sulfur, oxidized nitrogen and photochemical oxidants. Model development and evaluation for the 1994 growing season. SMHI report RMK No. 82. Swedish Met. And Hydrol. Inst., SE-601 76 Norrkoping, Sweden.

[Roemer *et al.* 1996] Roemer M., Boersen G., Builtjes P. and Esser P. (1996). The budget of ozone and precursors over Europe calculated with the LOTOS model. TNO publication P96/004, Apeldoorn, The Netherlands.

[San Jose *et al.* 1994] San José R., Rodriguez L., Moreno J., Palacios M., Sanz M.A. and Delgado M. (1994) Eulerian and photochemical modelling over Madrid area in a mesoscale context, *Air Pollution II, Vol. 1Computer Simulation, Computational Mechanics Publications, Ed. Baldasano, Brebbia, Power and Zannetti*., pp. 209-217.

[San Jose *et al*. 1996] San José R., Cortés J., Moreno J., Prieto J.F. and González R.M. (1996) Ozone modelling over a large city by using a mesoscale Eulerian model: Madrid case study, *Development and Application of Computer Techniques to Environmental Studies, Computational Mechanics Publications, Ed. Zannetti and Brebbia*, pp. 309-319.

[San Jose *et al.* 1997] San José R., Prieto J.F., Castellanos N. and Arranz J.M. (1997) Sensititivity study of dry deposition fluxes in ANA air quality model over Madrid mesoscale area, *Measurements and Modelling in Environmental Pollution, Ed. San José and Brebbia*, pp. 119-130.

[Schmidt *et al.* 2001] Schmidt H., Derognat C., Vautard R. and Beekmann M. (2001). A comparison of simulated and observed ozone mixing ratios for the summer 1998 in Western Europe. Atmospheric Environment, 35, 6277-6297.

[Stockwell *et al.* 1977] Stockwell W., Kirchner F., Kuhn M. and Seefeld S. (1977). A new mechanism for regional atmospheric chemistry modeling. J. Geophys. Res., 102, 25847-25879.

[Walcek 2000] Walcek C. (2000) Minor flux adjustment near mixing ration extremes for simplified yet highly accurate monotonic calculation of tracer advection. J. Geophys. Res., 105, 9335-9348.

Comparison of two chemistry mechanisms Impact on the air quality predictions and comparison with observations

J. Arteta
Laboratoire de Météorologie Physique
OPGC-CNRS
24 Avenue des Landais – 63177
Aubière cedex
FRANCE
33 (0)4 73 4O 52 76
J.Arteta@opgc.univ-bpclermont.fr

S. Cautenet
Laboratoire de Météorologie Physique
OPGC-CNRS
24 Avenue des Landais – 63177
Aubière cedex
FRANCE
33 (0)4 73 4O 52 76

ABSTRACT
The ESCOMPTE experiment (Expérience sur Site pour COntraindre les Modèles de Pollution et de Transport d'Emissions) was a great measurement campaign conducted over Southern France (including urban and industrial zones) in June and July 2001. In order to study the impact of chemical mechanisms on the redistribution of anthropogenic and biogenic emissions and on the oxidizing capacity of the atmosphere, we use an "online" coupling between the RAMS meso-scale model and two chemical mechanisms: (i) a condensed chemical mechanism - MOCA2.2, (ii) an explicit chemical mechanism - RACM. In these cases of complex circulations (sea breeze associated with topography) with high urban and industrial areas, this online coupling is an essential step to well simulate the processes which involve peaks of pollution. Two Intensive Observation Periods characterized by various meteorological conditions were simulated: IOP2a and IOP2b in June 2001. Many primary species (NO_x, SO_2, CO, VOC) or secondary species (O_3, NO_y …) are compared with aircrafts and surface stations measurements for the numerical results from both chemistry models. We point out the impact of different chemical mechanisms on the production of species involved in the oxidizing capacity such as ozone, radicals and peroxides under urban and industrial areas. We highlight that theses two chemical mechanisms produce very close results for most of the pollutants, despites of their big differences.. We show the reduced and detailed mechanisms are almost the same for all the main atmospheric pollutants, as in spatial distribution as in temporal evolution. The differences between both mechanisms are only visible for VOCs because these compounds are the heart of RACM mechanism. For air quality modeling, a reduced mechanism is satisfactory, and has the advantage to be fast for using.

KEYWORDS
meso-scale modelling, chemical mechanisms, air pollution, gas-phase

1. Introduction

Control and prevision of pollution peaks on urban and sub-urban areas have become important human health issues. Despite of all national and inter-national agreements, increasing human activities provide a huge inrush of more or less toxic species onto the low-level layers of atmosphere. With the increase of computers calculation capacities, scientifics have made great progress on the comprehension and the simulation of dynamical and chemical processes which occur in the arrival, the persistence and the end of these high pollution periods. Dynamics and thermodynamics are well known to be important factors in the transport of chemical species contributing to the air quality. They strongly influence the evolution of concentration and the distribution of chemical species. However, theses parameters are also very dependent on chemical mechanisms used [Müller *et al*, 1995], emissions, dry deposition on surface, evaluation of actinic fluxes. Lots of chemistry schemes, with always more species and reactions, have been elaborated during the last decades (EMEP [79 species, 141 reactions; [Simpson *et al*, 1997]], RACM [77 species, 327 reactions; [Stockwell *et al*, 1997]], MCM [2400 species, 7100 reactions; [Jenkin *et al*, 1997]], …). All of these models give good results, but is such sophistication necessary to predict pollution peaks, principally due to primary and secondary species (Ozone, NO_x, SO_2, CO …)? Furthermore, how do these schemes, tested and validated most of the time with 0-Dimension meteorological models in idealized cases [Kuhn *et al*, 1998]; [Gross *et al*, 2003]; [Jimenez *et al*, 2003], behave coupled with 3D meso-scale model, in which lots of parameterizations influence the spatial and temporal redistribution of chemical species?
Indeed, in the low layers of troposphere, the phenomena of emissions and deposition are extremely important, and strongly vary grid- point with another of the studied domain. A meso-scale modeling with nested grids, coupled to two different gas phase chemical schemes, as well as a module of emission and dry deposition [Wesely, 1989], realized on the domain covered by measurement campaign ESCOMPTE [Cros *et al.*, 2004], will allow to simulate the three-dimensional redistribution of the atmospheric pollutants, and thus to determine the real impact of the chemical model in simulations of quality of the air.

2. Simulations framework

2.1. Meteorological model

To drive this study, we used the Regional Atmospheric Modeling System (RAMS) model version 4.3 (http://www.atmet.com, [Cotton *et al.*, 2003]). RAMS is a paralleled, meso-scale, non-hydrostatic weather forecast model allowing spatio-temporal integration from emissions scale up to meso-scale. This model is principally used for regional scale simulations and air quality applications. Many previous investigations on regional pollution have been made using the RAMS model [Lyons *et al.*, 1995]; [Millan *et al.*, 1997]; [Edy Cautenet, 1998]; [Cautenet *et al.*, 1999]; [Poulet *et al.*, 2004], [Taghavi *et al.*, 2004]).

The model was used with two nested grids (two-ways nesting) (**fig.1**). With this configuration, each grid takes in account different part of the atmospheric dynamics. The coarse grid (grid 1), witch covers Southern France, a part of Northern Spain and a part of Northern Italy (field ranging from 41.45°N to 46.17°N and 2.0°W to 8.5°E) is principally devoted for synoptic circulation. This domain includes the cities of Lyons, Turin, and Barcelona in the north, east, and southwest respectively, witch are the most important sources of pollutant in this West European continent. Moreover, it comprises the Pyrenees, Massif Central, and Alps mountains. This topography introduces a complex circulation associated with sea breeze. This grid has 36 square meshes of 15 km. The fine one (grid 2 : 42.76°N to 44°N, 4.5°E to 6.2°E)(**fig.2**), covers the ESCOMPTE domain (including the cities of Marseilles, Toulon, Avignon, Alpilles hills, and the Durance and Rhone valleys), and is devoted to local circulation. It has 47 meshes of 3 km. The vertical resolution is the same for both grids: 35 levels whose 15 levels from surface to 1500 meters, which ensures a fine description of the boundary layer. The time resolution is 15 seconds for the coarse grid, and five seconds for the fine one.

Figure 1: Grid 1 and the nested grid 2

Figure 2: Zoom on the grid 2

Meteorological fields are initialized and 6-hourly nudged by the ECMWF (European Center for Medium-Range Weather Forecasts) database. This nudging is done at the lateral limits of the coarse domain. Simulations start on June 20, 2001 at 0000 UTC and runs during 6 complete days. The soil vegetation model includes 30 classes issued from the USGS (United States Geophysical Survey) database with a 1 km resolution. A subgrid-scale scheme called "patch configuration" allows us to keep the 1 km information within our 3 km-mesh. The topography also has a 1 km resolution and is provided by USGS too. The sea surface temperature is obtained from satellite and from in-situ OOM (Observatoire d'Océanographie de Marseille) data.

2.2. Emissions databases

As shown by Taghavi *et al.* [2005], emissions play a critical role in air quality modelling. For the first grid we used the GENEMIS emission database for all anthropogenic species, and the GEIA database for biogenic ones. Theses inventories provide hourly and spatially averaged values. The 1° x 1° spatial resolution has been interpolated to our 3 kms x 3 kms grid. This method cannot provide a detailed view of the local emissions, but the first grid is just used as a driver for the grid two. So, the most important is to model background values, not local peaks. For grid two, the emission inventory has been made for different IOPs during ESCOMPTE campaign [François *et al.*, 2005]. The spatial resolution is 1 km × 1 km in the horizontal direction. The emissions data include hourly values of 170 species. All emissions factors of anthropogenic species are calculated from data of 1999. All the available local and regional characteristics for specific sources of the ESCOMPTE region are taken into account. All biogenic emissions factors have been updated with data of 2000, specifically for the ESCOMPTE region, and in some cases they have been corrected from in situ measurements.

For more information about the assessment methodology of both emission databases, one can refer to a detailed document in the ESCOMPTE database (http://medias-mip.fr/escompte /data/index). A comparison between the

ESCOMPTE, CITEPA (PRQA, 1994), and GENEMIS inventories is explained in detail in François *et al.* [2004] for anthropogenic emissions.

2.3. Deposition model

In the atmospheric boundary layer, chemical field concentrations are affected by lots of processes due to the presence of ground and vegetation. The main process is the deposition of pollutant with act as a sink. Two ways are distinguished for this deposition: dry deposition and wet deposition. In our simulations, dry deposition is based on the parameterization described by Wesely [1989]. This method is a three-resistance approach:

$$V_d = (r_a + r_b + r_c)^{-1}$$

where r_a is the aerodynamic resistance, mainly controlled by atmospheric turbulence; r_b is the bulk resistance, representing the transport in the fluid sub layer near the plant surface; and r_c is the canopy resistance. The resulting chemical resistance is a function of the considered pollutant (14 in our model), land-use, surface condition (dew or rain or not), and season [Wesely Hicks, 2000].

2.4. Meteorological conditions of the 22 and 25 June 2001

The 3D redistribution of pollutants is very dependant on the typical meteorological conditions on the ESCOMPTE domain. The dynamics over this domain are driven by north wind which is channelled by the Rhone valley, but also by the topography on the west of the domain (Alps Mountains). We also have lots of sea breezes conditions. In order to compare accurately our chemical results, we should study different dynamical situations. We focus on two special days: the 22 June and the 25 June, because theses days are well documented, and also because they represent typical dynamical conditions observed in this region. For 2d map, we show values at 18:00 UTC because at this hour, dynamical phenomena are well developed and the peak of photolysis has been produced about 13:00 UTC – 14:00 UTC. So at this hour, the impact of all photochemical processes is weaker and the chemical fields obtained represent the result of all of these processes.

June 22 is a typical summer Mistral condition. We have on the northeast of the domain the Mistral wind, and a weak see-breeze along the coast. The two flows combine themselves to form a moderate speed wind blowing parallel to the littoral.

On June 25, there is no more Mistral wind, but a highly developed sea-breeze, intensified by a southwest flow. Wind enters far inland.

Figures 3 and 4 show wind simulated (black arrow) and measured (red arrows) for respectively the 22 June (**fig. 3**) and the 25 June (**fig. 4**) at 18:00 UTC at ground level.

Detailed comparisons between the observed and modelled values for temperature, humidity and wind are shown in Taghavi [2003].

3. Chemical mechanisms used

The aim of this study was to use different chemistry schemes with the same modelling of meteorological conditions and to compare the results of simulations to observations. But generally, changing the chemistry scheme requires heavy changes in the program code. To avoid this problem, an interpreter, SPACK, was coupled on-line. It allows us using any gas phase chemistry scheme without any changes in the code. Mechanism is read one time during model initialization, and production/destruction expressions for all species are constructed and kept into memory. This coupling has been validated by the inter-comparison protocol proposed by Kuhn *et al.* [1998] and Poppe *et al.* [1996]. Our results have been compared to the results obtained by Kuhn and are in very good agreements.

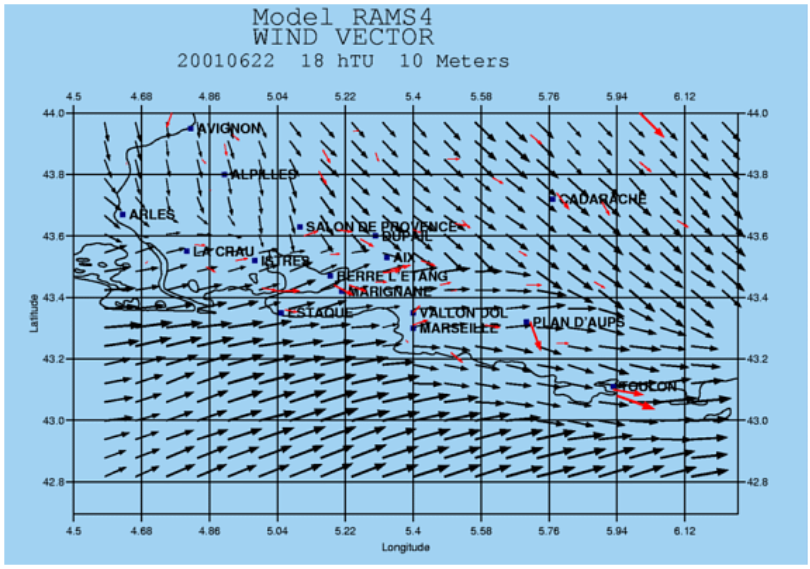

Figure 3: Wind of the 22 June 2001 at 18:00 UTC

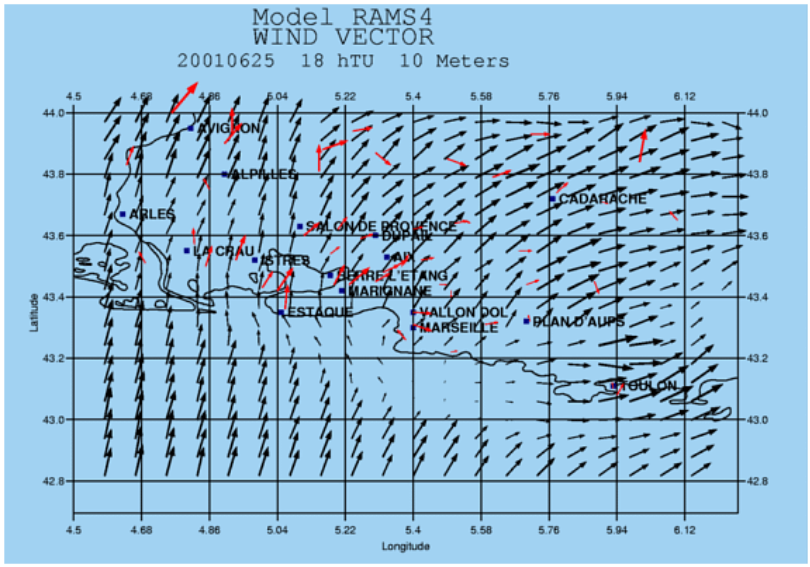

Figure 4: Wind of the 22 June 2001 at 18:00 UTC

3.1. MOCA condensed

We used first a condensed version of the MOCA2.2 scheme ([Aumont *et al.*, 1996]; [Taghavi *et al.*, 2005]). This mechanism takes 12 stable inorganic species, 5 inorganic intermediates, 10 stable organic species, and 2 organic intermediates into account, including isoprene, propene, ethene, and ethane, and is based upon a set of 65 chemical reactions (including 11 photolytic reactions). It accounts for the main processes driving the ozone concentration in a polluted zone. The hydroperoxyl / aldehyde conversion describes the degradation of the various organic compounds from anthropogenic emissions. The three main pathways of isoprene oxidation (strongly emitted by the Mediterranean vegetation) are taken into account. This chemical module calculates PAN concentration, which allows a realistic representation of NO_y transport. Lastly, the model includes NO_3/N_2O_5 equilibrium for night chemistry. Figure 5 gives us a schematic representation of this scheme.

3.2. RACM (Regional Atmospheric Chemistry Mechanism)

Secondly, we used the RACM scheme [Stockwell *et al.*, 1997]. This model is a completely revised version of the RADM1 (Regional Acid Deposition Model) [Stockwell *et al.*, 1986] and RADM2 [Stockwell *et al.*, 1990] models, developed in order to incorporate new data. The mechanism includes 17 stable inorganic species, 4 inorganic intermediates, 32 stable organic species and 24 organic intermediates for a total of 237 reactions (including 23 photolytic reactions). Hundreds of VOCs (Volatile Organic Compounds) are grouped into 16 anthropogenic and 3 biogenic model species. This grouping is principally based on the reactivity of the VOC toward HO. Alteration of alkanes and alkenes

and also well represented. This mechanism is of course more realistic than MOCA, but it requires more informatic resources.

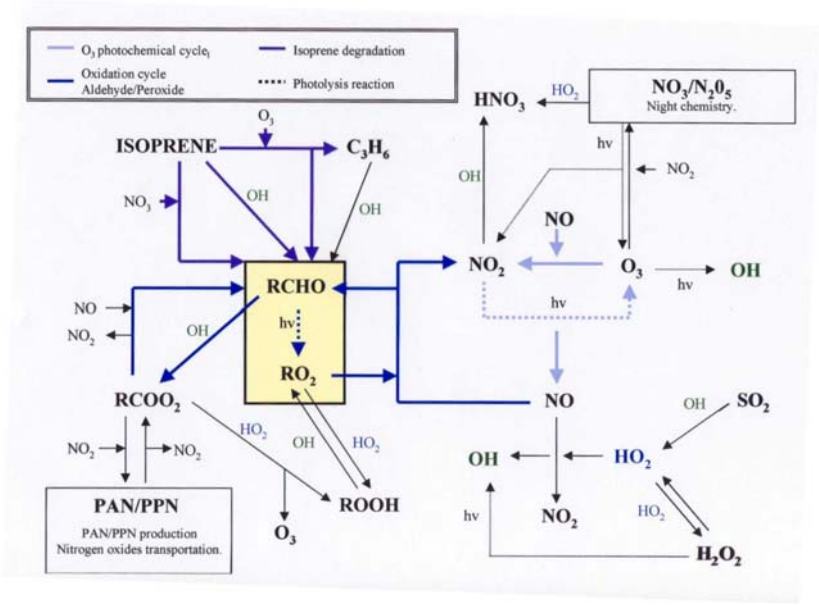

Figure 5: schema of the MOCA condensed mechanism

3.3. Other chemical related parameterizations

The chemical time resolution is one second for both grids. At each time step and each mesh, chemical rates are evaluated from the temperature, pressure and humidity calculated in the RAMS model. Photolysis rates have been calculated by the TUV (Tropospheric Ultraviolet and Visible radiation) model offline [Madronich Flocke, 1987] which takes solar incident radiation and molecular properties of atmospheric gases into account and tabulated. These rates are updated every five minutes. Actinic fluxes are estimated by the d-Eddington approximation ([Joseph *et al.*, 1976]; [Wiscombe, 1997]). For the MOCA mechanism, three photolysis reactions, not integrated in the Madronich's program, have been added in this model with the calculation of new quantum yield and absorption efficiency [Aumont *et al.*, 1996]. For RACM, we added 15 reactions (cross sections and quantum yields from Stockwell *et al.*, [1997].
The chemical solver is the QSSA (Quasi Steady State Approximation), [Hesstvedt *et al.*, 1978], which is faster than a matrix solver like the Gear solver [Gear, 1971] but is nevertheless quite accurate ([Shieh *et al.*, 1988]; [Dabdud *et al.*, 1995]; [Saylor Ford, 1995]).

4. Results and discussion

4.1. SO2

SO_2 is a key compound in atmospheric pollution because this specie is only emitted by fire and human activities. It is also a stable species, and his chemistry in gas-phase is very simple. Sulfur dioxide is only degraded into sulfuric acid. So, obviously, the 2 mechanisms (RAMS4 = MOCA-condensed; RAMS5 = RACM) give almost same results, concentration fields are principally directed by emissions. This specie is used as validation of our simulations, to be sure that both mechanisms work well.
For both days, and both models, we can clearly see the impact of all the industrial emissions around the Berre pond and the Fos-Berre bay. Depending on the wind direction, SO_2 peaks are located along the littoral, and impact the city of Marseilles (**fig. 6 and 7**), or transported inland, polluting rural areas like La Crau or Salon de Provence (**fig. 8 and 9**). Fields pattern are of course almost the same for the both mechanisms.
If we look daily evolution of the sulfur dioxide concentration for the 25 June (**fig. 10**), we can see that both mechanisms give same results. Even if we correctly reproduce daily variation of SO_2 concentration, we observe overestimation SO_2 values during the night, and an underestimation during the day. Different reasons can explain theses results. The first is the very long lifetime of SO_2. So measurement can be affected by very long-range transported SO_2 (this compound may easily travel over distances of much more than 300 km), which cannot be taken into account with meso-scale modeling. The second is a negative bias in the emission database. At last, a large part of measured SO_2 is due to aerosols, which are not taken into account in our simulations.

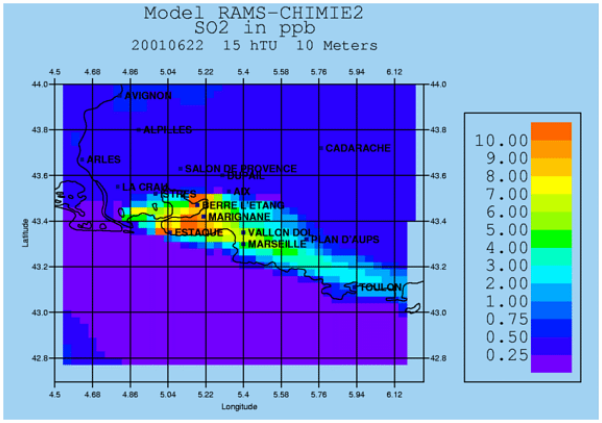

Figure 6 : SO_2 map for MOCA (22 June 2001 at 15 UTC)

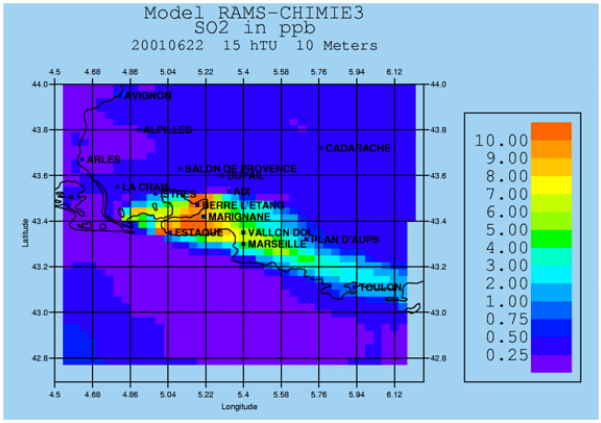

Figure 7 : SO_2 map for RACM (22 June 2001 at 15 UTC)

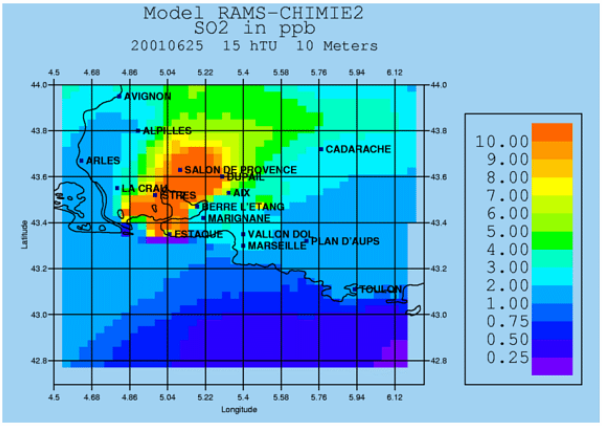

Figure 8 : SO_2 map for MOCA (25 June 2001 at 15 UTC)

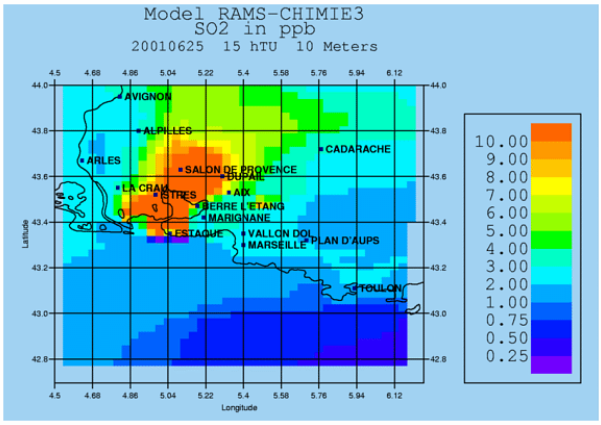

Figure 9 : SO_2 map for RACM (25 June 2001 at 15 UTC)

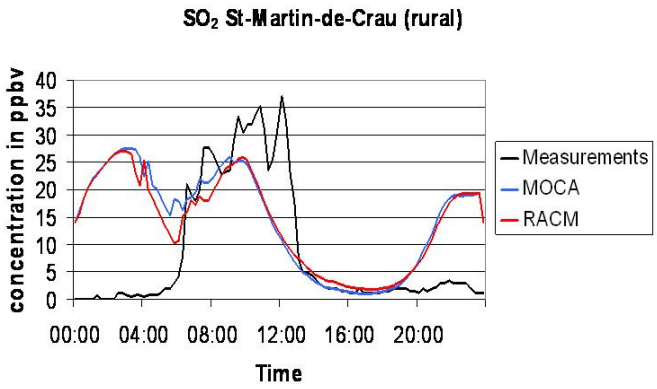

Figure 10 : Time evolution of SO_2 concentration

4.2. NOx

Atmospheric concentration of NO_x is one of the main drivers (with VOCs) of the ozone production. So a good simulation of NO_x field is important. Even if the main pathways of NO_x production are the same in the two mechanisms (i.e. photodissociation), there are some differences, especially in the treatment of organic nitrogen and the reactions with NO_3 and VOCs oxidation. As shown by Jimenez *et al.* [2003] with 0D model, predicted values for NO_x concentrations for both MOCA and RACM mechanisms are almost identical. The same characteristics are found with meso-scale modeling.

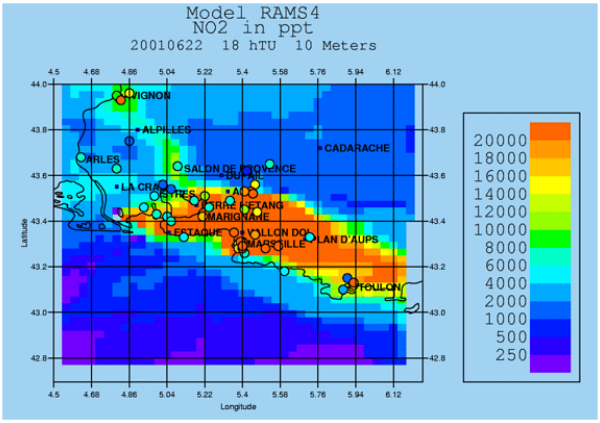

Figure 11 : NO_2 map for MOCA (22 June 2001 at 18UTC)

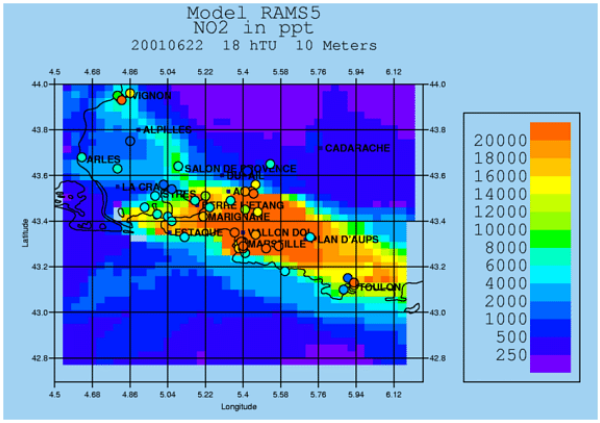

Figure 12 : NO_2 map for RACM (22 June 2001 at 18 UTC)

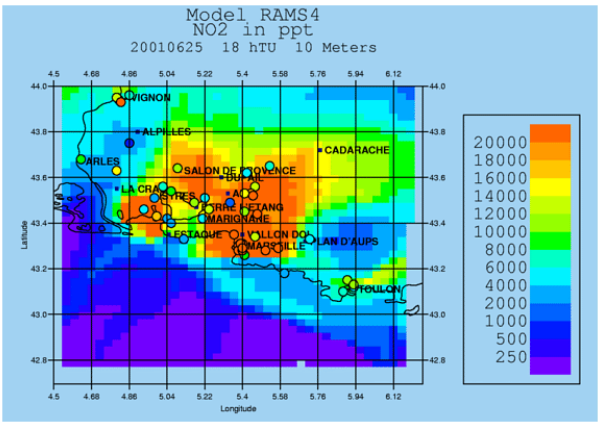

Figure 13 : NO_2 map for MOCA (25 June 2001 at 18 UTC)

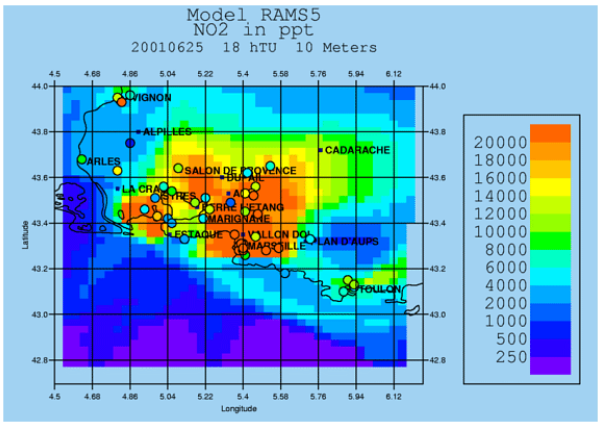

Figure 14 : NO_2 map for RACM (25 June 2001 at 18 UTC)

For the figures 11, 12, 13, and 14, the colour spots at each station represent the measurement in this place.

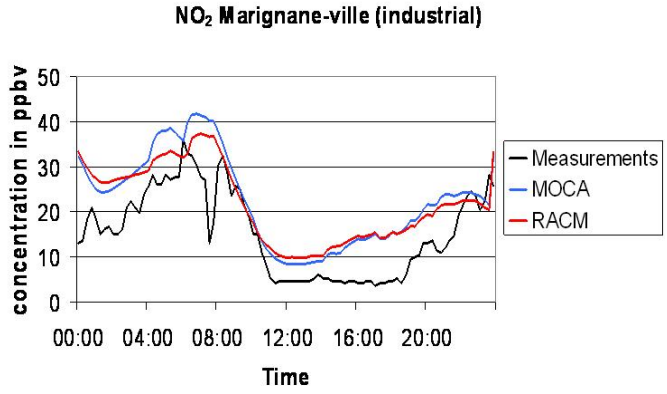

Figure 15 : Time evolution of NO_2 concentration

Concerning NO_2, results for both mechanisms are in good agreements with measurements (the colored point onto the maps), but the spatial variability of the measurement cannot be reproduced by our setup resolution (3x3 km) (**fig. 11 to 14**). For both meteorological conditions, values around the Berre pond and the city of Marseilles are almost the same. We can suppose that these areas are essentially directed by emissions. It is not the case for cities like Toulon or Arles. We see that for these stations, the results for both mechanisms are close together and in good agreement with measurement too. We can just focus the little bit higher NO_2 background concentration for MOCA-condensed, especially the 22 June. Time evolution (**fig. 15**) shows that simulations done with the two mechanisms are also close together all along the day. So we see that differences between the MOCA-condensed and RACM mechanisms are negligible.

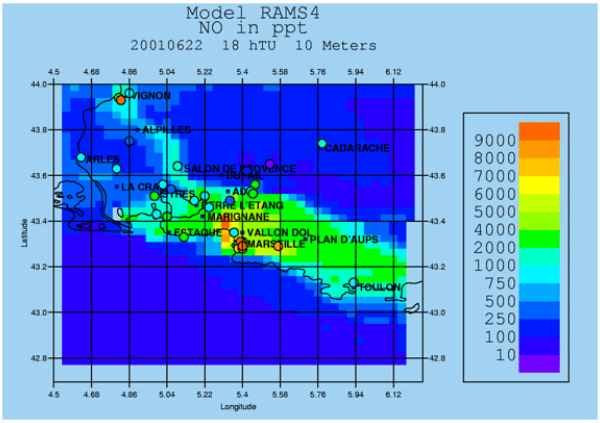

Figure 16 : NO map for MOCA (22 June 2001 at 18 UTC)

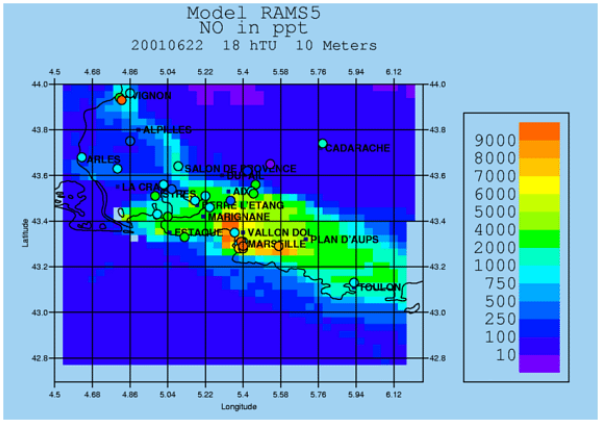

Figure 17 : NO map for RACM (22 June 2001 at 18 UTC)

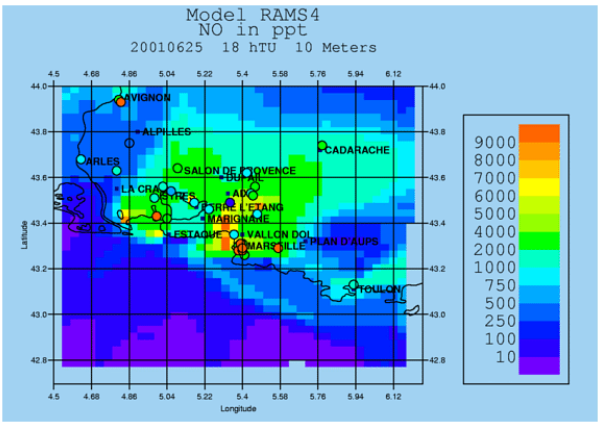

Figure 18 : NO map for MOCA (25 June 2001 at 18 UTC)

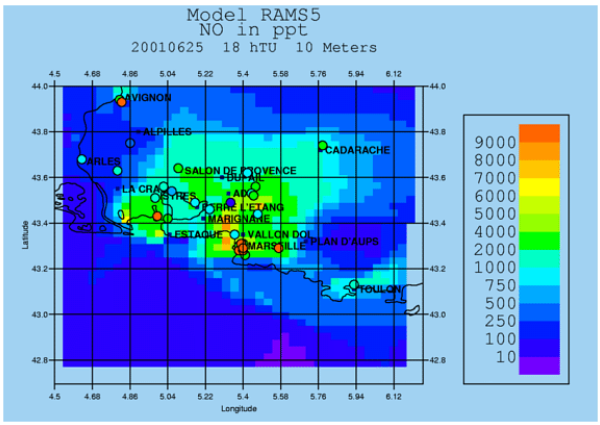

Figure 19 : NO map for RACM (25 June 2001 at 18 UTC)

For the figures 16, 17, 18, and 19, the colour spots at each station represent the measurement in this place.

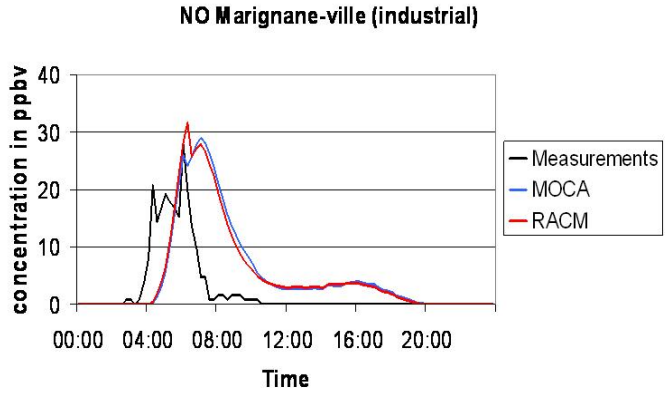

Figure 20 : Time evolution of NO concentration

The same conclusion can be formulated for NO fields. It's very interesting to see that a condensed mechanism like MOCA, with his much reduced set of reactions, can well simulate such short-life species, even in areas not directly directed by emissions (**fig. 16 to 19**). The same tendency to have higher background values for MOCA-condensed is visible. Time evolution shows a little shift for the NO peak, maybe due to our meteorology, or a shift in the emission database

4.3. Ozone

Ozone is the main atmospheric pollutant. For both mechanisms, and both days, modeled values are in good agreement with the measurements (**fig. 21 to 24**). But, some differences appear. For the 22 June, MOCA seems to reproduce better the ozone values near 70 ppb around the Berre-pond and all the high emissions areas, but over-estimated rural values of about 10 ppb. RACM, well simulates these values, but underestimates, some largely, values near the Berre-pond.

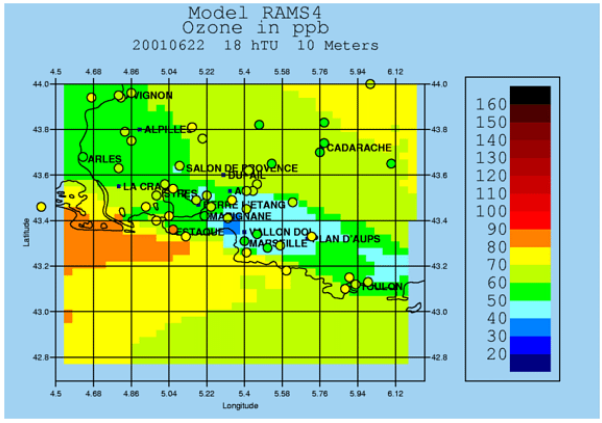

Figure 21 : O_3 map for MOCA (22 June 2001 at 18 UTC)

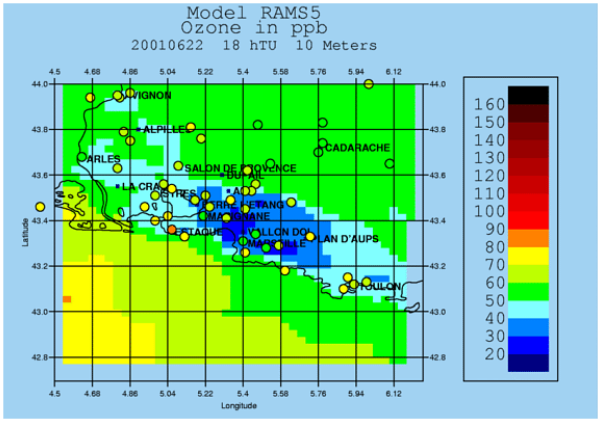

Figure 22 : O_3 map for RACM (22 June 2001 at 18 UTC)

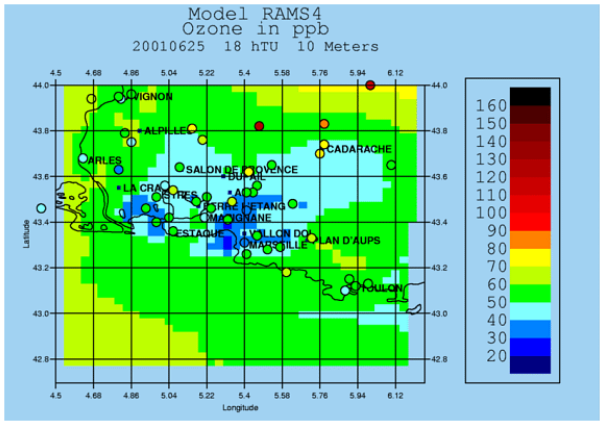

Figure 23 : O_3 map for MOCA (25 June 2001 at 18 UTC)

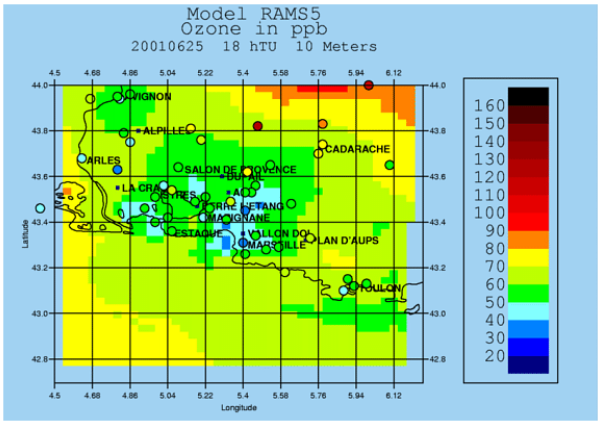

Figure 24 : O_3 map for RACM (25 June 2001 at 18 UTC)

For the figures 21, 22, 23, and 24, the colour spots at each station represent the measurement in this place.

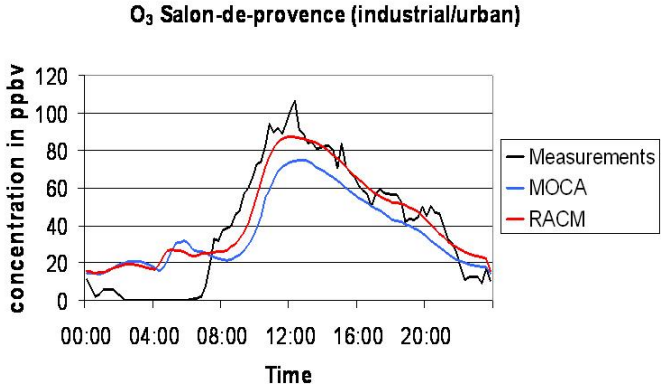

Figure 5 : Time evolution of O_3 concentration

It's the inverse for the 25 June. MOCA mechanism underestimates ozone values, predicting concentration of about 10 ppb less than measurements. RACM values are very good, except near the city of Arles. The high ozone values measured in the northeast are underestimated by both mechanisms. But it's not a chemical problem. In fact, the peak is well simulated, with the good values, but it is located some kilometers northeastern, probably due to our meteorology. Sea-breeze is too strong. Daily variations of ozone are also well simulated (**fig. 25**). Furthermore, we can see some difficulties to reproduce very low values during the night. We also remark the differences between the both mechanisms during the day, with more than 10 ppb between MOCA and RACM.

4.4. Peroxydes

All peroxides, and especially hydrogen peroxide (H_2O_2) and hydroperoxide radical (HO_2) are the main drivers of the oxidizing capacity of the atmosphere. Theses photochemical products serve as precursors of odd-oxygen, and indicate how the mechanism is able to degrade VOCs and produce secondary pollutants as ozone. For 22 June and 25 June (**fig. 26 to 29**), RACM produces more peroxides over the land, and less over the sea. So we can suspect biogenic VOCs as responsible. But time series (**fig. 30**) show that MOCA produces higher daily variations in the RO_2 concentration than RACM. Unfortunately, there is no measurement to know the good mechanism for peroxides.

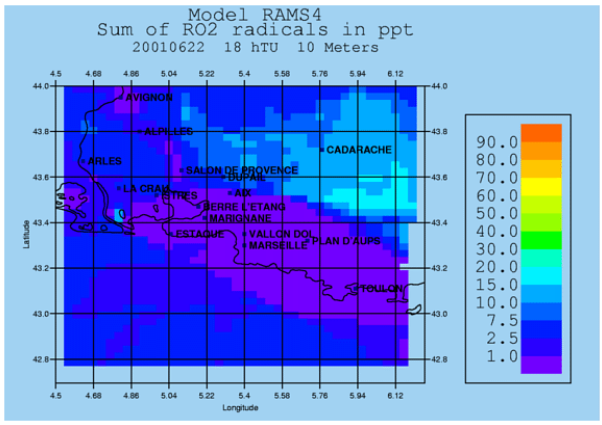

Figure 26 : RO_2 map for MOCA (22 June 2001, at 18 UTC)

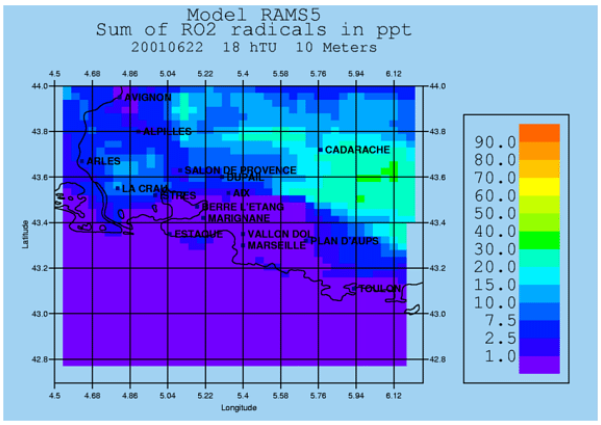

Figure 27 : RO_2 map for RACM (22 June 2001, at 18 UTC)

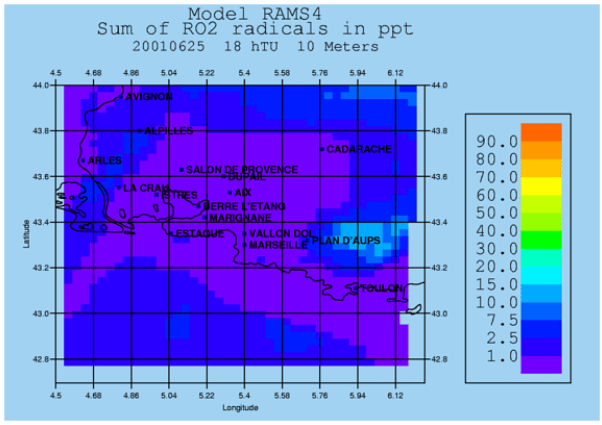

Figure 28 : RO_2 map for MOCA (25 June 2001, at 18 UTC)

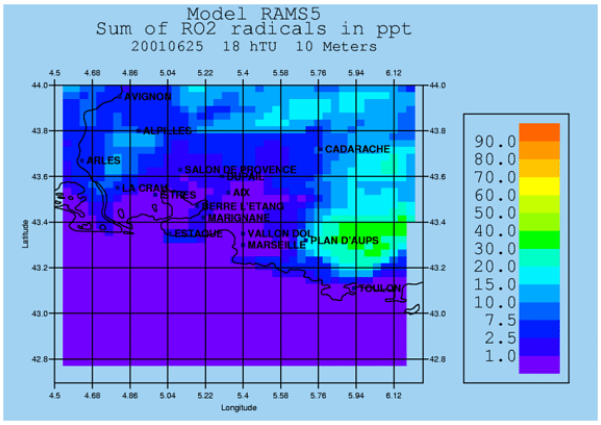

Figure 29 : RO_2 map for RACM (25 June 2001, at 18 UTC)

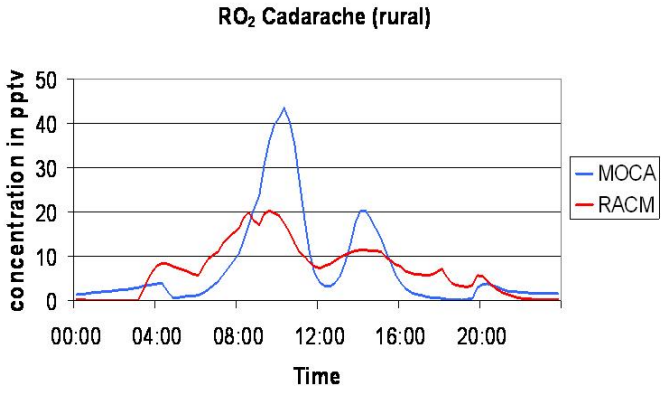

Figure 30 : Time evolution of RO_2 concentration

4.5. NOy

NO_y regroup all nitrogen compounds except NO_x. We can see higher concentrations for MOCA than for RACM, especially the 22 June 2005 (**fig. 31 to 32**). Background values for MOCA are about 5 times higher. This difference

shows the different treatment of NO_3 in the two mechanisms. In RACM, a huge part of the NO3 reacts with organic peroxy radical, whereas in MOCA, we have an accumulation of this specie in the atmosphere during daytime. This impact is less significant during the 25 June 2005 (**fig. 33 to 34**) because organics peroxy radicals are mainly due to the oxidizing of biogenic VOCs, not emitted by sea.

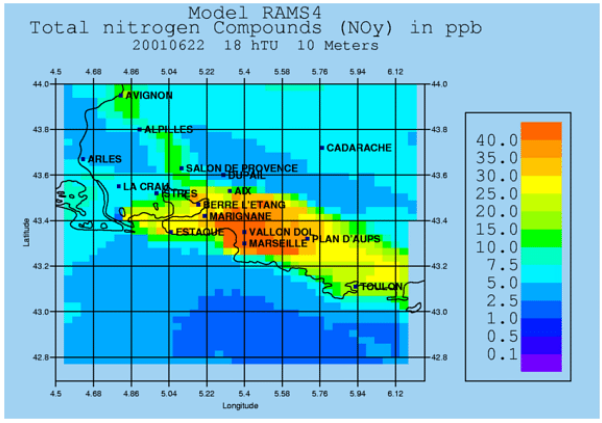

Figure 31 : NO_y map for MOCA (22 June 2001 at 18 UTC)

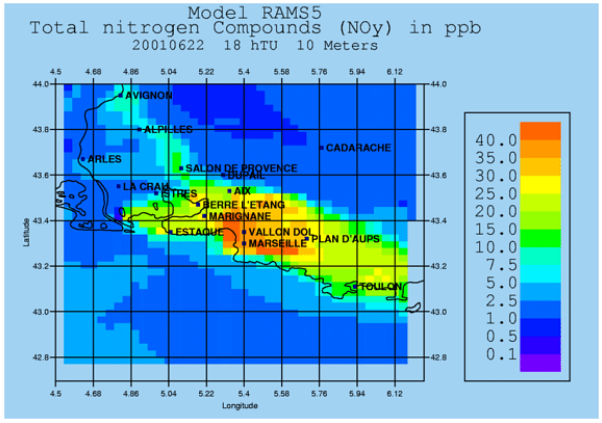

Figure 32 : NO_y map for RACM (22 June 2001 at 18 UTC)

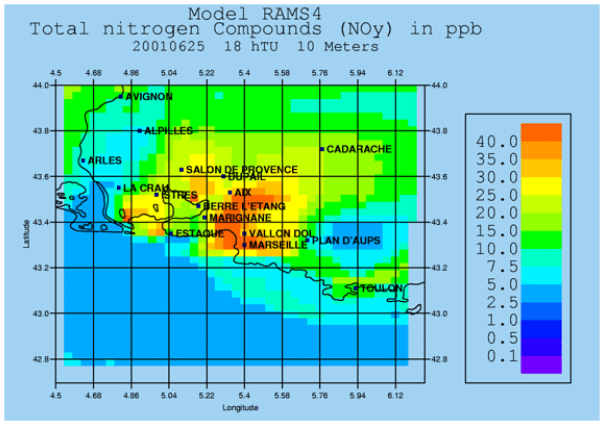

Figure 33 : NO_y map for MOCA (25 June 2001 at 18 UTC)

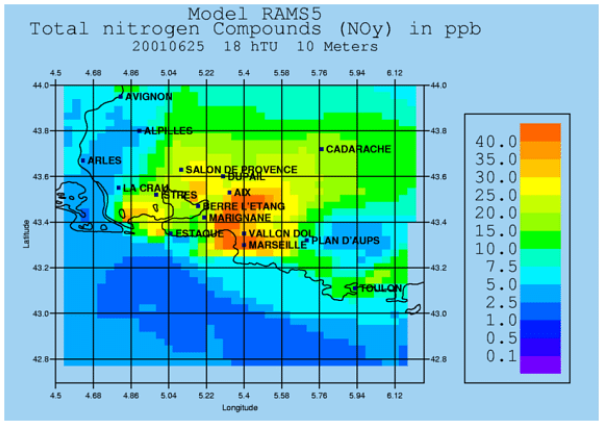

Figure 34 : NO_y map for RACM (25 June 2001 at 18 UTC)

So this day, concentrations of NO_y are more dependent of anthopogenic emissions along the Berre-pond which are transported by the sea breeze. However, the concentration pattern for both mechanisms is the same, with values ranging from 1 to 7 ppb in rural areas and from 10 to 40 ppb in high emissions areas.

4.6. VOCs

The main difference between our two models concerns VOCs. MOCA includes a very limited development in the treatment of VOCs, especially for the biogenic ones. Only 10 VOCs are considered, as RACM uses more than 30 organic compounds. As expected, results for the two mechanisms are totally different. For Total Anthropogenic Hydrocarbons (TAH) (**fig. 35 to 38**), RACM produces values 3 to 6 times higher than MOCA, especially around the Fos-Berre petrochemical installations. Unfortunately, there are no usable measurements to validate these results, but viewing the local installations (high oil refinery), it seems that values simulated by RACM (up to 15 ppb) are more in agreement with reality and values commonly measured than MOCA's ones (only 3-5 ppb). Figure 39 confirm the higher values for TAH given by RACM than these given by MOCA all along the day.

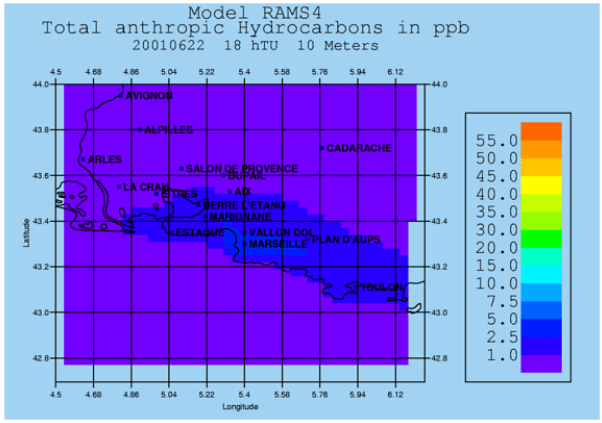

Figure 35 : TAH map for MOCA (22 June 2001 at 18 UTC)

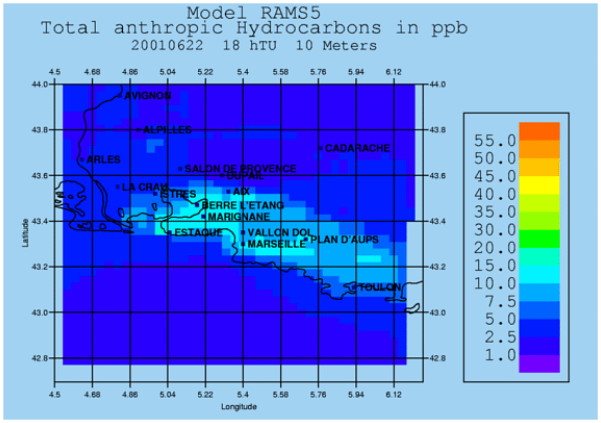

Figure 36 : TAH map for RACM (22 June 2001 at 18 UTC)

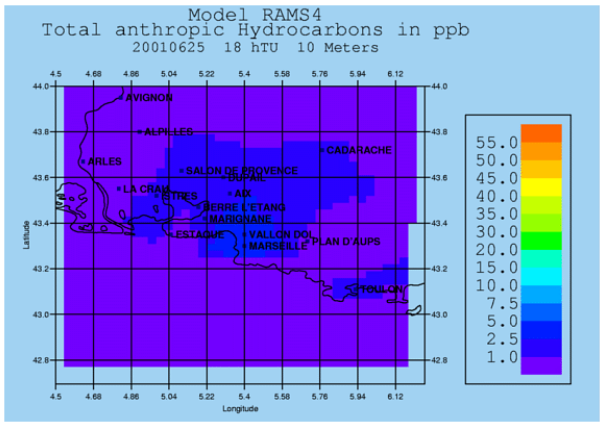

Figure 37 : TAH map for MOCA (25 June 2001 at 18 UTC)

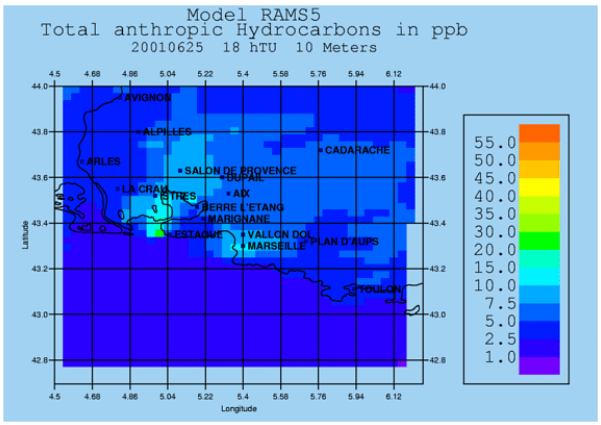

Figure 38 : TAH map for RACM (25 June 2001 at 18 UTC)

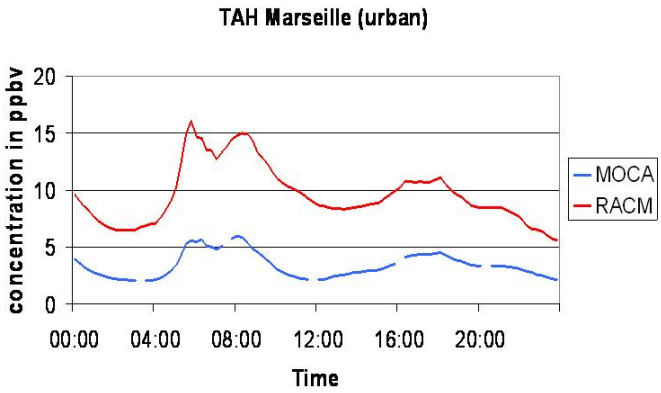

Figure 39 : Time evolution of TAH concentration

For Total Biogenic Hydrocarbons (TBH), results are quite different. In the MOCA mechanism, only isoprene is considered, and in the ESCOMPTE domain there are high emissions of this species. RACM considers isoprene, but also all terpenes. However, the higher values for total biogenic carbon are predicted by MOCA (**fig. 40 to 43**). In MOCA, isoprene is emitted, but cannot be degraded rapidly, so we have accumulation in the atmosphere. RACM, because of his high concentrations of peroxides, can rapidly degrade biogenic VOCs onto high reactive fragments. However, we note values predicted by both mechanisms are close, with only up to 2.5 ppb of difference. Figure 44 confirm the higher values for TBH given by RACM than these given by MOCA all along the day.

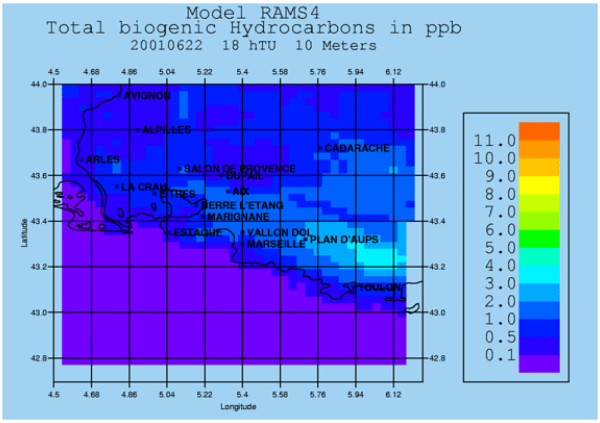

Figure 40 : TBH map for MOCA (22 June 2001 at 18 UTC)

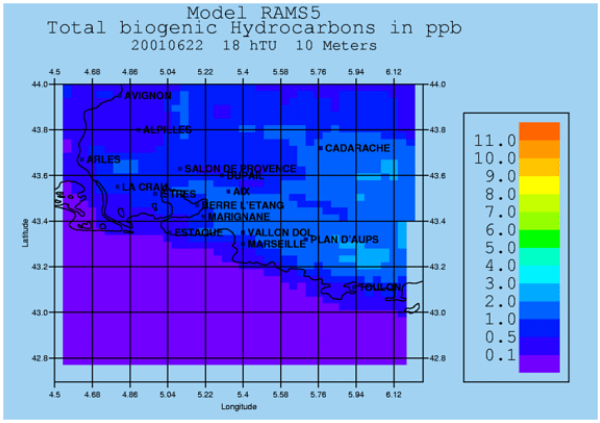

Figure 41 : TBH map for RACM (22 June 2001 at 18 UTC)

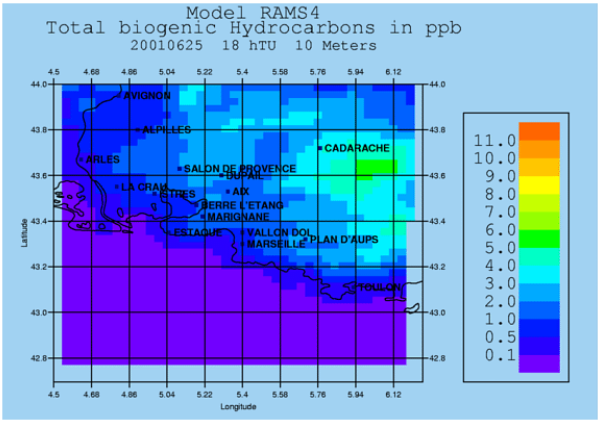

Figure 42 : TBH map for MOCA (25 June 2001 at 18 UTC)

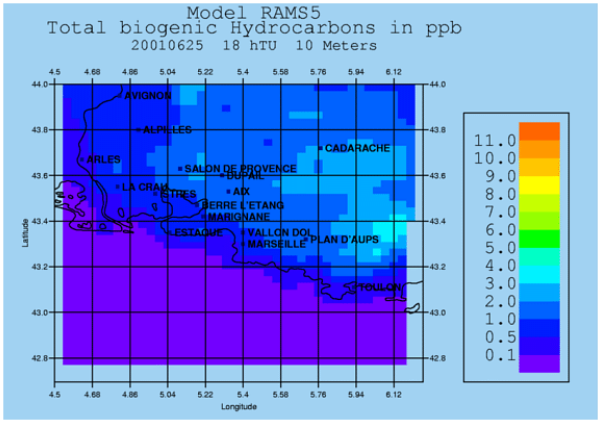

Figure 43 : TBH map for RACM (25 June 2001 at 18 UTC)

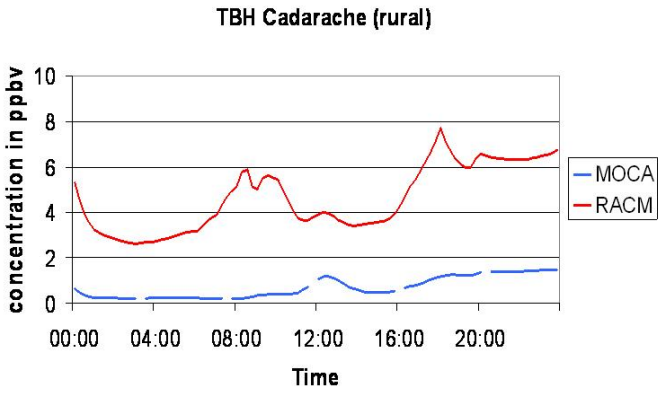

Figure 44 : Time evolution of TBH concentration

5. Conclusion

The aim of this study was to compare two chemical mechanisms coupled online with the same meso-scale model, with the same parameterizations for photolysis rates and deposition , in order to determine if a detailed mechanism (RACM) is better than a reduced one (MOCA) for air quality prediction. The results of the two mechanisms were compared to measurements, to validate the simulations. It appears that results given by the reduced and detailed mechanisms are almost the same for all the main atmospheric pollutants, as in spatial distribution as in temporal evolution. The differences between both mechanisms are only visible for VOCs because these compounds are the heart of RACM mechanism. For air quality modeling, a reduced mechanism is satisfactory, and has the advantage to be fast for using.

Detailed mechanisms should be reserved for special predictions, for example prediction of concentration of compound highly volatile or for particular studies.

ACKNOWLEDGMENTS

This modelling study is supported by funding of the French Centre National de la Recherche Scientifique (Programme National de Chimie Atmosphérique). This work makes use of the RAMS model, which was developed under the support of the National Science Foundation (NSF) and the Army Research Office (ARO). Computer resources were provided by CINES (Centre Informatique National de l'Enseignement Supérieur) project amp2107. The authors also wish to thank the computer team of the laboratoire de Météorologie Physique de l'Université Blaise Pascal (France); A.M. Lanquette, F. Besserve and Ph. Cacault.

REFERENCES

[Aumont *et al*., 1996] Aumont B.,A. Jaeker-Voirol, M. Martin and G. Toupance, Tests of some reduction hypotheses made in photochemical mechanisms. *Atmos. Environ.*, **30**, 2061-2077, 1996.

[Cautenet *et al.*, 1999] Cautenet S., D. Poulet, C. Delon, R. Delmas, J.M. Grégoire, J.M. Pereira, S. Cherchali, O. Amram and G. Flouzat, Simulation of carbon monoxide redistribution over Central Africa during biomass burning (Experiment for Regional Sources and Sinks of Oxidants (EXPRESSO)), *J. Geophys. Res*., **104**, 30641-30657, 1999.

[Cros *et al.*, 2004] Cros B., P. Durand, H. Cachier, Ph Drobinski, E. Frejafon, Ch. Kottmeier, P.E. Perros, J.L. Ponche, D. Robin, F. Saïd, G. Toupance and H. Wortham, The ESCOMPTE Program: an Overview, *Atmos. Res.*, **69**, 3-4, 241-279, 2004.

[Cotton *et al.*, 2003] Cotton W.R., R.A. Pielke Sr, R.L.Walko, G.E.Liston, C.J. Tremback, H. Jiang, R.L. McAnely, J.Y. Harrington, M.E. Nicholls, G.G. Carrio, and J.P. McFadden, Rams 2001: Current status and future directions, *Meteorol. Atmos. Phys.*, **82**, 5-29, 2003.

[Dabdud *et al.*, 1995] Dabdud, D. and J. H. Seinfeld, Extrapolation techniques used in the solution of stiff odes associated with chemical kinetics of air quality models, *Atmos. Environ.*, **29**, 403, 1995.

[Edy Cautenet, 1998] Edy, J. and S. Cautenet, Biomass burning: local and regional redistribution, *Air Pollution Modeling and its application.* 63- 69.Plenum Press, New-York, 1998.

[François *et al*., 2005] François S., S. Fayet,E. Grondin and J.L. Ponche, The Air Quality Oriented Atmospheric Emission Inventories of the ESCOMPTE Program: Methodology and Results., *Atmos. Res.*, 2005.

[Gear, 1971] Gear, C. W., The automatic integration of ordinary differential equations, *ACM Comm*., **14**, 176, 1971.

[Gross *et al*, 2003] Gross A. and Stockwell W.R., Comparison of the EMEP, RADM2 and RACM Mechanisms, *J. Atmos. Chem.*, **44**, 151-170, 2003

[Hesstvedt *et al.*, 1978] Hesstvedt E., Hov Ø. and Isaksen I.S.A., Quasi-steady-state approximation in air pollution modeling: Comparison of two numerical schemes for oxidant prediction, *Int. J. Chem. Kinetics*, **10**, 971-994, 1978

[Jenkin *et al*, 1997] Jenkin M.E., Saunders S.M. and Pilling M.J., The tropospheric degradation of volatile organic compounds: A protocol for mechanism development, *Atmos. Environ.*, **31**, 81-104, 1997.

[Jimenez *et al*, 2003] Jimenez P., Baldasano J.M. and Dabdub D., Comparison of photochemical mechanisms for air quality modelling, *Atmos. Environ.*, **37**, 4179-4194, 2003

[Joseph *et al.*, 1976] Joseph, J. H., Wiscombe, W. J., and Weinman, J. A., The delta-eddington approximation for radiative flux transfer, *J. Atmos. Sci*., **33**, 2452–2459, 1976.

[Kuhn *et al*, 1998] Kuhn M., Builtjes P.J.H., Poppe D., Simpson D., Stockwell W.R., Andersson-Sköld Y., Baart A., Das M., Fiedler F., Hov Ø., Kirchner F., Makar P.A., Milford J.B., Roemer M.G.M., Ruhnke R., Strand A., Vogel B. and Vogel H., Intercomparison of the gas-phase chemistry in several chemistry and transport models, *Atmos. Environ.*, **32**, 693-709, 1998

[Lyons *et al.*, 1995] Lyons, A.W., C. J. Tremback and R. A. Pielke, Applications of the regional atmospheric systems (RAMS) to provide input to photochemical grid models for the lake Michigan ozone study (LMOS), *J. Appl. Meteor.*, **34**, 1762 – 1785, 1995.

[Madronich Flocke, 1987] Madronich S., Photodissociation in the atmosphere. 1. Actinic flux and the effects of ground reflections and clouds, *J. Geophys. Res.*, **92**, 9740-9752, 1987.

[Millan *et al.*, 1997] Millan, M.M., R. Salvador, E. Mantilla and G. Kallos, Photooxidant dynamics in the smtag307 Mediterranean basin in summer: Results from European research projects, *J. Geophys. Res.*,**102**, 8811 – 8823, 1997.

[Müller *et al*, 1995] Müller J.F. and Brasseur G., IMAGE: A three-dimensionnal chemical transport model of the global troposphere, *J. Geophys. Res.*, **100**, 16445-16490, 1995

[Poppe *et al.*, 1996] Poppe D., Andersson-Sköld Y., Baart A., Builtjes P.J.H., Das M., Fiedler F., Hov Ø., Kirchner F., Kuhn M., Makar P.A., Milford J.B., Roemer M.G.M., Ruhnke R., Simpson D., Stockwell W.R., Strand A., Vogel B. and Vogel H., Gas-phase reactions in atmospheric chemistry and transport models: A model intercomparison, EUROTRAC Special Publication, International Scientific Secretariat, Garmisch-Partenkrichen, 1996.

[Poulet *et al.*, 2004] Poulet D, S. Cautenet and B. Aumont, Simulation of the chemical impact of the bush fires emissions, in Central Africa, during the EXPRESSO campaign *In revision to J. Geophys. Res.*, 2004.

[Saylor Ford, 1995] Saylor, R. D. and G. D. Ford, On the comparison of numerical methods for the integration of kinetic equations in atmospheric chemistry and transport model, *Atmos. Environ.*, **29**, 2585, 1995.

[Shieh *et al.*, 1988] Shieh D. S.-S., Y. Chang and Carmichael G. R., The evaluation of numerical techniques for solution of stiff ordinary differential equations arising from chemical kinetic problems, *Env. Software*, **3**, 28-38, 1988.

[Simpson *et al*, 1997] Simpson D., Olendrzynski K., Semb A., Støren E. and Unger S., Photochemical Oxidant Modelling in Europe : Multi-annual Modelling and Source-receptor Relationships, *EMEP MSC-W Report 3/97*, Norwegian Meteorological Institute, Oslo, Norway, 1997.

[Stockwell *et al.*, 1986] Stockwell W.R., A homogeneous gas phase mechanism for use in a regional acid deposition model, *Atmos. Environ.*, **20**, 1615-1632, 1986

[Stockwell *et al*, 1997] Stockwell W.R., Kirchner F. and Kuhn M., A new mechanism for regional chemistry modeling, *J. Geophys. Res.*, **102**, 25847-25879, 1997.

[Stockwell *et al.*, 1990] Stockwell W.R., Middleton P., Chang J.S. and Tang X., The second generation regional Acid Deposition Model chemical mechanism for regional air quality modelin, *J. Geophys. Res.*, **95**, 16343-16367, 1990

[Taghavi *et al.*, 2004] Taghavi M, S. Cautenet and G.Foret, Simulation of ozone production in a complex circulation region with nested grids, *Atmos. Chem. Phys.*, **4**, 825-838, 2004.

[Taghavi *et al.*, 2005] Taghavi M., S. Cautenet and J.Arteta, Impact of an high resolution emission inventory on modeling accuracy, *Atmos. Res*. (Special issue ESCOMPTE), **74**, 65-88, 2005.

[Taghavi, 2003] Taghavi M. Etude de la pollution en zone urbaine et péri-urbaine à l'aide d'une modélisation méso-échelle durant la campagne ESCOMPTE. Impact de la dynamique et des inventaires d'émission. Thèse de doctorat d'Université, n° 1454, Clermont II, Novembre 2003.

[Wesely, 1989] Wesely M.L., Parameterization of surface resistances to gaseous dry deposition in regional-scale numerical models, *Atmos. Environ.*, **23**, 1293-1304, 1989

[Wesely Hicks, 2000] Wesely M.L. and Hicks B.B., A review of the current status of knowledge on dry deposition, *Atmos. Environ.*, **34**, 2261-2282, 2000

[Wiscombe, 1997] Wiscombe, W. J., The delta - m method; Rapid yet accurate radiative flux calculations for strongly asymmetric phase functions, *J. Atmos. Sci.*, **34**, 1408, 1997.

Simulation of a severe ozone episode over Marseille metropolitan area in the frame of ESCOMPTE modelling exercise

Claudio Carnevale, Veronica Gabusi, Marialuisa Volta
DEA – University of Brescia
Via Branze, 38
25123 Brescia, Italy
+39 0303715 [449, 456, 460]
[carneval, gabusi, lvolta]@ing.unibs.it

ABSTRACT
Tropospheric ozone episodes are frequent in Mediterranean area characterized by relevant biogenic and anthropogenic emissions and high solar radiation levers. In the Marseille metropolitan area, the ESCOMPTE experimental campaign and modelling exercise have been performed in order (1) to analyse the photochemical pollution production and transport processes and (2) to design air quality control policies. The paper presents the simulation results performed by the TCAM model for the episode 21-26 June 2001 (IOP2).

KEYWORDS
Photochemical modelling system, ESCOMPTE modelling exercise, ozone episode simulation.

1. Introduction

Severe ozone concentrations often occur over Mediterranean countries, due to complex non-linear chemical reactions activated by high solar radiation and favoured by stagnating meteorological conditions [Sillman 1999]. These characteristics make photochemical smog to be typically a summer phenomenon, mainly occurring in domains nearby large urban areas. Such a complex phenomenology requires adequate models for analysing and designing effective emission reduction strategies. Several air quality models have been described and applied at the urban and regional scales for seasonal and episode simulations [Russel Dennis 2000].

This work describes the simulation of the ozone episode 21-26 June 2001, monitored during ESCOMPTE experimental campaign [Cros *et al.* 2004], and performed by the TCAM photochemical model [Volta Finzi 2005], in the frame of the ESCOMPTE modelling exercise.

2. The modelling system

TCAM (Transport and Chemical Aerosol Model) is a multiphase, three-dimensional Eulerian grid model, in terrain-following co-ordinate system. The model formalizes the physical and chemical phenomena involved in the formation of secondary air pollution in heterogeneous phase. The pollutant evolution is computed solving, for each cell of the computational domain, the following mass-balance equation:

$$\frac{\partial C_i}{\partial t} = -v_x \frac{\partial C_i}{\partial x} - v_y \frac{\partial C_i}{\partial y} + K_{xx} \frac{\partial^2 C_i}{\partial x^2} + K_{yy} \frac{\partial^2 C_i}{\partial y^2} - v_z \frac{\partial C_i}{\partial z} + \frac{\partial}{\partial z}\left(K_{zz} \frac{\partial C_i}{\partial z} \right) + E(x,y,z,t) + \\ + D(x,y,z,t) + S(x,y,z,t) + R(x,y,z,t) + A(x,y,z,t) \quad \textbf{(1)}$$

where:

C_i is the concentration of i species;

v_x, v_y and v_z are the wind components;

D_i and S_i are the deposition and emission terms;

K_{xx}, K_{yy}, K_{zz} are the diffusion coefficient along the x, y and z direction;

R_i is the heteerogeneous chemical term;

A_i is the term taking into account the aerosol processes (condensation, nucleation, acqueous).

The chemical and physical phenomena occur simultaneously in atmosphere but solving Eq. 1 for each domain cell would be too time and memory expensive [Bastrup-Birk *et al.* 1996].

To solve the equation system 1, TCAM implements a split operator technique allowing to separately treat the horizontal transport, the vertical phenomena (including transport-diffusion, emissions and deposition) and the chemistry (including the aerosol phase processes), using the relation:

$$C_i^{n+1} = A_{xy} A_z A_c A_c A_z A_{xy} \quad \textbf{(2)}$$

where C_i^n is the concentration of species i at time step n, A_{xy}, A_z and A_c are the horizontal transport, the vertical transport and the chemistry operators respectively. This approach ensures second order accuracy in time [Marchuk 1975].

2.1. **Horizontal transport module**

The horizontal advection and diffusion module is based on a finite difference scheme using Chapeau Function [Pepper *et al.* 1979], coupled with a nonlinear Forester filter [Forester 1977]. This scheme, 4th order accurate in space, is computationally efficient allowing mass conservation and suppression of negative concentrations.

The module computes the lateral turbulent diffusivities on the basis of the Pasquill-Gifford stability classes [Pasquill 1974].

2.2. **Vertical transport module**

The use of a terrain following coordinate system implies that vertical wind component needs to be corrected to take into account the vertical mass transport due to horizontal components:

$$V_z = v_z - v_x \frac{\partial h_t}{\partial x} - v_y \frac{\partial h_t}{\partial y} \quad \textbf{(3)}$$

where V_z is the corrected wind velocity and h_t are the height of the terrain above sea level.

The turbulent diffusion generally dominates the vertical transport of the pollutants [Holstag Nieuwstadt 1986]. The computation of K_{zz} is performed taking into account the meteorological parameters: the Monin-Obukhov length, the mixing height, the friction velocity and the convective velocity [Holstag Nieuwstadt 1986], [Scire *et al.* 1990]. The choice of the integration scheme is performed on the basis of the value of the vertical turbulent diffusivity coefficient K_{zz}: for high values, a fully implicit scheme is used, otherwise (stable classes, usually during the night) an explicit Cranck-Nicholson scheme is performed [Wille 1994].

2.3. **Dry and Wet deposition**

Dry deposition is an important removal process, acting on all pollutant. It is characteristic of lower level of atmosphere and it is mostly related to roughness, composition and type, amount and physiological state of the vegetation, atmospheric parameters (stability, turbulence intensity) and pollutant properties. The phenomenon is described by the equation [Seinfeld Pandis 1997]:

$$F_i = C_i \cdot v_{di} \quad \textbf{(4)}$$

where F_i is the removed pollutant flux, C_i is the concentration of the i species near the terrain and v_{di} is the deposition velocity, computed on the basis of atmospheric turbulence, molecular brownian diffusion, terrain retain capability, and, for aerosol species, of gravitational settling.

Wet deposition (of both gas and aerosol species) is described by the equation [Environ Corp. 2003]:

$$F_i = C_i \cdot \Lambda \quad \textbf{(5)}$$

where Λ is the scavenging coefficient computed separately for gases and aerosols.

2.4. **Gas phase chemical module**

A full mathematical description of the atmospheric chemistry is not possible because of the complexity and the large amount of reactions involving primary and secondary compounds. Air quality models implement simplified atmospheric chemistry by means of condensed chemical mechanisms [Dodge 2000], defined using either a lumped molecule or a lumped structure approach [Gery *et al.* 1989]. In the first case, organic compounds are grouped taking into account similar chemical and kinetic characteristic, while in the lumped structure approach, they are split into smaller reaction elements based on the types of carbon bonds in each species. TCAM allows the simulation of gas chemistry using either the lumped molecule schemes SAPRC90, SAPRC97, COCOH97 or the lumped structure mechanism CBIV.

The inclusion of photochemical reactions into a grid-based model constitutes a severe numerical challenge as the resulting system is characterized by eigenvalues ranging over 10 order of magnitude. The algorithm implemented in TCAM to solve the differential equation system is the Implicit-Explicit Hybrid solver [Sun *et al.* 1994], that splits the species into fast and slow ones, according to the reaction velocity. The fast specie system is solved by means of the implicit Livermore Solver for Ordinary Differential Equations (LSODE) [Hindmarsch 1975], while the slow specie concentrations are computed by a Adams-Bashforth explicit scheme [Wille 1994].

2.5. **Aerosol module**

The aerosol module implemented in TCAM is coupled with the COCOH97 gas phase chemical mechanism [Wexler Seinfeld 1991]. It describes the most relevant aerosol processes: the condensation [Seinfeld Pandis 1997], the evaporation [Seinfeld Pandis 1997], the nucleation of H_2SO_4 [Jaecker-Voirol Mirabel 1989] and the aqueous oxidation of SO_2 [Seinfeld Pandis 1997]. The module describes particles size evolution by means of a fixed-moving approach. A generic particle is represented with an internal core containing the non volatile material, like elemental carbon, crustal and dust. The dimension of the core of each size class is established at the beginning of the simulation on the basis of a logarithmic distribution and it is held constant during the simulation. The volatile material is supposed to reside in an outer shell of the particle whose dimension is computed by the module at each time step processing the total mass and the total number of suspended particles. Both shell and core fractions are supposed to be internally mixed. The module describes the dynamics of 21 chemical compounds, 12 inorganic (H_2O, $SO_4^{=}$, NH_4^{+}, Cl^{-}, NO_3^{-}, Na^{+}, H^{+}, SO_2(aq), H_2O_2(aq), O_3(aq), elemental carbon and other) and 9 organic (a generic primary and 8 classes of secondary organic species) split in 10 size bins.

3. **Episode simulation**

3.1. **Computational domain**

The Marseille area (South-East France) is characterized by complex terrain and meteorology. Three regions can be identified: (1) the high densely populated area along the Mediterranean coast including the cities of Marseille and Toulon, (2) the Fos-Berre high industrial emission area in West of the domain, separated by Marseille zone by a rural area, and (3) the strong biogenic emission area in the NE of the domain (Figure 1). Such domain, often affected by severe photochemical pollution episodes during summer season, has been deeply investigated by means of the experimental campaigns and modelling studies performed in the frame of the ESCOMPTE project [Cros *et al.* 2004].

3.2. **Episode selection**

The ESCOMPTE campaign has monitored four Intensive Observing Periods (IOPs). The period 21-26 June 2001 (IOP2) has been selected to be simulated with TCAM model, as it represents two typical meteo-chemical conditions. Analysing meteorological and chemical parameters, such period can be split in two sub periods, namely IOP2a (21-23 June) and IOP2b (24-26 June) [Cros *et al.* 2004]. The former is characterized by the conclusion of a Mistral episode, with a moderate wind blowing from NW to East and critical ozone levels over SE part of the domain. During the latter, the circulation is mainly due to local breezes (mountain - sea), and the ozone concentrations reach high values in suburban areas and in the valleys at North of Marseille.

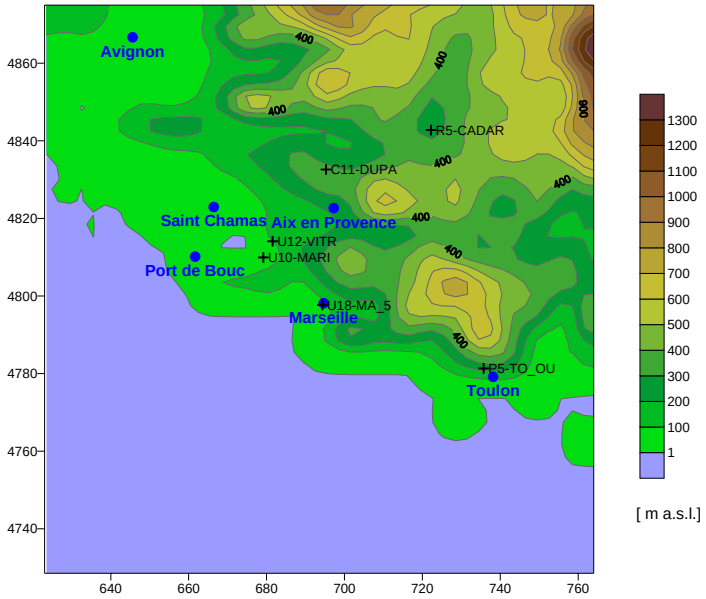

Figure 1: Simulation domain with main cities and monitoring stations selected for the model simulation assessment.

3.3. **Simulation Setup**

The TCAM model, implementing the SAPRC97 [Carter *et al.* 1997] chemical scheme, has been applied over a 144x150 km^2 area, subdivided according to a grid system having 48 per 50 cells with 3 km step size and 15 vertical layers of variable thickness (20, 50, 100, 170, 260, 380, 560, 840, 1220, 1750, 2400, 3300, 4500, 5700, 7000 m a.s.l.).

The 3D meteorological fields (wind, mixing height, humidity and temperature) are provided by means of a three-step procedure. (1) The available local measurements and the ALADIN fields (ESCOMPTE database) [Bubnova *et al.* 1993], have been collected and analysed. (2) The meteorological fields have been performed by RAMS prognostic model [Walko 2001]. (3) Finally, RAMS hourly meteorological fields have interpolated into TCAM grid system by means of CALMET model [Scire *et al.* 1990], in order to preserve continuity and mass consistence.

The hourly emission fields have been performed processing the ESCOMPTE point and area source inventory. Table 1 shows the diffuse and point source emissions in the simulation domain. With the exception of SO_2 emissions, area sources represent the primary pollutant sources. Table 2 presents the main VOC compound emission and the source apportionment during the episode: the high contribution of isoprene in the total amount of organics is underlined. The VOC classes have been mapped into SAROAD [US-EPA 1991a] species and lumped into SAPRC97 chemical mechanism classes. Figures 2 and 3 show the NOx and VOC emissions estimated for the domain during the simulated episode. The emissions from anthropogenic sources are mainly located in correspondence of main urban and industrial areas along the coast as well as along the road networks and the ship trajectories. The biogenic emission map highlights that such contribution, mainly estimated in the NE part of the domain, is comparable to anthropogenic emissions.

The boundary conditions have been estimated processing MOCAGE [Peuch *et al.* 1999] fields, provided in the frame of the ESCOMPTE project. The MOCAGE chemical species have been mapped in the SAPRC97.

Table 1: Total emission and source contribution [%] over the domain, computed for the IOP2.

Source Type	NO_x	CO	SO_2	VOC
Emissions (ton/period)	2,315	7,266	1,802	2,454
Area	78%	56%	13%	97%
Point	22%	44%	87%	3%

Table 2: Main VOC lumped group total emission and source contribution [%] over the domain, computed for IOP2.

Source Type	Formaldeyde	Alkanes	Aromatics	Isoprene	Olefins
Emissions (ton/period)	80	313	191	1,606	181
Area	39	6	3	0	1
Point	61	94	97	100	99

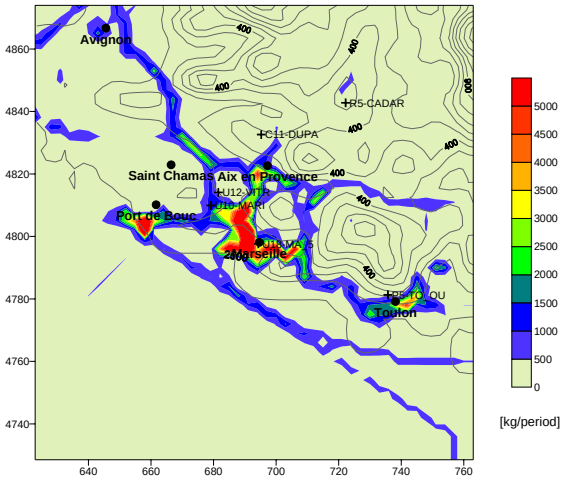

Figure 2: NOx emissions for the selected episode (kg/period).

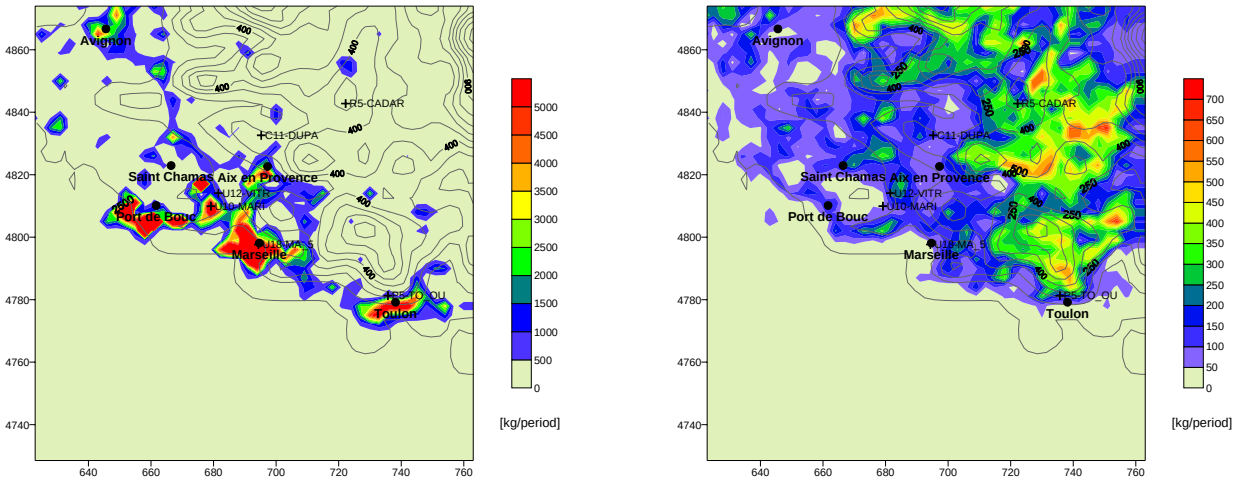

Figure 3:Anthropogenic (left) and biogenic (right) VOC emissions for the selected episode (kg/period).

3.4. **Validation**

In order to assess model performances, six monitoring stations, located in areas with different emission densities and ozone levels, have been selected (Figure 1): two are located in Marseille and Toulon urban areas (U18, P5), two in rural areas (C11, R5), and two in the region between Marseille urban area and the Fos-Berre industrialized zone. The rural stations are characterized by the highest ozone values occurring during the IOP2b (24-26 June): the breezes transport Marseille plume towards rural areas, where moderated NOx emissions are not able to reduce transported ozone masses. Urban sites show a more homogeneous behaviour, with a moderate decrease in the IOP2b.

3.4.1 **Ozone**

The simulation validation has been performed comparing computed and measured hourly ozone concentrations using the performance indexes suggested by [US-EPA 1991b]. These indexes include (1) correlation coefficient, (2) Mean Normalized Bias Error (MNBE) and (3) Mean Normalized Gross Error (MNGE). The errors have been calculated accounting a cut-off threshold of 60 ppb on the measured concentrations and their confidence level criteria are respectively ±0.05÷0.15 and 0.30÷0.35. The statistics reported in Table 3 show satisfying performance for all the indexes in the considered stations. The highest correlation values are computed in the urban and suburban stations (near 0.69÷0.74), while in the rural stations the correlation values are the lowest ones (0.46÷0.61). The MNBE index shows that the model underestimates high ozone concentrations in all the assessment sites.

Table 3: Validation performances (Correlation, Mean Normalized Bias Error and Mean Normalized Gross Error above 60 ppb) of the modelling system for the selected period: ground level ozone.

Code	Station	Correlation	$MNBE_{60}$	$MNGE_{60}$
U10	Marignane-Ville	0.69	-0.12	0.13
U12	Vitrolles	0.73	-0.07	0.17
U18	Marseille 5 Avenue	0.71	-0.13	0.14
C11	Dupail	0.61	-0.16	0.17
R5	Cadarache/Durance	0.46	-0.24	0.25
P5	Toulon Ouest/Olive	0.74	-0.04	0.08

The Figure 4 shows the good agreement between observed and computed concentrations for the IOP2a while the IOP2b is characterized by the ozone underestimation in the rural stations and the overestimation in the urban sites. Such behaviour can be ascribed to the difficulty of the meteorological processors to correctly reproduce at this scale the breezes occurred during the IOP2b.

The Figure 5 presents the mean ozone concentrations calculated during daylight hours (8-19) for the IOP2. The ozone map for the IOP2a shows the maximum impact in the coastal region, near Toulon; high concentrations are simulated in the valleys in the central part of the domain. During the IOP2b the highest values are calculated in the Marseille surroundings. The map also underlines the ozone accumulation in the rural areas of the domain due to the breezes phenomena as suggested by the time series analysis.

The ozone simulated maps are similar to those computed by other models performed during the ESCOMPTE modelling exercise (http://medias.obs-mip.fr/escompte/exercice/HTML/exe.html).

3.4.2 **Nitrogen oxides**

Figure 6 presents the comparison between measured and simulated nitrogen oxides time series time in a urban (Marignane-Ville) and a rural (Dupail) station. Measured values present high concentration peaks due to point emissions. In the Dupail rural station this phenomenon is clear during the IOP2b, when local breezes transport industrial plume towards the center part of the domain.

The model generally underestimates NOx concentration, in particular in the rural station. The lower performances observed in the IOP2b, confirms that the meteorological preprocessor roughly describes local meteorological regimes at this space resolution. The NOx day-night trend is consistent: during the day the concentration of NO2 are lower, because of the high ozone value, while, when the photochemical activity decreases, NO2 concentrations increase.

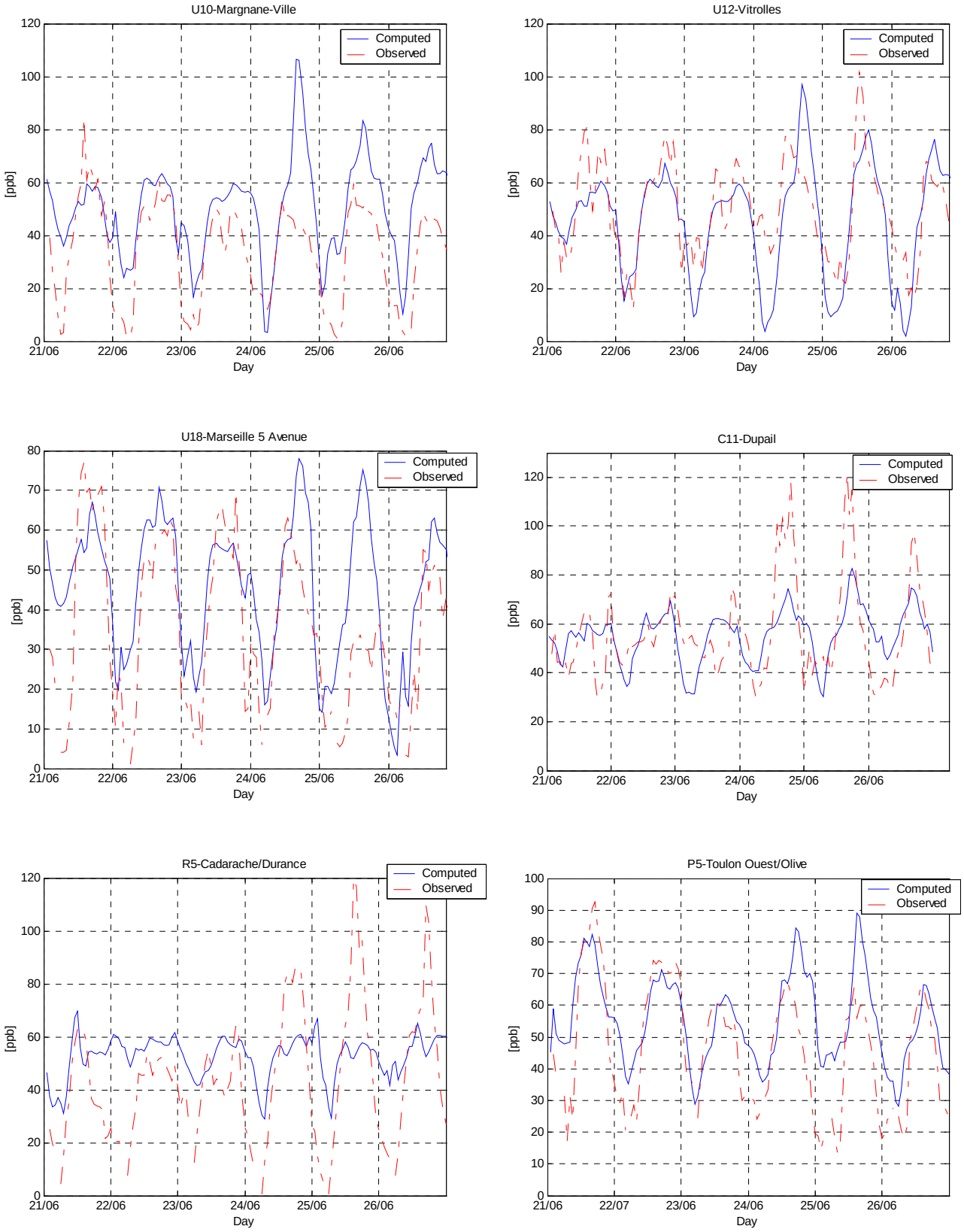

Figure 4: Computed and Observed ozone hourly concentrations.

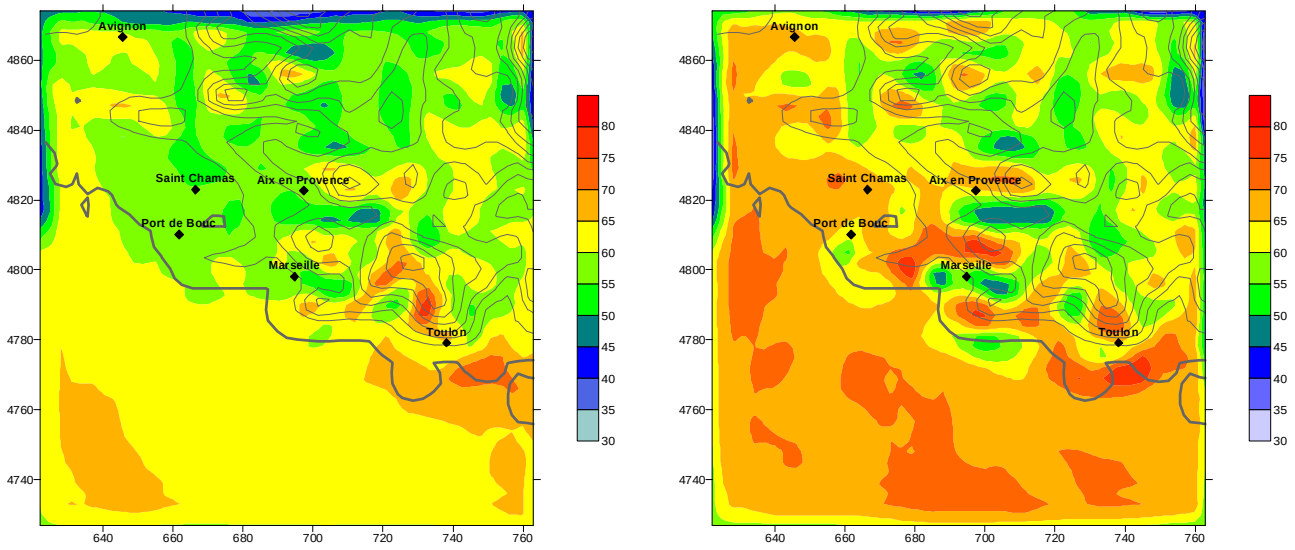

Figure 5: Mean hourly ozone concentration map (ppb) during light hours (8-19) in the periods 21-23 June (left) and 24-26 June (right).

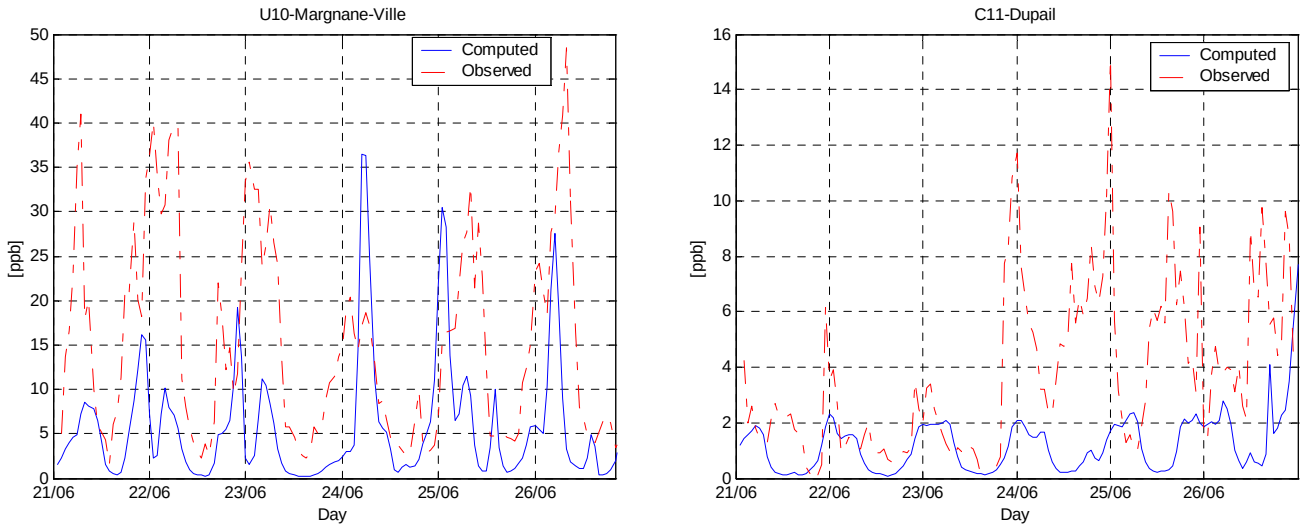

Figure 6: Computed and Observed NO_2 hourly concentrations.

4. Conclusions

The IOP2 monitored during the ESCOMPTE campaign over Marseille region has been performed by the TCAM photochemical model. The assessment analysis underlines high agreement between measured and simulates ozone concentrations during the first part of the episode when the meteorology is ruled by predominant wind circulations. The model performances decrease assessing the second part of the IOP2, characterized by local meteorological regimes roughly simulated by the meteorological processor at this space resolution. The modelling exercise reveals the key role of meteorological input driving simulations of severe ozone episodes over complex domain.

ACKNOWLEDGMENTS

The authors are grateful to Marco Bedogni (Milan Mobility and Environment Agency, Italy) and Guido Pirovano (CESI, Italy) for their cooperation in providing meteorological fields and boundary conditions. The authors also acknowledge ESCOMPTE project organizers, providing model input and validation databases.

REFERENCES

[Bastrup-Birk *et al.* 1996.] Bastrup-Birk, A., Brandt, J., Uria, I., Zlatev, Z. Studying cumulative ozone exposures in Europe during a seven-year period. Technical Report, National Environmental Research Institute, Roskilde, Denmark, 1996.

[Bubnova *et al.* 1993] Bubnova, R., Horanyi, A., Malardel, S. International project ARPEGE/ALADIN. *EWGLAM Newsletter*, **22**: 117130, 1993.

[Carter *et al.* 1997] Carter, W.P., Luo, D., Malkina, I.L. Environmental chamber studies for development of an updated photochemical mechanism for VOC reactivity assessment. Technical report, California Air Resources Board, Sacramento, 1997.

[Cros *et al.* 2004] Cros, B., Durand, P., Cachier, H., Drobinski, Ph., Frejafon, E., Kottmeier, C., Perros, P.E., Peuch, V.H., Ponche, J.L., Robin, D., Said, F., Toupance, G., Wortham, H. The ESCOMPTE program: an overview. *Atmospheric Research*, **69**: 241-279, 2004.

[Dodge 2000] Dodge, M.C. Chemical oxidant mechanisms for air quality modelling: critical review. *Atmospheric Environment*, **34**: 2103-2130, 2000.

[Environ Corp. 2003] Environ Corp. CAMx user's guide. San Raphael, 2003.

[Forester 1977] Forester, C.K., Higher order monotonic convection differences schemes. *Journal of Computational Physics*, **23**: 1-22, 1977.

[Gery *et al*. 1989] Gery M.W., Whitten, G.Z., Killus, J.P. A photochemical mechanism for urban and regional scale computer modeling. *Journal of Geophysical Research*, **94**: 12925-12956, 1989.

[Hindmarsch 1975] Hindmarsch, A.C. LSODE and LSODEI, Two new initial value ordinary differential equaton solvers. *ACM-SIGNUM Newsletter*, **15**: 10-11, 1975.

[Holstag Nieuwstadt 1986] Holstag, A.A.M., Nieuwstadt, F.T.M. Scaling the atmospheric boundary layer. *Boundary layer meteorology*, **36**: 201-209, 1986

[Jaecker-Voirol Mirabel 1989] Jaecker-Voirol, A., Mirabel, P. Heteromolecular nucleation in the sulfuric acid-water system. *Atmospheric Environment*, **23**: 2053-2057, 1989.

[Marchuk 1975] Marchuk, G. Methods of Numerical Mathematics Springer, 1975.

[Pasquill 1974] Pasquill, F., Atmospheric Diffusion, 2nd Edition. Halsted Press of John Wiley & Sons, 1974.

[Pepper *et al.* 1979] Pepper, D.W., Kern, C.D., Long, P.E. Modelling the dispersion of atmospheric pollution using cubic splines and Chapeau functions. *Atmospheric Environment*, **13**: 223-237, 1979.

[Peuch *et al.* 1999] Peuch, V.H., Amodei, M., Barthet, T., Cathala, M.L., Josse, B., Michou, M., Simon, P. MOCAGE: Modele de Chimie Atmospherique a Grande Echelle. *Actes des Ateliers de Modelisation de l'Atmosphere*, Toulouse, France, 1999.

[Russel Dennis 2000] Russel, A., Dennis, R. NARSTO Critical Review of Photochemical Models and Modeling. *Atmospheric Environment*, **34**: 2283-2324, 2000.

[Scire *et al.* 1990] Scire, J.S., Insley, E.M., Yamartino, R.J. Model formulation and user's guide for the CALMET meteorological model. Technical report, California Air Resources Board, Sacramento, 1990.

[Seinfeld Pandis 1997] Seinfeld, J.H., Pandis, S.M. Atmospheric chemistry and physics. John Wiley & Sons, 1997.

[Sillman 1999] Sillman, S. The relation between Ozone, NOx and Hydrocarbons in urban and polluted rural environments. *Atmospheric Environment*, **33**: 1821-1845, 1999.

[Sun *et al*. 1994] Sun, P., Chock, D.P., Winkler, S.L. An Implicit-Explicit Hybrid Solver for a System of Stiff Kinetic Equations. *Proc. 87th Air & Waste Management Association Annual Meeting*, 1994.

[US-EPA 1991a] US Environmental Protection Agency. Aerometric Information Retrieval System User's Guide, 1991.

[US-EPA 1991b] US Environmental Protection Agency. Guideline for regulatory application of the urban airshed model. Technical Report, EPA-450/4-91-013, 1991.

[Volta Finzi 2005] Volta, M., Finzi, G. GAMES,a comprehensive gas aerosol modelling evaluation system. *Environmental Modelling and Software*, in press, doi:10.1016/j.envsoft.2004.06.012

[Walko Tremback 2001] Walko, R. L., Tremback, C. J. RAMS Regional Atmospheric Modeling System - version 4.3/4.4, Users Guide Fort Collins, CO, USA, 2001.

[Wexler Seinfeld 1991] Wexler, A.S., Seinfeld, J.H. Second-Generation Inorganic Aerosol Model. *Atmospheric Environment*, **25**: 2731-2748, 1991.

[Wille 1994] Wille, D.R. New stepsize estimators for linear multistep methods. Technical Report, MCCM, 1994.

Simulating Evacuations Triggered by Earthquakes

Samia Abul-Rub
Al-Isra Private University
P.O. Box 22, 33
Al-Isra Private University Post Office
11622, Jordan
+962 79 5609975
s_aar@hotmail.com

Ghassan Al-Noubani
Al-Isra Private University
P.O. Box 22, 33
Al-Isra Private University Post Office
11622, Jordan
+962 77 7774055
al_noubani@isra.edu.jo

ABSTRACT
The latest Tsunami disaster is one example of how many places around the world suffer from natural disasters which obstruct human life and cause enormous types of damages. One of the major issues involved is such disasters is evacuation. Good evacuation planning reduces the risk of the most valuable loss- the human life.

In our work, we draw a mathematical model for the evacuation time involved in one of the major disasters- earthquakes with the long-term objective of minimizing the needed evacuation time. We study significant elements involved in any evacuation, as well as the effects of the factors of earthquakes on such an evacuation. Factors include the number of people involved in the evacuation, their estimated velocity, gender and age in addition to factors which relate directly to earthquakes such as the earthquake's magnitude and duration.

In conclusion, this study offers a flexible and stable model that calculates reasonable evacuation time for evacuations triggered by earthquakes. The model is applicable to all types of square-shaped rooms and takes into consideration the variations among the characteristics of the people involved in an evacuation, in addition to factors forced by earthquakes.

KEYWORDS
Modeling, earthquakes, evacuation factors, evacuation time

1. Introduction

One of the major issues involved in natural disasters, such as earthquakes, is evacuation. In this work, evacuations triggered by earthquakes are considered; evacuation time is studied based on a mathematical model, and conclusions are drawn on circumstances that lead to the fastest evacuation.

There are several factors which affect the time needed for evacuating a closed area. These factors include the number of people involved, the area and shape of the room to be evacuated, the number and size of egresses, the human velocity, and the human response time (considering aspects such as age and gender).

In addition to these general evacuation factors, there are factors which are specific to the problem under study – evacuations triggered by earthquakes. Such factors include: focal depth, distance from the earthquake's epicenter, earthquake's magnitude, earthquake's duration, and the nature of ground suffering an earthquake.

This research studies some components of the mathematical model used by [Buduardja *et al.* 1998] for calculating the needed evacuation time of a single square-shaped room having only one type of exits – a conventional door. However, more details are embedded in the model that, are believed, would help provide a more accurate translation of a real-life evacuation process. The weakness of the model drawn at Goshen College as described by its authors [Buduardja *et al.* 1998] is that it needs to utilize to different essential equations in order to decide the maximum room occupancy. However, there are also other considerations such as characteristics of the people involved in an evacuation as well as the nature of the alert that triggered the evacuation event.

It is believed that this study offers a model that calculates reasonable evacuation time that is applicable to all types of square-shaped rooms with exits formed by conventional doors. The model takes into consideration the variations among the characteristics of the people involved in an evacuation, in addition to factors forced by earthquakes.

2. The Mathematical Model

2.1. Defining Model Parameters

The model involves several parameters defined as follows:

N The number of people inside the room to be evacuated

T_{total} The total time required to completely evacuate everyone from inside the room to outside the room. T_{total} is measured starting from the time when the emergency notice is issued until everyone is outside the room

T_{exit} The time required for everyone to pass the exit door assuming that everyone has been in the ready-to-exit position

T_{delay} The total delay which involves response time, time to be ready, and other factors that cause more delay

T_{ready} The average time required for everyone to move to the ready-to-exit position from their initial position

$T_{respond}$ The average time required for everyone to respond to the emergency notice

T_{others} The time required for any other obstruction possibilities

T_{foe} The time added to the total evacuation time due to factors directly related to earthquakes

TD The duration of the earthquake

TD_{range} The delay forced by the duration of the earthquake

M The magnitude of the earthquake

M_{range} The delay forced by the magnitude of the earthquake

V_p The reasonable velocity of a human being in a panic situation

θ The human speed reduction factor under the situation where there are obstructions that may reduce the speed, such as movable furniture, raisers, slope …etc

S_e The distance calculated from the exit to the point between the nearest and the farthest distances from the exit

R The rate of people exiting, i.e. the average number of people exiting per unit of time

E The number of egresses

W_d The average frontal width of egresses

$T_{passing}$ The average time required by one person to pass the exit door

N_{ch} The number of children inside the room

N_w The number of women inside the room

N_m The number of men inside the room

Pr_{ch} The priority given to children

Pr_w The priority given to women

Pr_m The priority given to men

As can be seen from the above parameters, the model separates the total evacuation time into two elements: the time from when occupants first received the emergency notice until they pass through the exit door, and the time needed for people to go through the way out. The main objective is to evacuate as many people as possible.

2.2. **Details of the Model**

As mentioned earlier, the model separates the total evacuation time T_{total} into to the exit time T_{exit} and the delay time T_{delay}:

$T_{total} = T_{exit} + T_{delay}$ Equation 1

Furthermore, we define T_{exit} as the time required for everyone to pass the exit door. Hence T_{exit} should consider the number of people to be transported (N) taking into consideration priorities given, and the rate of people exiting R:

$T_{exit} = N / R$ Equation 1.2

where $N = N_{ch}*Pr_{ch} + N_w*Pr_w + N_m*Pr_m$ Equation 1.2.1

The rate of people exiting R can be calculated with the consideration of the frontal width of the exit W_d, the average frontal width of the people W_p, the number of egresses E, and the average time for each person to pass the exit $T_{passing}$.

Dividing the W_d by W_p will help determine the number of people that can escape through one exit at the same time.

In order to determine the amount of time required for each person to pass the door- $T_{passing}$, we divide the average distance traveled by each person when he/she crosses the exit S_p by the average velocity of a human being in a panic situation V_p:

$T_{passing} = S_p / V_p$ Equation 2

The average distance traveled by each person can be determined as the sum of the thickness of the door X and the average frontal width of humans:

$S_p = X + W_p$. Equation 2.1

The number of egresses E affects the throughput rate of people exiting. Therefore, we reach an equation for measuring the rate of people exiting R (assuming only conventional doors for exits):

$R = ((W_d / W_p) * E) / T_{passing}$ Equation 1.2.2

T_{delay} is defined as the average time required for everyone to move to the ready-to-exit position from his/her initial position. T_{delay} is very dependent on the room configuration, the room shape, and the location of people inside the room. Hence, the model should be general enough in order to cover the entire possible situations:

$T_{delay} = T_{ready} + T_{respond} + T_{foe} + T_{others}$ Equation 1.3

It is expected that the minimum T_{ready} should be the time needed for the person nearest the exit to travel from his or her position to the exit door, and the maximum T_{ready} is the time required by the person farthest from the exit to do the same action. However, as the farthest person is moving to exit, the nearest person has already exited. Based on those assumptions, the reasonable T_{ready} should be the average of those two. The best method to approximate the reasonable T_{ready} is the time needed by a person to travel from the distance between the nearest and the farthest distance from the exit door S_e.

The model also introduces another factor that may affect the velocity on the way to the exit door as θ. This factor would be 1 unless under the situation where raisers, slope, slippery surface…etc exist. The θ is ranging from 0 to 1 with 1 meaning that there is no reduction factor. We consider the movable furniture as velocity reduction factor because those do not change the path traveled by the people, but requires them to move them from their way. Thus, T_{ready} can be formulated as the following:

$T_{ready} = S_e / (\theta V_p)$ Equation 1.3.1

$T_{respond}$ is determined by the average time required by humans to respond to an emergency notice. In other words, it is the duration between the time emergency notice is issued and the time people start to react.

T_{others} introduces delays caused by other obstruction possibilities that may be present due to panic for example. T_{foe} introduces factors that are present due to the cause of evacuation. The problem specification defines earthquakes as the trigger to evacuation. The next section describes how T_{foe} is defined in the model.

2.3. **Evacuations Triggered by Earthquakes**

The evacuation time is highly affected by the nature of the earthquake itself. There are many factors that determine the effects made by an earthquake, such factors include [TheEpicenter 2005]:

1- The magnitude of the earthquake (M): which controls the whole process of evacuation to the extent that in cases of high magnitude (7 and above), no evacuation is possible. The magnitude of earthquakes depends on two elements:

a- The nature of the area hit by the earthquake: The magnitude of the earthquake differs depending on whether the area is rocky or sandy. In rocky areas, the earthquake's effects are more disastrous than in sandy areas, and the magnitude of earthquakes differs too depending on the nature of the plates; ocean plates absorb earthquake waves, so the damage is less than that of the continental plates.

b- The distance from the earthquake's epicenter: the larger the distance from the epicenter, the more time is available for evacuation.

2- The duration time of the earthquake (TD): affects the amount of damage caused by the earthquake; the longer the duration, the worse the damage caused, and therefore more time will be needed for evacuation.

The model considers both factors; magnitude and duration time as shown in the following equation:

$T_{foe} = M_{range} + TD_{range}$ Equation 1.3.2

2.4. **Assignment of Values**

In order to obtain a mathematical model that is close to real-world situations, constant values are assigned to some of the model parameters mentioned earlier. These values help verify the model; they are, however, subject to changes whenever necessary. The assignments are as follows:

V_p= (0.75-1.3) m/s. [Buduardja *et al.* 1998] assumed a value of 1m/s. The study varied the range by approximately +0.25 and -0.25 due to gender and priorities.

Pr_{ch}= 3, Pr_w= 2, Pr_m= 1. This as a common-knowledge social issue [Fordham 1999].

W_d= 1.0 m, X= 0.2 m, N= (1-100). These values were taken based on the available items for actual experiments.

W_{pch}= 0.3 m, W_{pw}= 0.45 m, W_{pm}= 0.5; based on the value of W_p assumed by [Buduardja *et al.* 1998].

$T_{respond}$= 2.0 seconds [Buduardja *et al.* 1998].

T_{others} = 1.0 seconds. [Buduardja *et al.* 1998] assumed a value of 0.0 seconds, however, the review of literature [Fordham 1999] [Wallenius 2001] showed delay caused by the time required for any other obstruction possibilities

M_{range} is assigned a value in seconds based on the range of M; (range 1-3, value = 20) (range 4-6, value = 30) (range >=7, no evacuation possible).

TD_{range} is assigned a value in seconds based on the range of TD; (range 1-3, value = 10) (range 4-6, value = 20) (range 7-10, value = 40).

The latter two assumptions of values are taken based on the damaged caused by an earthquake [TheEpicenter 2005].

3. Assumptions

The following assumptions are established in order to formalize the environment of the model:

- People are classified into three categories: men, women and children. [Fordham 1999] addressed the issue of gender in a disaster process and therefore the model was designed to be gender sensitive; i.e. gender-sensitive priorities are taken into consideration. This affects the total evacuation time in cases where lower priority gender is closer to exits. Obviously, another group 'elderly people' could have been incorporated, yet it was not possible to include for actual experiments.
- The number of people in the room does not exceed 100 persons; this was the maximum number that was available for actual experiments.
- There are no obstacles outside the room, so that outflow of people exiting the room depends only on the factors inside the room.
- There is only one type of exits – a conventional door.
- Evacuation priorities are given to different genders. Children are given the highest priority, followed by women the men. The influence of priorities is shown when a gender of a lower priority is closer to the exit.
- People want to reach the exit as fast they can. Panic is present [Alexander 1990].
- The evacuation is triggered by an earthquake. Therefore, characteristics forced by the trigger are highly considered [Edwards 1993].

4. The Simulation Process

The simulation process involved several considerations which are explained below. It should be noted that there was time stepping in the calculation of each trajectory.

4.1. Initial Positions

Initial positions are given to the assigned population by random (x,y) coordinates representing points within the 2-dimentional top view of the square shaped room.

4.2. Calculation of Path

The path a person takes towards an exit is calculated by following the Bresenham's line-drawing algorithm [Hearn Baker 1997] in which ($X_{initial}$, $Y_{initial}$) is taken to be the random initial position for each person mentioned in 4.1, and (X_{exit}, Y_{exit}) is the closest possible exit point to the person.

```
start
    for each person in the room
        give random initial position within the coordinates of the room (X_initial, Y_initial)
        locate the closest possible exit point (X_exit, Y_exit)
        locate the first midpoint
        while (X_exit, Y_exit) is not reached
                if midpoint is above the exact path
                        move towards lower available pixel
                        assign next midpoint to the right
                else
                        move towards upper available pixel
                        assign next midpoint to the top-right
end
```

Figure 1- Algorithm for Calculating the Path for Each Person towards the Exit

4.3. **Random Parameters**

In order to make a good approximation of the reality, random assignments where made to the parameters within the values stated in 2.4. However, certain patterns were also forced to examine the sensitivity of each parameter.

In each case, values were written to a file and then fed to the simulator. The results giving the total evacuation time, in addition to the values calculated for the time divisions given by the model were then save to another file for evaluation and comparison with values obtained by actual experiments.

5. **Case Studies**

The model was implemented, tested and visualized against a number of case studies:

5.1. **The Number of Egresses**

In this case, the number of egresses was varied among 1 and 3, other factors were kept fixed. This is shown in figure 2(a)(b).

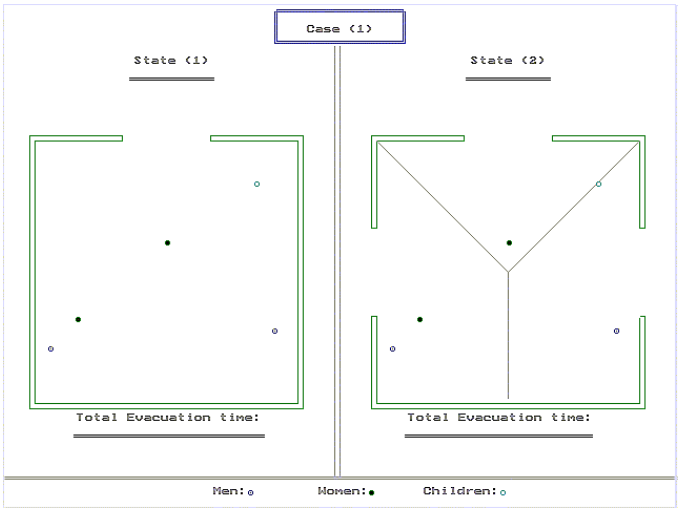

Figure 2(a) Initial state – Number of Egresses

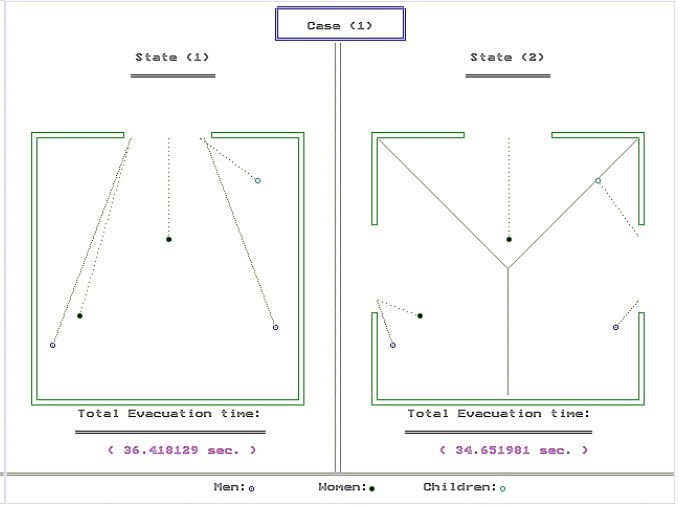

Figure 2(b) After evacuation – Number of Egresses

5.2. **The Number of People**

In this case, the number of people involved in the evacuation was varied among 5 and 10, other factors were kept fixed. This is shown in figure 3(a)(b).

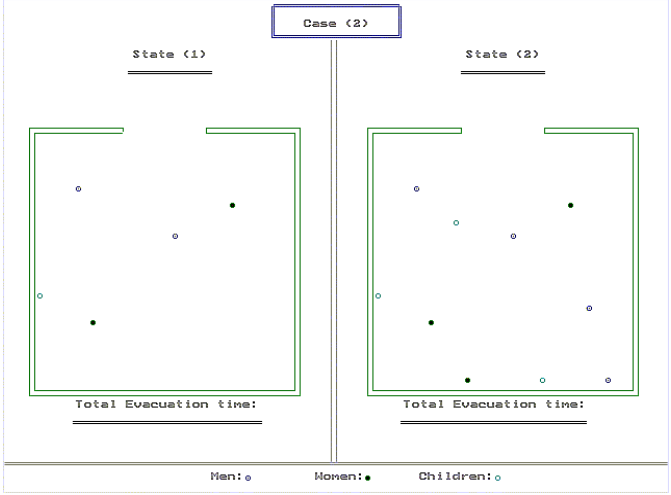

Figure 3(a) Initial state – Number of People

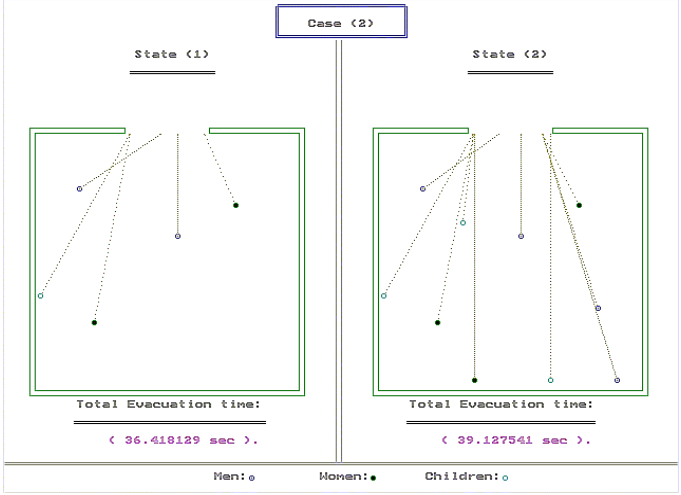

Figure 3(b) After evacuation – Number of People

5.3. **Gender Sensitivity**

In this case, the number of women and men involved in the evacuation was varied among 2 and 4, other factors were kept fixed. This is shown in figure 4(a)(b).

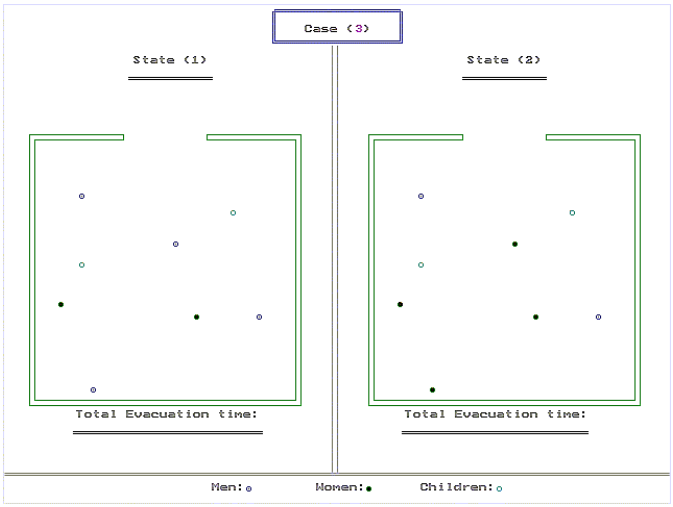

Figure 4(a) Initial state – Gender Sensitivity

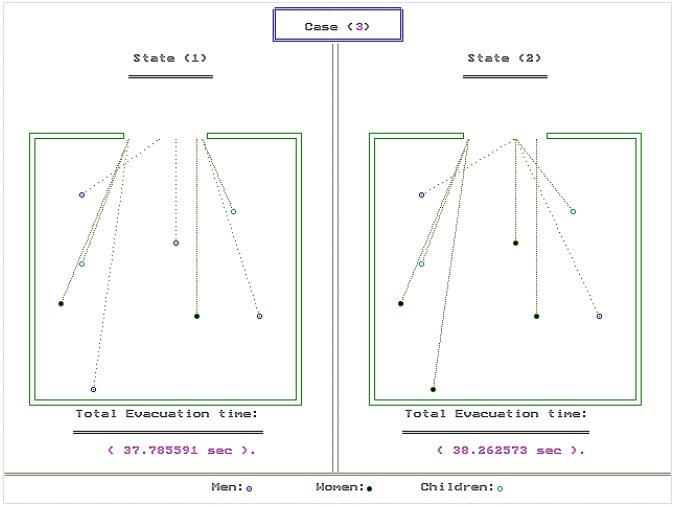

Figure 4(b) After evacuation – Gender Sensitivity

5.4. **The Number of Children**

In this case, the number of children and men involved in the evacuation was varied among 2 and 4, other factors were kept fixed. This is shown in figure 5(a)(b).

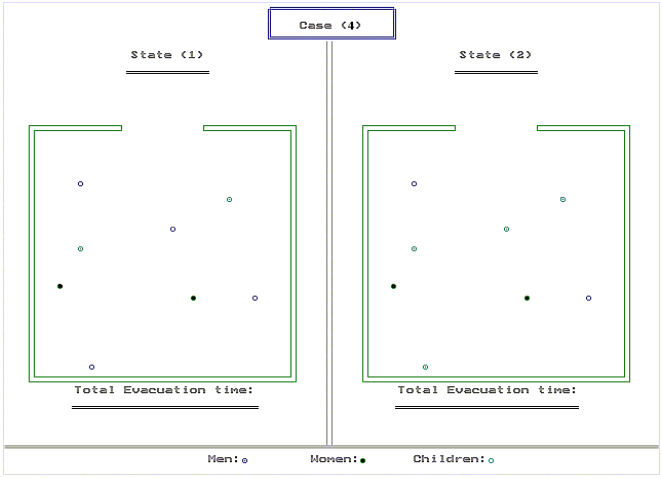

Figure 5(a) Initial state – Number of Children

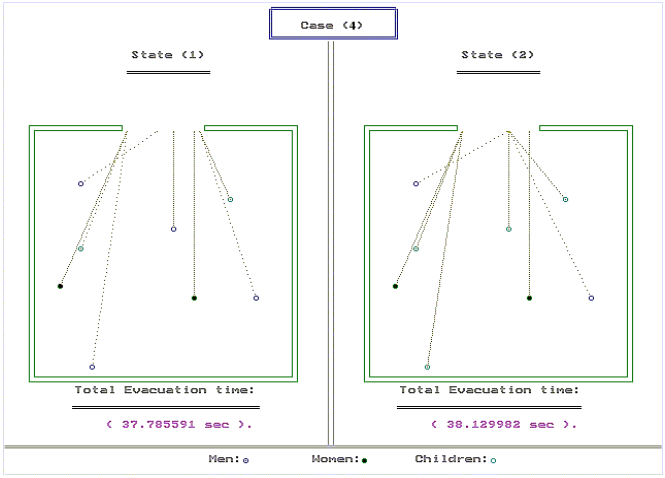

Figure 5(b) After evacuation – Number of Children

5.5. **The Average Velocity**

In this case, the average velocity for each individual was varied by +0.25, other factors were kept fixed. This is shown in figure 6(a)(b).

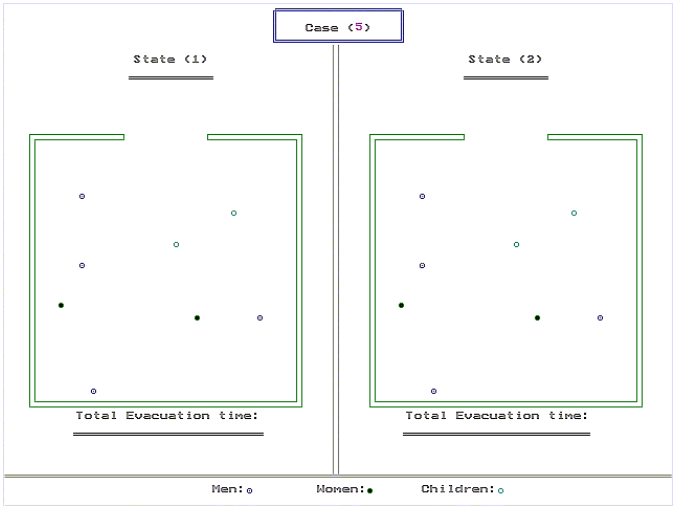

Figure 6(a) Initial state – Average Velocity

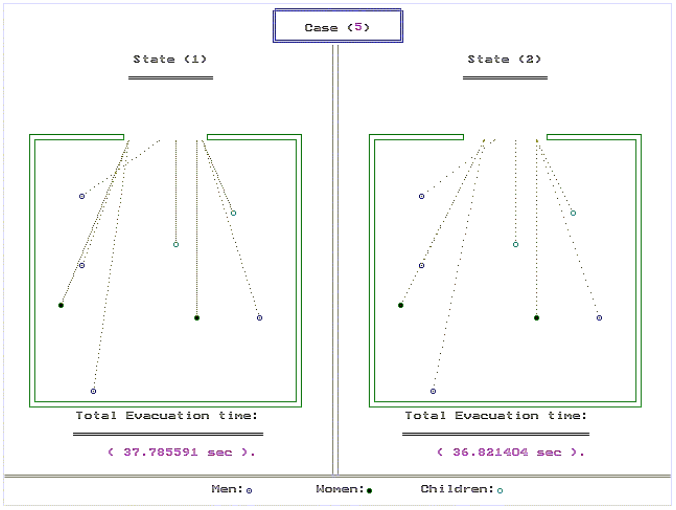

Figure 6(b) After evacuation – Average Velocity

5.6. **Earthquake Factors**

In this case, the magnitude and the duration time of the earthquake was varied among 2 and 5, other factors were kept fixed. This is shown in figure 7(a)(b).

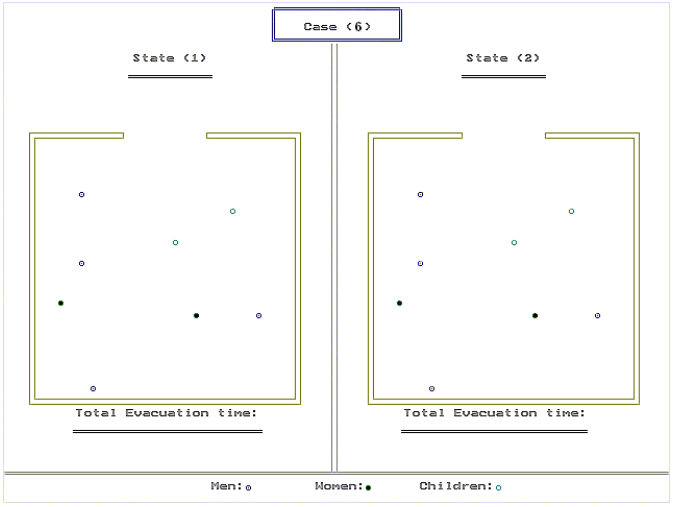

Figure 7(a) Initial state – Earthquake Factors

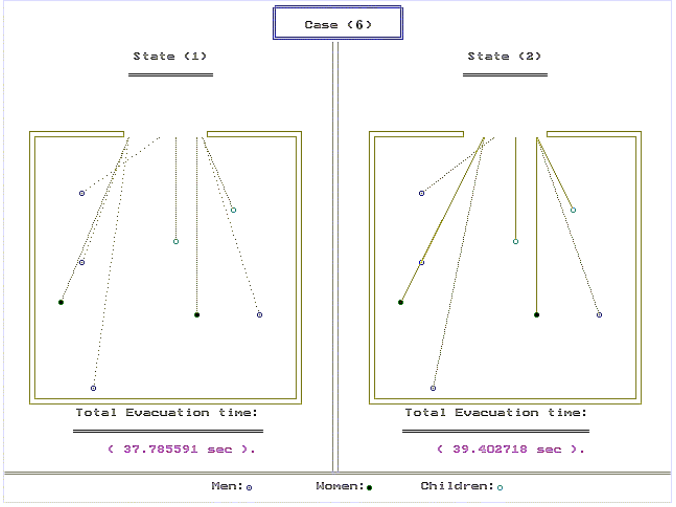

Figure 7(b) After evacuation – Earthquake Factors

6. **Testing**

Figure 8 shows the results obtained by actual experiment as opposite to those given by the model categorized by criterion. It should be stated that whenever a factor was tested, others were kept fixed with the mid-values mentioned in section 2.4. Also, the numbers show the average case scenario.

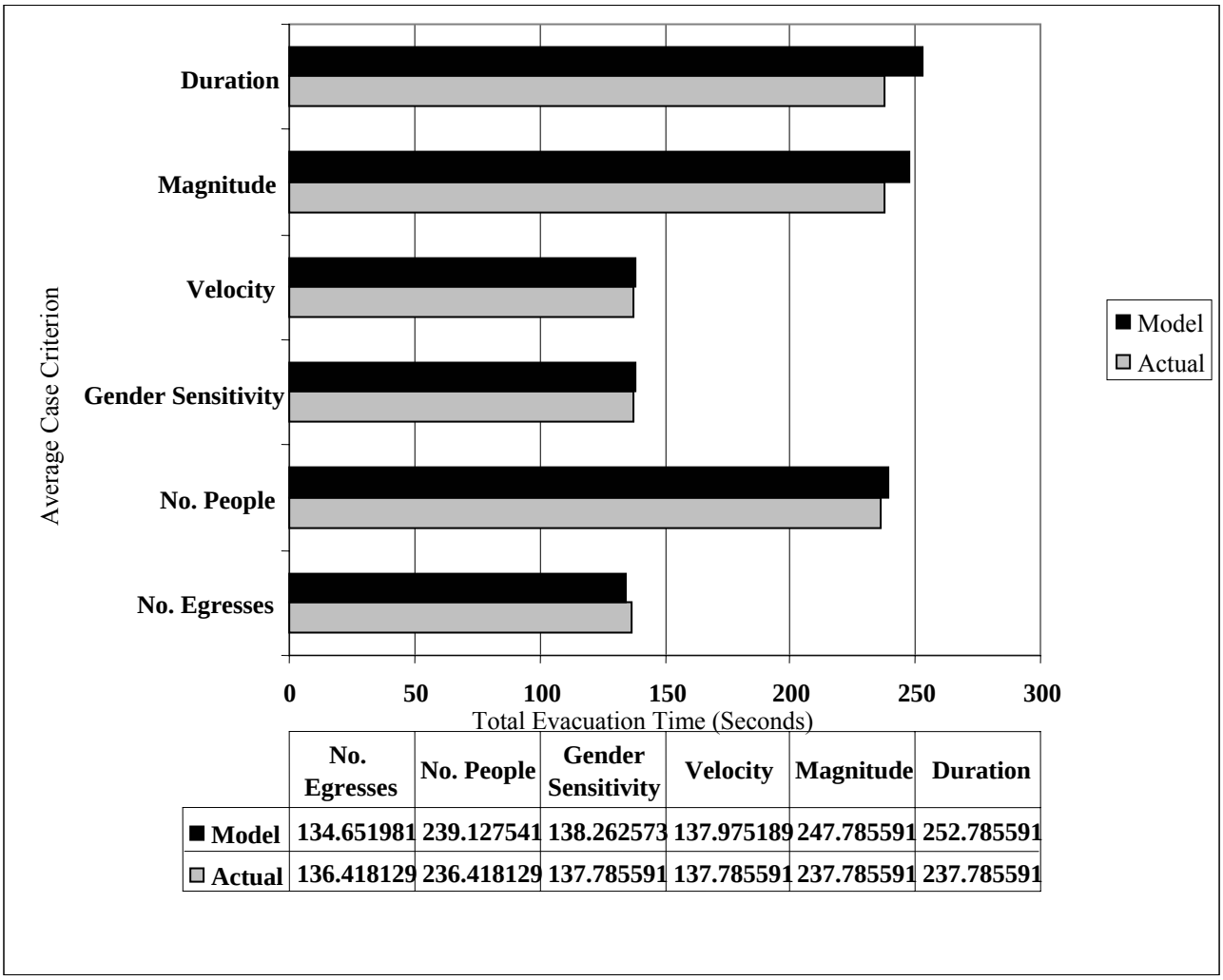

	No. Egresses	No. People	Gender Sensitivity	Velocity	Magnitude	Duration
Model	134.651981	239.127541	138.262573	137.975189	247.785591	252.785591
Actual	136.418129	236.418129	137.785591	137.785591	237.785591	237.785591

Figure 8 – Model Results as Opposite to Actual Experiment Results

7. **Conclusions**

The drawn model considers factors involved in evacuations triggered by earthquakes with the long-term objective of minimizing the time needed for evacuation. Factors include the number of people involved in the evacuation, their estimated velocity, gender and age in addition to factors which relate directly to earthquakes such as the earthquake's magnitude and duration.

The model is applicable to all types of square-shaped rooms and also takes into consideration the variations among the characteristics of the people involved in an evacuation, in addition to factors forced by earthquakes.

There are several desirable features about this model. The model is flexible since the values of parameters can be easily changed and tested as has been done in the above mentioned case studies. In addition, T_{others} offers great flexibility in handling special cases for square-shaped rooms. The model also guarantees stability since any parameter can be modified without affecting the integrity of the entire model.

8. **Recommendations for Further Work**

Further developments may be done to the model by taking into considerations the following:

- Obstacles that may face individuals inside and outside the evacuation area.
- Different kinds of exits, such as stairs, windows, electrical doors…etc. The frontal width for the exit may also be considered.
- Assigning values for M_{range} and TD_{range} based on a formula that takes into consideration M and TD.
- Introducing a new group 'elderly people' which will consequently have a different priority and speed. Therefore, an affect on the delay involved in an evacuation.
- Different designs of the evacuation area (other than the square-shaped).
- Developing the model to cover larger evacuation areas such as buildings.
- Developing the model to cover outdoor areas such as traffic, areas of a city…etc.
- Developing the model to cover the details for earthquake factors, such as focal depth and distance from epicenter.

ACKNOWLEDGMENTS

The contribution of Hikmat Al-Awawdeh and Nuha Al-Dawoud in this study is gratefully acknowledged.

REFERENCES

[Alexander 1990] Alexander, D. Behavior During Earthquakes: A Southern Italian Example**.** *International Journal of Mass Emergencies and Disasters*, **8**- 1: 5-29, 1990.

[Atwood 1993] Atwood, L.E. Perceived Impact of an Earthquake Prediction: The Third Person Effect. *International Journal of Mass Emergencies and Disasters*, **11**- 3: 365-378, 1993.

[Baldwin 1993] Baldwin, T.K. Earthquake Awareness in Southeast Missouri: A Study in Pluralistic Ignorance**.** *International Journal of Mass Emergencies and Disasters*, **11**- 3: 351-363, 1993.

[Bank *et al.* 1996] Bank, J., Carson, J.S. and Nelson B.L. Discrete-Event System Simulation, 2nd Edition, Prentice Hall, USA, 1996.

[Barlow 1993] Barlow, H.D. Safety Officer Accounts of Earthquake Preparedness at Riverside Industrial Sites. *International Journal of Mass Emergencies and Disasters*, **11**- 3: 421-435, 1993.

[Blanchard Boehm 1998] Blanchard-Boehm, R.D. Understanding Public Response to Increased Risk from Natural Hazards: Application of the Hazards Risk Communication Framework. *International Journal of Mass Emergencies and Disasters*, **16**- 3: 247-278, 1998.

[Buduardja *et al.* 1998] Budiardja, R.D., Christanday, G.S. and Hilman R. Modeling for Standard of Safety for Occupied Room. On-line at http://budiardja.org/writing/math_modeling/, 1998.

[Clark *et al.* 1993] Clark, L.V., Veneziano, L., and Atwood, D. Situational and Dispositional Determinants of Cognitive and Affective Reactions to the New Madrid Earthquake Prediction. *International Journal of Mass Emergencies and Disasters*, **11**- 3: 323-335, 1993.

[Dynes 2000] Dynes, R. The Dialogue between Voltaire and Rousseau on the Lisbon Earthquake: The Emergence of a Social Science View. *International Journal of Mass Emergencies and Disasters*, **18**- 1: 97-115, 2000.

[Edwards 1993] Edwards, M.L. Social Location and Self-Protective Behavior: Implications for Earthquake Preparedness. *International Journal of Mass Emergencies and Disasters*, **11**- 3: 293-303, 1993.

[Enander Claes 1999] Enander, A. and Claes, W. Psychological Reactions and Experiences Among Swedish Citizens Resident in Kobe During the 1995 Earthquake. *International Journal of Mass Emergencies and Disasters*, **17**- 2: 185-205, 1999.

[Farley 1998] Farley, J.E. Down But Not Out: Earthquake Awareness and Preparedness Trends in the St. Louis Metropolitan Area, 1990-1997. *International Journal of Mass Emergencies and Disasters*, **16**- 3: 303-319, 1998.

[Fitzpatrick Dennis 1991] Fitzpatrick, C. and Dennis, S.M. Motivating Public Evacuation. *International Journal of Mass Emergencies and Disasters*, **9**- 2: 137-152, 1991.

[Fordham 1999] Fordham, M. The Intersection of Gender and Social Class in Disaster: Balancing Resilience and Vulnerability. *International Journal of Mass Emergencies and Disasters*, **17**- 1: 15-37, 1999.

[Hearn Baker 1997] Hearn, D. and Baker M. P. Computer Graphics, 2nd Edition. Prentice Hall, New Jersey, 1997.

[Mesterton 1995] Mesterton, Michael, Gibbons. A Concrete Approach to Mathematical Modeling. Willey-Interscience Publication, New York, 1995.

[Neelamkavil 1991] Neelamkavil, F. Computer Simulation and Modeling, John Wiley & Sons, 1991.

[Stallings 1984] Stallings, R.A. Evacuation Behavior at Three Mile Island. *International Journal of Mass Emergencies and Disasters*, **2**- 1: 11-26, 1984.

[TheEpicenter 2005] The Epicenter Web Site. On-line at http://www.theepicenter.com, 2005.

[Wallenius 2001] Wallenius, C. Why Do People Sometimes Fail when Adapting to Danger? A Theoretical Discussion from a Psychological Perspective. *International Journal of Mass Emergencies and Disasters*, **19**- 2: 145-180, 2001.

Computer modelling and discrete event simulation of seaweeds trajectories

Jean-Baptiste Filippi[12]
filippi@batti.org

Teruhisa Komatsu[2]
komatsu@ori.u-tokyo.ac.jp

Kyushu Tanaka[2]
tanaka@ori.u-tokyo.ac.jp

[1] Corresponding Author

[2]Ocean Research Institute
The University of Tokyo
1-15-1 Minamidai, Nakano-ku
Tokyo 164-8639, JAPAN

ABSTRACT
Drifting seaweeds plays a major role in areas where they are present. We describe a computer model, Jeosim, that clarifies the roles of those seaweeds in relation to their transport using particle tracking algorithm. The Euler rule with trapezoidal approximation, used to calculates drifting paths, is implemented in JeoSim in discrete events fashion in order to simulate the path and movement of seaweeds. Preprocessing of the ocean currents is done with the Princeton Ocean circulation Model (POM). Simulated current constitutes the data that provides force and directions for the calculations of drifting paths. Along with the implementation of the particle tracking algorithm in discrete event fashion, the originality of the JeoSim software lies in its Object Oriented architecture which makes it especially suited to perform simulation of living, cross scale systems with complex behavior. Behavior of drifting seaweeds of the *Sargasso* family has been implemented in JeoSim, and experimented in East China sea following a drifting seaweed collection campaign in may 2002. Despite a relative low resolution ocean currents data, simulated results compares well with the observed distribution.

KEYWORDS Discrete event simulation, particle tracking, ecological modelling, modelling and simulation environment, models library, seaweeds

1 Introduction

Drifting seaweeds plays a major role in areas where they are present. They act as nursery for a vast amount of species, but also are a good bio-indicator of water quality. Such algae hosts moving ecosystems, and identifying the drift path is necessary in order to clarifying their roles. Particle tracking techniques have proven to be the most robust and common approach to identify drifting pathes [Reynolds 2003]. Mathematical models of particle tracking in the sea faces two main difficulties, the first is the lack of field data in order to evaluate the accuracy of such models. The second is the availability of ocean current data representing seasonal variability. These facts suggest that models should only retain such algorithm able to represent the minimum physics needed to reproduce the phenomena and avoid cumbersome procedures that have feeble scientific support, or that involves an excessive number of adjusting parameter. However, this minimum set of algorithms should be thoroughly tested and validated. Trajectory and spreading models usually uses resolutions of Lagrange particle tracking technique [García-Martínez and Flores-Tovar 1999], where particles simulate material transported by the water current, with various spreading mechanisms. The most common application of particle tracking spread models is the simulation of oil spills. Various works [García-Martínez and Flores-Tovar 1999], [Bennett and Clites 1987] shows that the common Euler approach used to solve Lagrange equations is very sensible to time stepping and might induce numerical errors that causes erroneous drift and exaggerate the spread. This report provides numerical experiment results that confirms the error introduced by a discrete time approach to an Euler resolution, and introduces a discrete event approach that is more suited to the simulation of ecological systems. The JeoSim model consists of two subsystems. The first is a three dimensional, sigma-coordinate hydrodynamic Model, the Princeton Ocean Model, that calculates ocean velocity fields in the area of interest. The second subsystem is a Lagrangian particle tracking spreading model that calculates material trajectories using the results from the hydrological model.

Moreover, the use of a fixed time step during the simulation causes coupling problems in case of an integration into a cross scale ecological model. Unlike oil spills models, drifting seaweeds has many different aspects of interest. Such models applied to ecological science requires an advanced software framework to be build upon, because the simulation is not one of an inert particle, but of a living organism with a behavior that evolves in time and influences the drifting path. Model is to be observed by different point of views, with various variables that must be taken into account (biomass, distribution, mortality,…). These require the integration of several temporal, geographical and abstraction scales, therefore using a thoroughly engineered software architecture to match with the desired complexity and flexibility.

The application presented in this report is the analysis and simulation of *Sargassum* Sea grass distribution in East China Sea to clarify ecological roles of this specie. Recently a lot of drifting seaweeds were found in the East China Sea surrounded by Taiwan, China and Japan in spring. The Kuroshio Current passes northeasterly along the surface layer above 200 m isobaths in the East China Sea. Tsushima Current is bifurcated southwest of Kyushu Island from the Kuroshio Current and enters the Japan Sea through Tsushima Straight. Origin of *Sargassum* species newly found as drifting seaweeds are thought to be geographically limited around Chinese coast in the East China Sea. *Sargassum* species were collected during on-site studies near Chinese coasts in East China Sea and Yellow Sea, and the zone further delimited with satellite imagery. Nevertheless, it is important to verify those assumptions with the use of simulation software to identify particle paths, distribution and the timing of the distribution. We will first describe the software architecture, before providing details about the underlying algorithms and finish by presenting the simulation experiment in east China sea.

2 General software architecture

The JeoSim Software needs the pre-processing of Ocean Currents with an Ocean Circulation Model. Because of the high processing power required by such models, it is often necessary to use a supercomputer. Most ocean Circulation models are written in Fortran [Mellor and Yamada 1982], with a few opportunities to integrate them into a monolithic software. Most of those models also offers routines for particle tracking [Pacanowski *et al.* 1991] [Mellor and Yamada 1982], but are not very convenient because the tracking calculations are usually made synchronously with the flow calculation. Given that an ocean flow simulation can take as much as one month on a supercomputer. Using pre-processed current flows provides a more flexible way to perform simulation of different scenarios. The separation between the tracking and the flow calculation also enables the use of any other data sets. To facilitate the use of the ocean circulation model, JeoSim provides a software interface for management of ocean model initialization data (bathymetry, temperature, salinity fields and wind stress). The biggest originality of the software lies in the particle tracking module. Because the purpose of this software is to simulate biological systems, Jeosim is not a straightforward Lagrangian particle tracking simulator, but includes interfaces with GIS, and the possibility to integrate particle tracking into cross scale models.

2.1 Modelling methodology

Jeosim is a tool designed for ecosystem modellers. Therefore, the user should focus only on modelling, while the associated simulation is generated automatically.

To do so, it is important to base the separation between modelling and simulation on a strong formal basis. This ensures that the model can be verified analytically, and that the traduction between the model and the simulation is mathematically correct.

The mathematical foundations of our discrete events approach lies in Systems Theory. The basics has been developed by Zeigler in the discrete event system specification (DEVS) formalism [Zeigler 1990]. In this formalism, models are constructed in a modular and hierarchical manner. DEVS formalism is based on the use of two kinds of models: basic and coupled. Basic models describe the behavior of basic system entities. Coupled models correspond to the structure and contain basic and coupled models as well as the link between them. Both basic and coupled models can be used as model components.

A basic DEVS model *BM* is a structure :

$BM = \langle X,S,Y, d_{\text{int}}, \mathbf{t}_a, d_{ext}, \lambda \rangle$, where:

- X: {(*p*,*v*)|(p∈ input ports, v∈ Xp)} is the set of input ports and values for the reception of external events,
- Y: {(*p*,*v*)|(p∈ output ports, v∈ Yp)} is the set of output ports and values for the emission of events,
- *S* is the set of internal sequential states,
- $d_{\text{int}} : S \rightarrow S$ is the internal transition function that will move the system to the next state after the time returned by the time advance function,
- $\mathbf{t}_a : S \rightarrow R^+$ is the time advance function, that will give the life time of the current state (returns the time to the next internal transition),
- $d_{ext} : Q \times X \rightarrow S$ is the external transition function that will schedule the states changes in reaction to an input event,
- $\lambda : Q \times X \rightarrow S$ is the output function that will generate external events just before the internal transition takes place.

The dynamic interpretation is the following:

- $Q = \{(s,e) | (s \in S, 0 < e < ta(s)\}$ is the total states set and parameter.
- *e* is the elapsed time since last transition, and s the partial set of states for the duration of *ta*(*s*) if no external event occur.

- δ_{int} : the model being in a state *s* at *ti*, it will go into *s'*, *s'* =δ_{int}*(s)*, if no external events occurs before *ti* + *ta*(*s*).
- δ_{ext} : when an external event occurs, the model being in the state *s* since the elapsed time *e* goes in *s'*, *s'* =δ_{ext}*(s,e,x)*.
    - The next state depends on the elapsed time in the present state.
    - At every state change, *e* is reset to 0.
- λ : the output function is executed before an internal transition, before emitting an output event the model remains in a transient state. A state with an infinite life time is a passive state (steady state), else, it is an active state (transient state). If the state *s* is passive, the model can evolve only with an input event occurrence.

The coupled DEVS model CM is a structure :

$CM = < X,Y,D,\{ M_d \in D \},EIC,EOC,IC >$, where:

- *X* is the set of input ports for the reception of external events,
- *Y* is the set of output ports for the emission of external events,
- *D* is the set of components (coupled or basic models),
- M_d is the DEVS model for each $_d \in D$,
- *EIC* is the set of input links, that connects the inputs of the coupled model to one or more of the inputs of the components that it contains,
- *EOC* is the set of output links, that connects the outputs of one or more of the contained components to the output of the coupled model,
- *IC* is the set of internal links, that connects the output ports of the components to the input ports of the components in the coupled models.

In a coupled model, an output port from a model $M_d \in D$ can be connected to the input of another $M_d \in D$ but cannot be connected directly to itself. Both coupled and basic models can stand alone and are stored in a models library for reuse and archiving.

A very important point for ecosystem modellers is that models specified in DEVS can be automatically simulated. To each component of a given model is attached a generic simulation component. The simulation process is driven by messages exchange between ports in order to generate output events from inputs of the studied system. In itself, the formalism is not adapted to suit specific needs, but it can easily be extended. Next section presents the adaptation of DEVS for spatially explicit models such as treated by JeoSim.

2.2 **DEVS formalism adapted to spatially explicit models**

The adapted method to suit spatially explicit models method consists in modelling each component of the studied system separately [Acquaviva *et al.* 2004]. The system is represented with thematic layers communicating if necessary for the simulation. This is similar to the GIS representation of a system where several layers, each representing a specific point of view of the reality, are superposed to represent the whole system. With this representation, a specialist of each discipline involved in the study can work in his own field of knowledge and model a part of the system. In this approach, the models that are developed are just automatically coupled. It implies an efficient tasks distribution, a simplified reuse of existing models and a more targeted reengineering process, see [Filippi and Bisambiglia 2003] for details about the software. Figure 1 represents the Object Oriented Architecture of the Software. In the specific problem a particle derives from a GeoAtomic model, which is a model with spatial attributes. Each particle/geoatomic model is associated to a simulator and the coupled models that contain those Geoatomics also have data layers that drive the simulation.

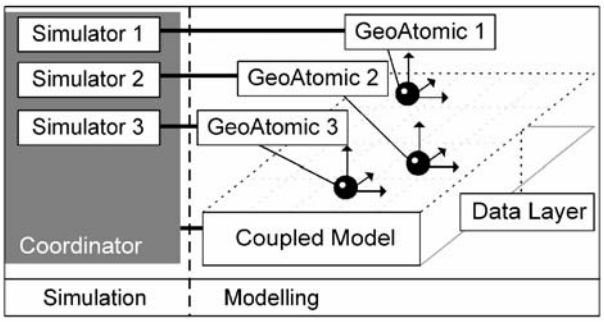

Figure 1: Architecture of the system

Thanks to the use of a strong theoretical base and the open architecture, JeoSim can be easily extended to include other biological processes that could occurs at different time and space scales. The next section presents in detail such adaptation for the case of the algae model.

2.3 The DEVS *Sargassum* algae model

A patch of algae is treated as a particle, that has a specific location, area and biomass. It has the following DEVS structure :

- X: {(*p*,*v*)|(p{*speed*}, v{*x-speed*,*y-speed*,*z-speed*})}
- Y: {(*p*,*v*)|(p{position, status},*v*{x, y, z}{attached, floating, sinking})}
- *S*:{*attached*,*floating*,*sinking*},*parameters*{*x*,*y*,*z*,*biomass*,*area-size*} ,
- δ_{int} : $S \rightarrow S$ updates position, and move to the next sequential state if appropriate.
- $\mathbf{t}_a$: $S \rightarrow R^+$ returns the time to next position update, or next state change,
- δ_{ext} : $Q \times X \rightarrow S$ receives new speed information in case of position or state update,
- λ : $Q \times X \rightarrow S$ outputs new position and state. Next section presents the particle tracking algorithm adapted for the algae dispersion model.

Next section presents the particle tracking algorithm adapted for the algae dispersion model.

3 Lagrangian discrete event particle-tracking trajectory model

JeoSim calculates trajectories based on the assumption that behavior of drifting Seaweeds, like oils pills, can be idealized by a large number of particles that moves in three dimensions in a water body by advection and spreading dynamics.

To determine the advective velocity field, JeoSim uses the 3D sigma coordinates Princeton Ocean Model [Mellor and Yamada 1982], that simulates ocean current, surface elevation, temperature, salinity and wind stress. The Princeton Ocean Model has been extensively tested and validated for the simulation of sea currents problems [POM 2005].

The velocities resulting from the hydrodynamic model is later used by the spread model to compute trajectories. The Lagrange particle tracking trajectory algorithm is based on the following vector equation:

$$\frac{\mathrm{d}\mathbf{x}_i}{\mathrm{d}t} = \mathbf{v}_a(\mathbf{x}_i, t) + \mathbf{v}_d(\mathbf{x}_i, t)$$

Where $\mathbf{x}_i$ is the I particle coordinate, $\mathbf{v}_a$ the advective velocity at the particle coordinate, and $\mathbf{v}_d$ is the random velocity fluctuation. The hydrodynamic model determines the advective velocities at discrete times, tn for t = 0..n and store it in a NetCDF [Unidata 2004] file for easy storing and analysis. The method most frequently used to solve is the system of Ordinaries differential equations is the Euler method. Generally, it is implemented in the following way:

$$\mathbf{x}_i^{n+1} \cong \mathbf{x}_i^n + \Delta t\left[\mathbf{v}_a(\mathbf{x}_i^n, t^n) + \mathbf{v}_d(\mathbf{x}_i^n, t^n)\right]$$

Where Δt is the time step, and n is the time index such that $tn = n\Delta t$. This method is first order accurate, and particle tracking trajectories may diverge greatly from real ones as times advances unless Dt is very small.

A very common method for achieve a better accuracy at an equivalent time stepping, is to use a trapezoidal approximation, which, uses a prediction-correction scheme such as:

(predictor) $\mathbf{x}_i^{n+1*} = \mathbf{x}_i^n + \Delta t[\mathbf{v}_a(\mathbf{x}_i^n, t^n)]$

(corrector) $\mathbf{x}_i^{n+1} \cong \mathbf{x}_i^n + \frac{\Delta t}{2}[\mathbf{v}_a(\mathbf{x}_i^n, t^n) + \mathbf{v}_a(\mathbf{x}_i^{n+1*}, t^{n+1}) + \mathbf{v}_d(\mathbf{x}_i^n, t^n) + \mathbf{v}_d(\mathbf{x}_i^{n+1*}, t^{n+1})]$

Nevertheless, in highly non uniform flows, such as found in oceans, this method stills require a relative small time step to keep a good accuracy in zones of high speed currents. One way to overcome this limitation, is the use of discrete event simulation, where there is no fixed time step, and the calculation is made instead for a step size Δq. Here *n* is an event index, and corresponds to an iteration with n = 0,1,2,3,.. being trajectories iterations indices. At each iteration, the time advance estimate, ta is computed to be the time taken by the particle to travel the distance Delta q. After each iterations, local time at the particle is updated to be tnext = t+ta.

With the trapezoidal rules, this gives the following implementation :

(step predictor)

$$t_a^* = \frac{\Delta q}{\mathbf{v}_a(\mathbf{x}_i^n, t)}$$

(predictor)

$$\mathbf{x}_i^{n+1*} = \mathbf{x}_i^n + t_a^*[\mathbf{v}_a(\mathbf{x}_i^n, t)]$$

(step estimate)

$$t_a = \frac{2\Delta q}{\mathbf{v}_a(\mathbf{x}_i^n, t^n) + \mathbf{v}_a(\mathbf{x}_i^{n+1*}, t+t_a)}$$

(corrector)

$$\mathbf{x}_i^{n+1} \cong \mathbf{x}_i^n + \frac{t_a}{2}[\mathbf{v}_a(\mathbf{x}_i^n, t^n) + \mathbf{v}_a(\mathbf{x}_i^{n+1*}, t+t_a) + \mathbf{v}_d(\mathbf{x}_i^n, t) + \mathbf{v}_d(\mathbf{x}_i^{n+1*}, t+t_a)]$$

4 Spreading calculations

Random velocities are obtained by random sampling in the range of velocities [-Ur, Ur], [-Vr, Vr] [-Wr, Wr] to simulate spreading of seaweed patches. Those ranges are assumed to be proportional to diffusion coefficients in x, y and y. Velocities diffusion has been estimated from a study from [Bograd *et al.* 1999], which uses satellites tracking of drifters in the northern Pacific to perform empirical estimates of diffusion coefficients. The relative diffusion coefficient is expressed by the following Formula: Du = Ur/U(rms) and Dv = Vr/V(rms). [Bograd *et al.* 1999] found an average Du to be 0.1 and Dv = 0.08. In the model, Dw = Wr/W(rms) is given by the mortality and loss of floatability of the seaweed. Therefore, it is not assumed to have additional random motion, because the mortality distribution in itself is random.

This extensive survey also suggest that the use of those overall diffusion coefficient are of a sufficient approximation for modelling studies. The general equation for Euler with dispersion is Vd= (Vx + Vd)/ dt. To estimate Vd, we then apply the diffusion coefficient to the RMS speed obtained from the flow calculation.

5 Numerical Experiments

The purpose of this section is to show and calculate the difference between Euler method, trapezoidal approximation, discrete Event and discrete time. To be able to verify the results against analytical ones, we neglect the diffusion coefficients in (1) the dispersion would only be dependant of the precision algorithm and truncation errors. The numerical experiment consist of a Lagrangian resolution of the circle equation. The analytical solution in this velocity field is :

$x_e(t) = \exp(at)[x_0 \cos bt - y_0 \sin bt]$

$y_e(t) = \exp(at)[x_0 \sin bt - y_0 \cos bt]$

Where x0 and y0 are initial position, and xe(t) and ye(t) are position at time t.

Figure 2a) presents the velocity field for a = 0 and b = 0.001, corresponding to a circular rotating flow, and the analytical solution of the particle path at a radius of 1000.

Figure 2b) presents the tracking in discrete time with Euler using dT of 60 seconds. It is clear that the Euler method causes an outward drift of particles with an error that is dependant of the flow speed.

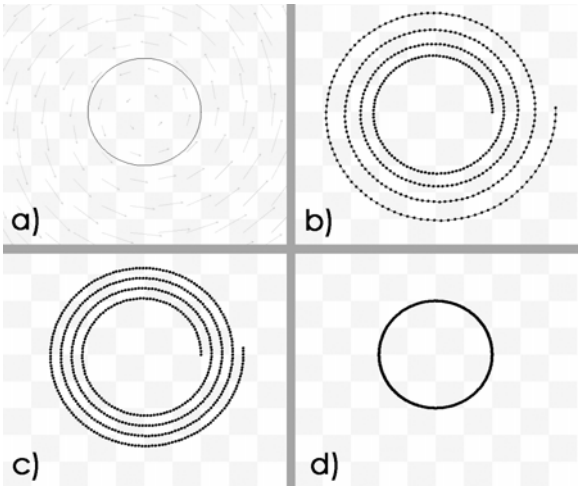

Figure 2: Particle trajectory simulation, a) Analytical solution, b) Euler resolution in discrete time, Dt = 60 seconds, c) Euler resolution in discrete event, Q = 60m, d) Euler resolution with trapezoidal interpolation, in discrete event, q = 60 meters

Figure 2c) presents the particle path with Euler, but in a discrete event Fashion, with a quantum of 60 meters, that means an original time step of 60 s (with speed = 1m/s), equal to the one shown in figure 2b). We can see from this figure, that here the error is independent of the flow speed, because whatever the flow speed is, the particle moves the same distance. This also means that the error would be high if compared with discrete time in areas where the flow speed is slow, because the calculations would be less frequent. Nevertheless using Discrete event simulation is interesting in turbulent flows, because the variability of the flow speed is high in space, but small in time. Using this technique will always keep the numerical errors within the same interval whatever the flow speed is. Numerically exaggerated diffusion is here of 500 meters after 3.5 hours, and 1200 Meters after 7 hours.

Figure 2d) presents the particle Path with the trapezoidal interpolation, in discrete event, with a quantum of 60 meters, that shows a path resolution almost identical to the analytical solution. This kind of resolution greatly limits the need for a big quantum, and is particularly well suited to be used in conjunction with discrete event simulation because the trapezoidal evaluation will be make with trapezoids of the same size, ensuring here too that the error is kept independent of the flow speed.

Euler method, like the trapezoidal approximation method provides no error in continuous flow, nevertheless in turbulent flows, such as found in Ocean. It is important to minimize the error and assume it the most constant over the surface to be able to quantify it, whatever the flow speed is. For it is assumed that the association of a discrete event simulation with trapezoidal Euler approximation is a good tradeoffs between computational efficiency and robustness. The next section presents the application of the algorithm into marine science through the simulation of seaweed propagation in East China Sea.

6 **Application**

In this section, Jeosim is applied to predict *Sargasso* distribution in East China sea. The aim of the simulation experiment is to have a better understanding of the *Sargasso* Path and validate the model and diffusion coefficients thanks to observation made onboard of the RV Hako-Maru (main research boat of the Ocean Research Institute) in march 2000. The Ocean Circulation simulation has been performed using the Princeton Ocean Model, a curvilinear sigma coordinates model that is very broadly used for flow calculations. The grid is 150 cells wide, 80 high and has 20 levels. With a spacing of 34.4 minutes per cell horizontally and 27.75 vertically on the grid. The studied region is bounded by 114 degrees east, 20 degrees west for longitudes and 5 degrees north, 42 degrees north for latitude. The model has been spinned up using boundaries condition provided by NCEP current reanalysis project [NCEP 2004]. NCEP data has been used to initialize the fields at a lower resolution, then run the simulation with flows updated at every time step from the NCEP dataset. Figure 3 presents the boundaries conditions used, the shaded area is the current data available in the NCEP dataset, while Yellow and Japan sea

currents are simulated. The bottom topography is the smoothed data from the National Geophysical Data Center database with 2 minute resolution (ETOPO2). The horizontal diffusivities are modelled using the Smagorinsky (1963) [Smagorinsky 1963] form with the 0.2 coefficient chosen for this application. The bottom stress is assumed to follow a quadratic law

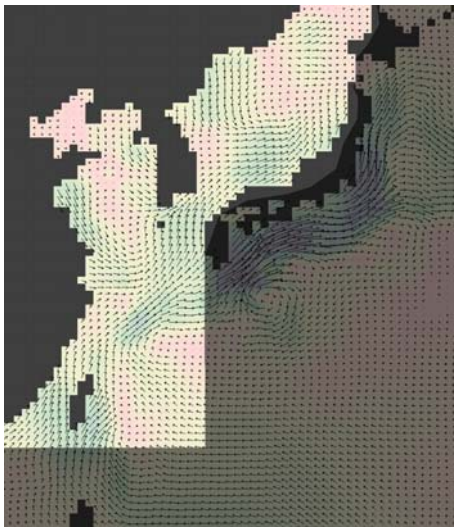

Figure 3: Simulated current (January 2001) and boundaries conditions of the Ocean current model

The currents in the shaded area are loaded and interpolated from the dataset at every time step for a period of 5 years, then the simulation is run using wind stress from NCAR reanalysis project [NCEP/NCAR 2004], and Levitus [Levitus 1982] Temperature and salinity field for two other years. The results retained are the calculations of the last simulated year, with weekly variability.

The particle tracking routines module is used thereafter to calculate the seaweed trajectories in the Kuroshio/Oyashio Region . Figure 4 shows an example of trajectories simulated using the two different schemes, but an equal amount of transitions. It appears that the discrete time method (Figure 4a)) is less accurate in high speed flows, resulting in an exaggerated drift. The discrete event method accuracy is independent of the current speed, and does not show an the exaggerated drift(Figure 4b)). In fact, most of the transitions of the discrete time simulation occurred in very slow current areas. This region is knows to be a trap in the pacific ocean [Hurlburt *et al.* 1996], where floating elements can stay up to two years. Using a discrete event method here might require a very small time step not to suffer from an exaggerated drift that might push the elements out of the current earlier than expected (Figure 4a)). Once diffusion is added to the model, several thousands of trajectories has to be calculated in parallel in order to represent the possible pathes of the particles, for this reason, the discrete event method seems to be the most appropriate.

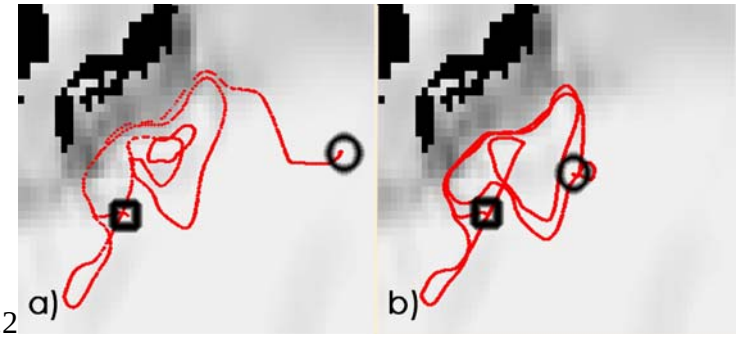

Figure 4: Six month trajectory simulation without diffusion, a) Euler method/discrete time, b) Trapezoidal interpolation method/ discrete event. Square represents the start position, circle the end position, shading shows the absolute flow speed.

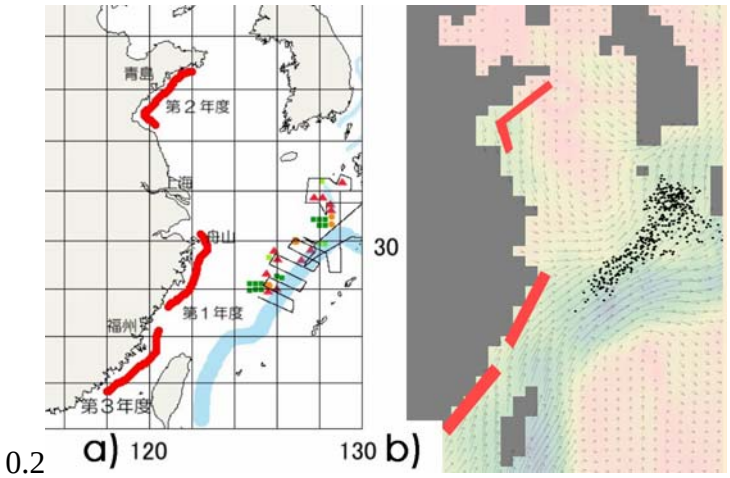

Figure 5: a) Distribution of drifting seaweeds in East China sea (circle squares and triangles maps to different *Sargassum* species). Coastal strokes corresponds to the supposed *Sargassum* origin, while the marine stroke represents the hot Kuroshio current flowing to the north east. b) Particles dispersion in east China sea (black dots), after 75 days of simulation using jeosim starting from March 15. Stokes corresponds to the release zones, shading represents the absolute flow speed.

The Laboratory of Behavior, Ecology and Observation Systems at the Ocean Research Institute (University of Tokyo) filed observation in the East China Sea using R/V Hakuho-Maru. They mapped geographical distribution of drifting seaweeds and collected samples of drifting seaweeds to detect the species. Figure 5a) shows the distribution of *Sargassum* in the East China Sea (triangles, squares and circles) as found by the Laboratory in May 2002. Origin of *Sargassum* species newly found as drifting seaweeds are thought to be geographically limited around Chinese coast in the East China Sea.

Figure 5b) presents the results of the simulation with a release date of 15 February, and a particle lifetime of 90 days. The numerical simulation using Jeosim provides results that prove to be very similar to the observation. In particular, it shows that the seaweeds are distributed on a path that is more north than the observation, which provides a good hint on where should be performed next observation.

7 Conclusion

This report has introduced a new combination of techniques that proves to be very well suited for the modelling of drifting ecosystems. The first advantage is that it directly uses the current fields calculated from the ocean circulation model. Currents are simulated only once, and particle tracking is made using the generated vector fields. Using subroutines integrated into the Ocean Model greatly limits the number of experiments and the ease of use because each time particle tracking is performed, currents have to be re-calculated, an ocean current simulation can takes up to 2 months. The second advantage is that the software is discrete event based, and not discrete time base, that means that the simulation has no time steps. Instead of calculating the distance travelled by a given particle for a fixed time, we calculate how long it takes for a particle to travel a fixed distance (like finite elements method). From a marine ecology point of view, the outcome of the research can be rather interesting because it will allow to study the *Sargassum* species that can be rather invasive and become an ecological problem. Future versions of the software will integrate the possibility to add a more complex behavior for the particles to represent the nesting of fish under those algae.

Acknowledgements

This research is supported by the Japanese Society for the promotion of Science.

References

[Acquaviva *et al.* 2004] Acquaviva, J., Filippi, J., and Bisgambiglia, P. (2004). A multi-layered modeling and simulation architecture. In *International Mediterranean Modeling Multiconference"*. CD-ROM, GISIG, Genoa, IT.

[Bennett and Clites 1987] Bennett, J. and Clites, A. (1987). Accuracy of trajectory calculation in a a finite-diference circulation model. *J. Comp. Phys.*, **68**(2), 272–282.

[Bograd *et al.* 1999] Bograd, S., Thomson, R., Rabinovich, A., and LeBlond, P. (1999). Near-surface circulation of the northeast pacific ocean derived from woce-svp satellite-tracked drifters. *Deep-Sea Research Part II*, **46**(11-12), 2371–2403.

[Filippi and Bisambiglia 2003] Filippi, J.-B. and Bisambiglia, P. (2003). Jdevs :an implementation of a devs based formal framework for environmental modelling. *Environmental modelling and Software*. A paraître, disponible sur http://www.sciencedirect.com.

[García-Martínez and Flores-Tovar 1999] García-Martínez, R. and Flores-Tovar, H. (1999). Computer modeling of oil spill trajectories with a high accuracy method. *Spill Science and Technology Bulletin*, **5**(5-6), 323–330.

[Hurlburt *et al.* 1996] Hurlburt, H., Wallcraft, A., Schmitz, W., Hogan, P., and Metzger, E. (1996). Dynamics of the kuroshio/oyashio current system using eddy-resolving models of the north pacific ocean. *Journal of Geophysical Research*, **101**(10), 941–976.

[Levitus 1982] Levitus, S. (1982). *Climatological atlas of the world ocean*. U. S. Government Printing Office.

[Mellor and Yamada 1982] Mellor, G. and Yamada, T. (1982). Development of a turbulence closure model for geophysical fluid problems. *Rev. Geophys. Space Phys*, **20**(4), 851–875.

[NCEP 2004] NCEP (2004). Ncep pacific ocean analysis. http://www.cdc.noaa.gov/cdc/data.ncep.pac.ocean.html.

[NCEP/NCAR 2004] NCEP/NCAR (2004). The ncep/ncar reanalysis project. http://www.cdc.noaa.gov/cdc/reanalysis/.

[Pacanowski *et al.* 1991] Pacanowski, R. C., Dixon, K., and Rosati, A. (1991). The gfdl modular ocean model user guide. *Technical Report, Princeton Geophysical Fluid Dynamics Laboratory*, **1**(2), 16.

[POM 2005] POM (2005). Priceton ocean model homepage, and pom applications. http://www.aos.princeton.edu/WWWPUBLIC/htdocs.pom/.

[Reynolds 2003] Reynolds, A. (2003). On the nonextensive statistical mechanics of tracer-particle motions in turbulence. *Physical Review Letters*, **91**. article 84503.

[Smagorinsky 1963] Smagorinsky, J. (1963). General circulation experiments with the primitive equations: I. the basic experiment. *Monthly Weather Review*, **91**, 99–164.

[Unidata 2004] Unidata (2004). Network common data form. http://my.unidata.ucar.edu/content/software/netcdf/.

[Zeigler 1990] Zeigler, B. (1990). *Object-Oriented Simulation with Hierarchical, Modular Models*. Academic Press.

A global eddy-resolving coupled physical-biological model: Physical influences on a marine ecosystem in the North Pacific

Yoshikazu Sasai
Frontier Research Center
for Global Change,
Japan Agency for Marine-Earth
Science and Technology
3173-25 Showa-machi,
Kanazawa-ku, Yokohama,
236-0001, Japan
+81 45 778 5575
ysasai@jamstec.go.jp

Akio Ishida
Frontier Research Center
for Global Change
Japan Agency for Marine-Earth
Science and Technology
ishidaa@jamstec.go.jp

Hideharu Sasaki
Earth Simulator Center,
Japan Agency for Marine-Earth
Science and Technology
sasaki@jamstec.go.jp

Shintaro Kawahara
Earth Simulator Center,
Japan Agency for Marine-Earth
Science and Technology
kawahara@jamstec.go.jp

Hitoshi Uehara
Earth Simulator Center,
Japan Agency for Marine-Earth
Science and Technology
uehara@jamstec.go.jp

Yasuhiro Yamanaka
Frontier Research Center
for Global Change,
Japan Agency for Marine-Earth
Science and Technology
galapen@jamstec.go.jp

ABSTRACT
Physical influences on a marine ecosystem in the open ocean are investigated using a simplified four-component ecosystem model embedded in an eddy-resolving ocean general circulation model (OGCM). Annual cycle of temperature, nitrate, and phytoplankton in the upper ocean is well reproduced with the climatological monthly mean forcing. A comparison with satellite ocean color data shows that the model is capable of a realistic description of the annual mean and regional patterns of surface chlorophyll. Simulated chlorophyll distribution at the surface shows a pattern influenced by the western boundary current (Kuroshio) and the meso-scale eddy. Nitrate distribution in the upper ocean in the Northwestern Pacific is mainly controlled by physical processes, especially meso-scale variability, including many anticyclonic and cyclonic eddies, fine scale fronts and filaments. The warm-core eddy entrains high-nitrate water from the surrounding filaments, creating condition for the spring.

KEYWORDS
Marine ecosystem, Physical processes, Eddy-resolving OGCM, North Pacific

1. Introduction

Marine ecosystems play important roles in global biogeochemical cycles. Dissolved CO_2 is converted from inorganic to organic carbon by the photosynthesis of the phytoplankton. Some of this organic carbon is exported from the euphotic zone into the deep ocean. The corresponding reduction of CO_2 in the surface ocean modulates the difference in partial pressure of CO_2 between the atmosphere and the surface ocean.

The conditions for biological production in the open surface ocean depend on the following major physical factors. Light is one controlling factor for biological production. Transport and mixing processes (e.g., winter convection, upwelling, diapycnic diffusion, and eddy-induced vertical motions) supply high nutrients from the deep layer into the euphotic zone. In winter season, the deepening of the mixed layer in mid-latitude and high-latitude regions supplies the nutrients from deep to the surface ocean. These features largely determine what types of phytoplankton develop and how much biological production occurs in the world ocean.

Distribution of nutrients and patterns of biological production are influenced by the physical processes, which vary from global to frontal scales. The first basin-wide simulation of the ecosystem in the North Atlantic presented by [Fasham *et al.* 1993] and [Sarmiento *et al.* 1993] is more realistic description of the physical environment. They used a seven-component nitrogen-based ecosystem model embedded in a general circulation model (coarse-resolution 2º) to investigate the physical-biological interactions that impact biogeochemical budget. However, these models could not investigate the role of meso-scale variability because of limited horizontal resolution. The eddy enhancement of export production over the basin scale has been examined using a simple four-component nitrate-phytoplankton-zooplankton-detritus (NPZD) ecosystem model coupled with an eddy-permitting (1/3º) resolution model [Oschlies Garçon 1999; Oschlies *et al.* 2000; Oschlies 2001] and an eddy-resolving (1/9º) model [Oschlies 2002]. Eddy-permitting and eddy-

resolving models improved the model physics and clearly reproduced the aspect of seasonal cycle of surface chlorophyll, especially the spatial pattern in mid and high latitudes and in coastal upwelling regions [Oschlies *et al.* 2000; Oschlies 2002]. By increasing horizontal resolution, the enhancement of export production is principally achieved through an eddy vertical transfer around the Gulf Stream and an eddy horizontal transfer along the flanks of the subtropical gyre [Oschlies 2002]. For the North Pacific, [Kawamiya *et al.* 2000] compared the simulated distribution of biological variables with the observation using an ecosystem model coupled with a general circulation model. [Hashioka *et al.* 2004] used a 3-D ecosystem-biogeochemical model to investigate the seasonal and horizontal variations of phytoplankton groups in the western North Pacific.

In this study, we simulate the seasonal variability of marine biology in the upper ocean using climatological forcing in an eddy-resolving (1/10º) general circulation model [Masumoto *et al.* 2004]. The ocean general circulation model is optimized and modified with the parallelization procedures for the Earth Simulator. The model can be run on the Earth Simulator for 50 model years within a month of wall-clock time. We investigate the physical influences on the biological production in the North Pacific by simulating realistic meso-scale variability, including the western boundary currents and meso-scale eddies.

2. Model Description

2.1. Physical Model

We used an eddy-resolving ocean model for the Earth Simulator (OFES) [Masumoto *et al.* 2004], which is based on the Geophysical Fluid Dynamics Laboratory's Modular Ocean Model (MOM3) [Pacanowski Griffies 2000]. The domain of this model covers from 75ºS to 75ºN with a horizontal grid spacing of 1/10º. There are 54 vertical levels, with varying distance between the levels from 5 m at the surface to 330 m at the maximum depth of 6,065 m. The model topography is constructed from the 1/30º bathymetry dataset created by the OCCAM Project at the Southampton Oceanography Centre.

A scale-selective damping of bi-harmonic operator is adopted for horizontal mixing of the momentum and tracers, to suppress computational noise with the horizontal scale of the grid spacing. The viscosity and diffusivity vary in space with the coefficients proportional to the cube of the zonal distance between the grids. The background horizontal bi-harmonic viscosity and diffusivity are -27×10^9 m^4 s^{-1}and -9×10^9 m^4 s^{-1}, respectively. For the vertical mixing, the KPP boundary layer mixing scheme [Large *et al.* 1994] is employed.

Monthly mean wind stresses averaged from 1950 to 1999 from the NCEP/NCAR reanalysis data are used for the climatological seasonal integration. The surface heat flux is calculated by the same bulk formula as in [Rosati Miyakoda 1988], using the monthly mean value from the NCEP/NCAR reanalysis outputs for the necessary datasets. Sea surface salinity is restored to the monthly mean climatological value of the World Ocean Atlas 1998 (WOA98). In the near polar regions (72º-75º), temperature and salinity are restored through the water column. The restoring time-scale is set to be 1 day at 75º. The model is integrated for 50 years from the annual mean temperature and salinity fields (WOA98) without motion [Masumoto *et al.* 2004].

2.2. Biological Model

The marine ecosystem model is a simple nitrogen-based Nitrate, Phytoplankton, Zooplankton, Detritus (NPZD) pelagic model [Oschlies 2001]. The evolution of any biological tracer concentration C_i in the OFES is governed by an advective-diffusive equation

$$\frac{\partial C_i}{\partial t} = -\nabla\cdot\left(uC_i\right)+\nabla\cdot\left(A\nabla C\right)+sms\left(C_i\right) \quad (1)$$

where the first term on the right-hand side account for advection, and the second term represents diffusion. Advection and diffusion are provided by the physical model (OFES). The last term is the source-minus-sink term due to biological activity. The biological model depicts in Figure 1. For the individual biological tracers, the source-minus-sink terms are given by

$$sms\left(P\right)=\overline{J}\left(z,t,N\right)P-G\left(P\right)Z-\mu_P P-\mu_{pp}P^2 \quad (2)$$

$$sms\left(Z\right)=\gamma_1 G\left(P\right)Z-\gamma_2 Z-\mu_Z Z^2 \quad (3)$$

$$sms(D) = (1-\gamma_1)G(P)Z + \mu_{pp}P^2 + \mu_z Z^2 - \mu_D D - w_S \frac{\partial D}{\partial t} \quad (4)$$

$$sms(N) = \mu_D D + \gamma_2 Z + \mu_P P - \bar{J}(z,t,N)P \quad (5)$$

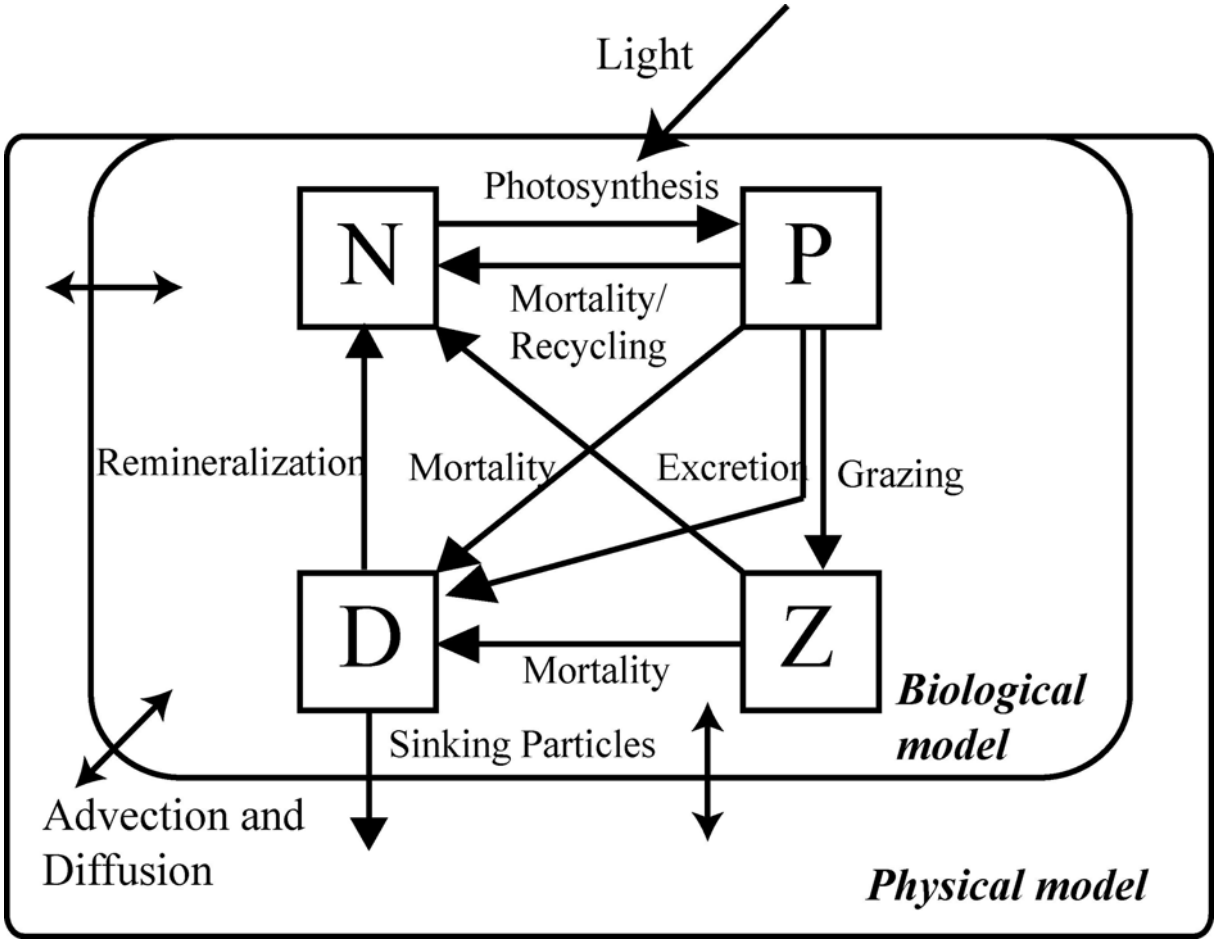

Figure 1. Schematic diagram of marine ecosystem in the physical model. See text for a description of ecosystem terms.

where $\bar{J}$ is the daily averaged phytoplankton growth rate as a function of depth z and time t, and G is the grazing function. Following [Hurtt Armstrong 1996], the phytoplankton growth rate is taken to be the minimum of light- and nutrient-limited growth,

$$\bar{J}(z,t,N) = \min\left(\bar{J}(z,t), J_{\max}\frac{N}{k_1+N}\right) \quad (6)$$

where $\bar{J}(z,t)$ denotes the purely light-limited growth rate averaged over 24 hours, and J_{max} is the light-saturated growth. $\bar{J}(z,t)$ is computed using the analytical method of [Evans Parslow 1985]. Following equation for zooplankton grazing [Fasham 1995] is,

$$G(P) = \frac{g\varepsilon P^2}{g+\varepsilon P^2} \quad (7)$$

The individual biological parameters are listed in Table 1.

Table 1. Parameters of the Marine Ecosystem Model

Parameter	Symbol	Value	Units
Phytoplankton (P) Coefficients			
Integration method for daily growth rate		*Evans and Parslow* [1985]	
Half saturation constant for N uptake	k_1	0.5	mmol m^{-3}
Specific mortality/recycling rate	μ_P	0.05	day^{-1}
Quadratic mortality rate	μ_{PP}	0.05	$(mmol\ m^{-3})^{-1}d^{-1}$
Zooplankton (Z) Coefficients			
Assimilation efficiency	γ_1	0.75	
Maximum grazing rate	g	2.0	day^{-1}
Prey capture rate	ε	1.0	$(mmol\ m^{-3})^{-2}d^{-1}$
(Quadratic) mortality	μ_Z	0.20	$(mmol\ m^{-3})^{-1}d^{-1}$
Excretion	γ_2	0.03	day^{-1}
Detritus (D) Coefficients			
Remineralization rate	μ_D	0.05	day^{-1}
Sinking velocity	w_S	5.0	$m\ d^{-1}$

The biological model is incorporated after the physical model is integrated for 50 years [Masumoto04]. The biological model coupled with the physical fields is integrated over a 5-year period. The initial nitrate field is taken from the climatological dataset (WOA98). The initial P and Z concentrations are set to 0.14 mmol N m^{-3} and 0.014 mmol N m^{-3} at the surface, respectively, decreasing exponentially with a scale depth of 100 m [Sarmiento *et al.* 1993]. D is initialized to 10^{-4} mmol N m^{-3} everywhere. Results are presented for the last one-year period (model years 55).

3. Results

Distribution of annual mean simulated chlorophyll concentration at the surface, compared with SeaWIFS sensor for annual mean of 2001, shows a pattern influenced by the western boundary current and meso-scale variability (Figure 2). The simulated phytoplankton concentration is converted to chlorophyll concentration using a ratio of 1.59 g chlorophyll per mol nitrogen. Overall, simulated chlorophyll distribution is in good qualitative agreement with observed chlorophyll, with low concentrations in the subtropical gyre and high concentrations in the upwelling and subpolar gyre. Simulated chlorophyll concentrations, however, are generally lower than the SeaWIFS data, especially off the coast and in the northern marginal seas (Okhotsk and Bering Seas).

The annual cycle of upper ocean temperature, nitrate, and phytoplankton concentrations at station A7 off Hokkaido, Japan (41º30'N, 145º30'E), in the Northwestern Pacific, is shown in Figure 3. This station is one of the stations along the A-line where the Hokkaido National Fisheries Research Institute has been conducting various cruises five or six times each year from 1987 [Saito *et al.* 1996]. The model clearly reproduces the annual cycle of temperature, nitrate, and phytoplankton concentrations in the subarctic North Pacific.

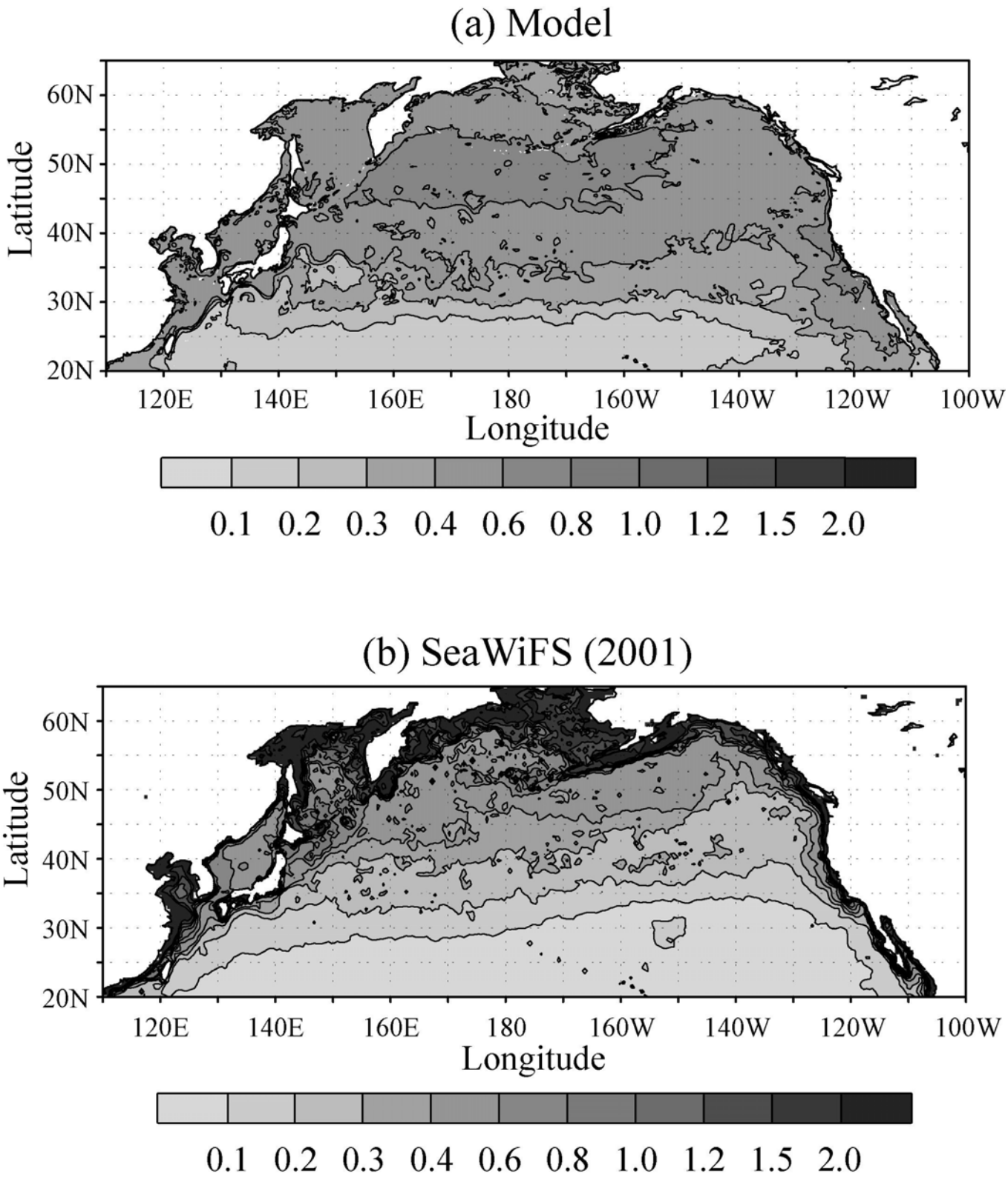

Figure 2. Comparison of (a) annual mean simulated chlorophyll concentrations in mg-Chl m^{-3} computed from nitrogen via a constant ratio of 1.59 g chlorophyll per mol nitrogen, with (b) the satellite SeaWIFS data.

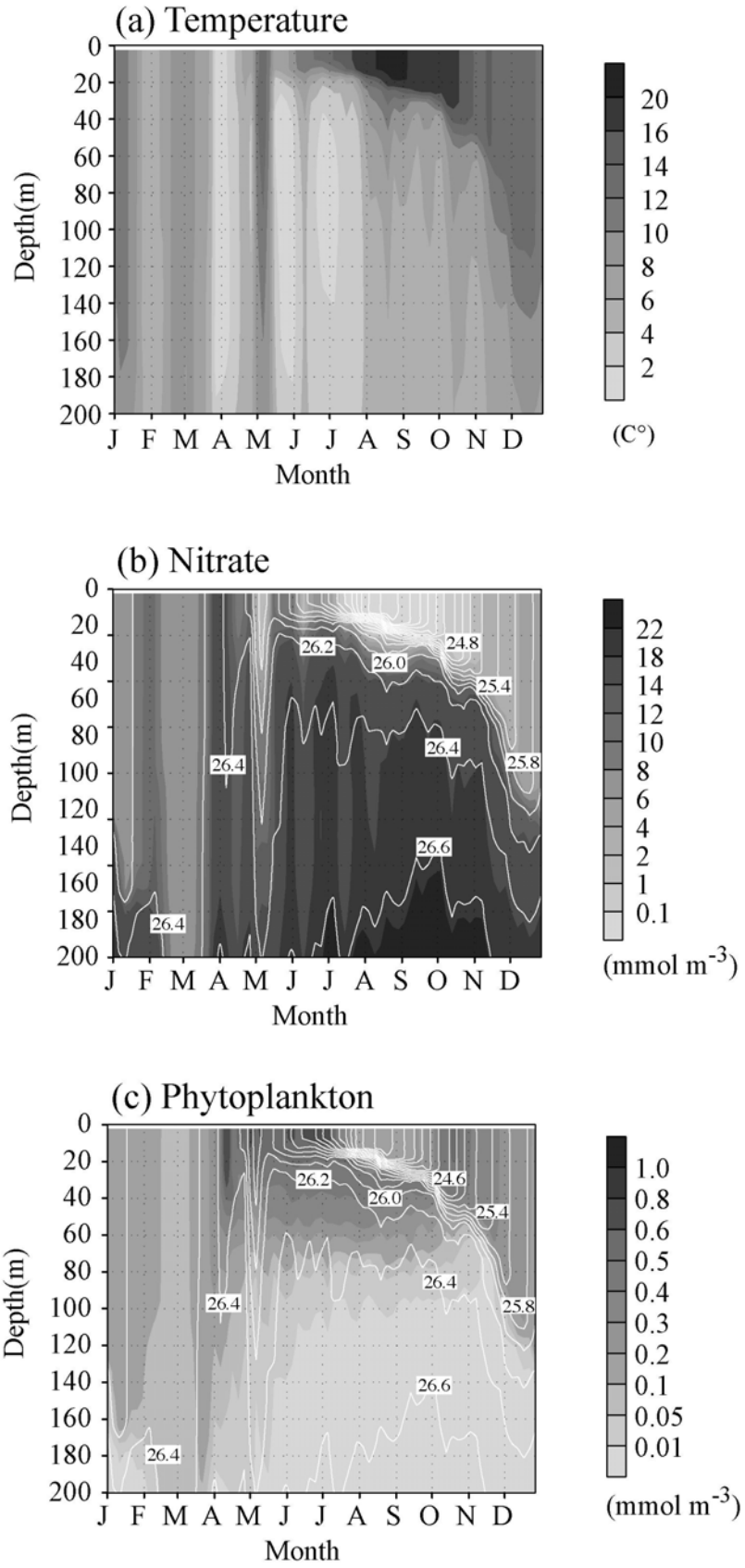

Figure 3. Vertical distributions of simulated (a) temperature (ºC), (b) nitrate concentration (mmol m^{-3}) and (c) phytoplankton concentration (mmol m^{-3}) at Station A-7 off Hokkaido, Japan (41º30'N, 145º30'E). Solid lines are potential density.

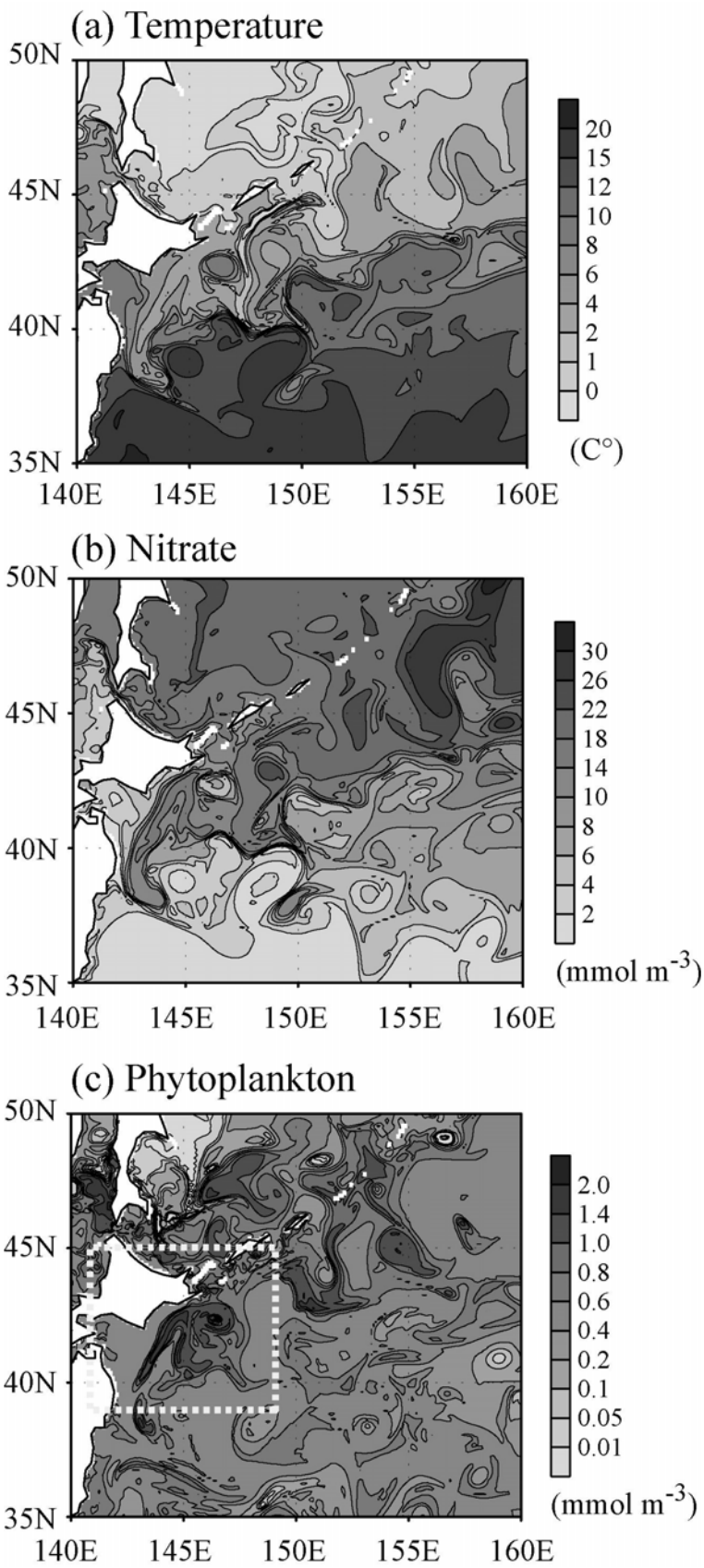

Figure 4. Snapshots of simulated (a) temperature (ºC), (b) nitrate concentration (mmol m^{-3}), and (c) phytoplankton concentration (mmol m^{-3}) at April, 11 in the northwestern Pacific. Dashed line area shows in Figure 5.

Simulated annual cycle of temperature, nitrate, and phytoplankton has almost the same range as observed in the Oyashio

region of the northwestern Pacific [Saito *et al.* 2002]. Simulated mixed layer depth (MLD) reaches to 260 m depth in winter season (Figure 3a). Before onset of spring bloom, high nitrate water is supplied by the winter MLD from lower to upper layer. Simulated nitrate concentrations reach maximum winter values of 18.0 mmol m^{-3} in the surface (Figure 3b). In April, a strong spring bloom occurs in this model (Figure 3c). Observed chlorophyll concentration reaches 5.6 mg m^{-3} at the surface, however, simulated chlorophyll is 1.3 mg-Chl m^{-3} (0.8 mmol m^{-3} x 1.59 g) during April to July. An ecosystem model coupled with a vertical one-dimensional mixed layer simulation reaches 4.6 mg-Chla m^{-3} during the spring bloom [Yamanaka *et al.* 2004]. In the subsurface (around 40 m depth), the maximum phytoplankton concentration occurs during summer season. Variability of potential density (solid lines in Figure 3b and 3c) shows the large physical influences, e.g., meso-scale variability.

Horizontal distribution of sea surface temperature (SST), nitrate and phytoplankton concentrations in the western North Pacific in April shows a typical pattern, which is influenced by the Kuroshio, the meso-scale eddy generation near the Kuroshio and Oyashio (Figure 4). Distribution of the simulated SST shows many anticyclonic and cyclonic eddies, fine scale fronts, and filaments in the Kuroshio Extension/Oyashio region (Figure 4a). Distribution of the simulated surface nitrate concentration is consistent with the simulated SST distribution (Figure 4b). The warm-core, anticyclonic eddy (42ºN, 146ºE) has low nitrate and the cold-core, cyclonic eddy (43ºN, 148ºE) has high nitrate. These eddies correlate with the Kuroshio and Oyashio. Simulated spring bloom occurs in the Oyashio region and the south of Okhotsk Sea (Figure 4c). This distribution is consistent with the simulated SST distribution below 4 ºC. In this region, the SST field may mainly control the pattern of phytoplankton concentration because there is enough nitrate concentration (14 - 18 mmol m^{-3}) for the spring bloom.

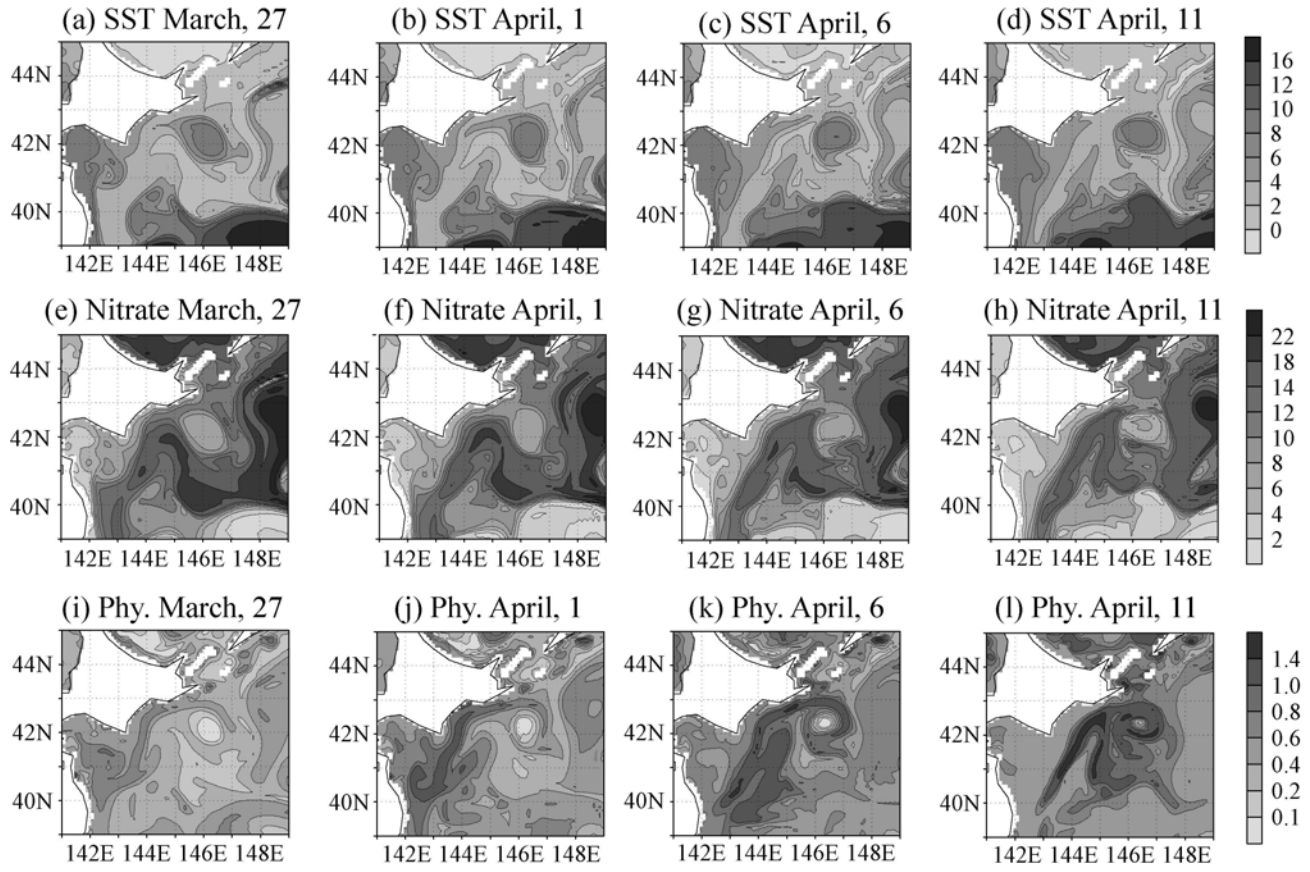

Figure 5. Snapshots of simulated surface (a)-(d) temperature (ºC), (e)-(h) nitrate concentration (mmol m^{-3}), (i)-(l) phytoplankton concentration (mmol m^{-3}) during spring in a subdomain off Hokkaido, Japan.

Snapshots of simulated SST, nitrate, phytoplankton concentrations are shown from March 27 to April 11 (Figure 5). The warm-core, anticyclonic eddy exists east off Hokkaido (42ºN, 146ºE). The length scale of the eddy is about 70 km and SST in the eddy remains above 10ºC (Figure 5a-d). High nitrate water spreads southward along the eddy (Figure 5e-h). The spring bloom begins close to coast of Japan (Figure 5i) and extends to eastern and northern regions (Figure 5j-l). Phytoplankton concentration along anticyclonic filaments around the eddy increases from 0.1 to 1.4 mmol m^{-3}. The high

nutrient supplied by the filament may play a role in this increase of phytoplankton around the anticyclonic eddy.

4. Conlusion

Fine-resolution models, such as an-eddy resolving global circulation models (e.g., OFES), drives the biological productivity controlled by the variable physical processes from the global to meso-scale. We investigated the physical influences on a marine ecosystem using a simple NPZD model coupled with the OFES. OFES illustrates that the spatial and temporal patterns of biological productivity are influenced by the western boundary current, meso-scale eddies, fine scale fronts and filaments in the North Pacific. Many anticyclonic (warm-core) and cyclonic (cold-core) eddies were generated along the Kuroshio, which is a strong western boundary current in the North Pacific. The ecosystem responds to the uplift and depression of the nutricline by these eddies. In the model, anticyclonic eddies take in high-nitrate water from the surrounding area and increase biological productivity around eddies. Using global eddy-resolving coupled physical-biological model, it is possible to capture the effects of relevant physical dynamics, such as the frontal and meso-scale variability, on the marine ecosystem. This paper focuses on the seasonal variability of marine biology in the upper ocean using OFES. Detailed analysis of the results from the model and investigation of the biological variability with the climate change remain as future work.

ACKNOWLEDGMENTS

We thank Drs. Masumoto, Kagimoto, Tsuda, Kanazawa, and Kitawaki for their efforts to develop the OFES on the Earth Simulator.

REFERENCES

[Evans 1985] Evans, G.T., and J.S.Parslow, A model of annual plankton cycles, *Biol. Oceanogr.,* **3**, 328-347, 1985.

[Fasham 1995] Fasham, M.J.R., Variations in the seasonal cycle of biological production in subarctic oceans: A model sensitivity analysis, *Deep Sea Res. I,* **42**, 1111-1149, 1995.

[Fasham 1993] Fasham, M.J.R., J.L.Sarmiento, R.D.Slater, H.W.Ducklow, and R.Williams, Ecosystem behavior at Bermuda Station ``S" and Ocean Weather Station ``India": A general circulation model and observational analysis, *Global Biogeochem. Cycles,* **7**, 379-415, 1993.

[Large 1994] Large, W,G., J.C.McWilliams, and S.C.Doney, Oceanic vertical mixing: A review and a model with a nonlocal boundary layer parameterization, *Rev. Geophys,* **32**, 363-403, 1994.

[Hashioka 2004] Hashioka, T., and Y.Yamanaka, Seasonal and regional variations of phytoplankton groups by top-down and bottom-up controls obtained by 3-D ecosystem model, *Ecological Modeling,* submitted, 2004.

[Hurtt 1996] Hurtt, G.C., and R.A.Armstrong, A pelagic ecosystem model calibrated with BATS data, *Deep Sea Res. II,* **43**, 653-683, 1996.

[Kawamiya 2000] Kawamiya, M, M.J.Kishi, and N.Suginohara, An ecosystem model for the North Pacific embedded in a general circulation model Part I: Model descriptions of biological variables, *J. Mar. Sys.,* **25**, 129-157, 2000.

[Masumoto 2004] Masumoto,Y., H.Sasaki, T.Kagimoto, N.Komori, A.Ishida, Y.Sasai, T.Miyama, T.Motoi, H.Mitsudera, K.Takahashi, and H.Sakuma, A fifty-year-eddy-resolving simulation of the world ocean: Preliminary outcomes of OFES (OGCM for the Earth Simulator), *J.Earth Simulator,* **1**, 35-56, 2004.

[Oshlies 1999] Oschlies, A., and V.Garçon, An eddy-permitting coupled physical-biological model of the North Atlantic: 1.Sensitivity to advection numerics and mixed layer physics, *Global Biogochem. Cycles,* **13**, 135-160, 1999.

[Oschlies 2000] Oschlies, A, W.Koeve, and V.Garçon, An eddy-permitting coupled physical-biological model of the North Atlantic: 2.Ecosystem dynamics and comparison with satellite and JGOFS local station data, *Global Biogeochem. Cycles,* **14**, 499-523, 2000.

[Oschlies 2001] Oschlies, A., Model-derived estimates of new production: New results point towards lower values, *Deep-Sea Research II,* **48**, 2173-2197, 2001.

[Oschlies 2002] Oschlies, A., Can eddies make ocean deserts bloom?, *Global Biogeochem. Cycles*, **16**, 1106, doi:10.1029/2001GB001830, 2002.

[Pacanowski 2000] Pacanowski, R.C., and S.M.Griffies, *MOM 3.0 Manual*, Geophysical Fluid Dynamics Laboratory/National Oceanic and Atmospheric Administration, 680pp, 2000.

[Rosati 1988] Rosati, A., and K.Miyakoda, A general circulation model for upper ocean circulation, *J. Phys. Oceanogr.*, **18**, 1601-1626, 1988.

[Saito 1996] Saito, H, H.Kasai, M.Kashiwai, Y.Kawasaki, T.Kono, S.Taguchi, and A.Tsuda, General description of seasonal variations in nutrients, chlorophyll-a and netplankton biomass along the A-line transect, western subarctic Pacific, from 1990 to 1994, *Bull. Hokkaido Natl. Fish. Res. Inst.*, **62**, 1-62, 1996.

[Saito 2002] Saito, H., A.Tsuda, and H.Kasai, Nutrient and plankton dynamics in the Oyashio region of the western subarctic Pacific Ocean, *Deep Sea Res. II*, **49**, 5463-5486, 2002.

[Sarmiento 1993] Sarmiento, J.L., R.D.Slater, M.J.R.Fasham, H.W.Ducklow, J.R.Toggweiler, and G.T.Evans, A seasonal three-dimensional ecosystem model of nitrogen cycling in the North Atlantic euphotic zone, *Global Biogeochem. Cycles*, **7**, 417-450, 1993.

[Yamanaka 2004] Yamanaka, Y., N.Yoshie, M.Fujii, M.N.Aita, and M.J.Kishi, An ecocystem model coupled with nitrogen-silicon-carbon cycles applied to station A7 in the Northwestern Pacific, *J. Oceanogr.*, **60**, 227-241, 2004.

Interspecific Separation of habitats in a Lattice Competition Model

Kei-ichi Tainaka
Dept. Systems Engineering
Shizuoka University
Hamamatsu, 432-8561
JAPAN
+81-53-478-1228
tainaka@sys.eng.shizuoka.ac.jp

Masashi Kushida
Dept. Systems Engineering
Shizuoka University
Hamamatsu, 432-8561
JAPAN
+81-53-478-1228
n/a

Yu Itoh
Dept. Systems Engineering
Shizuoka University
Hamamatsu, 432-8561
JAPAN
+81-53-478-1228
FZR02073@nifty.ne.jp

Tatsuya Togashi
Marine Biosystems Res. Center
Chiba University
Chiba, 263-8522
JAPAN
+ 81-43-290-2826
togashi@faculty.chiba-u.jp

Tatsuo Miyazaki
Marine Biosystems Res. Center
Chiba University
Amatsu-kominato, 299-5502
JAPAN
+ 81-470-95-2201
myzkt@faculty.chiba-u.jp

Jin Yoshimura
Dept. Systems Engineering
Shizuoka University
Hamamatsu, 432-8561
JAPAN
+81-53-478-1215
jin@sys.eng.shizuoka.ac.jp

ABSTRACT
Coexistence of competing species is extremely common in nature, whereas it is not so easy to know the mechanism of coexistence. According to the traditional perspective in theoretical ecology, spatial models do not promote the coexistence of multiple species. In the spatial models, each species is more or less clumped, and the incomplete segregation tends to reduce coexistence. Contrary to the traditional views, in the present article, we show that the complete separation of habitats induces coexistence. Our system is a lattice version of Lotka-Volterra competition model containing two competing species. Both species coexist, when intraspecific competition is stronger than interspecific competition. When the densities of both species approach zero, the living regions of two species are naturally and completely separated from each other, even though intraspecific competition is strong. Our result suggests that biological species may have a general property that naturally causes the isolation of habitats.

KEYWORDS
Habitat separation; Lattice model; Lotka-Volterra competition model

1. Introduction

The origin of biodiversity on the earth has long been a fundamental problem in ecology [Chessen & Warner 1981, Chessen 1985, Yoshimura & Clark 1991]. Species or individuals more or less compete with each other. Competition hinders the coexistence of species, resulting in the loss of biodiversity. Hutchinson [Hutchinson 1961] noted that the number of coexisting species should not exceed the number of limiting resources. However, coexistence of competing species which consume the same resource is extremely common in nature. In the present paper, we focus on the complete separation of habitats. If species live in different regions, they never compete with each other, even though intraspecific competition is stronger than interspecific one. We present a lattice model to demonstrate the complete separation.

Lattice models are widely applied in the field of ecology [Tainaka 1988, Matsuda et al 1992, Nowak et al 1994, Harada&Iwasa94, Nakagiri et al 2001, Ito et al 2004]. Spatial distribution of individuals usually differs from random distribution. In most cases, individuals of the same species form some clumping patterns; they huddle together. Non-randomness in spatial distribution influences not only on population dynamics, but also on evolutionary consequences. In most cases, segregation does not promote the coexistence of multiple species; examples are the basic contact process and the prey-predator model [Tainaka & Fukazawa 1992, Tainaka 1994] and so on. However, we know rare cases that local interaction (segregation) leads to the coexistence of multiple species [e.g. Tainaka 1988]. We believe that local interaction promotes the coexistence of multiple species. Traditional perspectives should have some missing points. In this article, we show that "complete separation" of habitats clearly promotes the coexistence. In contrast, incomplete segregation tends to reduce coexistence. This demonstrates why some of these studies show the opposite results.

2. Theoretical Rationale

Previously, co-workers in our laboratory presented the model of complete separation of habitats [Tainaka & Nakagiri 2000]. In this case, however, a specific interaction was assumed; the rock-paper-scissors relation was assumed among three species. In contrast, the model presented here may be applicable to many real ecosystems, since we only assume competition which is very common as an interaction between individuals [Silvertown et al 1992, Durrett & Levin 1998]. We deal with a lattice system called "lattice Lotka-Volterra model (LLVM)" [Tainaka 1988, Matsuda etal 1992]. The mean-field theory of this system corresponds to that of the so-called Lotka-Volterra model. In other words, in the case of LLVM, interaction is restricted to occur between adjacent lattice points (local interaction), whereas in the mean-field theory interaction globally occurs between any pair of lattice points (global interaction).

The LLVM model is an extension of the contact process (CP) which contains a single species. The CP model has been extensively studied from mathematical [Harris 1974, Liggett 1985] and physical [Katori & Konno 1991, Marro & Dickman 1999] aspects. In the CP, each lattice site is either empty (E) or occupied (X). The site X can be regarded as an individual; birth and death processes are respectively given by

$$X \rightarrow E \quad (\text{rate: } m) \tag{1a}$$

$$X + E \rightarrow 2X \quad (\text{rate: } r) \tag{1b}$$

The processes (1a) and (1b) simulate death and reproduction, respectively. The parameters m and r denote mortality and reproduction rates, respectively. The reaction (1b) occurs between adjacent lattice sites. The CP system evolves into a stationary state; the steady-state density increases with the increase of r (decrease of m).

In the next section, we explain our model which is an extension of the CP. Our model is composed of two species, while the CP model contains a single species. In our model, inter- and intra-specific competitions are assumed. The mean-field theory of the model corresponds to the Lotka-Volterra competition model. Computer simulation of our model illustrates that the isolation of microhabitats of both species naturally occurs, especially when their densities are low. In the final section, we discuss the mechanism of habitat separation, by which many species may express the similar form of habitat segregation.

3. Model

Our model is an extension of CP, and it is defined by

$$X \rightarrow E \quad (\text{rate: } m_x) \tag{2a}$$

$$X + E \rightarrow 2X \quad (\text{rate: } r_x) \tag{2b}$$

$$Y \rightarrow E \quad (\text{rate: } m_y) \tag{2c}$$

$$Y + E \rightarrow 2Y \quad (\text{rate: } r_y) \tag{2d}$$

and

$$X + X \rightarrow X + E \quad (\text{rate: } c_x) \tag{2e}$$

$$Y + Y \rightarrow Y + E \quad (\text{rate: } c_y) \tag{2f}$$

The reactions (2a) - (2d) are the same meaning as CP. The last two reactions represent the intraspecific competition. An example is the direct competition between a pair of plants; neighboring plants are competing to take sunlight or resources. The parameters c_x and c_y mean competition rates. Besides such direct competitions (2e) and (2f), our model contains tacit (indirect) competition: according to reactions (2b) and (2d), any pair of individuals competes to occupy the empty space E.

We describe the simulation method:

1) Initially, we distribute individuals on the square lattice; the initial distribution is not important, since the system evolves into a stationary state.

2) The reactions (2) are performed in the following two steps:

(i) We perform one-body reactions; that is, the mortality reactions (2a) and (2c). Choose one lattice point randomly. If the site is occupied by X (or Y), the site will become E by the rate m_x (or m_y). If the other sites are selected, then we skip this step.

(ii) We perform two-body reactions (2b), (2d), (2e) and (2f). Choose one lattice site randomly, and then randomly specify one of four neighboring sites. Let the pair react according to two-body reactions. For example, if the pair of sites is (X, E), the reaction (2b) may take place: the site E is changed into X with the probability (rate) r_x.

3) Repeat step 2) by L x L times, where L x L is the total number of lattice points (L = 100). This is called the Monte Carlo step [Tainaka88].

4) Repeat step 3) until the system reaches a stationary state.

4. Mean-field Theory

If the global interaction is allowed between any pair of lattice sites, the population dynamics of our system (2) is given by the mean-field theory:

$$\frac{dx}{dt} = -m_x x + r_x xe - c_x x^2 \tag{3a}$$

$$\frac{dy}{dt} = -m_y y + r_y ye - c_y y^2 \tag{3b}$$

where x, y and e are the densities of the sites X, Y, and E, respectively. The first, second and third terms on the right hand side denote death, birth and competition, respectively. By the use of the relation e=1-x-y, the equations (3a) and (3b) can be rewritten as

$$\frac{dx}{dt} = R_1 x(K_1 - x - ay)/K_1 \tag{4a}$$

$$\frac{dy}{dt} = R_2 y(K_2 - y - bx)/K_2 \quad . \tag{4b}$$

Here the parameters satisfy the following relations:

$$R_1 = r_x - m_x\,,\ R_2 = r_y - m_y\,, \tag{5}$$

$$K_1 = \frac{r_x - m_x}{r_x + c_x}\,,\ K_2 = \frac{r_y - m_y}{r_y + c_y}\,, \tag{6}$$

$$a = \frac{r_x}{r_x + c_x}\,,\ b = \frac{r_y}{r_y + c_y} \quad . \tag{7}$$

The equations (4a) and (4b) are called the Lotka-Volterra competition model, and its result is well known. Final stationary states are classified into four classes, depending on the values of parameters. Namely, (i) both X and Y coexist, (ii) X only survives, (iii) Y only survives, and (iv) either X or Y survives depending on the initial conditions. In this case, from the equation (7), the equations (4a) and (4b) have another state (v): both goes extinct, instead of class (iv). The condition for the coexistence is given by

$$K_1 > aK_2 \ \text{ and } \ bK_1 < K_2\,. \tag{8}$$

This can be explicitly expressed by

$$\frac{r_x(r_y - m_y)}{r_y + c_y} < r_x - m_x < \frac{(r_y - m_y)(r_x + c_x)}{r_y}\,. \tag{9}$$

If c_x = c_y =0, then the condition (9) is not satisfied. It is therefore necessary for the coexistence that intraspecific competition is stronger than interspecific one; in other words, the competition rates (c_x and c_y) should take large values for the coexistence.

5. Results

5.1. Symmetrical case

The population dynamics for lattice model is consistent with the prediction of mean-field theory. The system evolves into a stationary state. Four types of stationary states are observed: namely, (i) both X and Y coexist, (ii) X only survives, (iii) Y only survives, and (iv) both go extinct. If $c_x = c_y = 0$, both species cannot coexist [Neuhauser 1992]. With the increase of the values of c_x and c_y, both species become to survive together. In the present paper, we focus on the coexistence phase. There are six parameters. As a first attempt, we consider a symmetrical case: $r_x = r_y$, $m_x = m_y$, and $c_x = c_y$. We change the values of mortality rates (m_x and m_y), and fix the other parameters. In Fig. 1, steady-state densities of both species are depicted against the mortality rate. This figure reveals that the densities decrease with increasing the mortality rate. We find a phase transition: when the mortality rate exceeds a critical value, both species goes extinct.

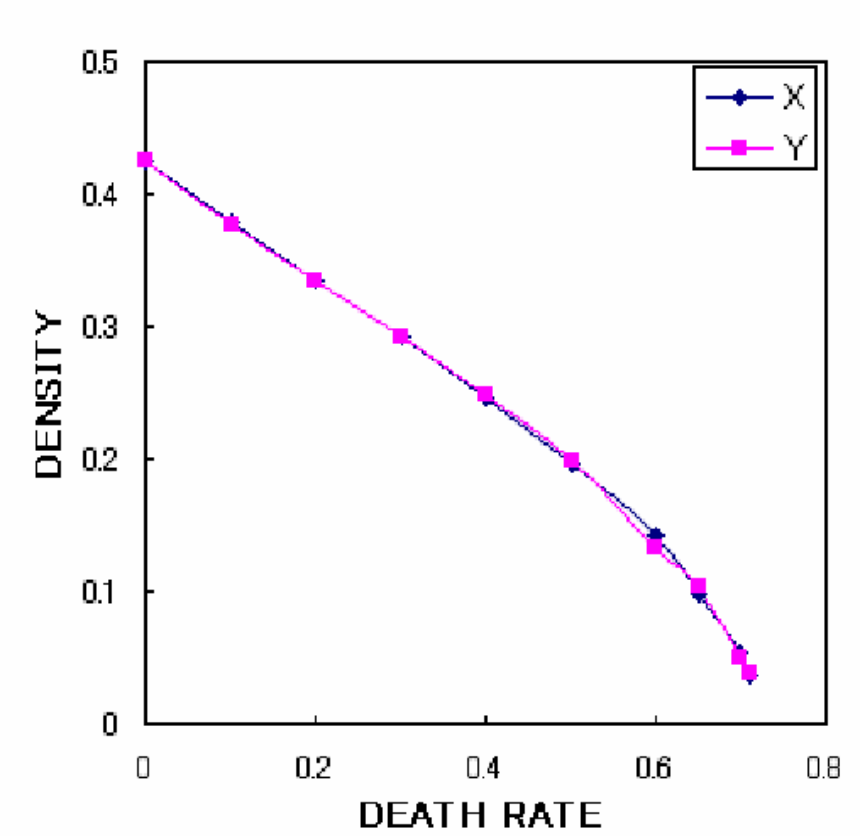

Fig. 1. The steady-state densities of species X and Y are depicted against the mortality rate of both species. Both densities become zero, when the mortality rate exceeds a critical value.

Spatial pattern at the stationary state exhibits specific properties (Fig. 2). Indeed, the densities decrease with increasing the mortality rate. In the case of Fig. 2(b), the system locates near the critical state of phase transition. We find from this figure that a kind of habitat segregation occurs: the species X and Y live separately. We analyze the segregation by the use of correlation function, F(r,jk), where r is the distance between a pair of individuals of species j and k (j,k=X or Y) (Fig. 3). Namely, F(r,jk) means the probability finding the species j at the distance r apart from an individual of species k. Note that they are scaled by overall densities, so that we always have F(r,jk)=1 for the uniform random distribution. The distance r takes discrete values (Fig. 3). The distance r=1 is most important, since the correlation function is usually a decreasing function of distance. Previously, F(1,XX) has been defined as the clumping degree of X [Tainaka 1994, Ito et al 2004], and F(1,XY) as the degree of coexistence of both species [Tainaka et al 2003]. In the case of present article, it may be necessary

to calculate not only for the shortest distance but also for several values of distance. Because our model (2) contains the direct competition which occurs in the same species; according to reactions (2e) and (2f), we expect that F(1,XX) takes a smaller value compared to F(2,XX).

(a) (b)

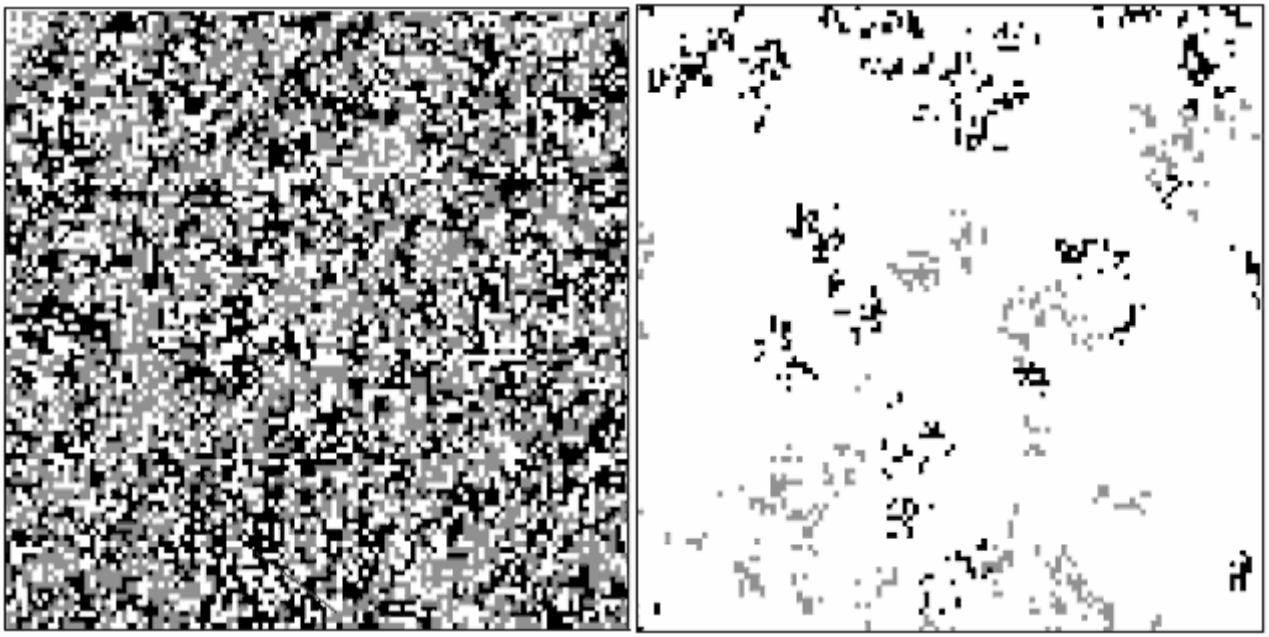

Fig. 2. Typical stationary patterns. (a) high density case; the mortality rate of both species is equal to 0.2 which is a relatively small value. (b) low density case (near extinction); the mortality rate of both species takes a large value (0.71).

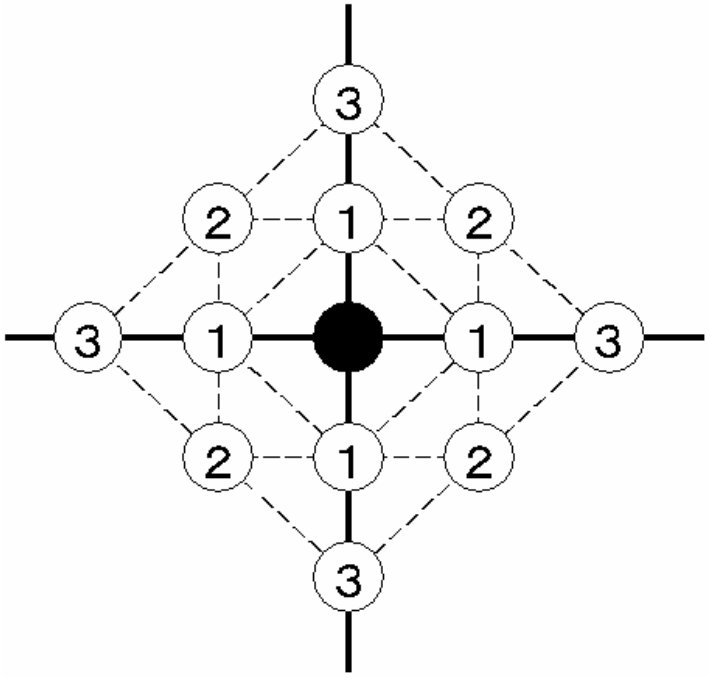

Fig. 3. Schematic illustration of distance *r* (numerals in circles). The shortest distance (*r*=1) means the nearest neighbor, and *r*=2 means the next nearest-neighbor, *etc*.

Figure 4 shows the correlation functions F(r,XX) for r=1,2,3. In the case of (a), the correlation functions are plotted against the mortality rate. In (b), they are plotted against the steady-state density (log-log plot). The functions F(r,XX) represent the degree of clumping. If F(r,XX) takes a large value, say F(r,XX)>1, then the species X is clumped. In contrast, if F(r,XX)<1, the species distributes uniformly. From Fig. 4, we find the following nontrivial results:

i) The value of F(r,XX) is always larger than unity.

ii) F(r,XX) takes the highest values for r=1 among three values of r, that is, F(1,XX)>F(2,XX)>F(3,XX).

In spite of the intraspecific competitions (2e), the above results are obtained. These unexpected results are discussed later. It is also found from Fig. 4 (a) that the degree of clumping of species X (or Y) increases with the increase of the mortality rate m. Fig. 4 (b) reveals that the correlation functions are proportional to $K^{-\beta}$:

$$\mathrm{F}(r,\mathrm{XX}) \propto K^{-\beta}, \tag{10}$$

where K, the equilibrium density (steady-state density of species X or Y), is sufficiently low. The value of power β is nearly unity regardless of the value of r. When the steady-state densities approach zero, F(r,XX) approaches infinity. In Fig. 5, F(r,XY) for r=1,2,3 are plotted against the steady-state densities. This figure implies that the degree of coexistence decreases with the increase of the mortality rate. Hence, if the densities of both species become zero, both species live separately.

(a) (b)

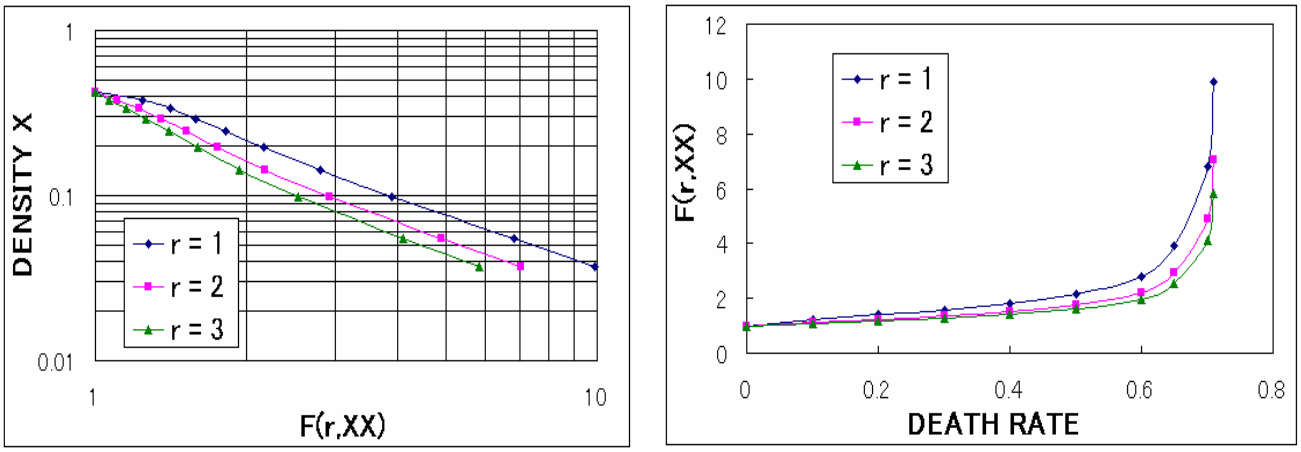

Fig. 4. The degree of clumping in terms of correlation functions F(r,XX), where r=1,2,3. If the distribution of individuals is random, the correlation functions equal unity. (a) The values of F(r,XX) are plotted against the mortality rate of both species. These values diverge near the extinction threshold. (b) The relation between the correlation functions and the densities plotted in Fig. 1 (log-log plot). The plots are almost on lines, indicating a kind of power law; all powers are nearly unity.

5.2. Asymmetrical case

Next, we consider asymmetry case, where the parameters are not equal with respect to the exchange between species X and Y. Fig. 6 shows the phase diagrams of competition rates, c_x and c_y under local and global interactions. Model parameters are set as $r_x = r_y = 0.7$ and $m_x = m_y =$ 0.5. Here the coexistence region of global interaction is much wider than that of local interaction. This implies that the local interaction (segregation) does not promote, but rather reduce the coexistence of both species. In the case of local interaction, species X and/or Y are usually endangered even in the coexistence region.

It should be noted that a qualitative result of habitat separation is almost unchanged even in asymmetrical cases. In Fig. 7, a typical stationary distribution of species is displayed, where the density of X (black) is very low. Similarly, a kind of habitat isolation can be observed. In Fig. 8, steady-state densities of both species are depicted against the mortality rate. This figure reveals that the density of species X monotonically decreases with the increase of mortality rates ($m_x = m_y$). We find

extinction of both species: with increasing the mortality rates, the species X first goes extinct, and Y goes extinct later. Moreover, we find the crossover of both densities. When the mortality rates take a small value, the density of X is larger than that of Y. In contrast, when they take a large value, the density of Y becomes larger compared to X. Such a crossover does not always appear.

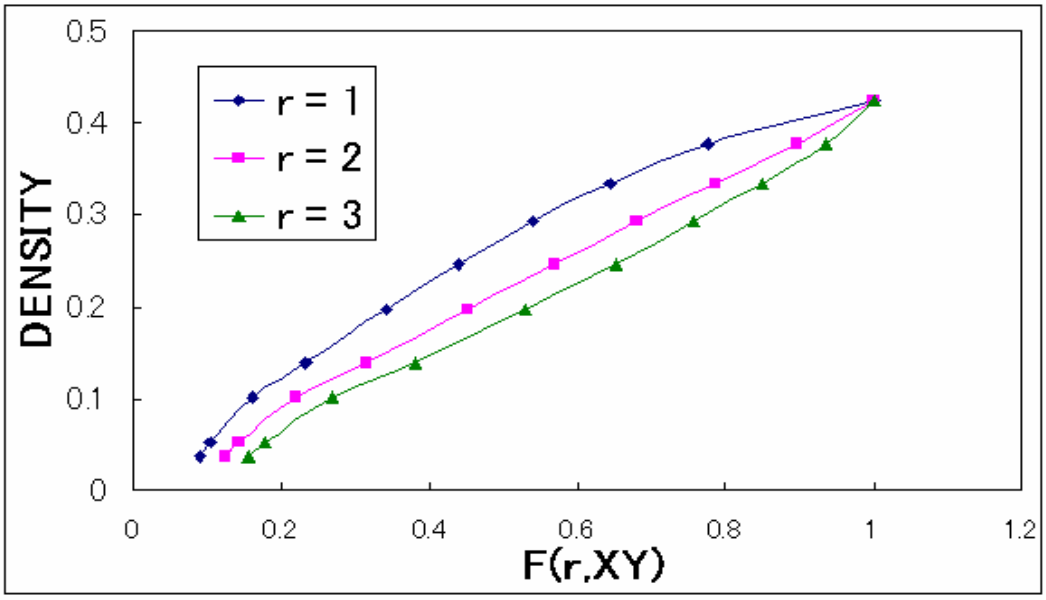

Fig. 5. The results of correlation functions F(*r*,XY) for *r*=1,2,3. These values indicate the degree of coexistence.

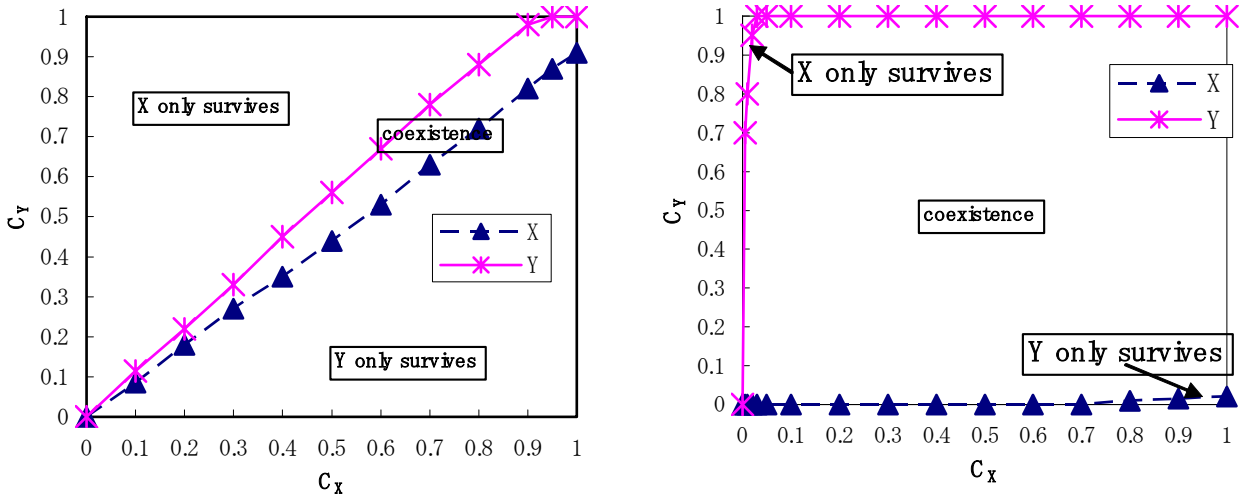

Fig. 6. The phase diagrams of competition rates, c_x and c_y with local (lattice; left) and global interactions (mean-field; right). Model parameters: $r_x = r_y = 0.7$ and $m_x = m_y = 0.5$.

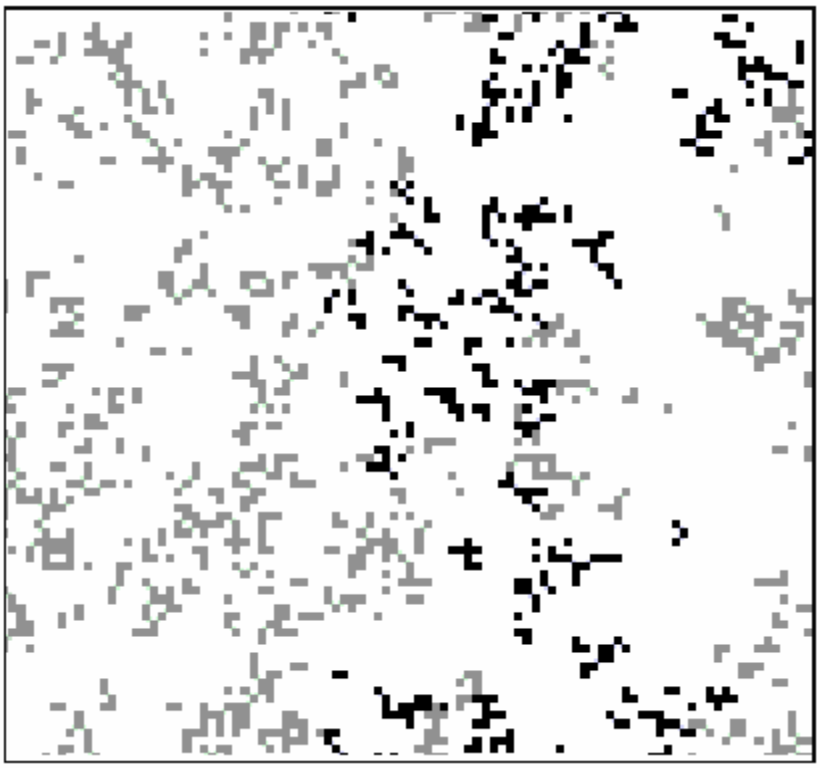

Fig. 7. A typical stationary pattern in the asymmetrical case. Model parameters are: (r_x, r_y, c_x, c_y, $m_x = m_y$) = (0.6, 0.61, 0.6, 0.64, 0.5). The species X (black) is endangered.

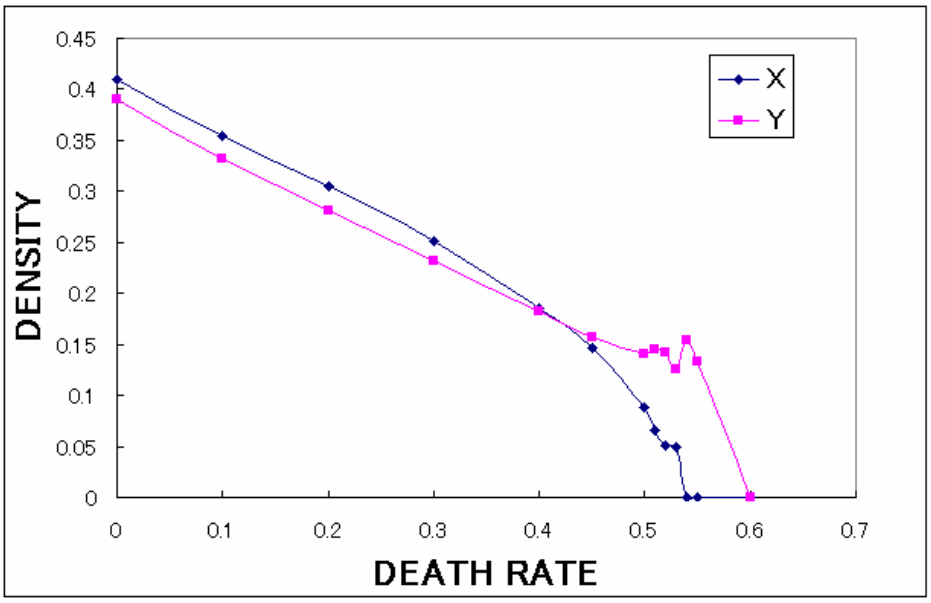

Fig. 8. The results of steady-state densities in the asymmetrical case. Parameters (r_x, r_y, c_x, c_y, $m_x = m_y$) take the same values as used in Fig. 7. The horizontal axis denotes the mortality rates of both species ($m_x = m_y$).

In Fig. 9, correlation functions F(r,XX) for r=1,2,3 are also calculated against the steady state densities (Fig. 8). As well as in Fig. 4 (b), Fig. 9 reveals that the correlation functions satisfy the similar power law (Eq. 10); the value of power is nearly unity. In other words, when the density of X approaches zero, the species X becomes strongly clumped. Such a clumping behavior may cause the separation of microhabitats of both species. In Fig. 10, F(r,XY) for r=1,2,3 are plotted against the steady-state densities. This indicates that the degree of coexistence decreases with the increase of the density of X. It is not clear in the limit of extinction threshold (zero density) whether F(r,XY) approaches zero or not. If F(r,XY) approaches nonzero values, then the separation of habitats is not perfect. Nevertheless, both species live separately.

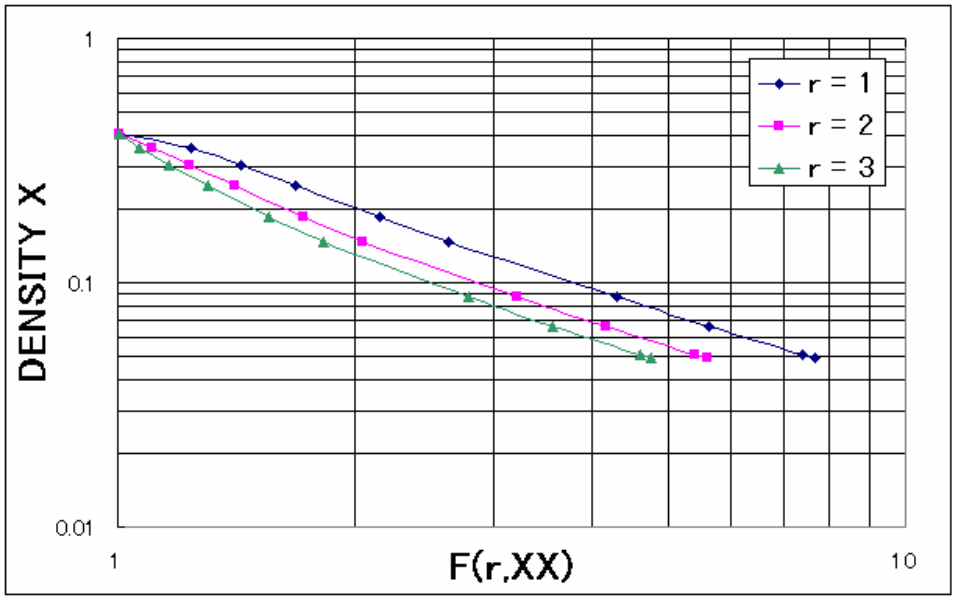

Fig. 9. Same as Fig. 4(b), but in the asymmetrical case. The degree of clumping satisfies the similar power law (all powers nearly take unity).

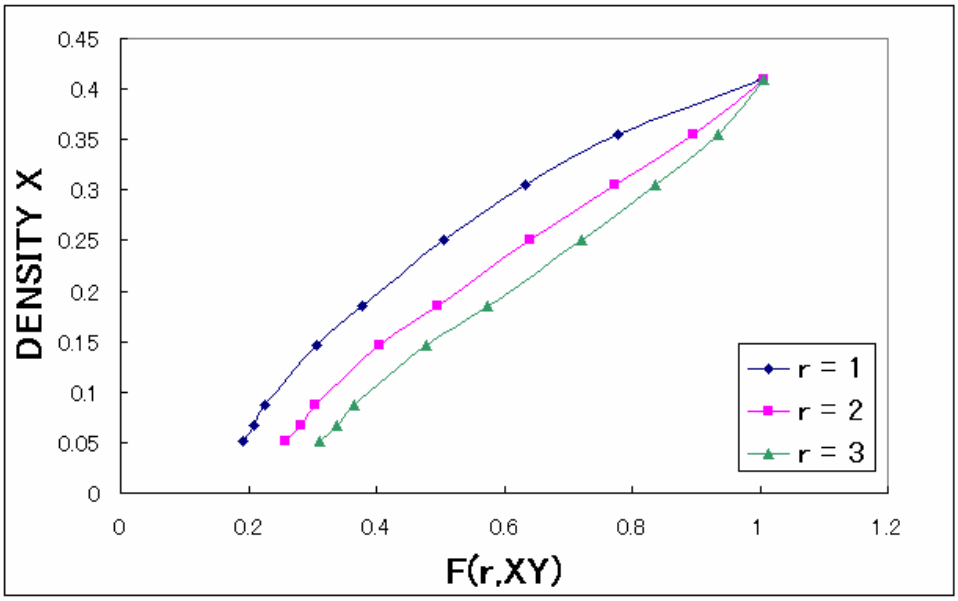

Fig. 10. Same as Fig. 5, but in the asymmetrical case.

6. Discussion

We have developed a spatially explicit model of competition. The population dynamics of our model is well predicted by the mean-field theory which is equivalent to the Lotka-Volterra model. As shown in the phase diagram (Fig. 6), the local interaction (lattice model) does not promote the coexistence of both species. We have evidence of "complete separation" of habitats. Our lattice system evolves into a stationary state. Depending on the values of mortality rates, the stationary pattern of two species exhibits a kind of phase transition (extinction): when the densities of both species become close to zero, the complete habitat separation takes place.

Our system (2) explicitly contains the intraspecific competition; that is, reactions (2e) and (2f). On the other hand, the system implicitly contains the other type of competition. Namely, in the reactions (2b) and (2d), individuals compete to get the resource (empty site E). The latter implicit competition emerges not only between both species X and Y but also between individuals of the same species. Although our system has direct intraspecific competitions, (i) the species X and Y live separately (habitat separation), (ii) we always have $F(1,XX)>F(2,XX)>F(3,XX)$, and (ii) the degree of clumping of endangered species infinitely increases.

We first dealt with the symmetrical case for which the values of parameters never change with respect to the exchange between species X and Y. Computer simulations reveal that interspecific segregation of habitats completely occurs. When densities of both species approach zero, $F(r,XX)$ diverges but $F(r,XY)$ approaches zero for $r=1,2,3$. The qualitative result of habitat segregation does not change for the asymmetrical case. In this case, however, it is not clear whether separation of habitats is quantitatively complete or not. When the density of species X approaches zero, then $F(r,XX)$ indeed diverge, but it is not clear whether $F(r,XY)$ approach zero or not.

We discuss a fundamental problem whether the local interaction promotes the coexistence of species or not. This problem is still unsolved. Fig. 6 clearly reveals that the local interaction (lattice model) does not promote the coexistence of both species. The coexistence region of global interaction is much wider than that of local interaction. In contrast, we illustrate the complete separation of habitats. This implies that the local interaction promote the coexistence of both species. Although we never carry out a full analysis of emerging properties of space on coexistence, the property of complete separation should be served for the coexistence of multi-species. We have shown the occurrence of habitat segregation under the condition that the densities of species are very low. Such a condition is not specific, since each species usually has a low density on the Earth.

Finally, we discuss the origin of habitat separation. If a species is endangered, the degree of clumping becomes large. As in the extinction of the passenger pigeon in the USA [Schorger 1955], the density of critically endangered species may be overestimated due to clumping, despite it is actually near extinction. The mechanism of cluster formation may be very simple; the enhancement in clumping degree may be originated in the fact that “offspring are located near their mother”. For this reason, many species potentially have the mechanism of habitat segregation.

ACKNOWLEDGMENTS

This work was supported in part by the Grant-in-Aids of the Japan Society for the Promotion of Science.

REFERENCES

[Chessen & Warner 1981] Chessen, P. L. and Warner, R. R. Environmental variability promotes coexistence in lottery competitive system. *Am. Nat.*, **117**: 923-943, 1981.

[Chessen 1985] Chessen, P. L. Coexistence of competitors in spatially and temporally varying environments: a look at the combined effects of different sorts of variability. *Theor. Pop. Biol.* **28**: 263-287, 1985.

[Yoshimura & Clark 1991] Yoshimura, J. and Clark, C. W. Individual adaptations in stochastic environments. Evol. Ecol. 5, 173-192, 1991.

[Hutchinson 1961] Hutchinson, G.E. The paradox of plankton. *Am. Nat.*, **95**: 137-145, 1961.

[Tainaka 1988] Tainaka, K. Lattice model for the Lotka-Volterra system. *J. Phys. Soc. Japan*, **57**: 2588-2590, 1988.

[Matsuda *et al* 1992] Matsuda, H., Ogita, N., Sasaki, A. and K. Sato, K. Statistical mechanics of population: the lattice Lotka-Volterra model. *Prog. Theor. Phys.*, **88**: 1035-1049, 1992.

[Nowak *et al* 1994] Nowak, M.A., S. Bonhoeffer, S. and May, R.M. More spatial games. *Int. J. Bifurcation and Chaos*, **4**: 33-56, 1994.

[Harada & Iwasa 1994] Harada, Y. and Iwasa, Y. Lattice population dynamics for plant with dispersing seeds and vegetative propagation. *Res. Popul. Ecol.*, **36**: 237-249, 1994.

[Nakagiri *et al* 2001] Nakagiri, N., Tainaka, K. and Tao, T. Indirect relation between species extinction and habitat destruction. *Ecol. Mod.*, **137**: 109-118, 2001.

[Ito *et al* 2004] Itoh, Y., Tainaka, K., Sakata, T., Tao, T. and Nakagiri, N. Spatial enhancement of population uncertainty near the extinction threshold. *Ecol. Mod.*, **174**: 191-201, 2004.

[Tainaka & Fukuzawa 1992] Tainaka, K. and Fukazawa, S. Spatial pattern in a chemical reaction system: prey and predator in the position-fixed limit. *J. Phys. Soc. Japan*, 61: 1891-1894, 1992.

[Tainaka 1994] Tainaka, K. Intrinsic uncertainty in ecological catastrophe. *J. Theor. Biol.*, **166**: 91-99. 1994.

[Tainaka & Nakagiri 2000] Tainaka, K. and Nakagiri, N. Segregation in an interacting particle system. *Phys. Lett.*, **A 271**: 92-99, 2000.

[Silvertown *et al* 1992] Silvertown, J., Holtier, S., Johnson, J. and Dale, P. Cellular automaton models of interspecific competition for space – the effect of pattern on process. *J. Ecology*, **80**: 527-534, 1992.

[Durrett & Levin 1998] Durrett, R. and Levin, S. Spatial aspect of interspecific competition. *Theor. Pop. Biol.*, **53**: 30-43, 1998.

[Harris 1974] Harris, T. E. Contact interaction on a lattice. *Ann. Prob.*, **2**: 969-988, 1974.

[Liggett 1985] Liggett, T.M. *Interacting Particle Systems.* Springer-Verlag, New York, 1985.

[Katori&Konno 1991] Katori, M. and Konno, N. Upper bounds for survival probability of the contact process. *J. Stat. Phys.*, **63**: 115-130, 1991.

[Marro&Dickman 1999] Marro, J. and Dickman, R. *Nonequilibrium Phase Transition in Lattice Models.* Cambridge Univ. Press, 1999.

[Neuhauser 1992] Neuhauser, C. Ergodic theorems for the multitype contact process. *Probab. Theory and Rel. Fields*, **91**: 467-506, 1992.

[Tainaka etal 2003] Tainaka, K., Terazawa, N. Yoshida, N. Nakagiri, N. Takeuchi, Y. The effect of mutualism on community stability. *J. Phys. Soc. Japan*, **68**: 956-961, 2003.

[Schorger 1955] Schorger, A.W. *The passenger pigeon: its natural history and extinction.* University of Oklahoma Press, Oklahoma, 1955.

Bond and Site Destruction of Habitat in Model Ecosystems

Nariyuki Nakagiri
Department of Human Science and Environment,
University of Hyogo
1-1-12 Shinzaike-honcho
Himeji, 670-0092
JAPAN
+81-792-92-9240
nakagiri@shse.u-hyogo.ac.jp

Kei-ichi Tainaka
Department of systems engineering,
Shizuoka University
3-5-1 Jyouhoku
Hamamatsu, 432-8561
JAPAN
+81-53-478-1228
tainaka@sys.eng.shizuoka.ac.jp

Taro Hayashi
Department of systems engineering,
Shizuoka University
3-5-1 Jyouhoku
Hamamatsu, 432-8561
JAPAN
+81-53-478-1228

Jin Yoshimura
Department of systems engineering,
Shizuoka University
3-5-1 Jyouhoku

JAPAN
+81-53-478-1228
jin@sys.eng.shizuoka.ac.jp

ABSTRACT
Human activities have often caused the mass extinction of biospecies in recent history. The conservation of biodiversity is one of the most important problems in this century. So far, many authors have studied the effect of habitat destruction on ecosystems, especially on prey-predator systems. These works have mainly dealt with *site destruction*, where species cannot live in the destroyed site. Recently, co-workers in our laboratory have introduced *bond destruction* that blocks the interaction between lattice sites. This work assumed that only the reproduction of prey was prohibited, and reveals that the predator indirectly went extinct. Such extinction was not be predicted by mean-field theory. In the present article, we study the case that the reproduction of predator is disturbed by destruction, and apply two methods; bond and site destructions. It is found that with increasing extent of destruction, prey always increased. On the other hand, the predator either increased or decreased. These results are qualitatively explained by mean-field theory. However, we find that the extinction thresholds for bond and site destructions are much smaller than those predicted by mean-field theory. This may come from the fragmentation of habitat; by the connection of destructions, habitats are fragmented.

KEYWORDS
Habitat destruction, fragmentation, prey-predator system, lattice model, mean-field theory

1. Introduction

Habitat loss is one of the primary causes of species extinction. Even if the destruction of habitats is limited to local and small areas, its accumulation increases the risk of extinction. Habitat destruction and fragmentation are the root causes of many conservation problems [Frankel Soule 1981, Debinski 2000, Soule 1987]. The present article is designed to illustrate such a relation between extinction and habitat fragmentation.

There is abundant literature on habitat loss and fragmentation [Boswell et al 1998, Fahrig 2003, Kondoh 2003]. In particular, the effect of habitat loss on two-species (prey-predator) systems has been studied by many authors [Swihart 2001]. These works mainly studied *site destruction*, where species cannot live in the destroyed sites [Bascompte Sole 1998]. In contrast, co-workers in our laboratory have introduced *bond destruction* by which interactions between neighboring lattice sites are prohibited where species cannot live in the destroyed site [Tao et al 1999, Nakagiri 2001]. The barriers, destroyed lattice link, were randomly located between adjacent lattice points with probability D. The barrier (destruction) interrupted the reproduction of preys, while it caused no direct damage to the predators. This system exhibited extinction of predators with the increase of the barrier density D. On the other hand, an initial suppression of prey later led to the increase of prey. These results could not be explained by a mean-field theory [Nakagiri 2001, Nakagiri 2004].

In the present paper, we study the case that destructions prohibit the reproduction of predator. We compare the results between bond and site destructions. We report that with increasing destruction *D*, preys always increased, whereas predators either increased or decreased. These results are qualitatively explained by mean-field theory. However, we find that the

extinction thresholds of D for bond and site destructions are much smaller than those predicted by mean-field theory. This may come from the fragmentation of the habitat; by the connection of destructions, habitats are fragmented. The connection of small destructions enlarges the effect of habitat loss. Moreover, we obtain a kind of paradox that the extinction threshold for bond destruction becomes large compared to site destruction. This is just opposite to the prediction of percolation theory: the transition points of bond and site percolations are given by D=0.5 and $D \approx 0.6$, respectively [Stauffer 1985, Sahimi 1993].

2. The Model

2.1. Destruction Models

In this article, we consider the case that the destruction of habitat prohibits only the reproduction of predators. We apply both bond and site destructions to a predator-prey system; in the bond destruction the interaction is interrupted between lattice sites, while in the site destruction a lattice site is destroyed. Consider a square lattice that contains both prey (X) and predator (Y). Each lattice site has one of three states; namely, a vacant site (O) or occupied by prey (X) or predator (Y). We assume the following interactions [Hofbauer Sigmund 1988, Tainaka Fukazawa 1992, Satulovsky Tome 1994, Sutherland Jacobs 1994, Tainaka 1994, Nakagiri 2001, 2004]:

$$Y + X \xrightarrow{p} 2Y \qquad \text{(1a)}$$

$$X + O \xrightarrow{r} 2X \qquad \text{(1b)}$$

$$Y \xrightarrow{m_Y} O \qquad \text{(1c)}$$

$$X \xrightarrow{m_X} O \qquad \text{(1d)}$$

The above interactions respectively represent the predation (p), reproduction of prey (r) and the death (m_X, m_Y) of predator. The interactions of equation (1a) and (1b) occur between adjacent lattice points.

The destruction is defined in two different ways: bond and site destructions. First, we explain the bond destruction. We randomly put the *barriers* (destructions) between two neighboring lattice sites. The probability whether the barrier exists or not is called *barrier density D*. Thus, D measures the intensity of habitat destruction. When the barrier exists, the interaction (1a) between the both sides of the barrier is prohibited. In contrast, the reactions (1b) – (1d) are not affected by the barrier. Hence, the destruction disturbs the reproduction of predator (Y), while prey (X) receives no direct effect.

Next, we explain the site destruction. If a site is destroyed, only predators cannot live in this site. In contrast, prey can survive, irrespective of destruction. The intensity D of destruction is defined by the probability of destruction in each site. Hence, each site is classified into five cases; namely, predator site (Y), prey in destroyed site ($\mathrm{X} \cap \mathrm{D}$ or $\mathrm{X_D}$), prey in living site ($\mathrm{X} \cap \overline{\mathrm{D}}$), empty destroyed site ($\mathrm{O} \cap \overline{\mathrm{D}}$) and empty living site ($\mathrm{O} \cap \overline{\mathrm{D}}$). It should be emphasized that predators cannot live in the destroyed sites. The locations of destructed site are fixed throughout the simulations.

It is known that the so-called percolation transition occurs [Stauffer 1985, Sahimi 1993, Boswell et al 1998]. When D takes an extremely small value, no destructions may connect with each other. On the contrary, when D takes a large value (near unity), almost all destructions are connected. Below, we call cluster for a clump of connected destructions and percolation in the case that the largest cluster reaches the whole size of system (meaning). The probability of percolation takes a nonzero value, when D exceeds a critical point D_C. The percolation threshold is given by $D_{BC} = 0.5$ for bond destruction and $D_{SC} \approx 0.6$ for site destruction. Percolation ecologically means that the habitat region of species X may be fragmented into small segments for $D > D_C$.

2.2. Simulation Method

We apply a method of lattice Lotka-Volterra model (LLVM) [Tainaka 1988, Matsuda et al 1992, Itoh Tainaka 1994, Tainaka Nakagiri 2000]. Evolution method of lattice model is defined as follows:

(i) Initially, we distribute two species, X and Y, on a square lattice randomly with no overlap of X and Y.

(ii) Each interaction process is performed in the following two steps.

(1) We perform the two-species interaction, i.e. reactions (1a) and (1b).

(a) Bond destruction model: Select one square-lattice point randomly, and then specify one of the nearest-neighbor points. The number of these points is called the coordinate number (z); for a square-lattice, this is given by z=4. When the pair of selected points are Y and X, and when there is no barrier between them, then the latter point will become Y by a probability p. On the other hand, the barrier never affects the reaction of X: when the selected points are O and X, the former point becomes X.

(b) Site destruction model: Select one square-lattice point randomly, and then specify one of the nearest-neighbor points. When the pair of selected points is Y and X, and when X is not located in the destroyed site, then X will become Y by a probability p. If X locates in the destroyed site, no predation occurs. On the other hand, when the selected points are the pair of O and X, then O becomes X; the reproduction of X occurs irrespective of destruction.

(2) We perform the one-species interaction (i.e. reaction (1c)). Choose one lattice point randomly. If the point is occupied by a X or Y species, then it will become O by a probability m_X or m_Y, respectively.

(iii) Repeat step (ii) LxL times, where LxL is the total number of Square-lattice sites in the repeating steps, the next site is chosen randomly from all sites. This step is called a Monte Carlo step [Tainaka 1988]

(iv) Repeat step (iii) for 1000-2000 Monte Carlo steps. At time t=0, the value of *D* is jumped from 0 to a nonzero value. Here we employ periodic boundary conditions, where the edges of lattice are connected to the opposite edges. Note the corner point is next to the opposite corner.

3. Mean-field Theory – Analytical Results

3.1. Bond Destruction

We study a predator-prey system by mean-field theory (MFT) which is equivalent to Lotka-Volterra equations [Hofbauer Sigmund 1988, Takeuchi 1996]. This theory is valid, when the interactions (1a) and (1b) occur globally (between any pair of lattice points), and when the total lattice sites LxL is infinitely large. The dynamics of global interaction (MFT) is given by

$$\dot{P}_X = 2rP_X P_O - 2p(1-D)P_X P_Y - m_X P_X ,$$

$$\dot{P}_Y = 2p(1-D)P_X P_Y - m_Y P_Y , \qquad (2)$$

where P_X, P_Y and P_O are densities of X, Y and O, respectively ($P_O = 1 - P_X + P_Y$), and the dots denote the derivatives with respect to time *t* which is measured by Monte Carlo Step [Tainaka 1988]. In the above equations, the effect of barrier connection (cluster formation) is neglected; the factor (*1-D*) in (2) denotes the probability that the barrier is absent. This factor can be obtained from the coordinate number *z,* which is the number of nearest neighbors (*z=4* for square lattice). Let *j* be the numbers of barriers around a given lattice point ($j \in \{0,1...,z\}$). The *effective* coordinate number <*4-j*> takes into account the effect of barriers. The mean value <*4-j*> can be obtained by

$$\langle 4-j \rangle = \sum_{j=0}^{4} (4-j)\binom{4}{j}(1-D)^{4-j} D^{j} .$$

It follows that <j>= 4(1-*D*). Thus, the probability that the barrier is absent is given by <*j*>/*4=1- D*.

The densities of both P_X and P_Y reach the stationary values. When $m_Y < 2p(1-D)$, they are expressed by

$$P_X = \frac{m_Y}{2p(1-D)},$$

$$P_Y = r\frac{1-m_Y/(2p(1-D)) - m_X/2r}{p(1-D)+r}, \qquad (3)$$

When $m_Y > 2p(1-D)$, the predator goes extinct (P_Y=0). According to the linear stability analysis [Hofbauer Sigmund 1988], the steady-state densities (3) are stable, if $m_Y < 2p(1-D)$. Hence, we can answer the effect of habitat destruction.

We consider the case that a perturbation is applied to our system. By the perturbation, the intensity D of destruction is suddenly increased from D=0 to D=0.3. Just after the sudden increase of destruction, the abundance of predator Y always

decreases (short-term response), but the steady-state density of X is increased. On the other hand, the long-term response (steady-state density) shows unexpected results: the steady-state density of Y is not always decreased. With increasing *D*. the abundance of predators increases, if the intensity D of destruction is slightly increased. However, when the intensity D is largely increased, the predator decreases and goes extinct. The extinction threshold D_{B0} of the predators is given by $m_Y = 2p(1-D_{B0})$. It follows that $D_{B0} = 1 - m_Y / 2p$. Note that X never becomes extinct for any value of *D* (0<*D*<1).

3.2. Site Destruction

In the case of site destruction, there are four types of sites; namely, O, Y, X and X_D where X_D is the cells where the prey lives in the destroyed site (sanctuary). The MFT is represented by

$$\dot{P}_X = 2rP_X(1 - P_X - P_Y) - 2p(P_X - P_{XD})P_Y - m_X P_X, \quad (4a)$$

$$\dot{P}_{XD} = 2rP_X(D - P_{XD}) - m_X P_{XD} \quad (4b)$$

$$\dot{P}_Y = 2p(P_X - P_{XD})P_Y - m_Y P_Y, \quad (4c)$$

where P_X, P_Y and P_{XD} are densities of X, Y and X_D, respectively. The dots denote the derivatives with respect to time *t*. In the above equations, the effect of barrier connection is neglected; the factor *D* in (4b) denotes the probability of the barrier. The densities of both P_X and P_Y reach the stationary values:

$$P_X = \frac{2rD + rm_Y / p - m_X + \sqrt{(2rd + rm_Y / p - m_X)^2 + 4rm_X m_Y / p}}{4r},$$

$$P_Y = \frac{-2rP_X + (2r - m_X)P_X}{2rP_X + m_Y}. \quad (5)$$

Hereafter, we set $m_X = 0$. When $m_Y > 2p(1-D)$, we have P_X =1 and P_Y=0. According to the linear stability, the steady-state densities (5) are stable if $m_Y < 2p(1-D)$. Hence, we can answer the result of the perturbation experiment. By the perturbation, the intensity D of destruction is suddenly increased from D=0 to D=0.3. After the perturbation, the abundance of predator Y always decreases, but the steady-state density of Y is unchanged by *D*; during a long period, the predator population recovers the same density as before the perturbation. However, the steady-state density of X is increased with increasing *D*. Note that X never becomes extinct for any value of *D* (0<*D*<1).

4. Simulation Results

4.1. Bond Destruction

First, we carried out a perturbation experiment: before the perturbation (for *D*=0), the system evolves into a stationary state, after the perturbation, the predator Y decreases, whereas prey increases. Later, the abundance of predators increases. In Fig. 1(b), the result of mean-field theory (global interaction) is also illustrated. This theory predicts well the time-dependences of local interaction, however the steady state levels are different. In Fig. 2 we depict typical stationary spatial patterns for different values of *D*. If the intensity *D* of destruction is large, the predator Y becomes extinct. Fig. 3 shows steady-state densities of both species X and Y against *D* together with the results of MFT. Here the plots (curves) denote the simulation results of local interaction (theoretical results of MFT). The lattice model in Fig. 3 reveals the following results:

(1) With the increase of barrier density *D*, the density P_X of prey increases. Especially, we have $P_X \approx 1$, when *D* takes a larger value than the extinction point of predators D_{B0}.

(2) With the increase of *D*, the predator density P_Y increases, but it conversely decreases for large values of *D*. the predator density takes a peak. When $D \geq D_{B0}$, the predator becomes extinct; D_{B0} is the extinction threshold for bond destruction ($P_Y = 0$ for $D \geq D_{B0}$).

(a) Lattice model

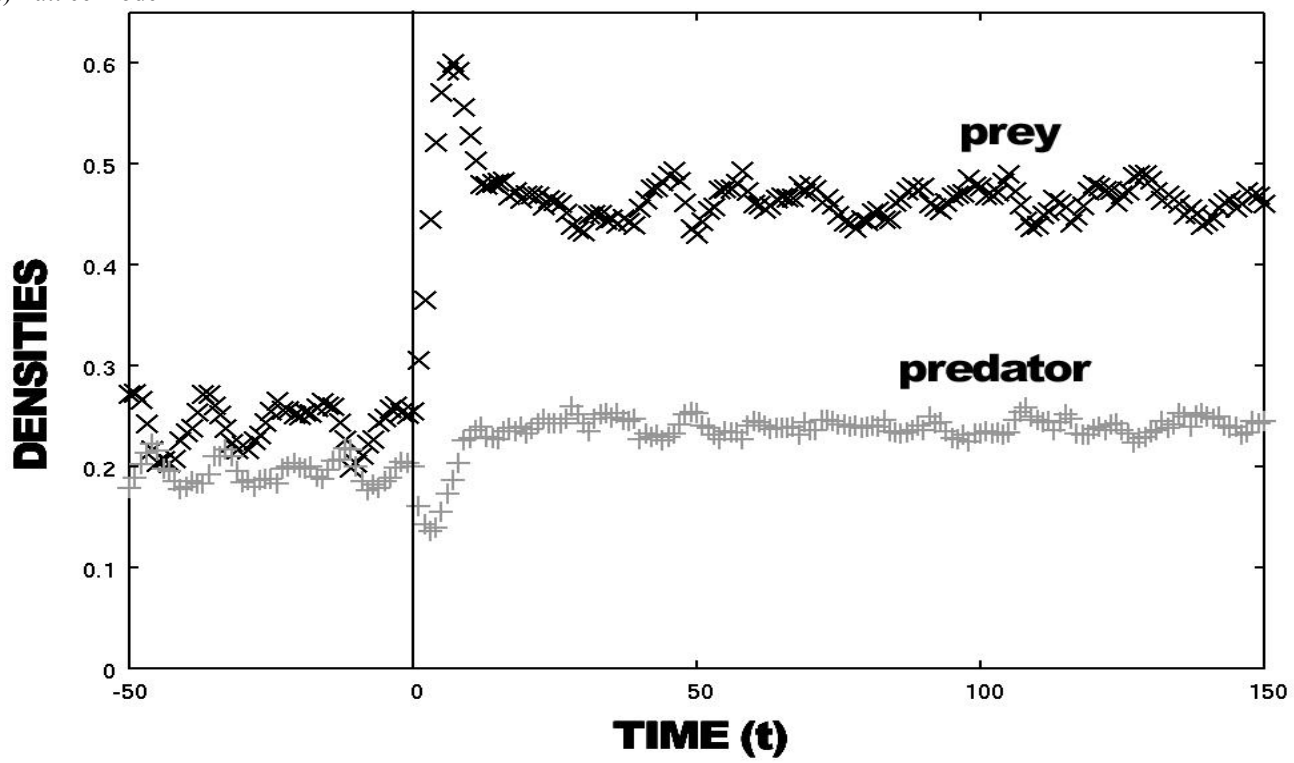

(b) MFT

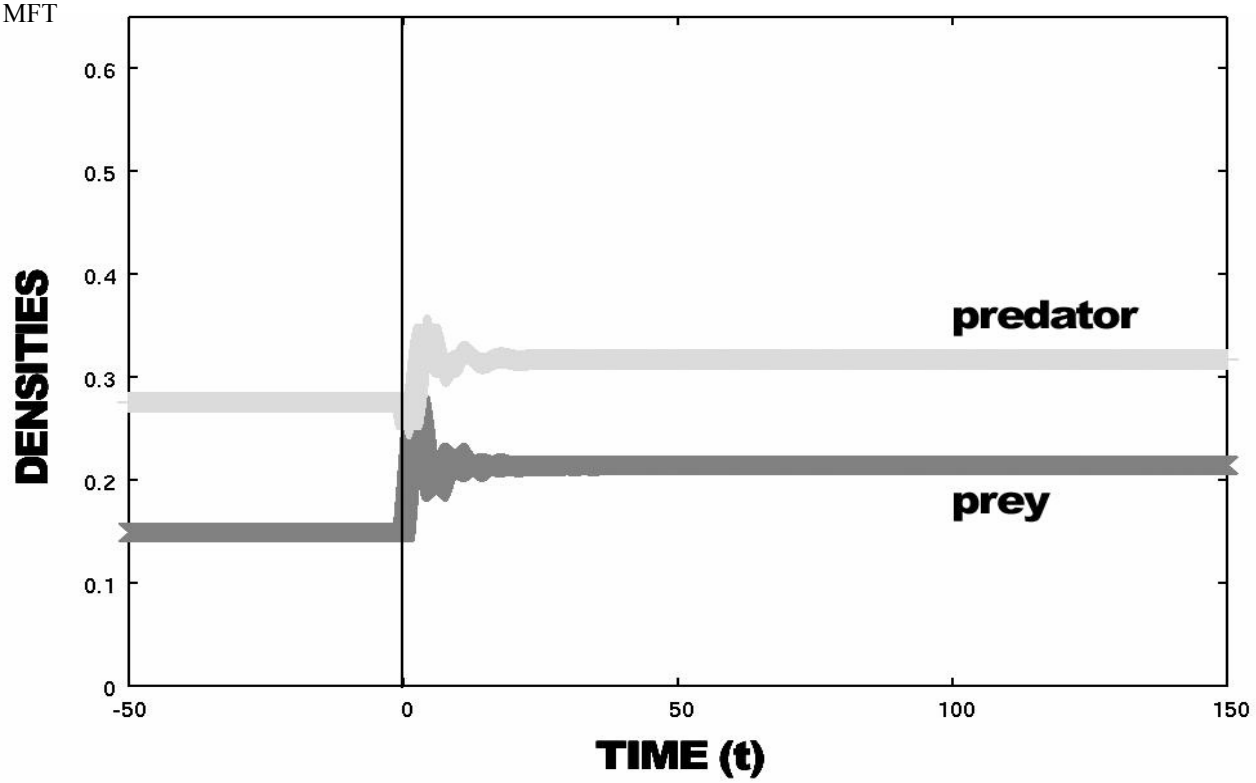

Fig.1: An example of population dynamics for bond destruction. (a) lattice model and (b) MFT (100x100). The time dependence of both species X and Y are shown. At time t=0, the barrier density D increases from 0 to 0.3. We put r=1.0, p=2.0, m_X=0.05, m_Y=0.6.

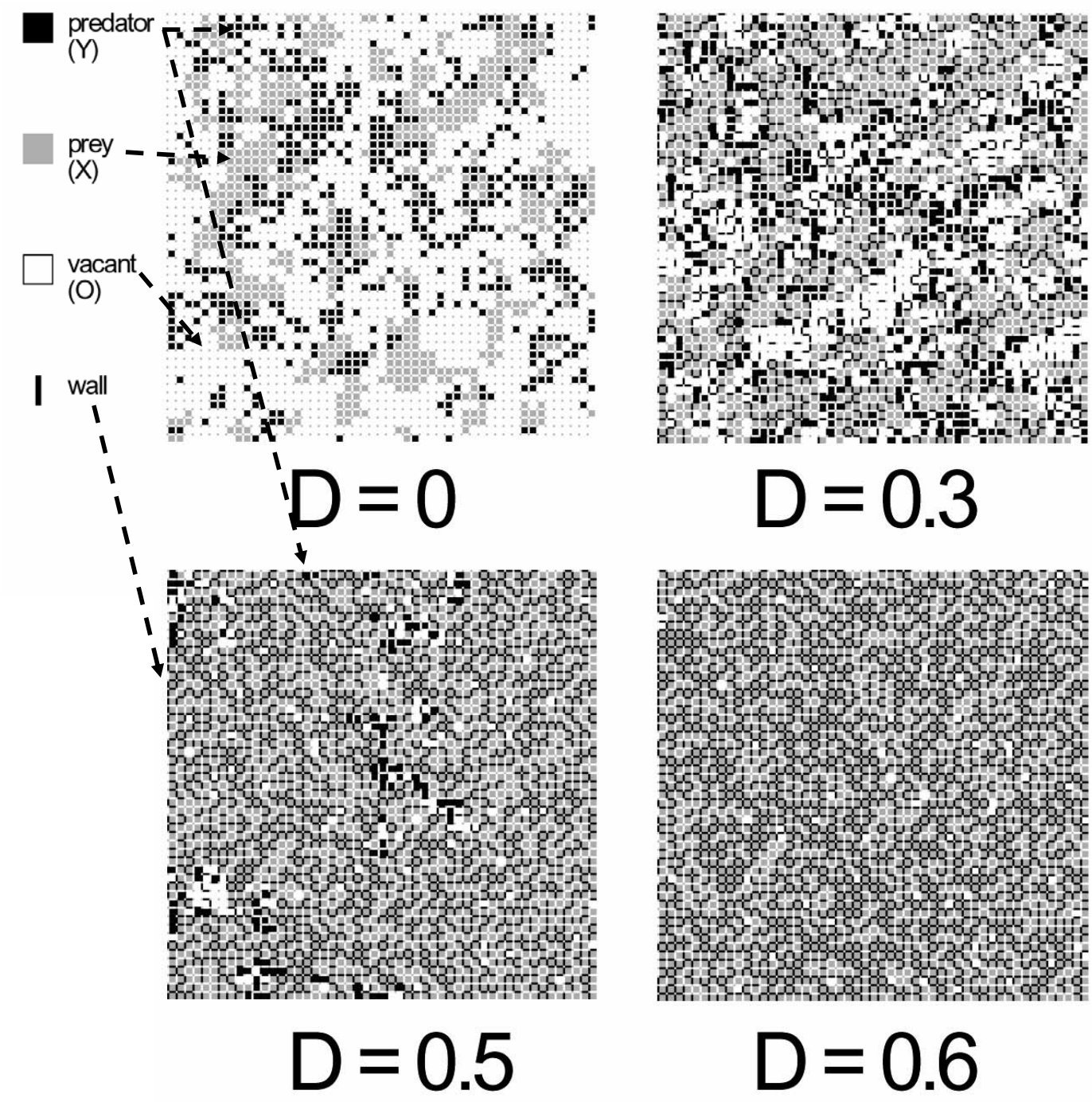

Fig. 2. Typical spatial patterns in stationary state for bond destruction. Model parameters are set as (r=1.0, p=2.0, m_X=0.05 and m_Y=0.6). The predator Y, prey X and the vacant site O are indicated by black, grey and white respectively, and the barriers are represented by bold lines between sites.

(a) prey X

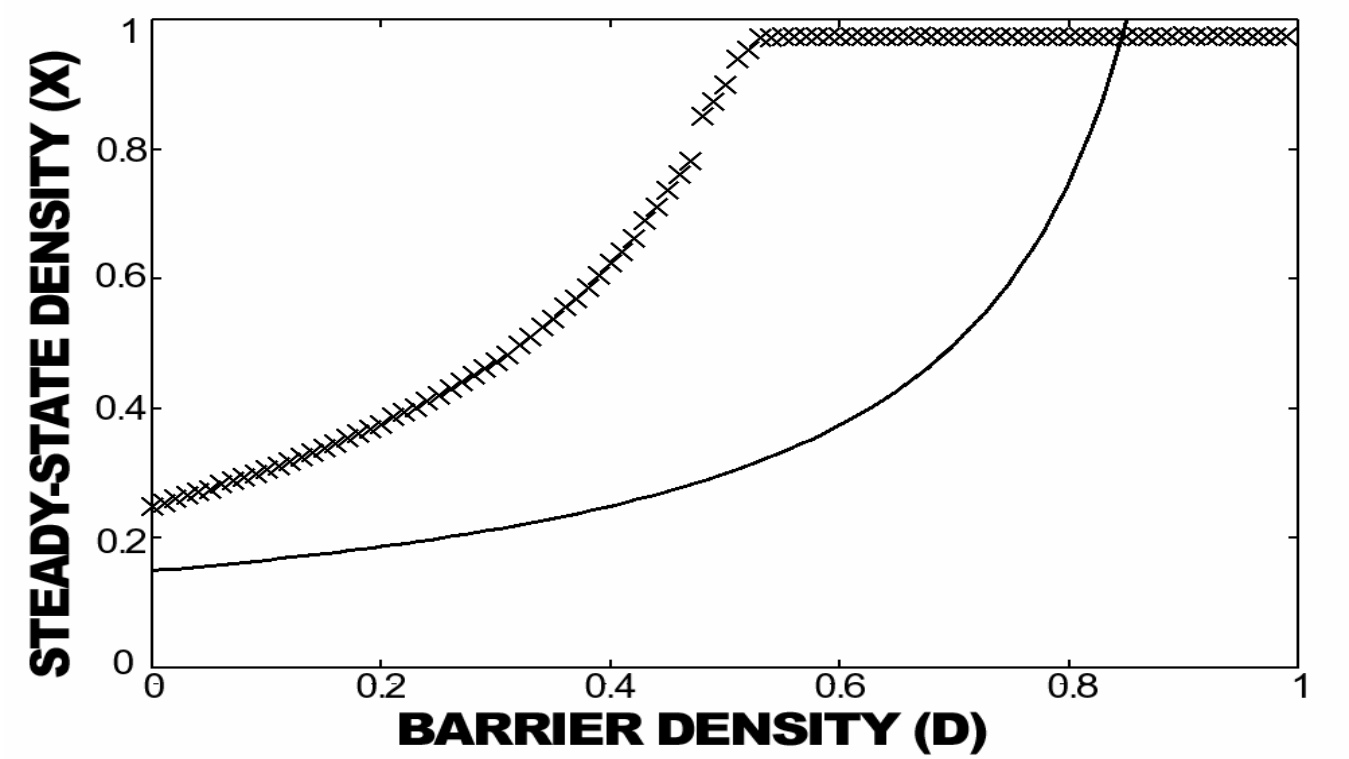

(b) predator Y

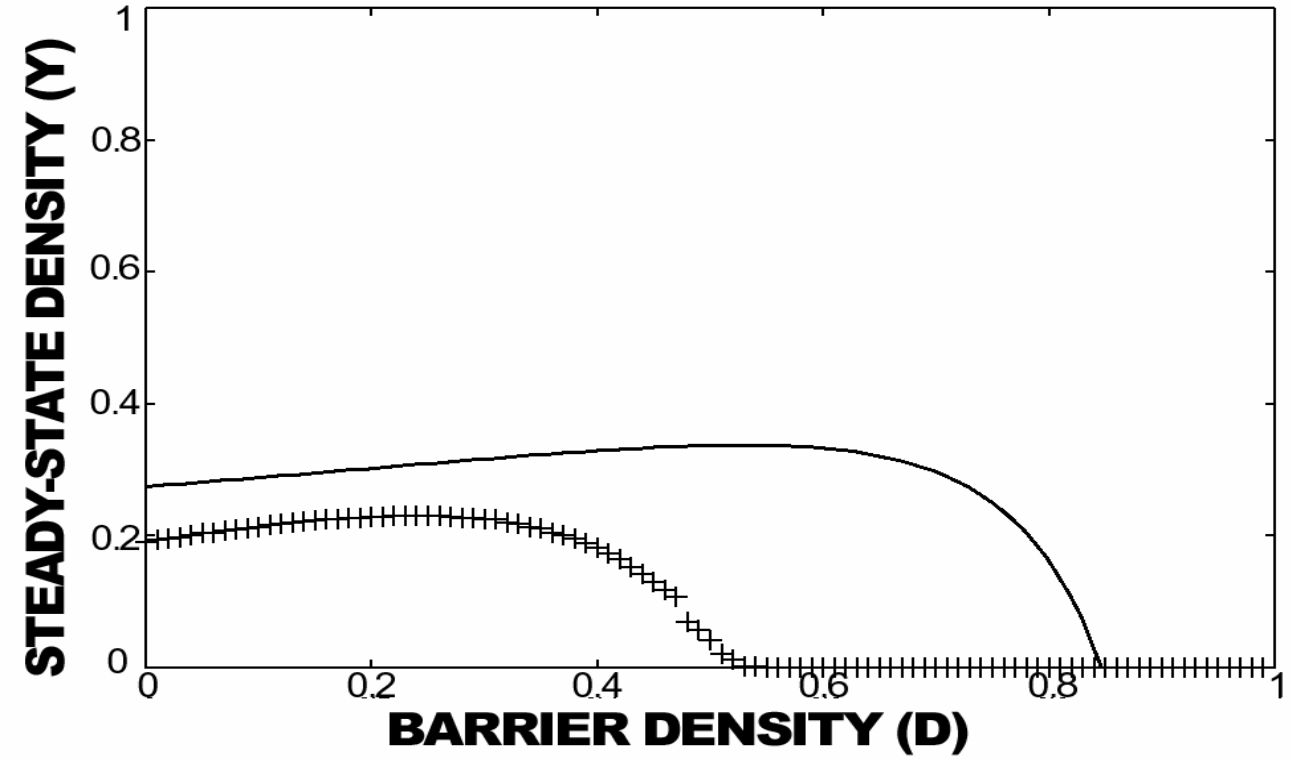

Fig.3. The results of bond destruction. The steady state density of prey X (a) and predator Y (b) are plotted against the barrier density *D*. Each plot is obtained by the long-time average in the stationary state ($500 < t \leq 1500$) with 100x100 lattice. The solid lines represent theoretical results of MFT.

The mean-filed theory (MFT) sufficiently predicts the population dynamics of both species, and the extinction of predators. However, extinction point D_{B0} takes a value much higher compared to the lattice model (Figs. 3). Moreover, we find from Fig. 3(a) or 3(b) that the density P_X (or P_Y) for the lattice model is much smaller (or larger) than that predicted by MFT. When the species Y goes extinct ($D>D_{B0}$), our system (1) becomes the contact process of X (and O)[Harris 1974]. In this case, the preys (X) occupy approximately the whole lattice points. Note that the mortality rate m_X of prey is assumed to have a very small value. In addition, the extinction point D_{B0} for the lattice model is found to be close to the critical value D_{BC} of percolation transition. This result suggests that the connection of barriers leads to the fragmentation of habitat, and the effect of destructions becomes severe.

4.2. Site Destruction

We perform the perturbation experiment of site destruction model. Fig. 4 illustrates a typical example of time dependence of densities of both species, where the value of D is increased from 0 to 0.3 at time t=0. The results of the dynamics are qualitatively identical to those of bond destruction. Typical spatial patterns in the stationary state are illustrated in Fig.5, and steady-state densities are plotted in Fig. 6. From Fig.6, we find that:

The profiles of steady-state densities for site destruction (Fig. 6) are almost the same as those for bond version (Fig. 3). However, extinction point D_{S0} of predator for site destruction takes a smaller value compared to the bond version. In the case of site destruction, however, the extinction threshold D_{S0} is much smaller than the percolation transition point ($D_{SC}\approx 0.6$). The mechanism of this paradox is discussed in the next section.

5. Discussion

To study habitat destruction, we compare bond and site destructions. We find unintuitive results: not only prey but also predator increase with the increase of intensity D of destructions, so long as D takes small values. When the value of D is large, the species Y deceases and goes extinct with increasing D; even though there exists a lot of prey, predators go extinct. The extinction of predators can be explained by mean-field theory (MFT). Let D_{B0} and D_{S0} be the extinction thresholds of predator for bond and site destructions, respectively. We find that both D_{B0} and D_{S0} for MFT take similar values. However, it is found that these values for lattice model is much smaller than those predicted by MFT.

The difference between lattice simulations and MFT may come from the percolation of destruction (fragmentation of habitat). The connection of destructions plays an important role in the lattice systems. If destructions are connected, the habitat is fragmented. When the intensity D of destruction exceeds a critical value, the so-called percolation transition occurs [Stauffer 1985, Sahimi 1993]. Because of percolation (fragmentation), the species easily go extinct. According to the percolation theory, the percolation threshold is given D_{BC}=0.5 and $D_{SC}\approx 0.6$ for bond and site destructions, respectively. Thus, the percolation threshold for bond destruction is smaller than that for site destruction. However, Figs. 3 and 6 reveal the opposite result: the extinction threshold for bond destruction is larger, compared to that for site version. This paradox is accounted by the percolation not of destroyed sites but of living sites. For example, we consider the case of site destruction. In this case the living site can be regarded as *sanctuary*. We must discuss the connection of sanctuary sites instead of destroyed sites. The percolation of sanctuary sites occurs, when D<0.4. Namely, the fragmentation of sanctuary occurs for D>0.4! Similarly, in the case of bond percolation, living region is fragmented for D>0.5. Hence, we can explain the mechanism of paradox.

So far, we have considered a simple press perturbation such that barrier density is jumped from zero to a nonzero value of D. Now we can consider more general cases. D is increased from D_1 to D_2. If $D_1 < D_2 < D_{B0}$, then the species Y can survive. However, If $D_1 < D_{B0}$ (or D_{C0}) $< D_2$, then the species Y becomes extinct. Even if the difference between D_2 and D_1 is very small, the extinction can occur. The present work shows the extinction of Y by direct effect. Recall that previously we studied the case that the destruction prohibits the reproduction of prey. In this work, the predator Y indirectly went extinct with the increase of D. In real fields, such a direct and indirect extinctions may occur. It is necessary to take care of not only one species but also all species in a particular ecosystem.

(a) Lattice model

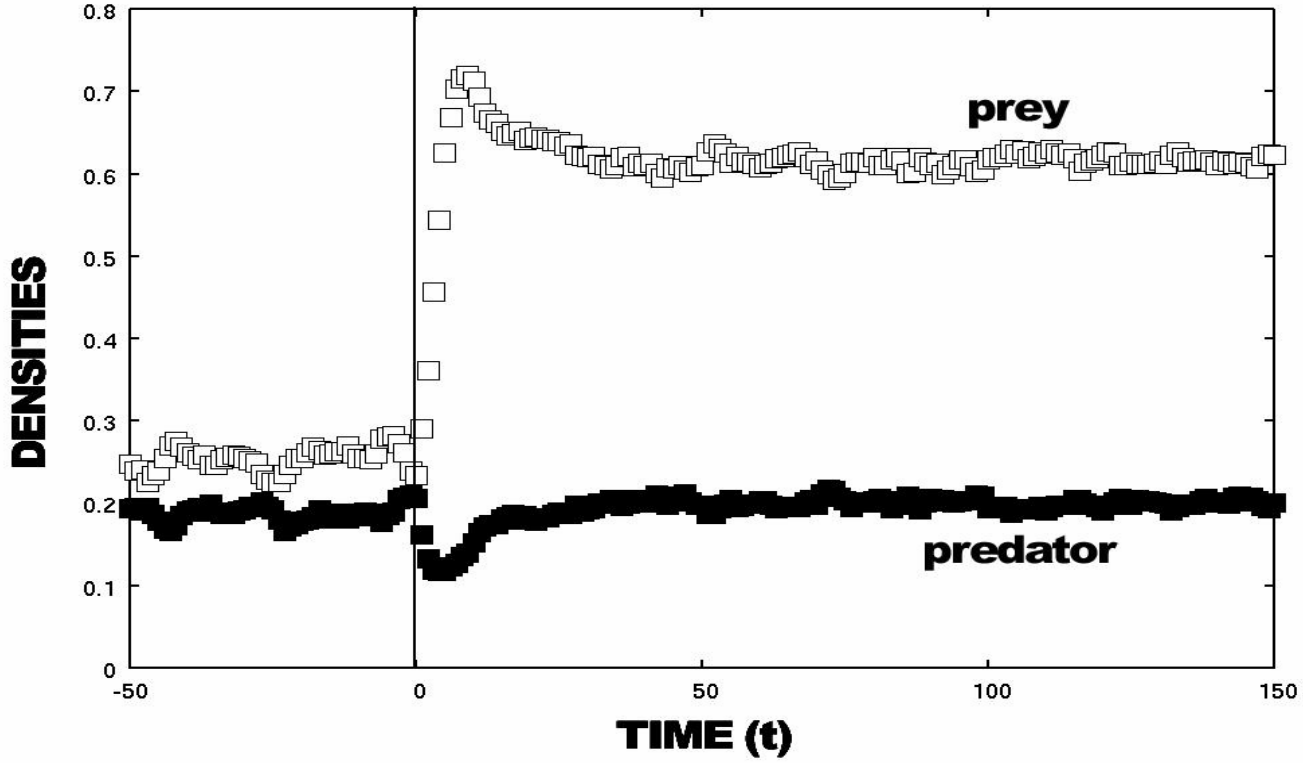

(b) MFT

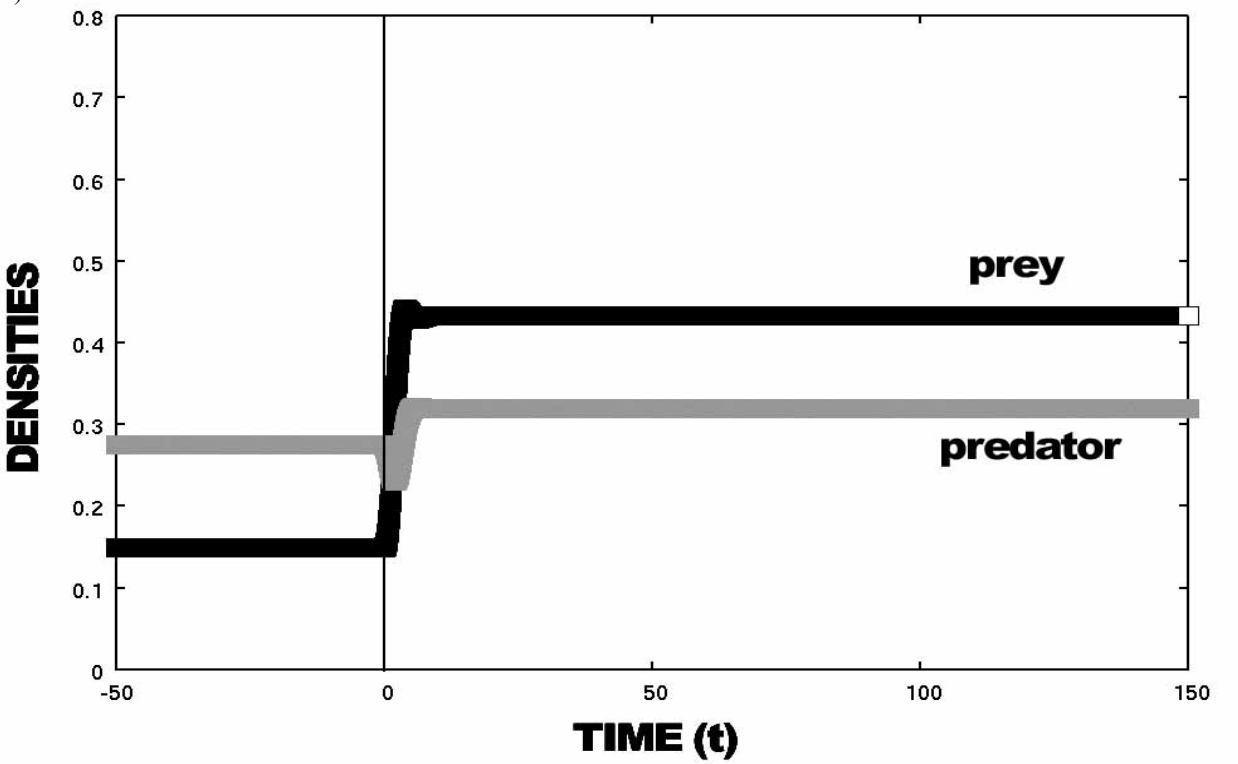

Fig.4 An example of population dynamics for site destruction. (a) lattice model and (b) MFT (100x100). The time dependence of both species X and Y are shown. At time t=0, the value of D increases from 0 to 0.3. We put r=1.0, p=2.0, m_X=0.05, m_Y=0.6.

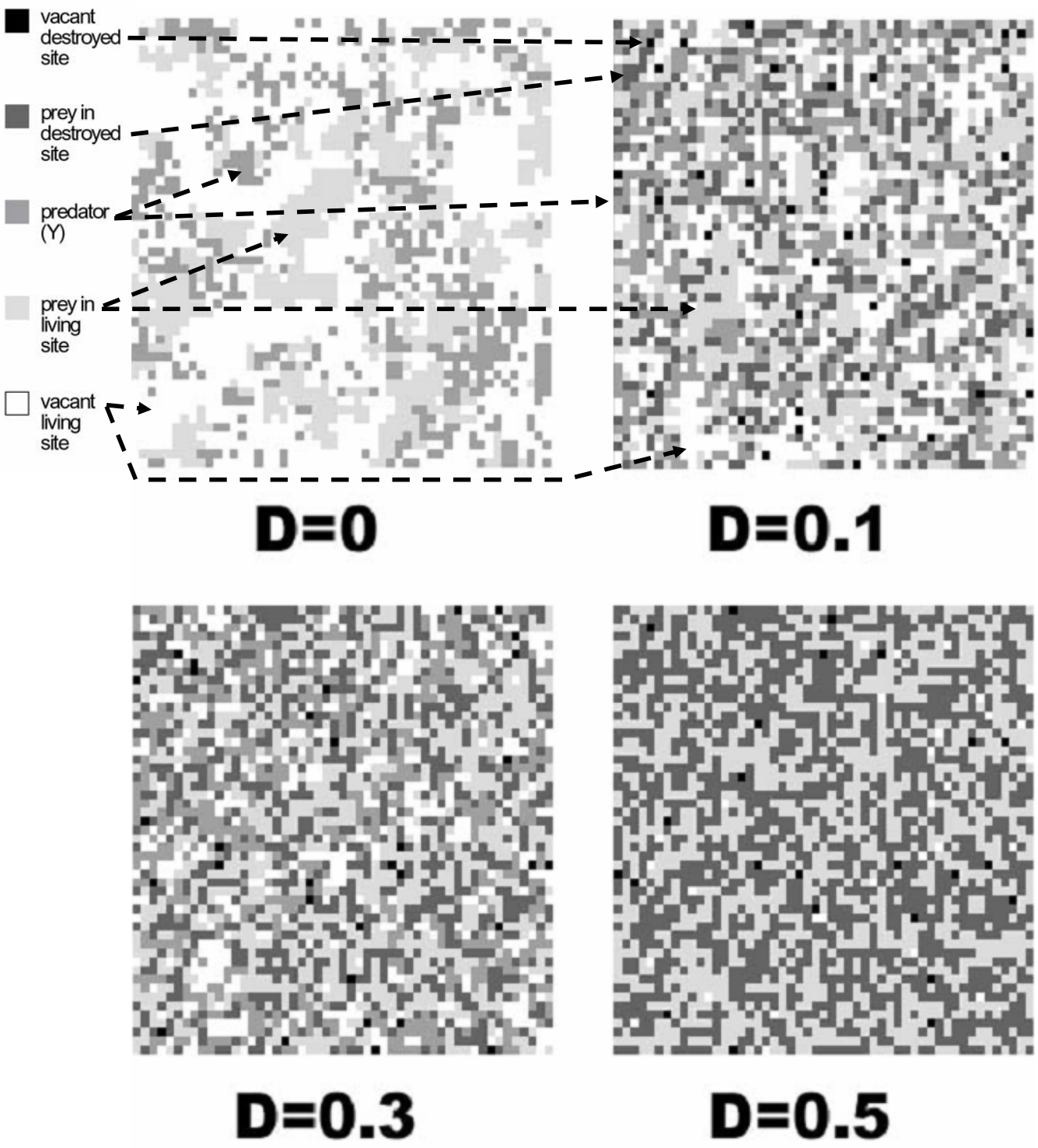

Fig. 5. Typical spatial patterns of site destruction model for various values of D (r=1.0, p=2.0, m_X=0.05 and m_Y=0.6); vacant destroyed site (black), prey in destroyed site (X_D: dark grey), predator Y (grey), prey in living site (light grey) and the vacant living site (white).

(a) prey X

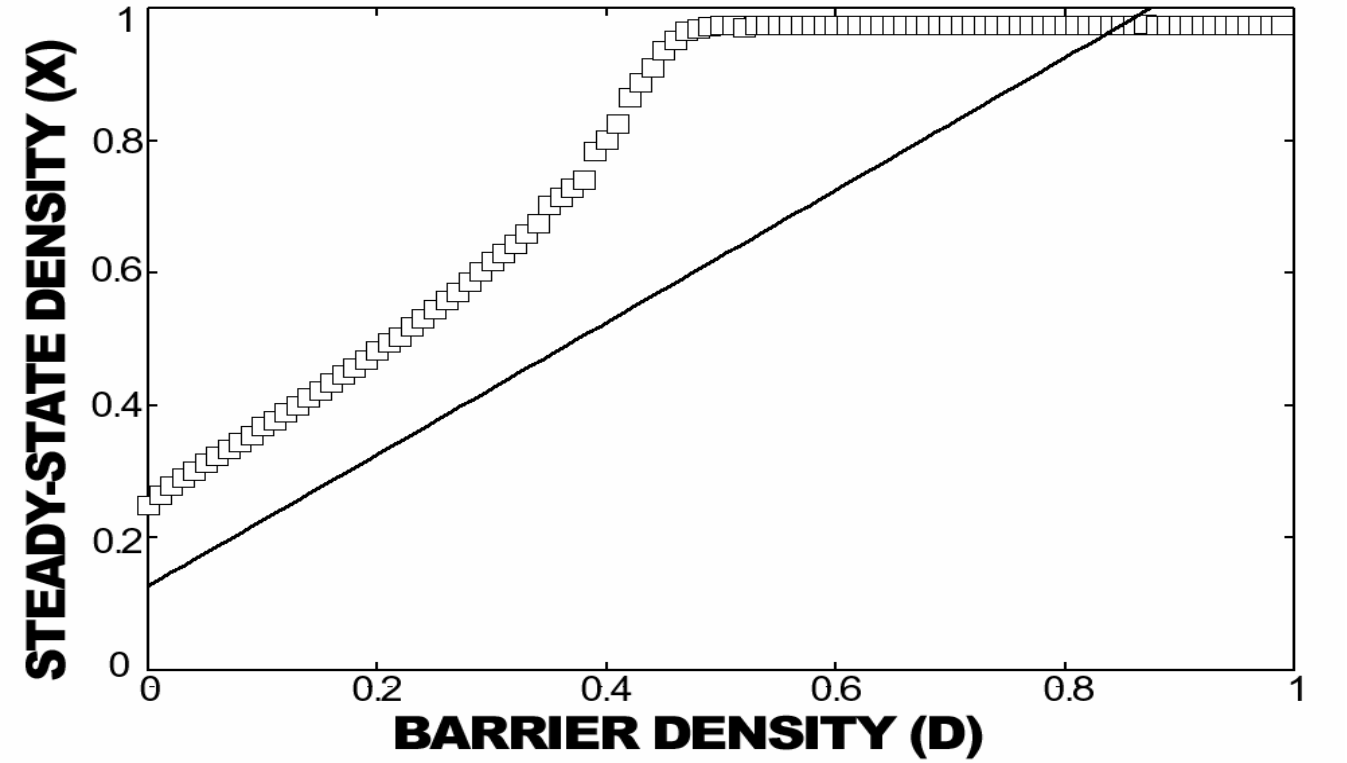

(b) predator Y

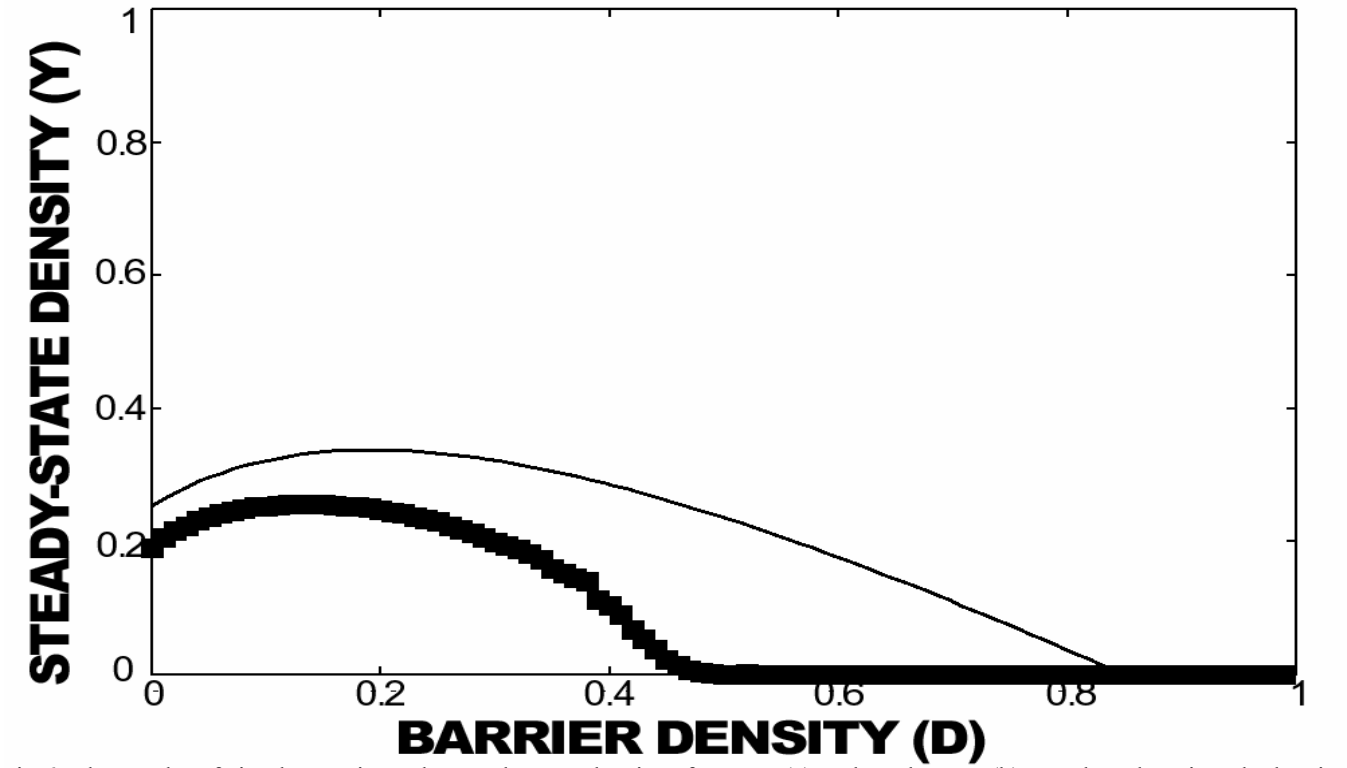

Fig.6. The results of site destruction. The steady state density of prey X (a) and predator Y (b) are plotted against the barrier density D (r=1.0, p=2.0, m_X=0.05 and m_Y=0.6). The curves denote the theoretical results of MFT.

ACKNOWLEDGMENTS
This work is supported in partly the by the Grant-in-Aids of the Japan Society for the Promotion of Science to K.T. and J.Y.

REFERENCES
[Bascompte and Sole 1998] Bascompte, J., Sole, R.V. Effects of Habitat Destruction in a Prey-Predator Metapopulation Model. *Journal of Theoretical Biology,* 195:383-393, 1998.

[Boswell et al98] Boswell, G. P., Britton, N. F., Franks, N. R. Habitat fragmentation, percolation theory and the conservation of a keystone species, *Proceedings of Royal Society of London Series B,* 265-1409:1921-1925, 1998.

[Debinski 1999] Debinski, D. M., Holt, R. D. A Survey and Overview of Habitat Fragmentation Experiments. *Conservation biology,* **14**-2:342-355, 1999.

[Fahrig 2003] Fahrig, L. Effects of Habitat Fragmentation on biodiversity. *Annual Review of Ecology, Evolution, and Systematics,* **34**:487-515 2003.

[Frankel Soule 1981] Frankel, O.H., Soule, M.E. Conservation and Evolution. Cambridge University Press, Cambridge, 1981.

[Harris 1974] Harris, T. E. Contact interaction on a lattice. *Ann. Prob.,* **2**: 969-988, 1974.

[Hofbauer Sigmund 1988] Hofbauer, J., Sigmund, K. 1988. The theory of evolution and Dynamical Systems. Cambridge University Press, Cambridge, 1988.

[Itoh Tainaka 1994] Itoh, Y., Tainaka, K. Stochastic limit cycle with power-law spectrum. *Phys. Lett.,* **A 189**:37-42, 1994.

[Kondoh 2003] Kondoh, M. Habitat fragmentation resulting in overgrazing by herbivores, *Journal of Theoretical Biology,* **225**:453-460, 2003.

[Matsuda et al 1992] Matsuda, H., Ogita, N., Sasaki, A. and K. Sato, K. Statistical mechanics of population: the lattice Lotka-Volterra model. *Prog. Theor. Phys.,* **88**: 1035-1049, 1992.

[Nakagiri 2001] Nakagiri, N. Indirect relation between species extinction and habitat destruction, *Ecological modeling,* 137:109-118, 2001.

[Nakagiri 2004] Nakagiri, N. Indirect relation between species extinction and habitat destruction, *Ecological modeling,* 174:103-114, 2004.

[Tao et al 1999] Tao, T., Tainaka, K., Nishimori, H. Contact Percolation Process: Contact process on a destructed lattice. *J. Phys. Soc. Japan,* **68**: 326-329, 1999.

[Sahimi 1993] Sahimi, M. Applications of percolation theory. Taylor and Francis, London, 1993.

[Stauffer 1885] Stauffer, D. Introduction to percolation theory. Taylor and Francis, London, 1985.

[Swihart 2001] Swihart R.K., Feng Z., Slade N.A., Mason D.M., Gehring T.M. Effects of habitat destruction and resource supplementation in a predator-prey metapopulation model. *J. Theor. Biol.,* **210**-3:287-303, 2001.

[Tainaka Fukazawa 1992] Tainaka, K. and Fukazawa, S. Spatial pattern in a chemical reaction system: prey and predator in the position-fixed limit. *J. Phys. Soc. Japan,* 61: 1891-1894, 1992.

[Satulovsky Tome 1994] Satulovsky, J. E., Tome, T. Stochastic lattice gas model for a predator-prey system. *Phys. Rev.* **E 49**:5073-5079, 1994.

[Soule 1987] Soule, M. E. Viable populations for conservation. Cambridge University Press, Cambridge, 1987.

[Sutherland Jacobs 1994] Sutherland, B. R., Jacobs, A. E. Self-organization and scaling in a lattice prey-predator model. *Complex System* **8**:385-405, 1994.

[Tainaka 1994] Tainaka, K. Intrinsic uncertainty in ecological catastrophe. *J. Theor. Biol.* **166**: 91-99. 1994.

[Tainaka 1988] Tainaka, K. Lattice model for the Lotka-Volterra system. *J. Phys. Soc. Japan,* **57**: 2588-2590, 1988.

[Tainaka Nakagiri 2000] Tainaka, K. and Nakagiri, N. Segregation in an interacting particle system. *Phys. Lett.,* **A 271**: 92-99, 2000.

[Takeuchi 1996] Takeuchi, Y. Global dynamical properties of Lotka-Voltera systems. World Scientific, Singapore, 1996.

Prediction of blood nutrient supply to tissues of economical interest in Ruminants: a first step with the prediction of portal blood flow

Jean Vernet
Unité de Recherches
sur les Herbivores
INRA
Theix
63122 S^{t}-Genès Champ^{le}, France
+33 04 73 62 42 24
Jean.Vernet@clermont.inra.fr

Hélène Lapierre
Dairy and Swine Research and
Development Centre
Agri. and Agri-Food Canada
Lennoxville, QC,
Canada J1M 1Z3
+1 819 565 9174
lapierreh@agr.gc.ca

Pierre Nozière
Unité de Recherches
sur les Herbivores
INRA
Theix
63122 S^{t}-Genès Champ^{le}, France
+33 04 73 62 46 86
Pierre.Noziere@clermont.inra.fr

Stéphanie Léger
Laboratoire
de Mathématiques
Université de Clermont-Fd II
24, avenue des Landais, BP 26
63177 Aubière Cedex
+33 04 73 40 63 63
Stephanie.Leger@math.univ-bpclermont.fr

Daniel Sauvant
UMR INRA-INAPG
Physiol. Nutrition et Alimentation
INRA
16 rue Claude Bernard
75231 Paris Cedex 03
+33 01 44 08 17 55
Daniel.Sauvant@inapg.inra.fr

Isabelle Ortigues-Marty
Unité de Recherches
sur les Herbivores

Theix
63122 S^{t}-Genès Champ^{le}, France
+33 04 73 62 42 29
Isabelle.Ortigues@clermont.inra.fr

ABSTRACT
Within a research program developed to model the fluxes and exchanges of blood nutrients between the major organs and tissues in Ruminants, the initial objectives were 1/ to create a bibliographic database on blood nutrient fluxes and 2/ to apply methods of meta-analysis to establish the law of response of the portal blood flow (PBF) as a function of the dry matter intake (DMI).

The conceptual model of the database was divided in 6 parts: 1/ the identification of the sources of information, 2/ the dietary conditions, 3/ the infusion of substrates, 4/ the methods of measurement and determination, 5/ the results of net blood nutrient fluxes and 6/ any other experimental information.

An initial dataset was constituted from 79 publications corresponding to 113 treatments on bovine and 118 on ovine. A meta-analysis was carried out according to the following steps: 1/ choice of an exponent of the body weight, 2/ selection and coding of the groups of treatments, 3/ global meta-analysis approach, 4/ within-group meta-analysis approach. Each type of meta-analysis included a covariance analysis of PBF vs DMI, and a statistical analysis of the residuals. One global response law was established on the pooled ovine and bovine populations. Two within-group of treatments response laws were established on ovine and on bovine separately.

The within-group approach brought more precision and reliability than the global one with lower residual variation. Consequently it allowed to detect differences in slopes between the ovine and the bovine population, which was not possible with the global approach. The increase of PBF with DMI was thus significantly higher in bovine than in ovine.

KEYWORDS
Database, meta-analysis, response laws, net nutrient fluxes, organs and tissues

1. Introduction

Research conducted in animal nutrition to improve animal performances and health as well as the quality of livestock products increasingly requires the ability to integrate knowledge on complex mechanisms [Sauvant 1992]. In particular, the metabolism of the different organs and tissues of the whole body has to be related in order to better understand the factors which regulate the metabolism of the productive tissues of economical interest (muscle and adipose tissues in growing animals raised for meat; mammary gland in dairy cows raised for milk). Each organ and tissue has its own requirements and functions which respond to different signals [Lobley Lapierre 2003]; [Ortigues-Marty *et al.* 2003]. Responses of productive tissues depend on the amount and the nature of their nutrient supply in interaction with hormonal signals. The nutrient supply to each tissue will obviously be related to feed intake and composition. It will also be linked with the metabolic utilization of nutrients in other tissues, in a coordinated response driven by the physiological priorities (or status) of the animal.

The present research program is thus aiming at modeling the fluxes and exchanges, from blood circulation, of nutrients between the major organs and tissues of the animal (digestive tract, liver, muscle, udder, adipose tissues) in relation with feed intake and composition. The objective is to develop a research tool to predict the supply of energetic and nitrogenous nutrients to peripheral tissues (muscle, udder) that will be used to better control and ultimately improve meat and milk yields and qualities. The initial step of this program consists of quantitatively reviewing all the experimental information existing on the net fluxes of nutrients among tissues and organs in ruminants in order to establish quantitative response laws. Subsequently, these laws will be included in a model of tissue metabolism and nutrient exchanges. The present paper describes the inter disciplinary approach developed to answer a biological question, consisting of determining the quantitative response laws relating portal blood flow (PBF) to dry matter intake (DMI). The PBF variable was selected in a first step because it is known to have a major quantitative influence on the results of blood nutrient fluxes.

The first objective which called upon computer and modelling expertise consisted in creating a bibliographic database of net nutrient fluxes across the splanchnic tissues, alone or in combination with other tissues such as the hind-limb or the mammary gland, in ruminants, called FLORA (standing for FLuxes of nutrients through Organs and tissues in Ruminant Animals). The data to be input concerned the animals, the diets (with key parameters of the chemical composition and nutritional value of the feeds and diets), the experiments with a description of the experimental treatments, the methods of measurement and determination of blood nutrients and the results of net nutrient fluxes. The principles and relevance of databases are well-known [Lescourret 1992]. In particular, they make it possible to store important volumes of data which can then be handled easily by means of powerful software [Microsoft 2002a].

The second objective which required statistical expertise consisted in applying statistical methods used in meta-analyses in order to establish quantitative response laws [Sauvant 2005], [St-Pierre 2001]. These powerful methods allow drawing quantitative conclusions which cannot be obtained as soundly with traditional bibliographic reviews. A pre-requisite condition for good practices is that the experiments gathered for a meta-analysis must relate the same experimental factors. Additionally, some meta-analytical methods have been developed specifically to distinguish between the global, and within-study variations and thus reduce the impact of biases on the prediction equations [Sauvant 2005].The within-study variations strictly include variations due to the influence of experimental treatments, all other conditions being identical. On the other hand, the global variations include both the influence of experimental treatments and the influence of changes in the conditions of result acquisition (e.g. type of animal, measurement methods, research team…). . Advantages and weakness of studying the global or the within-study variations will be discussed, in particular when combining data from different populations and when testing linear or quadratic responses.

The present paper presents the meta-analytical methods used to study the response of the PBF to DMI. The portal vein drains the digestive tract, the spleen, the pancreas and associated mesenteric fat and its blood flow has already been shown to be related to DMI [Lescoat *et al.* 1996]. The study was carried out from a set of publications available on ovine and bovine. In animal sciences, in order to combine data from different species, it is usual to divide the results by the live weight of the animal raised at a certain power [Brody 1945]. The choice of the exponent for the weight is a key element to compare species. Conventionnally, results are often expressed according to the weight raised to power 0.75 [Brody 1945], [INRA 1988]. This has also been the case for blood flows in the portal vein until now ([Ortigues 1991], [Rémond *et al.* 1998] but some authors advise on the use of another exponent ([Berthelot 2000]. The present work therefore includes a systematic exploration of the possible exponents of the weight (i.e. ranging between 0.5 and 1.2).

2. Material and methods

2.1. The Flora Database

For the conception of the FLORA database, the choice was made of a relational database in order to structure information in an optimal way and to structure relationships between the different pieces of information. FLORA was initially designed by using the Merise method which is now largely used in many fields, including agriculture [Lescourret 1992]. It was then implemented under Access which is usable on microcomputers and which offers a significant processing capability [Microsoft 2002a].The conception of FLORA was based on the structure of a first experimental database, built for a study carried out on 6 multicatheterized lambs [Vernet *et al.* 2002]. Constraints for FLORA were 1/ to gather all data published on net splanchnic nutrient fluxes (energetic and nitrogenous) measured in multicatheterized animals, 2/ to precisely describe the experimental treatments and conditions including the amounts and the composition of the diets fed to these experimental animals and 3/ to ensure the traceability of the data and results, in particular to know if they were specified in the publication, calculated from other results or estimated.

2.2. Meta-Analyses

The present study was carried out on a data file which included 79 publications, dating from 1965 to 2003 and corresponding to 231 treatments, including 113 on bovine and 118 on sheep. The data on fasting animals were withdrawn. The response law of PBF [liter per hour and per kg body weight raised to exponent e, l/(h.kg BW^e)], was established as a function of DMI [g per

day and per kg body weight, raised to exponent e, g/(d.kg BW^e)]. All data were expressed per kg BW^e of the animals in order to allow comparisons between species of different body weights [Brody 1945].

The first two steps of the meta-analysis were interdependent. The first step was to compare different exponents of the body weight. The exponents e= 0.5, 0.6, 0.7, 0.8, 0.9, 1.0, 1.1 and 1.2 of BW, as well as the exponents e=0.66 and 0.75 conventionally used in animal nutrition [Ortigues-Marty *et al.* 2003], were tested both graphically and by ANOVA using the specie as the main factor. The best exponent of the body-weight was the one which reduced the most any significant species effect on the explanatory variable.

The second step involved the constitution, the selection and the coding of groups of treatments within each publication. This step aimed at selecting, among all the experimental treatments cited in the publications available, the treatments which involved a change in the dependent variable of interest [Sauvant 2005]. Thus in the present case, only the treatments, within each publication, implying a change in DMI were kept. Thereby they constituted a group of treatments. An additional and necessary precaution within each group was to select treatments where the explanatory variable DMI was not biased by other factors, in particular the nature of the diet and the physiological stage of the animal. This selection was carried out based on the scientific objectives of the studies and on the within publication standard deviations of the explanatory variable (DMI).

The interdependence between these two steps lays in the fact that the selected groups were used for the choice of the exponent of the body weight and conversely, the selection of the groups was made on the basis of a particular exponent of the body weight.

A comparative meta-analysis was then carried out based on 1) a GLOBAL approach and 2) an WITHIN- group of treatments approach. Both GLOBAL and WITHIN meta-analyses were carried out on the selected groups of treatments (n=8 on sheep and n=7 on bovine), as detailed in section 3.2.2. For both meta-analysis approaches, the dependent and the explanatory variables (Y and X) were centered on their means and were thus expressed as $Y - \overline{Y}$ and $X - \overline{X}$, with $\overline{Y}$ and $\overline{X}$ being the means of all the selected treatments.

In the GLOBAL meta-analysis approach, the two covariance models $\mathbf{(Y - \overline{Y}) = \alpha + \beta\,(X - \overline{X})}$ and $(Y - \overline{Y}) = \alpha + \beta(X - \overline{X}) + \delta(X - \overline{X})^2$ were used to test linear effects only and both linear and quadratic effects, respectively.

In the WITHIN-group meta-analysis approach, the following covariance model $(Y - \overline{Y}) = \alpha + \alpha i + \beta\,(X - \overline{X})$ was applied, where α and β were coefficients common to all groups of treatments, and where αi corresponded to the effect of the group of treatments i. Concerning the covariance model, it should be stressed that because of the presence of only 2 treatments in the majority of the selected groups of treatments, the βi term representing the slopes of the groups of treatments could not be added to the model. This same reason precluded the possibility of testing any quadratic effect.

Analysis of the model residuals was then carried out by checking the standardized residuals (their distribution, their numerical value, their contribution to the residual variance, their leverage as well as the Cook's distances ([St-Pierre 2001], [Sauvant 2005]).

The Minitab software was used to complete the meta-analyses because of its graphic and statistical capacities [Minitab 2003].

3. Results

3.1. The Flora Database

Accounting for the above mentioned constraints led to a conceptual model of the data which was divided into 6 parts (Figure 1). They are briefly described here as more details on the conception and elaboration of the Flora database are available elsewhere [Vernet Ortigues-Marty 2005].

Figure 1 The different information in the FLORA database

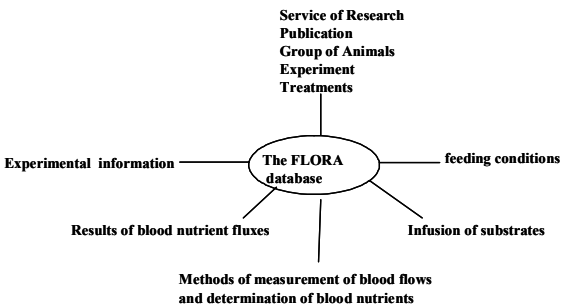

The first part of the model was used to identify the source of information and to depict the publication (number, title and source), the group of animals (number, specie, sex and physiological stage) and the experimental treatments (number, name, duration, nature of the treatment). To identify the source of information and facilitate the subsequent structuring of the data, two objects were created: SPEG (for administrative Service of the person who inputs the publication, Publication, Experiment and Group of animals) and SPEGT (for Service, Publication, Experiment, Group of animals and Treatment). The group of animals was a set of animals which were submitted to particular experimental conditions and for which some results of net nutrient fluxes were reported in the publication. This part also described the publication and its relationship with the author (name of the author), the group of animals and the experimental treatment.

In order to later establish laws of response between blood nutrient fluxes and feeding conditions of the animals, the second part of the model described the feeding conditions. This part was composed of the diets (name, percentage of concentrate, percentage of forage), the ingredients (type of conservation, plant family and plant specie), the feed composition of the diets (i.e. the centesimal composition of the diet in feeds, the intake, the chemical composition (e.g. the content in vegetable walls) and the nutritional values (e.g. the energy and nitrogen content) of the diets and ingredients.

In some studies, in order to follow the transformation of particular ingredients or molecules which occurs in the metabolism of the animal, some substrates (e.g. glucose, casein) were infused into the animal in particular anatomical sites, by means of blood catheters or digestive cannulas during the experiment. So, the third part of the model dealt with the supply of substrates. and described the nature of the substrates, whether they were administered alone or in a mixture, the corresponding supply in energy or nitrogen, the characteristics of the infused solutions (pH, molarity, osmolarity) and the infusion conditions (duration and rate of infusion).

The methods of measurement and determination may vary according to the team of research and the date of publication. They are supposed to affect the results. So, the fourth part of the model described the methods of measurement of the blood flows, the methods of determination of the concentrations and net fluxes of nutrients present in blood (or plasma) as well as the methods of determination of the nutrients and the pH of the rumen fluid. The choice was made to classify methods according to their principle, which proved convenient and feasible in most cases. Moreover, methods were detailed to the maximum by indicating the compartment of measurement (blood or plasma), the techniques of deproteinisation, the refrigeration and the freezing of the samples,…

The fifth part of the model was very important because it described the results. These latter could be divided into three types: the results of blood flows (e.g. the blood flow in the portal vein), the results of net fluxes of blood (or plasma) nutrients and the results of the parameters of the rumen fluid (e.g. pH, volatile fatty acids,…). The first two types of results could be connected to different anatomical sites (blood vessels or organs). Corresponding to theses type of results, three relationships were built, with some difficulties due to the high number of necessary branches and the necessity to put several properties in the relationships themselves.

Last, in order to be able to explain certain influent or aberrant data, it was important to memorise all the information available in the publication. So, the sixth part of the model described information on the experimental period, the catheters implantations, the blood sampling protocol, the statistical analyses and the meal frequency.

3.2. Meta-Analyses

3.2.1 Choice Of An Exponent For The Body Weight

In order to allow the combination of data obtained from different animal species of widely different body weights, the choice of an exponent for the body weight of the animal is an essential step. Ten exponents were tested. Figure 2 shows the graphs obtained with exponents 0.66, 0.75 and 1.0 (data for other exponents not shown). Graphically, the best overlap on DMI between the ovine and bovine data was obtained with the exponent 1.0. The DMI [expressed as g/(d.kg BW^e)] was significantly different between the 2 species, as tested by a one-way factorial ANOVA, with the exponents 0.5, 0.6, 0.66, 0.70, 0.75, 0.80 and 1.2. On the other hand, it was not significantly affected by the animal species with exponents 0.9, 1.0 and 1.1, with a higher probability being obtained for the exponent 1.0. (P= 0.85). On those bases, it was then decided to use the exponent e=1 in all subsequent analyses.

Figure 2 Influence of the exponent of body-weight on the variation of portal blood flow (PBF) with dry matter intake (DMI) within the selected studies (data are expressed per kg BW^{e} with e = 0.66 (a), 0.75 (b) and 1.0 (c), one point represents one treatment, several points connected together by a line represent one group of treatments)

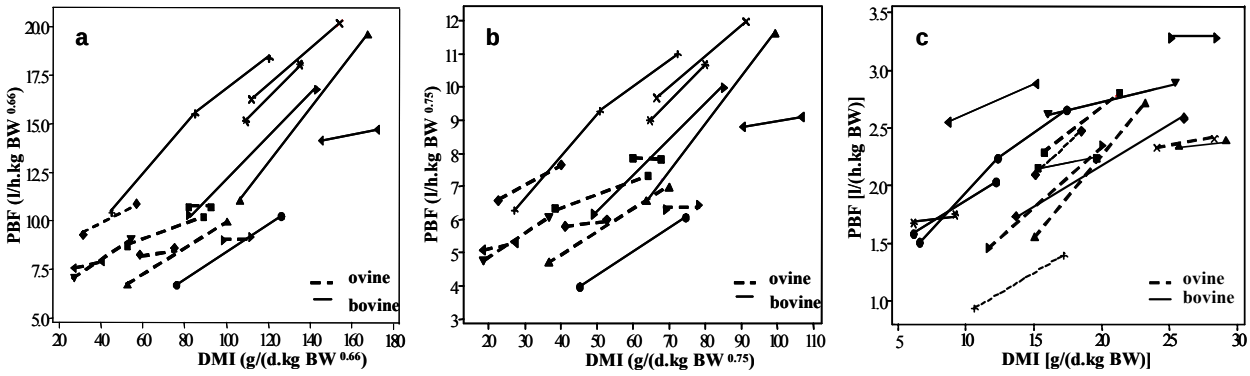

3.2.2 *Selection Of The Appropriate Groups Of Treatments*

In order to establish a response law where the explanatory variable DMI was not biased by other factors, in particular the nature of the diet and the physiological stage of the animal, a rigorous selection of the experimental studies which aimed strictly at testing the influence of changes in DMI was carried out (Table 1). The publications, and within the publications, the groups of treatments with a "strict" DMI effect were kept for the analysis while those with a confusion of effects between DMI and other variables were rejected. Thus, each selected study was subdivided into only one or several groups of treatments according to whether there were one or 2 factors of variation in the study. It was the case, in particular, for the studies with a 2x2 factorial design which were divided into two or several groups of treatments. Coding of the studies was then carried out to easily identify groups of treatments which varied only on the explanatory variable DMI and which were homogeneous on the other variables (e.g. the nature of the diet).

Table 1 Examples of selection and coding of groups of treatments within publications

Publication n^{o}	Treatment name	Treat^{t} no	Diet	DMI [g/(d.kg BW $^{1.0}$)]	Comment	Group of Treatments n^{o}
131	Alfalfa silage – low intake	1	Alfalfa silage	67	This publication was divided into 2 distinct groups of treatments according to the nature of the diet	131-1
131	Alfalfa silage – high intake	2	Alfalfa silage	91		131-1
131	Bermudgrass silage – low intake	3	Bermudgrass silage	65		131-2
131	Bermudgrass silage – high intake	4	Bermudgrass silage	80		131-2
112	Low level of concentrate	1	27% [25% cracked corn + 75% grain:urea (100:1)] + 73% hay	75	This publication which had a confusion of DMI and diet composition effects was removed from the analysis	-
112	High level of concentrate	2	63% [36% cracked corn + 64% grain:urea (100:1)] + 37% hay	64		-
24	1 fold maintenance	1	100% dactyle hay	15	This publication gave birth to only one group of treatment	24-1
24	0.5 fold maintenance	2	100% dactyle hay	9		24-1

The identification of those groups of treatments could also imply to select a limited number of experimental treatments within a study. At this stage, out of the initial dataset, only 16 groups of treatments (8 on bovine and 8 on ovine) and 34 treatments were kept for the analysis. Except for 2 groups of treatments which had 3 levels of DMI, all other groups had only 2 levels.

Following this first selection, another selection was made on the standard deviation of DMI within groups of treatments to keep only the groups of treatments which had a sufficient variation on the explanatory variable. In that step, knowledge of nutrition experts was called upon to fix a minimum threshold of standard deviation below which groups of treatments would be rejected. This minimum threshold was set at 1.5 g/(d.kg BW) within a group of treatment. On the whole, out of the initial dataset, only 15 groups of treatments (7 on bovine and 8 on ovine) and 31 treatments were kept for the analysis.

For the selected groups of treatments, several aspects could be underlined (Figure 2c): 1/ for most groups of treatments, PBF increased with DMI, 2/ the mean slope appeared visually to be different between the 2 species, it appeared to be higher in bovine than in ovine, 3/ within specie, the average DMI across all treatments were also similar between ovine and bovine (17.65 ± 8.10 vs 17.15 ± 5.71 g/(d.kg BW)), 4/ the ranges of DMI and PBF were similar in ovine and in bovine (for DMI: from 6.10 to 29.15 g/(d.kg BW) in ovine vs from 6.54 to 28.33 g/(d.kg BW) in bovine), but 5/ the ranges of DMI and PBF varied greatly between the groups of treatments considered . Thus, in order to allow the study of the within-groups variations independently of the among-groups variations, the centering of the variables was considered to be necessary (see part 2.2); 6/ it should be pointed out that only 1 out of the 15 groups of treatments presented 3 levels of DMI. Finally, it may be indicated that selected bovine population corresponded to growing cattle (varying between 199 and 349 kg of body-weight). In the ovine population, 6 groups of treatments were adult non producing ewes and castrated sheep varying between 44 and 82 kg of body-weight) while 2 groups of treatments corresponded to growing animals, varying from 32 to 40 kg body -weight.

3.2.3 Global Meta-Analysis Approach

The first type of meta-analysis was carried out following a global approach.. First linear response laws were tested separately for the ovine and bovine populations. Comparisons of the slopes β carried out by t-test indicated that the differences between ovine and bovine were not significant. Consequently, the two animal populations were pooled for the global meta-analysis.

Following the variance-covariance analysis testing for linear effects, three significant points could be underlined: 1) the proportion of the explained variance was low (table 2), 2/ the α constants were not significantly different from zero, 3/ the DMI variable had a significant influence on PBF as indicated by the probability for the β constant.

Table 2 Main results of the covariance analysis of $PBF - \overline{PBF}$ vs $DMI - \overline{DMI}$ in a global approach

Population	Nb of treat^{ts}	Adjusted R^2	P for $\alpha \neq 0$	P for $\beta \neq 0$
Ovine+bovine	31	42.00	0.974	0.0001

The linear response laws of PBF as a function of DMI, established on centered variables were as follows:

For ovine + bovine: $$PBF - \overline{PBF} = 0.0026\ (SD = 0.0773) + 0.0540\ (SD = 0.0113)\ (DMI - \overline{DMI})$$

R^2 = 42.00%, RSD = 0.4302, n = 31 treatments, $\overline{PBF}$ = 2.233 (SD = 0.101) l/(h. kg BW), $\overline{DMI}$ = 17.40 (SD = 1.25) g/(d.kg BW), $\overline{BW}$ = 175.8 (SD = 23.7) kg

The existence of quadratic response laws was also tested. However, the quadratic term was not significant (P = 0.668) .

The statistical analysis of the residuals of the linear models was necessary to ensure the normality, the absence of biases from the model and the selected studies, and the absence of aberrant or influent observations. This analysis showed three significant points. Initially, the normality of the model was checked by plotting the histogram of the residuals and the Henry straight line (graphs not shown). Both graphs showed a normal distribution of the data. Second, the standardized residuals did not exceed the usual limit (Figure 3, -2, +2). Finally, it was necessary to look at aberrant and influent observations: the leverage effects, the contributions to the residual variation and the Cook's distances were studied (graphs not shown). In both species, the graphs showed an acceptable homogeneity between the treatments and no abnormal point.

Figure 3 Residual analysis in the global approach: standardised residuals vs dry matter intake (DMI) in ovine + bovine

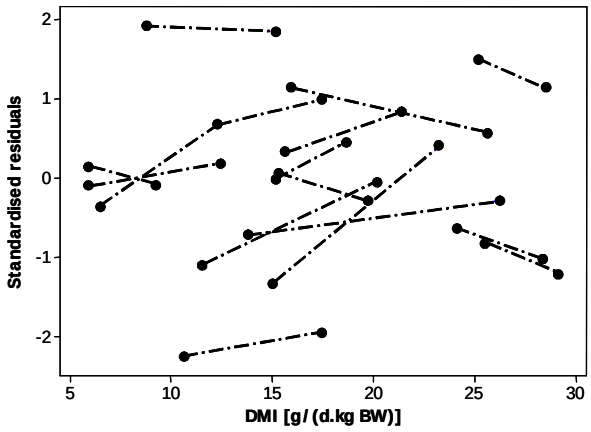

3.2.4 *Within-Group Meta-Analysis Approach*

As with the global approach, the two separate analyses: on ovine alone and on bovine alone were first carried out.

In the two populations, the proportion of the explained variance was high (Table 3). The α constants were not significantly different from zero in ovine and bovine. In all cases, more than half of the individual intercepts (αi) were significantly different from zero. The DMI variable had also a significant influence on PBF as indicated by the probability for the β constant. It should be stressed here that considering the fact that most of the selected groups of treatments had two treatments, it was not possible to test within-group slopes.

Table 3 Main results of the covariance analysis of $PBF - \overline{PBF}$ vs $DMI - \overline{DMI}$ in within-group approach

Population	Nb of groups of treatments	Nb of treatments	Adjusted R^2	P for $\alpha \neq 0$	Proportion of αi different from zero (P<0.05)	P for $\beta \neq 0$
Ovine	8	16	95.61	0.991	6/8	0.0001
Bovine	7	15	93.15	0.321	5/7	0.0001

The response laws of PBF as a function of DMI, established in within-group of treatments and on centered variables were then as follows:

For ovine: $$[PBF - \overline{PBF}] = 0.0003\ (SD = 0.0500) + \alpha i + 0.0500\ (SD = 0.0083)\ [DMI - \overline{DMI}]$$

R^2 = 95.61%, RSD = 0.114, n = 8 groups of treatments and 16 treatments, $\overline{PBF}$ = 2.376 (SD = 0.543) l/(h.kg BW), $\overline{DMI}$ = 17.64 (SD = 8.10) g/(d.kg BW), $\overline{BW}$ = 54.40 (SD = 18.02) kg

For bovine: $$[PBF - \overline{PBF}] = -0.0414\ (SD = 0.0388) + \alpha i + 0.1027\ (SD = 0.0110)\ [DMI - \overline{DMI}]$$

R^2 = 93.15%, RSD = 0.149, n = 7 groups of treatments and 15 treatments, $\overline{PBF}$ = 2.080 (SD = 0.565) l/(h.kg BW), $\overline{DMI}$ =17.15 (SD = 5.71) g/(d.kg BW), $\overline{BW}$ = 305.30 (SD = 45.70) kg

Contrary to the global meta-analysis, comparisons of the slopes β carried out by t-test indicated significant differences between ovine and bovine (P<0.001). Because of these differences, the two animal populations were not pooled.

For the reasons already mentioned (see part 3.2.3.), the residual analysis was also necessary in the within-group approach. Initially, the normality of the model was checked by plotting the histogram of the residuals and the Henry straight line (graphs not shown). For ovine, the distribution showed some insufficiency in the class of the null residuals but was considered acceptable with the limited number of observations available. For bovine, the normality was correct. The standardized residuals were plotted against DMI (Figures 4a and 4b) and did not exceed the usually allowed limits (-2, +2). The figures illustrate the fact that the standardized residuals are independent of DMI. It was also checked that the standardized residuals were independent of the diet composition (metabolisable energy and nitrogen contents). Finally, it was necessary to look at aberrant and influent observations: the leverage effects, the contributions to the residual variation and the Cook's distances were studied (graphs not shown). In both species, the graphs showed an acceptable homogeneity between the treatments and no abnormal point.

Figure 4 Standardised residuals of the within-group of treatments model vs dry matter intake (DMI) in ovine (a) and bovine (b)

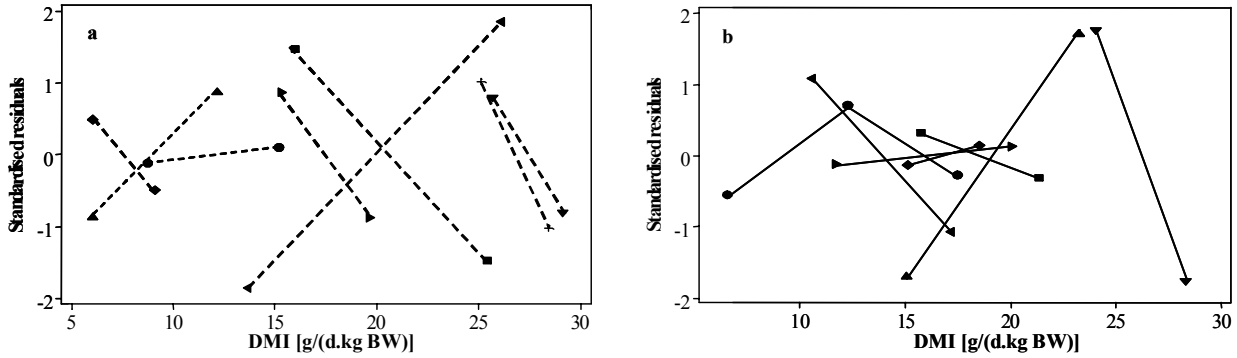

4. Discussion and conclusion

4.1. The Flora Database

The Flora database answered the three principal constraints. First, all information was taken into account, which satisfied the requirements of exhaustiveness and precision in the description of the experimental studies. Second, a minimal description of the diets and of their ingredients was carried on, mainly based on the values of the French and American tables of feed composition [INRA 1988], [NAS 1969]. Third, the traceability of the data was ensured by adding a criterion "reported, calculated or estimated" which accompanied the data as well as comments whenever it was judged necessary.

Overall, it may be concluded that the use of a relational database is more complicated than a simple spread sheet like Excel, as used by [Ortigues Visseiche 1995] in earlier work, and it also demands more expertise. However, it was a powerful tool. Besides the present work, FLORA has already been used successfully for a quantitative and qualitative study of literature data to establish response laws of the net hepatic glucose release in the ovine (n= 41 publications) by meta-analysis [Vernet *et al.* 2004], [Microsoft 2002b]. At the present time, approximately 150 publications were available in FLORA. They were input by 3 different teams of Research by means of a tool developed under Excel. It may finally be added that a reliable and exhaustive data extraction from publications required widely different expertise and experience which should not be underestimated and which was greatly facilitated by a team work.

4.2. Meta-Analyses

4.2.1 *General Points*

In the meta-analysis process presented here, several points were noteworthy. First, to combine data from animal species of different weights, the results were divided by the body weight raised to a certain exponent. Methods based on graphical observation and on one factor ANOVA were used in a first step to test the exponents of the body weight because of their easiness. Other methods can be imagined, for example, those which consist in seeking the best common fit of the data between species. The best possible exponent of the weight proved to be 1.0, in agreement with results obtained by [Berthelot 2000]. These results point to the limits of applying the conventionally used exponents (0.66 and 0.75, see [Ortigues 1991] for review; [Rémond *et al.* 1998] and to the necessity of testing the influence of the exponent with different types of results. This first step led to an overlap of the data of the 2 species which will then allow to test the effect of specie (independently of their body-weight differences). Subsequently, slopes of the within-group relationships were shown to be different according to the species.

Second, the selection of studies, and within studies the selection of groups of treatments, was a key aspect. The initial set of data available here consisted of 79 publications on both ovine and bovine. It was decided to carry out a very strict selection of studies based on the scientific objectives of the experiments: only experiments which were designed to study the strict influence of DMI on PBF were selected. Out of this pre-selected set, a second selection was applied on the standard deviations of the explanatory variable, in order to keep only the groups of treatments which presented a sufficient variation on DMI. The selection was done to the detriment of the number of observations kept for the analysis (n = 15 groups of treatments). However, in this first step towards the establishment of response laws, it gave the insurance to keep only the publications which studied the variable of interest (DMI). It avoided confusions of effects which could have been difficult to study such as a confusion between the level of intake of the animals and the nature of the diet.

Finally, the analysis of the residuals which was carried out here complies with good practices of meta-analyses. [Sauvant 2005]. No back and forth stepwise approach had been necessary, probably because of the very strict selection of studies and groups of treatments and also because there was no particular variation of the residuals according to DMI or to other significant variables of the composition of the diet.

4.2.2 *Comparison Between A global And A Within-Group Approach*

The present study allowed to compare the global and the within-group approaches. Seven points were worth to be underlined. First, the two methods led to different results. With the first method, the response law was of the form: PBF = $\alpha + \beta$ DMI. With the second method, the law was of the form: PBF = $\alpha + \alpha i + \beta$ DMI where αi depended on the group of treatments.

Second, the relations obtained in the 2 approaches did not apply to the same populations. Thus, with the within-group relationship, the slopes of the ovine and bovine populations were significantly different ($P<0.001$). Consequently, two relationships were established, one in ovine and one in bovine. With the global approach, the slopes in ovine and bovine were not significantly different. Consequently, only one global relationship was established for the ovine + bovine population. So, the within approach allowed to detect differences in slopes between the ovine and the bovine population, which was not possible with the global approach.

Third, the comparison of the within and global relationships showed that in ovine the slopes were not statistically different ($P<0.001$). In bovine, the slope of the within-group relationship was significantly higher than that of the global one (0.103 vs 0.054, $P<0.001$). There would remain to be determined whether those differences are due to specie or to the physiological stage of the animals (growing vs. adult). In our data, there was a confusion of effects between the specie and the physiological stage, since bovine were all growing animals whereas ovine were primarily nonproductive adult animals. So, it was not possible to study these two factors separately.

Fourth, the standard deviations of coefficients, residual standard deviations and explained variances were significant elements for the comparison of the 2 approaches. Thus, the standard deviations on the coefficients of the regression were 0 to 2 fold lower in within-group than in global relationships. Concerning the residual standard deviations, they were 2.9 fold to 3.8 fold lower in within-group than in global relationships. Moreover, the part of explained variance was higher in within-group in ovine and bovine than in global relationships (95.6% and 93.1% vs 42.0%).

The present results showed clearly that relationships obtained with a within-group approach were more precise, and more robust than those obtained with an global approach. All these elements justify the importance of carrying out a within-group as compared to a global approach.

Fifth, the importance of carrying out the statistical analysis at the within-group level [Sauvant 2005] was also made obvious by the present set of data which included animals of widely different body weights, and published studies from widely different research teams using quite different methodologies (e.g. methods of blood flow measurement). The fact that some αi terms were non significantly different from zero illustrated those methodological effects, even though they could not be attributed to any single methodological reason (e.g. measurement of blood flow, chemical determination methods) to date. In this context, the choice of establishing a response law on centered variables was also justified by differences in the distribution of the DMI levels between the groups of treatments in a given specie.

Sixth, the question of a linear or a curvilinear response between PBF and DMI is an important one biologically. Some nonlinearity in the response of PBF with DMI has already been reported. In fact, it appears significant to consider distinct responses depending on the level of DMI, i.e. one for low levels of DMI (below maintenance), one for average levels of DMI (from 1 to 2.5 times maintenance) and one for the highest levels of DMI (above 2.5 times maintenance, as measured in dairy cows). Indeed, when the feeding level is low (below maintenance), PBF does not vary much with DMI ([Nozière 2000], [Ortigues 1991] [Lomax 1983], [Webster 1975]). For average feeding levels, PBF seems to increase linearly with DMI [Rémond 1998]. For high feeding levels, the response does not exist in the bibliography because few measurements were carried out at such levels. However, a decreasing marginal response is physiologically possible. In our data, low feeding levels were not explored since the data of starving animals were withdrawn and those of under-fed animals were very few. Average

feeding levels were explored. High feeding levels were not explored since no data from dairy cows were included. These reasons probably explain why linear effects were significant whereas quadratic effects were not-significant. Lastly, it should be recalled that the test of the quadratic effects could only be realized in the global approach.

Finally, it should be stressed that the two methods did not lead to the same conclusions and interpretations. The global approach led to the establishment of a quantitative response law making it possible to predict a value of Y for any value of X, provided that this value of X was located in the range of initial variation and that the experimental conditions (type of animal, feeding conditions, methods of measurement) were compatible with those used for the establishment of the response law. It was not the case for the second method. Indeed, the latter only made it possible to predict a variation of Y for a variation of X. No general law was obtained since the intercept depended on the groups of treatments. The preceding analyses showed clearly that the αi terms were generally significantly different from zero. Thus, the precision and the reliability of the within-group approach response law were obtained to the detriment of its generalization.

4.2.3 *Within Group Meta-Analysis for the Response Law of Portal Blood Flow With Dry Matter Intake*

The response law which was established quantified the significant increase in PBF with an increment in DMI. Such a positive relationship is well known [Lescoat *et al.* 1996], however, the strength of the present approach laid in the robustness of the quantification of the slope, within the limit of the range of DMI values available. The αi terms were significant for the majority of the groups of treatments but no explanation could be found so far for those differences of intercept. Consequently, the response laws were known except for the αi term. The βi terms could not be included in the model and only a general slope was considered. The slope of the relationship on centered variables was significantly higher on bovine than on ovine (0.103 vs 0.050, $P<0.001$). For example, an increase in DMI of 10g/(d.kg BW) caused a rise in PBF of 1.03 and 0.50 l/(h.kg BW) in bovine and ovine, respectively. On bovine, the slope was significantly higher than that obtained by Lescoat who compiled the results from 89 treatments (28 publications) by linear regression (0.103 vs 0.060, $P<0.05$, [Lescoat *et al.* 1996]). It is significant to note that the slope of the global relationship was not significantly different from that of the relationship of Lescoat in bovine (0.054 vs 0.060, $P<0.05$). Such differences were already observed between simple regression which do not distinguish between within-studies and global variations and more rigorous within-studies meta-analyses [St-Pierre 2001].

4.3. *Conclusions*

The approach presented here will be applied to the net flux of all blood nutrients of interest. Preliminary responses have already been established for the net hepatic glucose release [Vernet *et al.* 2004]. The response laws that will be obtained are expected to precisely quantify the rates of changes of the explained variables in a more general way than could be made from only one experimental study. This approach will provide a comprehensive integration of quantitative knowledge on the supply and the net flux of nutrients of different organs and tissues and their coordinated response to changes in feed supply or physiological status. The current and future response laws will be used in compartmental mechanistic models on the same subject to define the relationships between compartments (and associated fluxes) and to help to set initial values or parameters. Understanding those mechanisms will contribute to improve the prediction of nutrient supply and utilisation to tissues of economical interest. This research work is complementary to that developed to predict the tissue characteristics involved in product quality [Hoch 2003].

REFERENCES

[Bertelot 2000] Berthelot, V. Contribution du propionate à la synthèse des acides gras impairs et ramifiés du tissus adipeux chez l'agneau: Facteurs de variation alimentaires et métaboliques, INRA-INA-PG, soutenue le 03/11/2000 à Paris.

[Brody 1945] Brody, S. Bioenergetics and growth. Reinhold Publishing Corporation, New York, 1945.

[Hoch 2003] Hoch, T., Jurie, C., Agabriel, J., Micol, D., and Picard, B. Modelling muscle characteristics of beef cattle for different animal types and muscles: Influence of age and energy supply on fiber type, surface and enzymatic activity, Proceeding of the 54th Annual Meeting of European Association for Animal Production, Rome (Italie), 2003.

[INRA 1998] INRA Alimentation des bovins, ovins et caprins. INRA, Paris, 1988.

[Lescoat *et al.* 1996] Lescoat, P., Sauvant, D., and Danfaer, A. Quantitative aspects of blood and amino acid flows in cattle. Reprod. Nutr. Dev., **36**: 137-174, 1996.

[Lescouret 1992] Lescourret, F., Pérochon, L., Coulon, J. B., Faye, B., and Landais, E. Modelling an information system using the MERISE method for agricultural research: the example of a database for a study on performances in dairy cows. Agric. Syst., **38**: 149-173, 1992.

[Lobley Lapierre 2003] Lobley, G. E. and Lapierre, H. Post-absorptive metabolism of amino acids, Progress in Research on energy and protein metabolism, Rostock-Warnemünde, Germany, EAAP Publ. no 109, 737-756, 2003.

[Lomax Baird 1983] Lomax, M. A. and Baird G. D. Blood flow and nutrient exchange across the liver and gut of the dairy cow. Brit. J. Nutr., **49**: 481-495, 1983.

[Microsoft 2002a] Microsoft Corporation Microsoft Access 92-2001, 2002.

[Microsoft 2002b] Microsoft Corporation. Microsoft Excel SP3. 1985-2001, 2002.

[Minitab Inc. 2003] Minitab Inc. Minitab for Windows release 14. 2003.

[NAS 1969] NAS United States-Canadian Tables of Feed Composition. Washington, D.C., 1969.

[Nozière *et al.* 2000] Nozière, P., Rémond, D., Bernard, L., and Doreau, M. Effect of underfeeding on metabolism of portal-drained viscera in ewes. Brit. J. Nutr., **84**: 821-828, 2000.

[Ortigues 1991] Ortigues, I. Adaptation du métabolisme énergétique des ruminants à la sous-alimentation. Quantification au niveau de l'animal entier et de tissus corporels. Reprod. Nutr. Dev., **31**: 593-616, 1991.

[Ortigues *et al.* 2003] Ortigues-Marty I., Obled C., Dardevet D., and Savary-Auzeloux I. Role of the liver in the regulation of energy and protein status, Progress in research on energy and protein metabolism, Rostock-Warnemünde, Germany, EAAP Publ. no 109, 83-98, 2003.

[Ortigues Visseiche 1995] Ortigues, I. and Visseiche, A. L. Whole-body fuel selection in ruminants: nutrient supply and utilization by major issues. Proc. Nutr. Soc., **54**, 235-251, 1995.

[Ortigues-Marty *et al.* 2003] Ortigues-Marty, I., Vernet, J., and Majdoub, L. Whole body glucose turnover in growing and non-productive adult ruminants: meta-analysis and review. Reprod. Nutr. Dev., **43**: 371-383, 2003.

[Rémond *et al.* 1998] Rémond, D., Ortigues-Marty, I., Isserty, A., and Lefaivre, J. Technical note: measuring portal blood flow in sheep using an ultrasonic transit time flow probe. J. Anim. Sci., **76**: 2712-2716, 1998.

[Sauvant 1992] Sauvant, D. La modélisation systémique en nutrition. Reprod. Nutr. Dev., **32**: 217-30, 1992.

[Sauvant 2005] Sauvant, D. Les méta-analyses de données expérimentales: application en nutrition animale. INRA Productions Animales, **18**, 63-73, 2005.

[St-Pierre 2001] St-Pierre, N. R. Invited review: Integrating quantitative findings from multiple studies using mixed model methodology. J. Dairy Sci., **84**: 741-55, 2001.

[Vernet *et al.* 2002] Vernet, J., Majdoub, L., and Ortigues-Marty, I. Relevance and elaboration of a base of experimental data of net blood nutrient fluxes across tissues and organs. Anim. Res., **51**: 465-477, 2002.

[Vernet *et al.* 2004] Vernet, J., Gely, G., Leger, S., Nozière, P., Sauvant, D., and Ortigues-Marty, I. Lois de réponse de l'émission nette de glucose par le foie chez l'ovin: méta-analyse, 11èmes Renc. Rech. Ruminants, INRA, Institut de l'Elevage, Paris, 2004.

[Vernet Ortigues-Marty 2005] Vernet, J. and Ortigues-Marty, I. Conception and elaboration of a bibliographic database of net blood nutrient fluxes across organs and tissues in ruminants. 2005, submitted.

[Webster *et al.* 1975] Webster, J. F., Osuji, P. O., and White, F. The influence of food intake on portal blood flow and heat production in the digestive tract of sheep. Brit. J. Nutr., **34**: 125-139, 1975.

Global Sensitivity Analysis to Improve Models in Agronomy

A. Penciolelli **C. Hue**
Inra Centre de recherches de Toulouse
UMR 1248 Arche
BP27 F31326 Castanet Tolosan Cedex
056128(5496,5025)
(penciol,chue)@toulouse.inra.fr
http://www.inra.fr

ABSTRACT
In this paper, we show through two examples how a global sensitivity analysis of model output can be used to improve agronomic models. Such an analysis measures the variation of a model output as a function of the variations of its inputs. The first example presents a bio-physical crop model and shows how global sensitivity analysis can improve model calibration or the choice of experimental design. The second example presents a bio-decisional model for irrigation and explains how global sensitivity analysis can guide the evaluation of the decisional inputs underlying that global sensitivity analysis requires knowledge of the correlation structure of model inputs and parameters.

KEYWORDS
Global sensitivity analysis, crop models, parameter estimation, model calibration, input data estimation

1. Introduction

For some decades now, simulation models have been developed to encapsulate understanding and to generalize experimental results on complex agronomic systems (soil, plant, climate and human practices). In this domain, the term *biophysical* model refers to a model which describes the soil-plant-atmosphere system while a *bio-decisional* model takes into account in addition human practices through decision rules. Both can concern different scales of times (from the second up to several decades) or space (from part of a field in site specific management up to the watershed scale needed to tackle some environmental questions).

Our research team includes agronomists, statisticians and computer scientists and aims at developing methods for the elaboration, the use and the evaluation of models for the management of environmental resources (e.g. water or permanent meadows). Recently, a tool box for crop models has been developed. It contributes to the diffusion of some methods that researchers hesitate to program on their own but use if they are easily available. One tool provides a method for performing global sensitivity analysis whose principles are described in the second section. In section three, we show how such a sensitivity analysis can help in the crucial step of model calibration for a *biophysical* model. In the last section, we show how it can help to choose which input data are interesting to estimate in a *bio-decisional* model.

2. Methods for Global Sensitivity Analysis of Model Outputs

Sensitivity analysis studies how sensitive a model output is with respect to elements of the model which are subject to uncertainty or variability. These elements, called factors, are for example the model parameters, or the input variables, but can also be different possible choices of the model structure. The output is supposed to be scalar. The book [Saltelli *et al.* 2000] is a comprehensive reference on this subject.

Local sensitivity analysis is performed by estimating the partial derivatives of the output with respect to each input factor around given nominal values. It gives a local measure of the output sensitivity which may vary with the nominal value. This value should then be chosen very carefully taking into account the goal of the sensitivity analysis.

Global sensitivity analysis (GSA) apportions the output variability to the variability of the factors when they vary in their whole uncertainty domains. This uncertainty is generally described using probability densities for factors. Methods for GSA can be decomposed into four steps:

1. definition of the factors and of their distribution;
2. generation of a sample of factor values;

3. evaluation of the model output for each element of the sample;
4. estimation of the effect of each factor on the model output.

Two main approaches can be distingued to perform the last step. The first one uses a model approximation, e.g. a linear regression model. The second one is based on a direct decomposition of the output variance and does not rely on any model approximation. Because of the strong non linearity of crop models we adopt here the second approach. In such variance-based methods as in analysis of variance, the output variance is decomposed into factorial terms called importance measures:

$$V(Y) = \sum_{i=1}^{s} D_i + \sum_{i<j} D_{ij} + ... + D_{1...s} \quad (1)$$

where: - s is the number of factors,

- $V(Y)$ denotes the total variance of the output variable Y considered,
- $D_i = V(E(Y|X_i))$ [1] the importance measure for factor X_i,
- $D_{ij} = V(E(Y|X_i,X_j)) - V(E(Y|X_i)) - V(E(Y|X_j))$ the importance measure for the interaction between factors X_i and X_j
- and analogous formulae for the higher order terms.

The sensitivity indices are computed by dividing the importance measures from (1) by the total output variance:

$$S_i = \frac{D_i}{V(Y)} \quad (2)$$

$$S_{ij} = \frac{D_{ij}}{V(Y)} \quad (3)$$

Consequently, they sum to one and can be interpreted as the proportion of variance explained by the various factorial terms. The indices S_i for i=1,...,s are called the first order indices and measure the main effect of each factor on the output variance without taking into account the interaction with the other factors.

The total sensitivity index of a given factor X_i takes into account the main effect and the effect of all its interactions with other factors. It is defined by:

$$ST_i = \frac{D_i + D_{i,\sim i}}{V(Y)} \quad (4)$$

where $D_{i,\sim i}$ indicates all interactions involving the factor X_i.

The main difficulty in evaluating these indices is that they contain integrals of high dimension. In the two following sections, we use the extended fast (EFAST) algorithm proposed in [Saltelli *et. al.* 1999] to estimate the first-order and total sensitivity indices. It performs a judicious deterministic sampling to explore the factors space which makes possible to reduce to one the dimension of the integrals via Fourier decomposition.

3. Global Sensitivity Analysis for Biophysical Crop Model Calibration

Biophysical crop models are systems of equations describing the dynamics of crop growth and development at a daily time step and at the field scale. They often contain several or even tens of state variables, with an equation describing the rate of change of each state variable. They provide agronomic outputs and outputs describing the environmental impact of the system. Crop model calibration, i.e. the estimation of its parameters, is a major problem because of the large number of parameters compared to the amount of training data.

Moreover, the structure of the data is often complex: in a given field, several different variables may be measured, and some of these variables may be measured at several different dates during the season. On the other hand, there is in general supplementary information about parameter values, e.g. when parameters have a clear physiological meaning.

---

[1] $E(Y|X_i)$ denotes the expectation of Y conditional on a fixed value of X_i and the variance is taken over all factors which are fixed in the conditionnal expectations.

Whatever the estimation algorithm used, it appears to us that a global sensitivity analysis can help answer two types of question:

1. Given a data base, on which parameters should we focus our attention?
2. Given some parameters to estimate, which variables and at which date shall we measure?

3.1. The MINI-STICS Model

The model considered here is part of the STICS model [Brisson *et al.* 1998]. It simulates with five state variables sunflower development over a period of 20 days, starting at the stage Maximal Acceleration of Leaf growth. The vector of explanatory variables has 75 elements and includes soil characteristics, daily climatic variables, management operations and initial conditions. The parameter vector has 14 elements to estimate.

3.2. The Sensitivity Analysis Implementation

To test our calibration algorithms on the MINI-STICS model, we have mainly worked with two different sets of data. The first contains measurements of the two variables leaf area index (LAI) and volumetric soil water content (HUR) at days 10 and 20. The second contains measurements of LAI at day 2 and three measurements of the fraction intercepted radiation (PARI) at days 2, 8 and 15.

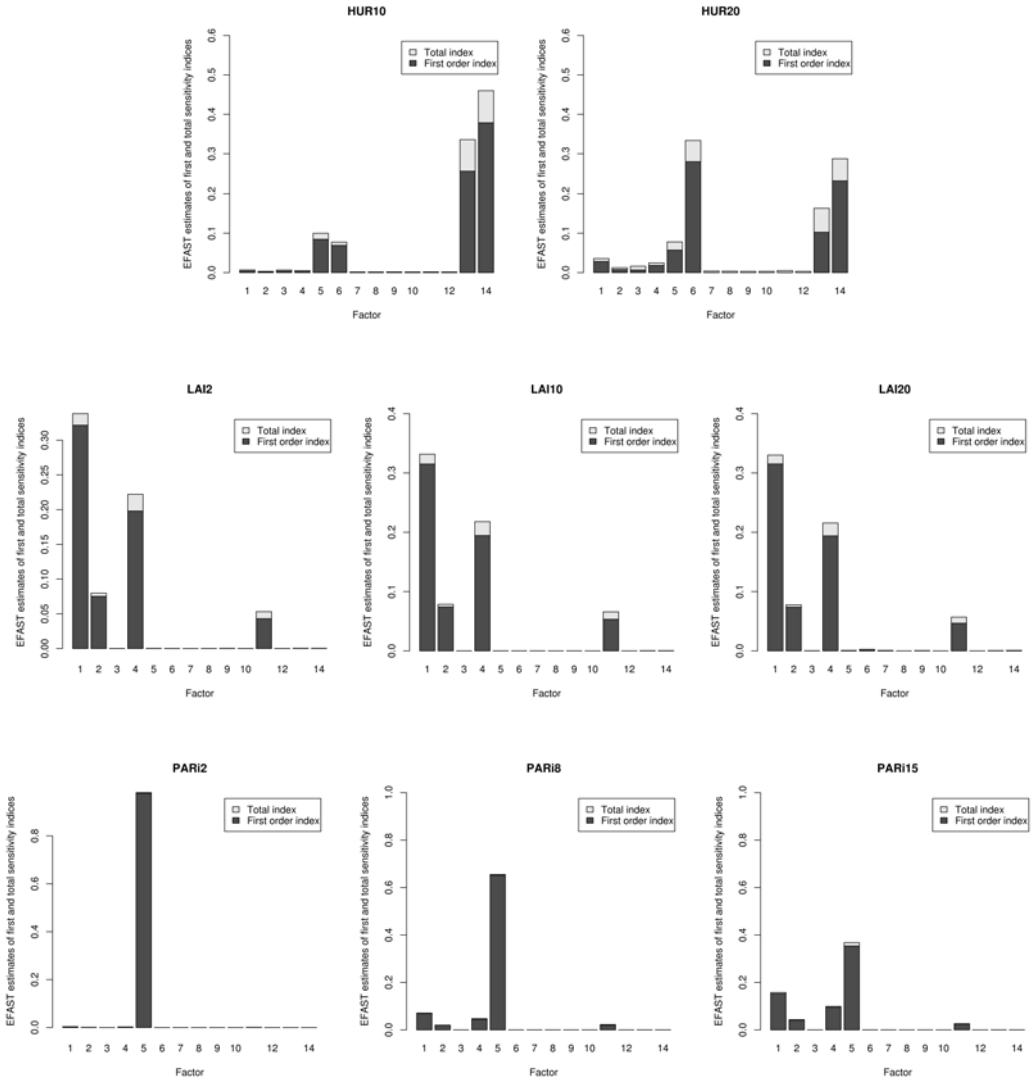

Figure 1. First order (dark grey) and total (light grey) sensitivity indices after averaging over 14 input conditions (soil, climate and management) considering successively output HUR10, HUR20, LAI2, LAI10, LAI20, PARI2, PARI8, PARI15.

We would like to understand before running the estimation algorithms how the choice of data set affects the quality of the parameter estimates. One way to answer this question is to perform GSA of this model. A major interest of this approach is that it only considers outputs generated by the model and is thus independent of the real measurements. It could then be run before the measurements are made.

For the EFAST method as for all global sensitivity analyses methods, the model output is considered to be scalar. We performed eight independent GSA by setting the output to each of the eight variables[2] . This set of analyses shows, for a given factor, how the order of sensitivity indices vary with the type and the date of the output considered.

In the context of model calibration, the input factors for this analysis are the 14 parameters of the model. We suppose here that these parameters are not correlated, which seems a reasonable assumption according to the model construction. As we use a Bayesian approach for parameter estimation, we have worked with experts to define prior distributions for all the parameters. The input intervals have been defined in accordance with these priors: they are of the form $[\mu-2\omega,\mu+2\omega]$ where μ and ω are respectively the mean and the standard deviation of our Gaussian prior. To reproduce the variability of the input conditions (soil and climate), we ran the sensitivity analyses for 14 different input conditions randomly chosen according to distribution laws established with experts.

3.3. **Results and Conclusion**

Figure 1 shows the first order and total indices averaged over the 14 input conditions for each of the eight outputs considered.

We first remark that the factors with the largest indices are different according to the measurement considered. For instance, for LAI2, LAI10 and LAI20 the two factors with the largest indices are factors 1 and 4 whereas for HUR10 and HUR20 factors 13 and 14 have the largest indices.

Secondly, for a given measurement type, the day at which the measurement is made may or may not influence the sensitivity indices:

1. For LAI, the sensitivity indices are the same whether day 2, 10 or 20 is considered. The four dominant factors 1, 4, 2 and 11 are precisely the four parameters used in the LAI dynamic equation.
2. For PARI, the measurement day has a strong influence. Only factor 5 has significant indices for measurement at day 2. Four other factors (1, 4, 2 and 11) appear more and more significant as the measurement day increases. Again, the knowledge of the model equations helps to analyze these results. The PARI variable is in fact a function of LAI and of the fifth parameter. Only this parameter is significant at the beginning and the LAI parameter (1, 4, 2 and 11) indices increase as the number of cycles of the model increases.
3. For HUR, the four most significant indices are the same at day 10 and 20 but their relative importance varies.

To illustrate question of type 1 enounced at the beginning of this section, we can conclude for instance that the data base 1 containing measurements LAI10, LAI10, HUR10 and HUR20 is much more adapted to estimate parameters 13 and 14 than the other data base. To illustrate how such analyses help answer question of type 2, we can conclude for instance that parameter 5 can be estimated with measurements of PARI at time 2.

4. **Global Sensitivity Analysis for Bio-Decisional Model Inputs Estimation**

A bio-decisional model is the association of a biophysical model and a decision model. As presented in paragraph 3, the biophysical model represents crop development at a daily time scale and at the field scale. The decision model expresses farming practices with a set of "IF...THEN..." rules. Unlike the preceding example, we are not interested here in the parameters of the biophysical model, but rather on the spatial variability of the decision model inputs and on their effects on the prediction of water withdrawals assessment.

4.1. **The ADEAUMIS Model**

ADEAUMIS [Leenhardt *et al.* 2004] is a bio-decisional model at the regional scale, which has been developed to assess water withdrawals due to maize irrigation in the Neste system (South West of France). To take into account spatial variability within the area, simulation units have been defined, within which meteorological data and farming practices are considered to be homogeneous.

---

[2]An interesting theoretical extension of actual global sensitivity analysis methods would be to take into account vector outputs.

The inputs for each simulation unit are listed in Table 1 and the output is the water withdrawal. Meteo-France provided meteorological data from the Auch Station from 1985 to 2004 and a survey done by INRA Toulouse in 2004 of 30 farmers of the Neste system, provided the information necessary for defining the intervals for the other inputs.

We would like to know which inputs, given their variations for the Neste system, will have the most effect on water withdrawals calculated by the model. The objective is to concentrate efforts on obtaining an accurate spatial description of the most important inputs.

4.2. **The Sensitivity Analysis Implementation**

A direct way to perform the sensibility analysis with EFAST would be to study 5 factors: meteorological data, "waiting time" (W_time), "sowing day", "return rule" and "dose". But using those factors does not take into account that sowing only takes place in spring when there is no irrigation and that the "return rule" and the "dose" are strongly correlated.

Table 1. Simulation unit inputs and their range of variation.

Input	Min	Max	Description
Meteo	1985	2004	Meteorological data for the year
W_time	4	15	Length of period without irrigation after rainfall
Sowing day	1-04	31-06	Sowing day
Return rule	4	12	Frequency of irrigation
Dose	18	50	Amount of water at each irrigation round

The factors we took into account for the sensitivity analysis are listed in Table 2. Knowing there is no irrigation during spring, we created two meteorological factors: "spring" which cover the sowing period and "summer" which covers the irrigation period. W_time was used as a factor for sensitivity analysis since it has no correlation with the other inputs. The sowing day is calculated using the meteorological data in "spring" and a sowing index as follows: the meteorological data determines a set of possible sowing days and the sowing index (S_index) selects the sowing day within that set (the higher the index is, the later the sowing day is selected). We also linked "return rule" and "dose" by a linear relation to build the factor "irrigation strategy" (I_strategy) which is an index which goes from 0 for "small dose and short return rule" to 1 for "high dose and long return rule" [Maton *et al.* 2005].

Table 2. Factors for GSA and their range of variation.

Factor	Min	Max	Description
Spring	1985	2004	Meteorological data for the spring period
Summer	1985	2004	Meteorological data for the summer period
W_time	4	15	Length of period without irrigation after rainfall
S_index	0	1	Sowing index
I_strategy	0	1	"dose" and "return rule" correlation index

4.3. **Results and Conclusion**

Results of the EFAST algorithm with these new factors are presented in figure 2. The first result is that the "summer" factor has the highest total sensitivity index and "irrigation strategy" has the highest first order sensitivity index. This means that "summer" can have a stronger effect than "irrigation strategy" in specific contexts which remain to be determined. The second result is that the "spring" factor can have a significant effect in interaction with other factors, probably the "sowing index" since there is no irrigation during "spring". There is need for further research of those interactions to identify situations where "summer" may have a stronger effect than "irrigation strategy" and "spring" may have a significant effect.

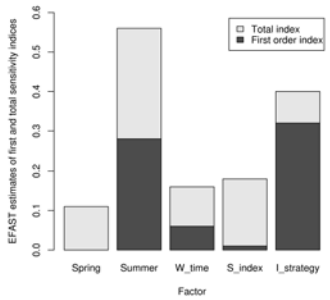

Figure 2. First order (dark grey) and total (light grey) sensitivity indices for ADEAUMIS factors

5. Conclusion

Following a description of global sensitivity analysis, we have illustrated the usefulness of such methods through two agronomic models. The first illustration shows that global sensitivity analysis can help on the one hand in the calibration step and on the other hand to choose experimental design. The second shows that it can help to determine which input variables are important to estimate more precisely and show an example of how to take into account the correlation structure of inputs.

ACKNOWLEDGMENTS

We thank R. Faivre for helping us to appropriate GSA methods, D. Wallach and M.-H. Charron-Moirez for their work on the tool box. This work was supported by funding from the ADEAUPI project.

REFERENCES

[Brisson *et al.* 1998] N. Brisson, B. Mary, D. Ripoche, M.H. Jeuffroy, F. Ruget, B. Nicoullaud, P. Gate, F. Devienne, R. Antonioletti, C. Dürr, G. Richard, N. Beaudoin, S. Recous, X. Tayot, D. Plénet, P. Cellier, J.M. Machet, J.M. Meynard and R. Delécolle. Stics : a generic model for the simulation of crops and their water and nitrogen balance. *Agronomie*, 18:311-346, 1998.

[Leenhardt *et al.* 2004] D. Leenhardt, J.L. Trouvat, G. Gonzalès,V. Pérarnaud, S. Prats and J.E. Bergez. Estimating irrigation demand for water management on a regional scale i. adeaumis, a simulation platform based on bio-decisional modelling and spatial information. *Agricultural Water Management*, 68:207-232, 2004.

[Maton *et al.* 2005] L. Maton, D. Leenhardt, M. Goulard, and J.E. Bergez. Assessing the irrigation strategies over a wide geographical area from structural data about farming sytems. *Agricultural systems*, to appear, 2005.

[Saltelli *et al.* 1999] A. Saltelli, S. Tarantola, and K. P.-S. Chan. A quantitative model-independent method for global sensitivity analysis of model output. *Technometrics*, 41:1, 1999

[Saltelli *et al.* 2000] A. Saltelli, K. Chan, and E.M. Scott, editors. *Sensitivity analysis*, Wiley, 2000.

Distributed fire spreading simulation using OpenMOSIX

Eric Innocenti Fabrice Bernardi Alexandre Muzy
Laurent Capocchi Jean-François Santucci
University of Corsica
SPE Laboratory, UMR CNRS 6134
Quartier Grossetti
20250 Corte, France
+33 4 95450208
{ino, bernardi, amuzy, capocchi, santucci}@univ-corse.fr

ABSTRACT
Parallel discrete event simulation of complex phenomena like fire spreading is known to be a challenge. We describe in this paper a distributed model and the techniques we used for implementing such a simulation on a cluster of workstations. The need in adapted methodologies in this area is a recurrent problem. Simulation times obtained do not allow developping effective prediction tools. Realistic large-scale simulations are obtained to the detriment of precision and simulation time. This is due to the physical models increasing complexity which is in constant opposition with the available computing resources. We show that an OpenMOSIX cluster could form a basis for a good distributed engine, easily adaptable for spatial model in large-scale simulations.

KEYWORDS
Distributed computing, parallel algorithms performances, discrete event simulation, fire spread simulation, MOSIX.

1. Introduction

These last years, the international community has known an increase of ecological and technological disasters. Many countries were devastated by destructive forest fires or suffered of fatal floods. However, the means of prevention and fight are each day more effective. The use of computer tools is largely accepted in this domain and spreads with the development of new technologies. Their use makes it possible the improvment of the traditional methods and generates development techniques helping to understand and control the time evolution of these phenomena. Among those, computer simulation allows the rise of new concepts adapted to the study of such systems [Ingalls 2002]

This work is related to the simulation of complex phenomena integrating space dynamics. We treat the design of a computer model for distributing simulation of fire spread. The need of adapted methodologies in this area is a recurrent problem. Indeed, the simulation times obtained are still too important and do not allow developping effective prediction tools. Obtaining realistic high speed simulations seems to be viable only to the detriment of the precision of the model. This is due to the physical models increasing complexity which is in constant opposition with the available computing resources. We try to find solutions to these problems by combining modeling and simulation concepts, objects and parallel computing techniques. This work relies upon the combination of simulation formalisms to specify discrete event simulators [Zeigler *et al.* 2000], and upon an innovative modeling method. The developed model allows an optimal use of parallel computing resources available and thus a gain in terms of performances. We discuss the techniques founded on OpenMOSIX for distributing the fire spread simulation.

This paper is organized as follows. First, we introduce the essential software paradigms we use in our development (Section 2); second, we describe both the modeling and simulation structures (section 3); third, we explain the fire spread implementation details and analyze the simulation results (section 4); finally, we give some conclusions and some perspectives of work (section 5).

2. Related Works

2.1. Cellular Modeling

Many methods can be used to design a model in the computer simulation domain. Among those, methods founded on models inspired by cellular automata are often used [Gardner 1970]. Many examples implementing advanced cellular models can be found in the litterature [Rennard 2000, Hoffmann and Al 2000, Chopard Masselot 1999, Sipper 1994, Maniatty and Al 1994].

History of Cellular Automata (CA) begins in 1940 with Stanislas Ulam (1909-1984), a polish mathematician. He studied the evolution of complex systems generated on the basis of elementary behaviors. He quickly realized he could build complex behavioral structures in a two-dimensional space split in cells, starting from very simple rules. In its first experiment cells could have two states: on or off. Then, evolution of a cell results from the current state and from the rules relative to the neighbors cells. Many extensions and modifications of the basic model can be found in the litterature [Bandini *et al.* 2001,

Worsch 1997, Di Gregorio Serra 1999, Sipper 1999, Talia 2000]. All of them imply variations of the structural and behavioral rules [Langlois Phipps 1997]. For example, modification of the neighborhood definition is allowed. If we consider models based on a two dimension cellular automata, [Rennard 2000] references the following neighborhood illustrated Figure 1.

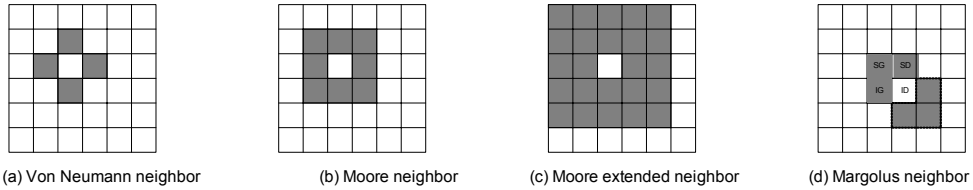

Figure 1. *The most used two-dimensional neighborhoods for cellular automata.*

2.2. Discrete Event Simulation and DEVS formalism

Discrete event simulation implements models whose state variables evolve in time in a discrete way. Contrarily to continuous simulations, this kind of approach is based on state changes ocurring on the time axis. These changes represent the events of the simulation. They are executed in the timestamp order of their occurrences according to the simulated time.

2.2.1 Event Driven Simulation

Discrete event simulation implies the development of models where the simulation time progresses by jumps of events occurrences [Erard Déguénon 1999]. In this case, only the significant moments where the model evolves are considered, i.e. during the process of simulation, only events generating a change of the value of the state variables are computed. For that, it is necessary to implement a scheduler to chronologically order the events. Each time progression implies a treatment, and all events are productive. The time progresses more or less quickly according to the computed events. Execution of an event at the head of the scheduler can generate additions or suppressions of other events. Event driven simulation is illustrated figure 2.

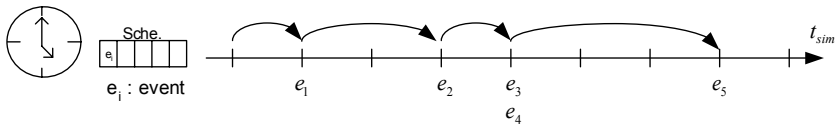

Figure 2. *Events driven simulation.*

Two types of events can occur: external and internal events. External event occurrences are not controlled by the model. Internal events on the other hand, come from the events programmed by the model. This distinction on the principal types of events can led to the definition of two state transition functions: the external transition function 'δ_{ext}', and the internal transition function 'δ_{int}'. This kind of approach is specified by [Zeigler 1976, Zeigler *et al.* 2000], with the DEVS (Discrete eVent System specification) formalism. In the case of event driven simulation events management algorithms are implemented at the simulator level. They constitute the synchronization kernel of the simulation process and are integrated in the simulators. The interested reader can find a detailed description of these algorithms in [Coquillard Hill 1997, Balci 1988, Overeinder *et al.* 1991]. Algorithm 1 is an example of an event driven simulator.

```
Event approach program
        Scheduler.initialisation() ;
        t=0 ;
        While scheduler not empty and t<>tfinal
                Get the first event in the scheduler ;
                Update clock simulation ;
                Execute the traitment associated to the event ;
        End while
        Get simulation results ;
End
```

Algorithm 1. *Discrete event simulator.*

The different treatments can generate new events inserted in the scheduler, as well as the suppression or the report of events. The execution of the treatments does not modify the clock of the simulator. Only the synchronization kernel is entitled to manage the time.

2.2.2 DEVS formalism

Developed in the beginning of the 1970's, DEVS is an abstract universal formalism used for discrete event modeling [Zeigler 1976].
A basic DEVS atomic model is a structure: DEVS = (X_M, Y_M, S, δ_{ext}, δ_{int},λ, ta),

Where,

X_M is the set of ports and input values,

Y_M is the set of ports and output values,

S is the set of system's states,

δ_{ext} is the external transition function,

δ_{int} is the internal transition function,

λ is the output function,

ta is the advance time function.

Components of the model are described via the descriptive variables. S represents the set of state variables. X is the set of input variables and Y the set of output variables. The atomic models are influenced by internal and external events. Atomic model activity is described by the internal transition function δ_{int}, the output function λ and the external transition function δ_{ext}. External events are generated on the input ports of the atomic model and imply the model response to the outside. Internal events are programmed if there is not external events occurrence during ta. The reader interested in more details will benefit from the new reference book for DEVS [Zeigler *et al.* 2000].

2.3. MOSIX/OpenMosix

MOSIX is a clustering tool developed by the team of the Professor Amnon Barak at the University of Jerusalem [Barak La'adan 1998]. It is designed as a set of patches applied to the Linux kernel operating system. MOSIX distributes the application tasks homogeneously through the workstation cluster, giving a solution to the distribution problem of load balancing. Although MOSIX is more than twenty years old, its development is mainly associated to its implementation on the GNU/Linux platform. MOSIX relies upon algorithms performing statistics and upon procedures that guarantee correct operations, even in the case of incidents (High Performance Clusters). MOSIX assigns a process to a node, according to the resources available. The objective is to optimize the use of each workstation in the cluster. A MOSIX cluster is fully decentralized, and can be compared to a "Peer to Peer" network. Each workstation manages its own processes comparing them to the other processing nodes and there is not hierarchy between the different workstation of the cluster. We used MOSIX for its simplicity of implementation. Indeed, using MOSIX only requires a patched Linux kernel and configuration files used to define the cluster.

3. Distributed Modeling and Simulation Framework

3.1. Model definition

With the development of parallel computing, spatial distributed models are well suited for large scale simulations on distributed parallel architectures. They offer a boundless execution support in terms of memory and they guarantee the highest exploitation of the computers power. Simulation models must be parallelized using the principles of the domain decomposition [Leduc 1999]. This technique consists in sharing the computer model which represents the spatial area to be simulated in different sub-elements. For this reason, the propagation domain represented by the simulation model is broken down into different sub-domains; it is quite common to consider as much as sub-domains than desired processes. Sub-domain computations are executed in parallel and at the level of each local process.

Distribution of the simulation model raises problems of neighborhood coherence while the simulation runs, due to data localized on the common interfaces of the sub-domains. Indeed, the spatial discretization implies knowing the values around an element situated on a mesh of the domain. Hence, when decomposing the model, each sub-domain must receive one or several layers of cellular elements called "ghost cells" and coming from the neighbors sub-domains. They constitute the boundary overlapping elements of a distributed simulation domain and they allow the simulator to calculate the value of the border elements. These elements are updated at each time step on the values calculated by the process taking care of the sub-domain. [Leduc 1999] emphasizes that message passing is the main type of communication in distributed models and represents a restrictive factor for the performances of the simulation. Figure 3 illustrates the domain division implemented, and the mechanisms of messages passing we will employ in order to guarantee the global coherence of the simulation.

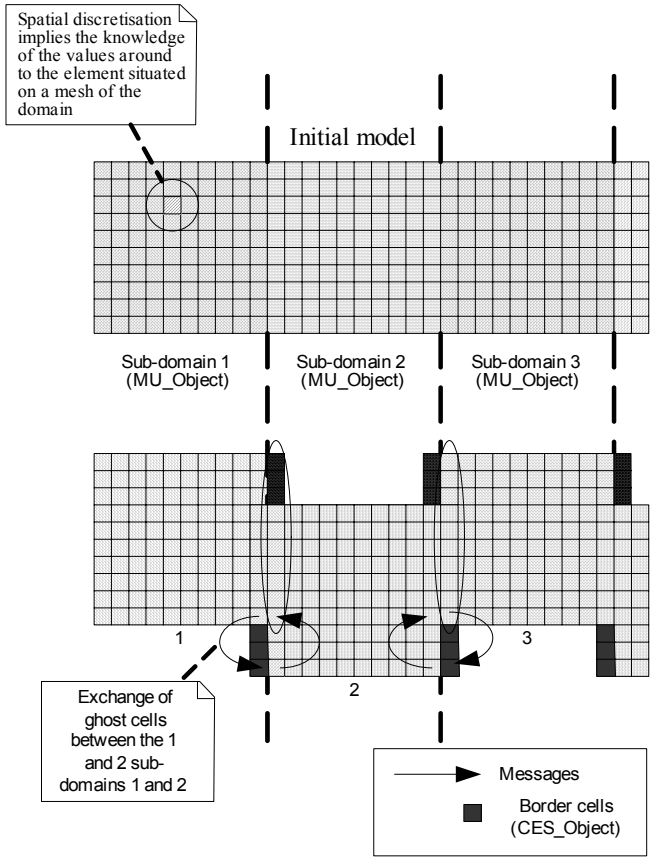

Figure 3. *Division of the model for distributing fire spread simulation.*

The different sub-domains of the distributed model are implemented in an evolved cellular automaton (MU_Object) and the data exchanged are used to update the attributes of the elementary cellular objects (CES_Object) established as "ghost cells".

3.2. Distributed architecture of the simulation

Distributed discrete event simulation brings a lot of interest because it provides structural framework and services allowing the simulation of large-scale models impossible to exploit on traditional computer architecture. Performances often depend

on the method used to process communication during the synchronization of the information needed for the accuracy of the simulation. This communication is founded on message-passing principles. Implementations of these techniques are numerous and varied [Reinefeld *et al.* 1998]. However, code reuse is compromised since the distribution code get tangle with simulator code providing the basic services for the simulation.

We consider distribution as a nonfunctional property of an application, i.e. like a specific device of execution, advisable to compose separately in order to "build" the application. It is necessary to develop a composition mechanism to make this assembly. On the basis of this consideration, we propose to distribute the simulation as an aspect which can be added to the simulator when the simulation is distributed. Subsequently, the distribution of the simulation avoids mixing the basic functional services of the simulator, with those corresponding to the distribution. This considerably improves the evolution of model components. The communication techniques for synchronizing are numerous and diverse, and the installation of a mechanism for choosing a type of communication is also necessary. We design the simulator using the Decorator pattern [Gamma *et al.* 1994], to control the distribution as a sequence of functions executed in a specific order. The objective is to dynamically associate additional responsibilities to simulator objects. Figure 4 illustrates this scheme.

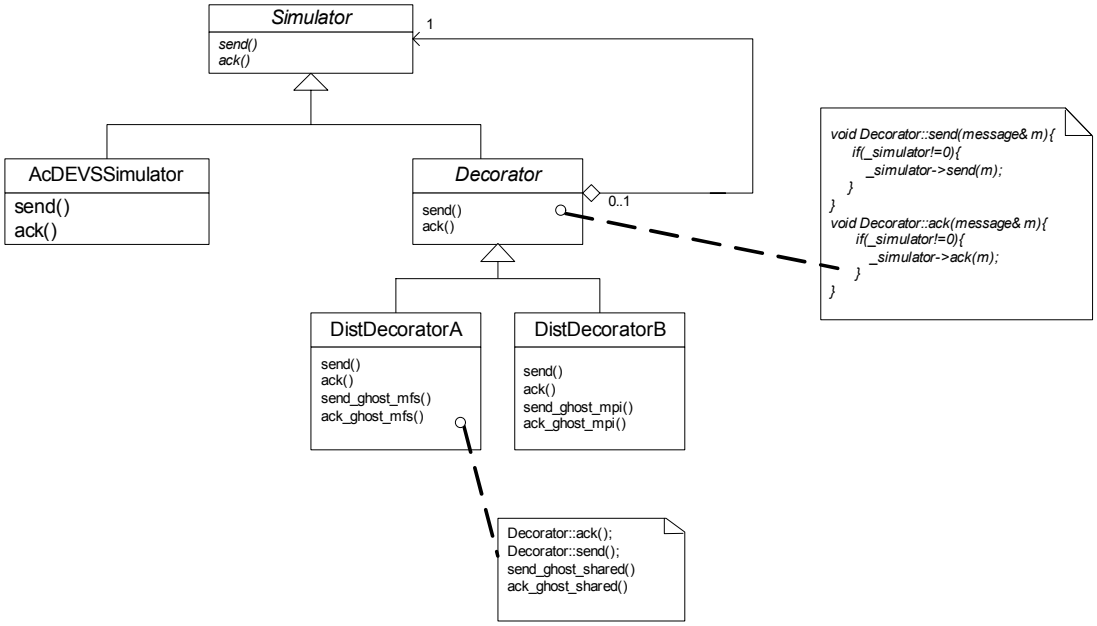

Figure 4. *The Decorator pattern.*

In order to simulate the distributed model, we describe it as a set of autonomous logical components executed on several machines without centralized control, and cooperating in order to ensure the simulation of the spreading phenomenon. The need of distributed collective information (ghost cells) implies to exchange common information, and to avoid causality error at each time step and for each node. Communication management between the different nodes implies to use adequate methodology. The Decorator pattern facilitates adaptation according to the execution context. It makes it possible to install a composition mechanism in order to assemble AcDEVSSimulator objects (Simulator) and the various possible methods of communication (Classes DistDecoratorA and DistDecoratorB). The DistDecoratorA and DistDecoratorB objects implement the communication methods for exchanging the ghost cells, respectively send_ghost_mfs(), ack_ghost_mfs() and send_ghost_mpi() and ack_ghost_mpi(). These methods are called after execution of the local treatments implemented in the methods ack() and send() of the concrete component AcDEVSSimulator, being used to ensure the communications between the parents simulators and coordinators on each node.

4. Application to fire spreading

4.1. Modeling and simulating fire spreading

Physical models are used to improve decision-aid. The physical model we use (1) has been validated against numerous experiments [Santoni *et al.* 1998, Dupuy 1995]. Then, the propagation of fire results from the evolution of a front of flame in a domain of 1 m² of pine needles, without slope, nor wind. A preliminary numerical study makes it possible to solve the model using the explicit method of finite differences, leading to a system of differential equations. The domain of propagation is then divided into elementary components constituting the ground and the plants, each one being described by

the following algebraic equation:

$$T_{i,j}^{k+1} = aT_{i-1,j}^{k} + aT_{i+1,j}^{k} + bT_{i,j-1}^{k} + bT_{i,j+1}^{k} + cQ\left(\frac{\partial \sigma_v}{\partial t}\right)_{i,j}^{k+1} + dT_{i,j}^{k} \qquad (1)$$

Where $T_{i,j}$ represents the temperature of a cell of the cellular automaton. Coefficients a,b,c, and d depend on the time step and on the space step considered. The parameters of the model are given starting from experimental statements of temperature obtained. The numerical results were compared to experimental data for various ignitions and the quality of the predictions is remarkable [Santoni *et al.* 1998]. However, the precision of these models make them difficult to be simulated under real-time constraints.

4.2. Distributed implementation on a Linux cluster

The distribution of the simulation model implies to divide the propagation plan into several sub-domains. The simulation treatments are then distributed onto a cluster of workstations, each node executing its own part of computing. This kind of models allows to simulate more realistic large-scale domains and to overtake the limits imposed by the finite dimension of the computers memory.

One of the major problems is the problem of the load balancing (Dynamic Load Balancing) [Lan *et al.* 2002, Tonguz Yanmaz 2003, Ghanem *et al.* 2004]. We tackled this problem using automatic migration of processes on nodes. We retained the openMOSIX environment for implementing the distributed model. OpenMOSIX (Multicomputer OS) dynamically controls the load balancing on a cluster of computers.

The experiments rely on the Knoppix/MOSIX distribution. The distribution of the computing resources is executed for the different experiments in a transparent way. Figure 5 illustrates the physical architecture developed for distributing the simulation. The fire front is divided in equal areas distributed on the workstations network. Each node computes a part of the fire front and communicates with the others.

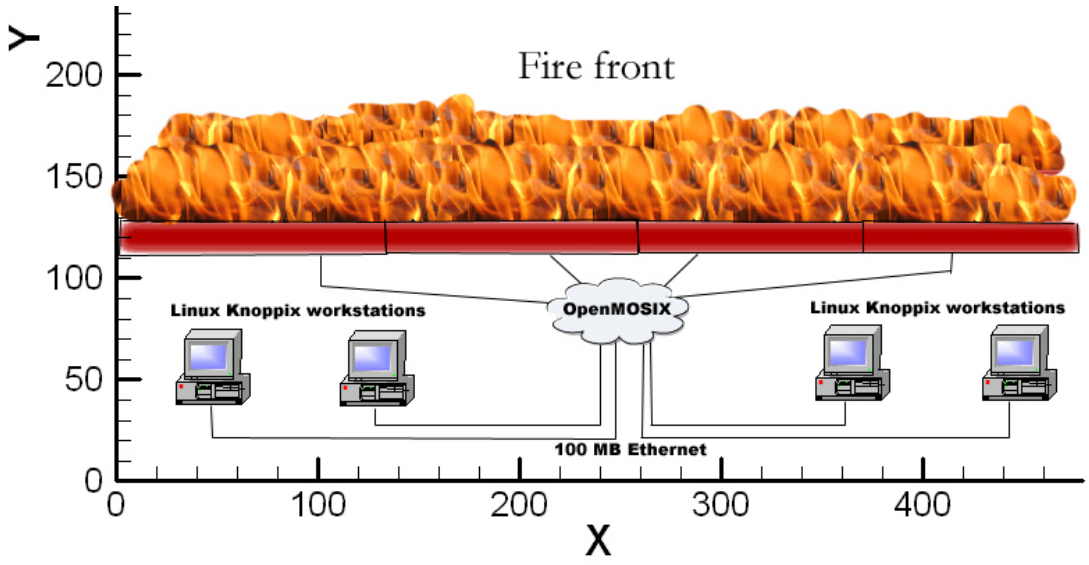

Figure 5. *Division of the propagation domain for distributing the simulation of fire spreading.*

Figure 6 sums up the performances obtained for a line ignition on a domain of 115 200 pine needles components (240 X 480), respectively for one, two, three and four nodes.

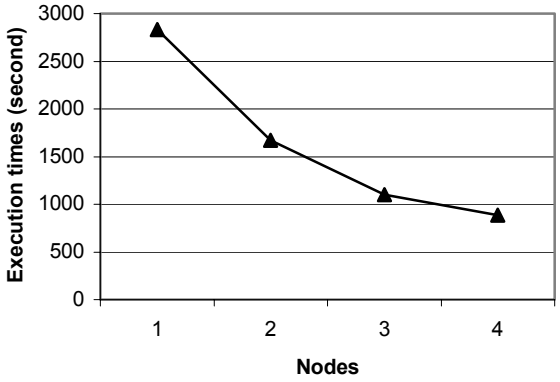

Figure 6. *Performances of the distributed simulation on a cluster of workstations*.

The simulation presents honorable performances. The object-oriented architecture easily implements distributed models of propagation. This development offers a reference application for developing future large-scale models we plan to specify.

5. Conclusions and prospects

This work proposes a methodology for modeling and simulating spatial complex phenomena on distributed architecture. The proposed methodology takes into account many concepts coming from existing works in the domain. We associate techniques and methods of discrete event simulation (DEVS), distributed computing (Ghost cells) and oriented-object programming (Design patterns), in order to simulate large-scale fire spreading. Modeling such spatial systems is facilitated by the use of enhanced cellular automata. The conception of the distributed model raises many design problems. Solutions are based on design patterns and enable to define a modular architecture adjustable to various contexts of execution. The model integrates object technologies and parallelization techniques in a modular and extensible way. Hence, the simulation kernel, more precisely the methods dealing with message exchanges for the distributed simulation, has to be enhanced. This study gives an overview of the performances we can reach using such methods in the domain of parallel and distributed simulation of fire spread, and constitutes a first stage. The validity of the approach and the encouraging results show that openMOSIX cluster could form a basis for a good distributed engine, easily adaptable for spatial model in large-scale simulations.

REFERENCES

[Balci 1988] Balci, O. (1988). The Implementation of Four conceptual Frameworks for Simulation Modeling in High-Level Languages. Technical Report SRC-88-009. System Research Center, Virginia State University.

[Bandini *et al.* 2001] Bandini, S., Mauri, G., Serra, R. (2001). Cellular automata : From a theoretical parallel computational model to its application to complex systems. Parallel Computing, 27, pp. 539-553.

[Barak La'adan 1998] Barak, A., La'adan, O. (1998). The MOSIX Multicomputer Operating System for High Performance Cluster Computing. *Journal of Future Generation Computer Systems,* Vol. 13, No. 4-5, pp. 361-372.

[Chopard Masselot 1999] Chopard, B., Masselot, A. (1999) Cellular automata and lattice Boltzmann methods: a new approach to computational fluid dynamics and particle transport. Future Generation Computer Systems, Vol.16, N°2--3, pp.249-257.

[Coquillard Hill 1997] Coquillard, P., Hill, D., R., C. (1997). Modélisation et Simulation d'Ecosystèmes. Des modèles déterministes aux simulations à évènements discrets. Masson.

[Di Gregorio Serra 1999] Di Gregorio, S., Serra, R. (1999). An empirical method for modelling and simulating some complex macroscopic phenomena by cellular automata. Future Generation Computer systems 16, pp. 259-271.

[Dupuy 1995] Dupuys, J., L. (1995). Slope and fuel load effects on fire behaviour : Laboratory experiments in pine needles fuel beds. International journal of wildland fire.

[Erard Déguénon 1999] P.J. Erard, P. Déguénon. (1999). Simulation par évènements discrets. Concepts et réalisations en Simula, Ada et Smalltalk. *Presses Polytechniques et Universitaires Romandes*.

[Gamma *et al.* 1994] Gamma, E., Helm, R., Johnson, R., et Vlissides, J. (1994). Design patterns. Elements of Reusable Object-Oriented Software. Addison Wesley. ISBN:0-201-63361-2.

[Gardner 1970] Gardner, M. (1970). Mathematicals Games, The fantastic combinations of John Conway's new solitaire game « life ». Scientific American 223, pp.120-123.

[Ghanem *et al.* 2004] Ghanem, J., Dhakal, S., Abdallah, C., T., Hayat, M., M., Jerez, H. (2004). Load Balancing in Distributed Systems with Large Time Delays: Theory and Experiments. Dans proceedings IEEE Mediterranean conference on control and automation, Turkey

[Hoffmann *et al.* 2000] R. Hoffmann, K., P., Völkmann, S., Waldschmidt. (2000). Global cellular automata GCA: an universal extension of the CA model. ACRI 2000 work in progress session, Karlsruhe, Germany.

[Ingalls 2002] Ingalls, R., G. (2002). Introduction to simulation. *Proceedings of the 2002 Winter Simulation Conference*. E. Yücesan, C-H. Chen, J.L. Snowdon, J.M. Charnes, eds. pp. 7-16.

[Lan *et al.* 2002] Lan, Z., Taylor, V., Bryan, G. (2002). Dynamic Load Balancing of SAMR applications on Distributed Systems. Journal of Scientic Programming, Vol 10(4), pp. 319-328.

[Langlois Phipps 1997] Langlois, A., Phipps, M. (1997). Automates cellulaires, application à la simulation urbaine. Edition Hermes.

[Leduc 1999] Leduc, T. (1999). Modélisations par réseau d'automates cellulaires et simulations parallèles du phénomène de subduction-érosion en tectonique des plaques. Thèse de doctorat en systèmes informatiques. Université Paris 6.

[Maniatty *et al.* 1994] B. Maniatty , T. Caraco, « TEMPEST: a fast spatially explicit model of ecological dynamics on parallel machines ». Proceedings of the 1994 simulation multiconference on Grand challenges in computer simulation, p.114-119, April 1994, San Diego, California, United States.

[Overeinder *et al.* 1991] Overeinder, B., J., Hertzberger, L., O., Sloot, P., M., A. (1991). Parallel Discrete Event Simulation. Dans W.J. Withagen, editor, The Third Workshop Computer systems, Faculty of Electrical Engineering, Eindhoven University, pp.19-30.

[Reinefeld *et al.* 1998] Reinefeld, A., Gehring, J., Brune, M. (1998). Communicating Across Parallel Message-Passing Environments. Journal of Systems Architecture, Vol. 44, pp. 261-272.

[Rennard 2000] Rennard, J., P. (2000). Introduction aux automates cellulaires. http://www.rennard.org/alife, pp 1-25.

[Santoni *et al.* 1998] Santoni, P., A. (1996). Propagation des feux de forêts : Modélisation dynamique et résolution numérique, validation sur des feux de litière. Thèse de Doctorat, Université de Corse.

[Sipper 1994] Sipper, M. (1994). Non-Uniform Cellular Automata: Evolution in Rule Space and Formation of Complex Structures. Dans proceedings of the 4th International Workshop on the Synthesis and Simulation of Living Systems \ Artificial Life IV, R. A. Brooks and P. Maes (eds.), pp. 394-399.

[Sipper 1999] Sipper, M. (1999). The emergence of cellular computing. In IEEE Computer, July, pp. 18-26.

[Talia 2000] Talia, D. (2000). « Cellular processing tools for high-performance simulation ». Computer. pp. 44-52.

[Tonguz Yanmaz 2003] Tonguz, O., K., Yanmaz, E. (2003). On the Theory of Dynamic Load Balancing, IEEE Global Telecom. Conf. (GLOBECOM'03), vol. 7, pp. 3626-3630, 2003.

[Worsch 1997] Worsch, T. (1997). Programming environments for cellular automata. Dans Proceedings Cellular Automata for Research and Industry (ACRI96), Springer, Berlin, pp.12.

[Zeigler 1976] Zeigler B.P., « Theory of Modelling and Simulation », Wiley, New York. 1976.

[Zeigler *et al.* 2000] B. P. Zeigler, H. Praehofer, T. G. Kim, « Theory of Modeling and Simulation: Integrating Discrete Event and Continuous Complex Dynamic Systems », Academic Press, January, 2000.

A Parallel Lake-Land-Atmosphere Hybrid Model using High Performance Computing (HPC)

Vimal Sharma
University of Guelp
Comp. Res. Lab. for Environment
Guelph, ON, Canada
+1-519-824-4120-ext 58272
vsharma@uoguelph.ca

David Swayne
University of Guelp
Comp. Res. Lab. for Environment
Guelph, ON, Canada
+1-519-824-4120-ext 58272
dswayne@uoguelph.ca

David Lam
Environment Canada
Nat. Water Res. Institute
Burlington, ON Canada

Wayne Rouse
McMaster University
Comp. Res. Lab. for Environment
Hamilton, ON, Canada

William Schertzer
Environment Canada
Nat. Water Res. Institute
Burlington, ON Canada

ABSTRACT
As well as atmospheric circulation, Canadian Regional Climate Model (CRCM) models atmosphere-land interaction. In this scheme, land is modeled by CLASS (Canadian Land Surface Scheme). CLASS models snow, vegetation, bare ground and composite of these fractions. CRCM currently lacks a lake component. With Canada possessing large lake mass, incorporation of lake component is essential for accurate climate change modeling. In this study, a prototype hybrid model using high performance computing has been tested to incorporate lake component in the existing scheme. A case study with 20 grid nodes using a benchmark dataset is presented. Preliminary results indicate that the proposed model can be an efficient, practical and viable option for lake-land-atmosphere interaction.

KEYWORDS
Lake-Land-Atmosphere interaction, CLASS, DYRESM, CRCM, high performance computing

1. Introduction

A very large number (millions) of small lakes and a dozen or so very large lakes have a significant, but unknown detailed effect on Canada's climate. Equally important is the potential impact of changes in Canada's climate on the quantity and quality of water, of which lakes constitute a significant portion

Regional climate models (RCM) are used in climate change studies. The current Canadian Regional Climate Model (CRCM) uses the Canadian Land Surface Scheme (CLASS) model for computation of heat and moisture fluxes associated with a land mass but is missing a lake component (Figure 3). To enhance the accuracy of the RCM there is definite need of incorporating a lake component in the system [Goyette 2000; Swayne 2003]. These models tend to be computationally intensive. The computational needs grow rapidly with finer grids. Finer grids are highly desired as they lead to increased accuracy of climate change models. The computational needs can be so high that computations may not be reasonably done using serial computers. Here arises the need for parallel computing. Parallel computing can be used to harness the collective computational power of many computer clusters available for the same problem. Depending on the size of the grid and number of processors available in the cluster, a group of nodes in a grid can be represented by individual processors that can be responsible for its computational needs.

Figure 1, shows the frequency distribution of lakes in western Canada. Each CRCM grid point (51 km CRCM grid resolution) further sub grids lake distribution by a 1 km^2 grid (Figure 2). A simulation study has to check to ensure that the behavior of a particular set of small to medium lakes is adequately represented. The problem complexity is enhanced by the fact that 0-dimensional or 1-dimensional models need to run depending upon presence of small, medium size lakes. Criteria for model choice have to be developed. These do not yet exist. With presence of a lake cell a decision has to be made about the choice of running of either one or both 0-D, and 1-D models. Over a period of time a small lake grid cell may appear or disappear depending on various environmental factors. This leads to the problem of how these results are to be incorporated.

In this paper, Section 2 presents a brief introduction of models is presented, Section 3 describes the proposed model design and lastly Section 4 presents a case study and preliminary results using the proposed design.

2. Background

In this section, a brief introduction to land and lake models used in the study are given. The land model being used is CLASS (Canadian Land Surface Scheme) and one-dimensional lake model is DYRESM.

2.1 CLASS

In late 80's, the Canadian Land Surface Scheme (CLASS) was developed at CCC (Canadian Climate Centre). It is a three layer physically, based land surface model. This surface scheme was developed to address shortcomings of land surface modeling within the Canadian GCM (General circulation model) [Verseghy 2000; Verseghy 1991; Verseghy 1993].

CLASS divides the soil column into three soil layers of depth 0.10, 0.25, and 3.75 m, to reproduce the soil thermal and moisture regime (Figure 3). The finite-difference one-dimensional heat conservation equation is applied to each layer for obtaining the change in average layer temperature $\bar{T}_i$ over a time step Δt is given by [Verseghy 1991]:

$$\bar{T}_i(t+1) = \bar{T}_i(t) + [G(z_{i-1}, t) - G(z_i, t)] \frac{\Delta t}{C_i \Delta z_i} \pm S_i \qquad (1)$$

where, $G(z_{i-1}, t)$ and $G(z_i, t)$ are the downward heat fluxes at the top and bottom of the layer, respectively, C_i is the volumetric heat capacity of the soil, Δz_i is the layer depth, and S_i is a correction term applied in case of freezing or thawing, or the percolation of ground water.

CLASS is recognized as potentially being able to represent the land grid modes, however, the current structure is inappropriate to represent a grid partially or totally covered by a lake [Goyette 2000; Swayne 2004] (Figure 3).

The current Canadian Regional Climate Model (CRCM) interacts with the Canadian Land Surface Scheme (CLASS) model for every land grid cell for computation of heat and moisture fluxes associated with a land mass, each time step. CLASS involves computation of heat and moisture fluxes for bare ground (fractional coverage by ground, FG), ground covered with snow (fractional coverage by snow, FSN), ground with canopy (fractional coverage by ground, FC) and ground with both snow and canopy, every time step for each grid node [Verseghy 2000]. Lake fraction (FK) is currently missing from the model (Figure 3).

The 51 km^2 node or grid square representative flux values are given by weighted average for each fraction (Figure 3). All the required inputs for the model are provided by the regional climatic model (RCM) and CLASS feeds back its results to the RCM for each node.

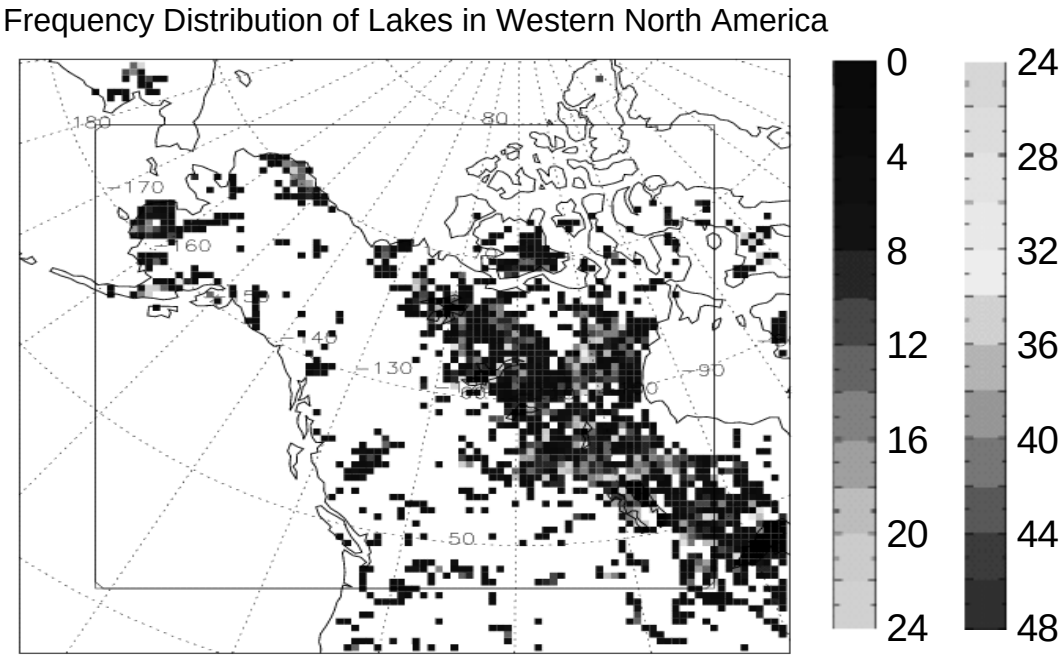

Figure 1: Lake fractional area based on CRCM 51 km grid resolution [Swayne 2004]

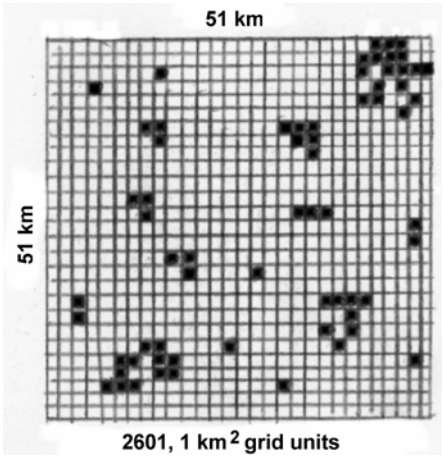

Figure 2: Lake Distribution AVHRR 1 km^2 resolution [Swayne 2004]

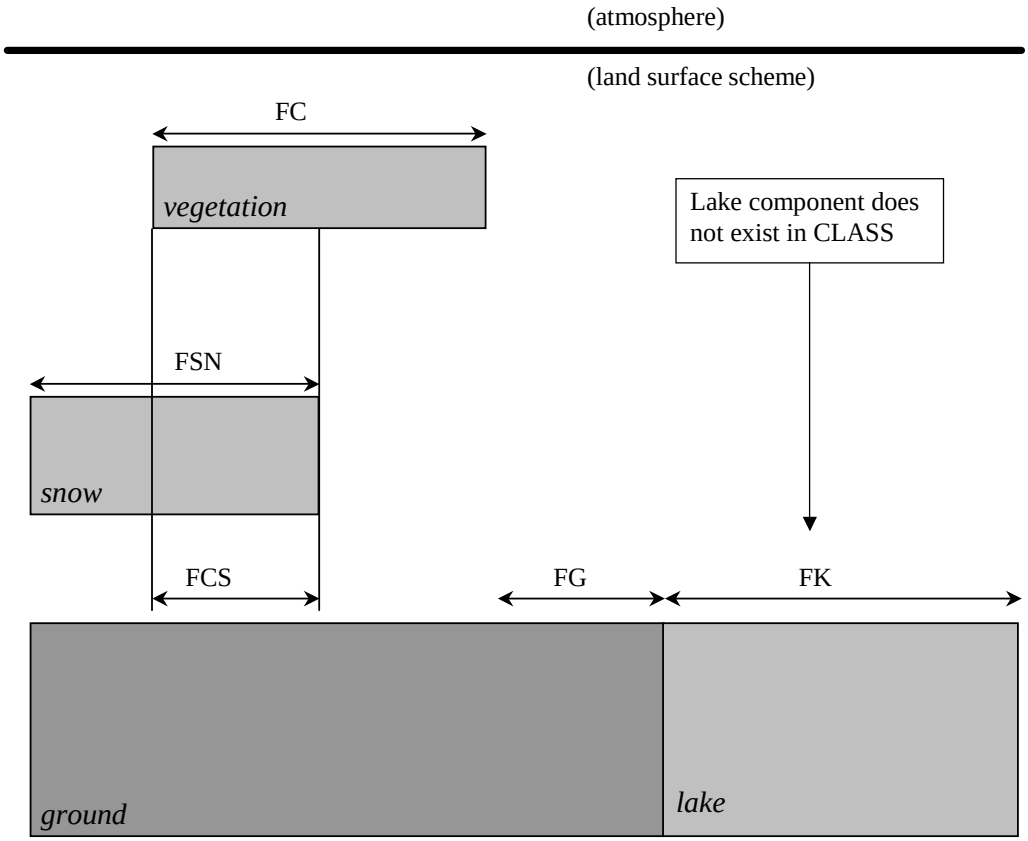

Figure 3: Layout of CLASS

2.2 DYRESM

Dynamic Reservoir Simulation model (DYRESM) is a one-dimensional hydrodynamic model for predicting the vertical distribution of temperature, salinity and density in lakes[Imberger 1980]; Antenucci 2002]. It has been developed by Centre for Water Research (CWR), Australia. The lake is modeled by series of horizontal layers of uniform property by variable thickness. The model is based on a Lagrangian layer scheme meaning that the series of horizontal layers are adjusted to stay within user-defined limits (instead of using a fixed grid approach).

Upper and lower limits are set on layer thickness and volumes to ensure that adequate resolution is achieved and excessive numbers of layers are not used. Any layer in excess of allowable volume is split in the required portions maintaining identical layer properties but with reduced volume. In the case of a layer volume below the allowable minimum, the layer is amalgamated with the neighboring layer of smallest volume.

The primary driving mechanisms for DYRESM are the surface heat, mass and momentum exchanges (Figure 4). These processes are responsible for majority of energy drivers for heating, mixing and stratifying the lake.

To incorporate a lake component to the existing system, combining the DYRESM model into the existing system is considered as a solution as DYRESM does not require calibration and has been tested around the world [Gal 2003;Boyce 1993; Han 2000].

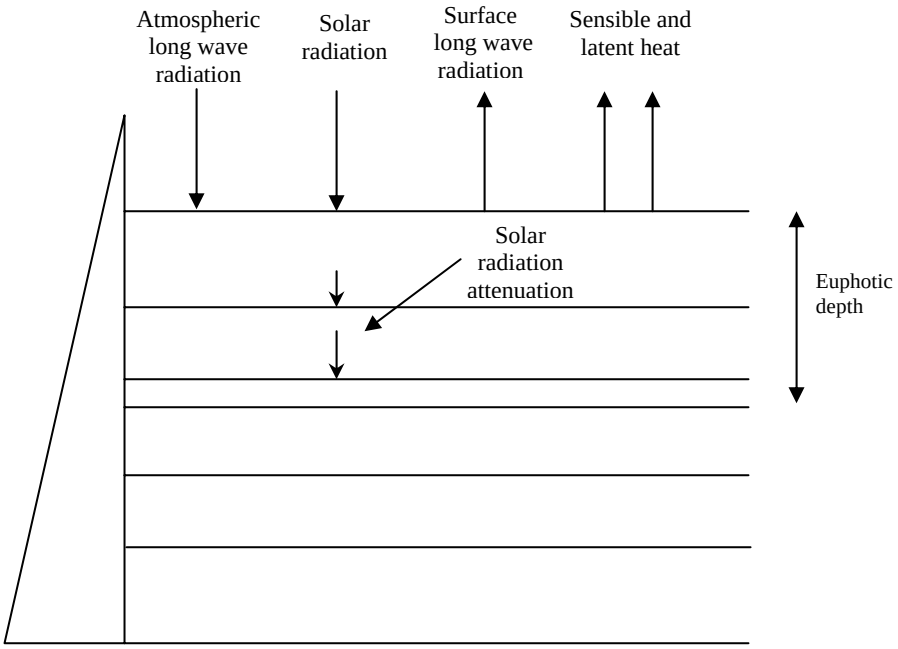

Figure 4: Layout of DYRESM [Antenucci 2002]

3. The Design

The implementation of the proposed hybrid model is run and tested on high performance computing (HPC) Guelph cluster of SHARCNET (The Shared Hierarchical Academic Research Computing Network). The cluster contains 27 Compaq Alpha ES40 nodes with 4 GB memory per node, running Red Hat Linux operating system. Each node has 4, 833 MHz processors.

Figure 3, represents a simple representation of CLASS's structure. As previously mentioned we are incorporating a lake component in this structure. As a solution, instead of using only the CLASS model in each grid's computation, the new hybrid model is employed to enclose the lake model in the system. The rationale for running two models in parallel is lowering of execution time and improving the possibility of modeling finer grid sizes. As the grid size is refined, the number of grid cell grows; any sequential solution will become impractical. In addition, there should be minimum change to existing tested code developed over the years. Therefore, solution as used by [Soulis 2000], serially combining two models cannot be used.

CLASS and DYRESM are two independent models, and therefore there is no need of communication between the two models before we synchronize them. In order to combine them, we have to synchronize them in a reasonable way. This makes parallel computation an ideal solution to the problem [Foster 1995]. Parallelism can provide a very simple and efficient mechanism for the purpose (Figure 5). Synchronization of the two models can be done at the end of computations for each iteration of the two models.

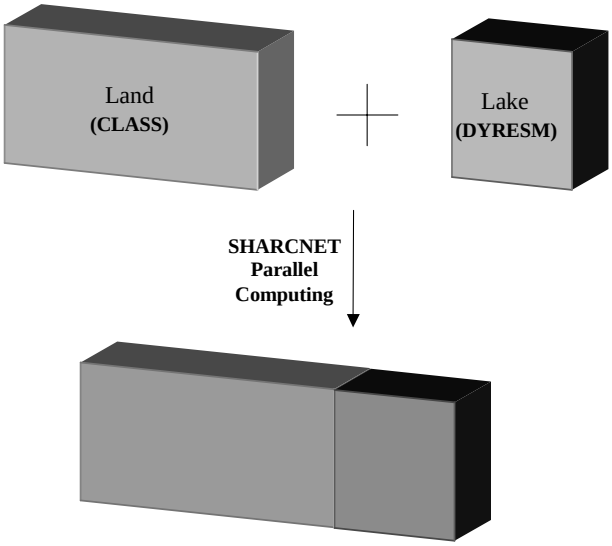

Figure 5: Schematic of proposed parallel hybrid model

Figure 6, illustrates the design of the hybrid model. Every grid node from RCM needs one single hybrid model for its data computation. The design in this study is a mix of *serial farm* and *parallel task* approaches. In *serial farm* design, a copy of a program, self-contained without any dependencies of communication with other grid nodes, is run on as many processors available in the cluster [Foster 1995]. Thus, as many copies of the program as the number of processors available maybe run concurrently.

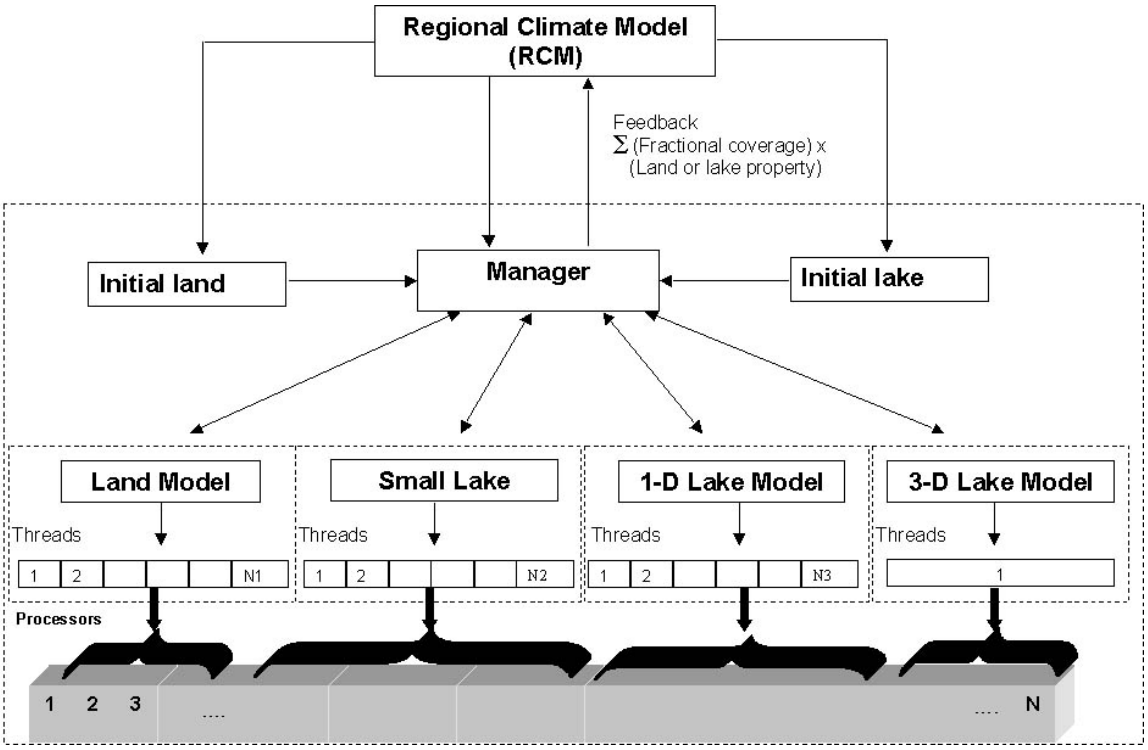

Figure 6: Design of proposed parallel hybrid model

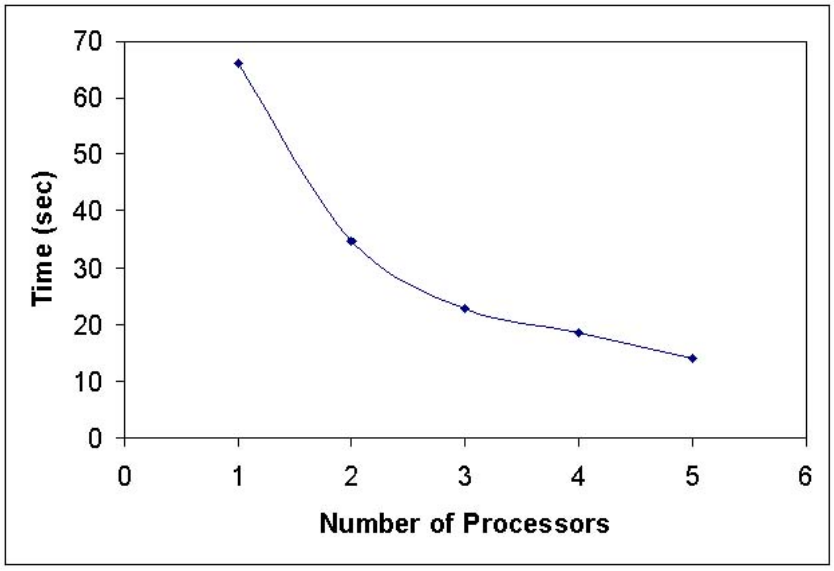

Figure 7: Preliminary results

On the other hand, a *parallel task* approach is to distribute the independent components in a single model to as many processors as there are the independent components. The components are computed in parallel and single node output is combination of result of each processor's result for assigned component. This leads to increased communication time per iteration. As well, interdependent or updated information must also be communicated to other components, which require it.

In our proposed design, computation of lake (0-d, 1-d, 3-d) and land (CLASS) components for a single grid node is done using parallel task approach by running the land and lake models concurrently on different processors, so that their combined result is the output of a grid node. These paired models are farmed out to as many processors available on the cluster, as there is no dependency of the pair on any other grid node (no horizontal flow), thereby, enabling the *serial farm* approach.

A manager program acts as an interface to take parameters from RCM and communicate to land and lake models. In addition, the manager is also adjusts the input/output data according to the requirements of respective land and lake models i.e. interpolation of input parameters to particular height as required by the model. It distributes copies of CLASS to the even numbered processors, and the copies of DYRESM to the odd numbered processors. As the number of processors available for computation is usually less than the number of grid nodes, we need to run multiple grid node computations on same processor. This is accomplished by multi-threading. Therefore, we run multiple copies of CLASS in multiple threads on even numbered processors and multiple copies of DYRESM in multiple threads on odd numbered processors. The maximum number of threads that can be created are limited by operating system constraints of 2GB memory per user. Each thread is given 2 MB of memory by the system; 1024 is the maximum number of threads that can be created and used per processor. The number of threads per processor as calculated as follows:

$$\text{Number of threads} = \frac{\text{Number of grid nodes}}{\text{Number of processors}} \tag{2}$$

The last processor additionally responsible for any residual grid nodes, and therefore .the equation (2) becomes

$$\text{Number of threads} = \frac{\text{Number of grid nodes}}{\text{Number of processors}} + \left(\text{Number of grid nodes \% Number of processors}\right) \tag{3}$$

Land and lake model(s) synchronize at end of each iteration by communicating their output to the manager, which computes the combined grid node output based on the fractional coverage of the grid node. This computed value is then available for RCM. This process is continued throughout the desired time period. To minimize the communication time, arrays of results from each processor are communicated to the manager after all the grid nodes for the processor are computed per iteration instead of communicating the results individually for each grid node.

4. Results and Conclusion

In the preliminary testing of the design, the two independent models, CLASS and DYRESM (1-d), are run in parallel on the Guelph SHARCNET cluster. To accomplish this, two processors per grid node are used, one running copy of CLASS and the other copy of DYRESM per grid node. The CLASS (land model) is run on the even numbered processor and the DYRESM (lake model) on the odd number processor for 20 grid nodes. The design can easily incorporate other lake components in the system for increased accuracy. In the preliminary testing, following simplifications were used:

1. The data feeding (input/output) is offline (no feedback to RCM).
2. Each grid node contains lake and land fractions.
3. Benchmark data set (107 days @15 min time step) for single node is used as input for all nodes by replicating the same data set for 20 grid nodes.

Preliminary results are presented in Figure 7. CLASS and DYRESM were run on the SHARCNET cluster with 20 grid nodes. The number of processors was varied from 1 to 5 for each model (total of 10 processors: 5 processors each computing land and lake components). Results indicate that the design performs as desired and significant decrease is observed in computation time required (about 65% less time required when using 5 processors as compared to 1 processor for each model). Also, it can be observed that as the number of grid nodes per processor decreases, the overhead cost becomes dominant over computational cost.

There is need to incorporate lake component in the current CRCM scheme without significantly changing the existing models. Also, a suite of lake models is needed to effectively model different sized lakes. In this study, a scheme to incorporate lake component using parallel computing is proposed. Preliminary results show that design can be an effective and viable solution. Further testing with suite of lake models and extended data set is needed.

ACKNOWLEDGEMENTS

This research is supported by SHARCNET, Canadian Foundation for Climate and Atmospheric Sciences, The Canadian Natural Sciences and Engineering Research Council, and Environment Canada.

REFERENCES

[Antenucci02] J. Antenucci and A. Imerito, "DYRESM- Science Manual," Centre for Water Research, The University of Western Australia, Dec.2002. Website:http://www2.cwr.uwa.edu.au/~ttfadmin/cwrsoft/doc/dyresm_science/index.html

[Boyce93] F. M. Boyce, P. F. Hamblin, D. Harvey, W. M. Schertzer, and R. C. McCrimmon, "Impact of heat load on Lake Ontario to deep cooling water withdrawls and to global warming," *J. Great Lakes Res.*, vol. 19, no. 3, pp. 603-616, 1993.

[Foster 1995] I. Foster, *Designing and Building Parallel Programs* Addison-Wesley Inc., 1995.

[Gal 2003] G. Gal, J. Imberger, T. Zohary, J. Antenucci, A. Anis, and T. Rosenberg, "Simulating the thermal dynamics of Lake Kinneret," *Ecol. Model.*, vol. 162, no. 1-2, pp. 69-86, 2003.

[Goyette 2000] S. Goyette, N. A. McFarlan, and G. M. Flato, "Application of the Canadian Regional Climate Model to the Laurentian great lakes region: Implementation of a lake model," *Atmosphere-Ocean*, vol. 38, no. 3, pp. 481-503, 2000.

[Han 2000] B.P. Han, J. Armengol, J. C. Garcia, M. Comerma, M. Roura, J. Dolz, and M. Straskraba, "The thermal structure of Sau Reservoir (NE: Spain): a simulation approach," *Ecol. Model.*, vol. 125, no. 2-3, pp. 109-122, 2000.

[Imberger 1980] J. Imberger and J. C. Patterson, "Dynamic Reservoir Simulation Model - DYRESM: 5," *Transport Models for Inland and Coastal Waters, Academic Press New York. 1981. Proceedings of a Symposium on Predictive Ability*, vol. August 18-20, p. 36, 1980.

[Swayne 2003] D. A. Swayne, D. C. L. Lam, M. MacKay, W. Rouse, and W. M. S. Schertzer, "Preliminary assessment of the interaction between the Canadian Regional Climate Model and lake thermal-hydrodynamic models," in *5th International Symposium on Environmental Software Systems (ISESS '03), May 27-30, 2003* 2003, pp. 161-177

[Verseghy 2000] D. L. Verseghy, "The Canadian Land Surface Scheme (CLASS): its history and future," *Atmosphere-Ocean*, vol. 38, no. 1, pp. 1-13, 2000.

[Verseghy 1991] D. L. Verseghy, "CLASS--A Canadian Land Surface Scheme for GCMS: I. Soil Model," *International Journal of Climatology IJCLEU*, vol. p 111-133, p. 44, 1991.

[Verseghy 1993] D. L. Verseghy, N. A. McFarlane, and M. Lazare, "CLASS-A Canadian land surface scheme for GCMS, II. Vegetation model and coupled runs," *Int. J. Climatol.*, vol. 13, no. 4, pp. 347-370, 1993.

[Swayne 2004] D. A. Swayne, "CFCAS Project Report", Computing Research Laboratory for Environment, University of Guelph. June2004.

[Soulis 2000] E. D. Soulis, K. R. Snelgrove, N. Kouwen, F. Seglenieks, and D. L. Verseghy, "Towards Closing the Vertical Water Balance in Canadian Atmospheric Models: Coupling of the Land Surface Scheme CLASS with the Distributed Hydrological Model WATFLOOD," *Atmosphere-Ocean*, vol. 38, no. 1, pp. 251-269, 2000.

Distributed-memory parallelization of a semi-empirical biogenic Volatile Organic Compounds emission model

Gerhard Smiatek
Institute for Meteorology and Climate Research (IMK-IFU)
Forschungszentrum Karlsruhe
Kreuzeckbahnstrasse 19
Garmisch-Partenkirchen, Germany
+49 (0)8821 183 282
Gerhard.Smiatek@imk.fzk.de

ABSTRACT
This paper describes parallelization of a grid-oriented semi-empirical biogenic volatile organic compound (BVOC) emission model (seBVOC). It uses distributed memory parallel (DMP) model relying on the MPI (message-passing-interface) library. The parallel version achieves nearly linear decrease in execution time as the number of processors is increased. However, with some numbers of processors the efficiency suffers from unequal load balance caused by different number of calculations within the grid cells. Application of variable domain decomposition improves the load balance adding up to 60% additional decrease of processing time.

KEYWORDS
BVOC, biogenic emissions, MPI, parallel processing

1. Introduction

Gridded environmental models provide favorable conditions for parallelization. The modeling area can easily be subdivided into smaller areas calculated in parallel following the Single Program Multiple Data (SPMD) principle. Often the modeled processes are also spatially independent and do not require information from neighboring cells. On the other hand environmental features vary in space and time. This might influence the number of required calculations within the grid cells and thus, result in a load imbalance limiting the performance of the parallel code.

The semi-empirical biogenic volatile organic compound model seBVOC is a grid-oriented model. It has been developed to assess regional volatile organic compound (VOC) emissions from the vegetation in high temporal and spatial resolution. Due to their high reactivity VOCs from biogenic sources (BVOC) play an important role in the chemistry of the atmosphere even in densely populated areas where VOCs from anthropogenic sources (AVOC) dominate. Therefore, they must be included in any air quality simulation using numerical chemistry transport models (CTM). The implementation of a parallel version of seBVOC was motivated by the increasing need of highly resolved BVOC emission inventories as well as the substantial requirement of computational power in the uncertainty assessment of the BVOC estimates with a Monte Carlo Study (MCS).

The article describes the seBVOC parallelization in the distributed memory parallel (DMP) approach using the standard message passing interface (MPI)[Snir et al. 1996] version 1.x and standard Fortran 90. Both are known to produce a portable code with good scalability. The article introduces in broad terms the models background, describes the parallelization approach and discusses the load balance problem.

2. Numerical model

The semi-empirical BVOC emission model (seBVOC) is based on the algorithm presented by [Guenther et al. 1993] and [Steinbrecher et al. 1997] and is discussed in detail by [Stewart et al. 2003]. In general, the emission E (in $\mu g m^{-2} h^{-1}$) of a distinct BVOC species k from a plant species l can be quantified as:

$$E_{kl} = A_l D_l \varepsilon_{kl} \gamma \tag{1}$$

where A_l is the area covered by the plant species (m^2), D_l the foliar biomass (gm^{-2}), ε_{kl} an average emission factor µg (g-dry weight)$^{-1}$h^{-1}) and γ an environmental correction factor. It corrects for effects of the actual temperature and solar radiation on

the emission as the emission factor is standardized for 30°C and 1000 μmol $m^{-2}s^{-1}$ photosynthetically active radiation (PAR). Isoprene emissions depend on temperature and solar radiation (synthesis emission) while monoterpene emissions are often temperature driven (pool emission). Monoterpene emissions of some trees (i.e., *Picea abies)* depend on both temperature and radiation [Steinbrecher et al. 1997].

The total emission can therefore be described as:

$$E_{kl} = E_{kl\_pool} + E_{kl\_synth} \tag{2}$$

where E_{kl_pool} is the pool emission and E_{kl_synth} the synthesis emission.

For synthesis emission the environmental correction factor is

$$\gamma_{synth} = C_L C_T \tag{3}$$

where C_L is the factor describing the response of the emission to PAR and C_T the response to the temperature. With empirical coefficients α (=0.0027) and c_{L1} (=1.066) as well as with the PAR flux I (μmol m^{-2} s^{-1}) C_L is calculated as:

$$C_L = \frac{\alpha c_{L1} I}{\sqrt{1+\alpha^2 I^2}} \tag{4}$$

and C_T is calculated as:

$$C_T = \frac{exp\dfrac{c_{T1}(T-T_S)}{RT_S T}}{1+exp\dfrac{c_{T2}(T-T_M)}{RT_S T}} \tag{5}$$

where R is the ideal gas constant(= 8.314 J K^{-1} mol^{-1}), C_{T1} a constant (=95000 J mol^{-1}), C_{T2} a constant (=230000 J mol^{-1}), T (K) is the leaf temperature, T_M (= 314 K) empirical coefficient, and T_S (=303 K) standard temperature. The correction factor for the pool emission is

$$\gamma_{pool} = exp(\beta(T-T_S)) \tag{6}$$

where T_S is the standard temperature (303 K), T leaf temperature (K), and β (= 0.09K^{-1}) a constant.

In seBVOC the light extinction within the canopy is taken into account by dividing the canopy into sunlit and shade fractions following the model presented by [de Pury et al. 1997]. The irradiance absorbed by the canopy I_c (μmol m^{-2} s^{-2}) is divided into sunlit I_{cSun} and shaded fraction I_{cSh} .The sunlit fraction is

$$I_{cSun} = I_{lbSun} + I_{ldSun} + I_{lbsSun} \tag{7}$$

where *lb* denotes the direct beam, *ld* the diffuse irradiance and *lbs* the scattered beam irradiance. The shaded fraction is calculated as:

$$I_{cSh} = I_c - I_{cSsun} \tag{8}$$

The Equations 7 to 8 are solved twice for visible and NIR (near infrared) part of the irradiance yielding I_c and I_{ir}. PAR I is assumed to be 0.45 x I_c.

The leaf temperatures are determined by the canopy energy budget [Dai et al. 2004]:

$$C_c \frac{\partial [T_l]_j}{\partial t} = 0 = [I_c]_j + [I_{ir}]_j - [H_c]_j - L[E_c]_j \quad (9)$$

where I_c is the summed net solar radiation absorbed by sunlit/shaded fraction of canopy (Wm^{-2}), I_{ir} is net NIR radiation absorbed by sunlit/shaded fractions of the canopy (Wm^{-2}), H_c is the sensible heat flux from foliages to canopy air (Wm^{-2}), and $L[E_c]$ is the latent heat flux from leaves to canopy air (Wm^{-2}). j denotes the integration for sunlit ($j = 1$) and shaded fractions of the canopy ($j = 2$). C_c is the canopy heat capacity ($J\ m^{-2}\ K^{-1}$) which is neglected for the steady state case. The numerical solution for leaf temperatures is calculated by application of the iterative Quasi-Newton-Raphson method.

The BVOC emissions are estimated for the sunlit and shadowed fractions of the canopy and then added. The seBVOC model can be run in a grid mode with mesh specification and meteorology input provided by the Fifth Generation NCAR/Penn State Mesoscale Model (MM5)[Dudhia 1993]. In the gridded approach the domain grid consist of n rows × m columns with a km by a km cell size.

SeBVOC has been coded in Fortran 90. The basic structure is (see Figure 1a):

- Initialize the 2D dimensions, modes and options
- Read required tabular input data (land cover, foliar biomass, leaf area index (LAI) and emission factors)
- Read gridded meteorology data for the term 0 (temperature, wind speed, solar radiation, humidity)
- Loop over columns, rows and land cover categories and calculate the light extinction (Equation 7), leaf temperature (Equation 9) and loop over the BVOC compounds and calculate the BVOC emission in each grid cell
- Iterate steps 3 to 4 for all required time terms. Time step is one hour.
- Write final 2D grid containing the BVOC emissions

3. **Distributed memory parallelism**

In the distributed memory parallel model each processor has its own dedicated computer memory. The data is exchanged between the processes via messages. Messages are sent and received via explicit calls. The MPI standard defines a set of functions and procedures that facilitate the message passing.

Parallelization with MPI involves domain decomposition. In a regional application the grid array consisting of n columns by m rows is divided into sub-grids which are distributed over the available processors. Each processor is responsible for BVOC calculation of its part of the array. At the current stage of the seBVOC development, the processors do not have to exchange data between neighboring areas. Thus, the communication is limited to provision of appropriate input data and communication of the results of a specific array. In that case both striped (column- or row-wise), in one dimension (1D), as well as block (check board) domain decomposition in two dimensions (2D) can be applied. The 1D partitioning is the simplest way and has the advantage to run on any number of processors. In seBVOC both 1D and 2D decomposition with an optimization option have been implemented.

The basic structure of the parallel code is (see Figure 1b):

- Initialize MPI and request the number of available processors (numbered from 0 to n)
- On 0 processor read the array dimensions of the meteorology input file and perform the domain decomposition according to the chosen 1D or 2D option
- On 0 processor read the tabular input data (land cover, emission factors, foliar biomass) and communicate the data to the processors 1 - n
- On 0 processor read the meteorology input of the term 0 and communicates appropriate array portions to the remaining processors
- On processors 1 - n receive the input data

- On processors 0 - *n* calculate the emission for all cells within their part of the array as shown in chapter 2 and communicate the resulting array to the processor 0
- On 0 processor receive the output and assemble the final output array.
- Iterate steps 4 - 8 are until the last required time term is reached
- On 0 processor write the BVOC emissions to the output file

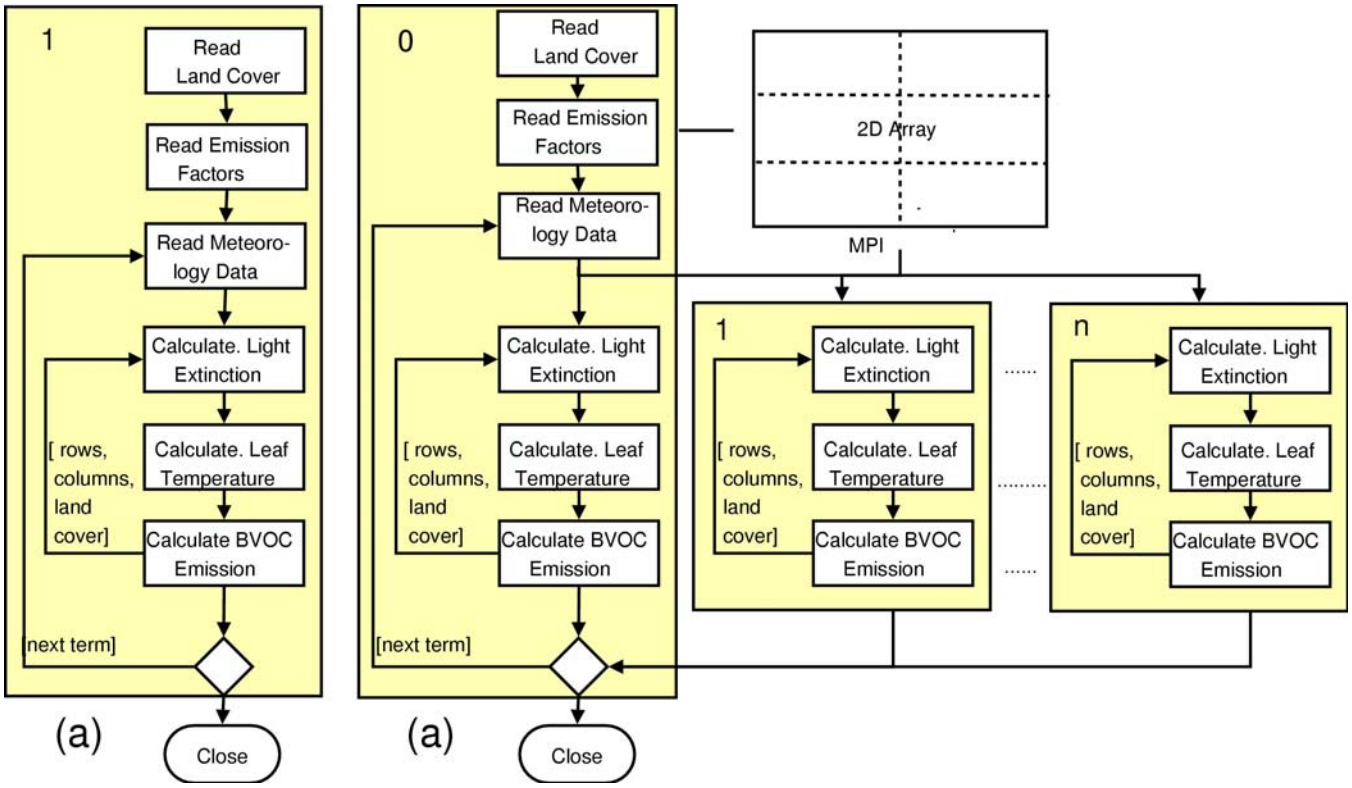

Figure 1. Schematic flow chart of the seBVOC sequential code with one processor (a) and parallel code (b) with 0,… n processors

4. **Results**

The parallel version of seBVOC has been applied in a modeling exercise aiming at the estimates of regional BVOC emissions from forest in Poland with a grid size of 10km by 10km (see Figure 4a). The available computing platform UHU is a SMP (symmetric multi-processor) Linux cluster. UHU is build with 100 rack mounted nodes. Each node is equipped with dual Intel Xeon 3.0 Ghz (50) and 3.2 Ghz (50) processors with 1GB of memory. UHU has a double internal Gigabit-Ethernet network: one service network for NFS communication and a second network for the MPI communication. The operating system is Linux with the kernel number 2.4. MPI is provided over Ethernet using LAM (Local Area Multicomputer) and MPICH (CH stands for Chameleon). The batch system on UHU is OpenPBS (Open Portable Batch System). There are two FORTRAN compilers available, the Intel Linux compiler 8.x and Portland Group Compiler (PGI) 5.x.

Figure 2a shows the speed-up and efficiency of the model run in 1D (column-wise) domain decomposition for one month in hourly resolution. The speed-up *s* of a parallel program is defined as:

$$s = \frac{t_{seq}}{t_{par}} \tag{10}$$

where t_{seq} is the execution time of the sequential code on the fastest processor and t_{par} is execution time of the parallel code.

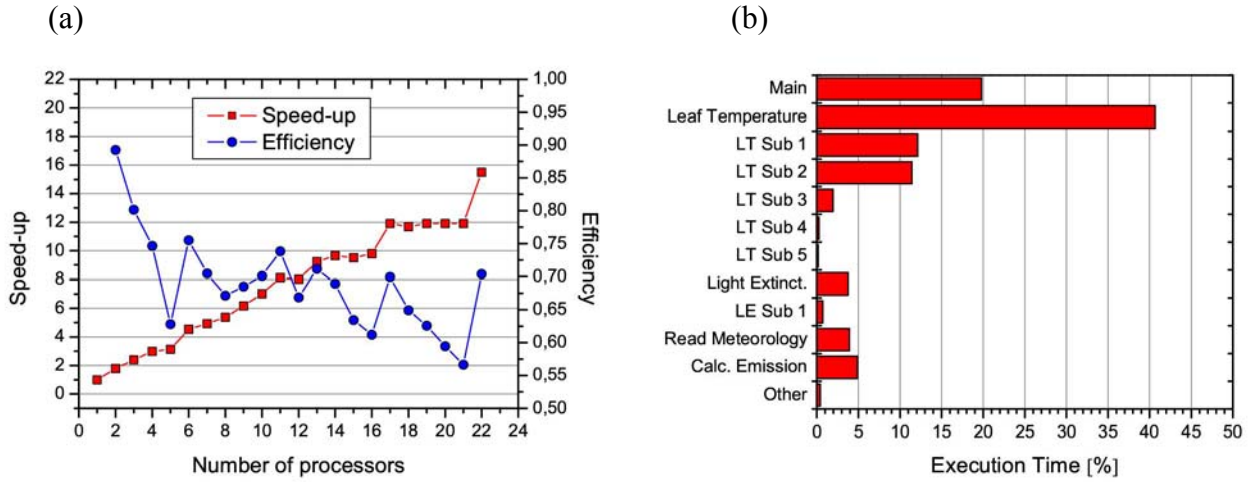

Figure 2. Scaling of seBVOC application for the area of Poland (Intel compiler and LAM) (a) and execution time spent in different parts of the model (b) (LT - leaf temperature function, LE -light extinction function)

The performance can also be linked to the efficiency e of a parallel program. Efficiency relates the speed-up s to the number of processors N used in the parallel run:

$$e = \frac{s}{N} \tag{11}$$

Due to the high data locality the parallel application scales nearly linear but there are some conditions where additional processors do not improve the speed-up. The efficiency suffers from unequal load balance. Figure 3a shows load balance in a test run with 8 processors. The domain consists of 66 rows and 72 columns. In 1D domain decomposition with 8 processors, 7 processors calculate 9 rows each and the last one has only 3 rows. In addition, the load imbalance results from the different number of calculations performed in single grid cells. Some grid cells are outside of the border (see Figure 4a) and do not require any calculations. However, the size of the domain cannot be changed due to some constrains resulting from the domain definition in the meteorology model MM5. Furthermore, the execution time in each grid cell depends on the number of tree species found in this cell, time of the day and the emission behavior of the tree species. This variability is rather typical in environmental modeling. The unequal load balance applies to both 1D and 2D domain decomposition.

Application of variable decomposition with variable number of rows and columns can improve the load balance. The key question here is which process within seBVOC could be used as measure to balance the load. Diverse code profiling tools (gprof = GNU profiler, pgprof = Portland Group profiler, Vampir = visualization and analysis of MPI resources) can be applied to the model code and provide appropriate information. They allow discovering which functions and procedures were how often executed and how much of the total execution time they have consumed. Figure 2b shows the execution time in the most important parts of seBVOC. It can be seen that the iterative calculation of the leaf temperature (Equation 9) required 40% and with all sub functions more than 60% of the total execution time. Thus, the number of leaf temperature calculations can be used as measure for a variable 1D decomposition. It depends solely on the number tree species found in a grid cell. Consequently, the number of calculations per model row or column can easily be accessed during the preprocessing of the land use, biomass and emission factors data and written out as an additional input file for seBVOC. The preprocessing is performed with a Geographical Information System (GIS)-based system.

Figure 4b shows the number of leaf temperature calculations which ranges between 0 and 12. It explains the unequal load in any 1D or 2D domain decomposition with constant number of rows and columns. In order to improve the load balance an

(a) (b)

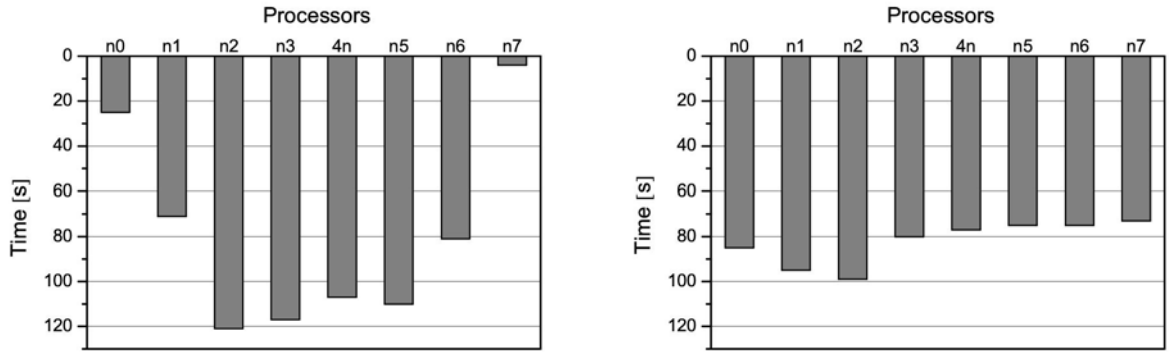

Figure 3. Processing time of a seBVOC run with 8 processors (Intel Compiler/LAM). Poor load balance (a) and improved load balance with an optimized row-wise domain decomposition (b)

Table 1. Speed-up (s) and efficiency (e) with different load balance optimizations and different MPI implementation options. Speed-up related to a single processor run of seBVOC compiled with the same compiler Intel or PGI

Processors	PGI/LAM						PGI/MPICH		Intel/LAM					
	1D R[1]		2D B[2]		1D RO[3]		1D RO[3]		1D R[1]		1D RO[3]		ID CO[4]	
	s	e	s	e	s	e	s	e	s	e	s	e	s	e
4	2.31	0.58	3.35	0.84	3.66	0.92	3.79	0.94	2,88	0.72	3.29	0.82	3.91	0.98
6	3.48	0.58	4.84	0.81	5.30	0.88	5.45	0.91	4.34	0.72	5.95	0.98	5.39	0.90
8	5.61	0.70	5.70	0.71	6.47	0.87	7.75	0.97	5.21	0.67	7.43	0.93	7.71	0.96
12	6.32	0.53	7.73	0.64	9.94	0.83	10.70	0.88	7.53	0.63	9.62	0.96	10.41	0.87
14	7.47	0.53	9.76	0.70	11.59	0.83	12.51	0.89	8.22	0.59	10.71	0.89	12.25	0.88
16	9.43	0.59	9.59	0.60	9.94	0.62	14.88	0.93	9.47	0.59	13.39	0.84	14.21	0.89

[1] row-wise decomposition
[2] block decomposition
[3] optimized row-wise decomposition
[4] optimized column-wise decomposition

optimization has been implemented in the 1D approach. It tries to use variable strips or columns in which the number of leaf temperature calculations is close as possible to an average calculated per available processor. Figure 3b shows the improved load balance and an a decrease of the processing time from over 120 s to below 100 s. Table 1 documents an additional speed-up in order of 10-60% with different numbers of processors. Thus, the parallel code reaches the same efficiency with lower number of processors. It must be pointed out, that in seBVOC application substantial differences in processing time decrease resulted from the choice of compiler, compiler version, compiler optimization options and the MPI implementation. On the UHU Linux cluster the seBVOC executable created with PGI and MPICH has shown to some extent higher performance (10%) than compiled with PGI and LAM (see Table 1). On the other hand the Intel compiler produced generally up to 30% faster code and better scalability. Due to the significantly faster memory access, in FORTRAN the 1D column-wise decomposition provides slightly higher performance. Thus, fastest runs were performed with the Intel/LAM in combination with optimized domain decomposition.

(a) (b)

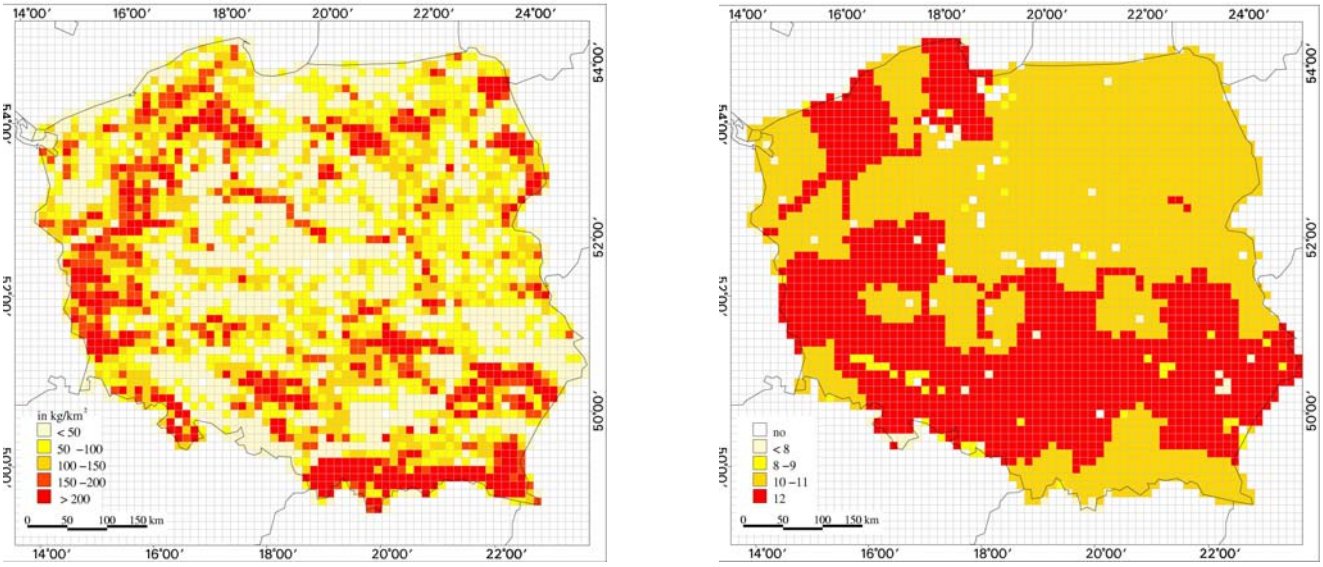

Figure 4. Monthly total BVOC emissions from forests in July 2000 in Poland (a) Number of leaf temperature calculations per grid cell 10 km by 10km (b)

5. Conclusions

A parallel version of the semi-empirical BVOC model using shared memory parallelization model and MPI library has been developed. Several compilers as well MPI implementations, such as LAM or MPICH can be selected when compiling the code. The application shows nearly linear scalability for small number of processors. On the UHU cluster choice of the compiler as well as the MPI implementation significantly influences the performance of the seBVOC model. A variable domain decomposition strategy taking into account the variability of environmental features, here the forest distribution within the specific modeling area, leads to an improvement of the processing time. Best performance has been reached with Intel/LAM combination and optimized domain decomposition. With the parallel version of seBVOC the computation time of a Monte Carlo Study was reduced from 3 months to less than one week [Smiatek Bogacki 2005].

REFERENCES

[Dai et al. 2004] Dai, Y., R. E. Dickinson, and Y.-P. Wang, A two-big-leaf model for canopy temperature, photosynthesis, and stomatal conductance, *Journal of Climate,* ***17*** (12), 2281-2299, 2004.

[de Pury et al.1997] de Pury, D .G. G., and G. D. Farquhar, Simple scaling of photosynthesis from leaves to canopies without the errors of big-leaf models, *Plant, Cell and Environment,* ***20***, 537 - 557, 1997.

[Dudhia 1993] J. Dudhia, A nonhydrostatic version of the Penn State-NCAR mesoscale model: Validation tests and simulation of an Atlantic cyclone and cold front, *Monthly Weather Review,* ***121***, 1993.

[Guenther et al.1993] Guenther, A., P. Zimmerman, P. Harley, R. Monson, and R. Fall, Isoprene and monoterpene emission rate variability: Model evaluation and sensitivity analysis, *J. Geophys. Res.,* ***98***, 12609-12617, 1993.

[Pacheco et al. 1997] Pacheco, P. S., and W. Ch. Ming, Introduction to message passing programming. MPI user s′ guide in Fortran. 55 pp., 1997

[Snir et al. 1996] Snir, M., S. Otto, S. Huss-Lederman, D. Walker, and J. Dongarra, MPI: The Complete Reference. Massachusetts Institute of Technology, 1996.

[Smiatek Bogacki 2005] Smiatek, G. and M. Bogacki., Uncertainty assessment of potential BVOC emissions from forests with Monte Carlo Method. Case study for an episode from 1-Jul-00 to 10-Jul-00 for Poland. *J*. Geophys. Res., 2005. (submitted)

[Steinbrecher et al. 1997] Steinbrecher,R., H. Ziegler, G. Eichstädter, U. Fehsenfeld, R. Gabriel, Ch. Kolb, R. Rabong, R. Schönwitz, and W. Schürmann, Monoterpene and isoprene emission in Norway spruce forests, in: Slanina, S. (ed), Biosphere-atmosphere exchange of pollutants and trace substances, EUROTRAC Vol. 4 , Berlin, 352-365, 1997.

[Stewart et al 2003] Stewart E. H., C. N. Hewitt, R.G.H Bunce, R. Steinbrecher, G. Smiatek, and T. Schoenemeyer. A highly spatially and temporally resolved inventory for biogenic isoprene and monoterpene emissions - model description and application to Great Britain. *J*. Geophys. Res. **108** (D20) : 4644, doi: 10.1029/2002JD002694, 2003

Emergent Social Ontology
Examples from Artificial Societies

Dr. Martin Neumann
Department of Social Sciences
University of Osnabrueck
Seminarstr. 33
40974 Osnabrueck, Germany
+ 49 (0) 5406/807844
martneum@Uni-osnabrueck.de

ABSTRACT
The problem of a realist social ontology has a long-lasting tradition. To employ a notion by Durkheim, this is the question regarding whether or not there is something like an emergent social 'sui generis'.
In this paper a survey of social simulation models will be analysed with regard to the question of how they could contribute to an explanation of a social 'sui generis'. Since this question is only implicitly addressed in concrete models, they have to be put into a theoretical framework. Two approaches will therefore be distinguished: The processes of production, and the reproduction of a social level of reality. Yet one class of models focuses on the reproduction of social order by the interplay of structure and agency. By conceptualising emergence as a concrete historical process, on the other hand, archaeological models will be utilised to study the very first production of a social 'sui generis'.

KEYWORDS
Modelling social theory, social ontology, model survey, models of structure and agency, archaeological models

1. Introduction

Since the very beginning of the development of sociological theories, there has been great debate as to what they should be concerned with. The debate can be characterised by two poles: individualism and collectivism. Individualism, on the one hand, claims that the social has no real existence. Instead, every social phenomenon should be explained in terms its of individual actors. Hence, it is a reductive approach to social reality. On the other hand, collectivism, or holism, as it is often called, insists on an autonomous reality of a social sphere. Such a social sphere is not reducible to any other form of reality. This distinction can be found throughout the history of sociology in various forms and notations. It is sometimes called the micro-macro link, sometimes the problem of structure and agency or system versus *Lebenswelt*. In some discourse it is also denoted as a problem of scope, but these are generally different aspects of the same debate [Knorr-Cetina 1981, Alexander 1987].

This paper will investigate whether Artificial Societies could contribute to the notion of a social ontology, that is, the holistic approach to social theories. Even though it is frequently claimed that simulation technologies provide a tool to overcome the classical micro-macro dichotomy [e.g. Epstein Axtell 1996, Epstein 1999, Sawyer 2003], an explicit reference to the notion of a social ontology is not very common in Artificial Societies. On the contrary, Epstein [1999] argued that Artificial Societies should aim at a microfoundation of social science. Social simulation models, however, are mainly employed in quantitative sociology and have only recently gained attention with regard to questions of sociological theory. Yet theoretical findings are only implicit in contemporary concrete models. Pointing to these theoretical implications of Artificial Societies, this paper shows that we are indeed justified in speaking of a Durkheimean social 'sui generis' – without being committed to metaphysics.

In order to show this, the paper proceeds as follows: First, a short outline of the theoretical problem will be given. Second, by the theoretical differentiation of the reproduction and the very first production of a social 'sui generis', the models considered will be distinguished into two classes: the class of models of structure and agency, which contribute to the former question, and archaeological models, which will be applied to the latter.

2. The Question of Social Ontology in Sociological Theory

The holistic approach to social reality is as old as sociology itself. Yet August Comte, the early protagonist of the very name of sociology, claimed that Society is no more decomposable into individuals than a geometrical surface is into its lines, or a line into points [Comte 1967 (1851)]. In the history of sociology, Emil Durkheim's notion to explain social

facts only by reference to another social fact [Durkheim 1984 (1895)] in particular marked a starting point for controversial debates. According to Durkheim social forces are as real as astronomical ones [Durkheim 1973 (1897)], determining, e.g. suicide rates by the degree of social integration. Society is claimed to be an autonomous entity 'sui generis'. Here the term 'sui generis' denotes his conviction that although society does not exist without individual human beings, social reality is not reducible to individual actors. Yet he holds the position that the composition of individual elements generates an ontologically new level of reality. Society emerges from the individuals. The notion of an emergent social reality is of central importance to the conception of a social 'sui generis' in the tradition of Emil Durkheim [Durkheim 1967, (1898), Esser 1993]. The emergent social ontology is a new form of reality driven by a new kind of laws.

A lack of space prevents a comprehensive review of the debate in the theory of social science regarding this fundamental claim. Durkheim's work, however, can be seen as setting the stage for a long lasting debate on the nature of the social sciences. As already pointed out by Parsons [Parsons 1937], he emphasised the social preconditions of the social contract, an idea that was recently further elaborated by the evolutionary account of Brian Skyrms [Skyrms 1996, Skyrms 2004]. Classical structural functionalist explanations drew attention to the explanatory power of the value system in constraining an individual action. Hence, the notion of a social reality was methodologically applied by the functionalist approach. It was not, however, able to gain ontological justification [Archer 1995]. Adherents of a social ontology therefore adopted a more defensive position [Gellner 1971, Mandelbaum 1973]. The work of Roy Bhaskar [Bhaskar 1975], Margaret Archer [Archer 1995], Geoffrey Hodgson [Hodgson 2002], Keith Sawyer [Sawyer 2002], or the systemic approach of Niklas Luhmann [Luhmann 1984] are just some of the more recent ontological foundations of a realistic approach to the science of society.

Critics of the structural functionalist explanation [Wrong 1961, Homans 1964], however, argued on ontological grounds that 'in principle' the foundation of social structure can only be found in man of 'flesh and blood'. Hence, the notion of a social reality is highly contested by adherents of methodological individualism, such as Watkins [Watkins 1958] or Collins [Collins 1981] and the rational choice theory [Esser 1985, Elster 1986]. Notwithstanding that recent theoretical developments tend towards more mediating positions [Bourdieu 1987, Giddens 1988], for the sake of the argument the theoretical problems ontological positions have to face, will now be considered:

A realist social ontology has to face the problem of how to legitimise the notion of a social reality. In fact, it implies "a complete break with empiricist assumptions, positivistic prescriptions and the underlying Humean notion of causality" [Archer 1995, p. 23]. Even though the reference to social facts is methodologically quite successful insofar as it improves empirical correlation, it is suspected of reification. Since it fails the empiricist existence criterion of being available to sense data, it is argued that a collectivistic terminology would introduce a mysterious social substance. Hence, within an empiricist framework it has to be suspected to be committed to metaphysics. To meet this criticism, a causal criterion of reality is proposed by protagonists of collectivism [Gellner 1971]. It stresses that even though social reality is not an entity located in space and time, social facts are held to be really existent since they prove to be causally efficacious. The positivist notion of causality, however, relies on observed regularities. This is the Humean notion of causality. Since society is an open system, causal explanations have to face the problem, that these regularities are commonly not generated [Archer 1995, p. 54]. Hence, there is a need for a different conception of causality.

3. The Question of Social Ontology in Artificial Societies

The conception and problems of social reality as described above perfectly match the research programme of Artificial Societies: Artificial Societies provide a virtual laboratory to investigate isolated causal structures. As they do not study empirical data they employ a concept of causality based on conditional sentences to investigate the implications of the model assumptions. Investigations of Artificial Societies are viewed as the "work at the discovery of conditional generalisations" [Doran 1997, p. 74] Hence, firstly Artificial Societies study causal structures and secondly they do not provide the Humean concept of causality as observed regularities. On the contrary, they allow the study of the often surprising results of nonlinear connections and complex interactions. Hence, the result of such a causal analysis might not be a regularity but even, for example, a chaotic attractor. By running a simulation, Artificial Societies allow the study of emergent features inherent in the model assumptions. Stemming from Distributed Artificial Intelligence, the notion of emergence is a central task of explanations provided by this research programme [Gilbert 1995, Epstein 1999, Lansing 2002]. For a comprehensive overview of the topic of emergence see, for example, [Stephan 1999]. Roughly speaking, it denotes the fact that simulation techniques allow the study of model behaviour that can not be derived by analytical mathematical solutions [Axtell 2000, Chaitin 2000]. Yet by studying Artificial Societies, a methodological conception of emergence meets the ontological concept of emergence, as employed in the Durkheimean tradition of social sciences. Thus, it should be expected that Artificial Societies enable the investigation of the notion of a social 'sui generis' in computational terms.

The objective of this task is not only to clarify the sociological theory, but also to meet one of the criticisms of Artificial Societies: Since they allow us to overcome the empiricist barrier, they are suspected of practising fact-free science [Smith 1995]. Even though there are models of concrete historical events, many Artificial Societies are theoretical investigations. The sugarscape model [Epstein Axtell 1996] may serve as a prominent example. Hence, it remains to investigate what the targets of the theories are. Critics [Helmreich 1998] argue that they simply reflect the prejudices of the researchers. A close examination of their relation to sociological theories, therefore, will improve their theoretical consistency. This could be denoted as intersubjective validity. Contributions to this research programme have already been provided, e.g. by Andrew Sawyer, investigating the contribution of Artificial Societies to the micro-macro mapping [Sawyer 2003], by Stephen Lansing, who re-examined the Positivismusstreit in German Sociology, [Lansing 2002], by Riccardo Boera [Boera 2004], who provided reasons to strengthen the interrelation between Sociology and the Complexity Theory, and by Thomas Kron [Kron 2002], who evaluated the Theory of Niklas Luhman by means of Artificial Societies.

4. Examples of Models

Since the question of a social ontology is only implicitly addressed in social simulation models they have to be regarded from a more theoretical point of view: Yet this task will be investigated in the following two different conceptualisations of modelling: First, models of structure and agency will be regarded. These employ an idealised interaction structure that can spontaneously generate social order at any space and time, regardless of its history. Second, it will be investigated how archaeological simulation models could contribute to the question of the social 'sui generis'. It will be argued that they allow the study of the very first emergence of society in early prehistory.

4.1. Emerging Social Order out of Interacting Agents

The problem of the emergence of a social 'sui generis' is implicitly addressed by the problem of the generation of social order by individual interactions, hence, by the dichotomy of structure and agency. Regarding this view, social order is an emerging macro feature of interactions on the micro level. If and how social order can be generated was studied by a series of models [Kron Dittrich 2002, Dittrich et al. 2003, Kron Schimank 2003] whereas "in a basic dyadic setting two agents build up expectations during their interaction process" [Dittrich et al. 2003]. The two agents can be interpreted as Ego and Alter, starting with no knowledge of one another. They build up a communication system by sending messages to each other. Ego starts by a random selection of a message, represented by a number. Alter replies to this message by sending another message to Ego. In the course of simulation they seek to maximise their expectation-expectation, that is Ego's expectation of what Alter expects Ego to do, and their expectation-certainty, that is Ego's expectation of what Alter might do.

This allows the study of the problem of double contingency [Parsons 1968] as the main problem of producing social order [Luhmann 1984]. As a reference point for analysing interactions, Parsons identified the problems that, firstly, actors both act and are the object of action and that, secondly, an actor is orientated towards himself and others [Parsons 1968]. Yet this problem can be studied by the notions of expectation-expectation and expectation-certainty.

Simulation runs of these models demonstrate that Luhmann's proposal [Luhmann 1984] that a self-organising process might produce a comparably stable social order does in fact hold. Social order, however, does not necessarily result from this, but is dependent on specific parameter constellations. In particular, the result depends on selection rules, the agents memory and the number of alternatives for action from which they can choose [Kron Dittrich 2002, p. 243]. Further, the basic dyadic setting was expanded to small world networks [Kron Schimank 2003] and a multi-actor world [Dittrich et al. 2003] to allow for "transitions from a more actor-oriented perspective of social interaction to a systems level perspective"[Dittrich et al. 2003]. In particular in the case of randomly chosen acting agents, it can be observed that order usually disappears [Dittrich et al. 2003]. To sum up, it can be said that by simulating the interplay of structure and agency to investigate communication systems, a fundamental problem of social order is identified: the question of scalability of social order [Lorentzen Nickles 2002, Dittrich et al. 2003]. Yet this result goes hand in hand with the above-mentioned problem of scope.

4.2. Historical Emergence

4.2.1 Conceptual Framework

In the following this problem will be investigated from a different angle in order to utilise another class of models. Following Peter Blau [Blau 1977], it will be proposed to conceptualise social structure as the distribution of a population among social positions. This is because social structure "nearly always includes the concepts that there are differences in social positions, and that there are social relations among these positions" [Blau 1977, p. 27]. Undoubtedly, social positions influence people's social relations, but they have to be distinguished from mere interaction. At different times the same position can be inhabited by different people. Yet positions gain an autonomous

reality. It shall therefore be proposed to conceptualise the emergence of a social 'sui generis' as the emergence of social positions, which have to be a concrete historical process that took place in time.

Archaeological findings indicate that this process might be located at the emergence of a social stratification in the Palaeolithic period [Mellars 1985, Aigner 1989, Kolb 1994, Renfrew 2001, Earle 2004]. No archaeological indicators for a social stratification can be found in earlier societies. In the course of cultural evolution, however, "egalitarian principles of burials were violated when extraordinary items of gold started to be placed with certain individuals, presumably to mark their social difference." [Earle 2004, p. 112]. It seems to be highly plausible that the process of social stratification goes hand in hand with the emergence of social positions. Thus, here we have an autonomous element of social reality, which evolved in the course of time.

4.2.2. Archaeological Modelling

Yet in the following archaeological models shall be analysed inasmuch they contribute to the modelling of the emergence of a social 'sui generis'.
Archaeological modelling is a growing discipline. The investigation, however, will concentrate on two models: The EOS model [Doran 1994] of the emergence of social complexity in the Upper Palaeolithic period of south–west Europe and the MÜE & ERB model [Müller 1991] of the emergence of the state. The EOS model deals with a very early time period of the evolution of social complexity. Its target system is the time period of 15 00 to 30 000 BC. MÜE & ERB covers the time period of 6000 – 1500 BC. While the EOS model is concerned with the beginning of the emergence of a social ontology, the emergence of the state might be seen as bringing this process to a close. Thus, the objective for this choice is to cover a considerable amount of the whole process.

4.2.2.1. The EOS Model

The target of the EOS model is to develop an agent-based model of a theory [Mellars 1985] of the growth of social complexity in the Upper Palaeolithic period of south–west Europe [Doran 1994], that is 15 000 to 30 000 years ago. In contrast to egalitarian societies, complexity is defined as containing centralised decision-making, ranking, role differentiation, and territoriality [Cohen 1985]. Hence, among other features, the evolution of social stratification is denoted by the notion of social complexity. Mellars stresses that a particular combination of ecological conditions led to a population concentration and comparably stable and long-lasting social groups. This was a crucial step towards the emergence of social complexity, i.e. the formation of hierarchies.

The model is an agent based model written in Prolog. Its main features are [Doran 1994]:

a) a two-dimensional simulated environment providing clusters of resources that can be gathered by the agents. When an agent acquires an instance of the resource their number at that locality is reduced by 1. Furthermore, the resources have a specific regeneration cycle and complexity, which is defined as the number of agents necessary to acquire them. The resource complexity ranges from 1 to 48.

b) a population of 32 to 50 agents. The agents are able to collect sensory data, move around in the environment, form plans for resource acquisition and communicate with each other about these plans. If the agent is not able to consume resources, its energy level falls below a certain threshold. Then it needs to gain resources. If the level reaches zero, the agent disappears from the simulation; i.e. he 'dies'.
The working memory of the agents contains a resource model, where the agents keep their beliefs about the location and type of resources and a social model, where an agent stores its beliefs about itself and other agents.
The agents' social model also contains the notion of a territory. Territories are not properties of the environment but exist as beliefs in the agents' social model: if one agent observes another agent collecting resources, then it will believe that the location where this occurs is the territory of this agent.

4.2.2.1.1. Simulation Results

In the course of the simulation, the agents act in the following manner: They start without any knowledge of groups or other agents. They collect information about their environment and, if they are able to collect resources individually, they do so. If there are resources that need co-ordinated activity, then they develop plans for collective resource gathering and will attempt to recruit others for the execution of the plan.

A lot of the agents' behaviour is dealing with the recruitment of a group. One agent sends out information about the resource and the others evaluate this information to decide whether or not to follow. Agents that are able to recruit others become group leaders. The agents whose plans are selected gain 'prestige'. This leads to a "semi-permanent leader-follower relationship" [Doran 1995, p. 106]. This group structure becomes part of the social model of the agents

involved. The agents may also leave a group or change from one to another. This process may be iterated, thus leading to a situation where a group leader becomes a participant of another group together with his group members. Yet by iterations of this process a social hierarchy is formed.

These hierarchies have the ability to persist from one time circle to another but they may also break down after a while. This is affected by how easily agents decide to operate independently of their leader and how long they believe to be part of a group when they are not in contact with it and how they operate in such a case [Doran 1994, p. 214].

Since the resources need the co-ordination of collective actions, the model performs three core processes. It is claimed [Doran 1994, p. 206] that this is due to population concentration. The processes are:

- Temporary planned co-operation between the agents,
- conversion of temporary into semi-permanent groups and, finally,
- the development of hierarchy structures.

Hence, the EOS model allows the study of mechanisms of the emergence of social stratification out of egalitarian groups of agents.

4.2.2.2. MUE & ERB

The target of MUE & ERB is the emergence of the state. This took place at circumscripted territories along river valleys. It went hand in hand with a new type of agricultural production, alluvial agrarian production, generating a remarkable surplus, unknown in former organisations of securing the subsistence of the society [Carneiro 1970]. As a result, it is highly probable that social differentiation took place, releasing a social class from direct agricultural production [Lenski 1973]. This process is under investigation in the model MUE & ERB.
MUE & ERB is an equation-based model written in DYNAMO. To calculate the number of persons that can be released from direct agricultural production, production is expressed in terms of subsistence minima, called C. Yet a production volume of C = 1 means that the production of one member of the society is sufficient to feed one member of the society. Let the production of one member of the social unit be denoted with P_i. It follows that, given a social unit of N members, the necessary minimal production volume has to be:

$\Sigma P_i \geq X = NC.$

This terminology leads straightforwardly to a calculation of the number of people who can be released from direct agricultural production. Given the number N of members of the social unit and their production volume P_i this number can be derived as:

$\Sigma P_i - N = V$ (virtual heads)

A fundamental assumption of the theory is that the redistribution of the surplus is performed by specialised institutions, which have to be supported from the surplus. These institutions are denoted by the term ‘power territory’ (PT), governed by a so-called ‘power territory ruler’ (PTR). PTs squat into the surplus [Müller 1989, p. 27] that is derived above. Hence, the maximum size of the social élite is V. However, since in this case no surplus could be redistributed, this is an extreme case of total exploitation. Typically, the PT system is legitimised by a specific competence from which they gain the privilege to distribute the produced surplus. By this operation they are qualified as the main social decision centre [Dye 1976, Müller 1979]. Social operations are performed by persons holding positions in the decision centre [Müller 1985]. This is identified with the PT system. The organisational structure of the PTs is modelled as a strict hierarchy with a PTR at the top, a number of suboligarchs and an even greater number of subordinates. Hence, it is an ideal type of hierarchy.

MUE & ERB is solely a redistribution model, regardless of how the surplus is utilised. Thus, first the generated production volume is calculated. This is done by multiplying the workforce by the labour productivity. Then access priorities to the produced values are formulated for three classes of the social unit: the working class, landlords, and the PT system. After this process, the remaining surplus is open for redistribution. Redistribution is governed by two variables reflecting two strategies of securing power: Both variables react to a comparison of the actual with the desired budget. One strategy is to enhance the revenues by expanding the territory of the PT under consideration. The other strategy is to save expenditures in the case of budget shortening. Yet they are dialectically opposed leading to a nonlinear dynamic.

4.2.2.2.1. Simulation Results

The simulation run starts roughly at the time when archaeological artefacts indicate first settlements. This is calibrated at 6000 BC. At this time the number of PTR positions remain a sleeping variable. At 1500 BC, however, the model shows a rapid growth of the number of PTR positions. Because of the nonlinear dynamics, this result cannot be calculated by means of analytical mathematics, but emerges as the variable changes its attractor. Sociologically, this is interpreted as the emergence of the state, containing centralised institutions with a bureaucratic structure.

Hence, with regard to the question of modelling social ontology, a fundamental feature of a social reality is created in the model: The emergence of social positions.

4.2.3. Discussion

The EOS model is concerned with the very beginning of the process of the emergence of a 'social sui generis', whereas the MUE & ERB model covers a very late period in this respect. It is the beginning of a process of social stratification that can be observed by the EOS model. The MUE & ERB model, on the other hand, enfolds the capacity of a position-generating process. "Now the growth motor is established which, presumably, will be active until nowadays" [Müller 1991, p. 89]. The fact that different periods are under consideration in the two models lead to different but complementary explanatory gaps regarding the question of how social positions could emerge in the early prehistory of human societies. Implications of modelling technologies, however, also have to be taken into consideration:
Within the EOS model the emerging hierarchies are not stable and depend on the individual agents that form the group. Yet it is criticised that the hierarchy remains an "implicit property of the agents' social model" [Gilbert 1995, p. 154]. Thus, the EOS model takes on a microsociological perspective on the emergence of social stratification. This leads to the result that the model is incapable of generating a social sphere of its own that is not reducible to properties of the agents. This is due primarily to the agent-based modelling technology. It remains an open question, however, as to whether this is a deficit of the model or a correct representation of social reality at around 20 000 BC.
Within MUE & ERB however no individual actors can be represented since the model is an equation-based model. In particular, social institutions are assumed as given and the emergence of the state is resulting out of their internal development. Thus, with regard to the question of the emergence of a social ontology, there is an explanatory gap in some respect complementary to that of the EOS model. While the EOS model remains on the level of agents, this model remains on the level of institutions. Thus, it adopts a macrosociological point of view. Since it is plausible, however, that institutions already existed at the time of the emergence of the state, in this case it might also be a correct representation of the respective social reality.
Hence, both models might be a more or less correct representation of their respective target system. With respect to the process of an emerging of social ontology, however, there remains an explanatory gap.

5. Conclusion and Perspectives

Since there is more need to argue why archaeological models could contribute to the question of a social 'sui generis' than is the case in models of structure and agency, the main focus of this survey was on the impacts of archaeological modelling to social theory. It has to be emphasised, however, that both accounts are by no means opposing. They can be regarded as complementary: While the focus of accounts on structure and agency is a timeless situation that could generate social order regardless of its history, the focus of archaeological models is a more concrete social innovation, namely the emergence of social stratification that took place in time. But once this took place, social orders have to be reproduced over time. Yet the accounts can be seen as models of the process of production of a social 'sui generis' on the one hand and its reproduction on the other.

The models demonstrate that no metaphysics is necessary to introduce the notion of a social 'sui generis'. However further research is needed in both accounts: At the moment, therefore, conclusions can only be provisional. In the case of the archaeological models the question is twofold: First, it can be questioned to what extent the explanatory gap is due to modelling techniques, namely to agent-based models on the one hand and equation-based models on the other. The impact of the methodology on social theory should be regarded. Hence, further research is needed to investigate the interrelation between the level of social structure that might be correctly represented by differential equations and an agent-based actor level. This research could investigate how social structure is shaped by person-position relations. In particular, the fact that actors can hold multiple positions has to be regarded.
It might also be the case, however, that the explanatory gap between the models is due to social change between the first emergence of social hierarchies in societies of hunters and gatherers and the establishment of a state in agricultural societies. In particular, there might be an impact of growing complexity simply by a growing number of actors. Research in this direction is currently undertaken by the NewTies project [http//www.new-ties.org].

Interestingly, exactly the complexity problem also arises in the case of the more abstract models of structure and agency. Social order emerges only in the dyadic setting but vanishes at least sometimes in the case of a multi-actor situation. Hence, in both accounts the problem of scale is of crucial importance. This is a fundamental finding that can be identified by the modelling approach to social theory.

ACKNOWLEDGEMENTS

I would like to thank Dr. Justus Lentsch and two anonymous referees for their fruitful comments and discussions. Moreover, this project is founded by the Fritz-Thyssen Stiftung. Their contribution is gratefully acknowledged.

REFERENCES

[Aigner 1989] Aigner, J. Frühe Siedlungen im arktischen Nordamerika. in *Siedlungen der Steinzeit*, Heidelberg: Spektrum, 1989.

[Alexander 1987] Alexander, J. Action and its environment. In: Alexander, J., Giesen, B., Munch, R., Smelser, N. (Ed.) *The Micro- Macro Link*, Berkley: University of California Press, 1987.

[Archer 1995] Archer, M. *Realist social theory: the morphogenetic approach.* Cambridge, Cambridge University Press, 1995.

[Axtell 2000] Axtell, R. Why Agents? On the varied motivations for Agent Computing in the Social Sciences. *Center on Social and Economic Dynamics Working Paper*, **17**, 2000.

[Bhaskar 1975] Bhaskar, R. *A realist theory of science.* Leeds: Leeds Books, 1975.

[Blau 1977] Blau, P. A Macrosociological Theory of Social Structure. *American Journal of Sociology*, **83**-1: 26-54, 1977.

[Boera 2004] Boera, R. Towards an Agent-Based Computational Sociology. Good reasons to strengthen Cross-Fertilization between Complexity and Sociology. In: Stoneham, L. (Ed.) *Advances in Sociology Research Vol. 2*, Nova Publishers, 2004.

[Bourdieu 1987] Bourdieu, P. *Die feinen Unterschiede. Kritik der gesellschaftlichen Urteilskraft.* Frankfurt a.M., 1987.

[Carneiro 1970] Carneiro, R. A Theory of the Origin of the State. *Science*, **169**, 1970.

[Chaitin 2000] Chaitin, G. A Century of Controversy over the Foundations of Mathematics. *Complexity* **5**-5: 12-21, 2000.

[Cohen 1985] Cohen, M. Prehistoric Hunter-Gatherers: The Meaning of Social Compexity. In: Price, T., Brown, J. (Ed.) *Prehistoric hunter-gatherers: the emergence of cultural complexity*, New York: Academic Press, 1985.

[Collins 1981] Collins, R. On the Microfoundations of Macrosociology. *American Journal of Sociology*, **86**, 1981.

[Comte 1967]Comte, A. *Système de Politique Positive.* Vol. 2, Osnabrueck: Otto Zeller, 1967.

[Dittrich et al. 2003] Dittrich, P., Kron, T., Banzhaf, W. On the Scalability of Social Order: Modelling the Problem of Double and Multi Contingency Following Luhmann, *JASSS* **6**-1, 2003.

[Doran 1994] Doran, J. Palmer, M., Gilbert, N., Mellars, P. The EOS Project: modelling Upper Palaeolithic social change. In: Gilbert, N., Doran, J. (Ed.) *Simulating Societies*, London, UCL Press, 1994.

[Doran 1995] Doran, J., Palmer, M. The EOS Project: integrating two models of Palaeolithic social change. In: Gilbert, N. Conte, R. (Ed.) *Artificial Societies: The computer simulation of social life*, London: UCL Press, 1995.

[Doran 1997] Doran, J. From Computer Simulation to Artificial Societies. *Transactions of the Society for Computer Simulation International*, **14**-2, 1997.

[Durkheim 1984] Durkheim, E. *Regeln der soziologischen Methode*, Frankfurt a. M.: Surkamp, 1984 (1895).

[Durkheim 1973] Durkheim, E. *Der Selbstmord*. Neuwied: Luchterhand, 1973 (1897).

[Durkheim 1967] Durkeim, E. Individuelle und kollektive Vorstellungen. In Adorno, T.-W. (Ed.) *Soziologie und Philosophie,* Frankfurt a. M.: Surkamp, 1967 (1898).

[Dye 1976] Dye, R. *Who's Running America? Institutional Leadership in the USA*. Engelwood Cliffs: Pr. Hill, 1976.

[Earle 2004] Earle, T. Culture Matters in the Neolithic Transition and Emergence of Hierarchy in Thy, Denmark: Distinguished Lecture. *American Anthropologist*, **106**, 2004.

[Elster 1986] Elster, J. (Ed.) *Rational Choice.* Oxford, 1986.

[Epstein Axtell 1996] Epstein, J., Axtell, R. *Growing Artificial Societies. Social Science from the Bottom Up.* Cambridge: MIT Press, 1996.

[Epstein 1999] Epstein, J. Agent-Based Computational Models and Generative Social Science. *Complexity* **4**-5: 41-60, 1999.

[Esser 1985] Esser, H. Soziale Differenzierung als ungeplante Folge absichtsvollen Handelns: Der Fall der ethnischen Segmentation. *Zeitschrift für Soziologie*, **14**, 1985.

[Esser 1993] Esser, H. *Soziologie: allgemeine Grundlagen.* Frankfurt a.M.: Campus, 1993.

[Gellner 1971] Gellner, E. Holism versus individualism. In: Brodbeck, M. (Ed.) *Readings in the Philosophy of the Social Sciences*, MacMillan, New York, 1971.

[Giddens 1988] Giddens, A. *Die Konstitution der Gesellschaft. Grundzüge einer Theorie der Strukturierung.* Frankfurt a. M., 1988.

[Gilbert 1995] Gilbert, N. Emergence in social simulation.. In: Gilbert, N. Conte, R. (Ed.) *Artificial Societies: The computer simulation of social life,* London: UCL Press, 1995.

[Helmreich 1998] Helmreich, S. *Silicon second nature: Culturing artificial lie in a digital world.* University of California Press, 1998.

[Hodgson 2002] Hodgson, G. Reconstitutive downward causation: Social structure and the development of individual agency. In: Fullbrook, E. (Ed.) *Intersubjectivity in Economics.* London, Routledge, 2002.

[Homans 1964] Bringing man back in. *American Sociological Review*, **29**-5, 1964.

[Knorr-Cetina 1981] Knorr-Cetina, K., Cicourel, A. V. (Ed.) *Advances in social theory and methodology*. London: Routledge, 1981.

[Kolb 1994] Kolb, M. Monumental Grandeur and the rise and fall of Religious Authority in Precontact Hawaii. *Current Anthropology*, **34**, 1994.

[Kron 2002] Kron, T. (Ed.) *Luhmann modelliert. Ansätze zur Simulation von Kommunikationssystemen,* Opladen, Leske + Budrich, 2002.

[Kron Dittrich 2002]Kron, T., Dittrich, P. Doppelte Kontingenz nach Luhmann – ein Simulationsexperiment. In: Kron, T. (Ed.) *Luhmann modelliert. Ansätze zur Simulation von Kommunikationssystemen,* Opladen: Leske + Budrich, 2002.

[Kron Schimank 2003] Kron, T., Schimank, U. Doppelte Kontingenz und die Bedeutung von Netzwerken für Kommunikationssysteme. *Zeitschrift für Soziologie*, **32**, 2003.

[Lansing 2002] Lansing, S. "Artificial Societies" and the Social Sciences. *Artificial Life*, **8**-3, 2002.

[Lenski 1973] Lenski, G. *Macht und Privileg: Eine Theorie der sozialen Schichtung,* Frankfurt a.M.: Surkamp, 1973.

[Lorentzen Nickles 2002] Lorentzen, K., Nickles, M. Ordnung aus dem Chaos – Prolegomena zu einer Luhmann'schen Modellierung deentropierter Strukturbildung in Multiagentensystemen. In: Kron, Thomas (Ed.) *Luhmann modelliert. Ansätze zur Simulation von Kommunikationssystemen*, Opladen: Leske + Budrich, 2002.

[Luhmann 1984] Luhmann, N. *Soziale Systeme. Grundriß einer allgemeinen Theorie*, Frankfurt a. M., Surkamp, 1984.

[Mandelbaum 1973] Mandelbaum, M. Societal facts. In: O'Neill (Ed.) *Modes of Individualism and Collectivism.* London, Heinemann, 1973.

[Mellars 1985] Mellars, P. The ecological basis of social complexity in the Upper Palaeolithic of southwestern France. In: Price, T., Brown, J. (Ed.) *Prehistoric hunter-gatherers: the emergence of cultural complexity*, New York: Academic Press, 1985.

[Müller 1979] Müller, N. *Empirische Herrschaftstheorie – Zur Beziehung zwischen Kontextdifferenzierung, politischer Herrschaft und politischer Sozialisation*, Köln: Westdeutscher Verlag, 1979.

[Müller 1985] Müller, N. Real structure modelling: a methodology for the description of large scale social units. *Social Science Information*, **24**-3: 603-624, 1985.

[Müller 1989] Müller, N. *Civilization Dynamics, Vol. 1: Fundamentals of a model oriented description.* Aldershot: Avebury, 1989.

[Müller 1991] Müller, N. *Civilization Dynamics Vol 2: Nine Simulation Models.* Aldershot: Avebury, 1991.

[Parsons 1937] Parsons, T. *The Structure of Social Action.* Glencoe: 1937.

[Parsons 1968] Parsons, T. Interaction. In: Sills, D. L. (ed.) *International Encyclopedia of the Social Sciences*, **7,** London, 1968.

[Renfrew 2001] Renfrew, C. Symbol before Concept: Material Engagement and the Early Development of Society. In: Hodder, I. (Ed.) *Arachaeological Theory Today*, Cambridge, Polity Press, 2001.

[Sawyer 2002] Sawyer, K. Durkheim's Dilemma: Towards a Sociology of Emergence. *Sociological Theory*, **20**-2, 2002.

[Sawyer 2003] Sawyer, K. Artificial Societies: Multiagent Systems and the Micro-Macro Link in Sociological Theory. *Sociological Methods and Research*, **31**-3: 325-363, 2003.

[Skyrms 1996] Skyrms, B. *Evolution of the social contract*. Cambridge, Cambridge University Press, 1996.

[Skyrms 2004] Skyrms, B. The Stag Hunt and the Evolution of Social Structure. Cambridge, Cambridge University Press, 2004.

[Smith 1995] Smith, J.M. Review of "The Origins of Order". *New York Review of Books*, **30**, 1995.

[Stephan 1999] Stephan, A. *Emergenz: von der Unvorhersagbarkeit zur Selbstorganisation.* Dresden: Dresden Univ. Press., 1999.

[Watkins 1957] Watkins, J. Historical Explanations in the Social Sciences. *The British Journal for the Philosophy of Science*, **8**, 1957.

[Wrong 1961] Wrong, D. *The oversocialized conception of man. American Sociological Review*, **26**-2, 1961.

How long does the spatial structure of an initial state influence the dynamics of a forest growth model ? A simulation study using the Capsis platform.

Goreaud François
Cemagref - LISC
24 avenue des Landais - BP 50085
63172 AUBIERE CEDEX 1
France
+33 (0)4 73 44 06 80
francois.goreaud@cemagref.fr

Courbaud Benoît
Cemagref - EPGR
2 rue de la Papeterie - BP 76
38402 Saint-Martin-d'Hères
France
+33 (0)4 76 76 27 62
benoit.courbaud@cemagref.fr

de Coligny François
INRA - AMAP
TA40/PS2, Boulevard de la Lironde
34398 Montpellier Cedex 5
France
+33 (0)4 67 61 71 68
coligny@cirad.fr

ABSTRACT
Spatially explicit Individual Based Models are more and more often used in forest modelling, especially because they take into account the influence of the spatial structure on the dynamics. However, they are potentially very sensitive to the initial spatial structure used for a simulation, which can be problematic if the initial state is not known, or is simulated in an unrealistic way.

The aim of our paper is to study this sensitivity to initial spatial structure in the case of the Mountain model, an individual based model of irregular spruce stands implemented in the Capsis platform. In order to characterise the influence of the initial spatial structure on the dynamics of the model, we simulated different initial spatial structures and compared the results of long term simulations.

We showed that the initial spatial structure can highly influence the dynamics of the model, not only during the first cycle of the evolution, but also at very long term in the evolution of the next generations. We also illustrated how some disturbances, such as a periodic gap opening through storms, can modify both the long term dynamics of the stand and the duration of the influence of the initial spatial structure.

KEYWORDS
Forest, tree, growth model, simulation, Monte Carlo, Spruce, spatial structure, initial state

1. Introduction

Individual Based Models (IBM) are more and more often used in forest modelling (*e.g.* [Ek Monserud 1979] [Tomé Burkhart 1989]), especially for complex forest stands with mixed tree species or irregularity in size or age. Because they consider each tree individually, individual based models can take into account the high variability of such stands [Spellmann 1992]. This was impossible with simpler stand level models, based on mean properties at the stand level such as density or total basal area [Houllier *et al.* 1991]. Different forest growth simulators have been recently developed to integrate both stand level and individual based forest models (*e.g.* [Pretzsch *et al.* 2002] [de Coligny *et al.* 2004]), and can be used either as management tools or for research purposes.

Some of these IBM are moreover spatially explicit, which means that they also consider each tree location. With such models, it is possible to characterise the local neighbourhood around each tree through competition indices. Many different competition indices can be found in the literature, taking into account the number, size and location of neighbouring trees [Biging Dobbertin 1995]. One advantage of such models is that they take explicitly into account the influence of the spatial structure of an ecosystem on its dynamics. This relation between spatial structure and dynamics is considered as an important process in many ecosystems, and has been thoroughly studied (*e.g.* [Begon *et al.* 1990] [Dieckmann *et al.* 2000]). For instance in forest stands trees located in aggregates are supposed to grow less than isolated trees, because of the competition for light or nutrients. However, spatially explicit models also have the drawback of requiring very detailed initial states, including the location of all trees at the beginning of the simulation. Such data are very seldom available for real forests. Therefore, most of the time it is necessary to simulate a "virtual" initial state, i.e. a set of numbers representing the species, diameter, and location of simulated trees ([Pretzsch 1997] [Goreaud *et al.* 2004]).

Precisely because they take into account the influence of the spatial structure of a forest stand on its dynamics, spatially explicit individual based models are likely to be very sensitive to the initial spatial structure used in a simulation. In real forest ecosystems, the influence of the spatial structure on the dynamics is usually supposed to be a short term influence, because many stochastic events (either natural disturbances such as storms, or human sylvicultural actions such as thinning) can modify the spatial structure and thus the growing conditions (*e.g.* [Pontailler *et al.* 1997] [Wolf *et al.* 2003]). However, ecological models do not always include as much stochasticity, and can sometime show a long term sensitivity to the initial spatial structure ([Dubé *et al.* 2001] [Goreaud *et al.* 2002] [Ménard *et al.* 2002]). This problem is quite general and can be encountered in other types of models, for instance cellular automaton or grid based models [Dieckmann *et al.* 2000].

This high sensitivity of individual based models can become a real problem if the spatial structure of the initial state is not known, or is simulated in an unrealistic way, because in that case it can lead to unrealistic simulation results. Unfortunately, this is often the case. Most of the time, the initial state of a simulation is simulated very simply, using random, clumped or regular patterns. Only very few studies propose to really fit a model of spatial structure on real data, or to estimate the realism of the spatial structure simulated as initial states for forest growth models ([Rathbun Cressie 1994] [Batista Maguire 1998] [Prévosto *et al.* 2003] [Goreaud *et al.* 2004]). In order to avoid this problem, some authors prefer not to consider the first part of a simulation, supposing it can be unrealistic because of the dependence on the initial state. This method however makes the implicit hypotheses (i) that the dynamics of the model will converge toward an equilibrium state independently of the initial state, which may not be the case, and also (ii) that the transition period is not too long.

Therefore, we believe it is important, before using a spatially explicit individual based model, to study how much it is sensitive to the initial state, and more precisely to estimate how long this influence can affect its dynamics.

The aim of our paper is to study this sensitivity to initial spatial structure in the case of the Mountain model, an individual based model of irregular spruce stands [Courbaud *et al.* 2001]. This model (detailed in section 2.1) is implemented in the Capsis platform (section 2.2), which facilitates the simulation work [de Coligny *et al.* 2004].

In order to characterise the influence of the initial spatial structure on the dynamics of the model, we simulated different initial spatial structures (section 2.3), and compared the results of the corresponding long term simulations. We hypothesised that significant differences will occur as long as the initial state has some influence on the dynamics. However, as our model is stochastic, we could not simply compare the evolution curves between two simulations. We therefore used Monte Carlo simulations to represent the variability of the results (section 2.4). We first used a given initial state to assess the intrinsic variability of the model (section 3.1). Then we used a set of simulations with an initial spatial structure corresponding to our null hypothesis of Complete Spatial Randomness (section 3.2). Then, when using different initial spatial structures (section 3.3) we considered that any additional variability corresponds to the influence of the initial spatial structure on the dynamics.

We also wanted to test if potential disturbances, such as storms, could affect the duration of this influence of the initial spatial structure on the dynamics. We therefore handled two sets of simulations : A first one without any disturbance (section 3), and a second one corresponding to disturbed dynamics with periodic gap opening through storms (section 4).

We finally discuss the consequences of such sensitivity on the use of the model.

2. Material & Method

2.1. The model "Mountain"

"Mountain" is a spatially explicit, individual based model simulating the dynamics of irregular mountain spruce stands [Courbaud *et al.* 2001]. Figure 1 summarises the different processes included in Mountain. Each tree is represented by its spatial co-ordinates, height, diameter at breast height, crown base height and crown base diameter. Competition interactions are modelled through the calculation of the radiation intercepted by every tree in the stand taking into account the shading effect of its neighbours in three dimensions [Courbaud *et al.* 2003]. Each year, the model simulates the individual height and diameter increments corresponding to a vegetation season, as functions of the initial dimensions of the tree and the amount of radiation intercepted. Regeneration is simulated in openings by a probability of installation of new seedlings on every ground cell with irradiance higher than a given threshold. Seedling growth depends on the irradiance of their ground cell, until they reach a height of 1.30 m. They are then recruited as trees with all the related attributes. Mortality is modelled with two processes : a first probability of mortality depending on the radiation intercepted by a tree, simulating competition effects; and a second probability of mortality depending on tree height, simulating senescence and disturbance effects.

The Mountain model has been fitted and validated on data from two experimental plots in the French Alps [Courbaud 1997]. It is implemented in the Capsis platform, freely available on the Capsis Project homepage (http://capsis.free.fr).

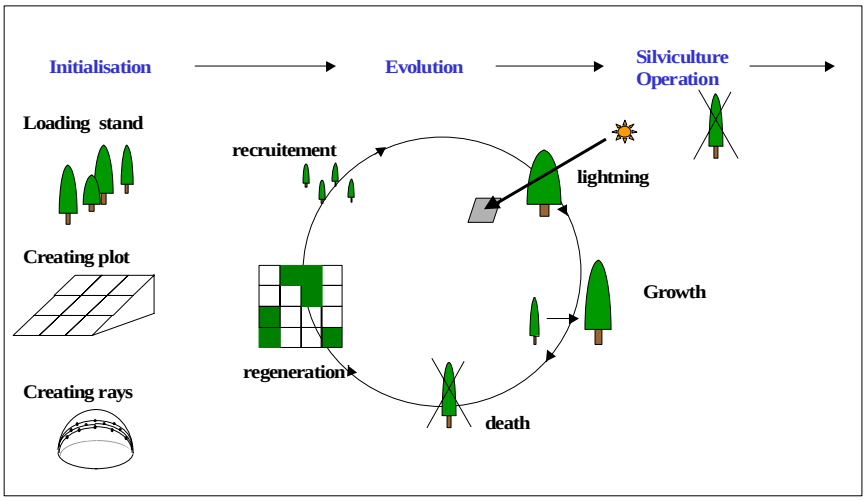

Figure 1 : The chain of processes successively simulated in the model mountain. The initialisation phase downloads or creates an initial stand, creates the ground cells and the light rays. During each vegetation season, the model first calculates radiation interception, then growth and mortality, and finally regeneration and recruitment. A scenario can alternate periods of growth and steps of silvicultural operations.

2.2. **The Capsis platform**

Capsis (Computer-Aided Projection for Strategies In Silviculture) is a generic forest simulator which has been developed by French researchers since 1994 ([Dreyfus Bonnet 1997] [de Coligny *et al.* 2004]). The objective of the Capsis project is to build a perennial, open and shared modelling platform (1) to contribute to the development and evaluation of models, (2) to share tools and methods, (3) to compare results of different models, (4) to transfer models to forest managers and (5) to serve as teaching material.

The version 4 of Capsis (figure 2) is generic enough to integrate very different kinds of models: stand models, distance independent or spatially explicit tree models, individual based or not, wood quality models, seed dispersal models, etc. It provides forest management tools to establish and compare different silvicultural scenarios. At the present time, Capsis hosts 25 models and 5 specific libraries which are all being co-developed by researchers and computer scientists. This shared forest modelling platform has already showed many advantages : allowing modellers to re-use sub-models and share specific tools and providing to foresters and students an easy-to-use software to compare different management strategies.

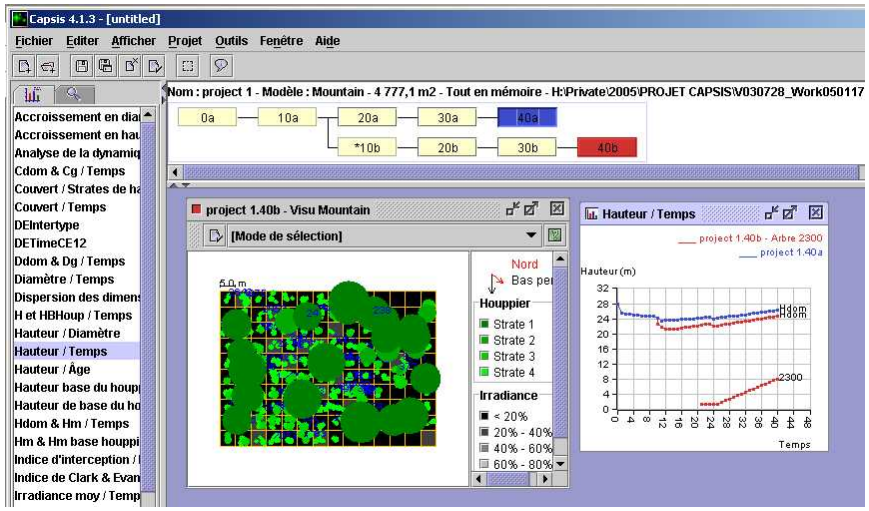

Figure 2 - A glance at Capsis4 : Project manager with two scenarios, a stand viewer, and a graphic.

In this paper, we simulated 1500 stand evolutions, each of them being quite long because of the computation of light rays trajectory for each trees (up to 5000 trees in a 1ha stand) at each time step. We therefore used the script pilot of Capsis to run the simulations on a cluster of 48 PCs, using approximately a total of 8300 h CPU time.

2.3. **Simulating different initial spatial structures**

In order to study the influence of the initial spatial structure on the dynamics of the model, we defined different initial states, composed of the same trees in terms of age and size, but with different spatial structures. We chose to consider a 1 ha young stand, composed of 5000 trees with the same 2cm diameter, and a mean height of 1.5m. Such a stand could correspond to a natural regeneration after a clear cutting. For all initial states we used exactly the same trees, and only modified their location. We used the classical point process formalism to simulate spatial patterns (*e.g.* [Diggle 1983] [Tomppo 1986] [Cressie 1993]), and the corresponding tools of the "spatial library" in Capsis [de Coligny *et al*. 2004].

We first ran a set of simulations with the same initial state (section 3.1), in order to characterise the variability corresponding to the intrinsic stochasticity of the model. For these simulations, we used one given realisation of a Poisson process as spatial pattern for the initial state. The locations of these trees correspond to the map in figure 3a.

We then used very classically as null hypothesis the Complete Spatial Randomness hypothesis (CSR), corresponding to the absence of constraint in the location of trees. This spatial structure is easily simulated by a Poisson process [Diggle 1983], for which the co-ordinates of each tree are random numbers. We have considered the variability resulting from this CSR initial states as a reference for our comparison work (c.f. section 3.2).

Finally, in order to simulate other very different spatial patterns, corresponding to highly variable spatial structure, we used a generalised Gibbs process with random values of the parameters, as defined in [Goreaud *et al*. 2002]. Gibbs point processes are classically used to simulate complex patterns [Diggle 1983]. The general principle of Gibbs processes is to define a pairwise cost function, whose values will lead either to aggregation, or to regularity, at various scales. When using it with random values of the parameters, we simulated very highly variable spatial structures, from aggregation to regularity, at different scales and intensity. Details of the algorithm can be found in [Goreaud *et al*. 2002]. Figure 3b and 3c illustrate two possible initial states, with the same trees, but very different spatial structures simulated with this Gibbs point process. When running a set of simulations with these highly different initial states, we have considered that the additional variability corresponds to the influence of the initial spatial structure on the dynamics.

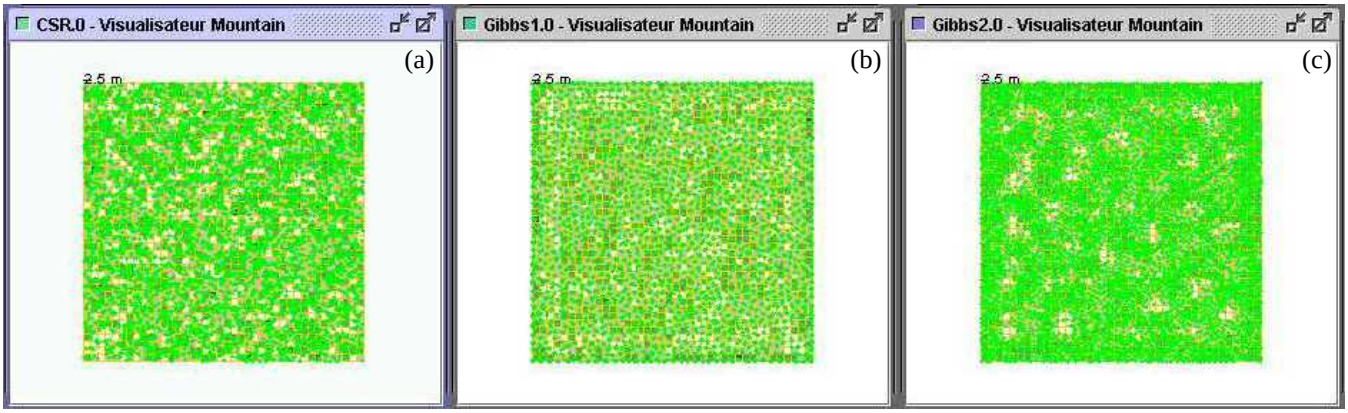

Figure 3 : Example of three initial states corresponding to the same trees, but to different spatial structure. (a) : Complete Spatial Randomness (CSR); (b) & (c) : Complex structures simulated with a Gibbs Process.

2.4. **Long term simulations**

Because we wanted to determine how long the spatial structure of the initial state can influence the dynamics of the Mountain model, we ran very long term simulations of 1000 years. The usual life time for trees is over 100 years, so a 1000 years period enables to simulate successive generations, and thus to let mortality and regeneration express themselves and modify the spatial structure of the stand. Note that such long term simulations are not realistic, and therefore must only be used to study the behaviour of a model [Shugart 1984], and not for predictive purposes.

We defined a few global variables to represent the dynamics of the stand, and followed their evolution during this 1000 years period. For each simulation, the model simulates the evolution of each tree, from its birth to its death. This corresponds to a huge amount of data. Therefore, we decided to focus on the evolution of some classical mean values at the stand level. In this paper, we have more precisely considered the evolution of : (i) N : the total number of trees in the stand; (ii) G : the total basal area, which is an indirect measure of the biomass of the ecosystem; (iii) Dg : the mean quadratic diameter, which characterises the mean evolution of each individual tree; and (iv) CE : the Clark & Evans index, which characterises the spatial structure of the stand (CE is a normalised measure of the distance to nearest neighbour : CE=1 for a random pattern, CE<1 for aggregation and CE>1 for regularity [Cressie 1993]).

For each set of parameters, we used 100 Monte Carlo simulations to represent the variability of the results. Indeed, the Mountain model is intrinsically stochastic, especially because the mortality and regeneration sub-models are probability models. For a given set of parameters and a given initial state, each simulation will lead to different choices of dying trees or regeneration locations, and thus to somehow different evolutions of the stand. Moreover, as the distribution of these curves does not follow a Gaussian distribution, it was not possible to use only the mean and standard deviation. In this simulation study, we thus obtained 100 different evolution curves for each variable of the stand, and we characterised the variability of these results by considering the max and min values of the simulated variables for each time step (see 3.3).

The different values for the parameters we used for these simulations are detailed in Table 1. They mostly correspond to the values obtained when fitting the model on two experimental plots in the French Alps [Courbaud 1997]. We used the same values of the parameters for all simulations, except for the parameters concerning disturbances. In the first set of simulation (section 3), those parameters were set to 0 so that no disturbance occur. Then, in section 4 we considered different values to assess the impact of disturbances on the dynamics.

Table 1 : Values of the main parameters of the simulations.

Main parameters	corresponding to :	value
Crown :		
treeLeafAreaDensity	Leaf area density	0.8 m^2/m^3
maxCrownRadius	Maximum crown radius	5 m
Growth :		
growthHmax	Maximum height	40 m
growthdHmax	Maximum height increment	45 cm/year
growthRH2	Height radiation threshold : over this value, height growth is maximum	40 %
growthDmax	Maximum diameter	90 cm
growthdDmax	Maximum diameter increment	8 mm/year
growthRD2	Diameter radiation threshold : over this value, diameter growth is maximum	80 %
Regeneration :		
seedlingStep	Time between two seeding events	10 years
limitEnergyInf	Sapling minimum radiation : under this value, no regeneration can occur	20 %
saplingPotHeightIncrement	Sapling maximum height increment	25 cm/year
recruitDensity	Sapling density	0.2 sap./m²
Mortality :		
deathPmax	Death maximum probability (for a tree with a null diameter increment)	0.5
deathLimitdD	Minimum diameter increment : under this value there is a risk of mortality	0.75 mm/year
Disturbances :		
gapRadius	Gap radius	0, 5, 10, 20 m
disturbanceStep	Gap frequency : number of years between 2 successive gap openings	5 or 10 years

3. **Influence of the spatial structure on the undisturbed dynamics**

In this first step of our study, we characterised the influence of the initial spatial structure of a simulation on the undisturbed dynamics of the stand modelled by the Mountain model. We therefore set the values of the parameters so that no disturbance occurs (i.e. no natural phenomenon such as storm, and no human actions such as thinning).

3.1. **Taking into account the intrinsic stochasticity of the model**

We have first considered a set of 100 simulations corresponding to 1000 years evolution of a stand with this undisturbed model, using always the same initial state, corresponding to the random pattern presented in figure 3a. At the beginning of each simulation the stand was always the same, but then progressively the stochasticity of the model led to different evolutions. Figure 4 shows the curves corresponding to the evolution of 4 global variables, that illustrate the evolution of the stand for these 100 simulations : the total number of trees, the total basal area, the mean quadratic diameter, and Clark & Evans index (see 2.4).

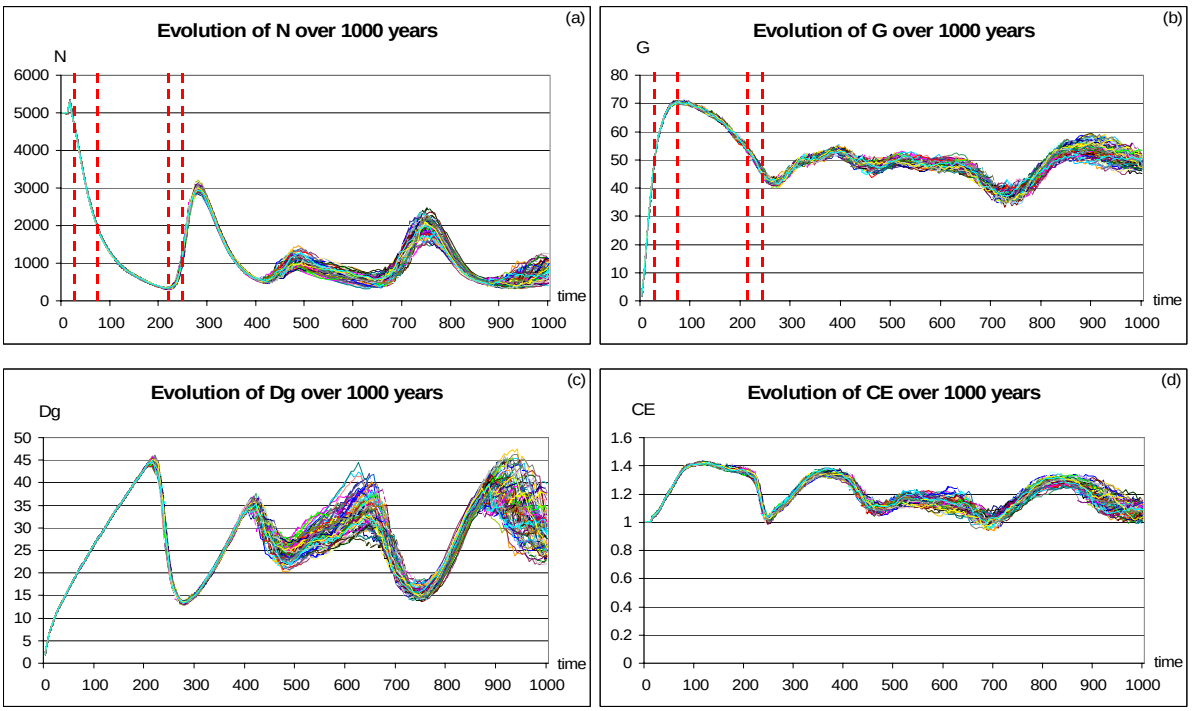

Figure 4 : Curves of 1000 years evolution for 100 simulations with the same initial state. (a) Number of trees in the stand, (b) total basal area, (c) mean quadratic diameter, (d) Clark & Evans index.

We can first notice that the simulations followed a rather cyclic evolution pattern, with a cycle of approximately 250 years. This cyclic evolution seems to correspond to 4 successive generations of trees, following more or less a regular stand dynamics. However, the third cycle does not seem to be very clearly defined. The first cycle is really characteristic to this regular stand dynamic, which is not surprising as our initial state corresponded to a very young and regular stand. However, we have also obtained similar cyclic evolution patterns with other initial states, and especially with initial states corresponding to real irregular experimental plots. Therefore, we believe that this cyclic evolution pattern characterises a potentially frequent behaviour of the model.

In the first cycle, we can identify the 4 main phases of forest dynamics [Oliver Larson 1996] : First the initiation phase (up to 30 years), corresponding to a progressive closure of the canopy with a fast increase of G (and fluctuations of N) ; then the stem exclusion phase (up to 75 years), with a fast decrease of N through competition and mortality (called self-thinning) but still an increase of G through the growth of surviving trees ; third the senescence phase (up to 220 years), with a decrease of both N and G, corresponding to the death of old and big trees ; and finally the renewal phase (up to 250 years) with a massive regeneration inducing an increase of N, whereas the death of the last old trees leads to a decrease of G. [Dubé *et al.* 2001], simulating northern hardwood forest succession over 1000 years, also obtained cyclic behaviour around 200-250 years.

There is however also a variability around this mean pattern, which is the result of the stochasticity of the model. This variability increases with time (which is quite usual with stochastic models) : at the beginning of the evolution the various simulated stands remained very similar, but then progressively the stochasticity of the model led to different evolutions. This is especially the case at the end of each cycle, when the regeneration process, which is highly stochastic, expressed itself on a wide area. As we used here always the same initial state, we have considered that this variability in the evolution curves really corresponds to the intrinsic stochasticity of the model, i.e. the use of random numbers when simulating mortality and regeneration.

3.2. **Null hypothesis of Complete Spatial Randomness**

The usual null hypothesis when studying the influence of spatial structure on the dynamics of ecosystems is the hypothesis of Complete Spatial Randomness [Cressie 1993]. This null hypothesis is more complex than a given initial state with a precise location of individuals, as we used in (3.1). Indeed, this null hypothesis corresponds to one given point process (the Poisson process), and thus to an infinite number of potential realisations. In each realisation, that can be used as an initial state, the locations of trees are different, but all realisations correspond to the CSR spatial structure. This stochasticity in the location of trees for a given spatial structure can bring an additional variability in the simulation results. Therefore, when using the model with the null hypothesis of CSR, the global variability of the results is composed of both the intrinsic variability of the model and the variability induced by the stochasticity of the CSR initial state.

In order to characterise this variability, corresponding to our null hypothesis, we have considered another set of 100 simulations corresponding to 1000 years evolution (with the undisturbed model) of a stand whose initial states all follow a completely random initial spatial structure simulated by a Poisson process. Figure 5 shows the curves corresponding to the evolution of the same 4 global variables than previously (the total number of trees, the total basal area, the mean quadratic diameter, and Clark & Evans index) for these 100 simulations.

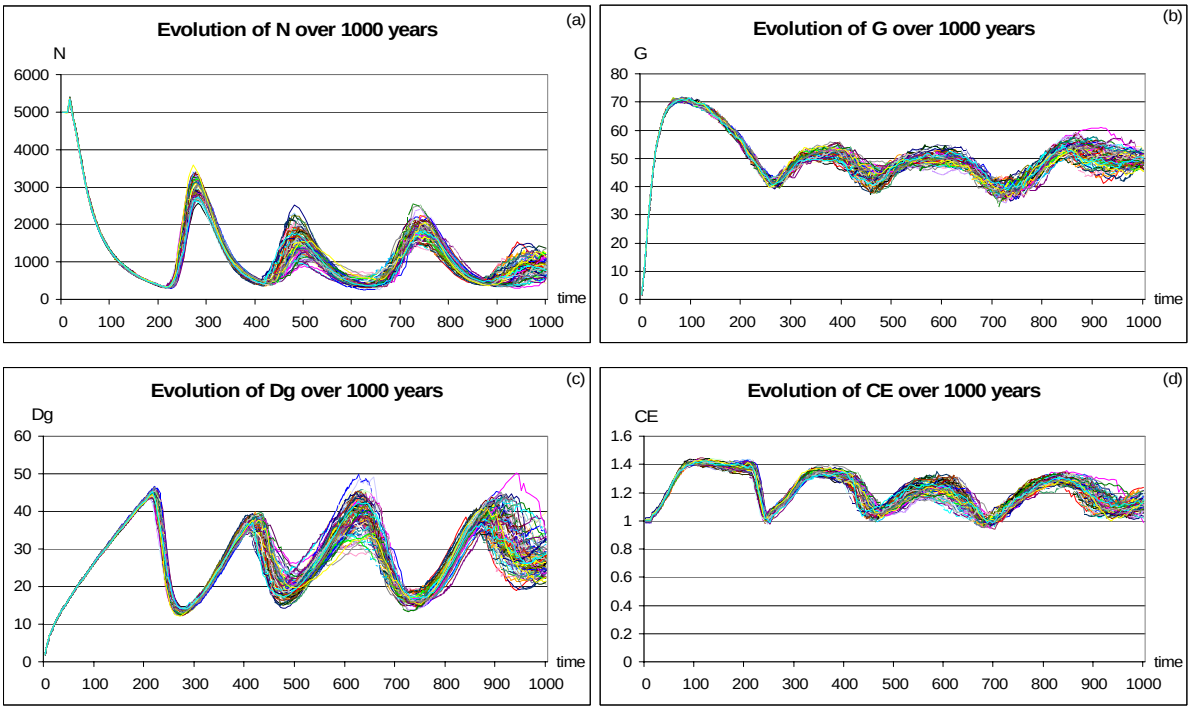

Figure 5 : Curves of 1000 years evolution for 100 simulations with a CSR initial spatial structure. (a) Number of trees in the stand, (b) total basal area, (c) mean quadratic diameter, (d) Clark & Evans index.

The results of these simulations are quite similar to those obtained previously, except for two details. First, as we expected, the evolution curves corresponding to our null hypothesis have a slightly higher variability, especially during the first cycle. This is due to the additional stochasticity induced by the different locations of trees in each initial state. Second, the evolution curve have a much clearer periodicity : each cycle is more precisely defined than when using the same initial state (cf. 3.1). We therefore hypothesised that this cyclic evolution was indeed characteristic of the dynamics of a stand with a CSR initial structure, and that the unclear third cycle obtained in (3.1) was only a specificity of the precise locations of trees used in the initial pattern. This difference illustrates the interest of using the CSR spatial structure as null hypothesis instead of a given initial state.

We therefore considered this variability, obtained with our CSR null hypothesis initial state, as a reference for our comparison work.

3.3. **Long term dynamics with a highly variable initial spatial structure**

We have then considered another set of 100 simulations, still corresponding to 1000 years evolution of a stand with the undisturbed model, but this time with very different initial states, corresponding to the same trees (in terms of size and age),

but to highly variable spatial structures simulated by a Gibbs process (c.f. 2.3). Figure 6 shows the curves corresponding to the evolution of the same 4 global variables (the total number of trees, the total basal area, the mean quadratic diameter, and Clark & Evans index) for these 100 simulations.

These results confirm that the initial spatial structure can highly influence the dynamics of the model. Indeed, these simulations followed the same overall evolution pattern than the previous ones corresponding to our null hypothesis (c.f. 3.2), but with a much higher variability around this global pattern. This high variability means that the differences in the spatial structure of the initial state have led to evolutions significantly different from those obtained under our null hypothesis. It seems to be especially true in the first cycle of the evolution, probably because the different initial spatial structures had already led to different competition contexts, and thus to some variability in the evolution of the global variables of the stand, whereas the simulations beginning with a CSR initial state had a very small variability of the competition context.

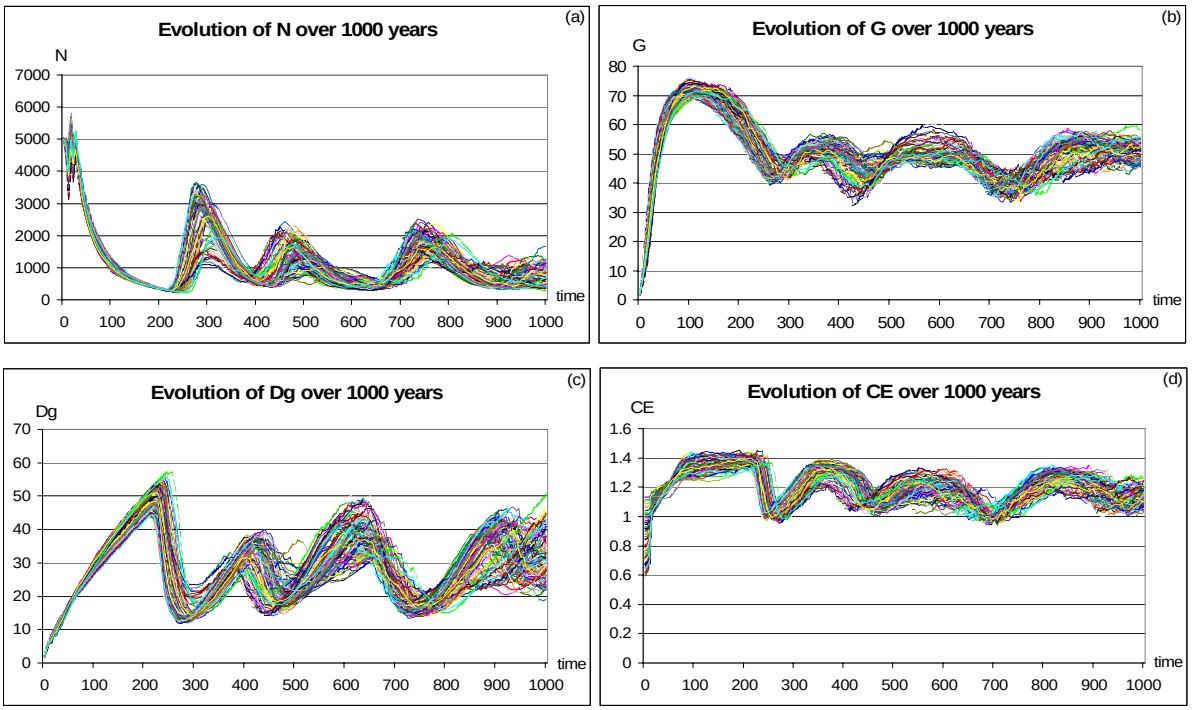

Figure 6 : Curves of 1000 years evolution for 100 simulations with a highly variable initial spatial structure simulated by a Gibbs process. (a) Number of trees in the stand, (b) total basal area, (c) mean quadratic diameter, (d) Clark & Evans index.

In order to clarify this phenomenon, we focused on the simulations corresponding to the most extreme initial states. Using the initial values of the Clark & Evans index, which characterises the spatial structure of the stand, we chose the 5 most aggregated (smallest values of CE) and the 5 most regular (highest values of CE) initial states, and compared their simulated evolution (figure 7). We obtained very different behaviours up to 1000 years, which confirms that the initial spatial structure can influence the dynamics of the model on a very long term.

We also noticed a very interesting phenomenon of alternative modification of the relative location of these curves. Thus, at the beginning of the first cycle, some trees of the most aggregated stands (blue) died rapidly, probably because the competition was too harsh in the centre of aggregates. Therefore, the total basal area became and stayed lower during the stem exclusion phase (until 75 years). Then, as the competition and the mortality increased, the mean and total basal area became lower in the most regular stands (green). We assume that, in aggregated stands the spatial structure had already led to an important differentiation, so that only small dominated trees died, whereas a lower differentiation in regular stands induced the death of bigger trees. Finally, the regeneration was larger in formerly regular stands, probably because more light was available everywhere in the stand. During the next cycles, the relative location of the curves swapped, which could be the result of an inversion in the spatial structure of the successive stands, as suggested by the Clark & Evans index. The precise interpretation of this phenomenon would however require to identify the different cohorts in the stand.

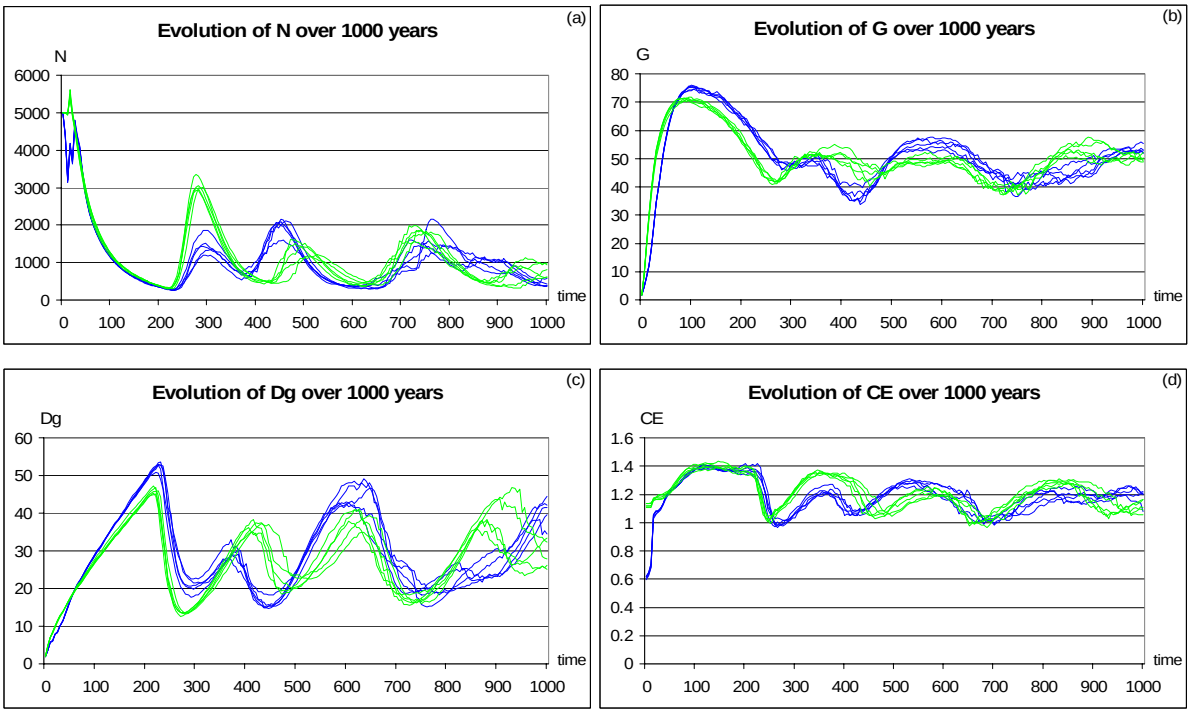

Figure 7 : Curves of 1000 years evolution for the 5 most aggregated (blue) and the 5 most regular (green) initial states. (a) Number of trees in the stand, (b) total basal area, (c) mean quadratic diameter, (d) Clark & Evans index.

3.4. **Quantifying the influence of the initial spatial structure**

In order to measure more precisely this increase of variability, we have used a very simple and classical Monte Carlo approach, comparing the min and max values of the different variables for both sets of simulations, corresponding either to our null hypothesis of CSR, or to highly variable spatial structure (figure 8). In fact, min and max values of a set of N simulations can be used to estimate a confidence interval corresponding to a significance level alpha of 1/(N+1). Unfortunately, this estimator is not very robust, and can lead to imprecise estimates of the confidence intervals. More precise estimates of the confidence intervals can be obtained by using order statistics (see for instance [Cressie 1993]), but this requires more simulations. In this paper, we chose to simply use min and max values to characterise the variability of the model, and we assumed that large differences of these min and max values are the result of a significant influence of the initial spatial structure on the dynamics.

First, when looking at the first cycle of the simulation (until 250 years), we can notice that there are very large differences of the variability of the results at all time step and for all variables. This corresponds to the direct effect of the differences in the initial spatial structures, who have led to different competition contexts for the trees of the first generation. We can thus conclude that the dynamics of the stand modelled in Mountain, mainly based on the competition for light, has not compensated for these different initial spatial structures.

Then, when looking at the next cycles, we can still point out some large differences of the variability of the results at some periods, even after a very long evolution (for instance 800 years). This means that the initial spatial structure can have a very long term influence on the dynamics of the model, even on the successive generations. We will discuss the implications of this result in section 5. We can also notice that this difference of the variability is larger at certain specific phases of the dynamics, and can differ from one variable to another. This is probably due to the fact that the stochasticity is mainly the result of the regeneration process, and that the impact of the regeneration is not similar for the different variables. For instance, a huge regeneration modifies the number of trees immediately, but as the new trees are small it does not modify the total basal area much.

In real forest stand, the spatial structure is usually not considered to have such a long term influence on the dynamics, and we therefore supposed it to be an artefact of the model. Indeed, real stand encounter many disturbances, and we can hypothesise that such stochastic events can shorten the influence of the spatial structure on the dynamics. This is what we have tested with the additional simulations presented in chapter 4.

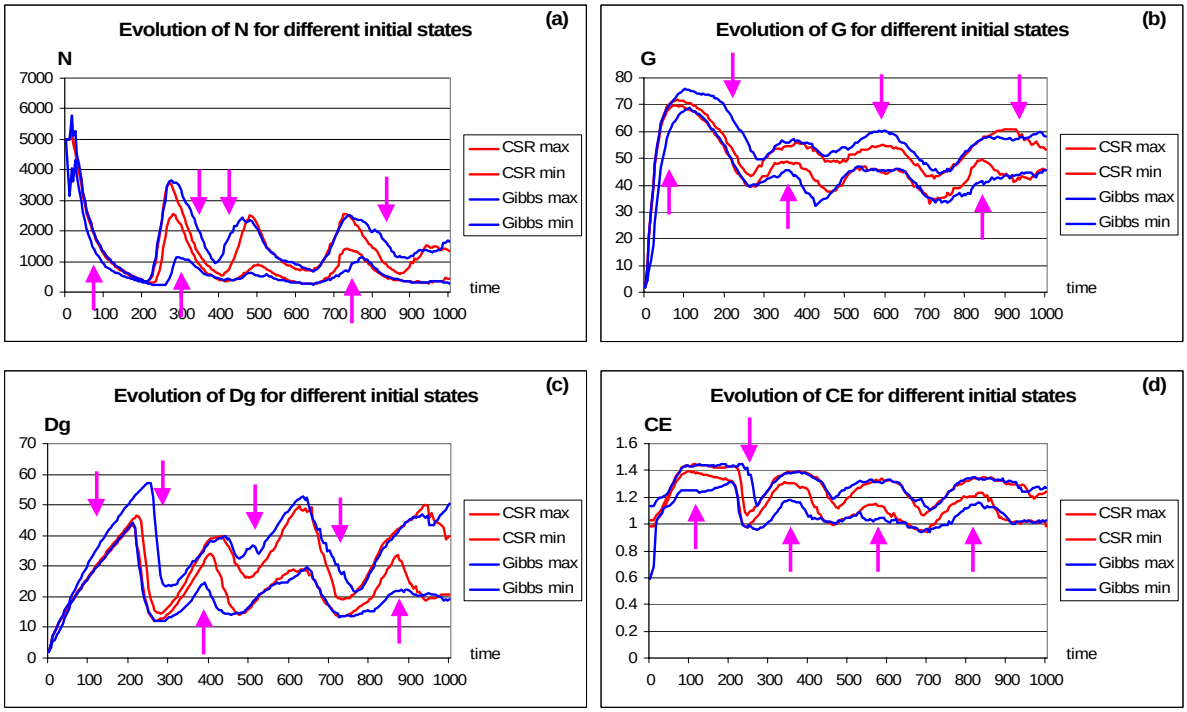

Figure 8 : Min and max values of the evolution curves for 100 simulations from a CSR initial spatial structure (red), and 100 simulations from a highly variable initial spatial structure (blue). Purple arrows point out the large differences of the variability. (a) Total number of trees in the stand; (b) total basal area; (c) mean quadratic diameter; (d) Clark & Evans index.

4. Taking disturbances into account

In this second step of our study, we characterised the influence of the spatial structure of the initial state of a simulation when the dynamics of the stand, modelled by the Mountain model, is periodically disturbed by storms. We therefore set the values of the parameters so that storms occurred, at different rhythms (every 5 or 10 years), leading to gap openings of different radius (5, 10 or 20 m).

We have first considered a disturbance corresponding to the opening of a 10m radius gap every 5 years, which is already a strong disturbance. We ran a new set of 100 simulations, corresponding to 1000 years evolution of a stand with very different initial states, with the Mountain model including this specific periodic disturbance. Figure 9 shows the curves corresponding to the evolution of the same 4 global variables (the total number of trees, the total basal area, the mean quadratic diameter, and Clark & Evans index) for these 100 simulations.

The simulation of this disturbance has completely modified the shape and the variability of the evolution curves. The different variables of the stand did not have cyclic evolution any more. The first 250 years still correspond roughly to the beginning of the first cycle simulated by the undisturbed model (see section 3), but then the disturbances have modified the stand sufficiently to avoid a new cyclic evolution of the stand, so that the variables converged toward equilibrium values, with small stochastic variations.

The variability of the curves is also smaller, and we have compared it to the corresponding variability when simulating the disturbed model with an initial state following CSR (figure 10). We can notice that the variability of the simulations with highly different initial spatial structures is slightly higher, but only during the 250 first years. We can therefore conclude that the disturbances have lowered the sensitivity of the model to the initial spatial structure, so that the influence of this spatial structure lasts less than 250 years in the disturbed model.

In order to characterise the sensitivity of the model to these disturbances, we have run other sets of simulations, corresponding to other values of the disturbance parameters : gap radius of 5, 10 or 20 m for 1 opening every 5 or 10 years. Table 2 presents the global behaviour of the simulations with these parameters. These results show that only large and frequent openings were able to modify the cyclic dynamics of the stand. We can conclude that small openings did not modify the spatial structure of the stand enough to influence its dynamics.

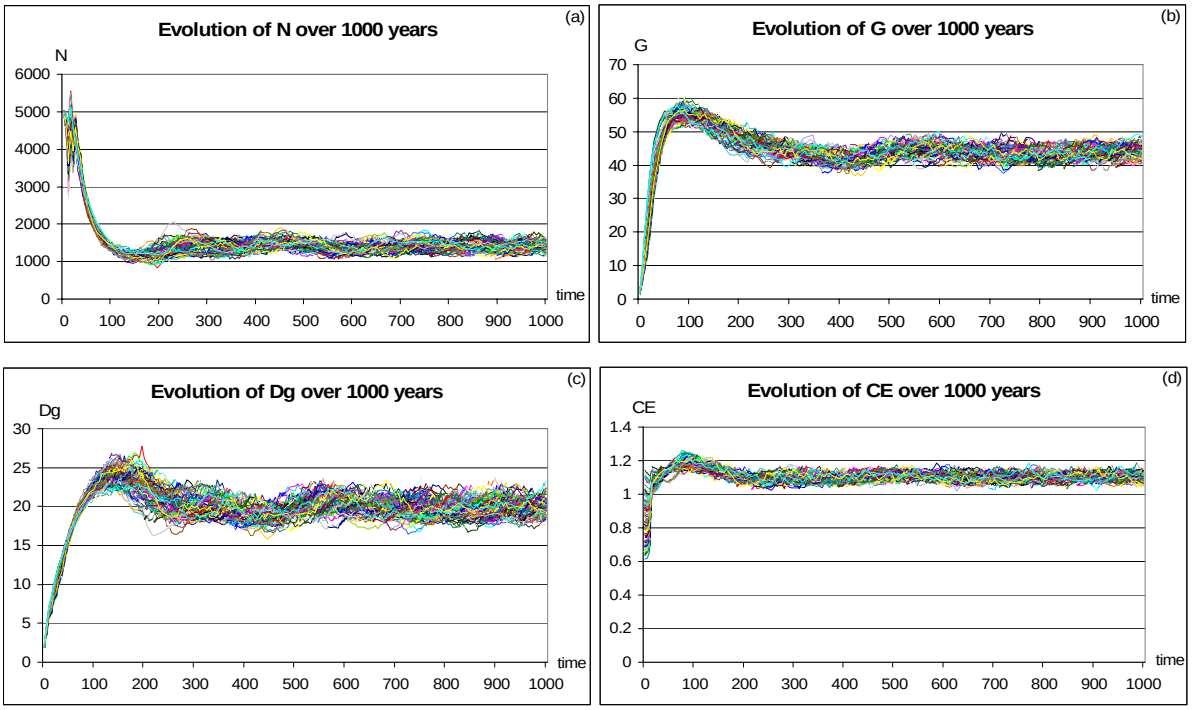

Figure 9 : Curves of 1000 years evolution for 100 simulations with a highly variable initial spatial structure simulated by a Gibbs process, and periodic openings of 10m radius gaps every 5 years. (a) Number of trees in the stand, (b) total basal area, (c) mean quadratic diameter, (d) Clark & Evans index.

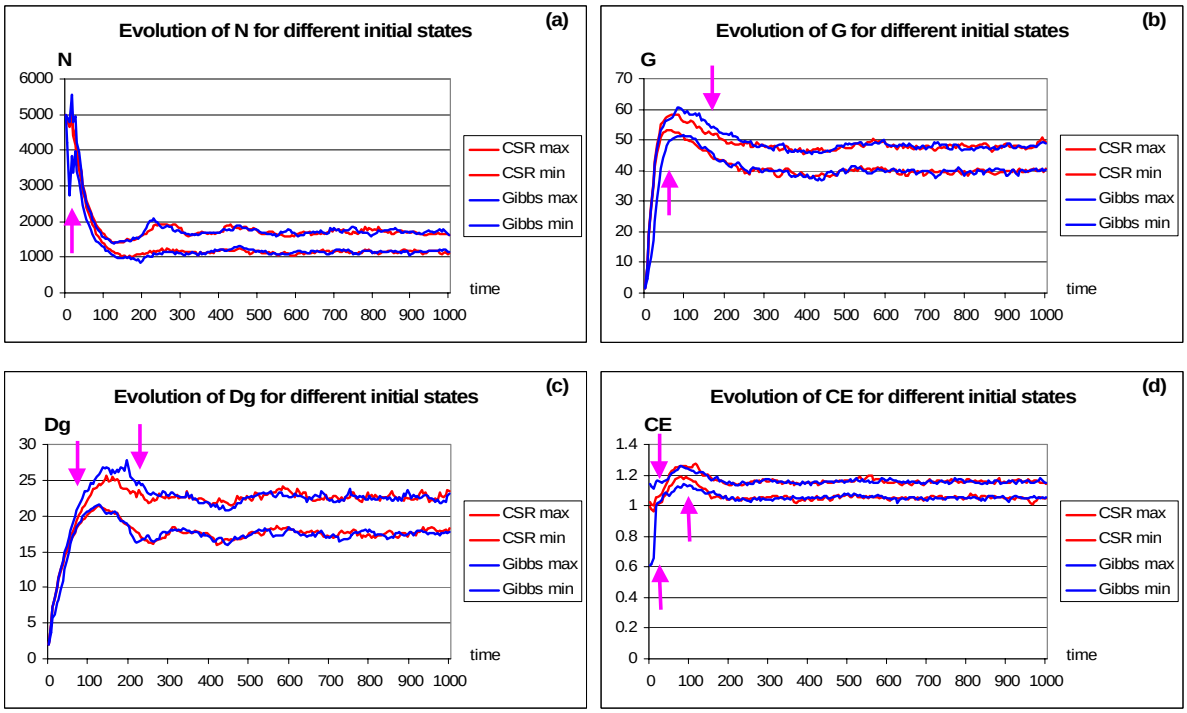

Figure 10 : Min and max values of the evolution curves for 100 simulations from a CSR initial spatial structure (red), and 100 simulations from a highly variable initial spatial structure (blue), with periodic openings of 10m radius gaps every 5 years. (a) Total number of trees in the stand; (b) total basal area; (c) mean quadratic diameter; (d) Clark & Evans index.

Table 2 : Global behaviour of the simulations for various disturbance parameters.

	Gap radius = 5m	Gap radius = 10m	Gap radius = 20m
1 opening every 5 years	cyclic evolution pattern	**convergence**	**fast convergence**
1 opening every 10 years	cyclic evolution pattern	cyclic evolution pattern	cyclic evolution pattern
without openings	cyclic evolution pattern		

5. **Discussion**

The long term sensitivity of forest models to the initial spatial structure has not been much studied and rises many questions ([Dubé *et al.* 2001] [Ménard *et al.* 2002]). In this paper, we have characterised this sensitivity for the Mountain model. We have shown that the initial spatial structure highly influences the dynamics of the undisturbed model, not only during the whole first cycle of the evolution (corresponding to the first generation), but also at a very long term at some periods in the evolution of the next generations. Such a very long term sensitivity is usually not expected in stochastic models, especially because the stochastic sub models (regeneration and mortality) highly modify the spatial structure and growing conditions of the stand. In our case, this long term sensitivity may come from the fact that the three biological processes of growth, mortality and regeneration are based on the same computation of available light, itself depending on the spatial structure of the stand. This potentially very long term sensitivity is an additional argument for not using long term simulation for prediction purposes

The importance of disturbances on the dynamics of forest stands has been more and more studied recently (*e.g.* [Pontailler *et al.* 1997] [Wolf *et al.* 2003] [Cordonnier 2004]). In this paper, we have illustrated how the addition of some disturbances in the model (such as a periodic gap opening through storms) can modify both the long term dynamics of the stand and the duration of the influence of the initial spatial structure. These results are consistent with those obtained by [Dubé *et al.* 2001], and [Ménard *et al.* 2002] with another forest model. We have also shown that small disturbances are not always sufficient to modify the dynamics of the stand or to lower the influence of the initial state. A finer exploration will be necessary to determine precisely the threshold values of these parameters.

These results confirm that long term simulations can be very interesting to study the behaviour of a model, but must not be used for predictions. Long term simulations of forest models are usually considered as not realistic at all, for different reasons. Firstly, forest stands growth models are usually fitted and validated on very short time periods (classically from 5 to 20 years). Their extrapolation on longer periods is not validated and can lead to errors accumulation. Secondly, the environmental conditions that are supposed to be constant in the model are likely to change during a long period [Dhôte Hervé 2000]. Thirdly, mortality and regeneration are very complex processes, that are still not well understood and not very precisely modelled. Other processes, such as different sorts of natural disturbances and human actions can not be planned on such a long period. In this paper, we pointed out the potential very long term sensitivity of forest models, that appears to be another argument for non using long term simulation in prediction purposes.

The potential sensitivity of forest growth models to the spatial structure of the initial state also questions the relevance of using simulated or virtual initial states, even for short term simulations. Indeed, if the model is sensitive to the spatial structure of the initial state, using an unrealistic initial spatial structure will lead to unrealistic results of the simulation. Unfortunately, the simulation of initial states for individual based models is usually very simply done, and very few authors evaluate the realism of these simulated initial stands ([Rathbun Cressie 1994] [Batista Maguire 1998] [Prévosto *et al.* 2003] [Goreaud *et al.* 2004]). Our results therefore confirm the need to improve the realism of the simulation of initial states for individual based models.

This study also points out the importance of disturbances, regeneration and mortality processes on both the simulated dynamics and the sensitivity of the model. These three stochastic processes are still not as well understood as growth, and thus the corresponding sub-models are often very simple. However, recent studies have illustrated their importance in the dynamics of a forest ecosystem. We therefore believe that a specific effort on the development of these sub-models, and on their integration in forest dynamics models could bring real improvement in the quality of the simulations, especially if we want to use simulations on longer periods.

Finally, our results rise some interesting questions on the long term dynamics of forest stands. Of course in this paper we obtained only some insights on the behaviour of the model, and not on the real forest ecosystem, as it is always the case with simulation studies [Pavé 1994]. This is all especially true because the model we studied has not been validated on its ability

to simulate long term dynamics, and such a very long term validation will probably remain impossible because it would require very long time measurements. It would however be very interesting to test on real stands the main qualitative results of the simulations, and especially the potentially long term influence of the initial spatial structure, and the role of disturbances in lowering this influence. Indeed, the influence of the spatial structure is usually considered as a short term process, precisely because many stochastic processes can modify the structure and the dynamics of a stand. However, this phenomenon has been rarely studied, and could have major implications on forest management. The combined use of real measures and simulation may facilitate the research work in this field.

ACKNOWLEDGMENTS

This study has been partly founded by the French ministry for agriculture. We are grateful to G. Bonnet and S. Bernard for their help when using the cluster of PCs, and to the OICMS referees for their constructive suggestions on the paper.

REFERENCES

[Ek Monserud 1979] Ek, A.R.; Monserud, R.A. Performance and comparison of stand growth models based on individual tree and diameter-class growth. *Canadian Journal of Forest Research*, 9 : 23-244, 1979.

[Tomé Burkhart 1989] Tomé, M.; Burkhart, H.E. Distance-dependent competition measures for predicting growth of individual trees. *Forest Science*, 35 : 816-831, 1989.

[Spellmann 1992] Spellmann, H. Concepts for mixed stand studies. *Proceedings from the IUFRO conference, held in Berlin-Eberswalde, 1992* : 10 p, 1992.

[Houllier *et al.* 1991] Houllier, F.; Bouchon, J.; Birot, Y. Modélisation de la dynamique des peuplements forestiers : état et perspectives. *Revue Forestière Française*, XLIII- 2 : 87-108, 1991.

[Pretzsch *et al.* 2002] Pretzsch, H.; Biber, P.; Dursky, J. The single tree-based stand simulator SILVA: construction, application and evaluation. *Forest Ecology and Management*, 162 : 3-21, 2002.

[deColigny *et al.* 2004] de Coligny, F.; Ancelin, P.; Cornu, G.; Courbaud, B.; Dreyfus, P.; Goreaud, F.; Gourlet-Fleury, S.; Meredieu, C.; Orazio, C.; Saint-André, L. Capsis : Computer-Aided Projection for Strategies In Silviculture : Open architecture for a shared forest-modelling platform. *In Proceedings of the IUFRO Working Party S5.01-04 conference (September 2002) Harrison, British Columbia, Canada* : 371-380, 2004.

[Biging Dobbertin 1995] Biging, G.S.; Dobbertin, M. Evaluation of competition indices in individual tree growth models. *Forest Science*, 41- 2 : 360-377, 1995.

[Begon *et al.* 1990] Begon, M.; Harper, J.L.; Townsend, C.R. Ecology : Individuals, Populations and Communities. *Blackwell Scientific Publications :* 945 p, 1990.

[Dieckmann *et al.* 2000] Dieckmann, U.; Law, R.; Metz, J.A.J. The geometry of ecological interactions. Simplifying spatial complexity. *Cambridge Studies in Adaptative Dynamics :* 564 pp, 2000.

[Pretzsch 1997] Pretzsch, H. Analysis and modeling of spatial stand structures. Methodological considerations based on mixed beech-larch stands in Lower Saxony. *Forest Ecology and Management*, 97 : 237-253, 1997.

[Goreaud *et al.* 2004] Goreaud, F.; Loussier, B.; Ngo Bieng, M.A.; Allain, R. Simulating realistic spatial structure for forest stands : a mimetic point process. *Actes des Journées Interdisciplinaires de Statistiques Spatiales, Paris, 2-3/12/04. On-line at http://team.univ-paris1.fr/jiss2004/index.php :* 22pp, 2004.

[Pontailler *et al.* 1997] Pontailler, J.Y; Faille, A.; Lemée, G. Storms drive successional dynamics in natural forests : a case study in Fontainebleau forest (France). *Forest Ecology and Management*, 98 : 1-15, 1997.

[Wolf *et al.* 2003] Wolf, A.; Møller, P.F.; Bradshaw, R.H.W.; Bigler, J. Storm damage and long-term mortality in a semi-natural, temperate deciduous forest. *Forest Ecology and Management*, 188 : 197-210, 2003.

[Dubé *et al.* 2001] Dubé, P.; Fortin, M.J.; Canham, C.D.; Marceau, D. J. Quantifying gap dynamics at the patch mosaic level using a spatially-explicit model of a northern hardwood forest ecosystem. *Ecological Modelling*, 142 : 39-60, 2001.

[Goreaud *et al.* 2002] Goreaud, F.; Loreau, M.; Millier, C. Spatial structure and the survival of an inferior competitor: a theoretical model of neighborhood competition in plants. *Ecological Modelling*, 158 : 1-19, 2002.

[Ménard *et al.* 2002] Ménard, A.; Dubé, P.; Bouchard, A.; Canham, C.D.; Marceau, D.J. Evaluating the potential of the SORTIE forest succession model for spatio-temporal analysis of small-scale disturbances. *Ecological Modelling*, 153: 81-96, 2002.

[Rathbun Cressie 1994] Rathbun, S.L.; Cressie, N. A space-time survival point process for a longleaf pine forest in Southern Georgia. *Journal of the American Statistical Association*, 89- 428 : 1164-1171, 1994.

[Batista Maguire 1998] Batista, J.L.F.; Maguire, D.A. Modeling the spatial structure of tropical forests. *Forest Ecology and Management*, 110 : 293-314, 1998.

[Prévosto *et al.* 2003] Prévosto, B.; Hill, D.R.C.; Coquillard P. Individual-based modelling of Pinus sylvestris invasion after grazing abandonment in the French Massif Central. *Plant Ecology*, 168 : 121-137, 2003.

[Courbaud *et al.* 2001] Courbaud, B.; Goreaud, F.; Dreyfus, P.; Bonnet, F.R. Evaluating thinning strategies using a Tree Distance Dependent Growth Model: Some examples based on the Capsis software "Uneven-Aged Spruce Forests" module. *Forest Ecology and Management*, 145 : 15-28, 2001.

[Courbaud *et al.* 2003] Courbaud, B.; de Coligny, F.; Cordonnier, T. Simulating radiation distribution in a heterogeneous Norway spruce forest on a slope. *Agricultural and Forest Meteorology*, 116 : 1-18, 2003.

[Courbaud 1997] Courbaud, B. Modélisation de l'éclairement et de la croissance de l'épicéa (Picea abies L. Karst) en forêt irrégulière de montagne. *PhD, Université Claude Bernard, Lyon I :* 244 pp., 1997.

[Dreyfus Bonnet 1997] Dreyfus, Ph.; Bonnet, F.R. CAPSIS (Computer-Aided Projection of Strategies in Silviculture) : an interactive simulation and comparison tool for tree and stand growth, silvicultural treatments and timber assortment. Connection between silviculture and wood quality through modelling approaches and simulation software. *IUFRO WP S5.01-04 second workshop. Berg-en-Dal, Kruger National Park, South Africa. August 26-31, 1996 :* 57-58, 1997.

[Diggle 1983] Diggle, P.J. Statistical Analysis of Spatial Point Patterns. *Academic Press, New York :* 148 pp, 1983.

[Tomppo 1986] Tomppo, E. Models and Methods for analysing spatial patterns of trees. *Communicationes Instituti Forestalis Fenniae n°138. The Finnish forest research institute Helsinki, Finland :* 65 p, 1986.

[Cressie 1993] Cressie, N.A.C. Statistics for spatial data. *Wiley Series in Probability and Mathematical Statistics :* 900 p, 1993.

[Shugart 1984] Shugart, H.H. A theory of forest dynamics. *Springer-Verlag, New York*. 1984.

[Oliver Larson 1996] Oliver, C.D.; Larson, B.C. Forest Stand Dynamics. *John Wiley & Sons, New York*. 1996.

[Cordonnier 2004] Cordonnier, T. Perturbations, diversité et permanence des structures dans les écosystèmes forestiers. *PhD, Université Paris XI :* 258 pp, 2004.

[Dhôte Hervé 2000] Dhôte J.F., Hervé J.C. Changements de productivité dans quatre forêts de chênes sessiles depuis 1930 : une approche au niveau du peuplement. *Annals of Forest Science*, 57 : 651-680, 2000.

[Pavé 1994] Pavé, A. Modélisation en Biologie et Ecologie. *Aléas, Paris*. 1994.

Modelling the colonisation dynamics of Scots pine in French areas. Impact of possible atmospheric carbon changes.

Robert A.
E.A. Gestion de la Biodiversité
Faculté des Sciences de Nice
Parc Valrose
06108 Nice Cedex 2, France
+33 (0)4 92 07 68 24
audrey.robert@unice.fr

Prévosto B.
U.R. Ecosyst. Méd. et Risques
C.E.M.A.G.R.E.F.
Le Tholonet P.O. box 31
13612 Aix-en-Provence, France
+33 (0)4 42 66 99 25
bernard.prevosto@cemagref.fr

Hill D. R. C.
Laboratoire I.M.O.S.
I.S.I.M.A.
Clermont-Ferrand /Les Cézeaux
P.O box 10125
63173 Aubière Cedex France
+ 33 (0)4 73 40 50 19
drch@isima.fr

Coquillard P.
E.A. Gestion de la Biodiversité
Faculté des Sciences de Nice
06108 Nice Cedex 2, France
+33 (0)4 92 07 68 23
patrick.coquillard@unice.fr

ABSTRACT
The purpose of this research was to explore the impact of the atmospheric CO_2 variations on Scots pine (*Pinus sylvestris* L.) dynamics occurring on two French sites : the Plateau de Caussols (Mediterranean bioclimate) and the Chaîne des Puys (Mountain-Oceanic bioclimate). To this end, we built a model (AFFORSIMulator) which simulates the extension of Scots pine forest on abandoned turf. It is an individual-based model, spatially explicit, which takes into account inter-tree competition for shared resources and the light occultation the trees endure from their neighbours. The individual growth is based on classical differential equations, weighted by the photosynthetic production calculated from both the atmospheric annual CO_2 concentration and the light value. Three scenarios simulating the variations of the atmospheric CO_2 through time were implemented. The results of the model mainly suggest that even if the Pine settlement is faster under Mediterranean conditions as opposed to Oceanic ones, stand parameters really depend on the way the atmospheric CO_2 will change through time. Surprisingly, the wood production may change in the near future, the Chaîne des Puys site becoming a greater wood producer that the Plateau de Caussols site in the context of a rapid variation.

KEYWORDS
Pinus sylvestris, atmospheric CO_2 variations, individual-based modelling, afforestation.

1. Introduction

The general pastoral abandonment that occurred in France, especially in uplands, during the second half of the 20th century resulted in tree colonisation on a large scale. Natural afforestation of former agricultural lands is assumed to be the main process responsible for the increase in woodland cover observed during the last decades in this country (about 10,000 to 40,000 ha per year, [D.E.R.F. 1995]).
Scots pine (*Pinus sylvestris* L.) is an abundant component of natural afforestation, especially in uplands and Mediterranean areas in southern France. For instance, the colonised areas in the Provence - Alpes Côte d'Azur region increased from 30,000 ha in 1878 to 250,000 ha in 1999 [Quézel Médail 2003]. Also, *P. sylvestris* is by far the most widespread species colonising abandoned turf or heathlands on flat areas and gentle slopes of the southern part of the French Massif Central.
The colonisation of former pastoral or agricultural lands on a large scale by Scots pines can rapidly lead to the closure of landscapes, to a drastic loss of biodiversity through extinction of resident species [Curt *et al.* 2003], [Higgins *et al.*1999] and to a greater risk of large fires.
The ecological and socio-economic implications of Scots pine colonisation in France raises the question of natural afforestation forecasting [Richardson 2000] in a context of environmental changes, such as atmospheric CO_2 increase. For this purpose, a forest dynamics model is an appropriate scientific tool. A modelling approach using the discrete event

simulation concept (AFFORSIMulator) has already been proposed by [Prévosto *et al.* 2003]. This is a spatially explicit individual-based model (IBM) that simulates the behaviour of each tree according to its local conditions, which depend on its neighbourhood. The competition process was based on differences in height between trees of the virtual stand. These competitive interactions were quantified with a geometric distance-dependent index (VASA) based on elevation angle sums. However, in the stands studied, some ecological factors (climate and soil parameters) were assumed to be constant. In addition, the afforestation process operated on a time scale short enough (decades) to assume that variations in atmospheric CO_2 concentration were of no consequence. The VASA index thus succeeded in representing the competition process driving the afforestation dynamics in these specific ecological and time scale conditions. However, for the purpose of exploring the consequences of atmospheric CO_2 variations on forest dynamics, VASA is no longer suitable since it is a highly lumped approach that does not allow any accurate integration of environmental variables, such as the amount of light a tree receives.
The present work is expected to gain insight into the mechanism of intraspecific competition of *P. sylvestris*. It aims at integrating a new parameter –called Light Relative Intercept (LRI) – in order to improve the biological realism of AFFORSIMulator, so that it could take into account certain environmental changes, while conserving its efficiency for the prediction of the internal dynamics of forest stands.

2. Materials and methods

2.1. AFFORSIMulator description

AFFORSIMUlator is based on the discrete event simulation concept (microsimulation). It is an individual tree-based model (IBM), spatially explicit and discrete in time (time step = 1 year). The kernel is clock guided and is of three-phase type ([Balci 1988]). Simulations start with stand characteristics corresponding to the state of simulated landscapes before grazing abandonment, i. e. some isolated trees accurately located in space and with their age and dimensions (initial conditions)

2.1.1 *Stand attributes*

Simulated forest stands are monospecific (*P. sylvestris*). This implies that all trees represented in the simulator are driven by the same dynamical processes, according to the theoretical knowledge of the biology and ecology of the species they belong to.
Stand attributes controlled by the model concern its density and basal area, but also the estimation of the colonised area it reaches through time. Simulations are running on a total area of 9 ha (300m*300m).

2.1.2 *Tree attributes*

For each simulated tree, social status is identified according to tree density in a neighbourhood radius of 5m around each subject tree. If no neighbours are located around the subject tree, the latter is considered as an isolated one, otherwise it is considered as within-stand tree and can undergo competition for resources.
Dimensions through time (trunk height, trunk circumference and crown diameter) as well as exact spatial locations (x, y and z coordinates) of each tree are known.

2.1.3 *Dynamic processes*

Regeneration, tree growth and tree mortality processes are computed each time step by functions classically used in IBM approaches applied to forest dynamics modelling.
Mortality process is managed thorough the computation of a probability of death for each tree which depends on age and the competition pressure it endures (intensity of VASA index, see the description hereafter). Recruitment process results from tree fertility, seed dispersion and seed survival processes: see [Prévosto *et al.* 2003] for description. Growth process concerns stem girth, stem height and crown diameter variation through time.
At each time step *t* VASA was computed as follows:

$$VASA_j = \sum_{\substack{i=1 \\ i \neq j}}^{n} (\varepsilon_i \theta_i) = \sum_{\substack{i=1 \\ i \neq j}}^{n} \varepsilon_i \arctan\left[\frac{|h_i - h_j|}{L_{ij}}\right], \qquad \text{(Eq. 1)}$$

where θ_i is the positive vertical angle between the horizontal plane and the line from the top of the subject tree *j* to the top of its neighbour i, h_i and h_j are the heights of the tress i and j, L_{ij} the distance between the trees i and j. $\varepsilon_i = 1$ if tree i is taller than tree j, and $\varepsilon_i = -1$ otherwise. Each neighbour i is localised in a 5m radius around the subject tree j. Therefore, VASA is the sum of positive and negative values depending on the relative competitive status of the subject tree and of each of its neighbours [Tomé & Burkhart89].
VASA was then integrated into the derivative form of the girth growth function (Eq. 2) [Prévosto *et al.* 2003].

$$G_t = \alpha_2 e^{\beta_2 VASA}\left(1 - e^{-age\left(\alpha_1 e^{\beta_1 VASA}\right)}\right)^{\gamma}, \quad \text{(Eq. 2)}$$

where $\alpha_2 e^{\beta_2 VASA}$ is the asymptotic girth (G_{max}) and $\alpha_1 e^{\beta_1 VASA}$ the growth rate.
Stem height and crown diameter growth partially depend on stem girth growth.

2.2. **Model calibration and hypotheses**

Data used to parameterise dynamic functions were recorded on two sites representative of two upland areas of France characterised by different bioclimates: the Chaîne des Puys (volcanic massif of the French Massif Central, mean altitude 900 m) and the Plateau de Caussols (southern part of the French Alps, mean altitude 1100 m).
Differences between site conditions are illustrated in the simulator through growth process: depending on thesite considered (Chaîne des Puys or Plateau de Caussols) tree growth does not exhibit the same sensitivity towards competition pressure, that is why growth function shape and parameters differ between site, according to observed growth patterns ([Prévosto *et al.* 2003], for the Chaîne des Puys site and for the Plateau de Caussols site).
Because of the lack of data concerning recruitment and mortality, we assumed that these processes exhibit the same modalities and parameters on both sites.
Site conditions are either considered constant or variable. As a matter of fact, atmospheric CO2 concentration and soil water content vary through time whereas the other limiting factors (Nitrate availability (NO3) and temperature) remain constant.

2.3. **Environmental changes implementation**

Atmospheric CO_2 concentration ($[CO_2]_{atm}$) is the main factor conditioning the amount of photosynthetic production a single individual is able to realise. In optimal conditions the photosynthetic production associated to a given $[CO_2]_{atm}$ (PPpot) can be estimated as described in figure 1.

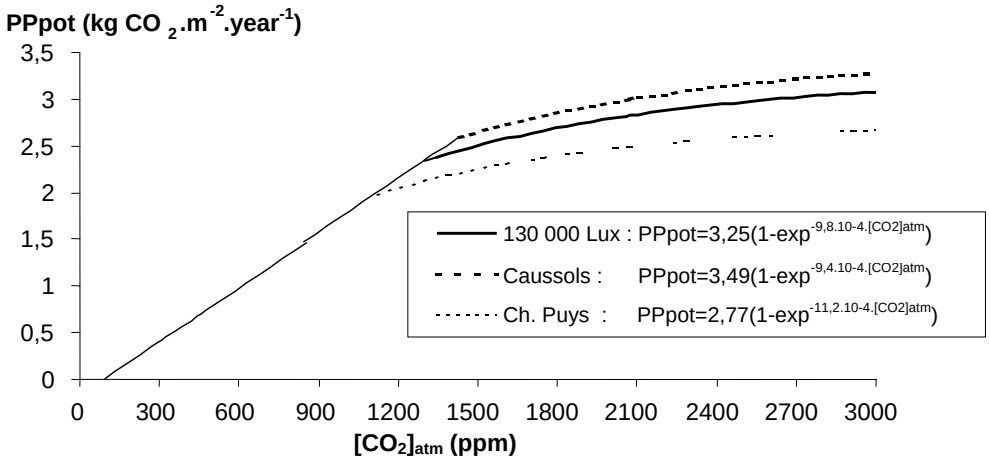

Figure 1: influence of the atmospheric $[CO_2]$ ($[CO_2]_{atm}$) on the net photosynthetic production (PPpot) . The graph shows relationship for a mean illumination of 130 000 Lux (illumination corresponding to Mediterranean areas), and relationships computed for the mean illumination characterising each study site (respectively 110 988 Lux for the Chaîne des Puys and 139 446 lux for the Plateau de Caussols). Whatever the conditions of illumination are, the relationship between PPpot and $[CO_2]_{atm}$ is first approximated by a linear relation (PPpot=19,15.10-4.$[CO_2]_{atm}$-0,1716).

We can then estimate the optimal variation of photosynthetic production (ΔPPpot) associated to a given $[CO_2]_{atm}$ in comparison to the photosynthetic production associated to the actual $[CO_2]_{atm}$ (PPref) as follows :

$$\Delta PPpot = \frac{PPpot - PPref}{PPref}, \quad \text{(Eq. 3)}$$

Light is the main limiting factor of photosynthesis process which conditions the fixation CO_2 by chlorophyll pigments. To illustrate the light occultation a tree suffers from its closest neighbours we built an index (LRI : Light Relative Intercept) which allows the estimation of the shadow produced, per unit area, by each neighbour located in a half-circle of 5m radius, centred on the subject tree and oriented to the south exposition. The shadowed area of each subject tree produced by a given neighbour (figure 2) depends on the solar elevation that can be deduced from the azimuth of the neighbour with respect to south exposure.

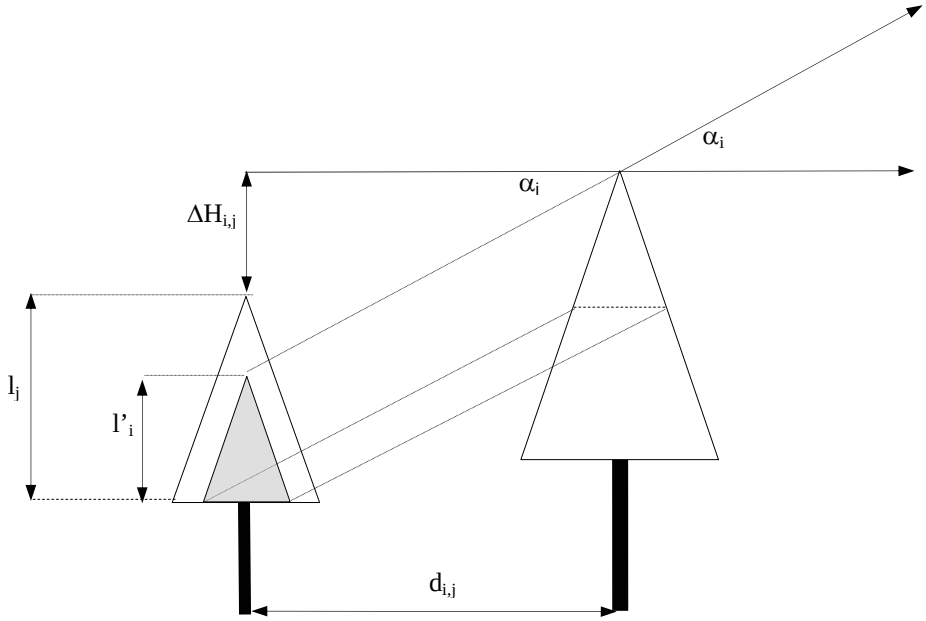

Figure 2. Light intercept between two neighbouring trees. From [Ung *et al.* 1997] after modifications.

LRI thus gives an approximation of the exact direct light occultation endured by each tree, and is calculated at each time step as follows:

$$LRI_j = \sum_{\substack{i=1 \\ i \neq j}}^{n} sh'_i / CA_j \ , \qquad \text{(Eq. 4)}$$

with $sh'_i = \beta . l'^2_i . \cos(\pi/2 - \alpha_i)$, (Eq. 5)

and $l'_i = \Delta H_{i,j} + l_j - d_{i,j} . \tan(\alpha_i)$, (Eq. 6)

where sh'_i is the area of the crown of the subject tree j shadowed by a neighbour i, CA_j is the crown area of tree j (conical area), l'_i is the length of the projected shadow produced by the ith tree on the crown of tree j [Ung *et al.* 1997], l_j is the length of crown of the j tree, $\Delta H_{i,j}$ is the height difference between respectively tree j and tree i, $d_{i,j}$ is the distance between trees i and j, α_i is the mean solar elevation deduced from the azimuth of tree i towards tree j according to south exposure, and computed from monthly data covering the tree growing season, β is a constant estimated as 0.291 in the Chaîne des Puys site and 0.306 in the Caussols site (see [Ung *et al.* 1997] for more details), n is the total number of competitors, located within the south-exposed half-circle – 5m radius – centred on the subject tree. The term $\cos(\pi/2 - \alpha_i)$ represents the variation of energy flux due to the incident angle of light on a flat surface.

An effective variation of the photosynthetic production (ΔPPeff) can be computed as:

$\Delta PPeff = \Delta PPpot \times SW$, (Eq. 7)

where SW ([0;1]) is a coefficient depending on LRI value. We assumed that SW obeys a negative saturation law. The fit of SW on data gave:

$$SW = \exp^{-LRI^{3,26}} \ , \qquad \text{(Eq. 8)}$$

If a tree is free from any shadow (SW=1) its growth is dependent onthe $[CO_2]_{atm}$ value, and is maximal. On the contrary, if a tree is completely shadowed (SW=0) its growth is minimal whatever the $[CO_2]_{atm}$ is. In intermediary situations, the growth depends on both competition index (VASA) , the light it receives (LRI), and the $[CO_2]_{atm}$.

The growth increment trees achieve at each time step in the simulator is then weighted as follows (example of growth parameterisation from "Chaîne des Puys" site conditions):

$$\frac{dG}{dt} = \left[\frac{2{,}77\left(1-\exp^{-11{,}2.10^{-4}.[CO_2]_{atm}}\right) - P\,Pref}{P\,Pref} \times \exp^{-IRL^{3{,}26}} + 1 \right] \times 0{,}03\exp^{(-0{,}02.VASA)} \times \exp^{(-0{,}05.\exp^{(0{,}02.VASA)}.Age)}$$ (Eq. 9)

3. **Materials and methods**

In order to explore the effect of the increase of $[CO_2]_{atm}$ on the dynamics of forest colonisation (forest growth and colonisation speed) during the next century, three scenarios were implemented with the simulator.
Scenario 1 (Sc1): constancy of $[CO_2]_{atm}$ through time to 325 ppm (actual concentration).
Scenario 2 (Sc2): linear increase of $[CO_2]_{atm}$ through time of +1,5 ppm/year (mean annual increase observed from 1750 till now).

Scenario 3 (Sc3): exponential increase of $[CO_2]_{atm}$ through time such as it reaches 940 ppm in 2100 (worst situation predicted by presentclimatic models).
We present here few results using single replicates, but representative enough of the behaviour of variables. In such conditions, the statistical aspect of simulations are not exposed in this paper.

3.1. **Forest growth under Sc1**

Results of simulation obtained with Sc1 allowed the comparison of model behaviour between the two bioclimatic situations (Ch. des Puys site and Pl. de Caussols site) since the only source of variation concerned the parameters used in individual growth functions.

Stand density simulated for each bioclimatic condition (figure 3) first increased till a maximum was reached. This phase illustrates the time that young trees need to colonise the available space. Stand density then decreased, the self-thinning process eliminating the less competitive trees. Stand density was always greater under Mediterranean bioclimate conditions than under Oceanic bioclimate conditions. Indeed, the maximum density was 1953 trees.ha^{-1} and 1500 trees.ha^{-1} 100 years later using the parameters estimated on the Pl. de Caussols site, whereas the maximum density was 1813 trees.ha^{-1} and 1225 trees.ha^{-1} at the end of the simulation using the parameters estimated on the Ch. des Puys site. These differences result from a greater competition pressure between trees under Oceanic conditions than Mediterranean ones.

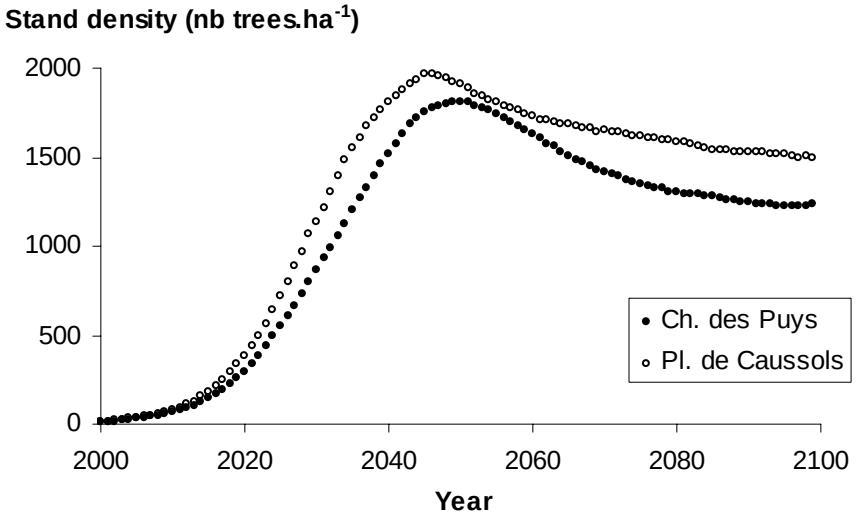

Figure 3 Stand density simulated by the model between 2000 et 2100 for each site conditions if no variation of atmospheric [CO2] occurs through time (Sc1).

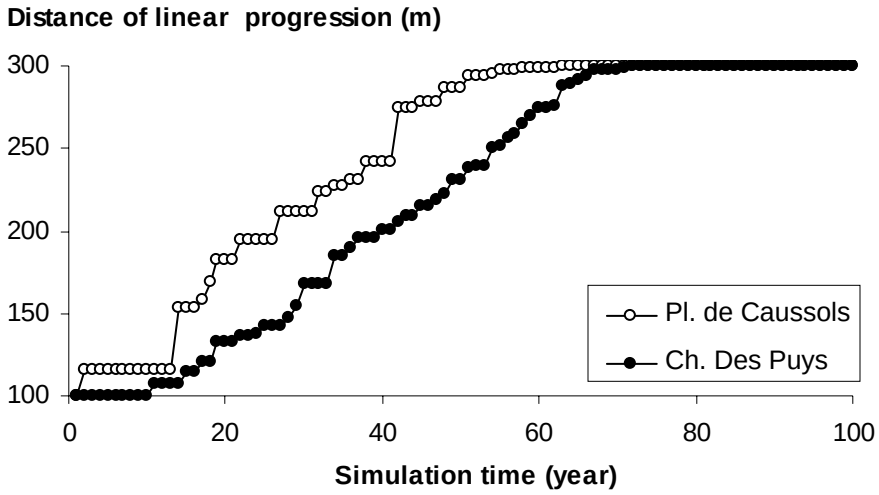

Figure 4 Colonisation speed (illustrated by the linear progression of trees from an initial line starting on the edge of the simulated area) simulated by the model between years 2000 et 2100 for each site conditions if no variation of atmospheric [CO2] occurs through time (Sc1).

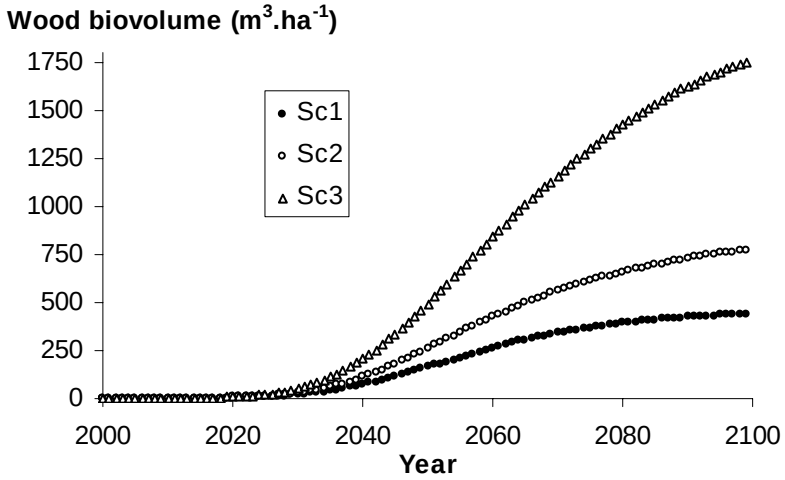

Figure 5 Wood biovolume simulated by the model for the Plateau de Caussols site between years 2000 et 2100 according to the three scenarios of atmospheric [CO_2] variation through time.

.

The speed of forest expansion simulated by the model (figure 4) was always greaterunder Mediterranean climatic conditions than under Oceanic ones. Indeed available space is totally colonised after 60 years of simulation using Pl. de Caussols parameters, and after 70 years of simulation using Ch. des Puys parameters.

These results showed that a Mediterannean climate would be more favourable to the extension of Scots pine forests in a mid-term time scale, even if trees would suffer fromsummer drought.

3.2. Effect of the increase of $[CO_2]_{atm}$ on tree growth

Wood volume increased through time whatever the bioclimatic conditions were, but the speeds differed according to the scenario simulated, especially after 30 years of simulation. Compared to biovolume produced after 100 years of simulation under Sc1, wood biovolume produced under Sc2 was almost doubled, and was 4 to 5 time greater under Sc3. The figure 5 exemplifies the Plateau de Caussols site.

3.3. **Comparison between site (wood volume)**

If no $[CO_2]_{atm}$ variation occurs (Sc1), wood volume remains greater under Mediterranean than Oceanic climate (figure 6a). However, when $[CO_2]_{atm}$ increases through time, whereas virtual stand tended to produce similar wood quantity after one century for Sc2 (figure 6 b), Sc3 shows an inversion after about 60 years : the wood production under Oceanic climate became greater than under Mediterranean climate (figure 6c).

4. **Conclusion**

The IBM spatially explicit approach aims at representing the impact of the heterogeneity of local conditions on tree growth through inter-tree interactions, and allows the simulation of the competition process for resource sharing. Concerning temperate stands, spatial competition indices were initially proposed to predict the wood production of even-aged pure stands [Mitchell 1969,1975] and later for uneven-aged pure or mixed stands [Ek Monserud 1975]. Thereafter, they were integrated into forest dynamics models for naturally regenerated stands, presenting more complex structures and more heterogeneous specific and/or size composition (see the review by [Porté Bartelink 2002]). By simulating the afforestation process we add a further source of complexity, *i.e.* the variation of structures (age structure, vertical and horizontal structures) over time. In the present case, this variation not only depends on the competition but also on nutrient availability we introduced through light index and $[CO_2]_{atm}$ variation.

The results of the model mainly suggest than even if the colonisation dynamics is faster under Mediterranean conditions than Oceanic ones, stand parameters really depend on the way the $[CO_2]_{atm}$ will change through time. These preliminary results showed that $[CO_2]_{atm}$ variation would induce major modifications either in wood production or stand density. Surprisingly the wood production may change in the near future, the Chaîne des Puys site becoming a greater wood producer than the Plateau de Caussols site in the context of Sc3. However, not only $[CO_2]_{atm}$ might be taken into account but also water and nitrate resources in the simulations. These aspects, considered as major by most biologists, could be the subject of further research.
We can consider AFFORSIMulator model as a scientific tool since it succeeds in reproducing the colonisation dynamics of Scots pine forests at landscape scale, and allows the apprehension of the effect of environmental changes. We also expect to use AFFORSIMulator as a tool for forest management since it will be able to forecast changes of landscape quality and helpful for wood harvesting with respect to the level of biodiversity.

a) Sc1 : constancy of $[CO_2]_{atm}$ through time

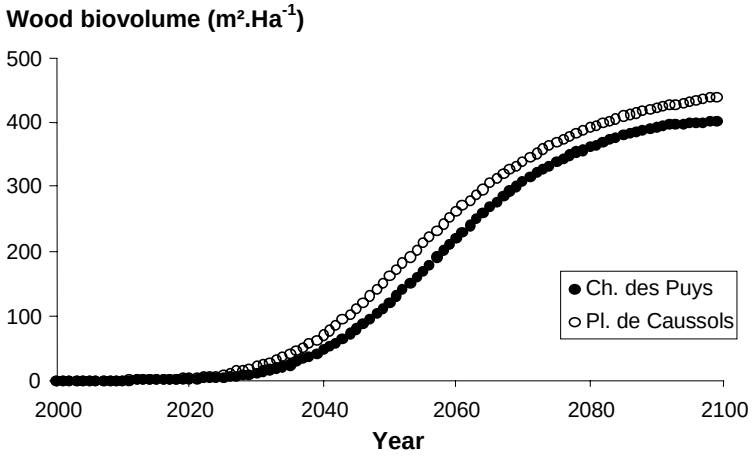

b) Sc2 : constant increase of $[CO_2]_{atm}$ through time

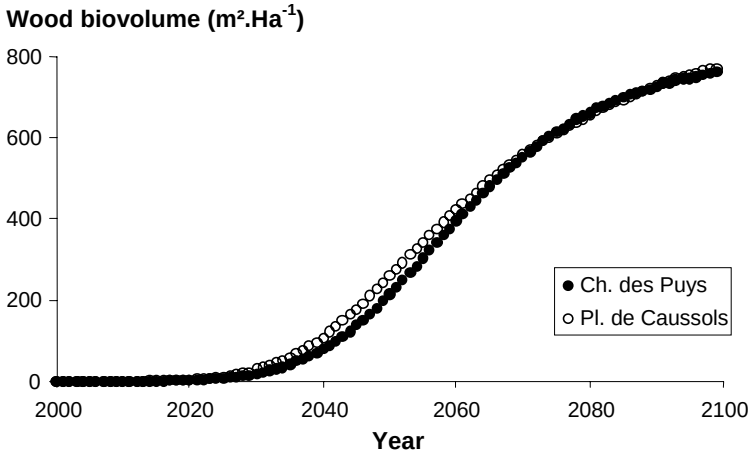

c) Sc3 : exponential increase of $[CO_2]_{atm}$ through time

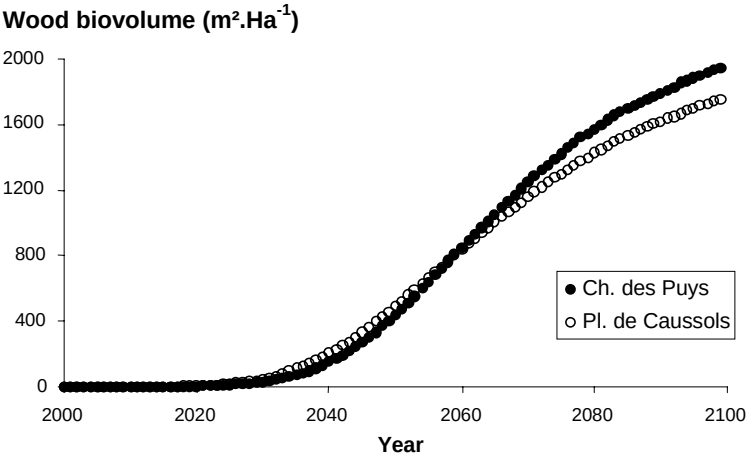

Figure 6 Wood biovolume simulated for each site by the model between 2000 et 2100,and according to the three scenarios of atmospheric [CO2] variation through time. (a) scenario 1 ; (b) scenario 2 ; (c) scenario 3.

REFERENCES

[D.E.R.F. 1995] D.E.R.F. Les indicateurs de gestion durable des Forêts Françaises. *Ministère de l'Agriculture et de la Pêche, Direction de l'Espace Rural et de la Forêt*, Paris, 1995.

[Quézel Médail 2003] Quézel P., Médail F. Ecologie et biogéographie des forêts du bassin méditerranéen. *Elsevier Ed.*, Paris, 2003.

[Curt *et al.* 2003] Curt T., Prévosto B., Klesczewski M., Lepart J. Post-grazing Scots pine colonisation of mid-elevation heathlands: population structure, impact on vegetation composition and diversity. *Ann. For. Sci.*, **60**: 711-724, 2003.

[Higgins *et al.* 1999] Higgins S.I., Richardson D.M., Cowling R.M., Trinder-Smith T.H. Predicting the landscape-scale distribution of alien plants and their threat to plant diversity. *Conservation Biology*, **13**: 303-313, 1999.

[Richardson 2000] Richardson D.M. Mediterranean pines as invaders in the southern hemisphere. In: Ne'eman G., Trabaud L. (Eds.). *Ecology, biogeography and management of Pinus halepensis and Pinus brutia forest ecosystems in the Mediterranean Basin*, Bachuys Publishers, Leiden, pp. 131-142, 2000.

[Prévosto *et al. 200*3] Prévosto B., Hill D. R. C., Coquillard P. Individual-based modelling of *Pinus sylvestris* invasion after grazing abandonment in the French Massif Central. *Plant Ecol.*, **168**: 121-137, 2003.

[Balci 1988] Balci O. The Implementation of four conceptual Frameworks for Simulation Modeling in High-Level Languages. *Technical Report SRC-88-009, System Research Center*, Virginia State University, 1988.

[Tomé Burkhart89] Tomé M., Burkhart H.E. Distance-dependent competition measures for predicting growth of individual trees. *Forest Sci.*, **35**: 816-831, 1989.

[Ung *et al.* 1997] Ung C.H., Raulier F., Ouellet D., Dhôte J.-F. L'indice de compétition interindividuelle de Schütz. *Can. J. For. Res.*, **27**: 521-526, 1997.

[Mitchell 1969] Mitchell K.J. Simulation of the growth of even-aged stands of white-spruce. *Bulletin of Yale University, School of forestry 75*, pp. 1-48, 1969.

[Mitchell 1975] Mitchell K.J. Dynamics and simulated yield of Douglas–fir. *Monographs Forest Science*, **17**: 1-38, 1975.

[Ek Monserud 1975] Ek A., Monserud R. Methodology for modelling forest stand dynamics. *Staff Paper Series No. 2, Department of Forestry, School of Natural Resources*, University of Wisconsin, Madison, 1975.

[Porté Bartelink 2002] Porté A., Bartelink H.H. Modelling mixed forest growth: a review of models for forest management. *Ecol. Model.*, **150**: 141-188, 2002.

Use of Netlogo as a rapid prototyping tool for the creation of more rigorous spatially explicit individual-based biological models

Jen Schellinck
Carleton University
1125 Colonel By Dr.
Ottawa ON Canada
K1S 5B6
(613) 520-2600 x 1129
jschelli@ccs.carleton.ca

Tony White
Carleton University
1125 Colonel By Dr.
Ottawa ON Canada
K1S 5B6
(613) 520-2600 x 2208
arpwhite@scs.carleton.ca

ABSTRACT
In this paper we discuss how the rapid creation of model prototypes at the first stage of the modelling process can improve the creation and validation process of individually based, socially explicit biological models. In particular, we suggest that use of a modelling environment like Netlogo can increase the likelihood that model parameters will be set based on empirical data. We begin the paper by reviewing current modelling practices with a focus on how researchers currently set their model parameters. Having established that modellers do not use prototypes currently, we go on to discuss the merits of the Netlogo modelling environment as a tool for rapid model prototyping. We then discuss our own use of a Netlogo based prototype and describe how it has been useful in planning our data gathering and modelling methods for a model of caribou (**Rangifer** tarandus) herd behaviour. In particular we describe how we used the Netlogo prototype as a stand-in for actually observing caribou in the field and then tested our field data plan by observing and gathering data on the prototype as we might observe and gather data on the actual caribou.

KEYWORDS
Individual-based, spatially explicit models, model creation and validation, rapid prototyping, Netlogo

1. Introduction

Rapid prototyping has been used for some time in computer science and engineering as a means of acquiring an initial idea of the resources and technology necessary for the creation of a computer system or piece of software. In this paper we suggest that rapid model prototyping could play a similarly beneficial role in the construction and validation of individually based, spatially explicit models (IBSEMs). In particular we believe that the use of prototype models will noticeably increase the ability of modellers to create appropriately detailed models with physically meaningful parameters that can be clearly validated and supported by empirical data.

Model validation is an important aspect of model construction. In the case of individually based, spatially explicit models, however, model validation is challenging [Wiegand 2004]. One source of difficulty is the numbers of parameters required by even the most simple IBSEM and the corresponding need to validate the settings for as many of these parameters as is possible [Letchet 1998]. Adding to this difficulty is the fact that each IBSEM has significantly different parameter requirements. Consequently, even for experienced researchers it can be difficult to anticipate what these parameters will be and how to go about collecting data that can be used to set them and/or verify the model once they are set.

Currently, researchers try to avoid or mitigate this problem by undertaking a planning phase before data gathering. We wish to go one step further and propose that IBSEM modellers formally make rapid model prototyping a regular and integral phase of their modelling process- where, by rapid prototyping, we do not simply mean the creation of a rudimentary or first pass model prior to data gathering but instead the creation and rigorous analysis of a model prototype using methods which will be further discussed in the rest of the paper.

The process of creating and analysing such a prototype has two principal benefits. The first benefit is that the construction of the prototype gives researchers the opportunity to evaluate which parameters will need to be included in the finished model and how the values for these parameters will be set. The second, and, we believe, larger benefit is that, once the prototype has

been created it can be used as a rudimentary stand-in for the natural phenomenon itself, allowing modellers to test their field data plans by gathering data from the prototype under different scenarios and then test their data analysis plan on the prototype data. They may then use the results of this prototype data analysis to judge whether or not their planned field research will be sufficient to obtain the data that they need to create an empirically substantiated model. It is this second use of the prototype that we believe is particularly novel and which will be of greatest benefit to researchers.

We will begin this paper by briefly reviewing existing individually based, spatially explicit models (IBSEMS), with a focus on the unique data requirements of IBSEMS and the current methods used to set model parameters. Once this analysis of existing models has been completed we will go on to discuss how the use of rapid prototyping may benefit modellers in this area. To illustrate this we will describe how we are using a prototype model to determine the data collection requirements for a model of caribou herd behaviour.

2. Current Model Generation Methods for IBSEMs

IBSEMS are models that involve multiple, often heterogeneous organisms and which situate these organisms (hereafter referred to as agents) in an explicitly spatial modelling environment. Relevant variables in the model are individual, rather than global in nature. For example, rather than considering average population density as a basic model variable, an IBSEM would provide individual representations of organisms with spatial coordinates and then derive population density values based on the locations of these agents in the model.

Because of their focus on individual organisms, these models are well equipped to answer questions about how the properties of individuals affect, and are affected by, their environment and the behaviour of other individuals. Because they are also, by their nature, highly detailed models, IBSEMs are particularly useful for making predictions about scenarios that do not necessarily occur currently in nature- for example, predictions about the possible effect of putting a roadway through an existing valley- and for studying environments that are too complex or large scale to be studied in a laboratory setting [Turner 1994]. As a result they are most widely used in areas of biology like ecology, where the subject of study often does not lend itself to controlled settings or laboratories, and where changes made to the environment are not easily, if at all, reversible.

When biologists began to use IBSEMS as a research tool, a number of papers were quick to criticize IBSEMS for not being adequately data driven (see [Grimm 1999], [Reynolds 1999] for some discussion of this and [Weigand 2004] for a contrasting viewpoint). As a result of this early criticism, empirical support for and validation of model parameter settings is currently a key component of the current modelling process. However, the relatively large number of variables necessarily incorporated into IBSEMs makes this a challenging task.

Based on the literature, different modellers have taken different approaches to parameter setting. In some cases, model parameters may be largely set based on empirical data gathered for the purpose of model generation. Frankenhausen and Enggist's model of alpine chamois habitat use [Frankenhausen 2004], for example, sets movement parameters of the chamois like velocity and turning angles based on field data gathered for the purpose of creating the model. Similarly, probability of transitions between a number of observed behaviours (lying, ruminating, standing, walking, feeding and running), are based on an analysis of transitions between behaviours observed in the field. Seymour et al, in their model of red fox predation [Seymour 2004] also set movement rates and movement patterns based on observations of red fox behaviour in the Lower Derwent valley in England although, in their case, searching ability and behaviour was determined by a combination of stochastic and data driven parameters.

In other cases, modellers set model parameters based on values available in the literature. For example, the model of roe deer behaviour in fragmented forest by Jepsen et al, sets parameters relating to reproduction, development, spatial behaviour, mortality and energy use using information taken from the existing literature [Jepsen 2004], Finally, in some cases model parameters are not set based on either field data or data from the literature, but instead are set solely by the researchers themselves, usually because the model is intended to be generalizable over multiple species of animals. In Zollner and Lima's model of animal dispersment [Zollner 2005], model parameters were completely set by the researchers. In an interesting variant on this, Turner et al's model of general ungulate behaviour [Turner 1993] has several parameters set without reference to empirical data and other model parameters set based on data gathered on ungulates and ungulate environments, but with approximate values only, so as not to reflect any particular ungulate.

Although the data driven methods for model creation discussed above are a clear improvement over earlier, more ad hoc methods, there are still challenges associated with constructing IBSEMs in this way. Most notably, it is difficult, in advance, to anticipate all of the aspects of the IBSEM that will need to have empirically supported parameters and also unlikely that information on every required variable will be readily available in the literature. As a result, researchers who are dedicated to

creating an empirically valid model may find themselves returning to the field again and again, in order to obtain the data they need to create a fully validated model.

While this is not in principle a problem, it may become a practical problem if it leads the researchers to exceed the available resources, in terms of both time and money, for a particular research project. Consequently, it is important for researchers, as much as possible, to anticipate data requirements in advance of doing field research. We suggest that the creation of a model prototype, and appropriate use of this prototype (as described in the following section) can greatly assist in this key research step.

3. Case Study: Use of a prototype for planning a model of caribou herd behaviour

We are currently using a rapid model prototyping to assist in the planning stages of a model of caribou herd behaviour. By a rapid model prototype we mean a simulation that has multiple agents with individual properties that are roughly analogous to the properties of the organisms of interest, and that displays global properties of interest to the researchers as a result of interactions between the agents. The simulation is not intended to become a model of the phenomenon, but instead is intended to be used to assist in the determination of the data collection and analysis required for eventual construct of an empirically based model of the phenomenon. Because of its limited role, the simulation does not need to meet the constraints that a model would need to meet and, as a result, can be created relatively quickly. At the same time the simulation is similar enough to an actual model that it can be a useful tool for planning data collection and analysis.

For the purposes of our own research, we have used the Netlogo modelling environment [Netlogo 2005] as a tool for prototype creation. Although there may be other pre-fabricated modelling environments available for use in this context, in our experience Netlogo has a number of features that make it particularly suited for rapid model prototype creation. In particular, it is very easy in Netlogo to create simulations that exhibit emergent behaviour as a result of interactions between agents [Resnick 1994]. This is a result of Netlogo's built in support for the creation of multiple heterogeneous agents, which, once created, are immediately set up to act simultaneously with each other and their environment. Also because of this support, only a few lines of code are required to create a fully operational multi-agent simulation.

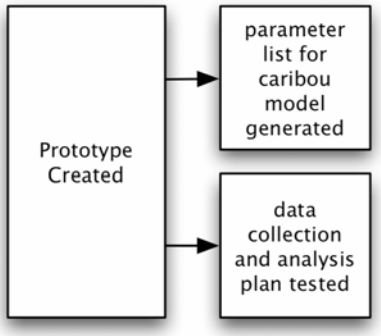

Figure 1: Two uses for the prototype

Currently, we are using our prototype model in two ways (see figure 1). The first is to investigate what sort of data will be required to provide empirically based values for the parameters of the actual model. The second is as a tool to test both the data collection plan and the methodology we intend to use to construct the final model based on the field data we have gathered. Although the first is perhaps a more obvious use of the prototype model, in this section we would particularly like to highlight the second use of the prototype as a stand-in for the natural phenomenon itself. This second use of the prototype has proven to be very useful for us, with respect to our ability to make a comprehensive data collection plan for the field data collection phase of the caribou herd model.

3.1 Creation of prototype

We created our netlogo prototype by assigning properties and actions to Netlogo agents based on ungulate properties that were frequently mentioned in the literature. In particular, we wanted our prototype to replicate the tendency for groups of ungulates to move as a cohesive group- reacting as a group to predators [Scotter 1995], fleeing as a group from predators, or disturbances [Harrington 1991] [Horejsi 1981] and moving as a group when grazing or travelling [Smith 1985].

Table 1- A sample of ungulon variables, actions and action rules

Ungulon Variables	Ungulon Actions	Ungulon Action Rules
Color	wave_tail	If a root is in eating range and uncovered, eat the root
Speed	Get_root_smell_info	
smell_range	Walk	If there are any ungulons in visual range with their tails waving, turn towards them and wave tail.
is_walking	Turn	
tail_is_waving	Dig_up_root	

Since the prototype was intended to be a tool for planning data collection and analysis, rather than a preliminary version of the final model, we named the agents in the model ungulons, to indicate that they were generally inspired by actual ungulates, but not meant to represent any particular ungulate species. We also included two more agent types in our simple prototype- predons (which were analogous to predators) and roots, which acted as a generic food source. It should be clear from this description that our prototype was both extremely simple and not overly connected to actual caribou herd properties and behaviours (see Table 1 for a description of some ungulon properties and behaviours). As stressed above, the prototype was intended to be used to help plan data collection for the actual model, and not to be used as a version of the model itself.

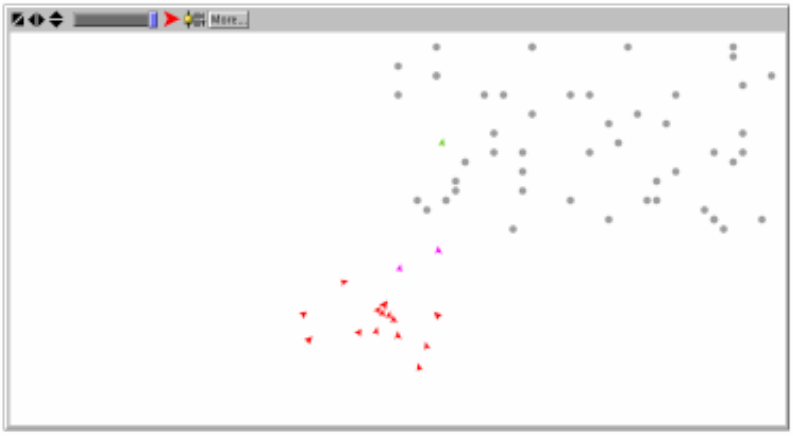

Figure 2: The ungulon prototype. Ungulons (pink and red triangles at bottom centre of screen) are orienting towards a predon (green triangle slightly top-right of screen), which is among the roots (grey circles in the top right quadrant).

The resulting prototype displayed, in a qualitative way, some of the group behaviours exhibited by caribou and other ungulates. In the absence of food or predators, the ungulons remained in a slightly moving group in the middle of their environment. In the presence of a field of roots they moved as a group towards this field and then moved about the field eating the roots. In the presence of predons, they stopped, and oriented towards the predons. Each ungulon had some probability of fleeing in the presence of the predons, which could in turn cause a stampede in the herd of ungulons (see Figure 2).

3.2 Parameter setting

To determine the data that would be required for the eventual model, we used the prototype to generate a record of the parameters that we anticipate will need to be set empirically in the final model (see Table 2). We did this by assuming that parameters similar to the ones required to generate appropriate behaviours in the prototype would at some point need to be set, based on empirical data, in the actual model. We went on to consider how these parameters might relate to actual real world properties and variables and planned our data collection requirements accordingly.

A point we would like to emphasize about parameter setting is that it is quite possible to generate fully functioning computer simulations by simply assigning a convenient value to the required parameters during creation of the simulation. Ultimately, however, for the simulation to become a model of a particular phenomenon, these parameters will need, as much as possible, to be set based on empirical data.

In our case, because we do not intend to use the netlogo prototype as a basis for the ultimate model, but instead plan to create the actual model in a programming environment with greater processing power and support for physically realistic interactions (for example, the Breve modelling environment [Klein 2002]), we will be able to set the parameters of the actual model based on our field data. By separating the prototype and the model construction stages we will be less likely to overlook variables that have been set initially in ad-hoc way for the convenience of initial testing of a preliminary model, or prototype.

Table 2: Parameters and information required

Environmental Parameters:
Size of environment/scale of model
Agent Physical Parameters:
Location vector (x and y co-ordinates)
Direction vector (heading)
Agent appearance (e.g. colour, other visual cues)
Agent Behavioural and Cognitive Parameters:
Types of behaviours: walking, running, turning, grazing, stampeding.
Internal cognition used to determine behaviour
Agent Action Parameters:
Walking velocity
Running velocity
Turning range
Agent Perception Parameters:
Smell range
Sight range
Environmental information acquired through each of these senses

3.3 Planning for data collection and model generation

We began the test of our data analysis plan by treating the graphic output of the netlogo prototype as a stand-in for observation of actual caribou in the wild. We gathering data and generated hypothesis from the prototype in a manner analogous to the way we planned to gather data and generate hypotheses while observing caribou. Once we had obtained the data from the prototype, we tested our data analysis plan on this prototype data to determine both what sorts of data and what sorts of data analysis techniques were required to create an adequate model of the prototype and, by extension an adequate model of actual caribou herd behaviour (see figure 3).

In order to ensure that knowledge of the prototype structure did not excessively interfere with the test, two researchers participated in this aspect of the project. One researcher set up a version of the rapid model prototype with precise parameter values, object properties and some aspects of the ungulon behaviour rules known only by that researcher. A second researcher then requested videos and data from the first researcher, thereby ensuring that the second researcher had no knowledge of the actual parameter settings for the prototype. The second researcher used the proposed field data collection plan, in conjunction with the videos and data to create a ‘model’ of the prototype (referred to as the prototype-model).

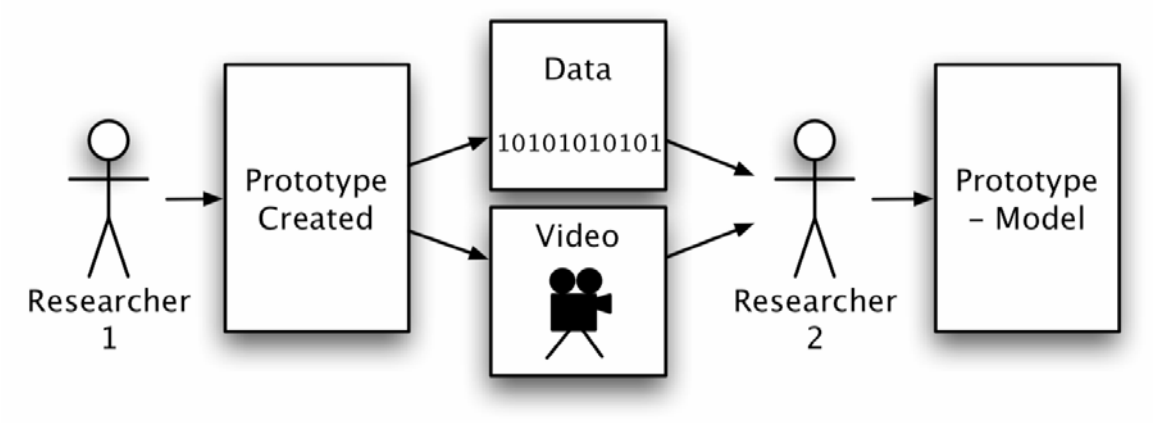

Figure 3: Testing our data collection and analysis plan, using the prototype

To give a more concrete example of the process followed by the second researcher, initial videotapes showed that ungulons had the capacity to change colour and might be one of three colours at any particular time- red, fuchsia and white. Videotapes also revealed that ungulons only turned fuchsia in the presence of predons. This led the researcher to hypothesise that this colour change was a reaction to perceived danger and that the reaction itself might also be perceived and used as a signal by other ungulons. Consequently, data was requested about colour of ungulons, location of ungulons and predons, orientation of ungulons to other ungulons and distance between ungulons, predons and other ungulons at each time step of the prototype run, both in the presence and in the absence of the predons. Data was obtained from the prototype by the first researcher and then supplied to second researcher, thus maintaining the integrity of the prototype.

As is the case when actually modelling, the second researcher was able to return to the first researcher if the currently available videos or data proved inadequate to test the hypotheses required to obtain the parameter settings, and the second researcher did in fact make further requests on several occasions. This was considered analogous to returning to the field to gather more data or doing a further literature review to determine if that data were available in the literature. Several iterations of this were required before the second researcher was able to begin generating a prototype-model.

As a result of this process we have now realized that we will need to put more emphasis on recording spatial variables than we had originally planned, during data collection, and as a result, will need to use a video analysis program like Tracker 3D [Grunbaum 2004] to obtain the spatial data required to construct a convincing model. Given the large amounts of data generated during the prototype modelling, and given that similar amounts and type of data would be generated by the video analysis, we further realized, during the data analysis phase, that storing the data in a customized database and performing some basic calculations on the data while it was being entered into the database would be to our advantage during data analysis.

As a result, during the data analysis test, we designed a MySQL database that would accommodate the required data. Placing the data in a database also allowed us to use SQL queries to test our hypotheses about the working of the prototype. Generally speaking, two main types of SQL queries were required. The first were queries that considered a behaviour or model of property of interest and then provided information about the conditions of the model one time step prior to these properties or behaviours. This sort of query was useful for seeking out possible patterns or causes of a particular behaviour or property of interest. The second were queries that tested hypotheses about causes by considering a particular property or behaviour and then providing information about the conditions of the model one time step after the property or behaviour was present, to determine if this property or behaviour consistently caused a second property or behaviour of the model in the time step after it was present.

As a result of the prototype testing, we plan to use our now established MySQL database, along with its supplementary Perl programs, to analyse the actual data for our caribou model. Based on our prototype data analysis experience we are further considering the use of genetic algorithms to assist in the data analysis which will allow us to better extract non-obvious patterns from the large amounts of data we expect to gather. We plan to first test the use of these genetic algorithms on the prototype data to determine how useful they will be in analysis of the actual data.

4. Conclusion

Use of IBSEMs as a tool for explaining biological phenomena has had a somewhat varied history. After the initial excitement felt by biological modellers at the introduction of IBSEMs began to diminish, biologists began to realize that there were unique challenges as well as unique benefits associated with using IBSEMs to model aspects of nature. Now, diverse efforts are being made to find ways to meet these challenges and overcome them, thus allowing IBSEMs to continue their contribution to biology.

In this paper, we have suggested that it is appropriate to confront model complexities as soon as the modelling project begins. We suggest that rapid model prototypes can act as an important guide through these model complexities, when modellers are determining what their data and modelling requirements will be. We have also tried to demonstrate in this paper that effort required for the creation of such prototypes, and their use, is minimal when compared to the need to gather more field data or redesign the model at the end of the modelling process. Because of this, we believe that the adoption of rapid model prototyping as a general practice will lead to significantly better models in this field.

REFERENCES

[Fankhauser 2004] Fankhauser R., Enggist P., Simulation of alpine chamois Rupicapra r. rupicapra habitat use. *Ecological Modelling* 175 (3): 291-302, 2004.

[Grimm 1999] Grimm V., Ten years of individual-based modelling in ecology: what have we learned and what could we learn in the future? *Ecological Modelling* 115 (2-3): 129-148, 1999.

[Grunbaum 2004] Grunbaum, D., 2004. Tracker 3D: Movement Analaysis Software. On line at http://peduncleii.ocean.washington.edu/%7Et3d/Tracker3D/

[Harrington 1991] Harrington, F.H., Veitch AM., Short-term impacts of low-level jet fighter training on caribou in Labrador. *ARCTIC* 44 (4): 318-327, DEC 1991.

[Horejsi 1981] Horejsi, B.L., Behavioral-response of barren ground caribou to a moving vehicle. *ARCTIC* 34 (2): 180-185, 1981.

[Jepsen 2004] Jepsen J.U., Topping C.J., Modelling roe deer (Capreolus capreolus) in a gradient of forest fragmentation: behavioural plasticity and choice of cover. *Canadian Journal Of Zoology-Revue Canadienne De Zoologie* 82 (9): 1528-1541, 2004.

[Klein 2002] Klein, J., breve: a 3D simulation environment for the simulation of decentralized systems and artificial life. *Proceedings of Artificial Life VIII, the 8th International Conference on the Simulation and Synthesis of Living Systems*. The MIT Press, 2002.

[Letcher 1998] Letcher B.H., Priddy J.A., Walters J.R., Crowder LB., An individual-based, spatially-explicit simulation model of the population dynamics of the endangered red-cockaded woodpecker, Picoides borealis. *Biological Conservation* 86 (1): 1-14, 1998.

[Netlogo 2005] Netlogo Home Page. On line at: http://ccl.northwestern.edu/Netlogo/

[Resnick 1994] Resnick, M., *Turtles, Termites and Traffic Jams: Explorations in Massively Parallel Microworlds*. MIT Press, 1994.

[Reynolds 1999] Reynolds, J.H., Ford DE. Multi-criteria assessment of ecological process models. *Ecology* 80 (2) 538-553, 1991.

[Scotter 1995] Scotter, G.W., Influence of harassment by wolves, Canis lupus, on Barren-ground Caribou, Rangifer tarandus groenlandicus, movements near the Burnside River, Northwest Territories. *Canadian Field-Naturalist* 109 (4): 452-453, OCT-DEC 1995.

[Seymour 2004] Seymour A.S., Harris S, White P.C. L.Potential effects of reserve size on incidental nest predation by red foxes Vulpes vulpes. *Ecological Modelling* 175 (1): 101-114, 2004.

[Smith 1985] Smith, W.T., Cameron RD., Reaction sof Large Groups of Caribou to a pipeling corridor on the Arctic Coastal Plain of Alaska. *ARCTIC* 38 (1) 53-57, 1985.

[Turner 1993] Turner M., Wu Y., Romme W., Wallace L., A landscape simulation-model of winter foraging by large ungulates. *Ecological Modelling* 69 (3-4): 163-184, 1993.

[Turner 1994] Turner M., Wu Y., Wallace L., Romme W., Brenkert A., Simulating Winter Interactions Among Ungulates, Vegetation, And Fire In Northern Yellowstone Park. *Ecological Applications* 4 (3): 472-486, 1994.

[Wiegand 2004] Wiegand, T., Revilla E., Knauer F., Dealing with uncertainty in spatially explicit population models. *Biodiversity And Conservation* 13 (1): 53-78, 2004.

[Zollner 2005] Zollner P.A., Lima S.L., Behavioral tradeoffs when dispersing across a patchy landscape *Oikos* 108 (2): 219-230, 2005.

Water and solute movement in soils – concepts and models for migration phenomena apart from classical convection-dispersion equation

S. Klepsch
Institute of Soil Science
BOKU Vienna *
Peter-Jordan Strasse 82
A-1190 Vienna, Austria
+43-1-47654-3105
sabine.klepsch@boku.ac.at

M. H. Gerzabek
Institute of Soil Science
BOKU Vienna
Peter-Jordan Strasse 82
A-1190 Vienna, Austria

W. Loiskandl
Inst. of Hydraulics and Rural Water Management, BOKU Vienna
Muthgasse 18
A-1190 Vienna, Austria

P. Bossew
Division of Physics and Biophysics
University of Salzburg
Hellbrunner Strasse 34
A-5020 Salzburg, Austria

* in cooperation with ARC Seibersdorf research GmbH, Austria

ABSTRACT
Several concepts for describing water and solute movement in the unsaturated soil zone are reviewed. The addressed models are mostly extensions of the classical convection-dispersion equation. Solute transport modelling is a prerequisite for risk assessments, in order to account for relevant processes determining the fate of hazardous substances to groundwater. Moreover, it is a necessary tool concerning prediction of water and nutrient availability for plants. Emphasis is on nonequilibrium concepts being able to predict accelerated migration of solutes through soil.

KEYWORDS
Water flow and solute transport, unsaturated soil zone, nonequilibrium models.

1. Introduction

Solute transport processes in soils are determined by various interactions of physical, chemical and biological phenomena. Modelling of water and solute movement through the unsaturated soil zone is necessary to estimate risks such as groundwater contamination, and to evaluate extents of contaminated surface soils with regard to their function as plant habitat. Numerous concepts have been developed to describe migration processes based on the convection-dispersion equation (CDE), and including diverse terms accounting for e.g. sorption, decay, fixation of solutes, or sink and source terms. This paper solely deals with "physical" concepts for solute transport, that often lead to nonequilibrium (NE) phenomena, i.e. processes that cannot be explained with the simple convection-dispersion equation leading to uniform flow. Processes with regard to sorption are not considered, since discussed extensively in numerous papers.

The complexity of real soils can only be accounted for by considering an (almost) continuous manifold flow regimes, caused by heterogeneous geometric soil properties (e.g. particle/pore size distributions) and physico-chemical properties (clay content, hydrophobic regions etc…). In reality, the complexity may only be described by probability distribution functions, leading to a stochastic model of the soil system. The concepts discussed here can be interpreted as reduction of stochastic descriptions to deterministic models, for example by dividing a continuous distribution of pore sizes into two discrete modes representing two pore regions. However, stochastic concepts are also out of the scope of this review.

For physical concepts "preferential" flow is an important issue and therefore treated extensively. Preferential flow denotes rapid movement of water and solutes in the soil, bypassing the soil matrix. Thus residence time of solutes is lower than that predicted by the CDE. It can result in reduced availability of water and nutrients to plants, and also in accelerated transport of pollutants to the groundwater. It occurs due to nonuniform flow fields with widely different velocities. Preferential flow paths may persist over years/decades and soil organic carbon be enriched in them (stemming from larger input of root-derived C

and illuviation of dissolved organic carbon). Causes for preferential flow can be e.g. root channels, channels produced by the soil fauna, non-capillary sized macropores due to shrinking and cracking of soils, structured field soils, tillage operations, flow instabilities due to entrapped air or transport from fine to coarse textured soil layers. It also might appear at seemingly homogeneous course-textured soils (e.g. [Gerke van Genuchten 1993]). Besides macropore flow, gravity driven unstable flow generally occurs in context with sandy textures. The wetting front breaks into discrete fingers, thus getting unstable, when either the saturated hydraulic conductivity increases with depth, soil is water repellent, or air pressure builds up at the wetting front of infiltrating water [Nieber et al. 1999]. A good review of gravity fingering is also given by [Glass & Nicholl96]. Generally, heterogeneity appears at macroscopic scale (above the representative-element-volume(REV)-scale), e.g. for soils with spatially variable hydraulic parameters, but also at a scale smaller than the REV, e.g. in aggregated or textured soils [Gerke Vogel 1994]. To account for preferential flow, numerous concepts have been developed during the last decades. Concepts for multiple pore water velocity regions, models considering swelling and shrinking processes, calculation of vertical flow along macropore walls by kinematic wave equations assuming gravity flow, boundary layer flow theory implementing viscous flow, application of Poiseuille's equation, Green and Ampt or Philip infiltration models, or the Chezy-Manning equation for turbulent flow, are examples applied to explain flow in macropores. The concepts described in the following chapters cover two-region-, and gravity flow-models (chapter 2), and extended concepts for water content, pressure head and hydraulic conductivity in chapter 3, including theories regarding influence of surface active substances and temperature on surface tension of water and hydraulic conductivity. Concepts for modelling swelling/shrinking behaviour of soils, including pore scale- and empirical considerations, are discussed in the last chapter.

2. Multi-Region Models

2.1. Two-Region Models (CDE-Type Preferential Flow)

A widely used model to account for physical "non-ideal" behaviour represents the two-region approach. This model concept is also useful for aquifers with varying hydraulic conductivity K (e.g. low (immobile region) and high (mobile) K layers). The division into two regimes – in comparison to a one-region model representing an average regime – is responsible for nonideality in breakthrough curves BTCs (early initial breakthrough and "tailing") in many cases. The processes in the two-domain model can be divided into: advective-dispersive transport from the bulk solution to the boundary layer; film diffusion (diffusive transport across the adsorbed water, initially controls solute uptake); and intra-aggregate diffusion (pore- and/or surface-diffusion in the immobile domain, responsible for solute uptake for the majority of the reaction period - whereas "solid" diffusion, besides chemical NE reaction, is defined to cause sorption nonequilibrium). TNE can be described by [Brusseau Rao 1990]

(a) a lumped (effective) dispersion coefficient replacing the hydrodynamic dispersion coefficient in the transport equation
(b) an empirical first-order mass transfer equation: knowledge of the porous medium's structure is not necessary when a kinetic approach for diffusive transfer (two region model) is used. The medium then is divided into two domains with low and higher permeability, respectively. Physical NE is often modelled by such a two-region (dual-porosity) type formulation [van Genuchten Wierenga 1976]. Water flow can be described in both domains and exchange of water and solutes is calculated by a coupling term in the CDEs. The mobile-immobile approach is one example of these models where water flow in the region with low permeability is neglected; and
(c) diffusive transfer via Fick's law: in diffusion models film diffusion and diffusion within the aggregate account for solute transfer. The geometric description of the medium is important (concerning the impact of film diffusion of e.g. inorganic ions it is cited in [Sparks 1989] that – in experiments – energetic mixing reduces or eliminates this effect. Film diffusion may be rate-limiting for the initial fast sorption but probably not important in long-term phenomena [Pignatello Xing 1996]).

For example, [Gerke van Genuchten 1993] used a dual porosity-model to calculate preferential flow for a given pore size distribution. Since many models are limited to conditions when flow and storage are negligible in one of the pore systems or when a simplified matrix block geometry (which is rarely available) has to be assumed, Gerke and van Genuchten distributed the medium of their dual-porosity model into two subregions – a macropore or fracture network and a less permeable pore system of aggregates or rock matrix blocks. In both pore systems calculation of water flow and solute transport is possible. Water and solute transfer between the two domains is given by quasi-empirical first-order rate equations. Thus the porous medium, from a macroscopic point of view, employs two flow velocities, pressure heads, water contents and solutions. Furthermore, two water retention functions and three hydraulic conductivity functions are presumed to characterise the dual-porosity system: $K_f(h_f)$, $K_m(h_m)$ as hydraulic conductivities of "fracture network" and matrix system, respectively (h…pressure head), and $K_a(h)$ as effective hydraulic conductivity for the exchange of water between the two pore systems (f...fracture-, m...matrix-pore region). One-dimensional vertical water flow in the fracture and matrix pore systems of a dual-porosity system is given by

$$C_f \frac{\partial h_f}{\partial t} = \frac{\partial}{\partial z}\left(K_f \frac{\partial h_f}{\partial z} - K_f \right) - \frac{\Gamma_w}{w_f} - S_f , \quad (1)$$

$$C_m \frac{\partial h_m}{\partial t} = \frac{\partial}{\partial z}\left(K_m \frac{\partial h_m}{\partial z} - K_m \right) + \frac{\Gamma_w}{1 - w_f} - S_m , \quad (2)$$

$$\Gamma_w = \alpha_w \cdot (h_f - h_m) \quad (\text{with } \alpha_w = \alpha_w * K_a ;\ \alpha_w * = \frac{\beta^*}{a^2} \gamma_w) \quad (3)$$

where t = time, $C_{f,m}$ = specific soil water capacity ($C = S_w S_s + \varepsilon \frac{\partial S_w}{\partial h}$, with S_s = specific storage coefficient and S_w = degree of fluid saturation), Γ_w = space- and time-dependent exchange term for water transfer (subscript w) between the two pore systems, w_f = volumetric weighting factor ($=V_{t,f} V_t^{-1}$; $V_{t,f}$ = total volume of fracture pore system, V_t = total volume), α_w = first order transfer coefficient for water, K_a = function of the "average" pressure head at interface between the two regions, β^* = factor representing the geometry of the aggregates, a = distance from the centre of a fictitious matrix block to the fracture boundary, γ_w = empirical coefficient, and $S_{f,m}$ = sink term for root water extraction. Geometrically based parameters will mostly be difficult to identify, and β, a and γ_w could be lumped into an effective hydraulic conductivity. Γ_w can also be expressed proportional to the difference of effective water contents in the fracture and matrix region, respectively, instead of pressure heads (and thus not requiring retention functions for the nonlinear pressure head/water content-relations in both regions) [Simunek et al. 2003].

Accordingly solute transport including linear adsorption and first-order decay in a dual-porosity medium leads to the following equations:

$$\frac{\partial}{\partial t}(\theta_f R_f c_f) = \frac{\partial}{\partial z}\left(\theta_f D_f \frac{\partial c_f}{\partial z} - q_f c_f \right) - \theta_f \mu_f c_f - \frac{\Gamma_s}{w_f} \quad (4)$$

$$\frac{\partial}{\partial t}(\theta_m R_m c_m) = \frac{\partial}{\partial z}\left(\theta_m D_m \frac{\partial c_m}{\partial z} - q_m c_m \right) - \theta_m \mu_m c_m - \frac{\Gamma_s}{1 - w_f} \quad (5)$$

where $c_{f,m}$ = solute concentration, $D_{f,m}$ = dispersion coefficient, $\mu_{f,m}$ = first order decay coefficient in the fracture and matrix region, respectively, Γ_s = solute (subscript s) mass transfer term, and $R_{f,m}$ = the dimensionless retardation factors given as $R_f = 1 + f\rho_b k/\theta_f$, $R_m = 1 + (1-f)\rho_b k/\theta_m$; ρ_b = bulk density**,** k = adsorption coefficient, f = fraction of sorption sites in contact with fractions, or mobile water (the factor f does not appear in the original paper of [Gerke van Genuchten 1993], apparently it has been lumped into the adsorption coefficient k). Γ_s is assumed to be influenced by convection as well as diffusion/dispersion (the latter being represented by the third term on the right-hand side of the next equation):

$$\Gamma_s = (1-d)\Gamma_w \Phi_f c_f + d\Gamma_w \Phi_m c_m + \alpha_s \cdot (1 - w_f)\theta_m (c_f - c_m) \quad (6)$$

with $d = 0.5\left(1 - \frac{\Gamma_w}{|\Gamma_w|}\right)$, $\Gamma_w \neq 0$, $\Phi_f = w_f \frac{\theta_f}{\theta}$, $\Phi_m = (1 - w_f)\frac{\theta_m}{\theta}$, and $\alpha_s = \frac{\beta}{a^2} D_a$, Γ_w = exchange term for water, *d* = dimensionless coefficient determining the direction of flow between the two pore systems, $\Phi_{f,m}$ = dimensionless coefficients relating the solute concentrations of the fracture and matrix pore system to the unit solute mass of the bulk soil, α_s = solute transfer coefficient, D_a = effective ionic or molecular diffusion coefficient of the matrix block near the interface.

The widely used "mobile-immobile" model calculates flow only in the mobile pore region and is thus a simplification of the equations shown above. For this concept, advective flow is negligible in the immobile domain, whereas in the mobile one solute transport is determined by advection and dispersion (diffusion). Within the scope of this two region model, a physically based estimate for the mass transfer coefficient α was presented by [Rao et al. 1980a,b], eliminating the disadvantage of the model, where this parameter otherwise can only be determined by curve fitting. [Rao et al. 1980b] found that tailing in BTCs through curves increased with increasing aggregate size and/or pore-water velocity for a given column length. Aggregate size determines mean diffusion path length and pore-water velocity, and column length determines time available for solute transfer between inter- and intra-aggregate pore-water regions. Based on the above equations, [Selim et al. 1999] computed the mass transfer coefficient as $\alpha = \Gamma \cdot \frac{2.6 \cdot D_e (1-F)\theta}{l^2}$ where Γ = a time-dependent variable that was estimated from [Rao et al. 1980a,b], F = fraction of mobile water content ($=\theta_m/\theta$), and l = width of cubic aggregates. [Brusseau Rao 1990] discuss in their review extensions of models such as the one by [Rao et al. 1980b] with e.g. terms accounting for film-transfer resistance (diffusion through a boundary "film" around the particle), treatment of non-spherical

geometries, or representation of aggregate size distributions by "equivalent aggregates". Regarding the impact of aggregate size distribution it can be stated that an increased number of smaller than average size aggregates (higher external surface area) cause a delay of BTC, whereas an increased number of larger than average size aggregates (higher individual volumes) lead to increased tailing.

A good comparison of dual porosity/permeability models and also the various descriptions the mass transfer factors is presented in [Simunek et al. 2003]. [Zurmühl Durner 1996] combined bimodal functions for hydraulic properties with a dynamic treatment of the factor f* (fraction of water filled pore space) in the mobile-immobile model. In doing so they were able to qualitatively recalculate results of a preferential transport experiment (from literature) in structured soils. In this case f* is responsible for a constant ratio of total hydraulic conductivity and dependent on both total water content and shape of the K(θ)-function. The variable immobile water content is hereby defined by $K(\theta_{im})/ K(\theta) = \varepsilon$ (a constant to be determined by a steady-state calibration experiment). [Flühler et al. 1996] discussed various concepts of lateral mass exchange between two discrete regions (as in the case of the two-region or double porosity models discussed before) and also multiple flow regions. The authors outlined the improvement of prediction of vertical solute distribution by incorporation of advective and diffusive water and solute exchange in the horizontal plane. For multiple flow regions, mass transfer is for example modelled by introducing velocity-coordinates, or pore class velocities and a phenomenological coefficient lumping the stochastic distribution of lateral average distances of pore clusters with different flow velocities, but also by a structural coordinate linking flow regions of different longitudinal average velocities. Also a mixing cell model subdividing soil into multiple flow regions representing various pore-size classes is noted, along with a generalised concept for arbitrary number of pore classes [Durner Flühler 1996]. With the latter concept the domains are arranged on a virtual one-dimensional structural coordinate ξ (without geometric interpretation) orthogonal to the direction of mean water flow. Flow velocity distribution over the pore domains is represented by the derivative of the macroscopic conductivity function, and thus bypass flow in macropores can be modelled if water redistribution along ξ is considered to be a slow process. Transport in flow direction within each domain was modelled by convection and diffusion, and solute mixing between the domains by convective-dispersive transport along ξ. Transport equation and macroscopic solute flux are given by (integration is over all water filled pores from zero to the volumetric water content θ(x))

$$\frac{\partial c}{\partial t} = -\nabla\left(v \cdot c - \tau D_0 \nabla c\right) - \frac{\partial}{\partial \xi}\left(w \cdot c - \alpha_\xi \frac{\partial c}{\partial \xi}\right) \qquad \text{and} \qquad J(x) = \int_0^{\theta(x)} \left[v(x,\xi)\cdot c(x,\xi) - D_0 \nabla c(x,\xi)\right] d\xi \tag{7}$$

where w = convective water flux in structural axis, α_ξ = domain interaction coefficient, and where v, c and w are functions of spatial and structural position. One-dimensional numerical modelling of transport of a solute pulse through soil columns under unit-gradient conditions revealed gradual change from convection-dominated to convective-dispersive transport, being slow for a wide pore-size distribution, small intensity of lateral mixing, and high water saturation. As noted by [Flühler et al. 1996], a disadvantage of these "interacting flow region" models is the problem of parameter identification, although they are capable of reproducing nearly any shapes of breakthrough curves or depth distributions of solute concentration.

When enhanced tailing by breakthrough curves occurs, a three-region model – or dual intra aggregate porosity model – may be more advantageous than a two-domain model. It considers an additional diffusive transfer between mesopores and micropores, since the aggregate itself is assumed to consist of two porosity regions. Nevertheless such multiple-region model require even more parameters which can hardly be measured in field soils. Moreover, other concepts might be required than those based solely on the CDE in order to account for accelerated flow in macropores which will be discussed in the following paragraphs.

2.2. Gravity Flow in Macropores

A concept implemented in the one-dimensional model MACRO [Jarvis 1991], [Jarvis 1994] is based on division of the simulated region into two flow domains: a high-conductivity/low porosity macropore domain coupled to a low-conductivity/high porosity domain for the soil matrix (CDE-type). Although this approach is also a two-region model, flow in macropores is treated differently. Since in this domain water retention curves are usually not known with sufficient precision, water movement is modelled by gravity flow. The hydraulic conductivity function is described by a simple power law expression of the degree of saturation in the macropores S_{ma} (the numerical equivalent of the analytical kinematic wave approach [Germann 1985]; total porosity in each soil layer is partitioned into micropores (mi) and macropores (ma) at a given water content (θ_b) and potential, characterised by a 'boundary' hydraulic conductivity K_b):

$$K_{ma} = K_{s(ma)} S_{ma}^{m*} \tag{8}$$

with K_{ma} = macropore hydraulic conductivity, $K_{s(ma)}$ = saturated hydraulic conductivity in macropores, $S_{ma} = \theta_{ma}/\varepsilon_{ma}$, θ_{ma} = macropore water content, ε_{ma} = macroporosity equivalent to the saturated water content θ_s minus θ_b, and m^* = empirical exponent. Thus a scaled macropore water content is used in the above equation, as opposed to the original model by [Germann

1985] where flux density q was given by $q = b\theta_{ma}^{m^*}$ and kinematic wave velocity by $C = \partial q/\partial\theta_f$ (as cited in [Simunek et al. 2003].

Water exchange is modelled by $S_w = \left(\frac{3\,D_w\,\gamma_w}{d^2}\right)(\theta_b - \theta_{mi})$ where d = effective diffusion pathlength (i.e. half aggregate width), D_w = effective water diffusivity ($D_w = \left(\frac{D_{\theta_b} + D_{\theta_{mi}}}{2}\right)S_{ma}$, $D_{\theta b}$ and $D_{\theta mi}$ = water diffusivities at θ_b and θ_{mi} , respectively; S_{ma} is introduced to account for incomplete wetted contact area between the two pore domains), and γ_w = scaling factor introduced to match approximate and exact solutions to the diffusion problem. Water exchange is driven by the difference between water content at the boundary micro-/macropores (saturated water content of the micropores), when the latter conduct water, and the average water content of micropores. In contrast, water exchange in the former described dual porosity model was based on pressure head differences (see equation 3) which might be numerically more unstable due to multiplication of nonlinear terms [Simunek et al. 2003]. The mass transfer term (U_e) of solutes between micropores and macropores is given by the following combined diffusion and mass flow formula

$$U_e = \left(\frac{3\,D_e\,\theta_{mi(m)}}{d^2}\right)(c_{ma} - c_{mi}) + S_w\,c' . \qquad (9)$$

Depending on the direction of water flow S_w the prime notation indicates either macro-pore or 'accessible water' in micropores (i.e. c' = c_{ma} if water flows from macropores to micropores), and D_e is an effective diffusion coefficient ($D_e = D_0 \cdot f^* \cdot S_{ma}$, f^* = impedance factor). The respective solute amounts stored in macropores and micropores, A_{ma} and A_{mi} are

$$A_{ma} = c_{ma}\theta_{ma} + f\rho s' \qquad (10)$$

$$A_{mi} = c_{mi}\theta_{mi(m)} + (1-f)\rho s' \qquad (11)$$

where f = mass fraction of solid material in contact with water in macropore domain and ρ = bulk density; a detailed definition of the model besides numerical techniques can be found in the technical description of MACRO.

Flow in macropores (such as cracks and root channels) principally depends upon surface boundary conditions, but not on water content unless the soil is close to saturation [Chen Wagenet 1992]. These authors described hydraulic conductivities of saturated macroporosity and of partially saturated macroporosity regions based on hydraulics of flow in tubes and channels. Within the defined range of macroporosity of 15 to 2500 μm the Reynolds number (Re) might increase for a liquid filled tube (the definition of $Re = U \cdot d/\nu_k$ is used, with U = average flow velocity, d = equivalent diameter of the macropore analogous to a tube and the kinematic viscosity of water $\nu_k = \nu_d/\rho_w$, with ν_d = dynamic viscosity of water and ρ_w = density of water). This indicates change from laminar (for Re below 1-10) to non-laminar (non-linear laminar and turbulent) flow behaviour. Applying the Hagen-Poiseuille equation for average velocity and taking Re = 3 as approximate upper limit for laminar flow a criteria radius (100 μm) between laminar and non-laminar flow was obtained by the authors. Above this radius the Hagen-Poiseuille equation cannot be applied. They suggest that for $Re > 3$ the Chezy-Manning equation approximately describes flow velocity in the tube. For modelling horizontal water movement from macropores into the soil matrix the Philip infiltration formula can be used.

Remark: [Germann 1990] presented a boundary layer infiltration model based on the kinematic theory, decoupling hydrodynamic dispersion of soil moisture from that of capillary potential. A "cubic" law for laminar flow of a thin water film along the walls of a fissure was presented and compared to hydraulic conductivity appearing in Darcy's law, for unit gradient flow conditions, assuming that seepage is dominated by flow in the widest pores. Viscosity is the only force counteracting flow-driven gradients (capillarity) in this model. Regarding applicability of laminar shear flow in porous media, [Germann 1990] also noted that at a critical waterfilm thickness F_{crit} can be expected above which turbulent flow might occur. The estimated Re (> 1000) corresponds to a F_{crit} of 1 mm. Nevertheless he added that roughness at the liquid-solid interface and tortuosity had been neglected in his study (note that [Chen Wagenet 1992] as cited above, wrote about a Re number three orders lower to define an approximate upper limit for laminar flow). Moreover it was noted that „a priori" no geometrical descriptions of preferred flow paths and no minimum fissure width were needed for the development of boundary layer approach to infiltration, and that extent and continuity in direction of flow seem to be as important as such a minimum width.

3. Extended Concepts Regarding Water Content, Pressure Head and Hydraulic Conductivity

3.1. Decoupling of Water Content and Pressure Head

Usually instantaneous equilibrium between water content (θ) and pressure head (h), represented by a "water retention function" θ(h), is assumed to exist while solving the Richard's equation for water flow through unsaturated media. [Ross Smettem 2000] presented a simple approach ("kinetic water content equilibration model") to account for nonequilibrium between the actual water content and the water content of the retention curve – a phenomenon resulting in deeper penetration of infiltrating water than compared to classical infiltration-theory-predictions. They combined Richard's equation with a first-order time constant equilibration model of infiltration into a hypothetical structured soil, requiring only one additional parameter. Due to this formulation, θ is decoupled from h. In order to account for macroporosity an exponential K(h) function was added to the hydraulic conductivity function. Defining $\theta_e(h)$ as (equilibrium) soil water retention, the change of actual water content θ with time ($f(\theta,\theta_e)$) is modelled as (k = discrete time step, τ = equilibration time, and $\Delta t = t^{k+1}-t^k$)

$f\left(\theta,\theta_e^{k+1}\right) = \left(\theta_e - \theta\right)/\tau$, and using the approximation $\Delta t = \int_{\theta_k}^{\theta_{k+1}} \frac{d\theta}{f\left(\theta,\theta_e^{k+1}\right)}$ leads to

$$\theta^{k+1} = \theta^k + \left(\theta_e^{k+1} - \theta^k\right)\cdot\left[1 - \exp\left(-\Delta t/\tau\right)\right]. \qquad (12)$$

[Ross Smettem 2000] successfully applied this model for downward flow through cores of a structured field soil. [Simunek et al. 2003] also note a disadvantage of this concept that the level of preferential flow is independent of the current θ.

3.2. Extensions of θ(h) / K(h) Relations

Interaction of all pores in the porous medium is assumed with the most common functions for hydraulic conductivity (e.g. van Genuchten-Mualem equations). Thus independent composite hydraulic distributions can be used to describe preferential water flow where some parts of the pore space is bypassed. Nevertheless for solute preferential flow it is necessary that additionally at least two different porous domains are regarded for, otherwise again a uniform flow regime will result (because in a one-region model average pore water velocity is determined by *total* water content). [Ross Smettem 1993] calculated soil hydraulic properties by summing over several overlapping pore-size distributions. They added exponential functions to water retention curves and hydraulic conductivity functions to model macropore contribution to water flow (as compared to [Ross Smettem 2000] where only for the latter one such a term was added). Another example for multi-modal pore systems, assuming van Genuchten-, Mualem-type relations for water retention and hydraulic conductivity was presented by [Durner et al. 1999] (cited in [Simunek et al. 2003], where also the respective equations are given).

Bimodal retention curves had been used by [Mohanty et al. 1997]. The concept has been developed for calculation of NE-water flow and solute transport in macroporous soils for situations near saturation, where gravity flow dominates. The equations for non-capillary hydraulic conductivity function above a critical pressure head h* (where flow changes from capillary dominated to gravity driven) are computed as

$$K_{nc}(h) = K^* + K^*\left(\exp^{(h-h^*)\delta} - 1\right) \quad \forall \quad h^* < h \le 0 \qquad \text{and} \qquad K_{nc}(h) = K^* + K^*\left(\exp^{(-h^*)\delta} - 1\right) \quad \forall \quad h > 0 \qquad (13)$$

where δ = fitting parameter representing effective macroporosity or other structural features contributing to non-capillary dominated flow, K_{nc} = hydraulic conductivity for non-capillary dominated flow domain, and K* = hydraulic conductivity corresponding to h^*. For $h \le h^*$ the original van Genuchten retention and conductivity functions are employed.

A simple but useful model for enhanced unsaturated hydraulic conductivity at conditions near saturation, as employed in the simulation model CATFLOW [Maurer 1997], is briefly shown. Soil macropores are very important for the whole migration process through the soil profile, and thus also infiltration is influenced by these pores to a great extent. A big problem is that their exact geometry can hardly be defined. Nevertheless, alternative models for calculating infiltration processes into macropores have been proposed (e.g. [Beven Germann 1981], [Bronstert 1994], [Germann Beven 1985]). When an infiltration surplus exists, a macropore-soil water content (in assumed vertical tubes) is adjusted, which moves into depth. A part of the macropore water content is adsorbed by the walls of the soil matrix. The models of [Beven Germann 1981] were compared to a more simple model of enlarged saturated hydraulic conductivity (K_s) in the macroporous zone by [Merz 1996]. Only slight differences between the model of [Beven Germann 1981] and calculation of an enhanced K_s could be investigated. In CATFLOW the following concept is used:

$$K_s^* = K_s\cdot\{1 + (F_{KS} - 1)\cdot(\theta - \theta_0)/(\theta_s - \theta_0)\} \qquad (\theta_0 < \theta < \theta_s) \qquad (14)$$

where K_s* = enhanced saturated hydraulic conductivity, θ_0 = limiting value of water content, and F_{KS} = macroporosity factor (to be defined at each knot of the simulated region).

3.3. Impact of Surfactants and Temperature on Surface Tension of Water

One very important effect is treated in the following paragraphs: the reduction of surface tension due to certain solutes. This effect is often neglected in standard literature and simulation tools. Nevertheless it can considerably influence water flow and also solute transport characteristics in unsaturated soil.

Surfactants (surface-active agents) used for remediation purposes but also many organic contaminants can decrease the surface tension of water and in turn also soil water retention curves. [Tschapek et al. 1978] estimated the surface tension σ of pure water as compared to that of soil solution. They investigated that σ of soils lacking organic matter (OM; subsoil and ignited surface soils) is similar to σ of pure water, whereas the investigated significant decrease of σ in surface soils might stem from the nature of OM. Reduction of σ due to humic (HA) and fulvic acids (FA) dissolved in water was also measured by [Chen Schnitzer 1978]. Furthermore a σ–decrease of the HA and FA solutions with increasing pH was investigated (explained by increased dissociation of acidic functional groups at higher pH resulting in formation of anionic hydrophilic groups), besides significant linear and inverse correlation between total HA/FA-acidity and σ. The authors suggested that at higher pHs presence of FA and HA improved soil wettability, but that at acidic and neutral pH and HA being predominant, water repellence was enhanced, and if FA occurred in sufficient amounts it could dissolve in water and improve wettability. A lowered σ due to soil surface active substances (SAS; in part soil humus and humic acid) considerably affects flow and solute transport in unsaturated porous media. Spreading of SAS is determined by its own properties and that of the underlying liquid [Tschapek Boggio 1981]. They review that a tangential force exerted by migrating SAS on the liquid influences flow behaviour of the underlying liquid, but is restricted to interfacial regions and should not affect bulk flow. Driving force for the spreading process is hypothesised as the gradient of the film disjoining pressure. Generally a non-uniform distributed surfactant monolayer on the free surface of a liquid (on an interface separating two non-miscible liquids) leads to gradients in surface tension creating shear stresses. Flow in the underlying liquid due to σ-gradients originating from concentration gradients is commonly known as Marangoni flow, see e.g. [Molenkamp98], whereas thermocapillarity denotes flow due to σ-gradients originating from temperature gradients. A counteracting process is the so-called Plateau-Marangoni-Gibbs effect, because when SAS are moved with the enhanced flow, a concentration gradient occurs, again resulting in a σ-gradient contrary to the movement.

[Henry et al. 1999] used a soluble and an insoluble surfactant (myristyl alcohol and butanol, respectively) to study the solubility effects on flow by a series of horizontal column experiments. They showed that myristyl alcohol induced σ-reduction was mainly limited to the original source zone and that a monolayer coverage is needed for significant σ-reduction. In contrast, butanol could depress σ significantly also at low concentrations, therefore the zone of depressed σ extended farther into the initially solute-free zone than in the case of myristyl as solute. Thus they demonstrated that surfactants need not form a condensed solid film at equilibrium spreading pressure π_e to be effective water movers.

[Renshaw et al. 1997] studied the effect that efficiency of surfactant enhanced remediation is limited by induced changes in physical characteristics of porous media due to sorption of the surfactant, leading to reduced permeability and altering the retardation of organic contaminants. The impact of surfactants depends on the concentration: below the critical micelle concentration (CMC) they exist as monomers with minimal effects on solubility of most organic compounds, whereas in the order of CMC lipophilic moieties of the monomers form micelles consisting of a hydrophobic nonpolar interior (thus attractive for nonpolar molecules and enhance apparent solubility of e.g. NAPLs) surrounded by a hydrophilic mantle. Furthermore, above CMC, the mobility of NAPLs can also be increased due to a reduced σ between organic and aqueous phases. The effect of σ-reduction can be counterintuitive in that pressure head can *increase* substantially while water content decreases due to presence of a surface tension depressing compound, as shown by [Smith Gillham 1999] for their sand column experiments (length: 2 m, boundary conditions: *constant flux* at top surface, water table 5 cm above column base). After butanol solution was applied and in order to keep constant flow, water content θ increases to provide enough flow to offset effects of higher υ, i.e. flow resistance. The authors argue that due to the higher viscosity of the solution, hydraulic conductivity K is lower than K of water at the same θ. [Smith Gillham 1994] earlier investigated by numerical modelling two effects when surfactants are present: a depressed capillary fringe due to lower σ (the air-entry pressure is smaller in this case) and large unsaturated flow perturbation associated with σ-changes within the solute front (see also [Henry Smith 2002]). In their numerical model, [Smith Gillham 1999] implied a pressure head scaled by relative surface tension:

$$h^*(\theta, c_0) = \frac{\sigma_0(c_0)}{\sigma(c)} h(\theta, c) \tag{15}$$

where h = measured pressure head at θ and concentration c, and h* = calculated scaled pressure head at the same θ and

reference concentration c_0, σ = surface tension at concentration c and σ_0 = surface tension at the reference concentration. They used the following relationships for surface tension:

$$\frac{\sigma}{\sigma_0} = 1 - b \cdot \ln\left(\frac{c}{a} + 1\right) \tag{16}$$

with a, b = compound specific constants, and for kinematic viscosity:

$$\frac{\upsilon(c)}{\upsilon_0(c_0)} = 1 - e \cdot \ln\left(\frac{c}{d} + 1\right) \tag{17}$$

where υ = kinematic viscosity at concentration c, υ_0 = kinematic viscosity at the reference concentration, and d, e = empirical (fitting) constants (in [Smith Gillham 1994] the effect of concentration-dependent υ was not regarded for).

The unsaturated hydraulic conductivity was scaled by the ratio of the concentration dependent relative viscosity:

$$K(\theta, c) = \frac{\upsilon_0(c_0)}{\upsilon(c)} K(\theta, c_0) \ . \tag{18}$$

[Smith Gillham 1999] investigated that lower σ has no obvious impact on residual θ or rewetted saturated θ, but causes a shift in the retention curve (volumetric θ versus pressure head relation) along the pressure head axis. Experimental and modelling results concerning the impact of dissolved organic carbon (DOC) on σ as function of concentration and weathering of the DOC extract was presented by [Totsche 2001], applying the previous equations for rescaling pressure head by σ and the relationship used by [Smith Gillham 1999]. [Totsche 2002] described the representation of surface activity of dissolved and colloidal phase organic carbon (DCOC) by a scaling factor within the water retention characteristics. The effect of DCOC on water flow and transport of nutrients and contaminants was shown.

In conclusion surfactants may considerably effect water flow and solute transport in porous media due to influence on flow driven by hydraulic head gradients, solute hydrodynamic dispersion, dependence of hydraulic conductivity on moisture content and viscosity, the hysteretic nature of moisture characteristic curves, dependence of capillary pressure on σ and concentration-dependent surfactant effects on σ [Henry Smith 2002].

Surface tension is not only a function of surface-active agents but also of temperature T and pH. [Philip de Vries 1957] studied pressure head as function of σ-changes associated with changes in temperature T. [Hopmans Dane 1986] investigated hydraulic properties under nonisothermal conditions. The above mentioned shift in retention curves can also be caused by changes in temperature. At increasing T hydraulic conductivity decreases since water amount at a given pressure head decreases. Counteracting, hydraulic conductivity increases because viscosity of liquids decreases due to decreasing cohesion (i.e. the force of attraction between two similar materials, which predominates in liquids; for explanation adhesion is the force of attraction between two unlike materials - the first molecular water layer in the soil is held by strong adhesive forces). More insight into the respective theory is given by e.g. [Hopmans Dane 1986], [Schubert 1982], [Karkare Fort 2002], [Grant 2000] or [Grant Bachmann 2002].

4. Modelling of Swelling Soils

The classical CDE might also not be a sufficient description of water and solute movement for soils exhibiting pronounced swelling/shrinking behaviour, e.g. due to high clay content. One cause of shrinkage may be generation of cracks, leading to preferential flow. Some physically based but also empirical concepts accounting for this effect are listed below.

4.1. Pore Scale Considerations

Lamellar swelling, or the interactions between charged clay surfaces and aqueous solutions can also be described by the disjoining pressure (interfacial force per unit area) formalism (DLVO; e.g. [Derjaguin Landau 1941], [Verwey Overbeek 1948]. Within this theory the equilibrium potential μ is defined to be a function of water film thickness and consists of three components, attractive short-range van der Waals forces besides repulsive short-range hydration- and long-range electrostatic-forces. [Tuller Or 2003] propose a modelling framework for upscaling pore scale processes to constitutive hydraulic properties in swelling soils. The authors demonstrate that their approach can be generalised to capture evolution of pore space as function of hydration state, solution composition, soil texture and clay type. Basis is the description of the additive disjoining pressure as being in equilibrium with the chemical potential of the bulk water phase (ρ = density of water, and h = equilibrium interlamellar spacing): $\mu = \rho^{-1} \cdot [\Pi_e(h) + \Pi_m(h) + \Pi_h(h)]$, $\Pi_{e,\ m,\ h}$ = potentials due to electrostatic repulsion between adjacent diffuse double layers (DDL), due to van der Waal's attractive forces, and due to hydration forces, respectively (the latter being a repulsive force preventing collapse of the diffuse double layer at short separation distances);

$\Pi_e(h) = 64 n_0 kT\gamma^2 e^{-\kappa h}$, $\Pi_m(h) = A_{ssl}/6\pi h^3$, $\Pi_h(h) = K_h e^{-h/\lambda}$ (empirically), with k = Boltzmann constant, $\gamma = \tanh(-ze\psi_0/4kT)$ (z = ion valence, e = elementary charge, ψ_0 = surface electrostatic potential), κ = inverse Debye screening length (dependent on electrolyte properties) representing effective thickness of the DDL; A_{ssl} = Hamaker constant; K_h = interaction energy parameter, and λ = characteristic length.

Silt and sand textural constituents were represented by rigid spheres, interspaced by the clay "fabric", leading to two basic configurations: reductive (mesopore volume decreases with increasing μ) and expansive (clay fabric expansion increases mesopore size) unit cells. Unit cell water saturation as function of bulk chemical potential was calculated by investigating liquid configurations in mesopores. Saturated and unsaturated functions for hydraulic conductivity have also been derived, by assuming individual contributions of flow in ducts, liquid films and corners bound by liquid-vapor interfaces. For upscaling to sample- and profile scales the authors plan to consider statistical representations of mesopores and grain sizes; spatial distributions of clay domains; sample position in soil profile to account for overburden and confining stress; and also the behaviour of the near surface layer with formation of crack networks, based on the work of [Chertkov 2000].

4.2. Hybrid Mixture Theory

Regarding modelling of swelling soils some other sophisticated theories have been developed, for example a theory by [Murad et al. 1995], and [Murad Cushman 1996] , [Murad Cushman 2000]. They used a *hybrid mixture theory* to upscale the colloids with vicinal water to form mesoscale swelling particles. An asymptotic expansion technique was applied to homogenise mesoscale particles and bulk phase water. In this way the macroscale solid phase was represented by a porous matrix consisting of swelling porous particles. Transport processes in clay soils, as opposed to non-swelling soils (silts and sands), are determined by water-mineral interactions to a high extent. Hydrated clusters of clay platelets form a bulk of platelets and vicinal adsorbed water, swelling under hydration and shrinking under desiccation. The properties of vicinal water vary with distance from the mineral surface since modified by hydration forces in the interlamellar spaces (e.g. [Grim 1968]). In the multiscale models with connected and disconnected bulk phase water [Murad Cushman 1996], clay minerals, vicinal water and bulk water were treated as separate phases to enable modelling of swelling.

4.3. Coordinate Transformation

[Garnier et al. 1997] modelled three-dimensional deformation and one-dimensional water flow in swelling/shrinking soils by applying a coordinate transformation in order to calculate different extents of deformation in vertical and lateral direction. When using a coordinate transformation, Richards equation is also applicable in swelling soils, as reviewed in their article (a coordinate frame fixed relative to the soil phase is used for the generalised water flow equation with such a transformation). Starting from the Richards equation

$$\frac{\partial(\rho_w \theta_w)}{\partial t} = \nabla \cdot (\rho_w \mathbf{K}_w \nabla \Phi) \tag{19}$$

where ρ_w = water density, θ_w = volumetric water content, $\mathbf{K}_w$ = hydraulic conductivity tensor and Φ = total water potential, description of the water flow in swelling soils in a coordinate frame ("Lagrangian") associated with the solid phase leads to

$$\rho_d \frac{\partial\left(\frac{\rho_w \theta_w}{\rho_d}\right)}{\partial t} = \nabla_s \cdot \left(\rho_w \mathbf{K}_{w/s} \nabla_s (\Phi) \mathbf{F}_s^{-1}\right) \mathbf{F}_s^{-1} \tag{20}$$

where ρ_d = dry bulk density, $\mathbf{K}_{w/s}$ = hydraulic conductivity tensor relative to the solid phase, subscript s indicates spatial derivatives with respect to Lagrangian coordinates, Φ = total water potential but with an overburden potential Ω included ($\Phi = h - z + \Omega$), and F_s = transformation gradient tensor with the components $F_{s,ij} = \partial x_i / \partial X_j$ (with x_i, X_j = spatial and material coordinate, respectively). With the relations $\vartheta = \theta_w \cdot (\rho_s/\rho_d)$ and $e = \rho_s/\rho_d - 1$ (with ρ_s = specific density of soil solids), the water flow equation can be expressed by

$$\frac{1}{1+e} \frac{\partial(\vartheta)}{\partial t} = \nabla_s \cdot \left(\rho_w \mathbf{K}_{w/s} \nabla_s (\Phi) \mathbf{F}_s^{-1}\right) \mathbf{F}_s^{-1} . \tag{21}$$

An elementary soil volume dV (=dXdYdZ) undergoing a deformation to dv (= dxdydz), yields $dv = \left(1 + e_r \big/ 1 + e\right) dV$, with the void ratios e_r and e of the elementary soil volumes dV and dv, respectively. Volume changes by using a dimensionless geometry factor r_s, being defined in z-direction, leads to $\left(1 - (dV - dv)\big/dV\right) = \left(1 - (dZ - dz)\big/dZ\right)^{r_s}$. The following relations for the changes in the spatial coordinates x, y, z are proposed by [Garnier et al. 1997], assuming isotropic soil deformation in directions

perpendicular to the z-axis, but anisotropic otherwise:

$$dx = dX\left(\frac{1+e}{1+e_r}\right)^{\frac{1}{2}\left(1-\frac{1}{r_s}\right)},\ dy = dY\left(\frac{1+e}{1+e_r}\right)^{\frac{1}{2}\left(1-\frac{1}{r_s}\right)},\ dz = dZ\left(\frac{1+e}{1+e_r}\right)^{\frac{1}{r_s}} \tag{22}$$

corresponding to $F_{s,11}$, $F_{s,22}$, $F_{s,33}$, respectively (the non-diagonal elements of F_s are equal to zero), and X, Y, Z = material coordinates. For the one-dimensional water flow simulations the swelling curve was calculated by the model of Braudeau. This model accounts for the three types of deformations generally investigated in swelling soils: residual, principal and structural deformation regimes (cited in [Garnier et al. 1997], where also the parametric formulas for the different deformation regimes are listed). It could be shown that the value of r_s controls the height of the soil surface, furthermore that it has significant effect on the distribution of water and on the total volume of water in the soil samples.

4.4. Empirical Relationships

Various models for the description of the so-called soil shrinkage characteristic curve (SSCC; relationship between specific volume and gravimetric water content) have been developed in the last decades, as e.g. stated in [Crescimanno Provenzano 1999]. Among these models is the "three straight lines" model, which defines three shrinkage zones, and having parameters with physical interpretation (which is a big advantage as compared to other functions for the SSCC using solely empirical parameters).

Regarding numerical simulations, models are useful that can be easily incorporated into existing software. Simple relationships for swelling and shrinkage are for example implemented in the model MACRO, accounting for changes in ε_{ma} and K_{ma} (see equation 8):

$$\varepsilon_{ma} = \varepsilon_s + p \cdot (\theta_b - \theta_{mi}) \tag{23}$$

$$K_{ma} = (K_{s(min)} - K_b)\left(\varepsilon_{ma} / \varepsilon_s\right)^{m*} \tag{24}$$

where p = slope of shrinkage characteristic, ε_s = minimum macroporosity given by θ_s - θ_b, θ_{mi} = micropore water content, $K_{s(min)}$ = minimum saturated hydraulic conductivity of a swelling soil attained when $\varepsilon_{ma} = \varepsilon_s$ (in a fully swollen soil; total porosity in any layer is held constant since the soil is assumed to be macroscopically rigid). A model concept to simulate water flow in cracked clay soils by employing a shrinkage characteristic was also implemented into SWAP (Soil-Water-Atmosphere-Plant; [van Dam 2000]; a brief description of these programs is given in Appendix 4). In this program an exponential relationship is used to describe the residual shrinkage stage: $e = \alpha_{sh} e^{-\beta_{sh} \nu} + \gamma_{sh} \nu$, where e = void ratio ($=V_p/V_s$, V_p = total pore volume, V_s = solid volume), ν = moisture ratio ($=V_w/V_s$, V_w = water volume), and α_{sh}, β_{sh}, γ_{sh} = dimensionless, empirical parameters.

Remarks:

– Swelling might be promoted by leaching with solutions containing Mg as proposed by [Zhang Norton 2002]. Thus saturated hydraulic conductivity can be reduced, where Mg^{2+} could also promote disaggregation and clay dispersion. The authors concluded that the greater hydration energy and larger hydration shell of Mg as compared to Ca causes these effects on soil aggregate stability and hydraulic conductivity.

– Swelling of soils could probably also be approximated by making use of the dual permeability model. Water content in the "slower" (matrix) region θ_m might be assumed to depend on a factor proportional to the volume of clay fraction, ξ_{clay}, and to the total water content. Looking at the mass transfer term in the two-region concept, this factor will be influenced by swelling, too, in addition to the dispersion factor and tortuosity.

5. Summary

Utmost exact definition of occurring physical and chemical properties of the soil itself and of the solutes investigated is needed, in order to be able to identify all relevant migration processes in the unsaturated soil zone. Models apart from the classical well known convection-dispersion equation are discussed as extension of the review by [Simunek et al. 2003]. Not addressed are sorption processes being also of high impact on the fate of solutes, such as mobile adsorbents, sorption kinetics, or dual mode sorption. In the last decades, prediction of solute translocation by mathematical modelling proofed to be a valuable tool in the field of soil science. However, the underlying concepts need to be understood clearly and simulation results have to be interpreted critically, because any model at most will remain only a simplification of reality.

REFERENCES

[Gerke van Genuchten 1993] Gerke, H.H. & van Genuchten, M.Th. A dual porosity model for simulating the preferential movement of water and solutes in structured porous media. Water Resources Research 29 (2): 305-319, 1993.

[Nieber et al. 1999] Nieber, J.L., Bauters, T.W.J., Steenhuis, T.S. & Parlange, J.-Y. Simulation of Experimentally Gravity-Driven Unstable Flow in Water Repellent Sand. AHPCRC Preprint 99-06, University of Minnesota, 1999.

[Glass Nicholl 1996] Glass, R.J. & Nicholl, M.J. Physics of gravity fingering of immiscible fluids within porous media: An overview of current understanding and selected complicating factors, Geoderma 70: 133-163, 1996.

[Gerke Vogel 1994] Gerke, H.H. & Vogel, T. Zweidimensionale Modellierung von Wasserbewegung und Stofftransport in heterogenen Bodensystemen. Mitteilgn. Dtsch. Bodenkundl. Gesellsch. 74: 261-264, 1994.

[Brusseau Rao 1990] Brusseau, M. L. & Rao, P. S. C. Modeling Solute Transport in Structured Soils: A Review, Elsevier Science Publishers B. V., Amsterdam, Geoderma, 46, 1990.

[van Genuchten Wierenga 1976] van Genuchten, M.Th. & Wierenga, P.J. Mass transfer studies in sorbing porous media I Analytical solutions. SSSA Proceedings 40(4): 473-480, 1976.

[Sparks 1989] Sparks, D. L. Kinetics of Soil Chemical Processes, Academic Press: San Diego, CA, 1989.

[Pignatello Xing 1996] Pignatello, J.J. & Xing, B. Mechanisms of Slow Sorption of Organic Chemicals to Natural Particles. Environ. Sci. Technol. 30(1), pp. 1-11, 1996.

[Rao et al. 1980a] Rao, P.S.C., Roston., D.E., Jessup, R.E. & Davidson, J.M.. Solute Transport in Aggregated Porous Media: Theoretical and Experimental Evaluation. Soil Sci. Soc. Am. J. 44: 1139-1146, 1980.

[Rao et al. 1980b] Rao, P.S.C., Jessup, R.E., Roston., D.E., Davidson, J.M. &. Kilcrease, D.P. Experimental and Mathematical Description of Nonadsorbed Solute Transfer by Diffusion in Spherical Aggregates. Soil Sci. Soc. Am. J. 44: 684-688, 1980.

[Selim et al. 1999] Selim, H.M., Ma, L. & Zhu, H. Predicting Solute Transport in Soils: Second-Order Two-Site Models. Soil Sci. Soc. Am. J. 63: 768-777, 1999.

[Zurmühl Durner 1996] Zurmühl, T. & Durner, W. Modelling Transient Water and Solute Transport in a Biporous Soil.WRR (32): 819-829, 1996.

[Flühler et al. 1996] Flühler, H., Durner, W. & Flury, M. Lateral solute mixing processes – A key for understanding field-scale transport of water and solutes. Geoderma 70: 165-183, 1996.

[Durner Flühler 1996] Durner, W. & Flühler, H. Multi-domain model for pore-size dependent transport of solutes in soils. Geoderma 70: 281-297, 1996.

[Jarvis 1991] Jarvis, N.J. MACRO - A Model of Water Movement and Solute Transport in Macroporous Soils. Reports and Dissertations No. 9, Dept. Soil Sci., SLU, Uppsala, Sweden, 1991.

[Jarvis 1994] Jarvis, N.J. The MACRO model (Version 3.1). Technical description and sample simulations. Reports and Dissert. 19, Dept. Soil Sci., Swedish Univ. Agric. Sci., Uppsala, Sweden, 51 pp, 1994.

[Germann 1985] Germann, P. Kinematic wave approach to infiltration and drainage into and from soil macropores. Trans. ASAE, 28, 745-749, 1985.

[Simunek et al. 2003] Simunek, J., Jarvis, N.J., van Genuchten, M.Th. & Gärdenäs, A. Review and comparison of models for describing non-equilibrium and preferential flow and transport in the vadose zone. Journal of Hydrology 272: 14-35, 2003.

[Chen Wagenet 1992] Chen, C. & Wagenet, R.J. Simulation of water and chemicals in macropore soils. Part 1. Representation of the equivalent macropore influence and its effect on soilwater flow. Journal of Hydrology 130: 105-126, 1992.

[Germann 1990] Germann, P.F. Preferential Flow and the Generation of Runoff 1. Boundary Layer Flow Theory. WRR 26(12): 3055-3063, 1990.

[Ross Smettem 2000] Ross, P.J. & Smettem, K.R.J. A Simple Treatment of Physical Nonequilibrium Water Flow in Soils. Soil Sci. Soc. Am. J. 64: 1926-1930, 2000.

[Ross Smettem 1993] Ross, P.J. & Smettem, K.R.J. Describing Soil Hydraulic Properties with Sums of Simple Functions. Soil Sci. Soc. Am. J. 57: 26-29, 1993.

[Durner et al. 1999] Durner, W., Priesack, E., Vogel, H.-J. & Zurmühl, T. Determination for parameters for flexible hydraulic functions by inverse modeling. In: van Genuchten, M.Th., Leij, F.J., Wu, L. (eds.), Characterization and Measurement of the Hydraulic Properties of Unsaturated Porous Media, University of California, Riverside, CA, pp. 817-829, 1999.

[Mohanty et al. 1997] Mohanty, B.P., Bowman, R.S., Hendrickx, J.M.H. & van Genuchten, M.Th. New piecewise-continuous hydraulic functions for modeling preferential flow in an intermittent-flood-irrigated field. Water Resources Research 33(9): 2049-2063, 1997.

[Maurer 1997] Maurer, T. Physikalisch begründete, zeitkontinuierliche Modellierung des Wassertansports in kleinen ländlichen Einzugsgebieten. Dissertation. Institut für Hydrologie und Wasserwirtschaft Universität Karlsruhe (TH). Heft 61, 1997.

[Beven Germann 1981] Beven, K. & Germann, P. Water flow in soil macropores II. A combined flow model. Soil Sci. 32: 15-29, 1981.

[Bronstert 1994] Bronstert, A. Modellierung der Ablußbildung und der Bodenwasserdynamik in Hängen. Mitteilungen des IHW, Universität Karlsruhe, Nr. 46, 1994.

[Germann Beven 1985] Germann, P. F. & Beven, K. Kinematic wave approximation to infiltration into soils with sorbing macropores. WRR 21(7): 990-996, 1985.

[Merz 1996] Merz, B. Modellierung des Niederschlag-Abfluß-Vorgangs in kleinen Einzugsgebieten unter Berücksichtigung der natürlichen Variabilität. Mitteilungen des IHW, Universität Karlsruhe, Nr. 56, 1996.

[Tschapek et al. 1978] Tschapek, M., Scoppa, C.O. & Wasowski, C. The surface tension of soil water. J. Soil Sci., 29, 17-21, 1978.

[Chen Schnitzer 1978] Chen, Y. & Schnitzer, M. The surface tension of aqueous solutions of soil humic substances. Soil Sci. 125(1): 7-15, 1978.

[Tschapek Boggio 1981] Tschapek, M. & Boggio, L. Surfactant and water migration in unsaturated sand. Z. Pflanzenernaehr. Bodenkd. 144: 30-40, 1981.

[Molenkamp 1998] Molenkamp, T. Marangoni Convection, Mass Transfer and Microgravity. Thesis, Rijksuniversiteit Groningen, NL, 1998.

[Henry et al. 1999] Henry, E.J., Smith, J.E. & Warrick, A.W. Solubility effects on surfactant-induced unsaturated flow through porous media. Journal of Hydrology 223, 164-174. 1999.

[Renshaw et al. 1997] Renshaw, C.E., Zynda, G.D. & Fountain, J.C. Permeability reductions induced by sorption of surfactant. WRR 33(3): 371-378, 1997.

[Smith Gillham 1999] Smith, J.E. & Gillham, R.W. Effects of solute concentration-dependent surface tension on unsaturated flow: Laboratory sand column experiments. WRR 35(4): 973-982, 1999.

[Smith Gillham 1994] Smith, J.E. & Gillham, R.W. The effect of concentration-dependent surface tension on the flow of water and transport of dissolved organic compounds: A pressure head-based formulation and numerical model. WRR 30(2): 343-354, 1994.

[Henry Smith 2002] Henry, E.J. & Smith, J.E. 2002. The effect of surface-active solutes on water flow and contaminant transport in variably saturated porous media with capillary fringe effects. Journal of Contaminant Hydrology 56: 247-270.

[Totsche 2001] Totsche, K.U. Einfluß gelöster organischer Substanzen auf den Bodenwasserfluß: Experimentelle Befunde und numerische Simulation. Mitteilungen der Deutschen Bodenkundlichen Gesellschaft, Band 96(1): 131, 2001.

[Totsche 2002] Totsche, K.U. 2002. Effect of dissolved and colloidal phase organic carbon on water flow in soils. 17th World Congress of Soil Science, Proceedings, Paper no. 1193.

[Philip de Vries 1957] Philip, J.R. & de Vries, D.A. Moisture movement in porous media under temperature gradients. Trans. Am. Geophys. Union. 38(2): 222-232. 1957.

[Hopmans Dane 1986] Hopmans, J.W. & Dane, J.H. Temperature dependence of soil hydraulic properties. Soil Sci, Soc. Am. J. 50: 4-9. 1986.

[Schubert 1982] Schubert, H. 1982. Kapillarität in porösen Feststoffsystemen. Springer Verlag, Berlin.

[Karkare Fort 2002] Karkare, M.V. & Fort, T. Effect of Temperature on Surfactant-Driven Water Movement in Wet Unsaturated Sand. Langmuir 18, 2190-2192, 2002.

[Grant 2000] Grant, S.A. Physical and Chemical Factors Affecting Contaminant Hydrology in Cold Environments. US Army Corps of Engineers. Engineer Research and Development Center. ERDC/CRREL TR-00-21, 2000.

[Grant Bachmann 2002] Grant, S.A. & Bachmann, J. Effect of temperature on capillary pressure. In: Environmental Mechanics, Water, Mass and Energy Transfer in the Biosphere (Raats, P.A.C., D.E. Smiles, and A.W. Warrick, eds.) Geophysical Monograph Series, v. 129. Washington, DC: American Geophysical Society, 199-212, 2002.

[Derjaguin Landau 1941] Derjaguin, B.V. & Landau, L. Acta Physiochim. 14: 633, 1941.

[Verwey Overbeek 1948] Verwey, E.J.W. & Overbeek, J.Th.G. Theory of Stability of Lyophobic Colloids. Elsevier, Amsterdam, 1948.

[Tuller Or 2003] Tuller, M. and Or, Dani. Hydraulic functions for swelling soils: pore scale consideration. Journal of Hydrology 272: 50-71, 2003.

[Murad et al. 1995] Murad, M.A., Bennethum, L.S. & Cushman, J.H. Transport in Porous Media 19, 93, 1995.

[Murad Cushman 1996] Murad, M.A. & Cushman, J.H. Int. J. Engng. Sci. 34(3): 313-338, 1996.

[Murad Cushman 2000] Murad, M.A. & Cushman, J.H. Thermomechanical theories for swelling porous media with microstructure. International Journal of Engineering Science 38. 517-564, 2000.

[Grim 1968] Grim, R.E. Clay Mineralogy, McGraw-Hill, New York, 1968.

[Chertkov 2000] Chertkov, V.Y. Modeling the pore structure and shrinkage curve of soil clay matrix, Geoderma 95, 215-246, 2000.

[Garnier et al. 1997] Garnier, P., Perrier, E., Jaramillo, R.A. & Baveye, P. Numerical model of 3-dimensional anisotropic deformation and 1-dimensional water flow in swelling soils. Soil Science 162(6): 410-420, 1997.

[Crescimanno Provenzano 1999] Crescimanno, G. & Provenzano, G. Soil Shrinkage Curve in Clay Soils: Measurement and Prediction, Soil Sci. Soc. Am. J. (63): 25-32, 1999.

[van Dam 2000] van Dam, Jos C. Field-scale water flow and solute transport. SWAP model concepts, parameter estimation and case studies. PhD-thesis, Wageningen University, Wageningen, The Netherlands. http://www.alterra.dlo.nl/models/swap/index.htm (28. 10. 2003), 2000.

[Zhang Norton 2002] Zhang, X.C. & L.D. Norton. Effect of exchangeable Mg on saturated hydraulic conductivity, disaggregation and clay dispersion of disturbed soils. J. Hydrol. (Amsterdam) 260:194–205, 2002.

Valuation of Irrigation Methods by Equal and Weighted Importance Models and the Analytic Hierarchy Process

Zorica Srdjevic
Department of Water Management
Faculty of Agriculture, University of Novi Sad
Trg D. Obradovica 8, 21000 Novi Sad
Serbia and Montenegro
+381 21 455 770
srdjevicz@polj.ns.ac.yu

Bojan Srdjevic
Department of Water Management
Faculty of Agriculture, University of Novi Sad
Trg D. Obradovica 8, 21000 Novi Sad
Serbia and Montenegro
+381 21 455 770
bojans@polj.ns.ac.yu

ABSTRACT
Selection of the best irrigation method for given field conditions is a multicriteria decision-making problem. It is commonly influenced by two types of factors: (i) objective factors such as crop density, growing conditions, water quality or topography, and (ii) subjective factors such as motivation or willingness of a decision maker to participate in decision process. In this paper the analytic hierarchy process is used to simulate a real life decision-making process influenced by both types of factors. The results are critically compared with the results obtained by two traditional techniques based on equal and weighted importance schemes of the decision factors. AHP demonstrated certain advantages by enabling the decision maker to simultaneously look at various diagrams and to semantically compare decision elements only two at a time, while controlling his level of consistency to remain under tolerant limit. The other two methods analyzed do not posses such capability. An illustrative example is given for four decision alternatives (irrigation methods: border, furrow, sprinkler and trickle) that are assessed across seven typical evaluating criteria (crop density, sensibility to diseases, growing conditions, slope, infiltration rate, water quality and skills of labor).

KEYWORDS
Irrigation method, decision making, analytic hierarchy process, multiplicative weighting methods

1. Introduction

The problem of choosing among different irrigation methods seems to be equally difficult to solve in either of two cases: farm is currently irrigated, or irrigation should be introduced as a new practice on a farm. For example, if furrow irrigation has already been implemented on farm, it may happen that new analyses indicate sprinkler irrigation as more advantageous method due to actual or foreseen changes in farm organization, modified objectives or anticipated prices changes on market. To make the decision is not easy, but to arrive to that point may be even harder if all relevant issues are included into analysis of alternatives. Selection of 'the most appropriate' irrigation method for given field conditions usually mean to perform some analytical procedure based on certain criteria and elements related to or influenced by water supply, soil, topography, crop, climate, energy and labor. [Holzapfel *et al.* 1985] suggested a procedure consisting of two steps: 1. analytical-technical, and 2. technical-economical. Following their work, only the first one is considered here to frame a discussion. The term 'given field conditions' can be understood as a data set describing parameters and phenomena for given field and anticipated irrigation strategy. Unfortunately, numerical data in many cases are not available or must be derived from primarily non-technical sources. Rigorous quantification of descriptive data is therefore necessary prior to an analytical procedure, which furthermore implies that experience gained through experimental work on different fields will be used. Dealing with categories of data such as crop density or infiltration rate is paradigm of this situation. As described in [Holzapfel *et al.* 1985], [Hamilton *et al.* 1953], [Srdjevic 1997], and [Todorovic and Steduto 2003], there are some possibilities to resolve afore mentioned problems successfully.

[Holzapfel *et al.* 1985] introduced an evaluating technique for selecting irrigation method that can be denoted as the multiplicative equal importance method (MEIM). It was used to find the best amongst four possible irrigation methods for given field conditions and crop pattern of corn and maize. Speaking in multicriteria analysis terms, field conditions correspond to evaluating criteria and irrigation methods to alternatives. Evaluation model in the MEIM is in a way analogous to product utility functions used in some standard multicriteria decision-making methods. Later on, it was argued by [Srdjevic 1997] that in practice the additive weighted importance method (AWIM) better supports robust decision-making;

the AWIM method has been introduced by [Hashimoto 1980], and successfully applied in risk-related water resources systems planning [Hashimoto *et al.* 1982].

Selection of most desired irrigation method is influenced by different factors but primarily by investments, production expenses, cost of irrigation system maintenance and irrigation system efficiency [Srdjevic 1997]. Important for making the decision are also real field conditions such as characteristics of the crop(s), water availability and quality, terrain topology, soil characteristics, labor skills etc. Some factors are qualitative and some are quantitative. Formulating the evaluation criterions is a problem itself, because they should reflect more or less conflict farmer's interests such as increasing net return, reducing total cost of agricultural production, improving soil quality, reducing prices of agricultural products, improving usage of human resources and machines, optimising water allocation etc. In other words, it is essential to include relevant decision factors, adopt proper evaluating methodology, and preserve consistency of the decision-making process at all its stages. The major issue is how to relate a variety of factors and determine dominance of one factor over another by investigating certain dominant/weak structures.

Different weighting methods has been used recently to manipulate objectives in related multicriteria decision-making problems, i.e. to simulate cognitive process of the decision maker while he is investigating possible alternative courses in irrigation, performing cost and benefit analyses or planning how to effectively allocate labor and equipment. The analytic hierarchy process (AHP) is one of these methods. It is considered as an efficient tool in supporting a part of these activities, namely selection of irrigation method, primarily because of its robustness and simplicity of use. AHP is a multicriteria decision-making method applicable to well-structured decision problems, that is to problems represented by the hierarchy, each level of it consisting of a finite number of elements. AHP search for the priorities representing the relative importance of the decision elements at each particular level. By additive aggregation it finally computes the priorities of the elements at the bottom level of the hierarchy, usually known as the alternatives. Their priorities are interpreted with respect to overall goal at the top of the hierarchy, and elements at upper levels such as criteria, sub-criteria, etc. are used to mediate comparison process. Theoretical foundation of the method is given in seminal Saaty's book [Saaty 1980]. Only basic properties of the method will be presented in section 3, necessary for understanding its applicability and comparative advantages in specific decision-making contexts such as the selection of an irrigation method.

This paper focuses on the valuation of results obtained by three different models applicable to irrigation method selection. It presents brief overview of relevant literature sources in subject area, and then expands the set of approaches for selecting most desired agricultural irrigation method. Finally, it presents the results obtained in case study application of two other (multiplicative and additive) methods and AHP under the same conditions.

2. The problem and solution methodologies – literature review

The acceptability of different irrigation methods is commonly evaluated by identifying an appropriate parameter set and computing on-field performance indices for irrigation methods within possible parameters' changes.

In [Holzapfel *et al.* 1985], 9 typical indices are defined to express acceptability or adaptability of any irrigation method to particular field conditions:

- Crop density index (I_1) - technical adaptability to crop density and type of sowing or planting.
- Canopy disease index (I_2) - susceptibility to disease of irrigated crops.
- Stem and root disease index (I_3) - susceptibility to disease of stem and root system of irrigated crops.
- Growth index (I_4) - adaptability to the growth habit of the crop.
- Slope index (I_5) - acceptability to field slope.
- Infiltration index (I_6) - adaptability to the infiltration characteristics of irrigated soil.
- Labor skill index (I_7) - adaptability to the skill level of available labor.
- Salt concentration index (I_8) - susceptibility to relative salt concentration in irrigation water.
- Suspended material index (I_9) - susceptibility to relative suspended material in irrigation water.

By assumption, indices can be scaled to range between 0 (irrigation method is not acceptable/adaptable) and 100 (irrigation method perfectly fits to certain field conditions). Parameters related to field conditions can be defined as relative, that is empirically normalized to fall within interval [0, 1]; for example, relative crop sensitivity to disease of value 0 should indicate that crop is tolerant, while value 1 should express situation when crop is very susceptible to disease.

Conceptually, functional relationship between any of afore mentioned indices and any normalized field parameter may be established for any irrigation method. The Fig. 1 illustrates assumed linear type of these relationships for four typical irrigation methods.

The following relation has been proposed for computing acceptability value of particular irrigation method:

$$(VIM)_j^{\,m} = \prod_{i=1}^{N} \left(\frac{(I_i)_j}{100} \right). \qquad (1)$$

VIM is the relative global acceptability value of irrigation method, I_i is the index of its acceptability/adaptability related to *i*-th field parameter, and *j* denotes the irrigation method itself. *N* is the number of indices used. Superscript *m* stands to simply indicate multiplicative type of relation (1). For example, $(I_1)_2$ stands for Crop density index I_1 and border irrigation method indexed as 2 (clarify Fig. 1). *N* is equal to 9 since all indices are used for evaluation. Obviously, VIM may range from 0 to 1; zero final value of VIM means that particular irrigation method is not suitable for specified field conditions; the opposite conclusion stands if VIM is equal 1.

Relation (1) is a core part of proposed procedure for ranking different irrigation methods for the same field conditions. It can be considered as an equal importance multiplicative approach with no preferences allowed for indices I_1 through I_N.

The alternative approach in computing VIM is proposed in [Srdjevic 1997]. It's starting point is the assumption that indices a priori may not have the same mutual (relative) importance. Having this in mind, while analyzing particular crop, field, labor and other conditions and constraints, it may be opportune to rank indices, and weight them appropriately, before multiplication (1) is performed. In this way one may define preferences among indices and build in so-called intentional strategy in the decision-making process.

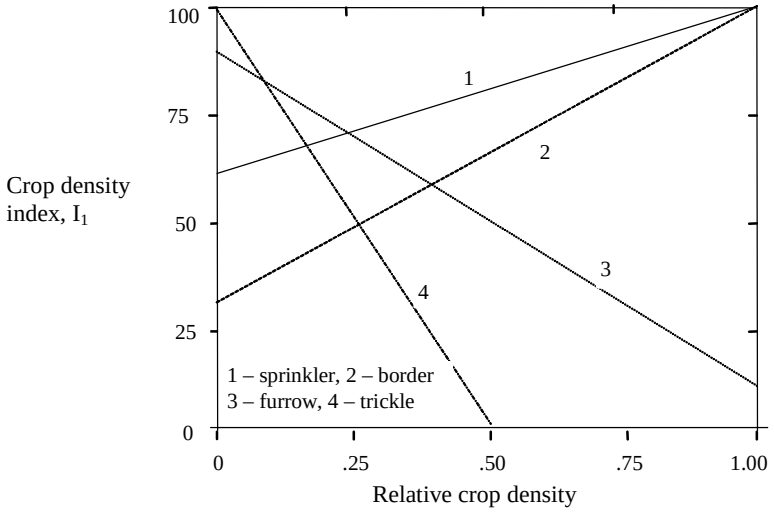

Figure 1. Crop density index vs. relative crop density (1).

Possible way to prepare weighting coefficient scheme is to set the preference list of indices with associated priority numbers *z*. For example, priority number $z = 1$ may declare the highest priority (most important) index, and $z = N$ the lowest priority (least significant) one. Corresponding weighting coefficients may simply be defined as reciprocal values: $w_1=1/z_1$, ..., $w_N=1/z_N$.

The weighted relative value of the *j*-th irrigation method is defined by relation (2):

$$(VIM)_j^{\,w} = \left(\sum_{i=1}^{N} \left[(I_i)_j / 100 \right] w_i \right) / \left(\sum_{i=1}^{N} w_i \right) \qquad (2)$$

where superscript *w* stands to indicate 'weighting type' of relation, and w_i is the weighting coefficient for *i*-th index; other symbols have the same meanings as before.

For equal importance scheme, relation (2) becomes:

$$(VIM)_j^{\,a} = \sum_{i=1}^{N} \left(\frac{(I_i)_j}{100} \right) / \mathrm{N} = \frac{1}{100N} \sum_{i=1}^{N} (I_i)_j \qquad (3)$$

Superscript *a* stands to indicate 'the averaging' in defined computation.

3. AHP in agricultural assessments

An assessment and selection of the most suitable irrigation method for given field conditions belong to the class of multicriteria decision-making practices. Within multicriteria analysis framework one may expect that different techniques might yield different rankings of decision elements. If irrigation methods are considered as the alternatives to be compared and ranked with respect to a set of criterions closely related to field conditions, a consequence is that two multicriteria models can produce different results – final selection of suitable irrigation method. As it was reported in [Srdjevic 1997], even simple models such as (1) – (3) can lead to a different final choice of the irrigation method. It is no strange that controversy constantly exists related to uncertainties about what method should be used, and whether a particular technique is better suited to certain situations than others [Hajkowicz and Prato 1998].

Reported successful stories on applications of the method in diverse areas of agriculture qualify this method as an efficient supporter of various decision practices in irrigation management (see for example [Mainuddin *et al.* 1997], [Raju and Pillai 1999], [Srdjevic *et al.* 2002], or [Koralov and Srdjevic 2004]).

3.1. A brief review of AHP

The essence of the analytic hierarchy process is decomposition of a complex problem into a hierarchy with goal (objective) at the top of the hierarchy, criterions and sub-criterions at levels and sub-levels of the hierarchy, and decision alternatives at the bottom level. After decomposing the problem, elements at given hierarchy level are compared in pairs to assess their relative preference with respect to each of the elements at the next higher level. The verbal terms of the fundamental Saaty's scale presented in Table 1 are used to assess the intensity of preference between two elements. The ratio scale and the use of verbal comparisons facilitate the weighting of quantifiable and non-quantifiable elements. Once the verbal judgments are made, they are translated into numbers by means of the fundamental scale 1 to 9. This procedure is repeated for elements at each level in downward direction.

Table 1. The fundamental Saaty's scale for the comparative judgments.

Numerical values	Verbal terms	Explanation
1	Equally important	Two elements have equal importance regarding the element in higher level
3	Moderately more important	Experience or judgement slightly favours one element
5	Strongly more important	Experience or judgement strongly favours one element
7	Very strongly more important	Dominance of one element proved in practise
9	Extremely more important	The highest order dominance of one element over another
2, 4, 6, 8	Intermediate values	Compromise is needed.

The AHP is simple mathematical method based on elementary operations with matrices. Its strong background is, however, in rational treatment of hierarchical relations between different criterions (objectives) and alternatives which all may be understood as decision variables. By creating appropriate hierarchies, and by performing particular step-by-step procedure while creating comparison matrices at different hierarchical levels, AHP computes and aggregates their eigenvectors in straightforward manner until the composite final vector of weight coefficients for alternatives is computed. The entries of final weight coefficients vector reflect the relative importance (value) of each alternative with respect to the goal stated at the top of hierarchy.

AHP additionally calculates inconsistency index as a ratio of the decision maker's inconsistency and randomly generated index. This index is important to assure the decision maker that his judgements were consistent and that final decision is made well. Inconsistency index less than 0.10 is assumed acceptable. Although higher value of inconsistency index requires re-evaluation of pair wise comparisons, decisions obtained in certain cases could also be taken as 'the best alternative' [Karlsson 1998].

4. Selecting irrigation method by different methods - An example

The two methods described in section 2 and the AHP method are used to solve the same problem: evaluation of four irrigation methods and select the most suitable one. To provide equal comparison framework, irrigation methods used here as the decision alternatives are the same as used in [Holzapfel *et al.* 1985] and [Srdjevic 1997]. In these earlier works, (respectively) 9 and 7 indices of acceptability/adaptability are used to evaluate global performance of irrigation methods across given set of field parameters.

For illustration purpose, herein a set of 7 field parameters is used as criteria set, the same crop (olive) pattern is assumed as well as the same field conditions. It is supposed that irrigated area is an olive field with slope of 1%. Soil of the field is sandy clay, with low infiltration rate. Quality of water that will be used for irrigation is good, and the labor skills are also considered good. The criteria selected for evaluating possible irrigation methods are: crop density (**cropden**), sensibility to diseases (**disease**), growing conditions (**growcon**), slope (**slope**), infiltration rate (**infrate**), water quality (**watqual**) and skills of labor (**labskil**). Decision alternatives are irrigating methods: **border**, **furrow**, **sprinkler** and **trickle**.

The decision hierarchy is given in Fig. 2. At the top of the hierarchy is a goal – the best irrigation method, criteria are set at the first level and the alternatives are at the second.

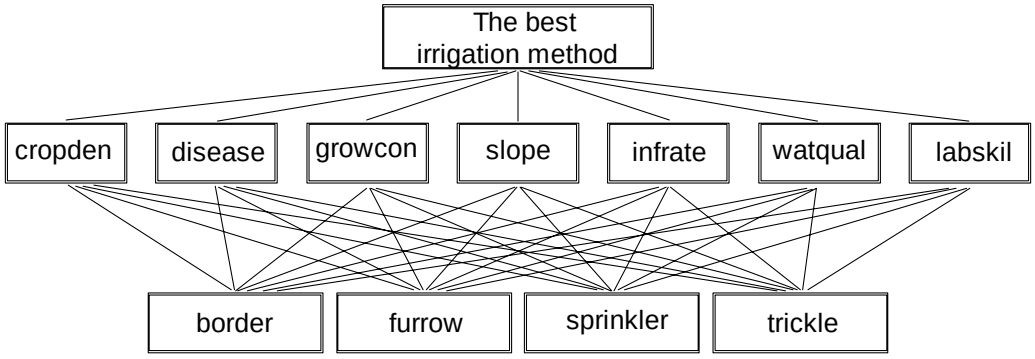

Figure 2. Hierarchy for the decision problem.

The AHP methodology says that weighting and prioritizing the criterions should be done firstly. By using Table 1 and by performing pair wise comparisons of criterions with respect to goal, the following matrix may eventually be created:

	cropden	disease	growcon	slope	inf rate	watqual	labskil
cropden	1	5	1	2	3	4	6
disease	1/5	1	1/5	1/5	1/4	1/4	1/3
growcon =	1	5	1	2	3	4	6
slope	1/2	5	1/2	1	3	2	4
inf rate	1/3	4	1/3	1/3	1	1/2	5
watqual	1/4	4	1/4	1/2	2	1	5
labskil	1/6	3	1/6	1/4	1/5	1/5	1

with corresponding set of criteria weights: **cropden**–0.272, **disease**–0.032, **growcon**–0.272, **slope**–0.171, **infrate**–0.097,**watqual**–0.115, and **labskil**–0.042. Note that sum of all weights is equal to 1.

The next step is to compare alternatives with respect to each criterion. For example, with respect to crop density, the following matrix of pair wise comparisons of alternatives can be created:

$$
\begin{array}{c} \\ \text{border} \\ \text{furrow} \\ \text{sprinkler} \\ \text{trickle} \end{array} = \begin{array}{c} \begin{array}{cccc} \text{border} & \text{furrow} & \text{sprinkler} & \text{trickle} \end{array} \\ \begin{bmatrix} 1 & 3 & 1/5 & 4 \\ 1/3 & 1 & 1/7 & 3 \\ 5 & 7 & 1 & 9 \\ 1/4 & 1/3 & 1/9 & 1 \end{bmatrix} \end{array}.
$$

(for **cropden** criterion)

Corresponding set of weights for alternatives is: **border**–0.195, **furrow**–0.097, **sprinkler**–0.660, and **trickle**–0.049, and again weights sum up to 1.

After similar comparisons of alternatives with respect to all criterions are completed, related weights are used as column-entries to create the following matrix:

$$
\begin{array}{c} \\ \text{border} \\ \text{furrow} \\ \text{sprinkler} \\ \text{trickle} \end{array} = \begin{array}{c} \begin{array}{ccccccc} \text{cropden} & \text{disease} & \text{growcon} & \text{slope} & \text{inf rate} & \text{watqual} & \text{labskil} \end{array} \\ \begin{bmatrix} 0.195 & 0.211 & 0.163 & 0.095 & 0.125 & 0.354 & 0.078 \\ 0.097 & 0.368 & 0.395 & 0.160 & 0.222 & 0.131 & 0.125 \\ 0.660 & 0.054 & 0.047 & 0.277 & 0.077 & 0.161 & 0.306 \\ 0.049 & 0.368 & 0.395 & 0.467 & 0.577 & 0.354 & 0.492 \end{bmatrix} \end{array} \qquad (4)
$$

The final step consists of creating a linear combination of products of criteria weights and corresponding columns in (4):

$$
\begin{array}{c} \\ \text{border} \\ \text{furrow} \\ \text{sprinkler} \\ \text{trickle} \end{array} = 0.272 \begin{bmatrix} 0.195 \\ 0.097 \\ 0.660 \\ 0.049 \end{bmatrix} + 0.032 \begin{bmatrix} 0.211 \\ 0.368 \\ 0.054 \\ 0.368 \end{bmatrix} + 0.272 \begin{bmatrix} 0.163 \\ 0.395 \\ 0.047 \\ 0.395 \end{bmatrix} + 0.171 \begin{bmatrix} 0.095 \\ 0.160 \\ 0.277 \\ 0.467 \end{bmatrix} +
$$

$$
+ 0.097 \begin{bmatrix} 0.125 \\ 0.222 \\ 0.077 \\ 0.577 \end{bmatrix} + 0.115 \begin{bmatrix} 0.354 \\ 0.131 \\ 0.161 \\ 0.354 \end{bmatrix} + 0.042 \begin{bmatrix} 0.078 \\ 0.125 \\ 0.306 \\ 0.492 \end{bmatrix}
$$

and computing so-called composite weight vector for alternatives:

$$
\begin{array}{c} \\ \text{border} \\ \text{furrow} \\ \text{sprinkler} \\ \text{trickle} \end{array} = \begin{bmatrix} 0.182 \\ 0.231 \\ 0.235 \\ 0.351 \end{bmatrix}
$$

The decision alternative with the highest composite weight coefficient is trickle – 0.351, so this one should be chosen as the best irrigation method for given field conditions. Computed the overall inconsistency index of 0.05 is acceptable and selection process is completed.

Table 2 summarizes the main results obtained by AHP and by two other models, MEIM and AWIM. It comes out that the two 'weighting' methods – AWIM (represented by relation (2)) and AHP – identify trickle as the best irrigation method for given field and crop conditions. Equal importance model MEIM (represented by relation (1)) puts a furrow method at the top and trickle method to the second place.

Table 2. Final ranking of irrigation methods.

Irrigation method	VIM ^{m} Rel. (1)	VIM ^{w} Rel. (2)	AHP
Sprinkler	0.183 (**3**)	0.637 (**4**)	0.235 (**2**)
Border	0.168 (**4**)	0.721 (**3**)	0.182 (**4**)
Furrow	0.265 (**1**)	0.812 (**2**)	0.231 (**3**)
Trickle	0.215 (**2**)	0.953 (**1**)	0.352 (**1**)

The AWIM model puts furrow irrigation to the second place, while AHP ranks it as the third, and sprinkler irrigation validates as the second best method (after trickle). Notice that weights of sprinkler and furrow obtained by AHP are very close and indicate that even small inconsistency may revert expectable and logical ranking (furrow is better irrigation method than sprinkler in this particular case).

Notice also that in case of models that perform VIM computations, normalization to 1 for values obtained by relations (1) and (2) is not allowed due to underlying concepts of MEIM and AWIM.

5. Conclusion

Analytic hierarchy process is recognized as an efficient decision-making tool. Its major advantage is that it formalizes and renders systematic what is largely a subjective decision process, and as a result facilitates 'accurate' judgments, that weights of criteria are also provided to decision maker, and that sensitivity analysis is easy to conduct by using computer [Narasimhan 1983]. AHP also provides to the decision maker the measure of his inconsistency while reasoning and comparing elements within the hierarchy of a problem. This appears to be more and more significant in solving real multicriteria and multiattribute problems when justification of the decision made is necessary to quantify and verify.

The AHP's advantages are recognized in various decision-making applications. In this paper it is demonstrated how to use AHP for selecting the best irrigation method for given field conditions and with respect to 7 selected criterions (crop density, sensibility to diseases, growing conditions, slope, infiltration rate, water quality and skills of labor). Four alternative irrigation methods (furrow, border, trickle and sprinkler) were evaluated and ranked. Assuming that olives are planted, AHP identified the trickle method as most suitable for irrigating given field.

In a competitive environment with the two more traditional evaluating methods introduced in earlier research, the results derived by AHP method appear to be trustworthy regarding both (1) the 'quality' of the final solution obtained in presence of conflict multiple criteria, and (2) attained high overall consistency index during the decision process. Additionally, AHP has certain advantages over the other two methods analysed in this paper because it enables decision maker to simultaneously look at various diagrams such as this in Fig. 1 and semantically compare decision elements contained in the hierarchy in Fig. 2. The rest will be done by the AHP in straightforward manner. Authors of this article do have very good experience with end-users in using this method such as walnut experts in evaluating walnut varieties, or water resources managers in prioritizing operational strategies for control of regional hydrosystems. In all cases the tool was well perceived.

REFERENCES

[Hajkowicz and Prato 1998] Hajkowicz S., Prato T. Multiple objective decision analysis of farming systems in Goodwater Creek Watershed. Missouri. Research Report No. 24, Center for Agricultural, Resource and Environmental Systems, University of Missouri, USA, 1998.

[Hamilton *et al.* 1953] Hamilton F., Schrunk J.. Sprinkler vs. gravity irrigation as a basis for choice of the best system. *Agricultural Engineering*, **34**- 4: 246-250, 1953.

[Hashimoto 1980] Hashimoto T. Robustness, reliability, resilience and vulnerability criteria for water resources planning. Ph.D. dissertation. Cornell University, USA, 1980.

[Hashimoto *et al.* 1982] Hashimoto T., Stedinger J.R., Loucks D.P. Reliability, resiliency and vulnerability criteria for water resources system performance evaluation. *Water Resources Research*, **18**-1: 21-26, 1982.

[Holzapfel *et al.* 1985] Holzapfel E.A., Marino M.A., Chavez-Morales J. Procedure to select an optimum irrigation method. *Irrigation and Drainage Engineering*, **111**-4: 319-329, 1985.

[Karlsson 1998] Karlsson J. A systematic approach for prioritizing software requirements. Ph.D. dissertation, No. 526. Linkoping, Sverige, 1998.

[Kolarov and Srdjevic 2004] Kolarov V., Srdjevic B. AHP evaluation of automatic irrigation machines by different prioritization methods. Journal *of Water Resources* '*Vodoprivreda*', **36**-209-210: 265-273, 2004 (in Serbian).

[Mainuddin *et al.* 1997] Mainuddin M., Gupta A., Onta P. Optimal crop planning model for an existing groundwater irrigation project in Thailand. *Agricultural Water Management*, **33**-1: 43-62, 1997.

[Narasimhan 1983] Narasimhan R. An analytical approach to supplier selection. *Purchasing and Materials Management*,19-1: 27-32, 1983.

[Raju and Pillai 1999] Raju K., Pillai C. R. S. Multicriterion decision making in performance evaluation of an irrigation system. *European Journal of Operational Research*, 112-3: 479-488, 1999.

[Saaty 1980] Saaty T.L. The Analytic Hierarchy Process, McGraw-Hill, Inc., 1980.

[Srdjevic 1997] Srdjevic B. On the use of systems analysis in horticultural crops irrigation. *Acta Horticulturae*, 449-1: 245-250, 1997.

[Srdjevic *et al.* 2002] Srdjevic Z., Srdjevic B., Potkonjak S., Zoranovic T. Allocation of land to agricultural crops in presence of irrigation and drainage: an approach based on the analytic hierarchy process. In: Proc. 'Melioration and Agriculture', Faculty of Agriculture, Novi Sad, Serbia and Montenegro, 222-239, 2002 (in Serbian).

[Todorovic and Steduto 2003] Todorovic M., Steduto P. A GIS for irrigation management. *Physics and Chemistry of the Earth*, 28: 163–174, 2003.

Track 2

METHODOLOGY

Algorithms for efficient implementations of the DEVS & DSDEVS abstract simulators

Alexander Muzy
Laboratory SPE CNRS UMR 6134
University of Corsica, Campus Grossetti, BP 52
20250 Corti
+33 495 45 02 07
a.muzy@univ-corse.fr

James J. Nutaro
Dept. of Electrical and Computer Engineering
University of Arizona
85716 Tucson
+01 865 241 1587
nutaro@ece.arizona.edu

1. Introduction

The Discrete EVent System Specification (DEVS) is a mathematical formalism for describing discrete event systems. DEVS is grounded in general systems theory. Within DEVS, discrete event systems are described by two kinds of structures. Atomic models describe the behavior of non-decomposable units via event-driven state transition functions. Each atomic model has a clearly defined set of inputs and outputs, and its state space is completely encapsulated. More complex models can be constructed from networks of atomic components. These network models, in turn, have well defined inputs and outputs, and they can be used as components within new network models. This allows for the modular and hierarchical construction of very large discrete event systems.

The hierarchical and modular structure of a DEVS model is reflected in the classical specification of the DEVS simulators [Zeigler et al., 2000]. Each atomic model is associated with a simulator object. The simulator is controlled by sending it messages such as “compute next state” and “compute next output”, and it makes requests such as “get time of next event”. A coordinator object is associated with each network model, and the coordinator can respond to the same types of messages as the simulator objects. The coordinator, as its name suggests, coordinates the execution of its component coordinators and simulators.

A direct implementation of the classical specification can be inefficient for simulating models that are comprised of numerous interacting subsystems [Muzy et al., 2002]. Memory inefficiencies result from using an excessive number of coordinator and simulator objects. Simulators are needed only for active components, whereas the standard description of the DEVS simulation algorithms calls for a simulator for every atomic model. Similarly, it is possible to replace the plethora of coordinator objects with a single coordinator object. This new coordinator uses recursion to manage the model hierarchy.

Time inefficiencies stem from the use of ensemble methods to determine the next event time and to route events through the model network (see, e.g., [Zeigler 2000]). This can be remedied by the use of more sophisticated event scheduling and event routing algorithms.

The efficiency of DEVS simulator implementations is beginning to receive significant attention [Hu and Zeigler, 2004; Lee and Kim, 2003; Wainer and Giambiasi, 2001]. Concerning cellular models, [Wainer and Giambiasi, 2001] shows that the simulation of cellular models can be improved by “flattening” the hierarchy of coordinator objects. In this flattened simulator, one coordinator manages all of the model’s atomic components. This can significantly reduce the cost of event routing, and it eliminates the need for multiple coordinator objects. [Lee and Kim, 2003] describe a similar solution that computes and stores possible event routes at compile time. [Hu and Zeigler, 2004] describe an improved scheduling algorithm for cellular models that are simulated using a hierarchy of coordinators and simulators.

We propose a new approach for implementing simulators for DEVS models [Zeigler et al., 2000] and Parallel Dynamic Structure Discrete Event (DSDEVS) models [Barros, 1997]. The simulation architecture and communication protocol have been designed to improve efficiency through:

- eliminating unnecessary simulator and coordinator objects,
- speeding up event scheduling by only storing references to active models,
- eliminating unnecessary internal synchronization messages (i.e., *-messages and d-messages [Zeigler et al., 2000]), and

- avoiding unnecessary event routing messages (i.e., y-messages and x-messages).

The algorithms described in this paper have been implemented in the adevs simulation engine [Nutaro, 1999], and they have been applied successfully to several large scale simulation problems (see, e.g., [Nutaro, 2003], [Jammalamadaka, 2003], [Muzy, 2004]).

2. Background

A DEVS atomic model is described by a structure [Zeigler et al., 2000] $< X, S, Y, \delta_{int}, \delta_{ext}, \delta_{conf}, \lambda, ta >$. X is the set of input events, S is the state set, Y is the set of output events, δ_{int} is the internal transition function, δ_{ext} is the external transition function, δ_{conf} is the confluent transition function, λ is the output function, and *ta* is the time advance function. The transition functions are triggered by events, and they operated on bags of inputs (denoted by X^b) and the state of the system when an event occurs.

A DSDEVS network is described by a structure [Barros, 1997] $< X_{DSDEVS}, Y_{DSDEVS}, \chi, M_\chi >$. X_{DSDEVS} is the set network of input events, Y_{DSDEVS} is the set of network output events, χ is the name of a special atomic model called the executive model, and M_χ is the executive model. The executive model is a special atomic model described by $< X_\chi, Y_\chi, S_\chi, \gamma, \Sigma^*, \delta_{ext,\chi}, \delta_{\text{int},\chi}, \delta_{conf,\chi}, ta_\chi, \lambda_\chi >$. X_χ and Y_χ are the input and output sets of the executive model, S_χ is the set of states, $\gamma : S_\chi \to \Sigma^*$ is the structure function, Σ^* is the set of network structures, and $\delta_{ext,\chi}$, $\delta_{int,\chi}$ and $\delta_{conf,\chi}$ are the executive model's external, internal, and confluent transition functions. ta_χ and λ_χ are the executive model's time advance and output functions. In effect, the state of the executive model describes the network structure. Structure changes can occur when the executive model changes its state.

3. Algorithms

Algorithm 1 describes a Root Coordinator (*Root*) that is used to drive a *Simulator*. The simulation starts by initializing the root coordinator's only child (i.e., the *Simulator*). The *Root* executes the main three functions of the *Simulator* until there are not more active models or the final simulation time t_{end} is reached. The first function, *network-compute-and-route-output()*, computes the output function of the imminent atomic models at the time of next event, t_n, and then routes any component output events. The second function, *atomic-model-delta-functions()*, computes the state transition function of the atomic models that are active (i.e., imminent or have received input) at t_n. The third function, *executive-delta-functions()*, computes the next states of the executive models that are active at t_n.

```
variables:
 tend   // total simulation time
 child // the Simulator

compute the initializations() function of the child
While (tn of the child < tend)
    compute the compute-and-route-output() function of the child
    compute the atomic-model-delta-functions() function of the child
    compute the network-executive-delta-functions() function of the child
endWhile
```

Algorithm 1. Root

Algorithm 2 sets out the main variables used in the *Simulator* to implement the *compute-and-route-output()*, *atomic-model-delta-functions()*, and *network-executive-delta-functions()* functions. A description of each variable is included in the algorithm as a comment. Subscripts are used to denote a version of the variable associated with a specific component model (e.g., D_1 indicates the set of current component models for executive model number 1).

```
Variables:
 parent                        // parent coupled model reference
 q                             // model state
 t_n                           // time of next event
 t_l                           // time of last event
 scheduler                     // priority queue of pairs (d,t_n,d)
 total-imminent-set            // set of imminent executive and atomic models
 receiver-set-temp             // set of intermediate event receivers
 receiver-set                  // set of final event receivers (executive models and atomic models)
 executive-imminent-set        // set of imminent executive models
 D                             // set of current component models
 D'                            // set of new atomic models
 D'- D                         // set of added atomic models
 D - D'                        // set of removed atomic models
 D ∩ D'                        // set of atomic models that have migrated from one network to another
 D_1 ∪ D_2... ∪ D_N            // set of all atomic models
```

Algorithm 2. Simulator variables

Algorithm 3 presents the function that sets up the initial states, simulation times, and model structures. The function *initializations()* initializes atomic model and network executive model states. Models with non-infinite next event times are then added to the scheduler. A similar function, called *structure-initializations()*, is used to initialize models that are added as the result of structure changes occurring during a simulation run.

```
Function initializations()
   t_l ← 0
   For each d ∈ D_1 ∪ D_2... ∪ D_N Do
      q_d ← q_0,d
      t_n,d ← ta_d(q_d)
      If(t_n,d < ∞) Then
         add (d,t_next,d) to the scheduler
      endIf
   endFor
endFunction initializations

Function structure-initializations()
   For each d ∈ (D'- D) – (D ∩ D') Do
      q_d ← q_0,d
      t_n,d ← ta_d(q_d)+t_l
      If(t_n,d < ∞) Then
         add (d,t_n,d) to the scheduler
      endIf
   endFor
endFunction structure-initializations()
```

Algorithm 3. Simulator: initialisations

The procedure for computing a next state of all active atomic components is shown as Algorithm 4. First, all of the models in the *total-imminent-set* are scanned. If the model is an executive model, then it is added to the *executive-imminent-set*. Otherwise, the model's state transition is computed.

```
Function atomicModelDeltaFunctions()
   For each d* of the total-imminent-set Do
      if d* is an executive model then add d* to the executive-imminent-set
      else compute the delta functions of d*
   endFor
endFunction atomicModelDeltaFunctions()
```

Algorithm 4. Simulator: Transition functions of atomic models

Algorithm 5 describes the function *compute-and-route-output()*. It begins by selecting the time $t_{n,d}$ of the first imminent model in the *scheduler*. This model is removed from the scheduler and added to the *total-imminent-set*. Next, all models having the same next event time are added to the *total-imminent-set* and removed from the *scheduler*. Then the output

function of every model of the *total-imminent-set* is computed. The result is stored in the model's output bag y^b. The contents of the output bags are routed and stored in one or more destination input bags x^b. The event routing algorithm is realized by the *route()* function, which is described in the next section. Finally, models that receive input events are added to the *receiver-set* and *total-imminent-set*.

Execution of state transition functions for models in the *total-imminent-set* is presented in Algorithm 6. If the input bag x^b for a model is not empty and that model is scheduled for an internal transition, then the confluent transition function $\delta_{conf,d^*}()$ will be computed. If the input bag x^b for a model is empty and that model is scheduled for an internal transition, then the internal transition function $\delta_{int,d^*}()$ will be computed. Otherwise, the elapsed time e_{d^*} is updated and the external transition function $\delta_{ext,d^*}()$ is computed. Finally, the last transition time t_{l,d^*} is updated. If the next transition time t_{n,d^*} is less than infinity, then the model reference and its next event time t_{n,d^*} are added to the *scheduler*.

Since state changes for executive models can result in structural changes, they must be handled differently. Computation of the state transition functions for network executive models is showed in Algorithm 7. It begins by ordering the *executive-imminent-set* by depth in the model hierarchy. The state transitions are then computed in the sorted order. The computation starts by recording the set of component models for the network managed by the executive model. The state transition function of the executive model is then computed as in the preceding paragraph. Every model that is in the old component set and not in the new component set is removed from the *scheduler* and deleted. Every model that is in the new component set but not in the old component set is initialised and scheduled via the *structure-initializations()* function.

```
Function compute-and-route-output()
   tn ← min{ tn,d / d ∈ D1 ∪ D2... ∪ DN }
   While(tn,d(scheduler) == tn)
      d* ← first (scheduler)
      add d* to the total-imminent-set
      remove (d*,tn,d*) from the scheduler
   endWhile
   For each d* of the total-imminent-set Do
      yb ← λd*(qd*)
      For each output event evj of yb Do
         add evj to xb of all receivers (atomic and executive models)
         // see the route method in section 5 for the implementation
         add the receiving models to the receiver-set
      endFor
   endFor
   total-imminent-set ← total-imminent-set ⋃ receiver-set
endFunction compute-and-route-output()
```

Algorithm 5. Simulator: compute and route events

```
Function compute_delta_functions()
   If( x^b_d* ≠ ∅ and tn,d* = tn) Then
      δconf,d* ( x^b_d* )
   Else If( x^b_d* = ∅ and tn,d* = tn) Then
      q'd* ← δint,d* (qd*)
   Else
      ed* ← tn − tl,d*
      q'd* ← δext,d* (qd*, ed*, x^b_d*)
   endIf
   tl,d* ← tn
   If(tn,d* < ∞) Then
      insert (d*,tn,d*) in the scheduler
   endIF
endFunction compute_delta_functions()
```

Algorithm 6. Simulator: compute and route events

```
Function networkExecutiveDeltaFunctions()
   D ← ∅
   D′ ← ∅
   For each n* of the executive-imminent-set Do
      D ← D ⋃ n* component model set
      compute the delta functions of n*
      D′ ← D′ ⋃ n* component model set
   endFor
   remove all d ∈ (D - D′) – (D ∩ D′) from the scheduler
   structureInitializations()
endFunction networkExecutiveDeltaFunctions()
```

Algorithm 7. Simulator: transition functions of network executive models

The performance of these algorithms in practice depends critically on the implementation of the supporting data structures. The essential data structures and their operations are

- set element insertion, element removal, containment tests, and iteration, and
- inserting, removing, and rescheduling items in the scheduler.

The set implementation used in adevs is based on a dynamic array that is backed by a hashtable for retrieval of specific items. Elements are inserted into a set by adding them to the end of the array and entering them into the hashtable. Items are removed by deleting them from the hashtable, removing them from the array. Holes in the array are filled by moving the item at the end of the array to the recently vacated position. Iteration is handled by simply looking at each array index in order. The scheduler in adevs is implemented using a binary heap. A hashtable that maps items in the heap to their indexes in the underlying array is used to support fast rescheduling. The data structures themselves have been chosen for their time complexity [Weiss 1993]. The C++ implementations have been carefully optimized ([Abrash 1997] provides an excellent series of essays on practical code optimization).

4. Recursive event routing

Event routing is achieved without a hierarchy of coordinators by employing recursion. Every model includes a reference to its parent model, except for the model at the top of the hierarchy. Every executive model contains a routing method that describes how events are routed within a single network model. Event routing begins when a model (atomic or network) generates an output or an input arrives to a network model. The immediate destinations for the event are determined using the network executive model's route method. If the destination is another atomic model within the same network, then the routing is finished. If the destination is a network model within the same network, then this procedure is repeated using the executive of that network model. If the destination is an output port of the current network model, then this procedure is repeated using the executive model of the current model's parent.

```
function route(parent,src,ev)
   compute the set of receivers for event ev using the parent's executive model
   For each model m in the receiver set
      if m is an atomic model or executive model
         add ev to the input bag x^b for model m
         add m to receiver-set
      else if m = parent
         route(parent of m,m,ev)
      else
         route(m,m,ev);
      end
   endFor
endFunction route()
```

Algorithm 8. Recursive event routing

To illustrate this recursive procedure, an example of a hierarchical model is presented in Figure 2. A coupled model *CM_2* contains two coupled models *CM_1* and *CM_3*. The coupled model *CM_1* contains an atomic model *AM_1*. The coupled model *CM_3* contains an atomic model *AM_2*. The atomic model *AM_1* is coupled to the atomic model *AM_2* through the three coupled models *CM_1*, *CM_2* and *CM_3*.

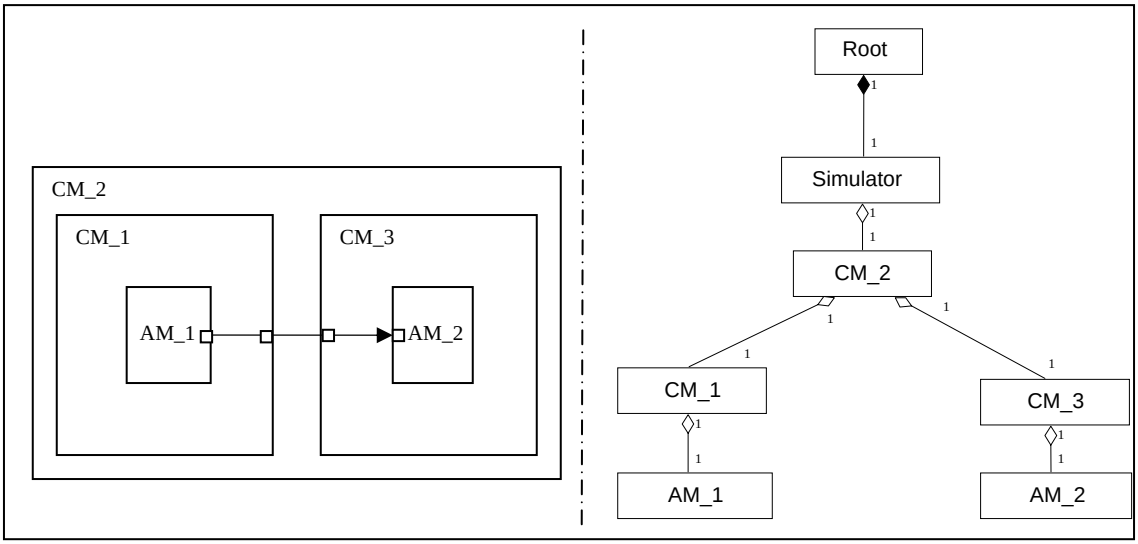

Figure 2. Models and associated simulator

Figure 3 depicts the event route that is computed using the recursive routing procedure. Here, the atomic model *AM_1* produces an output that should be consumed by model *AM_2*. Denoting the output of model *AM_1* by *ev*, the *route()* function is called recursively as follows: (1) route(*CM_1*,*AM_1*,*ev*), (2) route(*CM_2*,*CM_1*,*ev*), and (3) route(*CM_3*,*CM_3*,*ev*). The last call discovers the receiving model *AM_2*. The event *ev* is then added to *AM_2*'s input bag and *AM_2* is added to the *receiverSet*.

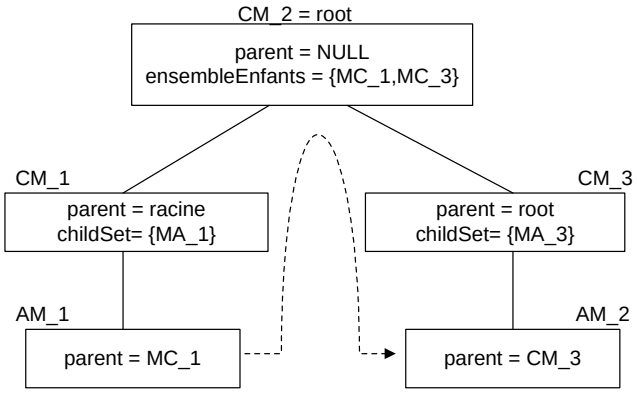

Figure 3. Implicit link tree

5. Conclusion

The simulation algorithms described here have been implemented in the adevs simulation library [Nutaro, 1999]. The performance of the simulation library has to be improved over its lifetime in three different ways. The first, and most significant, is via the application of the algorithms described here.

Secondly, the underlying data structures, and the set and scheduler implementations in particular, have been optimized for use in a simulation application. The use of dynamic arrays in particular takes advantage of the fact that most simulation

applications contain a fixed set of models. While dynamic structure modeling is supported, structure changes are relatively rare.

Thirdly, the liberal use of a performance profiling tool allowed for targeted optimization of the data structure implementations. One example of this is the choice of a closed hashing scheme for the hashtable implementation (see [Weiss 1993]). This choice was dictated by performance data obtained in a comparative study of different hashing schemes to solve some benchmark simulation problems.

The optimization of discrete event simulation software requires a balance between performance and ease of use. The design and implementation of adevs has evolved to support the best performance possible without exposing optimization tricks to the end user. One example of this is the computationally expensive use of a set difference operation to detect changes in a network's component set. An alternative implementation could allow for explicit add and remove operations within the executive model's transition functions. However, this would damage the abstraction of structure change being intrinsic to an executive model's change of state.

REFERENCES

Abrash, M., Graphics Programming Black Book Special Edition, The Coriolis Group Inc., 1997.

Barros, F. J., "Modelling Formalisms for Dynamic Structure Systems". ACM Transactions on Modelling and Computer Simulation, v. 7, 1997, p. 501-515.

Hu, X., and B. P. Zeigler, "A high performance simulation engine for large-scale cellular DEVS models". High Performance Computing Symposium (HPC'04), Advanced Simulation Technologies Conference (ASTC), 2004, p. 3-8.

Jammalamadaka, R., Activity characterization of spatial models: application to discrete event solution of partial differential equations: Computer science Master thesis, University of Arizona, Tucson, 2003.

Lee, W. B., and T. G. Kim, "Simulation speedup for DEVS models by composition-based compilation". Summer Computer Simulation Conference, 2003, p. 395-400.

Muzy, A., Elaboration of deterministic models for the simulation of complex spatial systems: Application to forest fire propagation [In french]: Computer science PhD thesis, University of Corsica, Corti, 2004.

Muzy, A., G. Wainer, E. Innocenti, A. Aïello, and J. F. Santucci, "Comparing simulation methods for fire spreading across a fuel bed". AIS 2002 - Simulation and planning in high autonomy systems conference, 2002, p. 219-224.

Nutaro, J., adevs (A Discrete EVent System simulator), Tucson, Arizona Center for Integrative Modeling & Simulation (ACIMS), University of Arizona, [http://www.ece.arizona.edu/~nutaro/index.php].

Nutaro, J., Parallel discrete event simulation with applications to continuous systems: Computer science PhD thesis, University of Arizona, Tucson, 2003.

Wainer, G., and N. Giambiasi, "Application of the Cell-DEVS paradigm for cell spaces modeling and simulation". Simulation, v. 76, 2001, p. 22-39.

Weiss, M., Data Structures and Algorithm Analysis in C, The Benjamin/Cummings Publishing Company Inc., 1993.

Zeigler, B. P., H. Praehofer, and T. G. Kim, Theory of modelling and simulation, Academic Press, 2000.

DEVS Coupling of Spatial and Ordinary Differential Equations: VLE Framework

Gauthier Quesnel
LIL
50, rue Ferdinand Buisson
BP 719
62228 Calais, France
quesnel@lil.univ-littoral.fr

Raphaël Duboz
UR RAP – IRD
Avenue Jean Monnet
BP 171
34203 Sète, France
duboz@ird.fr

David Versmisse
LIL
50, rue Ferdinand Buisson
BP 719
62228 Calais, France
versmisse@lil.univ-littoral.fr

Éric Ramat
LIL
50, rue Ferdinand Buisson
BP 719
62228 Calais, France
ramat@lil.univ-littoral.fr

ABSTRACT
In this article, we study the different ways to develop a multi-paradigm model of a hybrid system. VLE (Virtual Laboratory Environment) offers two ways: the DEVS mapping and the DEVS wrapping in order to manage existing models in VLE framework. We deal with the wrapping technique which consists in connecting existing simulators models to DEVS compliant simulators. Our approach is illustrated with several simple examples: an ordinary differential equations system in the case of wrapping and a spatial differential equations system in the case of mapping. The second aim of this article is to propose an approach to develop a multimodel of hybrid system in the formal and efficient application programming interface of VLE.

KEYWORDS
DEVS, Wrapping, Mapping, ODE, PDE, Quantized System, Cell-DEVS

1. Introduction

Nowadays, it is recognized that multimodelling is a powerful concept for modelling and simulation of large complex systems. At the end of 80's, P.A. Fishwick and B.P. Zeigler [Fishwick 1992] introduced the multimodelling basis concepts. One can define multi-models as large models which are composed of different types of models (i.e. different paradigms) [Fishwick 1995]. Concepts like refinement and hierarchical composition are basis of multimodelling. The first describes the decomposition of one model into several other ones in order to refine the behaviour of the composed model. The last defines the opposite process: it is say models aggregation. In this context, a major issue is how to deal with the coupling of heterogeneous models. Several works deal with the coupling of heterogeneous models. For a review of concepts and techniques, see the book of B.P. Zeigler *et al.* [Zeigler *et al.* 2000]. With DEVS, Discrete Event System Specification [Zeigler 1976], B.P. Zeigler has provided formal basis for coupled model construction in a network or graph manner. If models we want to couple are specified in a unique formalism, it does not appear unsolvable problems, whereas the coupling of models which are formally different can lead to several coupling strategies.

The work presented here takes place in the field of formally heterogeneous models coupling. To tackle this issue, we briefly recall concepts like mapping and wrapping. Then we give example of "formal" wrapping and show the feasibility with a particular and very simple application.

1.1. Heterogeneous Models Coupling

In their book, B.P. Zeigler *et al*. give formal basis for the specification of multi-formalism models. In the same way, H. Vangheluwe proposes a framework for multi-paradigm modelling and simulation [Vangheluwe *et al.* 2002]. In all those works, the DEVS formalism appears as the common denominator for the integration of heterogeneous models. DEVS provides two ways for integration of non-DEVS models into DEVS simulator: Mapping and Wrapping:

> ***Mapping***: Mapping concept means to find a total equivalence between an existing formalism and DEVS. We can find an example in Jacques and Wainer's works for the mapping of Petri nets into DEVS [Jacques 2002].
>
> ***Wrapping***: Wrapping means to build an algorithm that is compatible with DEVS abstract simulators i.e. to develop a functional interface between a particular model and a DEVS simulator.

In this paper, we propose to deal with wrapping. As we have applications in ecology [Duboz 2003], we need to address systems complexity. Wrapping seems to be a powerful mean to achieve it. We develop a free and open source platform: VLE, available on sourceforge.net website. Initially, VLE only deals with agent based modelling. This platform is now oriented

toward the integration of heterogeneous models. Actually, VLE uses the DEVS formalism and abstract simulators [Zeigler *et al.* 2000] for coupling models by integrating the concept of DEVS-Bus [Kim 1996]. VLE provides a framework for heterogeneous simulators coupling. Furthermore, VLE integrates XML applications to describe experiments and model coupling [Duboz 2002]. VLE is oriented toward the managing of existing models. Figure 2 shows the DEVS-Bus framework in the context of VLE.

We distinguish two layers: the top layer which is in concern with the formal integration and the simulation layer which is in concern with abstract simulators integration into DEVS-Bus.

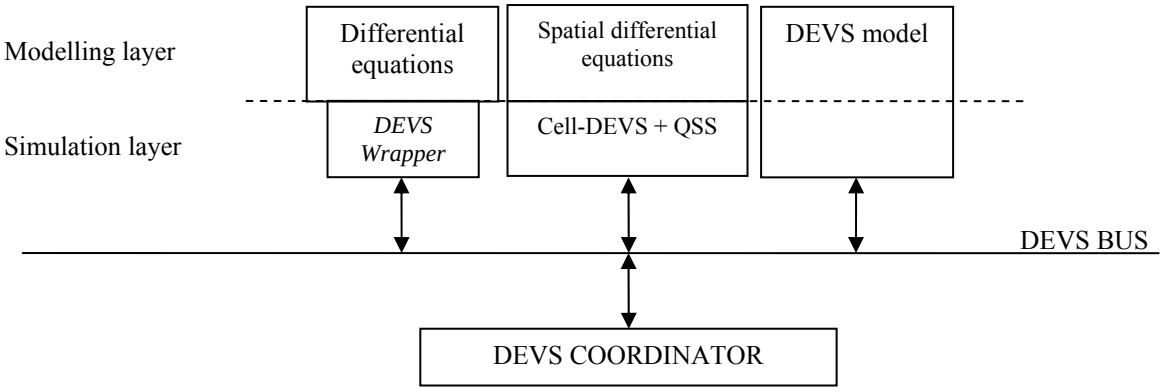

Figure 2: The use of DEVS-Bus for operational and formal coupling in VLE.

In this article, we discuss the articulation between the modelling and the simulation layer (Figure 2). It means that we address the issue of the wrapping of different pre-defined formal models into the VLE framework in order to simulate them.

In such a wrapping, the main difficulty is in concern with the connection of continuous time models or non timed models within the DEVS-Bus framework. Indeed, DEVS specifies discrete events based simulations. It may be difficult to connect simulators with another time scheduling or without explicit representation of what is an event. In this paper, we take an example with the coupling of a DEVS model with a Petri net and an ordinary differential equations system to illustrate this issue. Before presenting our example, we briefly present the formal basis of our works.

1.2. **DEVS and VLE**

A DEVS atomic model is defined as a structure:

$$M = \langle X, Y, S, \delta_{\text{int}}, \delta_{ext}, \lambda, ta \rangle$$

Where:

$X = \{(p,v) \mid p \in InPorts, v \in X_p\}$, is the set of input ports and values.

$Y = \{(p,v) \mid p \in OutPorts, v \in Y_p\}$, is the set of output ports and values.

S, is the set of sequential states.

$\delta_{\text{int}} : S \to S$, is the internal transition function.

$\delta_{ext} : Q \times X \to S$, is the external transition function.

$\lambda : S \to Y$, is the output function.

$ta : S \to \Re_0^+$, is the time advance function.

$Q = \{(s,e) \mid s \in S, 0 < e \leq ta(s)\}$,

Q is the set of total states,

e is the time elapsed since last transition.

A DEVS coupled model defines how to couple atomic models in order to build a new model. The property of closure under coupling guaranties that a DEVS coupled model is equivalent to an atomic one in an upper hierarchical level. Hierarchical decomposition and modularity are fundamental in the DEVS formalism [Zeigler *and al.* 2000]. In VLE, as in DEVS, we consider that δ_{int}, δ_{ext}, λ and ta are functions which encapsulate the dynamic and the behaviour of a model. We are particularly interested in formalism wrapping. Two questions are addressed:

1. "How to translate input and output event notions?"
2. "How to translate, δ_{int}, δ_{ext}, λ and ta?".

Indeed, if we are able to specify those functions considering a particular formalism, we can connect the associated simulators. Into the framework VLE, interaction between simulators and coordinators is given by the five "classical" DEVS functions [Zeigler *and al.* 2000].

```
EventList getOutputFunction(Time currentTime)
Time getTimeAdvance()
void init()
void processInternalEvent(InternalEvent event)
void processExternalEvent(ExternalEvent event)
```

1.3. **Wrapping**

Input and output events for non-DEVS formalism: If the designed formalism is based on the discrete events concept, it does not appear major problems. We just have to check that exchanged events are compatible in term of data type and semantics. If there is no notion of input and/or output event in the formalism we want to couple with a DEVS simulator, we need to find equivalence for those notions. We can propose various strategies for each formalisms, lets us give an example. What does an input or output event "means" for an Ordinary Differential Equation (ODE). In this case, input event can be seen as a perturbation on a particular variable of the ODE system. Therefore, the ODE model must incorporate the adequate behaviour in order to react in a good manner. For instance, the perturbation can be viewed as the definition of new initial conditions. As a consequence, the wrapper has to specify the type of input and output events it can accept. Then, some rules of translation (analogy) explicit how the data of the input events are interpreted in the target formalism.

In a more general way, the exchanged data related to events belong to a mathematical domain (For instance: $\Re^3$ or $\aleph^2 \times \Re$). When using a wrapper, this domain is constrained by the formalism encapsulated in the wrapper. If we consider a Coloured Petri nets (CPN) [Jensen 1997], we can imagine that attributes of coloured tokens take there values from information shared by input events. For outputs events, the wrapper of CPN must translate the arrival of a coloured token in a particular format to generate an output event. The rules of translation depend on the context of coupling, i.e. the models which are coupled with the wrapper [Quesnel 2005].

DEVS transition functions for non-DEVS formalisms: Transition functions specify the dynamic of state changes. These changes are triggered by two functions: the external transition function and the time advance function. Considering non-DEVS formalism, these functions we want to incorporate in a DEVS model must find an equivalent in the targeted formalism. In the case of the external transition function, we have to specify which functions are activated if an external event occurs. As the concept of state is specific to formalism, the state changes are described by the formalism. In other words, there are no major difficulties. In the case of time advance function, it can be more difficult. Indeed, we are facing the definition of time in formalisms. Time can be continuous, discrete or simply missing. In the latter case, the definition of time is given in the context of model coupling. The answer is then given by the context of model coupling.

2. **Wrapping and mapping in VLE**

In this section, we describe the shift from classical formalisms to a wrapper based on two examples: an ordinary differential equations system and a spatial differential equations system.

2.1. **ODE Wrapper**

In this section, we develop a wrapper to encapsulate an Ordinary Differential Equation system. The ODE system is resolved by the classical 4th order Runge-Kutta integration. This method is used in this paper in order to simplify the presentation. We can use any integration method. In VLE, we can deal with any ODE system following the form:

$$\frac{dx_i}{dt} = f_i\left(x_0,...,x_i,...,x_n\right)$$

Where equations are composed with different elements: variables, parameters, functions with parameters, operators (+, −, × or ÷) and real constants. The Runge-Kutta integration method can be change by another integration method like quantized methods QSS1 or QSS2 [Kofman 2001]. These last methods have the advantage to express with DEVS abstract simulator.

In the following sections, we discuss on wrapper signification for an ODE system, we define formally ODE Wrapper and we show an example.

2.1.1 Presentation

First, the equation parameters are initialised at time t_{min} and they don't change during the system resolution. This parameters are useful for us to perform some experiences with just modify their values.

The system variables can be modified at any moment. These modifications are named perturbation. In this wrapper, we define two types of perturbation: *additive* and *reset*. The aim of this property is to apply change on current state of model to manage incoming events. On each perturbation, the resolution algorithm is restarted (i.e. the perturbation defines new initial conditions).

Considering output event, we borrow an example from combined discrete and continuous formalism DEV&DESS [Zeigler *et al.* 2000]. We consider that output events are generated on thresholds. We distinguish three types of thresholds: a threshold on a value, on first derivative and on second derivate. Furthermore, we consider that an output event is generated at each time step of resolution of the integration method.

In the case of output events are generated when a threshold is reached, they are associated with a set of data which are built starting from the state of the system. The data types attached with event are specified by the modeller and they can depend on others models which are connected with the ODE wrapper.

After the translation of input and output events, we must define the transition functions. The internal transition function and the time advance function are related to the integration time step. At each time step, the state of system changes according to a numerical scheme.

According with the DEVS formalism, the output function is computed just before the internal transition function. In our example, the output function must generate an event if a threshold is reached. This computation is made possible thanks to an on line estimation of the derivatives. One can formalise this operation using a DEVS model.

2.1.2 Formal description

In this part, we formally define the ODE Wrapper:

$$M_{ode} = \left\langle X, Y, S, \delta_{\text{int}}, \delta_{ext}, \lambda, ta, \Omega, O \right\rangle$$

The set of states S, is define like:

$$S = \left(\vec{X}, \dot{\vec{X}}, \ddot{\vec{X}}, T \right)$$

Where:

$$\dot{\vec{X}} = \begin{pmatrix} \dot{x}_1 \\ \vdots \\ \dot{x}_n \end{pmatrix}$$

With $\omega \in \Omega$ set of definitions of thresholds, T a set of reached thresholds, $T \in \omega^p, T \subset \Omega, p \in \aleph$ number of reached threshold. $\omega = (i, \alpha, \sigma, v)$ defines of threshold with: i index of variable, α type of threshold (constant, derive1 and

derive2), $\sigma \in \{+,-\} \bigcup 0$. σ represents the direction of variation and v value of variable. $O = \{(p,\omega)\}$ defines the set of output port and threshold couple.

The internal transition is defined:

$$\delta_{\text{int}}\left(\vec{X},\dot{\vec{X}},\ddot{\vec{X}},\emptyset\right) = \left(\vec{X}',\dot{\vec{X}}',\ddot{\vec{X}}',T\right)$$

Where $\vec{X}'$, $\dot{\vec{X}}'$, $\ddot{\vec{X}}'$ are estimated variable at next time. We use Range-Kutta integration method to build estimated variables from $\vec{X}$ to $\vec{X}'$, $\dot{\vec{X}}$ to $\dot{\vec{X}}'$ and $\ddot{\vec{X}}$ to $\ddot{\vec{X}}'$. But all other integration method can be use.

$$\lambda\left(\vec{X},\dot{\vec{X}},\ddot{\vec{X}},\emptyset\right) = \varnothing$$

$$ta\left(\left(\vec{X},\dot{\vec{X}},\ddot{\vec{X}},\emptyset\right)\right) = \Delta$$

With $\Delta \in \Re$ is the integration step.

The previous functions show the integration of ODE. The following functions allow the management of events on the thresholds i.e. when $T \neq \varnothing$

$$\delta_{\text{int}}\left(\vec{X},\dot{\vec{X}},\ddot{\vec{X}},T\right) = \left(\vec{X},\dot{\vec{X}},\ddot{\vec{X}},\emptyset\right)$$

$$\lambda\left(\vec{X},\dot{\vec{X}},\ddot{\vec{X}},T\right) = \{(p,threshold(i,Xi))\}$$

$$ta\left(\left(\vec{X},\dot{\vec{X}},\ddot{\vec{X}},T\right)\right) = 0$$

Where i such as $\omega = (i,\alpha,\sigma,v) \in T$ and $(p,\omega) \in O$. In this article, we generalise the $ta(S)$ function if integration method don't use a synchronous method (for instance QSS2 [Kofman 2001]). If we use only a Range-Kutta integration, we can produce output events and next state of system in same time. In this case,

$$ta\left(\left(\vec{X},\dot{\vec{X}},\ddot{\vec{X}},T\right)\right) = \Delta$$

The external transition function is:

$$\delta_{ext}\left(\left((X_0,\ldots,X_i,\ldots,X_n),\dot{\vec{X}},\ddot{\vec{X}},T\right),e,(p,(i,v,\alpha))\right) = \begin{cases} \left((X_0,\ldots,X_i+v,\ldots,X_n),\dot{\vec{X}},\ddot{\vec{X}},T\right) if\ \alpha = additive \\ \left((X_0,\ldots,v,\ldots,X_n),\dot{\vec{X}},\ddot{\vec{X}},T\right) if\ \alpha = reset \end{cases}$$

$$ta\left(\left(\vec{X},\dot{\vec{X}},\ddot{\vec{X}},T\right)\right) = \sigma - e$$

Such as:

$$X = \{(p,(i,v,\alpha))\}, p \in InPorts.$$

Where $\dot{\vec{X}}'$ and $\ddot{\vec{X}}'$ are re-initialised. If $T \neq \varnothing$ then conflict between internal and external event. The modeller must determine priority management between internal and external events. σ is the time that rest in current state. This method allows system to advance if the wrapper receive external event between two steps.

2.1.3 Algorithms

In this part, we describe algorithms written into the ODE Wrapper of VLE framework. For the *processInternalEvent* function, we present only the detection of constant and positive threshold. The others cases are similar.

```
processInternalEvent(internalEvent : Event)

   If T = ∅ Then
       S' = S
       ODE.solveSystem()
       For each ω = (i, α, σ, ν) ∈ Ω Loop
              If σ = +, α = 'constant', X_i' ∈ S', X_i ∈ S, X_i' < ν < X_i Then T = T ∪ {ω}
              ...
       End Loop
   Else T = ∅
   σ = Δ
   End If
```

Two cases for advance time function: the transient state for the generation of output (ta is null) and the state of numerical integration. The variable σ is equal to Δ, the integration step, in the majority of case. If an external event occurs then σ is decrease with the time elapsed since last transition (e).

```
Time getTimeAdvance()

   If T = ∅ Then Return σ
   Else Return 0
   End If
```

The output function is active when the set of reached thresholds isn't empty. The outputs of the model are building from the set of threshold and are also only discrete. Contrary to HFS (Heterogeneous Flow Systems – [Barros 2002]) or FSPN (Fluid Stochastic Petri Nets – [Kulkarni 1993] [Horton 1998] [Tuffin 2001]), our ODE wrapper didn't process continuous outputs and continuous inputs. The aim of this paper is to show how to build a DEVS wrapper in VLE framework. HFS and FSPN are more efficient methods for modelling and simulation of hybrid systems. Our ODE wrapper is more similar to DTSS/DESS (Discrete Time System Specification / Differential Equation System Specification [Zeigler 2000]).

```
EventList getOutputFunction(currentTime : Time)

   Y = ∅
   If T ≠ ∅ Then
       For each ω = (i, α, σ, ν) ∈ T Loop
              Y = Y ∪ {(p, X_i) / (p, ω) ∈ O}
       End Loop
   End If
   Return Y
```

When an external event occurs on a variable of the differential equations system, a discontinuity appears. The derivative and the second derivative are undefined. The numerical integration method is reset.

```
processExternalEvent(externalEvent : Event)

   Let x ∈ X / x = (p, (i, ν, α))
   If α = additive Then
        X_i = X_i + ν
   Else If α = reset Then
        X_i = ν
   End If
   ∀Ẋ_i, ∀Ẍ_i are undefined
   σ = σ − e
```

2.1.4 Example

In this section, we develop an example of model for using ODE wrapper. We construct a toy model simulating the regulation of prey and predator population dynamic by an external intervention. All unit and parameters values are arbitrary.

We just want an illustration of our approach. We first consider a the prey-predator model defined by Lotka-Volterra [Lotka 1925]:

$$\frac{dX}{dt} = ax - bxy$$
$$\frac{dY}{dt} = -cy + dxy$$

With X the concentration of preys and Y the concentration of predators. Parameters $a=0.2$, $b=0.2$, $c=0.5$ and $d=0.5$ are arbitrary. We use these values in order to obtain a stable equilibrium between preys and predatory. Initial condition are $X=1$ and $Y=0.1$.

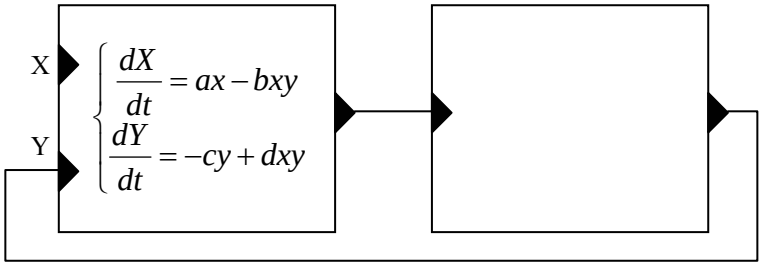

The ODE wrapper can receives disturbances from connected model on its input ports. This model send external event to the wrapper to decrease X variable by a constant: 1.2. ODE wrapper sends external events when Y variable reaches a constant threshold with value 3. The connected model who receives this events, wait 3 events and send an event to decrease X variable.

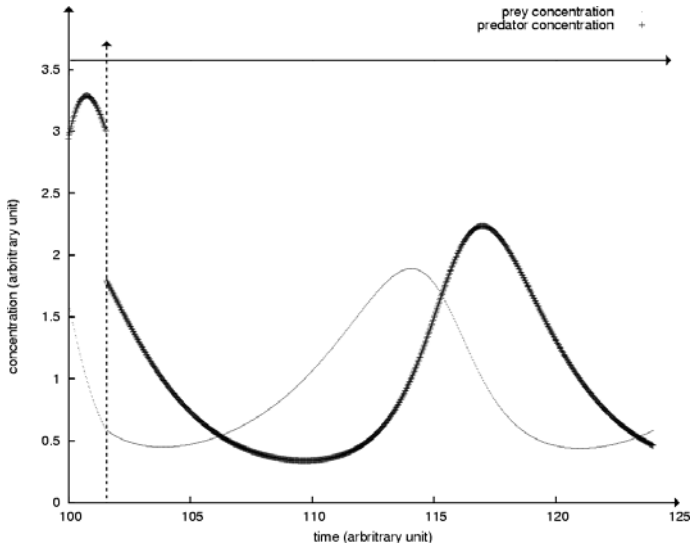

Figure 3: This figure shows a discontinuity in the predator concentration evolution. It corresponds to an event of predator uptake. At the same date, we can see another discontinuity in the evolution of prey concentration.

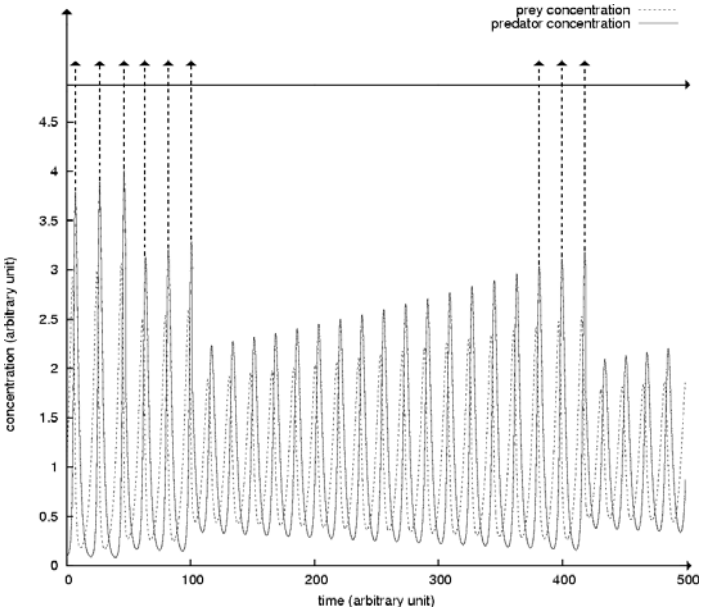

Figure 4: Oscillation of preys and predator concentration over time. Predator are taking off (-1.2 predators) if the concentration reach 3 times the arbitrary units of 3 predators. Taking predator introduce instabilities in the evolution of populations.

2.2. **CellQSS mapping in VLE : Spatial Differential Equations**

Another class of differential equations is partial differential equation. For this class, it's possible to use the previous tool, the ODE wrapper but, in this section, we propose another approach: the mapping technique in VLE framework. We will show that it is possible to generalize the use of DEVS formalism, Cell-DEVS and QSS with the partial differential equations with the derivative.

In the first part, we present the concept of quantification integrator and an extension of DEVS for cellular automaton. The first permits to propose a method to solve an ordinary differential equation. The mainly property of this method is to be express into DEVS framework. The second formalism is an extension of DEVS and proposes formalism for spatial process. In our case, the partial differential equation, we limit ourselves to the partial derivatives according to the time and the space.

2.2.1 Brief presentation of quantification integrators

Parallel to the traditional methods appeared new techniques of numerical resolution of differential equations based on the quantification of the output values rather than on the discretization of time. Thus, Kofman proposes in [Kofman 2001] [Kofman 2002] through QSS1 and QSS2 two methods of numerical resolution of first order differential equations. For the presentation of these two methods, let us consider the following system:

$$S\begin{cases} \dot{x}_i(t) = f_1(x_1(t),\ldots,x_n(t)) \\ \qquad\qquad \vdots \\ \dot{x}_n(t) = f_n(x_1(t),\ldots,x_n(t)) \end{cases}$$

The global idea is to approximate the functions $x_i(t)$ by constant piecewise functions (for QSS1) or of the affine piecewise functions (for QSS2) then to encapsulate each x_i in an atomic DEVS model. At an instant denoted t, each model has like state variable a constant for QSS1 or an affine function for QSS2. Lastly, it's appropriate for the models to compute an internal transition when their states move away too much the theoretical curve to integrate.

2.2.2 Another extension of DEVS: Cell-DEVS

The extension named Cell-DEVS was born from the following observation: many models use discrete spaces and use formalisms such as the cellular automata. Wainer and Giambiasi in [Wainer 01] developed Cell-DEVS. This extension must be able to describe and simulate models as a multidimensional cellular automata and discrete events. The dynamics of the cells is time-lag i.e. that the state of cell will be modified according to the state of its neighbour cells, but it will be known by neighbour cells after a certain time. The basic idea is to provide a simple mechanism of definition of the synchronization of the cells. As for any proposal for an extension, the authors offer at the same time the extension of the formalism which is

summarized with the addition of variables and their semantics, and the abstract simulator. In this paper, we propose a simplified structure according to the coupling with QSS formalisms.

Our Cell-DEVS atomic model is defined as a structure:

$$M = \langle X, Y, I, S, \delta_{\text{int}}, \delta_{ext}, \lambda, ta, \sigma, d, N \rangle$$

Where

X is the set of external input events;
Y is the set of external output events;
I is the interface of cell (list of neighbours);
$N = \{(\eta_i, s_i) / \eta_i \in I\}$ is the state of neighbourhood (it's a simplification compared to the original version);
S is the state variables used in each cell without the state of neighbourhood;
d $\in \boldsymbol{R}_0^+$ is the diffusion delay of the state;
$\delta_{\text{int}} : S \to S$ is the internal transition function;
$\delta_{ext} : Q \times X \to S$ is the external transition function, where Q is the state values defined as:

$$Q = \{(s, e) / s \in S \times d, e \in [O, ta(s)]\}$$

λ: S $\to Y$ is the output function;
ta: S x d $\to \boldsymbol{R}_0^+ \cup \infty$, is the state's duration function.

2.2.3 Integration of QSS into Cell-DEVS

By applying directly the principle of discretization of space and the transformation into linear system of order 1, it is already possible to integrate this kind of equation:

$\frac{\partial^n T}{\partial^n t} = \varphi\left(\frac{\partial^{n-1} T}{\partial t^{n-1}}, \ldots, \frac{\partial T}{\partial t}, T, \frac{\partial T}{\partial x_1}, \frac{\partial^2 T}{\partial x_1 \partial x_2}, \ldots, \frac{\partial^p T}{\partial x_1 \ldots \partial x_p}, \ldots\right)$ if an approximation of $\partial^p T / \partial x_1 \ldots \partial x_p$ is possible.

Let us show this assertion: let $f_i(t)$ the discretization of $\partial^p T / \partial x_1 \ldots \partial x_p$ then $f_i(t)$ will depend on $T(t, x), T(t, x-h), \ldots$ and will not depend on differential. Let us $T_1(t) = \frac{\partial T}{\partial t}, \ldots, T_{n-1}(t) = \frac{\partial^{n-1} T}{\partial t^{n-1}}$. Thus the previous equation becomes:

$$\frac{\partial^n T}{\partial T^n} = \varphi(T_{n-1}(t), \ldots, T_1(t), T(t), f_1(t), f_2(t), \ldots, f_p(t))$$

and it's possible to transform to a system:

$$\begin{cases} \dfrac{\partial T}{\partial t} = T_1 \\ \dfrac{\partial T_1}{\partial t} = T_2 \\ \dfrac{\partial T_2}{\partial t} = T_3 \\ \vdots \\ \dfrac{\partial T_{n-2}}{\partial t} = T_{n-1} \\ \dfrac{\partial T_{n-1}}{\partial t} = \varphi\left(T_{n-1}(t), \ldots, T_1(t), T(t), f_1(t), f_2(t), \ldots, f_p(t)\right) \end{cases}$$

Only ordinary differential equations are defined. Each equation depends on several ODE. In the case of spatial differential equation, if the space is discretized then these equations depend on neighbourhood.

2.2.4 Algorithms

In this part, we describe algorithms written with VLE framework. Before the description of algorithms, we define some variables of DEVS abstract simulator:

- t : the current time
- t_L : the time of last event
- t_N : the time of next event ($t_N = t_L + ta(S)$)
- e : the time elapsed since last transition
- σ : the time remaining in the current state ($\sigma = t - t_N = ta(S) - e$)

Each variable is indexed by the number of differential equation and by the index of cell. In the following, we omit to indicate the index of cell in order to simplify algorithms.

The internal transition function is identical to that of QSS. Indeed, if no event occurs before σ_i then the threshold q_i is reached and the gradient must be revalued.

```
processInternalEvent(internalEvent : Event)
```

Let i the current differential equation (i. e. $\sigma_i = 0$)

If $\dot{x}_i > 0$ Then $q_i = q_i + 1$ Else $q_i = q_i - 1$

$x_i = q_i \Delta q$

$\dot{x}_i = f_i(t)$

$\forall j \neq i, \sigma_j = \sigma_j - \sigma_i$

$\sigma_{\min} = \min_{i \in [1;n]} \sigma_i$

If $\left|\dot{x}_i\right| < \varepsilon$ Then $\sigma_i = +\infty$

Else If $\dot{x}_i > 0$ Then $\sigma_i = \dfrac{(q_i + 1)\Delta q - x_i}{\dot{x}_i}$

Else $\sigma_i = \dfrac{q_i \Delta q - x_i}{\dot{x}_i}$

The advanced time function is very simple. The duration of state without external perturbation is equal to the minimal of time to reach a threshold q_i.

```
Time getTimeAdvance()
   Return σ_min
```

When the gradient of one or more equations is modified by internal event (i.e. the state is modified), the values of variables of the system are posted to neighbour cells from the output function. Each cell has only one output port for the propagation of state of cell.

```
EventList getOutputFunction(currentTime : Time)
   Y = ∅
   If state is modified Then
       V = ∅
       For all differential equation f_i Loop V = V ∪ {X_i} End Loop
       Y = Y ∪ {(out,V)}
   Return Y
```

Two kinds of external event can occurs: one of neighbour cell have changed its state or another model coupled to CellQSS model makes a perturbation. In these two cases, the gradient of each function can be modified. So, one must to compute the state of system when external event occurs and the gradient function is compute too in order to estimate the new σ_i.

```
processExternalEvent(externalEvent : Event)
   If externalEvent is a change of state of neighbour Then
       Let p ∈ I , the name of neighbour
       Let v, the new state of current neighbour
       s_p = v where (p, s_p) ∈ N
   Else processPerturbation
   For all differential equation f_i Loop
       Let e_i = t − t_{L_i}
       If e > 0 Then x_i = x_i + e ẋ_i
       ẋ_i = f_i(t)
       If |ẋ_i| < ε Then σ_i = +∞
       Else If ẋ_i > 0 Then σ_i = ((q_i + 1)Δq − x_i) / ẋ_i
                Else σ_i = (q_i Δq − x_i) / ẋ_i
       T_{L_i} = t
   End Loop
```

In case of external perturbation, the gradient of each function is reset and the quantum is updated.

```
processPerturbation(externalEvent : Event)
   For all differential equation f_i Loop
       Ẋ_i = 0
       q_i = E(Ẋ_i / Δq)
       σ_i = 0
   End Loop
   σ = 0
```

2.2.5 Example

Let us consider the example of the equation of diffusion of heat on a bar [Fletcher 2000] for illustration of QSS and Cell-DEVS:

$$\frac{\partial T(t,x)}{\partial t} = K \frac{\partial^2 T(t,x)}{\partial x^2}$$

where K is the coefficient of diffusion.

We make an approximation of T(t,x) by its values in various points of the bar after having chosen a space step ∂x. Denoted $T_i(t)$ these values, the previous equation becomes:

$$\frac{\partial T_i(t)}{\partial t} = K \frac{T_{i-1}(t) - 2T_i(t) + T_{i+1}(t)}{(\Delta x)^2}$$

for all i from 1 to N, using, by example, an approximation of the second derivative in three points.

One of the traditional approaches (the explicit method, for instance) would now consist to approximating $\partial T_i(t)/\partial t$ by $(T_i(t+\Delta t) - T_i(t))/\Delta t$. But the equations form at this level a system of first order differential equations in $T_i(t)$. It is thus possible to solve them using a QSS method.

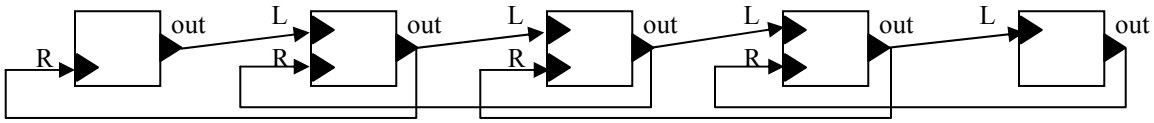

3. Discussion and Perspectives

The first question in this article is how to bring making of VLE wrapper from existing models. Several stages are necessary. The first part, we must find in study model, elements like time, states, events etc. Some models like Petri net can make problems because time does not exist in basic Petri net structure however time is a principal element of DEVS formalism. In this case, time must be recreated in the formalism in order to satisfy DEVS functions [Quesnel 2005].

Second stage is to define state of model. State S is an important element. The state can be accompanied of DEVS formalism elements. After state, we must define an internal transition function δ_{int} who allows changing state. An external transition function δ_{ext} can be defined to manage external events. We must attach each element to its DEVS function. Lastly, we must find in the model how an input event could come to disturb the current state.

This paper is a first step toward the integration of complex model such as multi-paradigm systems. If we consider pre-existing models which are not formalised, Wrapping techniques can be very useful to permits there reusability

In section 2, we defined two DEVS models used in VLE framework to model continuous systems. First, we use wrapping technique to develop a wrapper to an ODE formalism based on Runge Kutta integration method. Second, we develop a model based on mapping method to perform coupling between a cell automata, CellDEVS, and an ODE system, QSS, to build spatialized equation systems.

With these models, we offer to model continuous and discrete models. However, is VLE framework providing tools and models to build hybrid systems?

Hybrid systems are defined as systems using both continuous and discrete behaviour. Differential equations are used for representing continuous system, discrete event for discontinuities. There is some works on this type of systems like the Fluid Stochastic Petri Nets (FSPNs) defined by V.G. Kulkarni and K.S Trivedi [Horton Kulkarni 1998]. In this type of Petri net, some features are different from traditional Petri net.

- The tokens transport continuous variables.

- Two type of transition exist:
    - Stochastic: Transitions are fired after a random timed.
    - Classical but with condition: Transitions are fired fallow some conditions. The Conditions are function of continuous variables on tokens.

In next section, we study the implementation possibilities, in VLE framework, of hybrid system. We explain the Heterogeneous Flow System Specification (HFSS) defined by F.J. Barros [Barros 2002] and its potential integration in VLE.

The HFSS is a paradigm for simulating hybrid systems. HFSS is based on DEVS formalism and provides discrete and continuous input and output ports, a set of states, a transition function which depends on discrete and continuous inputs.

HFFS is defined by:

$$HFSS = \left(X, Y, S, \rho, \tau, q_0, \delta, \Lambda_c, \lambda\right)$$

Where:

$X = X_c \times X_d$ is the of input flow values, X_c the set of continuous input flow values, X_d the set of discrete input flow values.

$Y = Y_c \times Y_d$ is the of output flow values, Y_c the set of continuous output flow values, Y_d the set of discrete output flow values.

S is the set of partial states.

$\rho : S \to \Re_0^+$ is the time to input function.

$\tau : S \to \Re_0^+$ is the time to output function.

$q_0 = \left(s_0, e_0\right) \in Q$ is the initial state, with e is the time to transition function.

$\delta : Q \times \left(X_c \times X_d^{\emptyset}\right) \to S$ is the transition function

HFSS entries are continuous or discrete. Continuous input ports, using sampling, have an influence on continuous system. Discrete inputs can change the state of HFSS model. HFSS uses threshold to build discrete outputs and continuous output ports. The fundamental idea of HFSS paradigm is the discrete entries cause change of state on system and thus cause change between differential functions.

HFSS seems to be a technique to develop efficient hybrid systems in speed building and simulation. HFSS uses optimisation in simulator to increase simulation. However, the main critical remark for us is the incompatibility with DEVS formalism used in VLE framework. In DEVS we need two transition functions: an internal and an external to make models compliant with DEVS abstract simulator.

An alternative to HFSS i.e., to allow creation of hybrid systems and to create an equivalent to HFSS, is to use the GDEVS (Generalized Discrete Event Specification formalism [Giambiasi *et al.* 2000]). It's a compliant DEVS models that uses polynomials of arbitrary degree to represent the piecewise input-output trajectories of a discrete event model instead of DEVS who approximates the input, output, and state trajectories through piecewise constant segments. The input ports can change a coefficient to change state of continuous variables. A coefficient event is considered as an instantaneous event. The GDEVS model provides to VLE framework new methods to develop hybrid systems and a good replacement to HFSS.

REFERENCES

[Barros 2003] Barros F., "Dynamic Structure Multi-Paradigm Modeling and Simulation," A*CM Transactions on Modeling and Computer Simulation*, Vol. 13, No. 3, pp. 259-275, 2003.

[Barros 2002] Barros F., "Modeling and Simulation of Dynamic Structure Heterogeneous Flow Systems." *SIMULATION: Transactions of The Society for Modeling and Simulation International*, Vol. 78, No. 1, 18-27, 2002.

[Branicky 1997] Branicky M. S. and Mattson S. E., Simulation of hybrid systems. In Hybrid Systems IV, P. J. Antsaklis, W. Korn, A. Nerode, and S. Sastry, Eds. Lecture Notes in Computer Science, vol. 1273. Springer-Verlag, New York, 1997

[Ciardo 2003] Ciardo G., Dinol D.M. and Trivedi K.S., Discrete-Event Simulation of Fluid Stochastic Petri Nets, *IEEE Transactions on software engineering*, 25 (2): pages 207-217, 1999.

[D'Abreu 2003] D'Abreu M. C. and Wainer G. A., Models for Continuous and Hybrid System Simulation, Proceedings of the 2003 Winter Simulation Conference, pp. 642-649, 2003.

[Duboz 2003] Duboz R. and Ramat E., Towards the simulation of scale transfert in ecological modelling using computational emergence: Parametrization of classical population model with reactive agent model. *Systems Analysis Modelling Simulation*, volume 43, 793–814, 2003.

[Duboz 2002] Duboz R., Xml for the representation of semantic in model coupling. In F. J. Barros and N. Giambiasi, editors, AIS'2002. AI, *Simulation and Planning in High Autonomy Systems*, 267–270, Lisboa, Portugal, april 7-10, 2002.

[Fishwick 1995] Fishwick, *P.A. Simulation Model Design and Execution*. Number ISBN 0-13-098609-7. Prentice Hall, 1995.

[Fishwick 1992] Fishwick, P.A. and Zeigler B.P. A multi-model methodology for qualitative model engineering. *ACM transaction on Modeling and Simulation*, **2-**1:52–81, 1992.

[Fletcher 2000] C.A.J. Fletcher, Computational Techniques for Fluid Dynamics, Volume 1 and 2, Springer, 2nd Edition, 2000.

[Giambiasi *et al.* 2000] Giambiasi N., Escude B., Ghosh S. GDEVS: A generalized discrete event specification for accurate modeling of dynamic systems, *Transactions of the Society for Computer Simulation International* 17(3): 120-134, 2000.

[Horton Kulkarni 1998] Horton G., Kulkarni V.G. and Trivedi K.S., Fluid Stochastic Petri Nets: Theory, Application and Solution. European Journal of Operational Research, 105: 184-201, 1998.

[Kim 1996] Kim Y.J. and Kim T.G., A heterogeneous distributed simulation framework based on devs formalism. In Sixth Annual Conference On Artificial Intelligence, *Simulation and Planning in High Autonomy Systems*, 116–121, La Jolla, California, USA, 1996.

[Kofman 2001] Kofman, E. and Junco, S. (2001). Quantized state systems. A devs approach for continuous systems simulation. *In Transactions of SCS*, volume 18, 123-132, 2001.

[Kofman 2002] E. Kofman, "A Second Order Approximation for DEVS Simulation of Continuous Systems". *Transactions of SCS*, **78**-2, pp. 76–89, 2002.

[Kulkarni 1993] Kulkarni, V.G. and Trivedi, K.S., FSPNs: Fluid Stochastic Petri Nets. In 14th International Conference on Applications and Theory of Petri Nets, pages 24-31, 1993.

[Quesnel 2005] G. Quesnel, R. Duboz and E. Ramat, Wrapping into DEVS Simulator: A Study Case, International Mediterranean Modeling Multiconference, pp. 374-382, 2005.

[Lotka 1925] Lotka, A.J. *Elements of physical biology*. Baltimore: Williams & Wilkins Co, 1925.

[Tuffin 2001] Tuffin B., Chen D.S. and Trivedi K.S., Comparison of Hybrid Systems and Fluid Stochastic Petri Nets. Discrete Event Dynamic Systems, 11 (1-2), 2001.

[Vangheluwe *et al.* 2002] Vangheluwe, H., Lara, J., and Mosterman, P.J. An introduction to multi-paradigm modelling and simulation. In F.J. Barros and N. Giambiasi, editors, AIS'2002. Simulation and Planning in High Autonomy Systems, 9–20. *Society for Modelling and Simulation International*, Lisbon, Portugal, April 2002.

[Zeigler 1976] Zeigler, B.P. *Theory Of Modeling and Simulation*. Wiley Interscience, 1976.

[Zeigler et al. 2000] Zeigler, B.P., Kim, D. and Praehofer, H. Theory of modeling and simulation: Integrating Discrete Event and Continuous Complex Dynamic Systems. Academic Press, 2000.

Towards the Verification and Validation of DEVS Models

Yvan Labiche
Carleton University
Systems and Computer Engineering Dept.
1125 Colonel By Drive
Ottawa, ON K1S5B6, Canada
+1 613 520 2600 ext. 5583
labiche@sce.carleton.ca

Gabriel Wainer
Carleton University
Systems and Computer Engineering Dept.
1125 Colonel By Drive
Ottawa, ON K1S5B6, Canada
+1 613 520 2600 ext. 1957
gwainer@sce.carleton.ca

ABSTRACT
The creation of a simulation model, like the creation of any software product, is guided by principles and procedures that have been reasonably well established within the software engineering community. In the context of a simulation, we need to be able to characterize the dynamic behavior of the system, and such characterization should be expressed in a format that is as clear and unambiguous as possible. Wherever feasible, formal approaches should be used. One of these formal techniques, the DEVS formalism, has gained popularity in recent years. Although some efforts have been dedicated to the Validation and Verification (V&V) of DEVS models, this is an open research area with interesting opportunities for application of advanced software engineering techniques. Indeed, it appears that thanks to the characteristics of DEVS models and the fact that DEVS models can be executed (e.g., the CD++ toolkit allows the use of DEVS and Cell-DEVS formalisms) well-known software testing techniques are worth investigating for the V&V of DEVS models. In this article, we show these similarities and discuss open research paths in the field of DEVS modeling Verification and Validation by means of testing.

KEYWORDS
DEVS, Cell-DEVS, CD++, Verification & Validation, Testing

1. Introduction

In recent years, several efforts have been devoted to define modeling paradigms, improving the analysis of complex dynamic systems through simulation. The creation of a simulation model, like the creation of any software product, is guided by principles and procedures that have been reasonably well established within the software engineering community. A key prerequisite is the specification of a set of requirements, which, in a simulation context, means the characterization of the dynamic behavior of the System of Interest (SoI). It is essential that this characterization be expressed in a format that is as clear and unambiguous as possible. Wherever feasible, formal approaches should be used: e.g., Petri nets, Bond Graphs, Partial/Ordinary Differential Equations, etc. A formalism that gained popularity in recent years is called DEVS (Discrete Event systems Specification). It allows modular description of models that can be integrated using a hierarchical approach [Zeigler et al. 2000]. Different environments have been built to support modeling and simulation of discrete-event systems using DEVS, and a current effort is trying to standardize modeling environments [DEVSTD 2004]. One of them, the CD++ toolkit [Wainer 2002], allows the use of DEVS and Cell-DEVS [Wainer and Giambiasi 2001] formalisms. CD++ provides both graphical and programmatic (C++) ways of building simulation models [Christen et al. 2004].

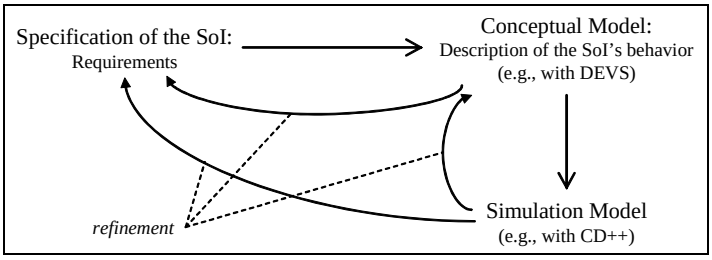

Figure 1 Deriving a simulation model: Life cycle

These activities can be organized in a life cycle (Figure 1), which begins with the definition of the requirements and follows with the definition of the conceptual and simulation models. As any software life cycle, this process is cyclic, allowing

refinement. Reasons for refinement include but are not limited to: changes to the level of granularity of the model to better address the goals of the simulation, modification and maintenance of the model(s) to fix defects.

Validation and Verification (V&V) of these different steps has already been identified as paramount for users of such technology [Sargent 2000]. A simulation model can be useful and effective only to the extent that there is enough confidence in the results which it generates. *Validation* is concerned with the fundamental issue of whether or not the simulation model is an acceptable representation of the SoI, when viewed from the perspective of the stated goals of the intended simulation study. Typically, the question to be answered is: "Are we simulating, or have we simulated, the right system?" As the simulation model is an evolution of the conceptual model (together with aspects of the requirements specification), it follows that the validation process needs to focus on the conceptual model. On the other hand, *Verification* is concerned with the transformation of the conceptual model into a simulation model. Here, the question one tries to answer is: "Are we simulating, or have we simulated, the system right?"

V&V activities do not constitute a particular phase of the life cycle, but are an integral part of it, and Validation and Verification (V&V) techniques have to be used throughout this life cycle. V&V activities must be as systematic as possible and must be documented correctly to increase our confidence into simulation results.

Testing, that is the execution of a system with actual values (as opposed to symbolic execution) is one well known technique, among others, that has been used to verify and validate software systems. Given that simulation models such as DEVS models have the interesting property of being "executable" (thanks to environments such as CD++) we are interested in using (possibly adapting) traditional software testing techniques to perform V&V of discrete-event models based on the DEVS formalism.

A first attempt at adding V&V capabilities to CD++ by means of testing was described in [Wainer et al. 2002], where a specific infrastructure for the execution of test cases on DEVS models is described. Specifically, test case data provided by the tester is translated into a DEVS model (a DEVS *Generator* model) that represents a component of an Experimental Framework created for testing purposes, and it is connected to the model under test to generate test input(s). Another DEVS model (called the *Transducer*) is created to collect the output(s) of the model under test and verify whether they correspond to the expected ones, i.e., whether there is a failure. Experiments did show that such infrastructure could indeed help the designer to find defects in the model(s).

Although these facilities provide basic infrastructure to carry out the tests, a systematic approach for the derivation of test cases is required: we want to trust the simulation models. Shortcomings uncovered during the execution of the simulation model imply either shortcomings in the requirements specification or shortcomings in the verification process. In order to ensure trust, we need to address different issues: How has this been achieved? What was the testing strategy followed? (if any) Are the results simply empirical evidence? Are there any measures of code coverage when executing a set of models (benchmarks?).

In this article, we address some of these questions, and provide general ideas on how to solve them in the long term, showing some open research questions and possible solution paths. Very recent efforts [Traoré and Zeigler, 2004] tried to formalize the concepts of Experimental Frameworks and their relationship with DEVS models. A discussion about the relation between these two efforts is outside the scope of this paper, and it could be addressed in future work. In our particular case, we are not focused on the formalization of the Experimental Framework concept, nor in the meta-modeling methods involved. Instead, we want to explore new techniques to incorporate automated testing facilities that are well-known in the Software Engineering community to the testing framework based on Experimental Framework originally presented in [Wainer et al. 2002].

In the following sections, we shortly describe the DEVS formalism and discuss some basic facilities already built into the CD++ toolkit (Section 2), and introduce some software testing terminology (Section 3). We then discuss how traditional software testing techniques pertain to the V&V of simulation models described in DEVS (Section 4). Conclusions are drawn in Section 5.

2. The DEVS formalism and CD++

The DEVS formalism was originally defined in the '70s as a discrete-event modeling specification mechanism. It is a systems theoretical approach that allows the definitions of hierarchical modular models that can be easily reused [Zeigler et al. 2000]. A real system modeled with DEVS is described as a composite of submodels, each of them being behavioral (atomic) or structural (coupled). Each model is defined by a time base, inputs, states, outputs and functions to compute the next states and outputs. It has been proved that DEVS models are closed under coupling, that is, when observing the I/O trajectories of a given atomic model, we can always find a coupled model that is semantically equivalent, although having different structure. This allows coupled models to be integrated to a model hierarchy, allowing model reuse. As a result, the security of the simulations is enhanced, testing time reduced, and productivity improved.

A DEVS atomic model is formally described by:

$$M = < X, S, Y, \delta_{int}, \delta_{ext}, \lambda, ta >$$

Each atomic model can be seen as having an interface consisting of *input* (**X**) and *output* (**Y**) *ports* to communicate with other models. Every *state* (**S**) in the model is associated with a *time advance* (**ta**) function, which determines the duration of the state. Once the time assigned to the state is consumed, an internal transition is triggered. At that moment, the model execution results are spread through the model's output ports by activating an *output function* (**λ**). Then, an *internal transition function* (**δ_{int}**) is fired, producing a local state change. Input external events (those events received from other models) are collected in the input ports. An external transition function (**δ_{ext}**) specifies how to react to those inputs, using the current state (S), the elapsed time since the last event (e) and the input value (X).

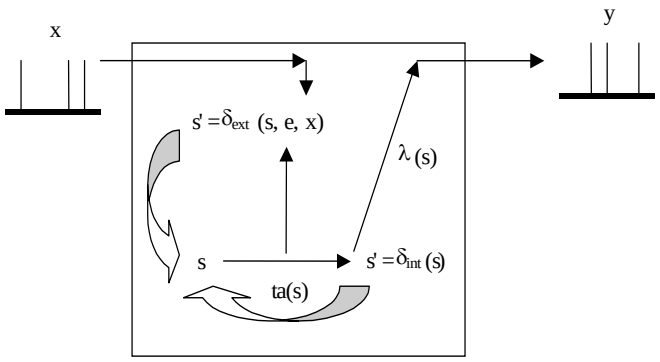

Figure 2. Informal description of an atomic model.

A DEVS coupled model is composed of several atomic or coupled submodels. They are formally defined as:

$$CM = < X, Y, D, \{M_i\}, \{I_i\}, \{Z_{ij}\} >$$

Coupled models are defined as a set of basic components (**D**), which are interconnected through the model's interfaces (***X***, ***Y***). The translation function (**Z_{ij}**) is in charge of converting the outputs of a model into inputs for the others. To do so, an index of influencees is created for each model (**I_i**). This index defines that the outputs of the model **M_i** are connected to inputs in the model M_j, where j is an element of I_i.

CD++ is a modeling and simulation tool that implements DEVS and Cell-DEVS theories. It allows to define models according to the specifications introduced in the previous section [Wainer 2002]. A set of independent applications related with the tool allows the user to have a complete toolkit to be applied in the development of simulation models.

The tool is built as a hierarchy of models, each of them related with a simulation entity. Atomic models can be described simply graphically or programmed in C++. CD++ provides a framework of CD++ classes with that purpose. A specification language allows to define the model's coupling, including the initial values and external events. Graph-based notations have the advantage of allowing the user to think about the problem in a more abstract way. Therefore, we have used an extended graphical notation to allow the user define atomic models behavior [Christen et al. 2004], based on the DEVS-graphs notation suggested in [Zeigler et al. 1996]. On the other hand, C++ classes increase flexibility, e.g., to define complex output functions. Figure 3 (a) represents a simple model using all the constructions available for the DEVS Graph notation in CD++.

Each state is represented by a bubble including an identifier and the duration for the state (TL). This specification allows defining the pair (state, duration) associated with internal transition functions. For instance, Figure 3 (a) shows a state called "Start", whose duration is 4 time units. Each model includes an interface with input/output ports, represented as arrowheads associated to a model definition. Internal transition functions are represented by arrows connecting two states. Each of them can be associated to pairs of ports with values (p,v) corresponding to the output function. The syntax for the output function values is **`p!v.`** For instance, the model in the figure represents a state change from *Process* to *Finish* after 10 time units. In that moment, the output function will execute, sending the value 1 through the port *out*. External transition functions are represented graphically by a dashed arrow connecting two states. The notation used to represent ports and expected values is similar to the one used for external transition, but replacing the exclamation mark by a question mark: **`p?v [`t_i`..`t_f`].`** Here, **`p`** and **`v`** represent the input port for the event and the value needed to trigger the associated input behavior, while **t_i`..`t_f** represent the initial and final expected external event times for the external transitions. These values represent the elapsed time value, as the external transitions can produce different state changes according to the elapsed time when an external event arrives. The model in Figure 3 (a) can be formally defined as illustrated in Figure 3 (b).

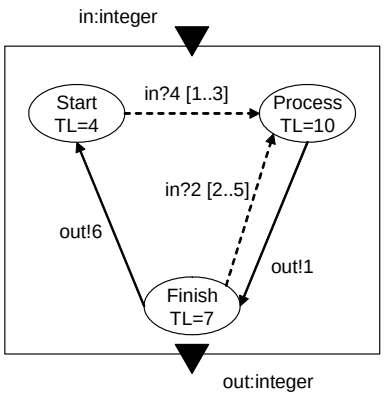

(a)

Server = < X, S, Y, δ_{int}, δ_{ext}, λ, ta >

X = { in / in ∈ Z };

Y = { out / out ∈ Z };

S = { Start, Process, Finish };

δ_{int} (Process) = Finish, δ_{int} (Finish) = Start;

δ_{ext} (Start, e, in) = { i = = 4 && 1 ≤ e ≤ 3 } ?
⇒ Process,

δ_{ext} (Finish, e, in) = { i = = 2 && 2 ≤ e ≤ 5 } ?
⇒ Process

λ(Finish) = (out = 6), λ(Process) = (out = 1);

ta (Start) = 4, ta (Process) = 10, ta (Finish) = 7.

(b)

```
[Server]
in: in
out: out
state: Start Process Finish
int: Process Finish out!1
int: Finish Start out!6
ext: Start Process  in 4 [1..3]
ext: Finish Process in 2 [2..5]
Start: 4
Process: 10
Finish: 7
```

(c)

Figure 3. Definition of an atomic model

CD++ defines an analytical notation for DEVS graphs, which can be executed by a model's interpreter. Figure 3 (c) shows the analytical specification for the model presented earlier in Figure 3 (a): Four lines (starting in "int:" or "ext:") define the state changes according to internal and external transition functions.

- After each atomic model is defined, they can be combined into a multicomponent model. Coupled models are defined using a specification language specially defined with this purpose. The language was built following the formal definitions for DEVS coupled models.

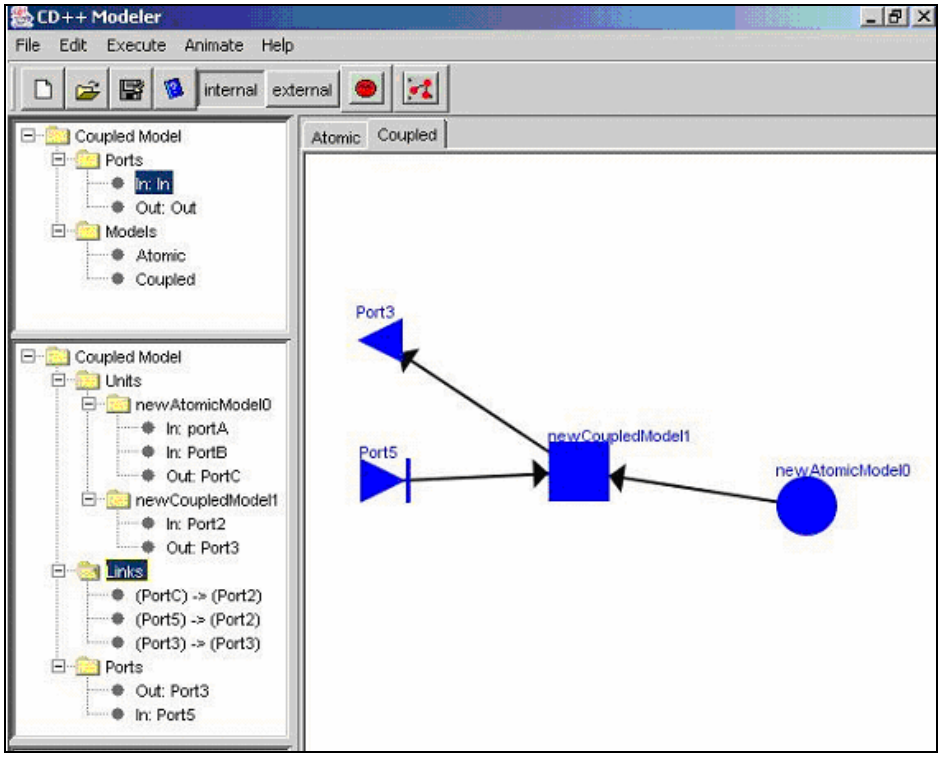

Figure 4. Analytical definition of Figure 3 (a) in CD++.

3. Software Testing Terminology

When testing a software system, the tester usually builds a *model* representing the software. The model can represent the structure of the software (e.g., the control flow graph of a procedure), in which case the testing technique is called *white-box*

(or *structural*), or its behavior (e.g., a finite state machine) in which case the technique is called *black-box* (or *functional*) [Beizer 1990]. A *criterion* is then selected among a set of possible criteria to drive the construction of test cases from the model. A criterion usually indicates how much the elements of the model should be exercised (we say covered) by the test set composed of test cases. The *coverage ratio* of a test set is the proportion of the elements of the model that are covered by the test set. A tester usually tries to achieve a 100% coverage ratio, in which case the test set is said to be *adequate* for the selected criterion. A typical criterion for the control flow graph and finite state machine models are the all-statements and all-transitions criteria, respectively [Beizer 1990, Binder 1999]. The decision of choosing a specific criterion rather than another can be driven by the so called subsumes relationship between criteria [Binder 1999]: We say that criterion C1 *subsumes* criterion C2 when, for every program, any adequate test set for C1 is also adequate for C2. For instance, in the context of a state machine, the all transitions criterion (requiring that all the transitions be exercised) subsumes the all states criterion, since whenever a test set covers all the transitions, it also covers all the states. It is then possible to establish a subsumes hierarchy, that is to analytically compare criteria. A subsumes hierarchy usually indicates that some criteria are more expansive (e.g., in terms of number of test cases in an adequate test set) than others. However, it is not informative as to whether one criterion is more effective at finding faults than another, even when the former subsumes the latter.

A typical testing infrastructure entails the system under test, a *driver* in charge of executing the test cases[1] (it drives the tests), and *stubs* simulating the behavior of any software or hardware device that is not yet available (e.g., not yet developed) during the testing campaign. In the end, the tester needs a mechanism to decide whether a test case has passed or not. In the latter case, the test case has revealed a failure. This mechanism is known as the test *oracle*, and it is usually assumed that the tester is able to build one: This is known as the oracle assumption [Howden 1987]. An oracle requires (1) a mechanism to compute the expected value of a test case execution from the specifics of the test case, and (2) a mechanism to compare the actual result with the expected one [Beizer 1990, Binder 1999]. Unfortunately, building an oracle is rarely an easy task. It may even be impossible to build an oracle at reasonable costs (i.e., a cost that is lower than the cost of building the system under test): This violates the oracle assumption. When this happens, alternatives have to be found [Weyuker 1982] (e.g., partial oracle that only checks that the output is within range).

One advantage of testing, which likely explains that this has been the main software V&V technique used in practice, is that it does imply the execution of the software system under test. A major drawback, though, is that one can prove the presence of bugs but never their absence with testing techniques [Dijkstra 1972]. It is then paramount to be systematic when testing (thus the use of criteria) in order to increase our (tester, user) confidence in the system. Such a use of a model and associated criterion is indeed encouraged and required for the certification of specific software systems (e.g., avionics systems [RTCA 1992]).

4. Verification and Validation of DEVS Models: Techniques and Issues

When one wants to model and simulate a discrete event system, a possible approach is to model the system using the DEVS formalism [Zeigler et al. 2000] and simulate it using the CD++ toolkit [Wainer 2002], as described in Section 2, and illustrated by the left swimlane in the UML activity diagram [Booch et al. 1999] of Figure 5 (also referred to as Figure 5(a)). The *DEVS model* is defined and the *CD++ toolkit* is used to produce *Simulation results*. If one wants to perform V&V activities for the discrete event system, several questions have to find an answer, following the terminology introduced in Section 3 (see Figure 5(b)): What model and associated criteria to be used (Section 4.1); What are the specifics of the testing infrastructure (Section 4.2); How to address the oracle problem in our specific context (Section 4.3); What additional issues can be considered (Section 0). In this section, we intend to describe existing testing strategies that pertain to these aspects in the context of the verification and validation of DEVS models.

[1] Note that this may require that the system under test possess (or be extended by) mechanisms to control and observe it (e.g., set it state, observe its outputs) [Binder 1999]. These mechanisms are usually used by the test driver.

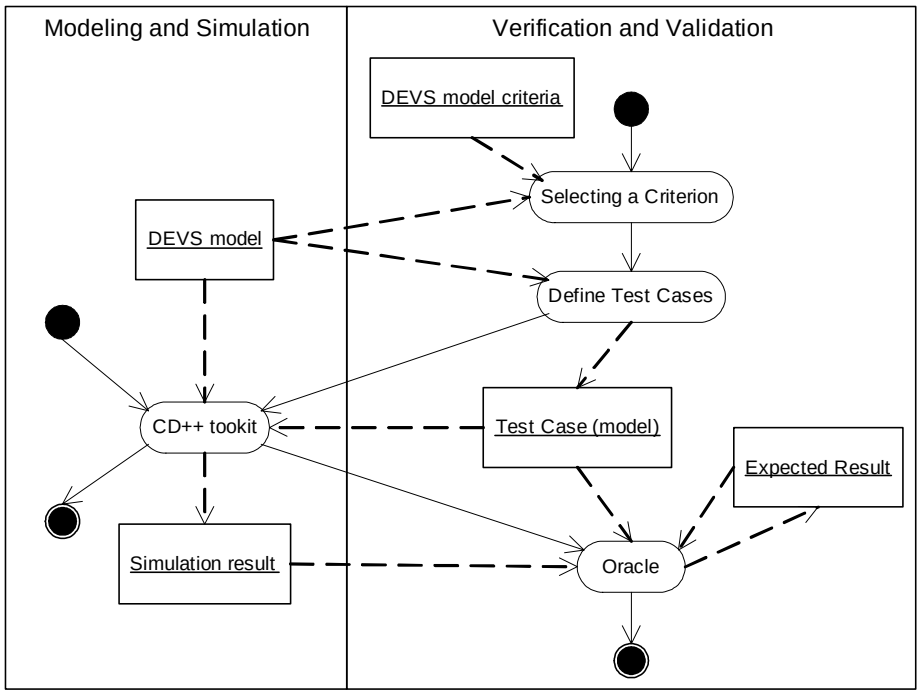

Figure 5 Modeling & Simulation (a) and Verification & Validation (b) activities

4.1. Model(s) and Associated Criteria

First, the model to be used to derive test cases is obviously the DEVS model that one is interested in validating/verifying. There likely exist a number of testing criteria that can be defined for DEVS models and it is important to decide which ones are pertinent (Section 4.1.1). Additionally, there exist two orthogonal black-box testing strategies (i.e., they can likely be combined with criteria identified in Section 4.1.1) that also seem to pertain to our context, namely testing from Boolean expressions and Category-Partition (Section 4.1.2).

4.1.1 Finite State Machines and Extensions

Since the DEVS models we want to validate and verify are based on the notation presented in Figure 3, which is essentially based on communicating finite state machines, it is paramount to investigate whether existing techniques for testing (extended) finite state machines or communicating finite state machines [Lee and Yannakakis 1996] can be used directly or should be adapted. Several directions for further investigations can be identified.

First, to what extent DEVS-like finite state machines have the appropriate characteristics to allow the use of the so called W-method [Chow 1978], that has been widely used in the telecom domain for protocol testing. The W-method requires the construction of a transition tree, for instance using a breadth-first or depth-first traversal of the finite-state machine. In the example state machine (DEVS model) in Figure 3(a), a breadth-first traversal[2] would lead to a tree with two paths: `Start-in-Process-in-Finish-in-Process` and `Start-in-Process-in-Finish-out-Start`, where the notation used to specify a tree path is a sequence of pairs `state-event`. The W-method then consists of two steps: The first one traverses the transition tree so that each path in that tree be covered by the test cases (this is the criterion), and the second one appends a state identification sequence (also known as characterization sequence) to each transition tree sequence (i.e., test case) in order to check the state that was reached. The characterization sequence is an input sequence that can distinguish between the behavior of every pair of states by simply observing the output(s) of the state machine. In other words, the output(s) produced by the finite state machine in response to the characterization sequence is unique to the states. The successful identification of the characterization sequence depends on the characteristics of the state machine (the interested reader is referred to [Chow 1978] for further details). Other similar techniques for state based testing from finite state machines exist (e.g., [Lee and Yannakakis 1996]), but they all test the same sequences (from the tree) and only differ with respect to the sequence added for the state identification problem. Note that the W-method, thanks to the characterization sequence, elegantly solves the oracle problem with respect to verifying the state reached at the end of a test case: One simply executes the characterization

[2] Using as a stopping criterion for the traversal the one suggested in [Chow 1978]: we stop traversing when a node in the tree corresponds to a state that is already present elsewhere in the tree.

sequence, and uniquely identifies the state reached at the end of the test case by simply observing the output(s); There is no need to add controllability and observability mechanisms to the system under test, which can really be considered as a black-box.

These strategies do not account for the timing aspects in DEVS models. Authors have thus extended the W-method for testing real-time systems, when the software behavior is specified as a timed input output automaton (TIOA) [En-Nouaary et al. 2002]. Such an automaton specifies behavior in terms of input and output actions that the machine receives from and sends to the environment, states (including an initial state), clocks and transitions. The TIOA formalism does have interesting similarities with DEVS formalism, although the mapping is not immediate, and some work has been done in finding equivalences between the two formalisms [Giambiasi et al. 2003]. Given that the Timed Wp-method seems to be applicable to communicating TIOA, it is thus worth investigating to what extent the Timed Wp-method can be applied (or adapted) to DEVS models.

Note that in a situation where the state-based behavior is not fully specified in the state machine (the DEVS model), it is necessary to complement any criterion explicitly based on the state-based behavior with the test of so-called sneak paths [Binder 1999]. For instance, it may happen that the response of a state to a specific event is not specified in the state machine, thus stating that the event is simply ignored (this is for instance a common practice when specifying UML statecharts). In such a situation, one would want to verify that when the system executes, is in that given state, and receives the specific event, the event is indeed ignored. If test cases are only derived from the behavior specified in the state machine (e.g., using a transition tree), this sneak path will not be exercised.

Last, in order to give insight to the DEVS designer/tester as to which criterion to use in a particular context, the identified criteria will have to be evaluated: see Section 4.4.

4.1.2 Boolean expressions and Category-Partition

Since, as pointed out in [Wainer et al. 2002] complex cellular models can be defined thanks to Boolean, relational and arithmetic operators, it seems clear that existing techniques for testing Boolean predicate expressions are relevant [Ammann et al. 2003, Weyuker 1994]. Different strategies to derive test cases from a Boolean formula exist (the interested reader is referred to [Ammann et al. 2003, Weyuker 1994] for details) and some are more cost-effective than others (i.e., less test cases and more fault detection capabilities). If a DEVS model involves complicated Boolean expressions, it will be necessary to complement the state-based criteria with such Boolean expression criteria. Similar combinations between Boolean expression testing and state-based testing criteria have been already suggested for UML statecharts [Offutt and Abdurazik 1999].

Another functional testing strategy that could be considered is Category-Partition [Ostrand and Balcer 1988]. It is the most well known extension of input domain partitioning and boundary value analysis[3] [Myers 1979]. The specification (e.g., a DEVS model) is decomposed into functional units to be tested independently (e.g., system operations or class public operations, depending on the context of application). Then, parameters and environment conditions affecting the function's behavior are identified. Categories for such parameters and conditions are defined such that they trigger a different behavior of the functionality, and are chosen to maximize the chances of finding errors. A category can be seen as a major property of the parameter or condition. Then, each category is partitioned into a series of distinct choices, i.e., partition classes, including all the possible values for the category. The set of categories and choices constitute the test specification from which it is possible to derive the test frames, that is a template to derive test cases. Each test frame is composed of a set of choices from all the categories, where each category contributes with, at most, one choice. Possible interaction among different choices belonging to different categories can be annotated in the test specification as constraints. A constraint indicates, for instance, that a choice belonging to a category cannot appear in the same test frame of another choice belonging to another category. This allows testers to reduce the number of possible test cases. Work has already investigated, with success, the combination of state-based criteria for UML statecharts and Category-Partition [Briand et al. 2004c].

Since there is evidence that traditional state-based criteria can be efficiently combined with Boolean expression testing or Category-Partition testing, it seems worth investigating the combination of state-based criteria for DEVS models (e.g., an adapted Wp-method) and those two black-box techniques. Again, an evaluation of the different strategies will be required, especially considering that in the case of combining state-based criteria with Boolean expression testing, initial empirical investigation showed the resulting combined criterion to have a low cost-effectiveness compared to other criteria (e.g., the W-method) [Briand et al. 2004a].

[3] A common approach to generating test cases from functional specifications is to partition the input domain of the function/method being tested into equivalent classes, and then to select an input for each class of the partition (and at the boundaries of the partitions), according to the principle that all elements belonging to an equivalence class are interchangeable for testing purposes.

4.2. Testing Infrastructure

Regardless of the selected criterion, testing data for a DEVS model will entail: (1) a sequence of inputs (possibly sent to different ports) to the model under test, as well as (2) delays between the inputs. For instance, referring to the model in Figure 3 (a), a test case could be: supposing the model is in the *Start* state, send the input value 4 at time 2 through port *in*, wait for 13 time units, and send an input with value 2 through the input port *in*. As a result, we expect the model should go from *Start* to *Process* at time 2, produce an output of the value 1 through the output port *out* and change to *Finish* at time 12, and then be back to *Process* at time 13.

It is then clear that such a test case can itself be modeled using the DEVS formalism, as illustrated in Figure 6. Similarly, a DEVS model could be in charge of collecting the outputs of the DEVS model under test, and play the role of the oracle, i.e., directly report on failures if erroneous data are received on correct data are not received in time. Such a strategy has already been experimented with [Wainer et al. 2002]. Note that it may be necessary to add output ports to the model under test (and perhaps input ports too) to observe (and control) the behavior of the model under test. This will especially required if, because of the specifics of the model, we cannot find a characterization sequence (recall Section 4.1.1).

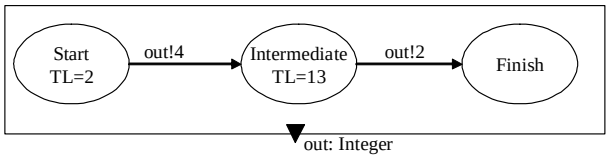

Figure 6 A test case for Figure 3(a) as an DEVS model

In terms of test scaffolding, that is test infrastructure, no stub seems to be required for the verification and validation of a DEVS model. CD++ can serve as the core of the testing infrastructure. Any other DEVS model simulator would do too. Note however that it is important that the simulator be able to execute without the user inputs (i.e., in a batch mode): we do not want the tester to stand by the computer while hundreds of test cases execute. Thanks to such environment, test cases generated according to the selected criterion can be transformed into a DEVS model that is connected to the input(s) of the model under test as discussed above.

4.3. Oracle

The oracle problem is acute in such V&V activities as in any other complex V&V activity (e.g., software), and there is no general solution: can the expected output be described (or computed) simply from the specifics of a test case or do we have to resort to the expertise of the modeler or any other expert in the problem at hand? Is it always possible to describe the correct result of the simulation as a formula or perhaps a DEVS model? The modeler (or expert) may not know the correct answer, and this might be the reason why s/he is performing a simulation. It is well known in the simulation community that interpreting simulation results is not an easy task, even for an expert. Nonetheless, there might exist simple cases for which the expected output is known, although the modeler is really interested in more complicated cases (e.g., longer runs): the model can then be tested against those simple cases and results can be extrapolated for the more complicated ones. If two different models can be built for the same problem, they can be used to test each other. (This is known as having a partial oracle). Executing a test case on each of them should produce the same result. The reader is referred to [Weyuker 1982] for a discussion on these alternative solutions to the oracle problem in the context of software testing. It is worth noting that as the complexity of the model under test increases, we can expect any interesting criterion (e.g., a cost-effective one) to produce a large number of test cases and it does not seem reasonable to ask the modeler or expert to look at them all and decide whether the outputs are correct. The tester should then strive for an oracle (even partial) as automated as possible.

An elegant solution to the oracle problem in a state-based context is the W-method, or its extensions, already introduced in Section 4.1.1. Recall that when the state machine has the right characteristics [Chow 1978] it is possible to use a characterization sequence to uniquely identify the state reached at the end of a test case. When possible, this simply eliminates the need to build an expensive oracle for the verification of the state reached. (Note that we still need an oracle to evaluate the outputs). However, as in the context of finite state machines for which the W-method can be applied, the machine may not possess those interesting characteristics. The W-method, i.e., the construction of test cases by traversing the stat machine, can still be used. It is the second part of the technique that cannot.

Another alternative to building expensive oracles has recently been suggested in the context of software testing. Contract, for instance defined according to the Design by Contract approach [Meyer 1997], can be transformed into code statements (called assertions), that are eventually inserted in the source code under test. Such assertions have been shown to be reasonable substitute for oracles [Briand et al. 2003], thus solving the oracle problem, and some work has already shown that contracts defined in OCL (in the context of UML) can be automatically instrumented in a Java implementation [Briand et al. 2004b]. Then, there is no need to build an oracle, which as we have seen before is not an easy task, and simply rely on the assertions to reveal failures. Choosing between oracles and assertions is a decision that can be driven for instance on the level

of confidence we would like to have in the simulation results. Indeed, those assertions are only reasonable substitute as experiments have shown that some faults, which are revealed by oracles are missed by assertions [Briand et al. 2003]. This seems an interesting avenue for further research though, especially since CD++ allows the designer to create C++ classes to describe complex behavior, i.e., to write code in addition to build a model, and combine the C++ classes with a DEVS model.

4.4. Other Considerations

Note that once a set of test cases have been identified when using a given criterion, such as the two examples described in Section 4.1.1 for the model in Figure 3(a), one issue still remains: How to identify real inputs (values for input ports and delays) for the DEVS model in order to exercise the set cases. For instance, what is a possible set of inputs to the DEVS model in Figure 3(a) that would trigger test case `Start-in-Process-in-Finish-in-Process`? As discussed previously, the following would do: send input 4 at time 2, wait during 12 time units, send input 2 after 1 time unit. Identifying actual input values to trigger a test case (i.e., a path in a model) is a well known issue in the software testing community, referred to as path sensitization [Beizer 1990], that often does not find an obvious answer: it is an un-decidable problem; no algorithm can solve this problem in all cases. People have thus investigated the use of heuristics techniques such as Genetic Algorithms (e.g., [Tracey et al. 1998]) .

In a standard process, when a modeler tests a DEVS model and results show failures, the model undergoes changes and the changed model should pass through a testing procedure too. One of the objectives is to verify that the changes haven't introduced new problems and this testing activity is known as regression testing. Regression testing techniques have been applied to procedural and object-oriented software as well as spread-sheets [Fisher II et al. 2002, Rothermel and Harrold 1997, Rothermel et al. 2000] and it will be interesting to see how they can be applied (or adapted) to DEVS models.

CD++ provides two main working approaches, as discussed in Section 2. The principles discussed so far apply to both approaches. In the case where the model is directly implemented in C++, additional strategies can be considered. First, the tester will be interested in structural coverage of the C++ source code [Beydeda et al. 2001, Binder 1999]. It is indeed usually admitted that functional and structural approaches are complimentary.

Another issue is that applying those testing techniques for the V&V of DEVS models assumes that the DEVS model simulator is trustworthy. How is this achieved is another challenge which seems to be similar to testing compilers [Boujarwah and Saleh 1997]. So far, given that the simulation engines are built using DEVS abstract simulation concepts [Zeigler et al. 2000], and that tool users did not report many problems related to the simulation engines[4], users have enough confidence in the simulation results. The strategy that has been adopted so far for the CD++ toolkit is to resort to a number of benchmarks models of varying complexities (which is very similar to compiler testing). Such a strategy may become an issue if DEVS models and CD++ are used to specify safety critical systems, such as an airborne system. Indeed, in such cases, not only users have to be convinced that the simulation results are trustworthy, but international certification organizations have to be convinced too. For specific such systems the tools used to develop them (in our case CD++) must be certified at the same level or criticality as the built system, and this requires a lot of effort [RTCA 1992].

Last, there is an increasingly stringent call for experimental evaluation of testing criteria. On the one hand, it may seem that if criterion C1 subsumes criterion C2, then a C1 adequate test set is guaranteed to find more faults than a C2 adequate test set for every program. This is unfortunately not true: there exist programs for which a C2 adequate test set finds more faults than a C1 adequate test set although C1 subsumes C2 [Frankl and Weiss 1993]. The analytical comparison of criteria (i.e., the subsumes hierarchy) is not sufficient and we have to resort to experimentations. For instance, it has been shown that the strategy suggested in [Chow 1978] for finite state machines and adapted by Binder to UML statecharts [Binder 1999] does not necessarily lead to interesting test sets [Briand et al. 2004a]. Similarly, combining state based criteria with Boolean testing, as suggested in [Offutt and Abdurazik 1999], has been shown to be very effective (more effective than other well-known state-based criteria), but at a very high cost [Briand et al. 2004a]. It will then be necessary, once some criteria have been identified for DEVS model, to empirically evaluate their cost and effectiveness.

5. Conclusion

Performing Verification and Validation (V&V) of discrete event system model (for instance specified in DEVS) has been identified as a paramount activity, as it can increase the confidence of the user in the simulation results and lead to the accreditation/certification of the simulated system. Because of the interesting capability of DEVS models to be executable, thanks to environments such as the CD++ toolkit, a natural approach is to consider software testing techniques to perform V&V of DEVS simulation models (testing requires the execution of the tested system).

[4] Since 1999, CD++ users reported only 3 errors related to the simulation engine, which were identified and fixed in a matter of hours.

As discussed in this article, DEVS models have many similarities with behavioral models that are used to specify and test software systems (i.e., finite state machines and extensions of it). It clearly follows that there are many avenues for research on applying (perhaps adapting) existing software testing techniques to the V&V of DEVS models.

In this article we tried to clarify what V&V of DEVS models, by means of testing, would entail in terms of applicable testing techniques and testing infrastructure. We identified a couple of testing techniques commonly used for software testing that seem to immediately apply to the testing of DEVS models. We also clarified some of the main issues that we will have to address in the future (e.g., the oracle problem). We showed that the DEVS formalism provides mechanism to help building a testing infrastructure. Our objective was not to be exhaustive, and we may have overlooked possible software V&V techniques (including testing) applicable to the V&V of DEVS models. Our findings in this preliminary investigation seem encouraging, although many issues remain to be investigated. Overall, we now have to do it and experiment the V&V of DEVS models by applying software testing techniques.

We have focused on testing techniques on purpose. Other software V&V approaches could be investigated too: symbolic execution, model checking, transformation of the model into other models amenable to automatic checks (such as Petri nets), etc.

Note that by trying to see how simulation can benefit from testing, we came to the conclusion that perhaps testing could also benefit from simulation. This will be investigated in the future as both authors get acquainted with each other's field.

ACKNOWLEDGEMENTS

Yvan Labiche and Gabriel Wainer are supported by NSERC operational grants.

REFERENCES

[Ammann et al. 2003] Ammann, P., Offutt, A.J. and Hong, H.S., "Coverage Criteria for Logical Expressions," *Proc. International Symposium on Software Reliability Engineering*, pp. 99-107, 2003.

[Beizer 1990] Beizer, B., *Software Testing Techniques*, Van Nostrand Reinhold, 2nd Ed., 1990.

[Beydeda et al. 2001] Beydeda, S., Gruh, V. and Stachorski, M., "A graphical class representation for integrated black- and white-box testing," *Proc. IEEE International Conference on Software Maintenance*, pp. 706-715, 2001.

[Binder 1999] Binder, R.V., *Testing Object-Oriented Systems - Models, Patterns, and Tools*, Addison-Wesley, 1999.

[Booch et al. 1999] Booch, G., Rumbaugh, J. and Jacobson, I., *The Unified Modeling Language User Guide*, Addison Wesley, 1999.

[Boujarwah and Saleh 1997] Boujarwah, A.S. and Saleh, K., "Compiler test case generation methods: a survey and assessment," *Information and Software Technology*, vol. 39 (9), pp. 617-625, 1997.

[Briand et al. 2003] Briand, L.C., Labiche, Y. and Sun, H., "Investigating the Use of Analysis Contracts to Improve the Testability of Object-Oriented Code," *Software - Practice and Experience*, vol. 33 (7), pp. 637-672, 2003.

[Briand et al. 2004a] Briand, L.C., Labiche, Y. and Wang, Y., "Using Simulation to Empirically Investigate Test Coverage Criteria," *Proc. IEEE/ACM International Conference on Software Engineering*, Edinburgh, pp. 86-95, May, 2004a.

[Briand et al. 2004b] Briand, L.C., Dzidek, W. and Labiche, Y., "Using Aspect-Oriented Programming to Instrument OCL Contracts in Java," Carleton University, Technical Report SCE-04-03, http://www.sce.carleton.ca/squall, 2004b.

[Briand et al. 2004c] Briand, L.C., Di Penta, M. and Labiche, Y., "Assessing and Improving State-Based Class Testing: A Series of Experiments," *IEEE Transactions of Software Engineering*, vol. 30 (11), pp. 770-793, 2004c.

[Chow 1978] Chow, T.S., "Testing Software Design Modeled by Finite-State Machines," *IEEE Transactions on Software Engineering*, vol. SE-4 (3), pp. 178-187, 1978.

[Christen et al. 2004] Christen, G., Dobniewski, A. and Wainer, G., "Modeling State-Based DEVS Models in CD++," *Proc. MGA, Advanced Simulation Technologies (ASTC)*, Arlington, VA, 2004.

[DEVSTD 2004] DEVSTD, DEVS Standardization Group, www.sce.carleton.ca/faculty/wainer/standard, [Last checked: December 2004]

[Dijkstra 1972] Dijkstra, E.W., "Notes on Structured Programming," in O. J. Dahl, E. W. Dijkstra and C. A. R. Hoare, Eds., *Structured Programming*, Academic Press, 1972, pp. 1-82.

[En-Nouaary et al. 2002] En-Nouaary, A., Dssouli, R. and Khendek, F., "Timed Wp-Method: Testing Real-Time Systems," *IEEE Transactions of Software Engineering*, vol. 28 (11), pp. 1023-1038, 2002.

[Fisher II et al. 2002] Fisher II, M., Jin, D., Rothermel, G. and Burnett, M., "Test Reuse in the Spreadsheet Paradigm," *Proc. International Symposium on Software Reliability Engineering*, pp. 257-268, November 2002.

[Frankl and Weiss 1993] Frankl, P.G. and Weiss, S.N., "An Experimental Comparison of the Effectiveness of Branch Testing and Data Flow Testing," *IEEE Transactions of Software Engineering*, vol. 19 (8), pp. 774-787, 1993.

[Giambiasi et al. 2003] Giambiasi, N., Paillet, J.-L. and Châne, F., "From timed automata to DEVS models," *Proc. Winter Simulation Conference*, New Orleans, LA, 2003.

[Howden 1987] Howden, W.E., *Functional Program Testing & Analysis*, McGraw-Hill, 1987.

[Lee and Yannakakis 1996] Lee, D. and Yannakakis, M., "Principles and Methods of Testing Finite State Machines - A Survey," *Proceedings of the IEEE*, vol. 84 (8), pp. 1090-1123, 1996.

[Meyer 1997] Meyer, B., *Object-Oriented Software Construction*, Prentice Hall, 2nd Ed., 1997.

[Myers 1979] Myers, G.J., *The art of software testing*, John Wiley & Sons, 1979.

[Offutt and Abdurazik 1999] Offutt, A.J. and Abdurazik, A., "Generating Tests from UML specifications," *Proc. 2nd International Conference on the Unified Modeling Language (UML'99)*, Fort Collins, CO, pp. 416-429, October, 1999.

[Ostrand and Balcer 1988] Ostrand, T.J. and Balcer, M.J., "The Category-Partition Method for Specifying and Generating Functional Test," *Communications of the ACM*, vol. 31 (6), pp. 676-686, 1988.

[Rothermel and Harrold 1997] Rothermel, G. and Harrold, M.J., "A Safe, Efficient Regression Test Selection Technique," *ACM Transactions on Software Engineering and Methodology*, vol. 6 (2), pp. 173-210, 1997.

[Rothermel et al. 2000] Rothermel, G.,Harrold, M.J. and Debhia, J., "Regression Test Selection for C++ Software," *Journal of Software Testing, Verification, and Reliability*, vol. 10 (2), pp. 77-109, 2000.

[RTCA 1992] RTCA, "Software Considerations in Airbone Systems and Equipment Certification," Radio Technical Commission for Aeronautics (RTCA), European Organization for Civil Aviation Electronics (EUROCAE), Standard Document no. DO-178B/ED-12B, December, 1992.

[Sargent 2000] Sargent, R.G., "Verification, Validation, and Accreditation of Simulation Models," *Proc. Winter Simulation Conference*, pp. 50-59, 2000.

[Tracey et al. 1998] Tracey, N.,Clark, J.A.,Mander, K.C. and McDermid, J.A., "An Automated Framework for Structural Test-Data Generation," *Proc. IEEE Conference on Automated Software Engineering*, pp. 285-288, 1998.

[Traoré and Zeigler 2004] Traoré, M.; Zeigler, B. "Conditions for model component reuse". Materials of the Dagstuhl Seminar 04041, Component-Based Modeling and Simulation. 2004.

[Wainer and Giambiasi 2001] Wainer, G. and Giambiasi, N., "Timed Cell-DEVS: modeling and simulation of cell spaces," in H. Sarjouand and F. Cellier, Eds., *Discrete Event Modeling & Simulation: Enabling Future Technologies*, Springer, 2001.

[Wainer 2002] Wainer, G., "CD++: a toolkit to develop DEVS models," *Software - Practice and Experience*, vol. 32 (3), pp. 1261-1306, 2002.

[Wainer et al. 2002] Wainer, G.,Morihama, L. and Passuello, V., "Automatic Verification of DEVS Models," *Proc. SISO Spring Interoperability Workshop*, 2002.

[Weyuker 1994] Weyuker, E., "Automatically Generating Test Data from a Boolean Specification," *IEEE Trans. on Software Engineering*, vol. 20 (5), pp. 353-363, 1994.

[Weyuker 1982] Weyuker, E.J., "On Testing Non-testable Programs," *The Computer Journal*, vol. 25 (4), pp. 465-470, 1982.

[Zeigler et al. 1996] Zeigler, B.,Song, H. and Kim, T., "DEVS Framework for Modeling, Simulation, Analysis, and Design of Hybrid Systems," *Proc. Hybrid Systems IV*, 1996.

[Zeigler et al. 2000] Zeigler, B.,Kim, T. and Praehofer, H., *Theory of Modeling and Simulation: Integrating Discrete Event and Continuous Complex Dynamic Systems*, Academic Press, 2000.

Combining DEVS and Logic

Mamadou K. Traoré
LIMOS CNRS UMR 6158
Université Blaise Pascal
Campus des Cézeaux
63177 Aubière Cedex, France
+33 473 405 046
traore@isima.fr

ABSTRACT
This paper presents an introduction to integrating formal methods in the DEVS framework. Formal methods are known to allow symbolic manipulation and reasoning. DEVS is a well-establish Modeling and Simulation (M&S) framework. Combining them makes it possible to formally specify models, automate their analysis as regard to design and use requirements, and develop rigorous proofs of their properties. Such a potential is very important for verification, validation and accreditation, a key issue in M&S. The paper presents the methodological approach we have defined for specifying logic-based simulation models, combining DEVS and the Z formalism. A case study is presented and we use the Z/EVES system for formal analyses.

KEYWORDS
DEVS, formal specification, modeling and simulation framework, symbolic reasoning, logic

1. Introduction

Semantics reasoning with models, through their specifications, is a challenge in M&S, while also a need. A huge gain can be obtained with a formal framework in which concepts can be sketched in their clearer abstract form, and formal way be defined to manipulate them and to reason about them. DEVS is a well-establish framework for M&S [Zeigler 1976] [Zeigler 1984] [Zeigler et al. 2000], based on systems theory. Systems are specified in DEVS in terms of atomic and coupled models, the former ones being the most basic entities that describe both systems structure and behavior. The latter are obtained by composing atomic models into larger models. However, DEVS doesn't involve specific abilities for symbolic reasoning and proofs. A promising way to enrich the framework with such a potential is to integrate formal methods in it.

A little work has been done in combining M&S and formal methods. Two means are briefly presented in [Kuhn et al. 2003] through which formal methods could be introduced successfully into the M&S field. In [Stevenson 2003] is proposed a direct formalization of DEVS in a mathematical theory (e.g., set theory or category theory). The advantage of this approach is that the underlying mathematical theory is more abstract and imposes fewer restrictions than a formal method that was not specifically designed for DEVS. However, no operational framework is really defined.

We provide here an approach combining DEVS and the Z formal specification language, which can directly map to the formal representation used by the Z/EVES theorem prover [Saaltink 1997]. Then, with the DEVS semantics and associated logic, we can easily integrate automatic techniques (i.e., syntax and type checking, schema expansion, precondition calculation, domain checking, and general theorem proving) into M&S. Section 2 briefly presents the DEVS framework. The basic models which support its specification structure are shown as well as their mapping onto simulation. Section 3 gives an overview of formal methods, and then focus on the Z formalism. The reasons for this focus are given. Z-DEVS is introduced in section 4. This new framework relies on a set of basic schema classes that we exhibit. Section 5 shows a case study where the framework is applied, driving towards formal analysis and checking. Concluding remarks are given in section 6.

2. DEVS Framework

Several approaches and methodologies for M&S trace their origins to general systems theory, which postulates that real systems show similar patterns of behavior despite their dissimilarities. The most developed appeal to general systems theory in the context of M&S is the DEVS framework. DEVS identifies three major conceptual elements: the system, the model, and the simulator (separation of concerns). Two major relationships hold: modeling, which deals with the relationship between systems and models, and simulation, which refers to the relationship between models and computers, as shown by figure 1.

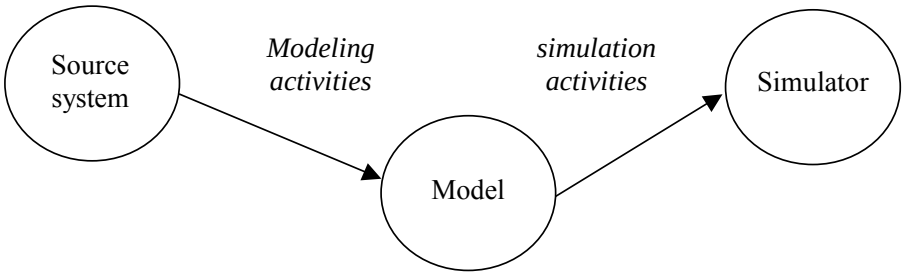

Figure 1. DEVS basic entities and relationships

2.1. **DEVS Models**

The basic complete specification of both the structure and the behavior of a system is given by an atomic model. Essentially, an atomic model is described by a set of inputs, outputs, states, and governing functions. Formally, an atomic model is defined as a structure:

$IOS = \langle X, Y, S, \delta_{int}, \delta_{ext}, \lambda, ta \rangle$, where
- X is the set of input values,
- S is the set of states,
- Y is the set of output values,
- $\delta_{int} : S \rightarrow S$ is the internal transition function,
- $\delta_{ext} : Q \times X \rightarrow S$ is the external transition function, where
  - $Q = \{ (s,e) / s \in S, 0 \leq e \leq ta(s)\}$ is the total state set,
  - e is the time elapsed since last transition,
- $\lambda : S \rightarrow Y$ is the output function,
- $ta : S \rightarrow R_{0,\infty}$ is the time advance function (that can take any positive real value, including 0 and ∞).

This model is supposed to be at any time in some state $s \in S$. When the elapsed time $e = ta(s)$ expires before any external event occurs, the system outputs the value $y = \lambda(s)$, and changes to state $\delta_{int}(s)$. One important constraint in DEVS is that output is only possible just before internal transitions. If an external event $x \in X$ occurs before the expiration time defined by ta(s), the system changes to state $\delta_{ext}(s,e,x)$. Thus, the internal transition function dictates the model's new state when no event occurred since the last transition. The external transition function dictates the model's new state when an external event occurs. In both cases, the model is in a new state s' with some new elapsed time defined by ta(s') and simulation goes on.

A coupled model is a composition of models (atomic or coupled in their turns) that presents the same external interfaces as do atomic models. By coupling together output ports of one model to input ports of another, outputs are transmitted as inputs and acted upon by the receiving model. Although arbitrary fan-out and fan-in of coupling is allowed, no self-loops are permitted. DEVS is closed under coupling, which means that a coupled model can itself be a component (equivalent to an atomic model) within a higher level coupled model, leading to hierarchical, modular model construction.

The semantics of DEVS models are supported by simulators and coordinators. Atomic models are mapped onto simulators and coupled models are mapped onto coordinators. All simulators and coordinators adhere to a generic message protocol that allows them to coordinate with each other to execute the simulation. A root coordinator is used to handle the simulation cycle, first initiating the simulation by an initialization message, and then leading the simulation loop by scheduling messages to provide the correct synchronization for the subordinate coordinator (or simulator). Abstract algorithms have been defined in [Zeigler et al. 2000] to characterize what simulators and coordinators have exactly to do.

3. **Formal Methods**

Formal Methods (FM) refer to the application of mathematical techniques for the specification, analysis, design and implementation of complex software and hardware. Use of FM can greatly increase our understanding of a system through at least one of the following techniques [Clarke and Wing 1996]: formal specification, and formal verification (model checking, or theorem proving). Here we review these techniques, and then we focus on the Z formalism for specific advantages.

3.1. **Formal Specification and Symbolic Reasoning**

Formal specification is the process of describing a system and its desired properties, using a language with a mathematically-defined syntax and semantics. The kinds of system properties might include functional behavior, timing behavior, performance characteristics, or internal structure. In this sense, DEVS is a satisfying formal language. But also, a formal

specification must involve rules for inferring useful information from the specification (the proof theory). This aspect is what DEVS misses. Some formal methods (such as Z) focus on specifying the behavior of sequential systems (states are described in terms of sets, relations and functions, and state transitions are given in terms of pre- and post-condition). Such methods perfectly fit our need to turn the IOS (Input Output System) level of DEVS specification into a logical specification (recall that atomic models are produced at that level). One must mention that it is through the specification process that developers uncover inconsistencies (e.g., all specified properties taken together lead to a contradiction), ambiguities (multiple interpretations of interest making it true), and incompleteness.

Formal specification techniques can be classified into the following five main paradigms [Lamsweerde 2000]:

- History-based specification characterizes the maximal set of admissible histories over time. The properties depicting the behavior of the system are specified by temporal logic assertions.
- State-based specification characterizes the maximal set of admissible system states. The properties depicting the states of the system are specified by invariants constraining the system objects at any snapshot, and pre- and post-assertions constraining the application of system operations at any snapshot.
- Transition-based specification characterizes the required transitions from system state to state. The properties of interest are specified by a set of transition functions which give for input states and triggering events (eventually guarded by necessary precondition) the corresponding output states.
- Functional specification characterizes the system as a structured collection of mathematical functions that are grouped, either by types then defining algebraic structures, or into logical theories (high-order functions). The properties of interest are specified as conditional equations that capture the effect of composing these functions.
- Operational specification characterizes the system as a structured collection of processes that can be executed by some more or less abstract machine.

Model checking relies on building a finite model of a system and checking by an exhaustive state space search that a desired property holds in that model. It can be used to check partial specifications, then providing useful information about system's correctness even if the system is not completely specified. Also, it can produce counterexamples which typically are subtle errors in design. The problem of model checking is the state explosion problem. However, efficient representation of state transitions can increase the size of the system that could be verified.

Theorem proving is a technique where both the system and its desired properties are expressed as logic-based formulas, in terms of axioms and inference rules. Theorem proving is the process of finding a proof of a property from these axioms and rules, and possibly derived definitions and intermediate lemmas. In contrast to model checking, theorem proving can deal with infinite state spaces, but it usually results in a slow and often error-prone process.

3.2. **Z Formalism**

We can give formal semantics to DEVS by introducing a mapping from DEVS specification to a well established formal method for simulation models development, in a way suggested by [Paige 1997]. Once a DEVS model is translated into a specification in a formal language, all the analysis and manipulations are performed on the formal specification. The clear advantage of this approach is that it is possible to reuse all the previous work on the FM for analyzing DEVS models.

We turn towards Z formalization of DEVS. The reasons for choosing the Z formalism are the following:

- It provides much simpler semantics.
- It is widely used in successful applications.
- It is widely disseminated in the FM community.
- It has an expressive power in logic.
- There are available powerful tools which support its specification (notably Z/EVES).

The Z formalism [ISO 2002] makes use of mathematical data types to model the data in a system. The notation of predicate logic allows to describe abstractly operations that cause change in the system state. A main ingredient in Z is the way of decomposing a specification into small pieces called schemas. Schemas are used to describe both static and dynamic aspects of a system. A schema, as shown in figure 2, consists of a box divided into two parts. The part above the dividing line is used to declare variables (mainly, the state space of the system), and the part below the line is used to specify the relationship between the values of these variables (the invariants and the operations of the system).

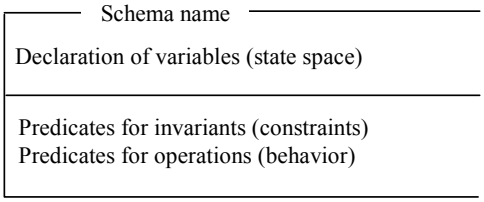

Figure 2. Structure of a Z schema

4. Introduction to Z-DEVS

One of the most important benefit in the DEVS framework is the separation of concerns. Our integrated framework, which we call Z-DEVS (read "the DEVS"), consists first in guaranteeing this separation of concerns. Thus, we have defined different schema classes for specifying the fundamental entities of the DEVS framework (i.e., models, and simulators). Moreover, the significant parts of these entities have been specified by specific primary classes of schema (to describe the state space, the transition and output functions…). So, these primary schema classes are assigned to certain roles, and are instantiated by aggregation in main schema classes. Z-DEVS models derive from main schema classes, and present a uniform interface to the modeler.

A main schema class in Z-DEVS is either a model class or a simulator class. Model classes describe structural and behavioral part of the DEVS model. Simulator classes describe concurrent, synchronous processes, which behavior are given by model classes. Models are integrated to their corresponding simulators by plugging model schemas to simulator schemas. This design leads to conformance with the principle of separation of concerns, as well as to conformance between semantic and supporting tools integration, as illustrated in figure 3.

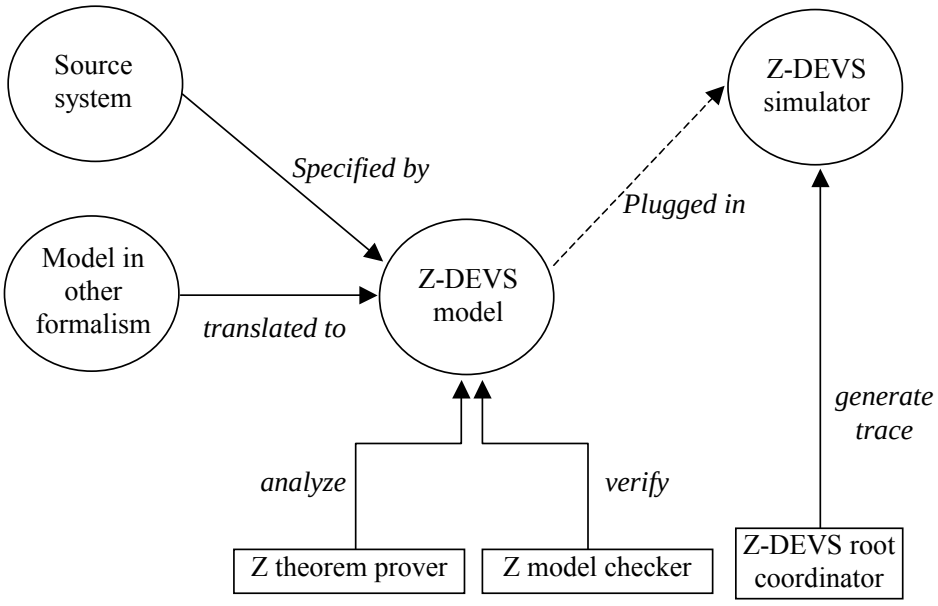

Figure 3. Z-DEVS framework

4.1. Z-DEVS Primary Schema Classes

The Z-DEVS specification is organized into primary schema classes and main schema classes. To specify a Z-DEVS model, the modeler must first define primary schemas, and then combine them to get the entire model. Each primary schema class is characterized by variables and invariants that describe the properties of the entity represented by the schema class.

This object-oriented style favors modularity and reusability of schemas. Modularity allows the modeler to focus on specific aspects of his model, and reusability allows him to take advantage of existing specifications and to build larger models by integrating existing schemas.

Basic components are represented by the following primary schema classes:

- The PARAMETER schema class: it specifies the parameters and constants used in the model.
- The INPUT schema class: its variables describe the data structure used to store the messages that are received on the model input ports, and its invariants characterize the set of admissible input segments of the model.
- The OUTPUT schema class: its variables describe the data structure used to store the messages that are sent along the model output ports, and its invariants characterize the set of admissible output segments of the model.
- The STATE schema class: it describes the set of variables that represents the total state space of the model, and the constraints and conservation laws which may prevail at each time on this state space.
- The INIT schema class: it gives the initial state of input, output and state variables.
- The DELTA_INT schema class: it describes the operations which realize state changes in the model, and the conditions under which these changes can occur.
- The DELTA_EXT schema class: it describes similar operations in the case they are triggered by an input.
- The LAMBDA schema class: it describes the operations for computing the model's output.
- The TIME_ADVANCE schema class: it describes how simulation time is advanced, depending on its current state.
- The PARAMETER schema class: its variables describe global data (such as constants), and its predicates describe the operations for manipulating these data (under eventual conditions).

4.2. **Z-DEVS Main Schema Classes**

Main schemas classes (atomic and coupled models, simulator and coordinators) can be defined encapsulating the primary schema classes. In the scope of this paper, only the ATOMIC schema class is defined (figure 4): it encapsulates the specification of the model, and is suitable for symbolic manipulation and reasoning at the conceptual level.

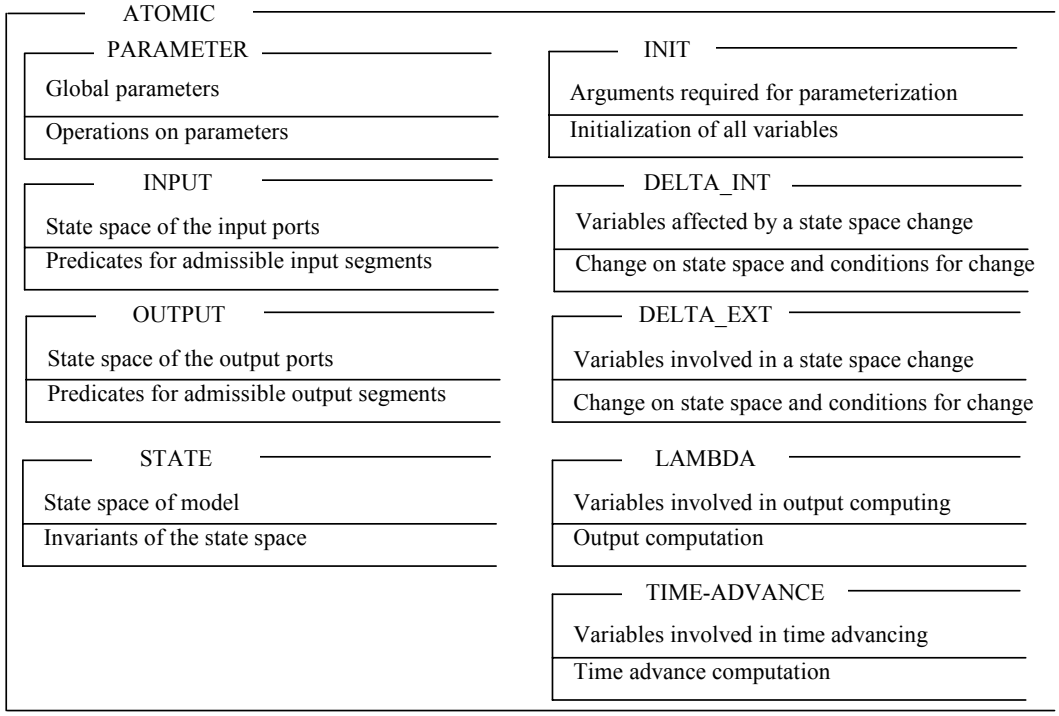

Figure 4. Z-DEVS atomic model schema class

5. **Case Study**

We apply hereafter the Z-DEVS specification to an academic example [Zeigler 1984], specifying a Z-DEVS model of a bus system, and performing simple partial proofs during the specification process. This is not an extensive verification and validation process, but an introduction to the potentials carried by the combination of DEVS and Logic.

5.1. **DEVS Model of a Bus System**

A bus shuttles between a downtown station and a university station, providing students and non-students with a transportation service. The growing number of users leads the university administration to set up a study to evaluate the performances of the bus system. We then consider a model for the UBS, with user identification possibilities. A user enters the model when he lines up in a station. He exits from the model when he gets off the bus at a station. A DEVS specification of this model is given hereafter, with comments in italic characters. Figure 5 is an illustration of possible internal transitions in the model. Situations are linked by dashed lines, an the corresponding values of the state variables are indicated.

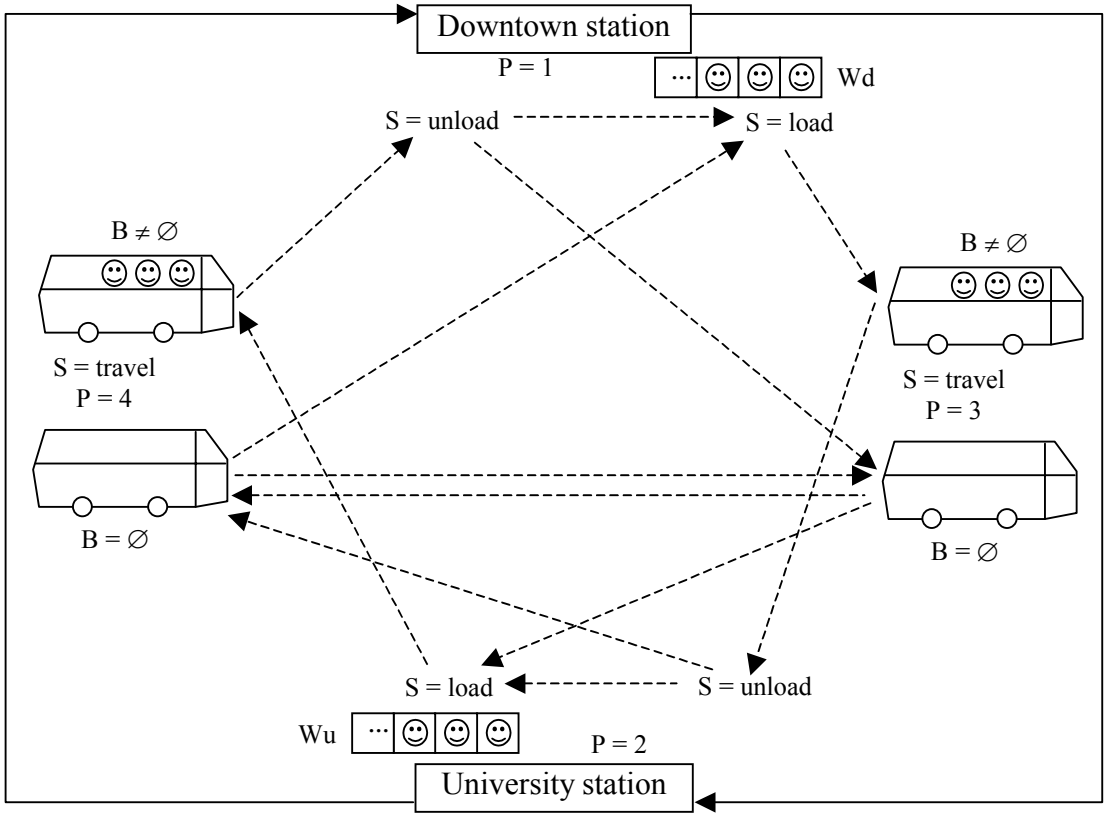

Figure 5. University Bus System

$IOS_{UBS} = <X, Y, S, \delta_{int}, \delta_{ext}, \lambda, t_a>$

The UBS is specified as an atomic model.

where X = {Hello1, Hello2} and Y = {Bye1, Bye2}

Hello1, Hello2, Bye1, and Bye2 ∈ {(identity, status) / identity is a string, and status ∈ {"student", "non-student"}}

S = {Wd, Wu, B, P, D, S}

Wd is the ordered list of users waiting at the downtown station,

Wu is the ordered list of users waiting at the university station,

B is the ordered list of passengers in the bus,

P ∈ {1, 2, 3, 4} is the current position of the bus (1: downtown station, 2: university station, 3: from downtown to the university, 4: from the university to downtown),

D is the duration of the current action,

S ∈ {"load", "unload", "travel"} is the current status of the bus,

τ is the current simulated time.

δ_{int}(Wd, Wu, B ≠ ∅, P = 4, D, S = “travel”, τ) = (Wd, Wu, B, P = 1, D = 0, S = “unload”, τ = τ + D)

If the bus arrives at the university station (the travel time is elapsed, then an internal transition must occur), it must stop to let the passengers get off,

δ_{int}(Wd ≠ ∅, Wu, B = ∅, P = 4, D, S = “travel”, τ) = (Wd, Wu, B, P = 1, D = ν, S = “load”, τ = τ + D)

If the bus is empty, the users waiting at the station can immediately start getting in it,

δ_{int}(Wd = ∅, Wu, B = ∅, P = 4, D, S = “travel”, τ) = (Wd, Wu, B, P = 3, D = β1, S, τ = τ + D)

If the bus was empty, and no one was waiting at the station, a stop is not required,

δ_{int}(Wd, Wu, B ≠ ∅, P = 1, D, S = “unload”, τ) = (Wd, Wu, B = rest(B), P, D = μ, S, τ = τ + D)

All the passengers in the bus must get off when the bus stops at the station. They do it, one by one,

δ_{int}(Wd, Wu, B = ∅, P = 1, D, S = “unload”, τ) = (Wd, Wu, B, P, D = 0, S = “load”, τ = τ + D)

When all the passengers get off the bus, the users waiting at the station can start getting in it,

δ_{int}(Wd = ∅, Wu, B, P = 1, D, S = “load”, τ) = (Wd, Wu, B, P = 3, D = β1, S = “travel”, τ = τ + D)

If there is no one waiting, the bus can start its travel to the other station,

δ_{int}(Wd ≠ ∅, Wu, B / ||B|| = α, P = 1, D, S = “load”, τ) = (Wd, Wu, B, P = 3, D = β1, S = “travel”, τ = τ + D)

Also if the bus is full, the bus can start its travel to the other station,

δ_{int}(Wd ≠ ∅, Wu, B / ||B|| < α, P = 1, D, S = “load”, τ) = (Wd = rest(Wd), Wu, B = B + first(Wd), P, D = μ, S, τ = τ + D)

If not, users can get in it, one by one.

Similar specifications are done at the following 8 lines for the case the downtown station is considered.

δ_{int}(Wd, Wu, B ≠ ∅, P = 3, D, S = “travel”, τ) = (Wd, Wu, B, P = 2, D = 0, S = “unload”, τ = τ + D)

δ_{int}(Wd, Wu ≠ ∅, B = ∅, P = 3, D, S = “travel”, τ) = (Wd, Wu, B, P = 2, D = ν, S = “load”, τ = τ + D)

δ_{int}(Wd, Wu = ∅, B = ∅, P = 3, D, S = “travel”, τ) = (Wd, Wu, B, P = 4, D = β2, S, τ = τ + D)

δ_{int}(Wd, Wu, B ≠ ∅, P = 2, D, S = “unload”, τ) = (Wd, Wu, B = rest(B), P, D = μ, S, τ = τ + D)

δ_{int}(Wd, Wu, B = ∅, P = 2, D, S = “unload”, τ) = (Wd, Wu, B, P, D = 0, S = “load”, τ = τ + D)

δ_{int}(Wd, Wu = ∅, B, P = 2, D, S = “load”, τ) = (Wd, Wu, B, P = 4, D = β2, S = “travel”, τ = τ + D)

δ_{int}(Wd, Wu ≠ ∅, B / ||B|| = α, P = 2, D, S = “load”, τ) = (Wd, Wu, B, P = 4, D = β2, S = “travel”, τ = τ + D)

δ_{int}(Wd, Wu ≠ ∅, B / ||B|| < α, P = 2, D, S = “load”, τ) = (Wd, Wu = rest(Wu), B = B + first(Wu), P, D = μ, S, τ = τ + D)

$\alpha \in \aleph$ is the capacity of the bus,

$\beta 1 \in \Re$ is the travel time from downtown station to university station,

$\beta 2 \in \Re$ is the travel time from university station to downtown station,

$\mu \in \Re$ is the time for a user to get in the bus,

$\nu \in \Re$ is the time for a user to get from the bus,

first (list) returns the first element of list,

rest (list) returns list, which has been reordered after its first element has been removed,

||list|| gives the number of element of list,

“list + element” performs an adding of “element” to “list”, and reorders “list”,

λ(Wd, Wu, B ≠ ∅, P = 1, D, S = “unload”, τ) = (bye1 = first(B), bye2 = ∅)

$\lambda(Wd, Wu, B \neq \emptyset, P = 2, D, S = \text{“unload”}, \tau) = (bye1 = \emptyset, bye2 = first(B))$

A passenger who gets off the bus at any station exits the system too,

$\lambda(Wd, Wu, B, P, D, \tau) = (bye1 = \emptyset, bye2 = \emptyset)$ in all other cases

$\delta_{ext}((Wd, Wu, B, P, D, S, \tau), e, (x1 \neq \emptyset, x2 = \emptyset)) = (Wd + x1, Wu, B, P, D = D - e, S, \tau = \tau + e)$

A user can line up at the downtown station, at any time.

Then, the time he enters the UBS is updated to the current time, and the time he enters the bus is set to $+\infty$

$\delta_{ext}((Wd, Wu, B, P, D, S, \tau), e, (x1 = \emptyset, x2 \neq \emptyset)) = (Wd, Wu + x2, B, P, D = D - e, S, \tau = \tau + e)$

Similar situation at the university station.

$\delta_{ext}((Wd, Wu, B, P, D, S, \tau), e, (x1 \neq \emptyset, x2 \neq \emptyset)) = (Wd + x1, Wu + x2, B, P, D - e, S, \tau + e)$

Situation where two users line up simultaneously at the downtown and the university station.

$t_a(Wd, Wu, B, P, D, S, \tau) = D$

5.2. **Z-DEVS model of the bus system**

We have translated the DEVS specification of the bus system into a Z-DEVS specification, as shown by the screenshots exhibited in figure 6 (many screenshots have been necessary to exhibit the entire Z-DEVS specification). These screenshots shows the results of on-going checks of syntax and proof in the columns at the left-hand side of the graphical user interface of the Z/EVES software tool.

The abstract set [User] is defined to represent the bus users, and we don't need to be more concise at this level, since the identification and the status of the bus users are useless for our purpose. Also, a STATUS type is defined to characterize what the bus is doing (traveling, loading, or unloading).

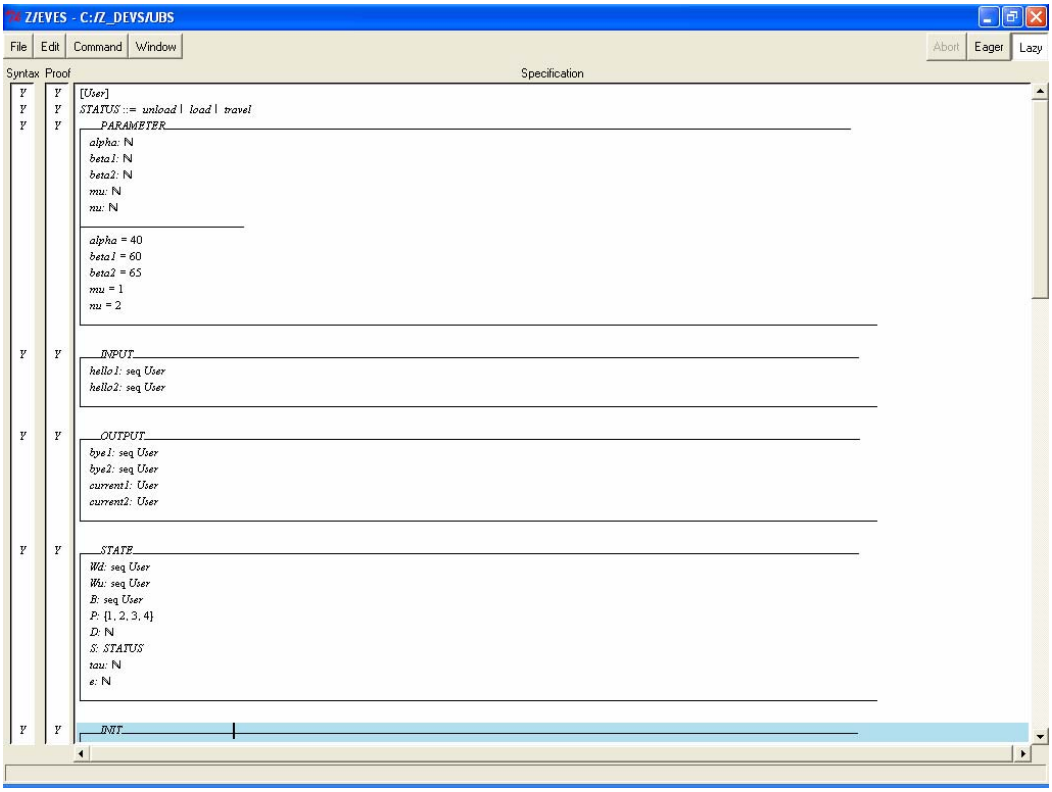

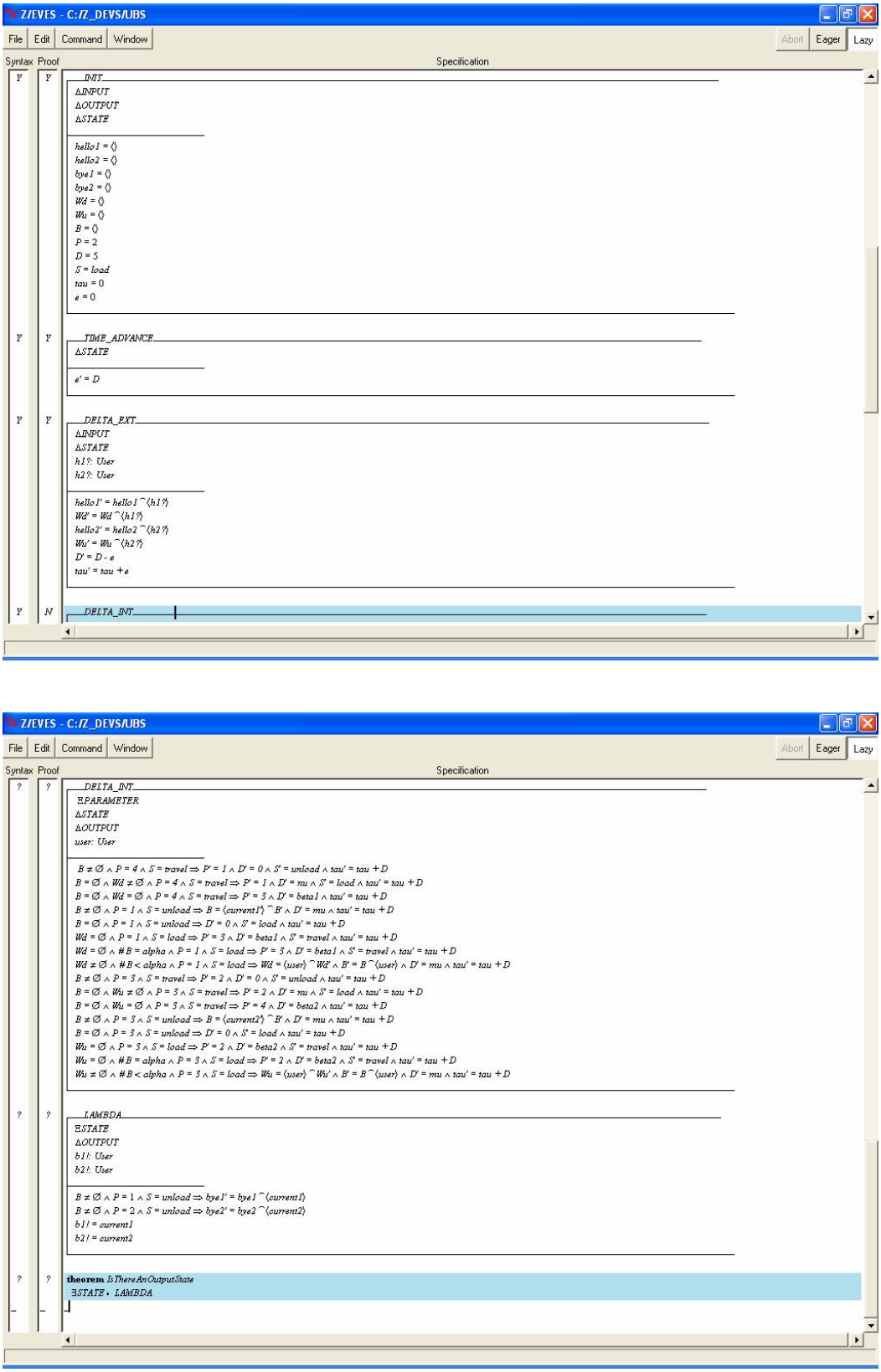

Figure 6. Z-DEVS model of the UBS

One can see that there is a slight difference between the object orientation of the approach that we have proposed and the way schemas are really implemented in Z/EVES. This is due to the fact that Z/EVES does not support the object-oriented programming style. To strictly map our approach onto an effective formal specification, a tool supporting the Object-Z principles [Smith 2000] is required, e.g. ZIMOO [Friesen et al. 1998]. However, it is possible to realize the modularity underlying the Z-DEVS specification process using any Z-supporting tool. Since the Z/EVES tool supports the standard Z specification paradigm, the surrounding schema box "atomic" is implemented using schema inclusion operators like Δ and Ξ.

5.3. **Analysis potentials**

Once the Z-DEVS model is built, possible analyses may consist in:

- Identifying ambiguities, conflicts and inconsistencies in the specification. A first step in identifying ambiguities, conflicts and inconsistencies in the specification is to run partial checks while doing the specification of the Z-DEVS model. The Z/EVES tool shows in a left-hand side column (the proof column) of its graphical user interface that the current specifications of the modeler are consistent or not (Y or N). This is very helpful to drive a complete and concise specification in an incremental specification process. More can be done after the specification is achieved (e.g., verifying that there is an initial state), since such a specification is opened to all the verification and theorem proving means that are available in a Z-supporting tool.
- Studying system behavior and producing traces of it.
- Demonstrating properties. We have tried to verify if there is a state in which an output value is computed. Figure 7 shows the result of the analysis of the corresponding theorem, that we have defined as follows:

theorem IsThereAnOutputState
•STATE ••LAMBDA

The proof window of Z/EVES shows that it is not possible to assert that a state in which there is an output is reachable in the current specification of the bus system (elsewhere, the formula frame would show "true"). If we return to the specification window of Z/EVES, we see that the proof is not complete (? in the proof column). Hence, additional information is needed.

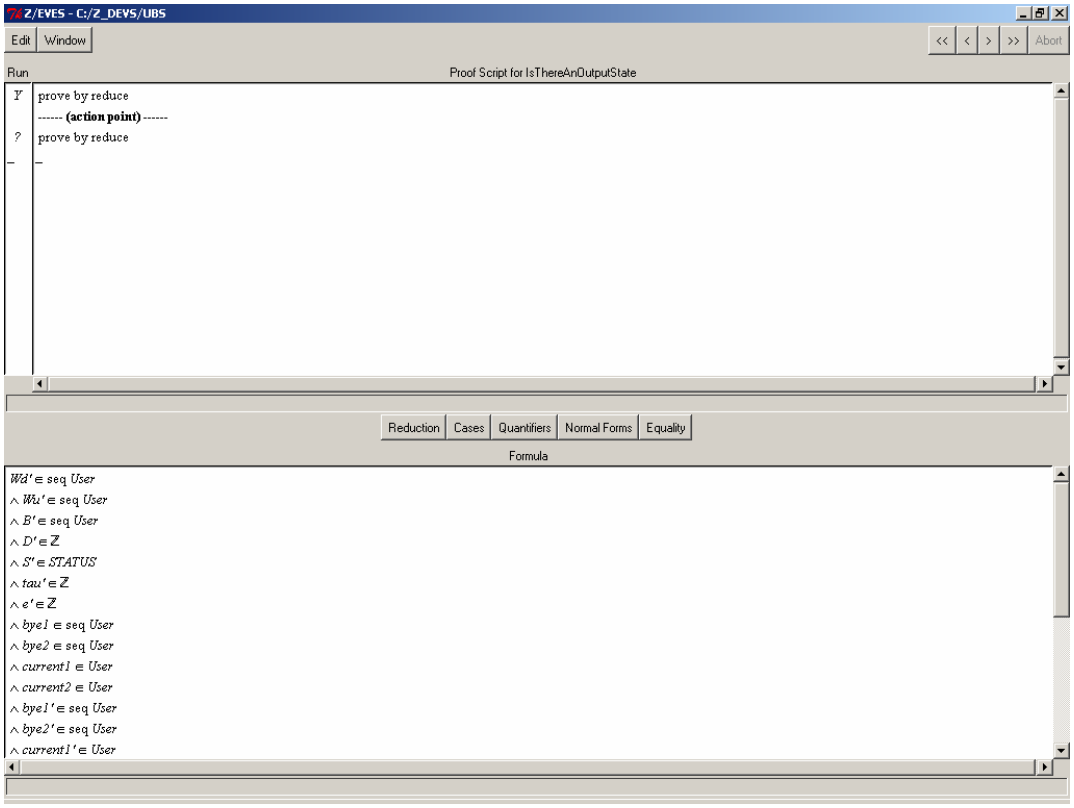

Figure 7. Proof process of the IsThereAnOutputState predicate

To study system behavior and produces traces of it, the modeler can use the Z-DEVS root coordinator to get the trajectories of his concern. To demonstrate properties, a Z-DEVS specification can be submitted to tests such that those performed to find hidden properties [McMillan 1992]. All of these aspects are not detailed in the present paper, both for the lack of space and for that each of them deserves a special focus.

Even if the paper focuses on DEVS atomic models only, coupled models are also considered in our ongoing work. There are two ways to deal with them: (1) due to the closure under coupling property of DEVS, each coupled model has an equivalent atomic model which we can deal with for formal verification; or (2) coupled models are specified in terms of concurrent components. This could be done in CSP and its equivalent Z specification can be produced, as presented in [Graeme 1992].

6. Conclusion

We have shown in this paper how DEVS and Z formalisms can be combined. Our goal is to extend the DEVS formalism and to turn it to a logical framework, in order to obtain simulation models of a better quality by making them accessible to formal analyses. Theorem-proving tools could be used to explore properties, often detecting conflicts between different requirements or missing assumptions. Then, ambiguities and inconsistency in requirements could be discovered early, when they can be corrected with much less expense than after code has been developed. This is an interesting prospect for VV&A in M&S.

Another prospect of this work is that, given a formal definition of requirements through experimental frames, and a formal specification of the model, theorem proving tools can be used to assist in proving that the specification meets the requirements, i.e., that the experimental frame can be applied to the model and the expected results correctly obtained. This can open the way to the management of models libraries in one hand, and experimental frames libraries in the other hand, and automatic selection, retrieval and matching processes.

Even the study presented here focuses on atomic models, the framework must also involve a higher specification level where coupled models can be created by connecting together atomic models. All these considerations are part of our future work.

REFERENCES

[Clarke and Wing 1996] Clarke, E., and J.M. Wing. Formal Methods: State of the Art and Future Directions. *ACM Computing Surveys,* **28**- 4: 626-643, 1996.

[Kuhn et al. 2003] Kuhn, D.R., D. Craigen, and M. Saaltink. Practical Application of Formal Methods in Modeling and Simulation. *Proceedings of SCSC'03 (invited). Summer Simulation Multiconference*, Montreal, Canada, 2003.

[Lamsweerde 2000] Lamsweerde, A.V. Formal Specification: a Roadmap. *International Conference on Software Engineering. Proceedings of the Conference on the Future of Software Engineering*, 147-159. 2000.

[McMillan 1992] McMillan, K.L. Symbolic Model Checking. An Approach to the State Explosion Problem. *Ph.D. Thesis in Computer Science, CMU-CS-92-131*, Carnegie Mellon University. 1992.

[Paige 1997] Paige, R.F. A Meta-Method for Formal Method Integration. *Proceedings of the 4th International Symposium of Formal Methods Europe*, 473-494. 1997.

[Smith 2000] Smith, G. The Object-Z Specification Language. *Advances in Formal Methods. Kluwer Academic Publishers*. 2000.

[ISO 2002] Information Technology. Z Formal Specification Notation - Syntax, Type System and Semantics. *ISO/IEC 13568*. 2002.

[Stevenson 2003] Stevenson, D.E. From DEVS to Formal Methods: a Categorical Approach. *Proceedings of SCSC'03, Summer Simulation Multiconference*, Montreal, Canada: 1-6. 2003.

[Zeigler 1976] Zeigler, B.P. Theory of Modelling and Simulation. *Wiley & Sons*, N.Y. 1976.

[Zeigler 1984] Zeigler, B.P. Multifacetted Modelling and Discrete Event Simulation. *Academic Press Inc.*, London. 1984.

[Zeigler et al. 2000] Zeigler, B.P., H. Praehofer, and T.G. Kim. Theory of Modeling and Simulation. Integrating Discrete Event and Continuous Complex Dynamic Systems. 2nd Ed. *Academic Press*. 2000.

[Graeme 1992] Graeme, S., and R. Duke. Specifying Concurrent Systems Using Object-Z. *Proceedings of the 15th Australian Computer Science Conference*: 1-14. 1992.

[Friesen 1998] Friesen, V., A., Nordwig, and M. Weber. Object-Oriented Specification of Hybrid Systems Using UMLh and ZimOO. *Proceedings of ZUM'98*: 328-346. 1998.

[Saaltink 1997] Saaltink, M. The Z/EVES system. *ZUM'97: Z Formal Specification Notation. Lecture Notes in Computer Science* 1212. *Springer-Verlag*: 72–85. 1997

.

Health, Uncertainty, and Insurance: A Social Simulation

Toshitaka Fukiharu
Faculty of Economics
Hiroshima University
1-2-1 kagamiyama
higashi-hiroshima, 739-8525, Japan
+ 81 82 424 7295
fukito@hiroshima-u.ac.jp

ABSTRACT

Insurance for the households in poor health is examined from the economic point of view. The household in poor health is defined as the one whose initial endowment of labor days is 300 days a year, for simplicity, compared with 365 days for the household in good health. In section 2, constructing general equilibrium (GE) model by the expected utility approach, medical insurance is examined when the health can be recovered by medical treatment, as seen in diseases. The introduction of insurance is shown to reduce the social welfare, as known as Moral Hazard, when the medical industry is under perfect competition. On the other hand, it is shown that the social welfare rises when the medical industry is a monopolist. In section 3, income compensation insurance is examined when the medical sector is left out of consideration. First, it is shown in simulation that when there is only one class of households regarding the probability of poor health, strict assumptions are required in order for them to make insurance contracts in GE model. Next, it is shown that when there are two classes of households, Adverse Selection emerges.

KEYWORDS

General equilibrium, expected utility, perfect competition, monopoly, Moral Hazard, Adverse Selection

1. Introduction

When Adam Smith, a moral philosopher, wrote *the Wealth of Nations* in 1776, the philosophy in economics was "small government", as expressed by "invisible hand"([Smith 1776]). It was replaced by "big government" philosophy after the great depression in the 1930s. Since the 1970s, however, "small government" philosophy revived. In this revival the theory of general equilibrium (GE) played an important role ([Lucas 1972]). The GE approach, initiated by Leon Walras in the 1870s, consists in solving a system of equilibrium conditions for all the markets in a society ([Walras 1877]). The existence of competitive GE model was proved in the 1950s utilizing the non-cooperative game, invented by Nash, who won a Nobel Prize in 1994 ([Nash 1950]). Lucas applied this approach to macroeconomics, asserting that governmental intervention through monetary policy is completely ineffective. He won a Nobel Prize in 1995. Utilizing simulation approach, Shoven and Whalley extended the applicability of GE models. For instance, a simulation-type GE model was applied to the evaluation of different taxing systems ([Shoven *et al.*1992]). In this paper, the simulation-type GE approach is applied to insurance problem.

The "small government" philosophy prevails in the US welfare policy. In the US, the national medical insurance system is rejected, although a few US Presidents, including Bill Clinton, advocated the introduction of the system. Thus, the advocates have criticized the existence of forty million lower middle incomes US citizens without medical insurance. (In the US, the lowest income citizens are covered by the Medicaid system.)

After Arrow initiated the medical economics, a lot of contributions have been made in this field ([Arrow 1963]). He won a Nobel Prize in 1972. While he stressed the positive side of medical insurance, Pauly pointed out its negative side, utilizing a simple partial equilibrium model ([Pauly 1968]). In the present-day textbooks on microeconomics, Pauly' argument of Moral Hazard is popular, and it is asserted that the medical insurance causes inefficiency of welfare: emergence of Dead Weight Loss, a triangle on the demand-supply diagram for the medical service market ([Layard *et al.*1978]). In the United States, the statistical estimation of this triangle (welfare loss) has been frequently conducted. In this paper, first, his argument is reconstructed in the simulation-type GE model for the purpose of elucidating the essence of medical insurance. Next, another important argument of Adverse Selection in insurance is examined in the same simulation-type GE framework. Akerlof examined the asymmetric information in the market for used cars, asserting that there may not exist equilibrium in such a market with asymmetric information, where sellers of used cars know the quality of them, and purchasers don't ([Akerlof 1970]). He won a Nobel Prize in 2001. Contributions by Arrow and Akerlof were synthesized by Rothschild and Stiglitz as

the economics of Adverse Selection in insurance market. Utilizing partial equilibrium model, [Rothschild *et al.*1976] asserted that there might not exist equilibrium in insurance market with asymmetric information, where sellers of insurance do not know the exact probabilities of poor health of the purchasers and they set the insurance fee by the average of those probabilities. Stiglitz also won a Nobel Prize in 2001. The present paper considers these problems concerning insurance markets using the simulation-type GE model.

In this paper, poor health, or sickness is defined by the loss of initial endowment of leisure (working hours), and the medical care recovers a part of the lost initial endowment, while it is supplied with medical service charge. In the argument of Moral Hazard, examining if the sum of households' utility level at the GE falls by the introduction of medical insurance makes final evaluation for GE model.

In Section 2 of this paper, first, it is assumed that medical service is supplied by the competitive medical sector, to examine if the Moral Hazard emerges. Here, medical insurance implies the fixed percent deduction of medical cost. Next, it is examined if the Moral Hazard emerges when the medical sector is a monopolist. In Section 3, the insurance system of income compensation is introduced into this model. For simplicity, medical service is left out of consideration in this section. First, it is assumed that there is only one class of households with the same probability of poor health. After examining the existence problem of GE in this case, we proceed to the case of two classes of households with the different probability of poor health. The Adverse Selection problem in the asymmetric information is examined. The main purpose of this paper, thus, is to evaluate if the simulation-type GE approach can add new insights to the classical contributions. In the final section, the conclusions are stated.

2. Moral Hazard Problem

When a person falls sick, one aspect of sickness is "bad feeling". The sickness, however, is not restricted to such a "feeling". Another important aspect is the loss of working hours. Thus, a doctor's services to patients are not only the alleviation of bad feeling but also the recovery of working hours. In consideration of this feature, Pauly's argument, it appears, needs reconsideration. His argument was constructed in the framework of partial equilibrium. In Figure1 x stands for the quantity

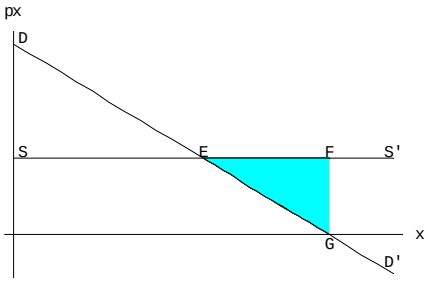

Figure1: Medical Service Market and Dead Weight Loss

of medical service, while p_x stands for the price of medical service. Demand function for medical service is depicted as DD', while the supply function is depicted as SS'. Without medical insurance the equilibrium for this market is determined at E. When all the medical service is covered by insurance, however, the equilibrium for this market is determined at G. According to Pauly, the dead weight loss, or loss of efficiency is measured by the triangle, EFG, using the argument of consumers' surplus. US economists conducted econometric estimations of the triangle: *e.g.* [Feldstein 1973].

When a part of the medical service charge is deducted by medical insurance, the increased medical service causes dead weight loss, as explained above. This, however, makes possible the recovery of working hours in the framework of this paper, which may well increase the consumption of goods. In other words, consumers' surplus in the consumable goods market may well increase as "external economy". Examining the sum of the two effects must make the final evaluation. The argument made so far calls for the analysis of medical insurance in the framework of general equilibrium (GE).

In this paper, sickness is defined by the loss of initial endowment of working hours (leisure), and the medical care recovers a part of the lost initial endowment, while it is supplied by medical sector with medical service charge. Computing GE allocations for the specified utility and production functions by Cobb-Douglas type, final evaluation is made by examining if the sum of households' utility level at GE is raised by the introduction of medical insurance. In subsection 2.1, the case in which there is no medical insurance is considered. In subsection 2.2 medical insurance is introduced, where the medical sector behaves as a competitive firm. In subsection 2.4 medical insurance is introduced, where the medical sector behaves as a monopolist.

2.1 No Medical Insurance Case: When Medical Sector Is Competitive

In this subsection, a GE model incorporating medical sector is constructed, where medical insurance is not available. At every moment, there are two types of households: the household with good health and the household with poor health. It is assumed that everyone knows that the distribution of households is constant in each year; a_1 households are of good health and a_2 households are of poor health. No one knows, however, whether each household is of good health or not before the beginning of the particular year. Only when the particular year starts, a_1 households know that they are of good health, while the remainder knows that they are of poor health. In this sense, every household knows that each household has the probability, $\alpha=a_2/(a_1+a_2)$, of being of poor health in each year. When the household is of good health, it has 365 days of initial leisure days. Its behavior is stipulated by traditional utility maximization under income constraint:

$$\max u\,[z_1, le_1]$$
$$\text{s.t. } p_z z_1=w\,(365-le_1)+Y_1 \qquad (1)$$

where $u\,[z_1, le_1]$ is the utility function, z_1 is the consumption of (aggregated) commodities, le_1 is the leisure consumption, p_z is the price of (aggregated) commodities, w is the wage rate, and Y_1 is the transfer of income from (and to) others, such as profit and tax, etc. In this section, since simulation approach is utilized, utility function is stipulated by

$$u\,[z, le]=z\times le. \qquad (2)$$

When the household is of poor health, it has H_0 days of initial leisure days, say H_0=300. It goes to a hospital to see a doctor, in order to recover a part of the lost leisure days. It is assumed for simplicity that a doctor can recover $x^{1/2}$ days of leisure for the households of poor health by supplying x medical treatment, while the doctor receives service charge p_x per one unit of medical treatment. Such household behavior is stipulated by the following utility maximization under income constraint:

$$\max u[z_2,le_2]$$
$$\text{s.t. } p_z z_2+p_x x=w\,(H_0+x^{1/2}-le_2)+Y_2 \qquad (3)$$

where $u[z_2, le_2]$ is utility function, z_2 is consumption of (aggregated) commodities, le_2 is leisure consumption, and Y_2 is transfer of income from (and to) others, such as profit and tax, etc. In this section, since simulation approach is utilized, utility function is stipulated by (2). Thus, the representative household's behavior is formulated by the following maximization of expected utility:

$$\max (1-\alpha)\,u[z_1,le_1]+\alpha\,u[z_2,le_2]$$
$$\text{s.t. } p_z z_1=w(365-le_1)+Y_1,\ p_z z_2+p_x x=w(H_0+x^{1/2}-le_2)+Y_2 \qquad (4)$$

The optimal values in (4) are the demand function for goods, $z_1^{d}[p_z,w,p_x,Y_1,Y_2]$ and the one for leisure, $le_1^{d}[p_z,w,p_x,Y_1,Y_2]$, when the household is in good health, the demand function for commodities, $z_2^{d}[p_z,w,p_x,Y_1,Y_2]$ and the one for leisure, $le_2^{d}[p_z,w,p_x,Y_1,Y_2]$, and demand function for medical treatment, $x^{d}[p_z,w,p_x,Y_1,Y_2]$, when the household is in poor health, Labor supply function when the household is in good health, $l_1^{s}[p_z,w,p_x,Y_1,Y_2]$, is defined by $365-le_1^{d}[p_z,w,p_x,Y_1,Y_2]$ and labor supply function when the household is in poor health, $l_2^{s}[p_z,w,p_x,Y_1,Y_2]$, is defined by $H_0-le_2^{d}[p_z,w,p_x,Y_1,Y_2]$.
The behavior of commodity-producing sector is stipulated by profit maximization where production function is given by:

$$z=f[l_g]= l_g^{1/2} \qquad (5)$$

where z is the output of (aggregate) commodities, and l_g is labor input. In this paper, this sector is a competitive firm, and the profit maximization under (5) gives rise to the labor demand function of the commodity-producing sector, $l_g^{d}[p_z,w]$, commodity supply function, $z^{s}[p_z,w]=f[l_g^{d}[p_z,w]]$, and profit function, $\pi[p_z,w]=p_z z^{s}[p_z,w]-w\,l_g^{d}[p_z,w]$. It is assumed that stocks of this firm is owned by the households with equal share, so that

$$Y_1=Y_2=\pi[p_z,w]/(a_1+a_2). \qquad (6)$$

The behavior of medical sector is stipulated by profit maximization in this section. The production function of medical service is given by:

$$x=g[l_x,z_x]= l_x^{1/2}\, z_x^{1/2} \qquad (7)$$

where l_x is the input of labor; *e.g.* nurses etc., z_x is the input of commodities; *e.g.* medicines etc. The medical sector aims at maximum profit. Since (7) implies constant returns to scale, the maximum profit is zero if any, and it aims at cost minimization. In order to provide the medical service demanded by the households in poor health, x, the medical sector has the demand function for the commodities, $z_x^{d}[x,p_z,w]$, the one for labor, $l_x^{d}[x,p_z,w]$, and the cost minimization function,

$c[x,p_z,w]= p_z\, z_x^{d}[x,p_z,w]+w\, l_x^{d}[x,p_z,w]$.

GE for this society is defined by the existence of p_x, p_z and w, satisfying the following.

$z^s=a_1\, z_1^{d} + a_2\, z_2^{d} +z_x^{d}$ (commodity market)

$a_1\, l_1^s+ a_2\, l_2^s=l_g^{d}+ l_x^{d}$ (labor market)

$p_x\, a_2x^{d} =c[a_2x^{d},p_z,w]$ (medical sector: perfect competition)

In what follows, p_x and p_z are actually computed by simulation where w=1. Suppose that

a_1=99, a_2=1, H_0=300. (8)

[Shoven *et al.*1992] asserted that Scarf algorism could always solve p_x, p_z and w. In this paper, however, utilizing the classical Newton method, p_x, p_z, $u_1=u[z_1,le_1]$, and $u_2=u[z_2,le_2]$ at GE are computed as:

p_x= 29.6923399007, p_z= 220.40876219, u_1^{CN}= 268.403187279 and u_2^{CN}= 201.4748019360 (9)

As is well known the Scarf algorism can find competitive GE from arbitrary initial position of p_x and p_z ([Scarf 1973]), while in the Newton method, it is required to find the initial positions of p_x and p_z to guarantee their convergence to (9). Note however, that we must construct a rather complicated computing program in the case of Scarf algorism ([Scarf 1973]), while we can use *Mathematica*'s ready-made function in the case to Newton method. As for *Mathematica* programming in this case, see [Fukiharu 2004a].

2.2 Medical Insurance Case: When Medical Sector Is Competitive

[Hellwig 2005] constructed an interesting GE model with insurance. His model examined Moral Hazard under competitive and Cournot-oligopolistic cases. Note, however, that competitive and Cournot-oligopolistic behaviors are assumed on insurance buyers: *i.e.* households in the present paper. Furthermore, his model does not incorporate the medical sector as in [Pauly 1968] and this paper. In this subsection, "fair" medical insurance is introduced into the GE model constructed in subsection 2.1. Suppose that (8) holds. In this medical insurance system, the household of poor health receives k% medical charge deduction: *i.e.* it pays $(1-k)\times p_x\times x$ for the medical service, x. Since there are a_2 such households, $a_2\times k\times p_x\times x$ must be supplied by the households of good health. Thus, $a_2\times k\times p_x\times x/a_1$ is the insurance fee for household of good health, if the "fair" insurance is to be constructed. Except for the specification of Y_1, no modifications in (1) and (2) are required for the household of good health. The modification in (3) is required for the household of poor health as follows.

$$\max u[z_2,le_2]$$

$$\text{s.t. } p_z\, z_2+(1-k)\, p_x\, x= w\,(H_0+x^{1/2}-le_2)+Y_2 \qquad (3\text{-}1)$$

If k=10/100, the household of poor health must pay 90% of the medical charge. This implies that $a_2\times k\times p_x\times x/a_1$ must be deducted from the household of good health's transfer function as the insurance fee. Thus, the specification of Y_1 must be modified as follows.

$Y_1=\pi[p_z,w]/(a_1+a_2)-a_2\times k\times p_x\times x/a_1$. (6-1)

With these modifications, as in subsection 2.1, we can compute the competitive GE values for the utility level of household in good health, u_1^{C}, and the utility level of household in poor health, u_2^{C} as follows.

u_1^{C}= 268.403175683520, u_2^{C}= 201.4756971621 (9-1)

As for *Mathematica* programming, see [Fukiharu 2004a].

If we define the social welfare as the sum of individual utilities, we have

$W^{C}=a_1u_1^{C}+a_2u_2^{C}$= 26773.390089830 < 26773.3903425860$=a_1u_1^{CN}+a_2u_2^{CN}=W^{CN}$ (10)

This result corresponds with Pauly' argument of Moral Hazard. By the introduction of medical insurance, the household of poor health becomes better off. However, since it affects the market price, it causes the decrease in efficiency of welfare. Division of W^{CN} and W^{C} by the number of total households imply the expected utility for each household in the society without medical insurance and the one with medical insurance. $W^{CN}>W^{C}$ implies that each household's expected utility in a society without medical insurance is greater than the one with medical insurance. In other words, market mechanism produces Pareto-optimality. From the viewpoint of social fairness, however, some economists may assert that as a social welfare, W^{CN} and W^{C}; simple sums of individual utilities should not be used. Rather, they may propose the social welfare as

the weighted sum of household's utilities, where the weight for the household in poor health's utility should be greater than the one for the household in good health. In this modification, made from the viewpoint of social fairness, the case with medical insurance may be better than the one without medical insurance. As is pointed out always, however, how to determine the weights for this modification is quite difficult. It must be pointed out that if the Rawls-type social welfare function is adopted the case with medical insurance is definitely better than the one without medical insurance ([Rawls 1971]).

2.1. **No Medical Insurance Case: When Medical Sector Is a Monopolist**

In [Hellwig 2005], the Cournot-oligopoly was assumed on households. In this subsection the medical sector is assumed to be a monopolist. The Japan Medical Association or The American Medical Association may become a monopolist in each country; if they can set the medical charges at will, although in Japan, the Japanese government sets the charges. For simplicity, suppose that the households with equal share holding own this sector. Thus monopolistic profit is distributed equally to each household. Other assumptions are the same as in subsection 2.1; *e.g.* the commodity-producing sector is assumed to be a competitive firm. In this modified GE model, what would happen to the above assertion: the introduction of medical insurance causes the welfare inefficiency?

First, the existence of monopolistic GE without medical insurance is examined and comparison is made with the result in subsection 2.1. As in subsection 2.1, suppose that (2), (5), (7), and (8) hold. From the same procedure as in subsection 2.1, the demand function for medical treatment is derived. Assuming that the medical sector provides the medical service demanded by the household of poor health, the minimum cost function for the medical sector is derived with p_x, p_z, and w, parameters. Using this minimum cost function, the *objective* profit function of the medical sector is given by the following function; $\pi_M[p_x,p_z,w]$.

$$\pi_M[p_x,p_z,w]=w^2/(4p_x)-p_z^{1/2}w^{5/2}/(2p_x^2) \qquad (11)$$

Medical sector's *objective* profit function, $\pi_M[p_x,p_z,w]$ is depicted as a function of p_x in Figure 2, when p_z=1/2 and w=1.

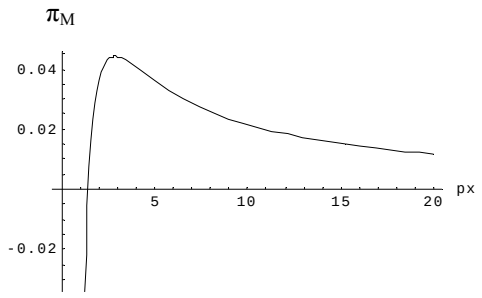

Figure 2: Objective Profit Function for the Medical Sector

The maximized monopolistic profit, $\pi_M[4p_z^{1/2}w^{1/2},p_z,w]$, is equally distributed to each household. Thus, we have

$$Y_1=Y_2=(\pi[p_z,w]+\pi_M[4p_z^{1/2}w^{1/2},p_z,w])/(a_1+a_2). \qquad (6\text{-}2)$$

Solving commodity market and labor market equilibrium conditions, with medical sector equilibrium condition replaced by

$$p_x= 4p_z^{1/2}w^{1/2} \quad \text{(medical sector: monopoly)}$$

we have

$$p_x^M= 59.3846767519,\ p_z^M= 220.408736728,\ u_1^{MN}= 268.40321054 \text{ and } u_2^{MN}= 201.470793567 \qquad (9\text{-}2)$$

In this computation, programming for the Scarf mechanism is not necessary, either. As in subsection 2.1, the traditional Newton method computes (9-2). As for *Mathematica* programming, see [Fukiharu 2004a]. Comparison between (9) and (9-2) shows that the households with poor health is worse off, while the households with good health is better off due to higher profit distribution. The social welfare, W^{MN}, is computed as the following.

$$W^{MN}=a_1u_1^{MN}+a_2u_2^{MN}=26773.388637908<26773.3903425860=a_1u_1^{CN}+a_2u_2^{CN}=W^{CN} \qquad (10\text{-}1)$$

Thus, inefficiency of welfare emerges due to the monopoly of medical sector.

2.2. **Medical Insurance Case: When Medical Sector Is a Monopolist**

When the medical insurance is introduced into this monopolistic model, what would happen? Following the definition of the medical insurance, medical service charges for the households of poor health is deducted 100×k%. The main modification in the computational programs is required for Y_1, as in what follows.

$$Y_1 = (\pi[p_z,w] + \pi_M[4p_z^{1/2}w^{1/2},p_z,w])/(a_1+a_2) - a_2\times k\times p_x\times x/a_1. \qquad (6\text{-}3)$$

With these modifications, from the equilibrium conditions with w=1, and k=10/100, we have utility levels for the household in good health, u_1^M, and the one for the household in poor health, u_2^M, as in what follows.

$$u_1^M = 268.4032101995,\ u_2^M = 201.471245896 \qquad (9\text{-}3)$$

Comparison among (9-1), (9-2), and (9-3) implies that the household of poor health with insurance in monopoly case is better off compared with non-insurance case, while it is worse off compared with insurance-in-competition case. The social welfare, W^M, is computed as in what follows.

$$W^M = a_1u_1^M + a_2u_2^M = 26773.3890556560 > 26773.388637908 = W^{MN} = a_1u_1^{MN} + a_2u_2^{MN} \qquad (10\text{-}2)$$

Note that W^M is greater than W^{MN}. In other words, the introduction of medical insurance into the monopolistic medical sector model makes this society better off, even if the social welfare is defined by the simple sum of individual utility levels. Since, however, the medical insurance in this paper is nothing but a subsidy to the households when the world is under uncertainty, this result could be foreseen from the traditional argument on the subsidy in monopoly. It is a standard result that in the certain economy with a monopolistic firm, a direct subsidy to the firm raises the total surplus in this economy. In other words, subsidy policy is not first best policy, but a second best policy in the certain world. It was shown in this paper that the same theorem holds in the uncertain world: an indirect subsidy policy makes the society better off in the monopolistic medical sector case.

3. **Adverse Selection Problem**

[Akerlof 1970] examined the asymmetric information problem in the market for used cars, asserting that there may not exist equilibrium in such a market with asymmetric information, where sellers of used cars know the quality of them, and purchasers don't. Constructing a partial equilibrium model, [Rothschild *et al.* 1976] asserted that there may not exist equilibrium in insurance market with asymmetric information, where sellers of insurance do not know the exact probabilities of diseases of the purchasers and insurers must set the insurance fee by the average of those probabilities. The problem arising from the asymmetric information is called the Adverse Selection problem. In this section, this problem is examined in the GE framework. The insurance in this section, the income compensation insurance, is different from the one in section 2. When a household suffers from accidents or illness, it has lower initial endowment of working hours as above. Each household is assumed to make a contract with the insurer, so that the household receives the contracted amount of money when it suffers from misfortunes. In order to elucidate the special feature of income compensation insurance, medical sector is left out of consideration. In subsection 3.1, assuming that the consequence of misfortunes is the loss of initial endowment as in section 2, the existence of GE with income compensation insurance is examined in a model without medical sector. As above, utility and production functions are assumed to be of Cobb-Douglas type. In this economy, there is a class of households with the same probability of misfortune, who maximize utility with leisure and (aggregate) commodities as variables, demanding the commodities, while supplying labor. As in section 2, under the insurance system of income compensation, the insurer imposes "fair" insurance fee. In subsection 3.2, it is extended to the case in which there are two classes of households with different probabilities of misfortune.

3.1. **One Class of Households Case**

In subsection 2.2, it was shown that in the case of medical insurance, the assumption on utility function, (2), suffices to prove the existence of GE. In this section, it is examined if (2) suffices to prove the existence of GE in the case of income compensation insurance. In the history of economics, the concept of utility has been at the center of discussion. Adam Smith dismissed the theory of price determination through utility. Although Leon Walras and two other marginal utility advocates revived this theory, there remained the skepticism over the concept of utility. In order to conquer the skepticism, economists devised the indifference curves. In other words, economists insisted that the *preference relation* suffices to construct the demand theory: *i.e.* the assumption of *ordinal* utility function. It is Gerard Debreu, a Nobel Prize winner of 1983, who proved that a utility function can be constructed from the *preference relation* ([Debreu 1959]). Thus, in microeconomics, or GE theory, the assumption of *strictly quasi-concavity* is imposed on utility function, which does not contradict the *ordinality*. A function, $F[X]$, is called *strictly quasi-concave,* if $F[X]$ satisfies $F[tX+(1-t)X'] > F[X]$ for $F[X'] \geqq F[X]$, $X \neq X'$, and $0 \leqq t \leqq 1$. Assumption (2) satisfies the *strictly quasi-concavity*. This holds in the case of certain world. In the case of uncertain world, however, it is known that the assumption of *cardinal* utility may be necessary ([Layard *et al.*1978, Chapter 13]). Thus, it is

examined if (2) suffices to prove the existence of GE in the case of income compensation insurance.

We start with the same assumptions except for the one on insurance: *e.g.* there is one class of households with the same probability of being in poor health, (8), etc. Suppose that in this economy, insurance is introduced where the insurer guarantees the "fair" insurance. Following [Rothschild *et al.* 1976], the insurer pays \$1 for \$$p_I$ insurance fee when an insurance holder is in poor health. Specifically, if a household plans to obtain \$ I_α when the household is in poor health, the household must pay p_I I_α, both in poor health and in good health. Thus, when the income compensation insurance is introduced, each household, with $\alpha=a_2/(a_1+a_2)$ probability of being sick, maximizes the following expected utility:

$$\max\ (1-\alpha)\, u[z_{1\alpha}, le_{1\alpha}] + \alpha u[z_{2\alpha}, le_{2\alpha}]$$

$$\text{s.t. } p_z z_{1\alpha} + p_I I_\alpha = w(365 - le_{1\alpha}) + Y_{1\alpha}, \text{ and } p_z z_{2\alpha} + p_I I_\alpha = w(300 - le_{2\alpha}) + I_\alpha + Y_{2\alpha} \qquad (12)$$

As explained above, in this model, the household selects the optimum insurance holding I_α, as well as optimum commodity consumption, and optimum labor supply. In what follows, first, we derive optimum z^d and l^s, given I_α. Deriving z^s and l^d from the firms' profit maximization, we derive equilibrium commodity price p_z, given I_α and w=1. This derivation provides the equilibrium expected utility level, $u_\alpha[I_\alpha]$, given I_α and w=1. Finally, the optimum insurance I_α is selected by maximizing the equilibrium expected utility level.

As computed in [Fukiharu 2004b], $p_z = 2\times 12145^{1/2}$, which is independent of I_α. We have indirect utility function $u_\alpha[I_\alpha]=(2360434675-12870\, I_\alpha+99\, I_\alpha^2)/(80000\times 12145^{1/2})$, which is depicted in Figure3.

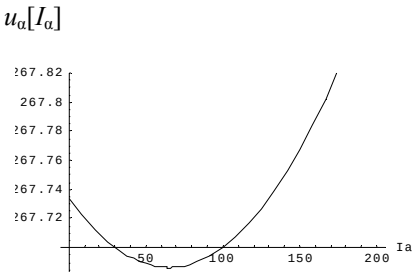

Figure3: Insurance-Dependent Indirect Utility Function When $u[z,le]=z\times le$

In Figure3, $u_\alpha[0]=u_\alpha[130]$, and I_α can be raised, while satisfying income constraint. Thus, there is no equilibrium.

In order to examine what strict assumption on utility function is required, suppose that the utility function is of the following form instead of (2).

$$u[z,le]=z^{1/2}\times le^{1/2} \qquad (2\text{-}1)$$

With this modification of utility function, the equilibrium expected utility level is computed as $u_\alpha[I_\alpha]=(99((-48645+I_\alpha)^2)^{1/2}+((42145+99\, I_\alpha)^2)^{1/2})/(20000\times 2^{1/2}\times 12145^{1/4})$, and $u_\alpha[I_\alpha]$ is depicted as in Figure4.

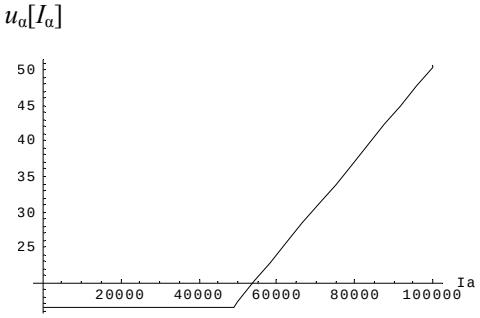

Figure4: Insurance-Dependent Indirect Utility Function When $u[z,le]= z^{1/2}\times le^{1/2}$

$u_\alpha[0]= u_\alpha[48645]$ and the selection of I_α, greater than 48645, is not feasible. Thus, no households purchase the insurance.

Suppose, then, that the utility function is of the following form instead of (2).

$$u[z,le]=z^{1/3}\times le^{1/3} \qquad (2\text{-}2)$$

With this modification of utility function, the equilibrium expected utility level is computed as $u_\alpha[I_\alpha]=(99((-48645+I_\alpha)^2)^{1/3}+((42145+99\,I_\alpha)^2)^{1/3})/(2000\times 2^{1/3}\times 5^{1/2}\times 2429^{1/6})$, and $u_\alpha[I_\alpha]$ is depicted as in Figure5.

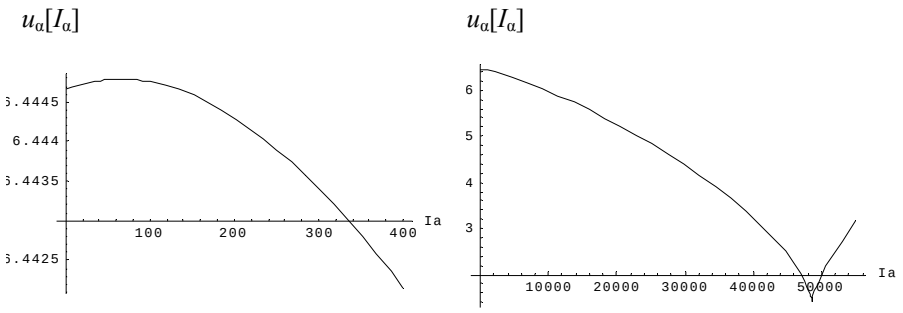

Figure5: Insurance-Dependent Indirect Utility Function When $u[z,le]= z^{1/3}\times le^{1/3}$

In the interval [0,48645], the equilibrium expected utility function, $u_\alpha[I_\alpha]$, has interior maximum as shown in the above diagram. When I_α is larger than 48645, $u_\alpha[I_\alpha]$ increases as shown in Figure5. However, $le_1^{\,d}$ becomes negative in this case, so that I_α, greater than 48645, is not feasible, and there exists GE with insurance when the utility function is specified by (2-2). The maximand of $u_\alpha[I_\alpha]$ is I_α=65.

A function, $F[X]$ is called *strictly concave,* if $F[X]$ satisfies $F[tX+(1-t)X']>t\,F[X]+(1-t)\,F[X]$ for $X\neq X'$, and $0\leqq t\leqq 1$. Note that (2-2) satisfies *strict concavity*; and it corresponds with the risk averter assumption: *i.e.* $u''(Y)<0$ where Y is income; for [Arrow1963] and [Rothschild *et al.*1976]. The *strict concavity* of utility function was assumed in [Lucas 1972] when Lucas proved the existence of GE with money, asserting that the monetary policy is completely ineffective. As pointed out by [Grandmont 1983] and [Fukiharu 1988], this strict assumption is indispensable in its proof: *i.e.* when the utility function is *strictly quasi-concave*, households do not hold paper money. Thus, in this subsection, it was ascertained that the assumption of *strict concavity* on utility function is indispensable for the existence of GE, when the transfer of financial assets is incorporated from the first period to the second period (in Lucas case), or from one situation, say, in good health, to another, say, in poor health (in our insurance case).

3.2. **Two Classes of Households Case**

[Akerlof 1970] considered the asymmetric information in the market for used cars, asserting that there may not exist equilibrium in such a market, where the sellers of used cars know the quality of them, while the purchasers don't. [Rothschild *et al.*1976] asserted that there may not exist equilibrium in insurance market with asymmetric information, where the sellers of insurance do not know the exact probabilities of diseases of the purchasers and the insurers must set the insurance fee by the average of those probabilities. In this subsection, following [Rothschild *et al.*1976], it is assumed that there are two classes of households with different probabilities of misfortune, and the sellers of insurance do not know the precise probabilities of misfortune of the purchasers and the insurers set the same insurance fee for all the purchasers.

Utility functions are specified by (11). There are two classes of households. Type A-households have the same characters as specified in subsection 3.1. Specifically, they have the probability α=1/100 of being unfortunate, and H_0=300. For simplicity, it is assumed that there are 100 class A-households. As in the preceding subsection, suppose that a_1 (=99) households in good health (or fortunate) and a_2 (=1) households in poor health (or unfortunate) in this class. In this section, another class of households is added. Suppose that there are 100 class B-households, with the probability β=1/10 of being unfortunate. For simplicity, suppose furthermore that b_1=90 fortunate households and b_2=10 unfortunate households in this class, and H_0=300. Thus, there are 200 households in this society, divided by two classes.

$$b_1=90,\ b_2=10,\ H_0=300. \qquad (8\text{-}1)$$

The behavior of class B households is stipulated in what follows.

$$\max\ (1-\beta)\,u[z_{1\beta},le_{1\beta}]+\beta u[z_{2\beta},le_{2\beta}]$$

s.t. $p_z z_{1\beta}+ p_I I_\beta=w(365- le_{1\beta})+Y_{1\beta}$, and $p_z z_{2\beta}+ p_I I_\beta=w(300- le_{2\beta})+I_\beta+Y_{2\beta}$ (12-1)

Equilibrium condition for the commodity market with two-class-household GE model is the following.

$z^s=a_1\times z_{1\alpha}{}^d+a_2\times z_{2\alpha}{}^d+ b_1\times z_{1\beta}{}^d+b_2\times z_{2\beta}{}^d$ (commodity market II) (13)

>From (13), the equilibrium commodity price p_z, when I_α and I_β are given and w=1, is computed as follows.

$p_z=(72285+ I_\alpha+10 I_\beta-100 I_\alpha p_I-100 I_\beta p_I)^{1/2}\ 2/3^{1/2}$ (14)

Equilibrium condition for the labor market with two-class-household GE model is the following.

$a_1 l_{1\alpha}{}^s+ a_2 l_{2\alpha}{}^s+ b_1 l_{1\beta}{}^s + b_2 l_{2\beta}{}^s = l_g{}^d$ (labor market II) (15)

>From (15), the equilibrium commodity price p_z, when I_α and I_β are given and w=1, is computed as follows.

$p_z=(72285- I_\alpha-10 I_\beta+100 I_\alpha p_I+100 I_\beta p_I)^{1/2}\ 2/3^{1/2}$ (16)

The same commodity price must prevail at equilibrium, so that from (15) and (16)

$p_I=(I_\alpha+10I_\beta)/(100(I_\alpha+I_\beta))$ (17)

must hold. Substitution of (17) into (16) gives rise to the constant equilibrium commodity price, $p_z=2\times 24095^{1/2}$. From (16) and (17), the indirect expected utility for household of class A, given I_α and I_β, is computed as $u_A[I_\alpha,I_\beta]$.

$$u_A[I_\alpha,I_\beta]= 99/(4000\times 5^{1/2}\times 4819^{1/6})\ \{((2 I_\alpha{}^2-97095 I_\beta+5 I_\alpha(-19419+4 I_\beta))^2/(I_\alpha+ I_\beta)^2)^{1/3}+$$
$$((198 I_\alpha{}^2+84095 I_\beta+5 I_\alpha(16819+36 I_\beta))^2/(I_\alpha+ I_\beta)^2)^{1/3}\} \quad (18)$$

The indirect expected utility function, $u_A[I_\alpha,I_\beta]$, is depicted in Figure6 ($0\le I_\alpha\le 1000$, $0\le I_\beta\le 1000$).

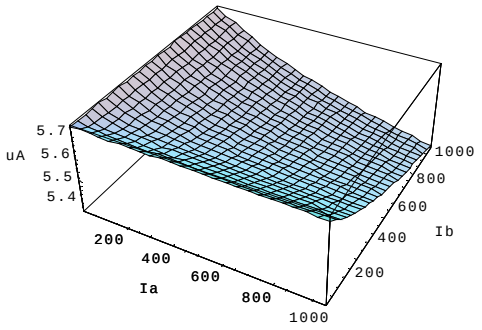

Figure6: Type A's Insurance Dependent Indirect Utility Function, $u_A[I_\alpha,I_\beta]$, ($0\le I_\alpha\le 1000$, $0\le I_\beta\le 1000$)

For instance, when I_β=1, $u_A[I_\alpha,I_\beta]$ has the local maximum at I_α=61.6467, while the global maximum is at I_α=0, as is clear from Figure7 ($0\le I_\beta\le 2$) and Figure8 (when I_β=1).

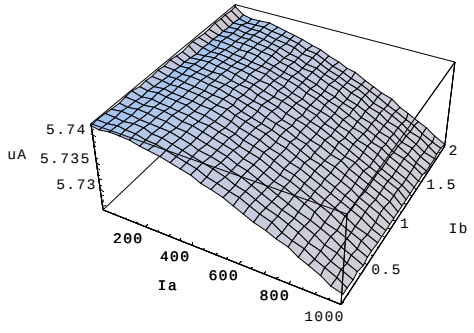

Figure7: $u_A[I_\alpha,I_\beta]$, ($0\le I_\alpha\le 1000$, $0\le I_\beta\le 2$)

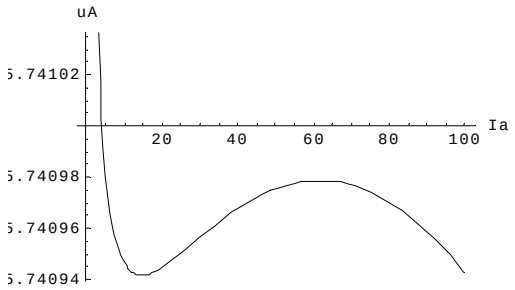

Figure8: $u_A[I_\alpha,1]$

When I_β is not small, however, $u_A[I_\alpha,I_\beta]$ has maximum at I_α=0, as is clear from Figure 9 ($50 \le I_\beta \le 100$) and Figure10 (when I_β=60).

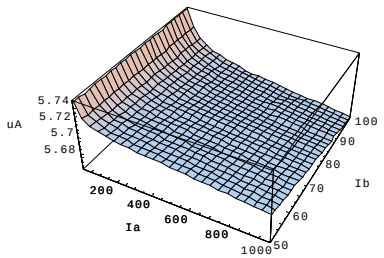

Figure 9 : $u_A[I_\alpha,I_\beta]$, ($0 \le I_\alpha \le 1000$, $50 \le I_\beta \le 100$)

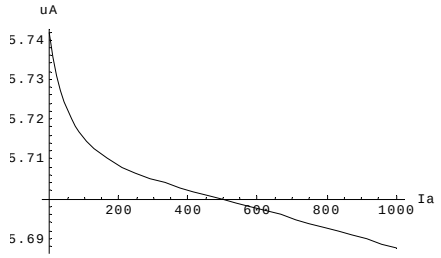

Figure 10: $u_A[I_\alpha,60]$

In the same way, the indirect expected utility for household of class B, given I_α and I_β, is computed as $u_B[I_\alpha,I_\beta]$.

$$u_B[I_\alpha,I_\beta]= 9/(400\times 5^{1/2}\times 4819^{1/6})\ \{((\ I_\alpha(-97095+ 2\ I_\beta)+5\ I_\beta\ (-19419+4\ I_\beta))^2/(\ I_\alpha+\ I_\beta)^2)^{1/3}+$$
$$((11\ I_\alpha(7645+18\ I_\beta)+5\ I_\beta(16819+36\ I_\beta))^2/(\ I_\alpha+\ I_\beta)^2)^{1/3}\}\quad (19)$$

The indirect expected utility function, $u_B[I_\alpha,I_\beta]$, is depicted in Figure11 ($0 \le I_\alpha \le 1000$, $0 \le I_\beta \le 1000$).

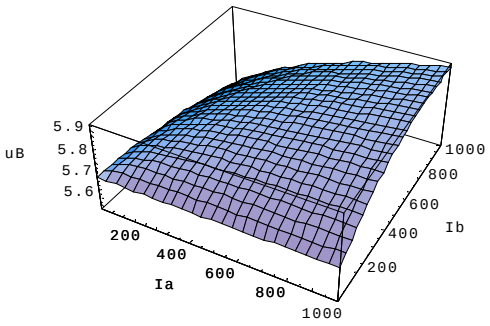

Figure 11: Type B's Insurance Dependent Indirect Utility Function, $u_B[I_\alpha,I_\beta]$, ($0 \le I_\alpha \le 1000$, $0 \le I_\beta \le 1000$)

Even when I_α is small, indirect utility function has maximum at $I_\beta \ge 65$, as is clear from Figure 12 ($0 \le I_\alpha \le 5$). This phenomenon emerges since insurance fee is cheap for class B households, who have higher possibility of misfortune. For instance, when I_α=1, indirect utility function has maximum at I_β=65.3268, as is clear from Figure 13 (when I_α=1).

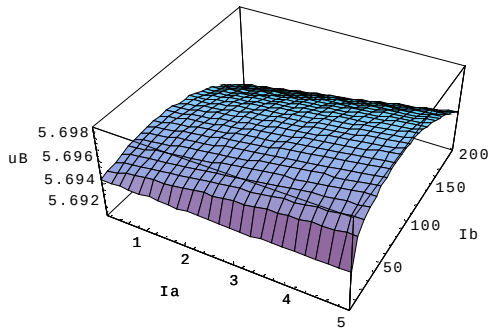

Figure 12: $u_B[I_\alpha,I_\beta]$, ($0 \le I_\alpha \le 5$, $0 \le I_\beta \le 200$)

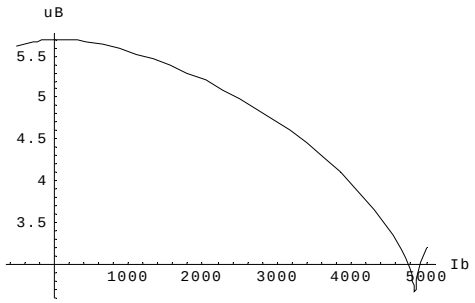

Figure 13: $u_B[1,I_\beta]$

Even if I_α is large, indirect expected utility has maximum at $I_\beta \ge 65$. For instance, when I_α=500, indirect utility has maximum at I_β=559.333. By simulation, it can be ascertained that the greater I_α becomes, the greater the maximand, I_β, becomes.

In this game-theoretic situation, equilibrium is on the boundary; *i.e*. I_α=0 and I_β=65. Indeed, when I_β=65, the indirect utility of class-A households is depicted as in Figure 10. On the other hand, when I_α=0 the indirect expected utility of class-B households has maximum at I_β=65, as is clear from Figure 13. In this way, the Adverse Selection emerges in this GE.

4. Conclusions

France, Germany, and Japan among advanced countries adopt the *national* medical insurance system, in which the insurer of medical insurance is the government. While [Arrow 1963] provided theoretical support, [Pauly 1968] pointed out defects in the medical insurance: Moral Hazard problem. Pauly argued that Moral Hazard emerges in the sense of welfare inefficiency. In section 2 of this paper, constructing simple GE model, this problem was examined in terms of simulation. In this paper, all the equilibria were computed using the traditional Newton method, instead of Scarf algorism. Note, first, that the Scarf algorism does not guarantee the existence of solutions in arbitrary GE model, while it guarantees that we can compute *competitive* general equilibria. Thus, it is an efficient approach to check the existence of *monopolistic* GE in terms of Newton method. So far, the existence problem has been solved for monopolistic GE model with *subjective* demand function. As shown in this paper, the demand function for medical service is *objective* and the existence of GE was guaranteed. Furthermore, we can use the ready-made *Mathematica* function in utilizing the Newton method, while we must newly program the Scarf algorism in utilizing it. In this section, it was ascertained first that the welfare inefficiency emerges under medical insurance with *competitive* medical sector. Second, it was shown, however, that medical insurance improves welfare if the medical sector is a *monopolist*. In section 3 of this paper, the Adverse Selection problem was examined in terms of graphical simulation. First, it was shown that in order to guarantee the existence GE with income compensation insurance, the stronger assumption on the utility function is required. This result extends the contribution by Grandmont. [Grandmont 1983] showed that when the transfer of financial assets is incorporated from the first period to the second period as in Lucas' Rational Expectations model, *non-ordinal* utility function must be assumed to guarantee the existence of GE. This paper showed the same result in our insurance case. Regarding the Adverse Selection, [Arrow 1963] had pointed out the asymmetry of information between the insurer and the insured. Synthesizing [Arrow 1963] and [Akerlof 1970], [Rothschild *et al*.1976] proved that the Adverse Selection emerges in the sense that there is no interior solutions in the partial equilibrium model with insurance. In this paper, it was shown utilizing graphical simulation that the Adverse Selection emerges in the sense that there does exist the unique boundary solution with no insurance for the insurance purchaser with lower probability of misfortune. In this way we may conclude that the simulation approach is quite effective in adding new insights to the classical contributions.

ACKNOWLEDGEMENT

The author appreciates the useful comments, made by anonymous referees. They greatly contributed in revising the draft of this paper.

REFERENCES

[Akerlof 1970] Akerlof, G. The Market for 'Lemons'. *Quarterly Journal of Economics*, 84: 488-500, 1970.

[Arrow 1963] Arrow, K.J. Uncertainty and the Welfare Economics of Medical Care. *American Economic Review*, 53: 841-73, 1963.

[Debreu 1959] Debreu, G. *Theory of Value*, Wiley, New York, 1959.

[Feldstein 1973] Feldstein, M.S. The Welfare Loss of Excess Health Insurance, *Journal of Political Economy*, vol.81, No.2, Part 1, March-April, 1973.

[Fukiharu 1988] Fukiharu, T. The Structure of Lucas-Type Neutrality of Money, *Kobe University Economic Review*, 34: 41-77, 1988.

[Fukiharu 2004a] Fukiharu, T. A General Equilibrium Approach to Medical Insurance. 2004. (*http://home.hiroshima-u.ac.jp/fukito/index.htm*).

[Fukiharu 2004b] Fukiharu, T. A General Equilibrium Approach to Adverse Selection II. 2004. (*http://home.hiroshima-u.ac.jp/fukito/index.htm*).

[Grandmont 1983] Grandmont, J-M. *Money and Value: A Reconsideration of Classical and Neoclassical Monetary Theory*, Cambridge University Press, Cambridge and London, 1983.

[Hellwig 2005] Hellwig, M.F. Nonlinear Incentive Provision in Walrasian Markets: a Cournot Convergence Approach, *Journal of Economic Theory*, 120: 1-38, 2005.

[Layard *et al.* 1978] Layard, P.R.G. and A.A. Walters, *Microeconomic Theory*, McGraw-Hill Book (U.K.), 1978.

[Lucas 1972] Lucas, R.E., Jr. Expectations and Neutrality of Money. *Journal of Economic Theory*: 103-124, 1972.

[Nash 1950] Nash, J.F. Equilibrium Points in N-person Games, *Proceedings of the National Academy of Sciences of the U.S.A*, 36: 48-49, 1950.

[Pauly 1968] Pauly, M.V. The Economics of Moral Hazard: Comment. *American Economic Review*, 58: 531-537, 1968.

[Rawls 1971] Rawls, J. *A Theory of Justice*, Oxford University Press, New York, 1971.

[Rothschild *et al.* 1976] Rothschild, M. and J.E. Stiglitz. Equilibrium in Competitive Insurance Markets: An Essay on the Economics of Imperfect Information, *Quarterly Journal of Economics,* 88: 44-62, 1976.

[Scarf 1973] Scarf, H. *The Computation of Economic Equilibria*, Cowles Foundation for Research in Economics, Monograph 24, Yale University Press, New Haven, 1973.

[Smith 1776] Smith, *A. An Inquiry into the Nature and Causes of the Wealth of the Nations* (ed. by E. Cannan), Modern Library, New York.

[Shoven *et al.*1992] Shoven, J.B. and J.Whalley. *Applying General Equilibrium*, Cambridge University Press, 1992.

[Walras 1877] Walras, L. *Eléments d'économie politique pure*, Lausanne, Corbaz, 1874-77.

Enhancing Theoretical Optimization Solutions by Coupling with Simulation

Bruno Bachelet
LIMOS UMR 6158
Université Blaise Pascal
Campus des Cézeaux - BP 10125
63173 Aubière CEDEX, France
+33 4 73 40 50 44
bruno.bachelet@isima.fr

Loïc Yon
LIMOS UMR 6158
Université Blaise Pascal
Campus des Cézeaux - BP 10125
63173 Aubière CEDEX, France
+33 4 73 40 50 42
loic.yon@isima.fr

ABSTRACT
When using optimization techniques based on mathematical models, we often need to make important simplifications. The solution thus provided, even if proven to be theoretically one of the best, might not be so good in practice. Simulation can be used to evaluate the actual performance of the solution. We propose here a coupling between optimization and simulation that tries to improve the solution provided by a mathematical model. This approach still focuses on optimizing the theoretical objective function, contrary to the common optimization-simulation coupling that focuses on improving the objective function evaluated from simulation. We propose to illustrate this approach on a routing problem, and present numerical results on the quality of the solution and the efficiency of both coupling approaches.

KEYWORDS
Optimization, discrete-event simulation, simulation optimization, routing problem

1. Introduction

The goal of this paper is to discuss a way to improve the practical quality of a solution provided by an optimization process. There are several advanced optimization techniques (mixed integer programming: branch-and-bound, branch-and-cut... [Nemhauser and Wolsey 1999], decomposition methods: Benders, Dantzig-Wolfe... [Lasdon 1970]) that can solve efficiently problems formalized with mathematical models. Major results have been stated to prove the optimality or the quality of the solution (approximation algorithms can ensure the solution found to be close to the optimal solution according to a given precision [Hochbaum 1997]), and to ensure the efficiency of the techniques (their complexity, their speed to converge to a solution...).

However, these methods have significant drawbacks when looking for their practical implementation. First, they are not robust to changes in the structure of the problem: adding a new kind of constraints might make the problem unsolvable with the previous optimization technique (e.g. linear constraints, solved with the simplex method, that become non-linear). Secondly, and more of concern in this paper, major simplifications on the modeling of the problem often have to be considered. As a result, a solution that is optimal in theory may not be so good in practice.

Therefore, we propose an optimization-simulation coupling called *model enhancement*, that attempts to reinforce the mathematical model in order to make the solution more adapted to practice than a straightforward optimization. This approach is mildly inspired by decomposition methods used for exact resolution of optimization problems, like Benders' decomposition or the column generation [Lasdon 1970].

Section 2 recalls the common optimization-simulation coupling sketch, usually called *simulation optimization*, and formalizes the problem that we propose to discuss in this article. Section 3 explains what straightforward optimization implies on the formulation and the solutions of the problem. Section 4 finally presents the idea of model enhancement, its goal and sketch. This proposition is illustrated in Section 5 through a routing problem. The approaches presented in the previous sections are implemented for this problem, and the quality of their solution and their computational efficiency are compared.

2. **Simulation Optimization**

An optimization problem can be expressed as finding the best solution x to a real problem (P_r), i.e. minimizing or maximizing a function $f_r(x)$. A solution x fits problem (P_r) if it satisfies a set of constraints that defines the space C_r of feasible solutions. For instance, x can represent the route of a bus in a city, C_r the constraints on this route (its length, the streets it can use...), and $f_r(x)$ represents the satisfaction of the customers using the route x.

$$(P_r)\begin{cases} optimize & f_r(x) \\ subject\ to & x \in C_r \end{cases}$$

During the modeling phase, the real problem (P_r) must be approximated. The common formulation of simulation optimization is expressed by problem (P_s). The fact that a function (resp. a space of solutions) b approximates another function (resp. another space of solutions) a is denoted $b \sim a$.

$$(P_s)\begin{cases} optimize & f_s(x) = g(x,\lambda),\ f_s \sim f_r \\ subject\ to & \left.\begin{array}{r} x \in C_s \\ \lambda \in \Lambda_s(x) \end{array}\right\} \sim C_r \end{cases}$$

C_s represents constraints on a solution x. It usually defines the basic structure of a feasible solution (e.g. the route of the bus must be a cycle in a graph representing the streets of the city). λ is a vector of measures (e.g. the travel times of the customers) that is returned by the simulation for a solution x (cf. Figure 1).

$\Lambda_s(x)$ is the set of feasible solutions for λ, according to a given solution x. It is defined by implicit constraints of the simulation model (given a solution x, the simulation returns the estimation λ), and by explicit constraints on some performance measures (e.g. the travel time of the customers must not exceed a given limit). That means $\Lambda_s(x)$ contains either one solution (x is feasible based on the simulation evaluation), or no solution (x is not feasible based on the simulation evaluation).

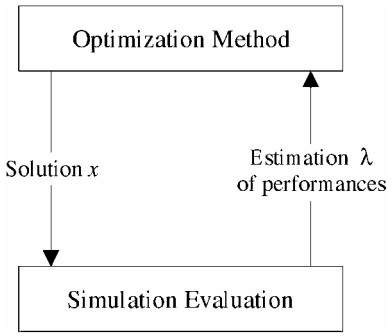

Figure 1: Simulation optimization sketch.

The objective function f_r of the real problem is approximated by f_s. We propose to parameterize this function on vector λ: $f_s(x) = g(x,\lambda)$. For instance, λ can represent estimated times of travel for solution x, and $g(x,\lambda)$ an estimation of the satisfaction of the customers for solution x according to these times.

Simulation optimization explores the set of solutions C_s to optimize f_s. For each solution x, the simulation estimates vector λ. If λ satisfies all the constraints in $\Lambda_s(x)$, the solution x is accepted, and the objective function $g(x,\lambda)$ is evaluated.

Several methods are proposed to solve problem (P_s). A classification in four major approaches can be found in [Merkuryev and Visipkov 1994] and [Azadivar 1992]: gradient based search, stochastic approximation, response surface and heuristic search. These methods are robust to changes in the objective function or in the constraints of the problem. However, they only represent a few optimization techniques and their efficiency and convergence are not always ensured.

3. **Straightforward Optimization**

Optimization techniques, independent of simulation, usually need a mathematical model (P_o). This representation is also an approximation of the real problem (P_r).

$$(P_o)\begin{cases} optimize & f_o(x),\ f_o \sim f_r \\ subject\ to & x \in C_o, C_o \sim C_r \end{cases}$$

However, we can reasonably assume that the simulation optimization problem (P_s) is closer to the real problem than the straightforward optimization problem (P_o): in our example, the optimization model (P_o) assumes that there is no waiting time at the bus stops, contrary to the simulation model (P_s) that inherently takes this data into account. For the purpose of model enhancement, we now make some assumptions on the structure of (P_o).

$$(P_o)\begin{cases} optimize & f_o(x) = g(x,\lambda) \\ subject\ to & x \in C_o \supset C_s \\ & \lambda \in \Lambda_o(x),\ \Lambda_o \sim \Lambda_s \end{cases}$$

- The constraints C_s describe the basic structure of a feasible solution. Hence, we can reasonably assume that the constraints defining C_o are approximations, and even relaxations, of the constraints defining C_s. It means that $C_o \supset C_s$. For instance, C_s can force a bus route to be an elementary directed cycle (i.e. without any loop), thus simulation optimization will explore the space of solutions more easily; whereas C_o can allow any kind of directed cycle, the space of solutions will be bigger, but straightforward optimization will solve the problem more easily.
- We consider that the objective functions f_o and f_s are identical: $f_o(x) = g(x,\lambda)$. However, we assume that the space of solutions Λ_o is an approximation of the space of solutions Λ_s, which implicitly makes f_o an approximation of f_s. In our example, $\Lambda_s(x)$ will be a statistical estimation of the travel times of the customers, whereas $\Lambda_o(x)$ will be a deterministic computation.

Depending on the structure of the problem, various optimization techniques can be considered to solve (P_o). However, once a particular method m has been chosen to solve the problem, it is difficult to deal with changes on the kind of constraints of the problem. For model enhancement purpose, we consider changes only on the constraints that describe Λ_o. Let us denote K_m the set of all the families of constraints that can be managed by method m. That means problem (P_o) is solvable by method m only if $\Lambda_o \in K_m$.

4. **Model Enhancement**

From the previous assumptions, if $\Lambda_o(x)$ is never empty, all solutions $x \in C_o$ are feasible solutions of problem (P_o). As $C_o \supset C_s$, any solution of the simulation optimization problem (P_s) is a feasible solution of (P_o). In particular, any optimal solution x_s^* of (P_s) is a feasible solution of (P_o). The idea of model enhancement is to find the family of constraints $\Lambda_o \in K_m$ such that the optimal solution x_o^* of (P_o) is one of the optimal solutions x_s^* of (P_s). We can state the model enhancement problem (P_e) as follows.

$$(P_e)\begin{cases} optimize & f_s(x_o^*) = g(x_o^*, \lambda_s) \\ subject\ to & \Lambda_o \in K_m, \Lambda_o \sim \Lambda_s \\ & (x_o^*; \lambda_o^*)\ optimal\ solution\ of\ (P_o) \\ & \lambda_s \in \Lambda_s(x_o^*) \end{cases}$$

(P_e) is a very hard problem. However, one way to find a good solution to the problem may be to approximate Λ_s by Λ_o as precisely as possible. Thus, λ_s and λ_o^* will have similar values and the theoretical evaluation $g(x_o^*,\lambda_o^*)$ of the optimal solution x_o^* of problem (P_o) will be close to its simulation evaluation $g(x_o^*,\lambda_s)$.

This approach is inspired by decomposition methods like Benders' decomposition or the column generation [Lasdon 1970], which propose to decompose a problem into two parts: the relaxed master problem, which is a relaxation of the original problem and the auxiliary problem, whose resolution provides useful information to enhance the relaxed master problem. Through an iterative process, the resolution of auxiliary problems will allow to add constraints or variables (depending on the decomposition approach) into the relaxed master problem, which will tend progressively to the original problem, and will provide an exact optimal solution.

We can propose a similar decomposition for model enhancement: (P_o) is the relaxed master problem, and simulation experiments act like resolutions of auxiliary problems that provide information to enhance the relaxed master problem. In our example, (P_o) does not consider waiting times at bus stops. The evaluation λ_s of its optimal solution x_o* using simulation provides estimations of these waiting times. Based on this information, we need to find a way to modify Λ_o so it better approximates Λ_s.

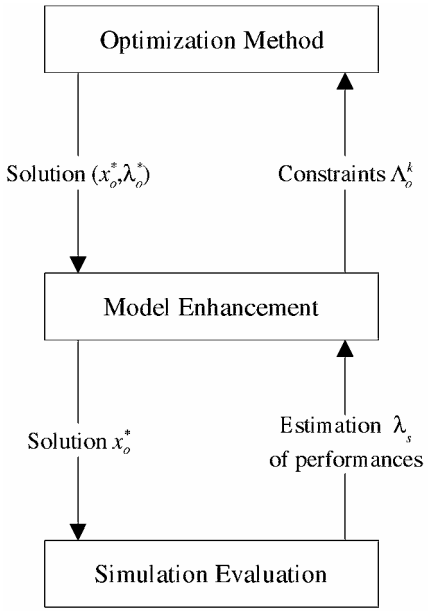

Figure 2: Model enhancement heuristic.

Algorithm 1 and Figure 2 describe a heuristic approach for model enhancement that iteratively modifies Λ_o, based on the simulation evaluation λ_s of an optimal solution of (P_o).

Algorithm 1: Model enhancement heuristic.

$k \leftarrow 0$;
let n be the maximal number of iterations;
let Λ_o^k be an approximation of Λ_s;

repeat
 let (x_o*,λ_o*) be an optimal solution of (P_o) with $\Lambda_o = \Lambda_o^k$;
 let λ_s be the simulation evaluation of x_o*;
 $\Lambda_o^{k+1} \leftarrow h(\Lambda_o^k,\lambda_s)$;
 $k \leftarrow k+1$;
until $| g(x_o*,\lambda_o*) - g(x_o*,\lambda_s) | < \varepsilon$ or $k \geq n$;

Function h represents the way to modify Λ_o at each iteration. It needs to be defined more precisely for any specific problem. In the next section, we propose to illustrate this heuristic with more details on the bus routing problem we mildly use as example in the first part of the article.

5. Study of a Routing Problem

We propose now to study a bus routing problem in order to illustrate the discussion of the previous sections. We detail the simulation optimization method, a straightforward optimization approach and the model enhancement heuristic for this problem. We also present a practical comparison of these three approaches.

5.1. Problem Presentation

We focus on the following problem: let us consider a public transportation company in an urban network, such as a bus company. Basically, this company needs to design low cost bus routes while satisfying potential customers.

Let us consider a directed graph $G = (V,E)$ where V is the set of vertexes and E the set of edges. Each vertex represents a potential bus stop or a crossroad in the real-life network. Each edge represents a road between two stops or crossroads.

We assume the customer demands are known, i.e. there is a description of the moves the customers need to perform in the urban network. A customer demand $d \in D$ is defined by a tuple $(o_d;s_d;Q_d;t_d^{min};t_d^{max})$, where $o_d \in V$ is the origin of the move, $s_d \in V$ the destination, Q_d the throughput of customers for this demand. t_d^{min} and t_d^{max} are reference times for the demand: t_d^{min} is the time it takes to a vehicle (such as a bus) to move from o_d to s_d; and t_d^{max} is the time of travel of a pedestrian from o_d to s_d.

In this article, we limit the problem to find a transportation system Γ that meets the following requirements:

- Γ is a set of directed cycles in graph G (for clarity reasons, we consider further only one bus cycle);
- the length of the bus route, i.e. the time it takes to the bus to move along the route, must be less than a given threshold T;
- Γ should maximize the satisfaction of the customers.

Let us denote t_d the time it takes to a customer with demand d to travel through the network. His satisfaction can be represented by a function $\Phi_d(t_d)$ defined as follows: if $t_d \leq 2t_d^{min}$ then the customer is fully satisfied and $\Phi_d(t_d) = 1$; if $t_d \geq 2t_d^{max}$ then the customer is not satisfied at all and $\Phi_d(t_d) = 0$; and between these two limits, the closer to the minimum, the better the customer is satisfied. Figure 3 illustrates the satisfaction function.

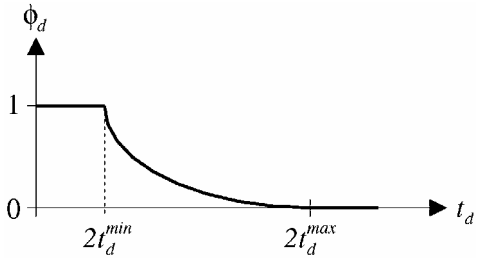

Figure 3: Satisfaction function for demand d.

Finally, we define w_i the time customers are waiting at a bus stop i. Back to our notations of the previous sections, λ is the vector of all the t_d and the w_i values. λ_o will be their theoretical estimation (from optimization) and λ_s their practical estimation (from simulation).

Let us denote x a solution to the problem, i.e. $x_e = 1$ if edge e is part of the bus route, and $x_e = 0$ otherwise. The objective is to maximize the satisfaction of the customers, i.e. function $g(x,\lambda) = \Sigma_{d \in D} Q_d \Phi_d(t_d)$.

5.2. **Simulation Optimization**

We propose to solve the problem using the tabu search metaheuristic in the simulation optimization sketch (P_s). The tabu search was first introduced by [Glover and Laguna 1997] and [Herz *et al.* 1997]. It searches for a good solution x in the space of solutions C_s. C_s represents bus routes with their length below T. Moreover, we force the structure of the bus routes in C_s to be a *geodesic* (the search is thus facilitated). A geodesic is a directed cycle defined by a given number of points called *control points*. Each control point is connected to its successor in the cycle by a shortest path (cf. Figure 4).

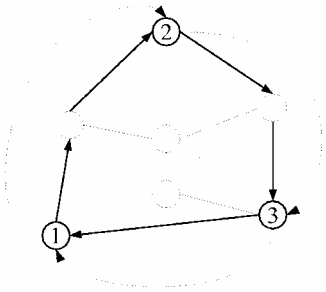

Figure 4: An example of 3-points geodesic.

Neighborhood structures for the heuristic rely on moving, adding or deleting a control point. The tabu list contains the control points that have been modified in the last few iterations. We have implemented a two-level heuristic using aspiration criteria (accepting a tabu move under some conditions) and diversification strategy (exploring another area of the space of solutions).

For a given solution x of the simulation optimization problem (P_s), simulation estimates the time of travel t_d of the customers with demand d and their waiting time w_i at bus stop i (reminder: all these values are stored in vector λ). Besides the implicit constraints of simulation, we consider no additional constraints in Λ_s that can discard a solution x based on its estimation λ. That means any solution $x \in C_s$ is a feasible solution of (P_s) (it is a necessary condition for model enhancement to work).

Discrete-event simulation is used to simulate the system, i.e. the bus and the customers are individual entities, whose moves are simulated to estimate the waiting times at the bus stops and the travel times of the customers (in order to evaluate their satisfaction).

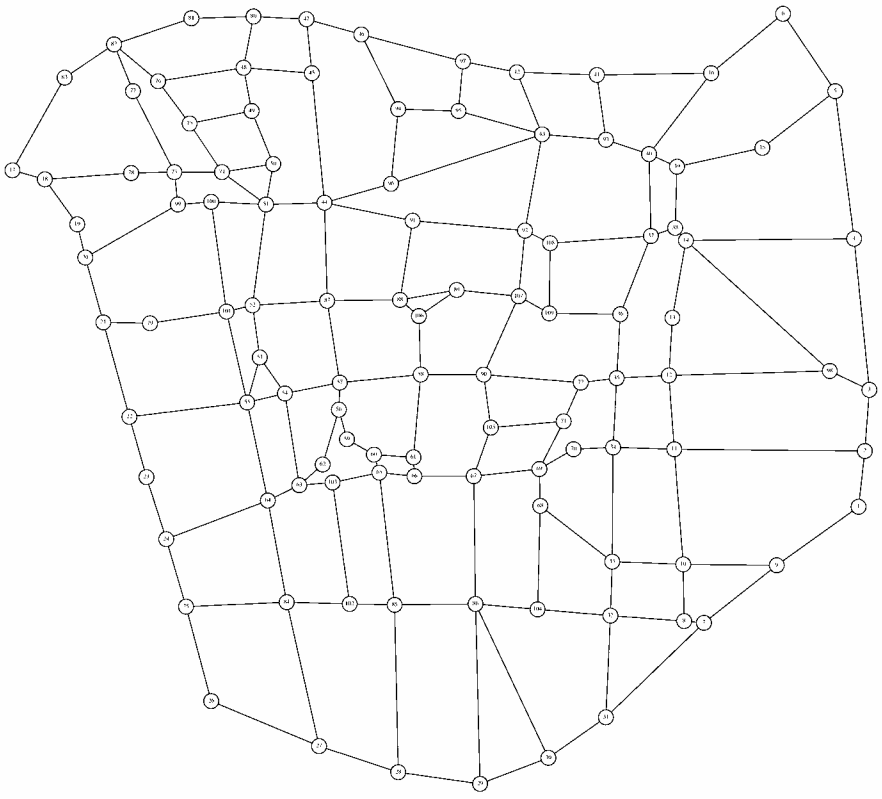

Figure 5: Graph modeling Clermont-Ferrand (France) downtown.

We consider now a graph with *109* vertexes and *392* edges that represents Clermont-Ferrand downtown (cf. Figure 5), with 12 customer demands. Table 1 presents numerical results for the simulation optimization on this instance. In order to test various problem structures, the number of control points in a geodesic varies. We also consider several maximal lengths T for the bus route. The tabu search has been implemented with C++ and the simulation model with the B++ Simulator framework [1] (cf. Figure 6). The tests have been performed on a Pentium Centrino 1.7 GHz with G++ 3.2 compiler.

[1] Information available at `http://frog.isima.fr/bruno/?doc=bpp_library+ch=simulator`.

Figure 6: Visual representation of the simulation.

Execution times can be more than a day. As our purpose here is only to know good practical solutions to compare with model enhancement's ones, we choose to limit the number of diversifications. Notice that the number of simulation evaluations to solve *(P_s)* is high, and without our restriction, it can reach more than *100000* evaluations. Hence, the solutions provided here are not always the best ones that simulation optimization can provide.

Control Points	Length Bound T	Best Evaluation $f_s(x_s^*)$	Number of Evaluations	CPU Time (hours)
5	700000	10.33	3793	5h04
5	800000	10.30	5203	7h04
5	900000	10.32	4807	6h08
5	1000000	10.32	7573	9h44
7	700000	10.32	8201	10h44
7	800000	10.34	6092	8h16
7	900000	10.32	6749	8h56
7	1000000	10.31	7883	10h28
10	700000	10.32	8843	11h20
10	800000	10.33	9706	10h12
10	900000	10.31	10732	13h52
10	1000000	10.34	8812	11h04
15	700000	10.31	6074	8h20
15	800000	10.32	8759	10h08
15	900000	10.33	10699	11h16
15	1000000	10.33	10302	11h08

Table 1: Simulation optimization numerical results.

5.3. **Straightforward Optimization**

Our bus routing problem is strongly related to the well-known Vehicle Routing Problem (VRP) class. Several straightforward optimization techniques can be considered to solve the problem [Toth and Vigo 2002]. Especially, [Yon *et al.* 2003] propose a mixed integer programming formulation. They show that the tabu search (as defined in the previous section) can provide solutions very close to the optimal solution (when known) or to the best known solution (when it takes to much time or memory to get an optimal solution using mixed integer programming).

Thus, we prefer to choose the tabu search as our method m to solve the optimization problem (P_o). It still searches a good solution x, but this time in the space of solutions C_o. With mixed integer programming, C_o would be larger than C_s ($C_o \supset C_s$), because instead of forcing the solution to be a geodesic, it would look for any directed cycle. With tabu search, it is easier to keep the geodesic structure, so $C_o = C_s$.

Λ_o is an approximation of Λ_s. The implicit constraints of simulation that define Λ_s are replaced by constraints to estimate the time of travel t_d of the customers with demand d. Other constraints fix the waiting times w_i to zero for any bus stop i, due to the assumption that there will be enough buses on the bus route for the waiting times to be insignificant. To sum up, Λ_o approximates the way to estimate the travel times and sets the waiting times to zero.

Control Points	Length Bound T	Straightforward Optimization Theoretical Eval. $f_o(x_o^*)$	Straightforward Optimization Simulation Eval. $f_s(x_o^*)$	Simulation Optimization Best Evaluation $f_s(x_s^*)$	CPU Time (seconds)
5	700000	11.99	10.29 (-0.4%)	10.33	5.0
5	800000	11.99	10.25 (-0.5%)	10.30	5.0
5	900000	11.99	9.62 (-6.8%)	10.32	5.1
5	1000000	11.99	10.08 (-2.4%)	10.32	5.3
7	700000	11.99	10.31 (-0.1%)	10.32	6.8
7	800000	11.99	9.92 (-4.1%)	10.34	7.1
7	900000	11.98	9.79 (-5.1%)	10.32	7.5
7	1000000	12.00	9.43 (-8.5%)	10.31	7.6
10	700000	11.97	10.18 (-1.4%)	10.32	7.7
10	800000	11.99	9.92 (-4.0%)	10.33	8.9
10	900000	11.99	10.05 (-2.5%)	10.31	9.4
10	1000000	12.00	9.33 (-9.8%)	10.34	10.3
15	700000	11.99	10.29 (-0.2%)	10.31	8.0
15	800000	11.99	10.01 (-3.0%)	10.32	9.0
15	900000	11.99	9.85 (-4.6%)	10.33	9.8
15	1000000	12.00	9.56 (-7.5%)	10.33	10.8

Table 2: Straightforward optimization numerical results.

Under the same conditions than problem (P_s), tests have been performed for (P_o). The problem is solved with tabu search. Table 2 shows the theoretical evaluation $f_o(x_o^*)$ of the best solutions x_o^* found for (P_o), and their simulation evaluation $f_s(x_o^*)$. The resolution is quite fast (around *10* seconds) compared to simulation optimization (several hours), but the solutions do not always have good simulation evaluations. Inside parenthesis is indicated the relative difference $(f_s(x_o^*) - f_s(x_s^*)) / f_s(x_s^*)$.

5.4. **Model Enhancement**

Simulation optimization provides good practical solutions, but needs a very long time to execute (cf. Table 4). At the opposite, straightforward optimization is very fast, but provides poor practical solutions. We describe now the model enhancement heuristic (as proposed in Section 4) applied to our bus routing problem, in order to improve the contraints defining Λ_o so problem (P_o) provides good practical solutions.

In problem (P_o), we assumed that the waiting times w_i are set to zero at any bus stop i. These constraints may make Λ_o a poor approximation of Λ_s. As the method used to solve (P_o) can deal with any constant waiting times $w_i \neq 0$, we propose to modify these theoretical waiting times at each iteration of model enhancement (in order to make Λ_o a better approximation of Λ_s).

Let us denote w_i^k the waiting times for problem (P_o) at iteration k, and $\lambda_s = (w\ t)$, composed of vectors $w = (w_i)_{i \in V}$ (the estimated waiting times) and $t = (t_d)_{d \in D}$ (the estimated travel times), the simulation evaluation of the current theoretical solution x_o^*. If $w_i \neq 0$, that means i was effectively used as a bus stop during the simulation. Thus, we propose to tend w_i^{k+1} to w_i as follows: $w_i^{k+1} \leftarrow w_i^k + \Delta(w_i - w_i^k)$. If $w_i = 0$, that means i is a vertex where customers never stop. However, we propose to tend w_i^{k+1} to the mean M of the waiting times (estimated since the start of the algorithm) as follows: $w_i^{k+1} \leftarrow w_i^k + \Delta(M - w_i^k)$.

$\Delta < 1$ is a progression step that needs to be tuned. One can choose Δ either constant, or variable according to the number of

iterations (in order to ensure some convergence). For this routing problem, we chose a constant $\Delta = 0.1$ and decide to stop the model enhancement after $n = 100$ iterations, or when there is some convergence, i.e. the difference between the theoretical evaluation $f_o(x_o^*) = g(x_o^*,\lambda_o^*)$ and the simulation evaluation $f_s(x_o^*) = g(x_o^*,\lambda_s)$ is less than $\varepsilon = 0.01$. Algorithm 2 summarizes the model enhancement heuristic for our bus routing problem.

Algorithm 2: Model enhancement heuristic for bus routing problem.

$k \leftarrow 0$;
for each vertex $i \in V$ do $w_i^k \leftarrow 0$;

repeat
 $k \leftarrow k+1$;
 solve (P_o) with waiting times w_i^k, $i \in V$;
 let (x_o^*,λ_o^*) be an optimal solution of (P_o);
 let $\lambda_s = (w\ t)$ be the simulation evaluation of x_o^*;
 update mean M of the estimated waiting times;

 for each vertex $i \in V$ do
  if $w_i \neq 0$ then $w_i^{k+1} \leftarrow w_i^k + \Delta(w_i - w_i^k)$;
  else $w_i^{k+1} \leftarrow w_i^k + \Delta(M - w_i^k)$;
 end for;
until $| g(x_o^*,\lambda_o^*) - g(x_o^*,\lambda_s) | < \varepsilon$ or $k \geq n$;

Under the same conditions than problems (P_s) and (P_o), tests have been performed for model enhancement. Table 3 indicates the theoretical evaluation of the best solutions x_e^* found. It shows that it is very close to the simulation evaluation of the same solution. In parenthesis, it indicates the relative improvement of the practical quality of the solution compared to straightforward optimization: $(f_s(x_e^*) - f_o(x_o^*)) / f_s(x_o^*)$. The number of iterations of the model enhancement process is also provided.

Control Points	Length Bound T	Model Enhancement: Theoretical $f_o(x_e^*)$	Model Enhancement: Simulation $f_s(x_e^*)$	Nb Iter.	Straight. Opti. $f_s(x_o^*)$	Simulation Opti. $f_s(x_s^*)$	CPU Time (minutes)
5	700000	10.48	**10.48** (+1.8%)	51	10.29	10.33	7'46
5	800000	10.38	**10.38** (+1.3%)	51	10.25	10.30	7'47
5	900000	10.20	10.20 (+6.0%)	45	9.62	**10.32**	6'53
5	1000000	10.23	10.23 (+1.5%)	49	10.08	**10.32**	7'20
7	700000	10.49	**10.49** (+1.7%)	46	10.31	10.32	8'24
7	800000	10.40	**10.41** (+4.9%)	46	9.92	10.34	8'33
7	900000	10.21	10.22 (+4.4%)	52	9.79	**10.32**	9'28
7	1000000	10.21	10.21 (+8.3%)	33	9.43	**10.31**	6'09
10	700000	10.47	**10.47** (+2.8%)	50	10.18	10.32	9'08
10	800000	10.41	**10.41** (+4.9%)	33	9.92	10.33	7'01
10	900000	10.12	10.12 (+0.7%)	56	10.05	**10.31**	12'18
10	1000000	10.05	10.05 (+7.7%)	64	9.33	**10.34**	15'00
15	700000	10.48	**10.49** (+1.9%)	51	10.29	10.31	10'02
15	800000	10.42	**10.42** (+4.0%)	44	10.01	10.32	9'17
15	900000	10.22	10.22 (+4.0%)	56	9.85	**10.33**	12'35
15	1000000	10.06	10.06 (+5.2%)	61	9.56	**10.33**	14'41

Table 3: Model enhancement numerical results.

The resolution is slower than straightforward optimization, but is really faster that simulation optimization (cf. Table 4). In fact, few calls to simulation evaluation are required, contrary to simulation optimization that needs a large amount of evaluations. The quality of the solution provided by model enhancement is usually close to the one provided by simulation optimization, and always improves the solution provided by straightforward optimization.

Control Points	Length Bound T	Simulation Optimization	Straightforward Optimization	Model Enhancement
5	700000	5h04	0h00'05s	0h07'46s
5	800000	7h04	0h00'05s	0h07'47s
5	900000	6h08	0h00'05s	0h06'53s
5	1000000	9h44	0h00'05s	0h07'20s
7	700000	10h44	0h00'07s	0h08'24s
7	800000	8h16	0h00'07s	0h08'33s
7	900000	8h56	0h00'08s	0h09'28s
7	1000000	10h28	0h00'08s	0h06'09s
10	700000	11h20	0h00'08s	0h09'08s
10	800000	10h12	0h00'09s	0h07'01s
10	900000	13h52	0h00'09s	0h12'18s
10	1000000	11h04	0h00'10s	0h15'00s
15	700000	8h20	0h00'08s	0h10'02s
15	800000	10h08	0h00'09s	0h09'17s
15	900000	11h16	0h00'10s	0h12'35s
15	1000000	11h08	0h00'11s	0h14'41s

Table 4: Execution times comparison.

Figure 7 shows the evolution and the convergence of both theoretical and simulation evaluations of solution x_o^* at each iteration k of the model enhancement process, for the search of a 10-points geodesic with $T = 1000000$. At the beginning, the theoretical evaluation is far from the simulation one, it is due to the fact that all the waiting times are considered to be zero in the theoretical model. Progressively, the waiting times information is injected into the theoretical model, which makes the theoretical optimization to provide various optimal solutions (that are not always very good in practice, which explains the variations in the first iterations). Finally, a good solution is found, with its theoretical evaluation very close to the simulation one.

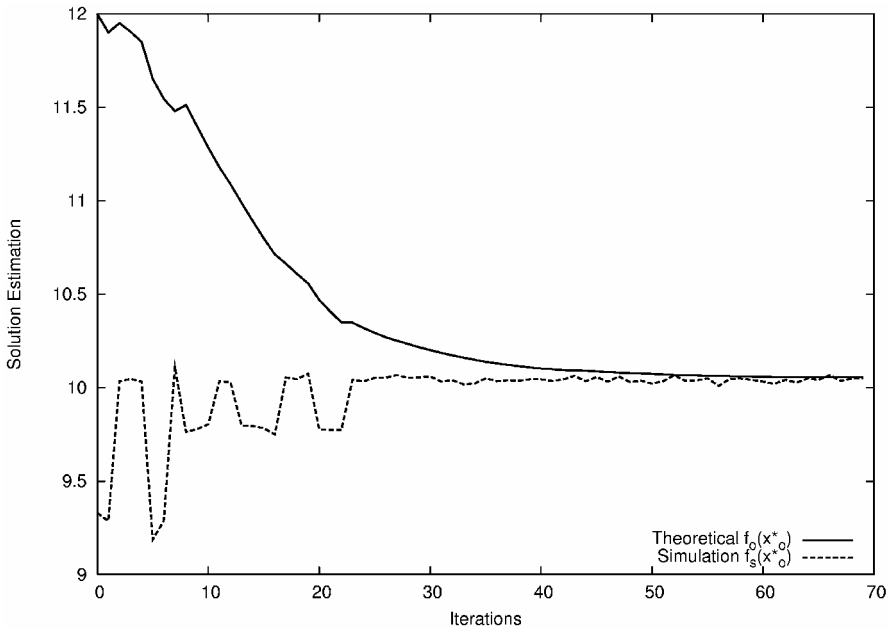

Figure 7: Solution estimation evolution with model enhancement, case 1.

The convergence seems to be achieved quite easily in this case. However, Figure 8 shows the same kind of evolution for the search of a 7-points geodesic with $T = 1000000$. As shown in this figure, the heuristic sometimes oscillates between several good solutions, thus the convergence is more difficult to achieve.

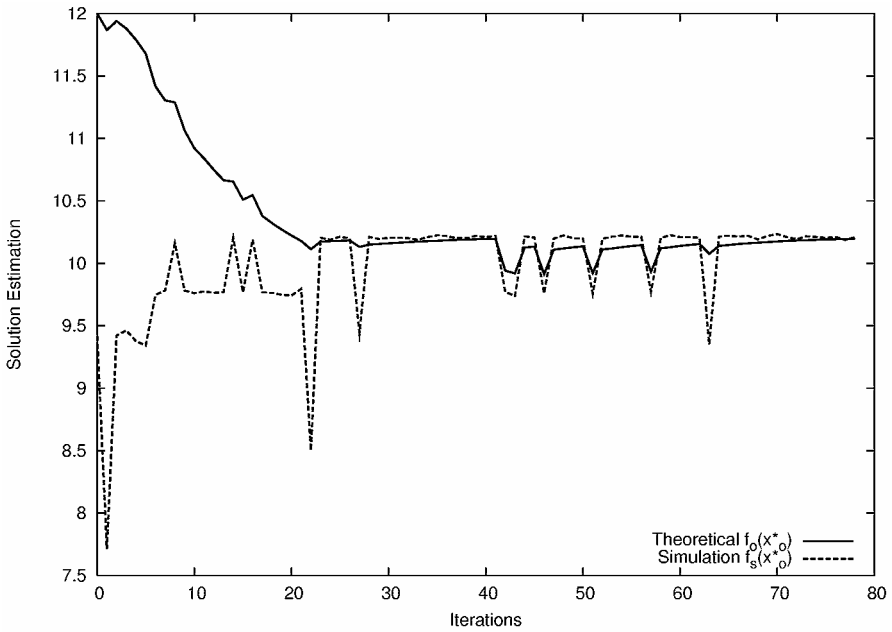

Figure 8: Solution estimation evolution with model enhancement, case 2.

6. Conclusion

Simulation optimization provides good practical solutions. However, it may take a long time to execute, with lots of simulation evaluations. At the opposite, for some problems, like the routing problem presented here, efficient theoretical approaches can efficiently solve simplified formulations. But, usually, they find solutions that are not so good in practice.

We propose in this article an approach called *model enhancement* that still focuses on the theoretical problem, and tries to improve its formulation in order to take into account practical aspects (estimated by simulation). The final goal is for the theoretical approach to provide good practical solutions.

We formalize model enhancement as problem *(P_e)* which, in some conditions, should provide the best practical solution (according to simulation evaluation). This problem seems actually very hard to solve. It proposes nevertheless a different way to think of optimization and simulation coupling. Therefore, we present a quite simple heuristic for model enhancement, illustrated on a routing problem. Experimental results show the potential of model enhancement, which needs further investigation.

ACKNOWLEDGMENTS

We would like to thank Antoine Mahul, PhD Student at Blaise Pascal University, Clermont-Ferrand, France, for his invaluable advice to formalize model enhancement.

REFERENCES

[Azadivar 1992] F. Azadivar. A Tutorial on Simulation Optimization. *Proceedings of the Winter Simulation Conference*, pages 198-204, 1992.

[Glover and Laguna 1997] F. Glover and M. Laguna. *Tabu Search*. Kluwer Academic Publishers, 1997.

[Herz *et al*. 1997] A. Herz, E. Taillard, and D. de Werra. Tabu Search. *Local Search in Combinatorial Optimization*, pages 121-136. Princeton University Press, 1997.

[Hochbaum 1997] D. S. Hochbaum. *Approximation Algorithms for NP-Hard Problems*. PWS Publishing Company, 1997.

[Lasdon 1970] L. S. Lasdon. *Optimization Theory for Large Systems*. MacMillan, 1970.

[Merkuryev and Visipkov 1994] Y. A. Merkuryev and V. K. Visipkov. A Survey of Optimization Methods in Discrete Systems Simulation. *Proceedings of the First Joint Conference of International Simulation Societies*, pages 104-110, 1994.

[Nemhauser and Wolsey 1999] G. L. Nemhauser and L. A. Wolsey. *Integer and Combinatorial Optimization*. Wiley-Interscience, 1999.

[Toth and Vigo 2002] P. Toth and D. Vigo. *The Vehicle Routing Problem*. SIAM Monographs on Discrete Mathematics and Applications, 2002.

[Yon *et al*. 2003] L. Yon, A. Quilliot, and C. Duhamel. Distance Minimization in Public Transportation Networks with Elastic Demands: Exact Model and Approached Methods. *Information Processing: Recent Mathematical Advances in Optimization and Control*. *Mathematical Sciences and Computing* series. Presses de l'Ecole des mines de Paris, pages 259-268, 2003.

Job arrival analysis for a cluster in a Grid environment

Emmanuel Medernach
Laboratoire de Physique Corpusculaire, CNRS-IN2P3
Campus des Cézeaux
63177 Aubière Cedex, France
+33 473 40 72 99
medernac@clermont.in2p3.fr

ABSTRACT
With Grids, we are able to share computing resources and to provide for scientific communities a global transparent access to local facilities. In such an environment the problems of fair resource sharing and best usage arise. In this paper, the analysis of the LPC cluster usage (Laboratoire de Physique Corpusculaire, CNRS-IN2P3, Clermont-Ferrand, France) in the EGEE Grid environment is done, and from the results a model for job arrival is proposed.

KEYWORDS
Grid, Workload analysis, Job arrival, Markov model

1. Introduction

Analysis of a cluster workload is essential to understand better user behaviour and how resources are used [Feitelson 02]. We are interested to model and simulate the usage of a Grid cluster node in order to compare different scheduling policies and to find the best suited one for our needs.

Briefly, we have some groups of users that each submits jobs to our cluster. These jobs are placed inside a waiting queue before being scheduled and then processed by a Worker Node. Each group has their own need and their own strategy to submit to the cluster.

We wish first to have good metrics that describes the group and user usage of the site, then to model the global behaviour (average job waiting time, average waiting queue length, system utilization, etc.) in order to know what is the influence of each parameter and to avoid site saturation, and finally to simulate jobs arrivals and characteristics to test and compare different scheduling strategies. The goal is to maximize system utilization and to provide fairness between site users to avoid job starvation.

As parallel scheduling for p machines is a hard problem, heuristics are used. Moreover we have no exact value about the duration of jobs, making the problem difficult. We need a good model to be able to compare different scheduling strategies.

First this paper describes the grid middleware used (section 2). Then the workload of the LPC computing resource, a Grid enabled cluster is presented (section 3) and the logs are extracted and analyzed statistically. A model is then proposed that describes the job arrival rate in section 4. We describe the simulation done (section 5) and validated it in section 6. A discussion is done in section 7 and section 8 concludes this paper.

2. Grid technology

The Grid gives new ways to share resources between sites, both as computing and storage resources. Grid defines a global architecture for distributed scheduling and resource management [England 04]. We would like to understand better such a system so that a model could be defined. With such a model, simulation might be done and a quality of service could then be proposed to the different users and groups.

In Grid world, resources are controlled by their owners. For instance different kind of scheduling policies could be used for each site. A Grid resource center provides to the Grid computing and/or storage resources and also services that allow jobs to be submitted by guests users, security services, monitoring tools, storage facility, software management, etc.

The Grid principle is to allow user a worldwide transparent access to computing and storage resources. This access aimed to be transparent by using LCG (Large Hadron Collider Computing Grid Project) middleware built on top of the Globus Toolkit [Foster 97]. Middleware acts as a layer of software that provides homogeneous access to different Grid resource centers.

2.1. LCG Middleware

The users Grid entry point is called an User Interface (UI). This is the gateway to Grid services. From this machine, users are

given the capability to submit jobs to a Computing Element (CE) and to follow their jobs status [Peris 04]. LCG-2 is organized into Virtual Organizations: dynamic collections of individuals and institutions sharing resources in a flexible, secure and coordinated manner.

Users submit their jobs to the Grid one by one. They could directly specify the execution site or let a Grid service choose the best destination for them. Users give only a rough estimation of the job running time that is a maximum job running time. In general this estimated time is overestimated and very imprecise [Zotkin 99].

The services of the Workload Management System (WMS) are responsible for the acceptance of job submits and the dispatching of these jobs to the appropriate CE, depending on job requirements and on available resources. The Resource Broker (RB) is the machine where the WMS services runs, at least one for each Virtual Organizations (VOs). (For more details see [Avellino 04] and [Andreetto 04]).

Users are then mapped to a local account on the chosen executing CE. A Computing Element is built on a homogeneous farm of computing nodes called Worker Nodes (WN) and on a node acting as a front-end to the rest of the Grid. When a CE receives a job, it enqueues it inside a batch queue, chosen depending on the job requirements, for instance depending on the maximum running time. A scheduler then proceeds all these queues to decide the execution of jobs.

2.2. Scheduling

The goal of the scheduler is first to enable execution of jobs, to maximize job throughput and to maintain a good fairness between user usage of the cluster [Feitelson 96]. At the same time scheduler have to avoid starvation, that is jobs, users or groups that take scarcely available cluster resources compared to others.

Scheduling is done on-line, that is the scheduler have no knowledge about all the job input requests but jobs are submitted to the cluster at arbitrary time. No preemption is done, the cluster uses a space sharing mode for jobs. For example, in a Grid environment long-time running jobs are common. The worst case is when the cluster is full of jobs running for days and at the same time receiving jobs blocked in the waiting queue. Short jobs like monitoring jobs relatively do not delay too much long jobs. For example, a 1 day job could wait 15 minutes before starting, but it is unwise that 5 minutes jobs have to wait the same 15 minutes. This results in production of algorithms classes that encourage the start of short jobs rather than the start of longer jobs. Short jobs have higher priority [Chiang 02]. Some other solution proposed is to split the cluster in static sub-cluster but this is not compatible with a sharing vision like Grids. Ideal on-line scheduler will maximize cluster usage and fairness between groups and users. Of course a good tradeoff has to be found between the two.

Our LPC cluster contains for now 140 CPUs managed by 2 CEs with the LCG middleware. We are using Maui as our cluster scheduler [Bode 00]. Currently the LPC Cluster is used mostly by Biomed users. Our cluster represents 75% of all the Biomed VO jobs during 2004. Another group is the Dteam VO, this group is responsible of sending test and monitoring jobs to our site. As seen on the figures 1(c) and 1(d), the total CPU time used by Dteam is small relatively to Biomed, but the jobs sent are important for the site monitoring. Soon there will be more groups from the LHC experiments.

3. Workload analysis

Workload analysis allows to obtain a model of the user behaviour [Calzarossa 93]. Such a model is essential for understanding how the different parameters change the resource center usage. Metacomputing workload [Chapin 99] like Grid environments is composed of different site workload. We are interested in modelling workload of our site which is part of the EGEE computational Grid. Our site receives only jobs coming from the EGEE Grid.

We have a cluster containing 140 CPUs since September 15. This can be visible in the figure (figure 1(a)), when we notice that the number of jobs sent increases. Statistics are obtained from the Portable Batch System (PBS) log files. PBS log files are well structured for data analysis. The PBS log format is quite similar to the Standard Workload Format described in [Chapin 99]. An AWK script is used to extract information from PBS log files. AWK acts on lines matched by regular expressions. In our case a line containing ‘;S;’ or ‘;E;’ means that a job starts or finishes. These matching lines include information like the arrival time of the job and its duration. We do not have information about user’s login time because users send jobs to our cluster from an User Interface (UI) of the EGEE Grid and not directly. During 163 days, our site received 108651 jobs from which 56799 Dteam jobs and 45523 Biomed jobs (figure 1(a)). It appears that jobs are submitted by bursts. From the logs, there are not many differences between CPU time and total time, so it means that jobs sent to our cluster are really CPU intensive jobs and not I/O intensive. Dteam jobs are mainly short monitoring jobs (figure 1(d)). We have 2850 days CPU time consumed by Biomed for 45523 jobs (Mean of one hour and half per jobs, figure 1(c)). Repartition of job duration for Biomed VO is shown on figure 1(b). What is not shown on this figure is that there are also 34017 Biomed jobs that run for less than half an hour and 5752 between 30 and 60 minutes. The longest queue allows jobs to run for less than 2 days CPU time or 3 days total time, so it explains the presence of a peak at 48 and 72 hours. There is a majority of jobs that do not stay waiting inside the queues before being executed. The queues are almost all the time empty for the moment, but as soon as other VOs will use our cluster the situation could change and the waiting factor may become important.

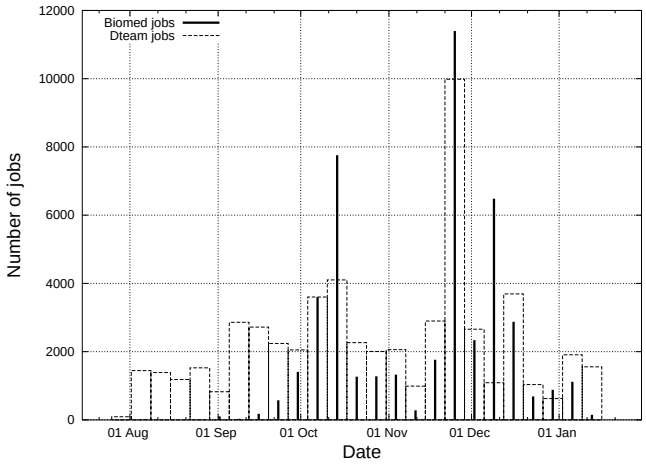

Figure 1(a) Number of jobs received per weeks

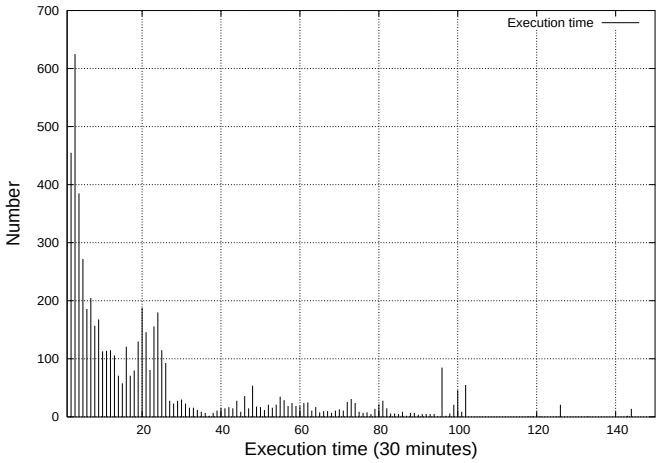

Figure 1(b) Execution time per jobs for Biomed

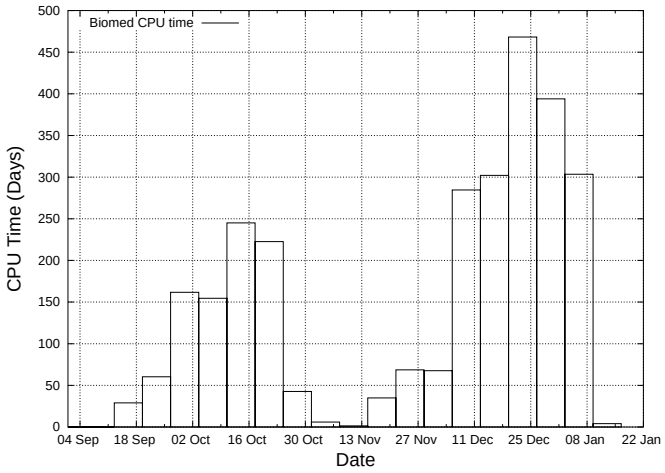

Figure 1(c) CPU consumed by Biomed jobs per weeks

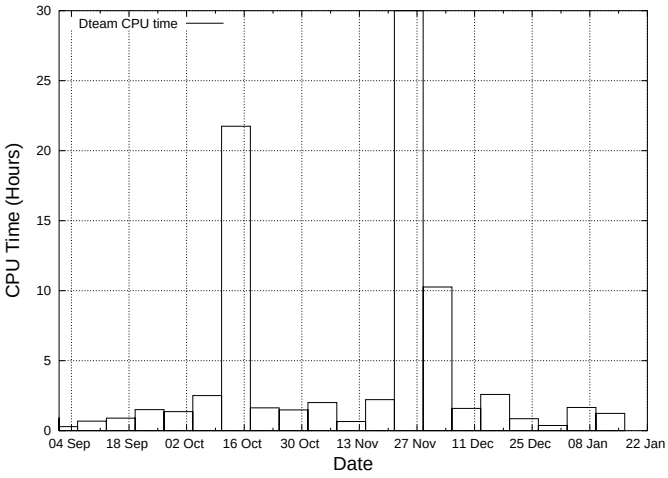

Figure 1(d) CPU consumed by Dteam jobs per weeks

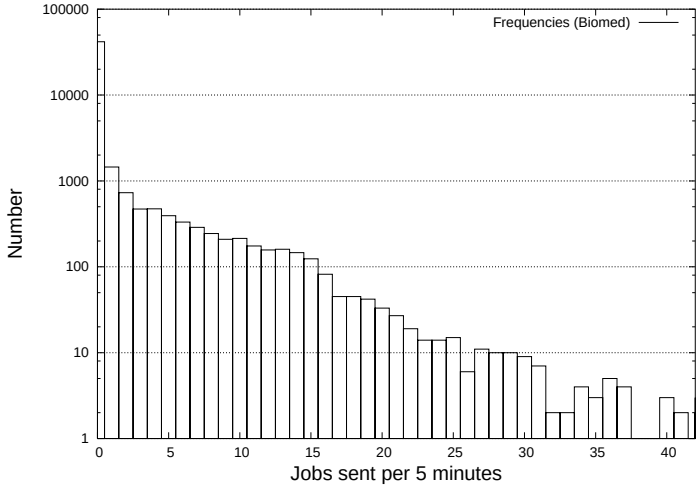

Figure 1(e) Biomed job arrival rate each 5 minutes

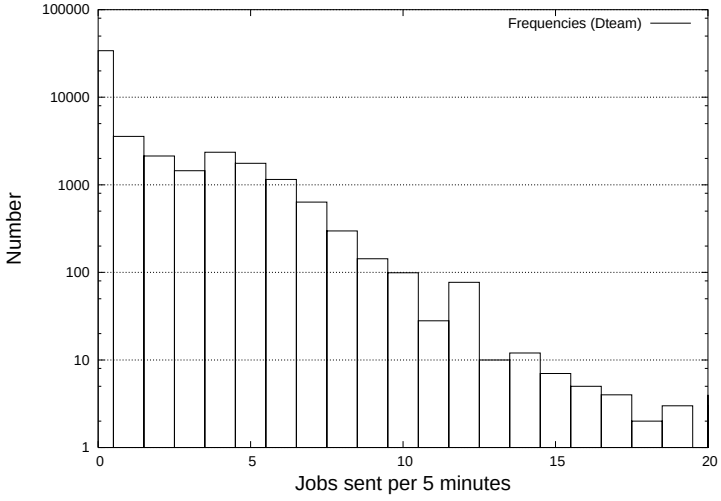

Figure 1(f) Dteam job arrival rate each 5 minutes

Figure 1: Biomed and Dteam cluster usage

Job arrival rate is a common measurement for a site usage. Figures 1(e) and 1(f) present the repartition of job arrival rate. They show that most of the time the cluster does not receive any jobs. Users usually submit groups of jobs and not stand-alone jobs. It explains the shape of the arrival rate: for instance the Dteam graph is relatively flat from 1 to 6 jobs per 5 minutes and then it seems that it exponentially decreases.

4. Workload modelling

Workload is composed with jobs arrival time and their durations for each users and groups. Workload could be modelled with two models, one model for job submittal process coupled with another model for job duration. First we look at modelling user login and submission behaviour. Secondly we validate the model proposed by comparing it to real user's behaviours.

4.1. Login analysis

In this section we begin to modelize user login/logout behaviour [Feitelson 02]. We neglect the case where an user has multiple login at the same time.

Let λ be instantaneous login rate and δ be instantaneous logout rate. A logout user has a probability during dt of λdt to login and a login user has a probability during dt of δdt to logout (see figure 2). We consider that the probability to have more than one event during dt is negligible compared to dt. λ and δ could be functions of time t.

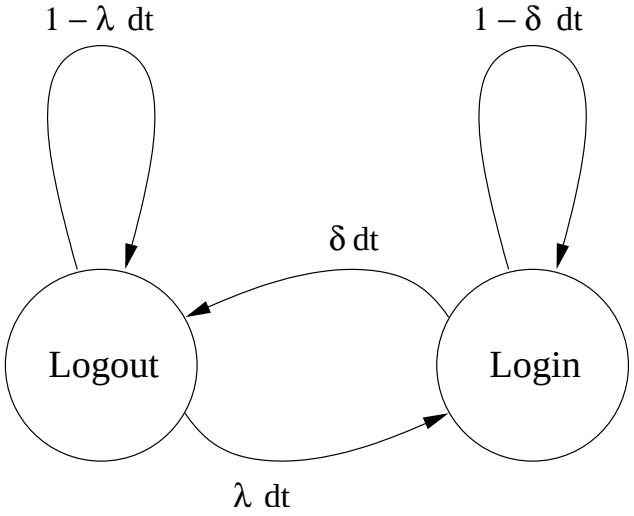

Figure 2: Login/Logout cycle

All these parameters can vary periodically over time as we see on the week job arrival (figure 1(a)) or during day time (work hours). The model proposed could be used more accurately with non-constant or periodic parameters at the expense of more calculation and more difficult fitting. For a study of arrival rate depending on arrival hours see [Cirne 01]. In the following we considered parameters to be constants. In this case, $1/\lambda$ is the logout mean time, $1/\delta$ is the login mean time. P_{Login} and P_{Logout} are the probabilities during time that the user is respectively logged or not logged. We obtain a state diagram evolving with time (see figure 2). At equilibrium, probabilities are

$$P_{Logout} = \delta/(\lambda + \delta),\ P_{Login} = \lambda/(\lambda + \delta) \quad (4.1)$$

4.2. Job submittal analysis

During period when users are logged they can submit jobs. We model the job submittal rate for one user as follows: During dt when the user is logged he has a probability of μdt to submit a job. With $\delta = 0$ we have a delayed Poisson process, and with $\mu = 0$ no jobs are submitted. The model is shown at figure 3.

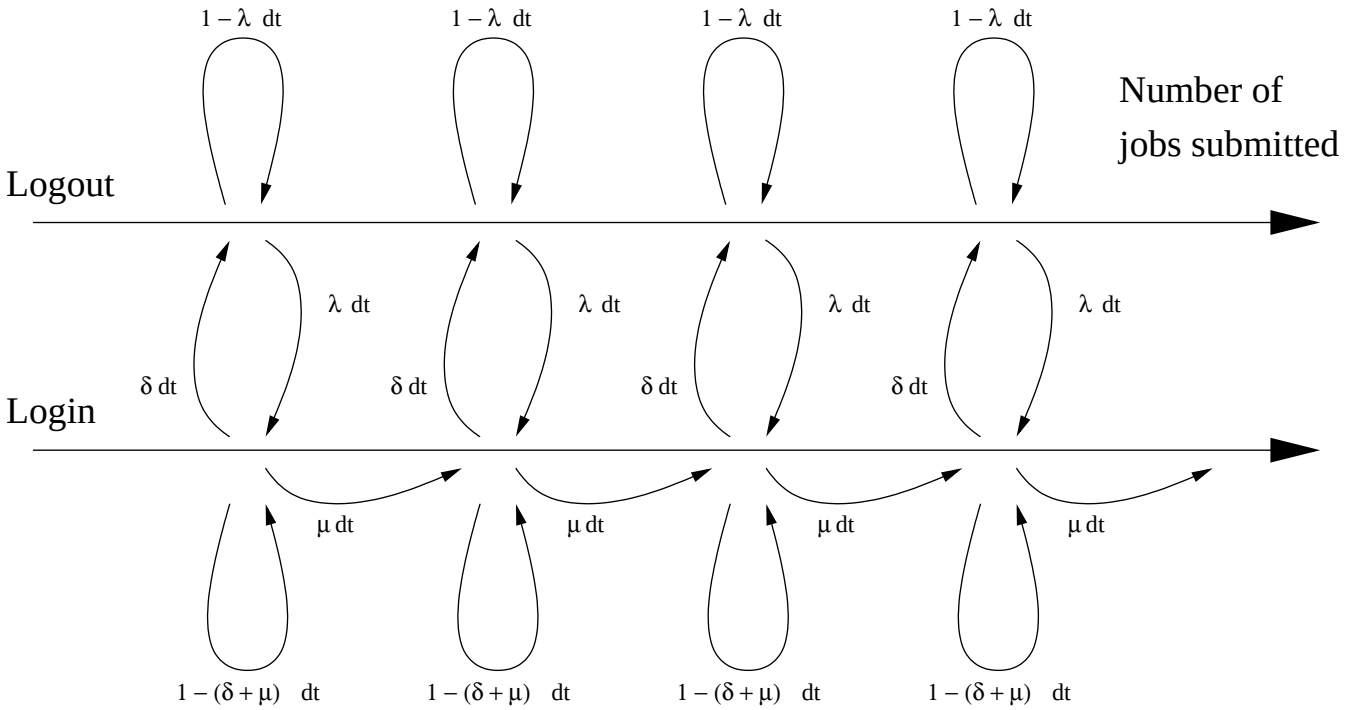

Figure 3 Markov modelling of jobs submittal

From the model, let Pn (t), Qn (t) and Rn (t) be defined as the following:

- Pn (t) is the probability to be in the state. “User is not logged and n jobs have been submitted between time 0 and t.”

- Qn (t) is the probability to be in the state ``User is logged and n jobs have been submitted between time 0 and t.".

- Rn (t) is the probability to be in the state ``n jobs have been submitted between time 0 and t.". This is the sum of Pn(t) and Qn(t).

These definitions result to the following recursive equation:

$$\mathcal{M} = \begin{pmatrix} -\lambda & \delta \\ \lambda & -(\mu+\delta) \end{pmatrix} \tag{4.2}$$

$$\begin{pmatrix} \mathcal{P}_0 \\ \mathcal{Q}_0 \end{pmatrix}' = \mathcal{M} \begin{pmatrix} \mathcal{P}_0 \\ \mathcal{Q}_0 \end{pmatrix} \tag{4.3}$$

$$\begin{pmatrix} \mathcal{P}_n \\ \mathcal{Q}_n \end{pmatrix}' = \mathcal{M} \begin{pmatrix} \mathcal{P}_n \\ \mathcal{Q}_n \end{pmatrix} + \begin{pmatrix} 0 \\ \mu \mathcal{Q}_{n-1} \end{pmatrix} \tag{4.4}$$

In case the parameters are constants we have:

$$\begin{pmatrix} \mathcal{P}_n \\ \mathcal{Q}_n \end{pmatrix} = e^{\mathcal{M}t} \int e^{-\mathcal{M}x} \begin{pmatrix} 0 \\ \mu \mathcal{Q}_{n-1} \end{pmatrix} dx \tag{4.5}$$

We take a look at the probability of having no job arrival during an arbitrary interval of time length t which is P0(t) plus Q0(t). R0(t) is the probability that no jobs have been submitted between arbitrary time length t. At arbitrary time we could be in the state Login with probability $\lambda/(\lambda + \delta)$ and in the state Logout with the probability $\delta/(\lambda + \delta)$. Finally we obtain the result from the results above:

$$\begin{pmatrix}\mathcal{P}_0(0)\\ \mathcal{Q}_0(0)\end{pmatrix} = \begin{pmatrix}\mathcal{P}_{Logout}\\ \mathcal{P}_{Login}\end{pmatrix} = \begin{pmatrix}\delta/(\lambda+\delta)\\ \lambda/(\lambda+\delta)\end{pmatrix} \quad (4.6)$$

$$\mathcal{R}_0 = \mathcal{P}_0 + \mathcal{Q}_0 \quad (4.7)$$

$$\mathcal{R}_0(t) = \frac{\mu\lambda}{\lambda+\delta}\frac{e^{-m_1 t} - e^{-m_2 t}}{m_1 - m_2} + \frac{m_1 e^{-m_2 t} - m_2 e^{-m_1 t}}{m_1 - m_2} \quad (4.8)$$

Where m1 and m2 are the opposite of the eigen values of M. (m1 + m2 = λ + δ + μ, m1 m2 = λμ)

With λ = 0 or μ = 0, we obtain that no jobs are submitted (R0(t) = 1). With δ = 0, this is a Poisson process and R0(t) = $e^{-\mu t}$. Note that during a period of t there are in average μP Login t jobs submitted. During login period, we have a Poisson process of parameter μ, so an average of μt jobs are submitted during login period t.

We have also for small period t, R0(t) = 1 - μP_{Login} t + o(t).

R0 (t) could be estimated by splitting the arrival processes in intervals of duration t and estimating the ratio of intervals with no arrival. The error of this estimation is linear with t.

Probability distribution of the duration between two jobs arrival is called an interarrival process. Interarrival process is a common metric in queuing theory. We have A(t) = P0(t) +Q0(t) with the initial condition that user just submits a job. This implies that user is logged.

$$\begin{pmatrix}\mathcal{P}_0(0)\\ \mathcal{Q}_0(0)\end{pmatrix} = \begin{pmatrix}0.0\\ 1.0\end{pmatrix} \quad (4.9)$$

$$\mathcal{A}(t) = \mu\frac{e^{-m_1 t} - e^{-m_2 t}}{m_1 - m_2} + \frac{m_1 e^{-m_2 t} - m_2 e^{-m_1 t}}{m_1 - m_2} \quad (4.10)$$

Let computes the mean interarrival time. Probability to have an interarrival time between t and t+dt is –A'(t)dt. The mean is

$$\tilde{\mathcal{A}} = \int_0^\infty -\theta\mathcal{A}'(\theta)d\theta = \int_0^\infty \mathcal{A}(\theta)d\theta \quad (4.11)$$

$$\tilde{\mathcal{A}} = \frac{1}{\mu\mathcal{P}_{Login}} \quad (4.12)$$

It is a hyperexponential distribution. This is coherent with other experimental fitting results [Li 04]. We have not solved the general recursive equation 4.4 but next section describe a simulation done in Scheme [Kelsey 98] directly using the Markov model.

There are too few samples to estimate precisely the user Interarrival distribution. Another problem is that for small period t we have from the PBS logs an error in the order of the second.

4.3. Job duration modelling

The jobs execution time distribution looks interesting because it shows the user job duration behaviour. This information has to be modelled for scheduling but a correct general model able to explain the distribution observed appears to be difficult to find. Jobs are a mixture of multiple applications applied to various data. Weibull distributions are commonly used probability distribution in the reliability engineering discipline. It has been also used with success for task completion time [England 04] as a failure process. Weibull distributions are distributions with a failure rate as a power function of time, instantaneous failure rate at time t is defined as the probability of failures between time t and t + dt given that no failure has occurred in the system until time t.

$$f(t) = C(\alpha+1)t^\alpha$$

and probability density function which is :

$$p(t) = C(\alpha+1)t^{\alpha}e^{-Ct^{\alpha+1}}$$

In our case no good results have been obtained with it.

Another way commonly used for modelling duration distribution is to use log-uniform distribution. Figures 4(a) and 4(b) show the fraction of Dteam and Biomed jobs with duration less than some value. Job duration has been modelled with a multistage log-uniform model in [Downey 99] which is piecewise linear in log space. In this case Dteam and Biomed job duration could be approximated respectively with a 3 and a 6 stages log-uniform distribution.

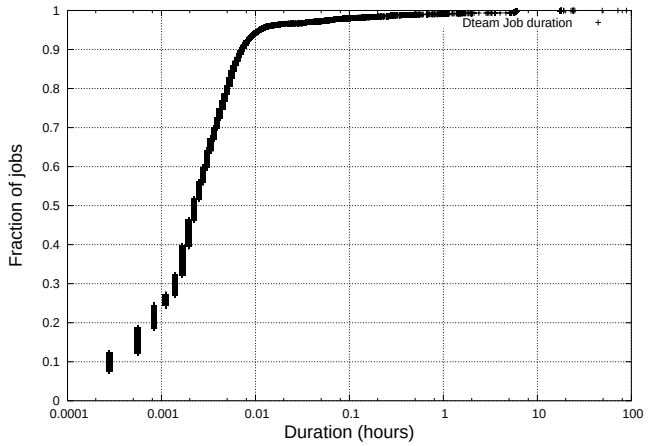

Figure 4(a)

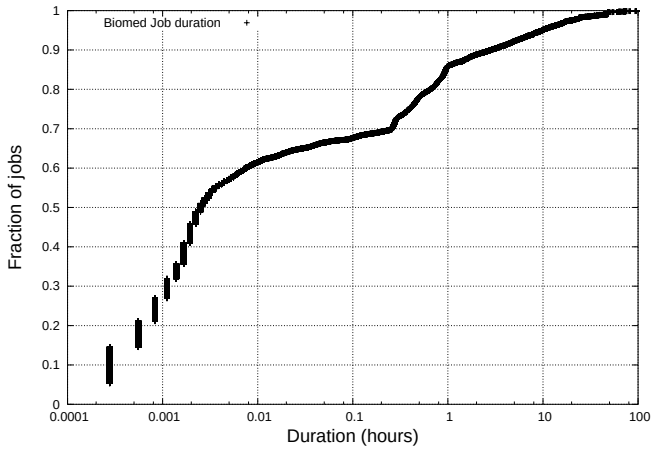

Figure 4(b)

Users submit their jobs with an estimated run length. For relationships between execution time and requested job duration and its accuracy see [Cirne 01]. To sum up estimated jobs duration are essentially inaccurate.

5. Simulation

Let compute distribution of the waiting time in a Markov state. If α is the sum of all exit rate of the current state, we have a probability of αdt during dt to go out. If p(t) is the probability to stay in the current state at time t, we obtain with p(0) = 1.0,

$$\frac{dp(t)}{dt} = -\alpha p(t) \quad p(t) = e^{-\alpha t}$$

We compute the waiting time inside a state with a time T = - log (p) / α before the next state where p is a random number between 0.0 and 1.0. We could then simulate the waiting time inside each state.

Scheme is a statically scoped and properly tail-recursive dialect of the Lisp programming language invented by Guy Lewis Steele Jr. and Gerald Jay Sussman. It was designed to have an exceptionally clear and simple semantics and few different ways to form expressions. A wide variety of programming paradigms, including imperative, functional, and message passing styles, find convenient expression in Scheme. Implementations of Scheme are required to be properly tail-recursive. Procedure calls that occur in certain syntactic contexts are `tail calls'. A Scheme implementation is properly tail-recursive if it supports an unbounded number of active tail calls. This allows the execution of an iterative computation in constant space, even if the iterative computation is described by a syntactically recursive procedure. Proper tail recursion was one of the central ideas in Steele and Sussman's original version of Scheme. Scheme procedures are objects in their own right. Procedures can be created dynamically, stored in data structures, returned as results of procedures, and so on [Kelsey 98].

We defined the states of the Markov chain as being functions, which when called return a pair containing a waiting time in that state and the next state. The frame of our Markov based simulation code is described below:

```
(define (waiting-time freq)
 (/ (log (random-simulation))
    (- freq)))

(define (markov-chain
         lambda-freq delta-freq mu-freq login?)
 (letrec
     ((logout-state
       (lambda ()
```

```
      (cons (waiting-time lambda-freq)
            login-state)))
   (login-state
    (lambda ()
      (cons (waiting-time (+ mu-freq delta-freq))
            (if (<= (* (+ mu-freq delta-freq)
                       (random-simulation))
                    delta-freq)
                logout-state
                submit-state))))
   (submit-state
    (lambda ()
      (cons 0 login-state))))
(if login?
    login-state
    logout-state)))
```

Events management is used to simulate properly a group of users. A heap composed of states is maintained to know which event will be the next to be produced. We had to pay special attention to the start time and the end time an user enter and leave the system definitely.

6. Validation

After running the simulation until a stop time equal to the user activity duration, we collect the events produced. Results are then processed in Scheme to obtain the distribution frequency and to compare it to real results. The norm used to compare distribution frequencies is the infinite norm on the cumulated probability distribution. During a period of t there are in average μP Login t jobs submitted. We evaluate the value of μP Login which is the average number of jobs submitted by seconds. We use that value when doing a set of simulation in order to fit a known real user probability distribution. We have two free parameters, so we vary P Login between 0.0 and 1.0 and lambda which the inverse is the average time an user is logout. Results obtained are shown in figures 5.

Figure 5(a) shows a corresponding Poisson fitting for Biomed user 1. Cumulatives errors made between our model and the real distributions are of the order of one percent for the first three figures. However a good norm to evaluate the goodness of fit is difficult to find, as the value of R0 is very near 1.0. For example for Biomed user 4 (figure 5(d)) results are good except for R0 and low frequencies which give the final 0.0878 cumulative error. Trying to fit the real distributions with our model take long time because of the two free parameters. An idea to evaluate μ would be to evaluate the job arrival rate during login periods, but we lack that login information.

To be able to completely simulate the node usage we need not only the jobs submittal process but also the job duration. It seems unlikely a general model for duration could be made because it depends highly on algorithms and data used by users.

Name	μ	δ	λ
Biomed user 1	0.0837	0.02079	2.1e-4
Biomed user 2	0.0620	0.01188	1.2e-4
Biomed user 3	0.0832	0.02475	2.5e-4
Biomed user 4	0.0365	1.4285e-3	1.075e-4

Figure 5

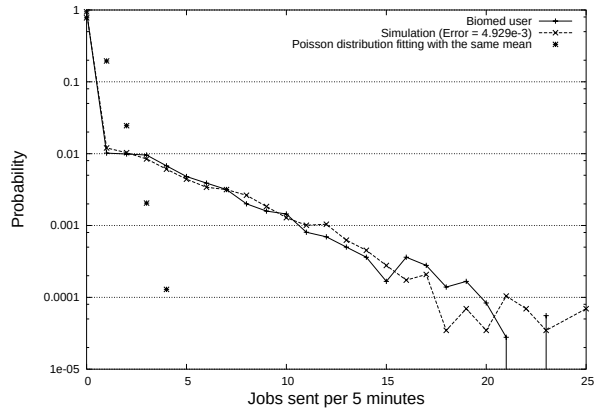

Figure 5(a) Biomed user 1

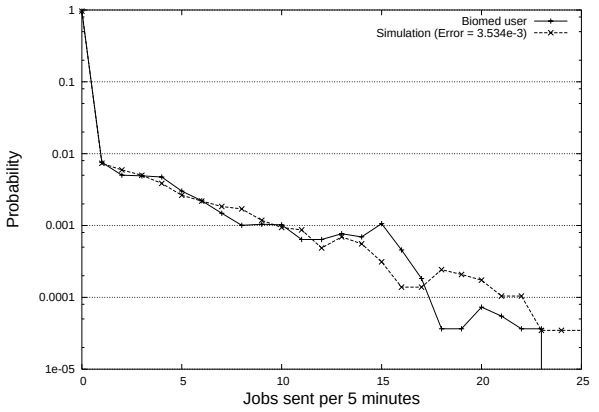

Figure 5(b) Biomed user 2

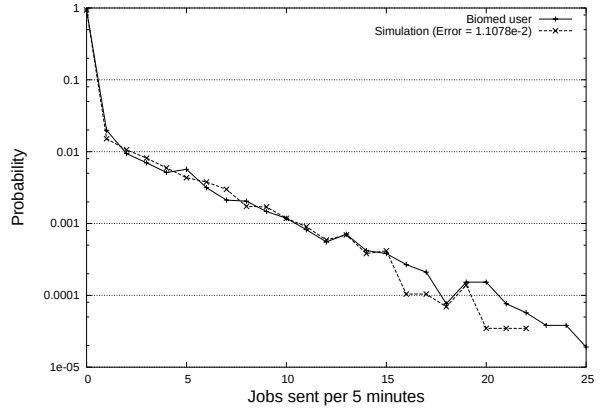

Figure 5(c) Biomed user 3

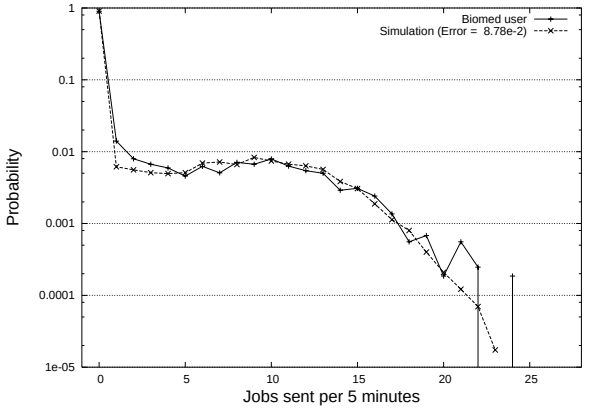

Figure 5(d) Biomed user 4

7. Discussion

Job arrival process is not a Poisson Law as shown in figure 5(a). Arrival processes are often modelled as Poisson processes for analytical simplicity. Errors introduced by modelling as Poisson processes in TCP arrival like web site traffic or file transfer are studied in [Paxson 95].

The fact an user could leave definitely the system could be modelled an additional state *Inactive* on our Markov model. We preferred not to add that state due to the complexity added with no real gain.

One benefits of the model proposed is that it could be also used to model the workload of a multi-user operating systems with user login and jobs submittal.

An interesting figure is job submittal rate depending on its rank for all users (figure 6) during their active period. It seems to be an exponential depending on user rank. We do not know if it is only a local property, or else it could be integrated on a general group model.

In order to completely characterize user's site behaviour, job arrival model presented in this paper need to be coupled with a general model of job duration, which is still an open problem. It is possible to use the Markov model described in this paper combined with a job duration model to simulate users and group's behaviours. This enables to compute saturation probabilities or to know the effect of having extra machines with some workloads.

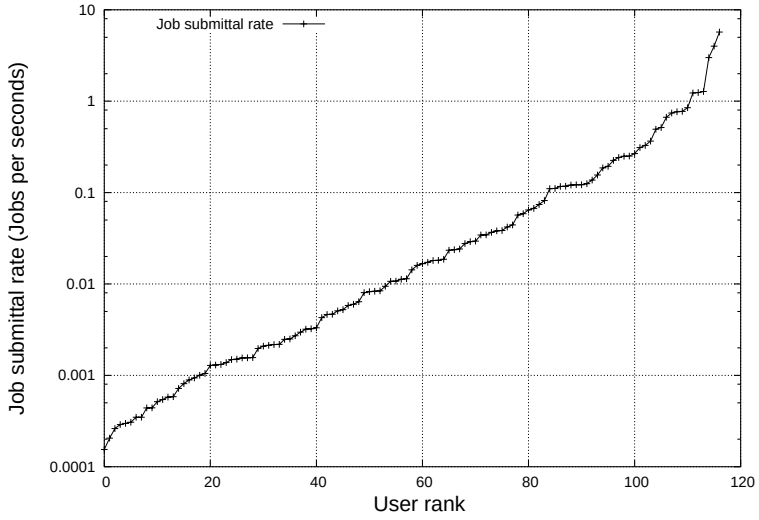

Figure 6

Scheduling could be regarded as some sort of risk assessment. This risk assessment may be based on probabilities obtained either from the logs or from some user behaviour models. For example, it could be wise to forbid that a group or an user takes all the cluster at a given time but instead to let some few percents of it open for short jobs or low CPU consuming jobs like monitoring. Scheduling algorithms are often optimized for maximising job throughput. However considering that Grid allows people to share computing resources, next scheduling strategies have to pay a special attention to the fairness issue both between resources providers [Attebury 04] and between resources consumers. In an on-line computing environment like Grids, meta-scheduling strategies have to take a lot of parameters into account. General on-line load balancing and scheduling algorithms [Azar 97, Azar 94, Bar-Noy 00, Lam 02] may be applied. The problem of finding the best suited scheduling policy is still an open problem. A better understanding of job running time is necessary to have a full model.

8. Conclusion

So far we have analyzed the workload of a Grid enabled cluster and proposed a Markov-based model that describes the process of jobs arrival. Then a numerical fitting has been done between the logs and the model. We find a very similar behaviour compared to the logs. Even bursts were observed during the simulation.

ACKNOWLEDGMENTS
This work was funded through contributions from the European Commission program EGEE, under contract INFSO-RI-508833. We also acknowledge the national funding agencies participating in EGEE for their support of this work. The cluster at LPC Clermont-Ferrand was funded by Conseil R'egional d'Auvergne within the framework of the INSTRUIRE project.

REFERENCES

[Feitelson 02] D. Feitelson. Workload modeling for performance evaluation, 2002.

[England 04] Darin England & Jon B. Weissman. Costs and Benefits of Load Sharing in the Computational Grid, 2004.

[Foster 97] Ian Foster & Carl Kesselman. Globus: A Metacomputing Infrastructure Toolkit. The International Journal of Supercomputer Applications and High Performance Computing, vol. 11, no. 2, pages 115--128, Summer 1997.

[Peris 04] Antonio Delgado Peris, Patricia M'endez Lorenzo, Flavia Donno, Andrea Sciaba, Simone Campana & Roberto Santinelli. LCG User guide, 2004.

[Zotkin 99] Dmitry Zotkin & Peter J. Keleher. Job-Length Estimation and Performance in Backfilling Schedulers. In HPDC, 1999.

[Avellino 04] G. Avellino, S. Beco, B. Cantalupo, A. Maraschini, F. Pacini, M. Sottilaro, A. Terracina, D. Colling, F. Giacomini, E. Ronchieri, A. Gianelle, R. Peluso, M. Sgaravatto, A. Guarise, R. Piro, A. Werbrouck, D. Kouril, A. Krenek, L. Matyska, M. Mulac, J. Pospysil, M. Ruda, Z. Salvet, J. Sitera, J. Skrabal, M. Vocu, M. Mezzadri, F. Prelz, S. Monforte & M. Pappalardo. The DataGrid Workload Management System: Challenges And Results. Kluwer Academic Publishers, 2004.

[Andreetto 04] P. Andreetto, S. Borgia, A. Dorigo, A. Gianelle, M. Mordacchini, M. Sgaravatto, L. Zangrando, S. Andreozzi,

V. Ciaschini, C. Di Giusto, F. Giacomini, V. Medici, E. Ronchieri, V. Venturi, G. Avellino, S. Beco, A. Maraschini, F. Pacini, A. Guarise, G. Patania, D. Kouril, A. Krenek, L. Matyska, M. Mulac, J. Pospysil, M. Ruda. Z. Salvet, J. Sitera, J. Skrabal, M. Vocu, V. Martelli, M. Mezzadri, F. Prelz, D. Rebatto, S. Monforte & M. Pappalardo. Practical approaches to Grid workload and resource management in the EGEE project. 2004.

[Feitelson 96] Dror G. Feitelson & Larry Rudolph. Toward Convergence in Job Schedulers for Parallel Supercomputers. In Dror G. Feitelson & Larry Rudolph, editeurs, Job Scheduling Strategies for Parallel Processing, pages 1--26. Springer-Verlag, 1996. Lect. Notes Comput. Sci. vol. 1162.

[Chiang 02] Su-Hui Chiang, Andrea Arpaci-Dusseau & Mary K. Vernon. The Impact of More Accurate Requested Runtimes on Production Job Scheduling Performance. In Dror G. Feitelson, Larry Rudolph & Uwe Schwiegelshohn, editeurs, Job Scheduling Strategies for Parallel Processing, pages 103--127. Springer Verlag, 2002. Lect. Notes Comput. Sci. vol. 2537.

[Bode 00] Brett Bode, David M. Halstead, Ricky Kendall & Zhou Lei. The Portable Batch Scheduler and the Maui Scheduler on Linux Clusters, USENIX Association, 2000.

[Calzarossa 93] Maria Calzarossa & Giuseppe Serazzi. Workload Characterization: A Survey. Proc. IEEE, vol. 81, no. 8, pages 1136--1150, 1993.

[Chapin 99] Steve J. Chapin, Walfredo Cirne, Dror G. Feitelson, James Patton Jones, Scott T. Leutenegger, Uwe Schwiegelshohn, Warren Smith & David Talby. Benchmarks and Standards for the Evaluation of Parallel Job Schedulers. In Dror G. Feitelson & Larry Rudolph, editeurs, Job Scheduling Strategies for Parallel Processing, pages 67--90. Springer-Verlag, 1999. Lect. Notes Comput. Sci. vol. 1659.

[Cirne 01] Walfredo Cirne & Francine Berman. A Comprehensive model of the supercomputer workload, 2001. [Li 04] Hui Li, David Groep & Lex Wolters. Workload Characteristics of a Multi-cluster Supercomputer, 2004.

[Kelsey 98] Richard Kelsey, William Clinger & Jonathan Rees (Editors). Revised 5 Report on the Algorithmic Language Scheme. ACM SIGPLAN Notices, vol. 33, no. 9, pages 26--76, 1998.

[Downey 99] Allen B. Downey & Dror G. Feitelson. The Elusive Goal of Workload Characterization. Perf. Eval. Rev., vol. 26, no. 4, pages 14--29, 1999.

[Paxson 95] Vern Paxson & Sally Floyd. Wide area traffic: the failure of Poisson modeling. IEEE/ACM Transactions on Networking, vol. 3, no. 3, pages 226--244, 1995.

[Attebury 04] Garhan Attebury, Vishvesh Sahasrabudhe & P. Sadayappan. On Fairness in Distributed Job Scheduling Across Multiple Sites. 2004.

[Azar 97] Yossi Azar, Bala Kalyansasundaram, Serge A. Plotkin, Kirk Pruhs & Orli Waarts. On-Line Load Balancing of Temporary Tasks. J. Algorithms, vol. 22, no. 1, pages 93--110, 1997.

[Azar 94] Yossi Azar, Andrei Z. Broder & Anna R. Karlin. On-line load balancing. Theoretical Computer Science, vol. 130, no. 1, pages 73--84, 1994.

[Bar-Noy 00] A. Bar-Noy, A. Freund & J. Naor. New algorithms for related machines with temporary jobs, 2000.

[Lam 02] Tak-Wah Lam, Hing-Fung Ting, Kar-Keung To & Wai-Ha Wong. On-line load balancing of temporary tasks revisited. Theoretical Computer Science, vol. 270, no. 1--2, pages 325--340, 2002.

Testing unrolling optimization technique for quasi random numbers

Romain Reuillon
LIMOS, UMR CNRS 6158
Blaise Pascal University
ISIMA, Campus des Cézeaux, BP 10125
63177 Aubière Cedex, France
+33 473 405 368
romain.reuillon@isima.fr

David R.C. Hill
LIMOS, UMR CNRS 6158
Blaise Pascal University
ISIMA, Campus des Cézeaux, BP 10125
63177 Aubière Cedex, France
+33 473 405 016
drch@isima.fr

ABSTRACT

Quasi Monte Carlo simulations are built on quasi random number generator (QRNG). Even if the use of a QRNG might lead to a faster convergence, for example with Monte Carlo integral computation, most of the simulation time can be taken by the number generation part. This paper present an optimization technique, called "unrolling" applied to QRNG. It consists in the generation and storage of random numbers in a compiled binary object file. After that, the library is used at the execution time by the simulator. We obtained good gains with "Unrolling" technique and QRNG, allowing a minimum gain factor of 4 on different computer architectures compared to the Sobol algorithm.

KEYWORDS

Quasi random numbers, unrolling, optimization, stochastic, simulation

1. Introduction

Monte Carlo simulations are stochastic simulations and are always based on a Random Number Generator (RNG). Running the RNG constitutes often a non negligible part of the simulation time. The "Unrolling" technique is a way to optimize the access to random numbers. This method consists in a pre-generation and storage of random numbers in an array of values. This array is directly included into the binary code during the compilation process. The convoluted RNG algorithm is so bypassed and the numbers are directly picked in sequence in the array. The "Unrolling" optimization is fully portable and is usable with generators written in any language. This method has been proved to be pretty efficient with small series of pseudo random numbers [Hill 2003]. Another type of generator is very interesting for stochastic simulations : Quasi Random Number Generators (QRNG). QRNG gain time by improving the convergence in numerous simulations [Papageorgiou 2001]. Pseudo-random numbers are well known and some good definitions were known since 1951 (see [Lelhmer 1951]). Quasi random numbers are a bit different and are also known as low discrepancy sequences, where the discrepancy is considered at the distance to perfect uniformity. This main characteristic helps in fastening convergence and with the lack of replication, quasi Monte Carlo simulations are naturally inclined to be unrolled in arrays stored in random access memory. Since the Van der Corput Sequence in 1935, many other sequences have been studied. The Halton sequence helped in obtaining results for various dimensions [Halton 1960]. In addition to these pioneering quasi-random sequence, the other best known sequences were given in 1960 by Hammersley [Hammersley 1960], in 1967 by Sobol [Sobol 1967, 1976], in 1980 by Faure in his thesis (see [Faure 1993] for details and in 1987 Niederreiter (see [Niederreter 1992]). In this paper we have mainly tested the unrolling technique on the GNU Scientific Library implementation of the Sobol algorithm. This is the fastest known implementation of the Sobol algorithm [Antonov and Saleev 1979], the latter being itself recognized as very interesting to fasten convergence. This implementation is valid up to 40 dimensions but is limited to 1 million drawings.

2. Convergence

Due to their good covering in N dimensional spaces, quasi random number generators are pretty efficient for integral computation [Jank 2005]. The PI computation is a good example to illustrate the astonish gain in term of convergence speed. In figure 1, QnD, ShNR and MT stand for three different types of Pseudo Random Number Generators (PRNG). They are respectively the Quick and Dirty [Numerical Recipes 1992], a linear congruential generator. The shuffled version of ran2 generator described in Numerical Recipes [Numerical Recipes 1992] and the Mersenne Twister generator of Makoto Matsumoto and Takuji Nishimura [Matsumoto and Nishimura 1997]. We have chosen the quick and dirty because it is a very fast but not very good generator. The two other ones are a lot slower but they provide a pretty good randomness quality. They both have passed the wall DIE HARD battery of tests from George Marsaglia [Marsaglia 1995]. More of that, the Mersenne Twister has a good space covering in 623 dimensions [Matsumoto and Nishimura 1997].

Figure *1* shows clearly that the QRNG allows a quick convergence in comparison to PRNG. It reaches, with only a few hundred million numbers, a precision of 10^{-7} that any of the PRNG never obtains even with two trillion generated numbers.

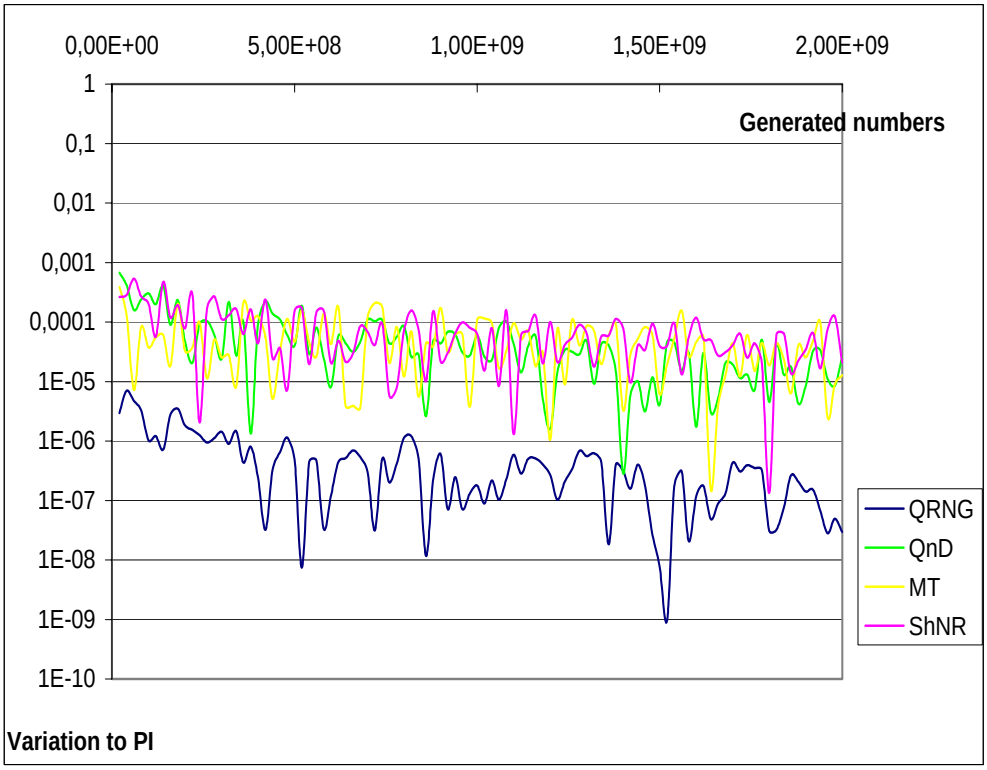

Figure 1 : Convergence comparison

3. Computing Effort

"QRNGs increase the convergence for integral calculation" doesn't necessarily mean that it reduces the computation time. We need to take into account the calculation effort taken to generate low discrepancy sequences and compare it with the one taken to generate pseudo random numbers.

The results of figure 2 have been obtained using an Intel Xeon 64 bits 3 GHz with 800 MHz internal bus and with DDR2 400 RAM. Two QRNG have been tested the Sobol [Sobol 1976] and the Neiderreiter [Neiderreiter, Bratley and Fox 1992]. The test consists in measuring the time needed to draw a million numbers with the different generators. Quasi random number generation is not way more resource consuming compared to pseudo random number generation. On our architecture the Sobol QRNG is as fast as the Mesrsenne Twister 19937 witch is reputed to be fast for a good PRNG.

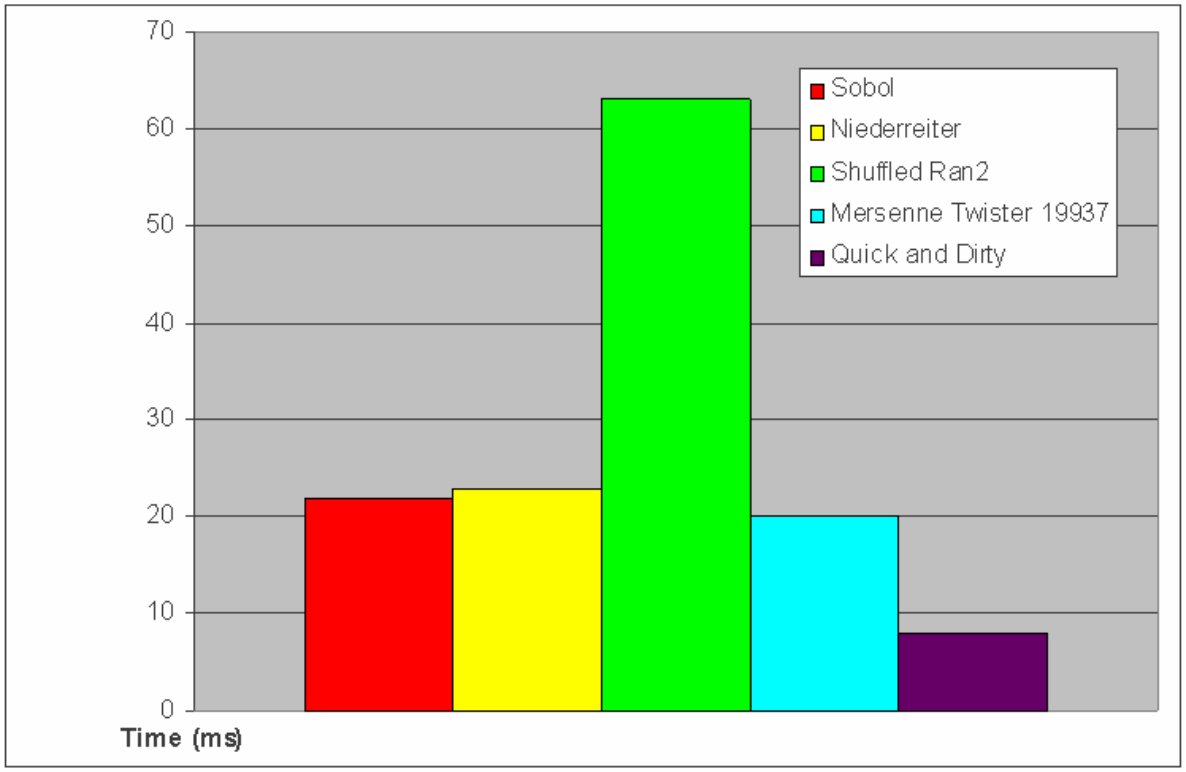

Figure 2 : Generation time in millisecond for 10^6 numbers on an Intel Xeon 3 GHz

4. Optimization

The unrolling technique is an optimization method for number generators [Hill 2003]. It consists in calculating in advance a sequence of number and storing it in a file formatted as a static array of a targeted language source code. Next step is to compile this array of numbers to obtain a binary object file, ready to be linked. Finally, the end-user code is linked to the binary file and directly access to the array instead of using a generator. The computation time is so decreased by bypassing the complex calculation of each value by the generator. The full "Unrolling" optimization process is described in the figure 3. The generation of the optimized generator source code can be done in any target language, independently from the generator language.

In order to evaluate the performances of the "unrolling" method applied to QRNG, we have written several programs. The tests we achieved were done with the C language but the technique is fully portable. To generate the source code with static arrays of random numbers, we have developed a program: QRNGUnroll. This program is able to unroll quasi random number sequences up to 40 dimensions using the Sobol algorithm. The program generates two source files: a header (UQRNG_1.h) and its corresponding implementation (UQRNG_1.c) of the static array of random numbers (the '_1' at the end of file names means one dimension). Both files are ready for separate compilation and this compilation is done automatically by the QRNGUnroll program. The result of the separate compilation (UQRNG_1.o) is then linked with the tests or application programs whose source code only includes the header file UQRNG_1.h containing: the declaration of the static array and the macroinstruction designed for accessing quasi random numbers (see appendix).

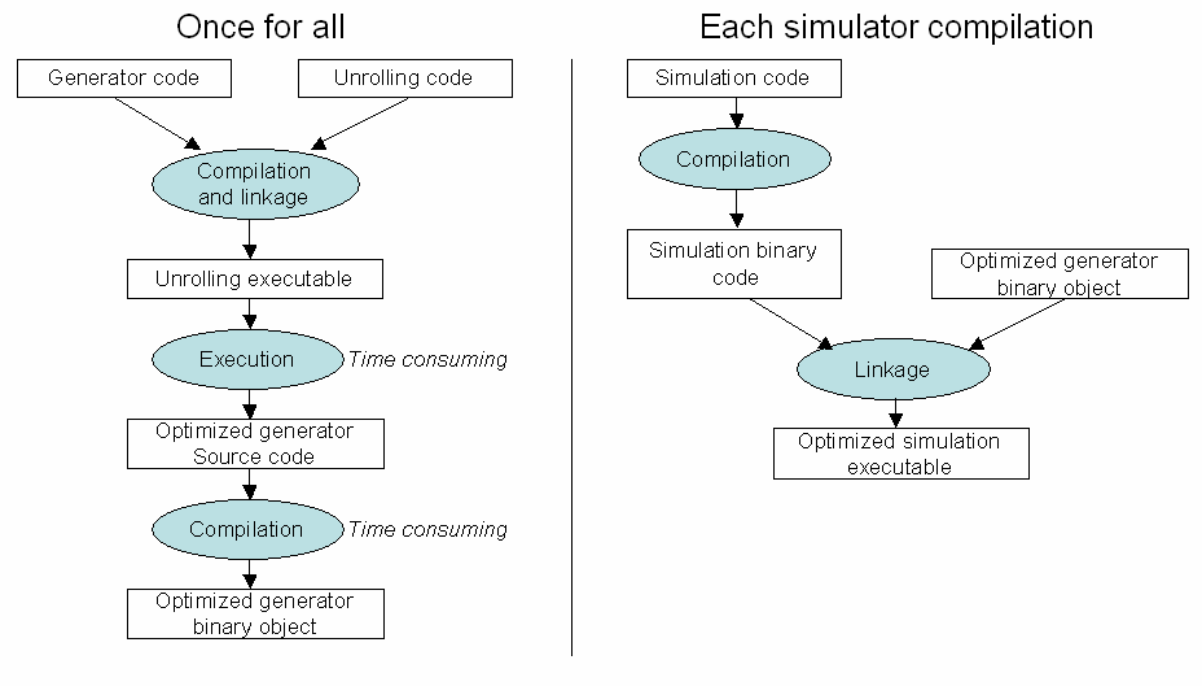

Figure 3: Unrolling optimization process

Due to the obligation to compile a big array, the unrolling technique is generally applicable for short and middle size series of number, depending on the amount of memory we own. According to figure 4, a source file containing 5 millions numbers, need 2 Go of random access memory to be compiled with gcc 3.4.

Size of the sequence	Size of the source code	RAM needed to compile / compilation time	Size of the binary executable
10^5	1,3 Mo	24 Mo / 0,6 s	392 Ko
10^6	14 Mo	210 Mo / 6 s	3,9 Mo
2.10^6	27 Mo	408 Mo / 12,5 s	7,7 Mo
3.10^6	41 Mo	1,15 Go / half an hour	12 Mo
5.10^6	69 Mo	1,95 Go / several hours	20 Mo

Figure 4: Unrolling and Memory Space Occupancy of the Compilation Process – Time given on an Intel Xeon 64 bits 3 GHz with 800 MHz internal bus and with DDR2 400 RAM running a Linux Fedora Core 3.

For some simulations, using QRNG allows a fast convergence and by consequence requires short sequences, short enough for the "unrolling" technique to be usable. Furthermore, the quasi Monte Carlo simulations don't imply the use of replications and thus it avoids the use of several uncorrelated sequences. With the unrolling technique we can compile, once for all, a binary object file containing a huge sequence of quasi random numbers. For the two reasons above, we can consider "unrolling" optimization technique as particularly well adapted for quasi random generation.

On the figure 5 the computing time for drawing a ten million numbers with several generators have been measured on different recent computer architectures and compared with an unrolled generator. The precise time is mentioned in millisecond under the graphical view. Each program has been compiled with the GNU C Compiler (gcc 3.4), and with the maximum optimisation level (option –O3).

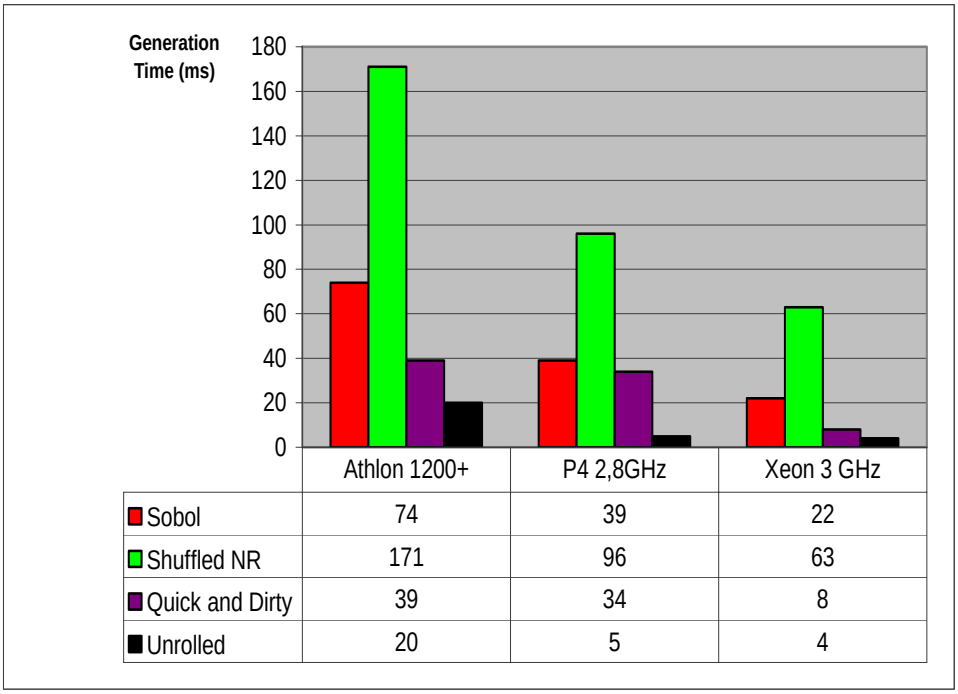

	Athlon 1200+	P4 2,8GHz	Xeon 3 GHz
Sobol	74	39	22
Shuffled NR	171	96	63
Quick and Dirty	39	34	8
Unrolled	20	5	4

Figure 5: Generation time of 10^6 numbers

Four generators have been tested: the Sobol QRNG, the Shuffled Ran2 and the Quick and Dirty of Numerical Recipes and an unrolled generator. The computer architectures used for the tests are, an AMD Athlon at 900 MHz, a Intel Pentium 4 at 2,8 GHz and an Intel Xeon 64 bits at 3 GHz. The results are pretty convincing. The unrolled generator is always faster than the others.

The “unrolling” technique allows a gain of a 5,5 factor for the Sobol QRNG, 15,8 factor for the Shuffled NR and 2 for the Quick and Dirty on the fastest and newest computer. The Pentium 4 is a bit slower in floating point calculation, that’s why it obtains bigger gain factors. In the computer improvement process, the memory speed increase with the CPU efficiency, that why the gain factor tends to be pretty independent of the architecture of the computer. A factor above 5 for the Sobol algorithm is pretty decent and shows how the unrolling is a way of decreasing significantly the computation time of quasi random simulations.

5. Conclusion

QRNG allow a fast convergence for integral calculation and thus they also reduce the global calculation time of simulations. In addition, QRNG are as fast as some statistically sound RNG. By decreasing by 5 the generation time for the Sobol algorithm in one dimension, the unrolling optimization technique we proposed, turned out to be pretty efficient on QRNG. The current implementation of the Sobol algorithm, in the GNU Scientific Library, only produces 1 million drawings up to 40 dimensions. The unrolling technique is interesting up to 5 millions drawings on a regular desktop computer. Moreover the “unrolling” optimization technique is particularly well adapted for Monte Carlo simulations since instead of storing less "efficient" (in terms of convergence) pseudo-random numbers, we can obtain a better precision with the same amount of stored quasi-random numbers.

However, for multiple dimensions, QRNG will be harder to optimize with this technique and it is precisely to evaluate multi-dimensional integrals that such sequences are used at their best (see [Halton 1960] and [L'Ecuyer 2003]). Still dealing with the limits of the unrolling technique, a user has to be aware that it implies: the creation of huge source files, the compilation time can be very long if the compiler has to swap and of course the efficiency of this technique depends on the available

RAM and of its access bandwidth. Another point is that the time needed to generate a 40 dimensions quasi randomized n-uple with the Sobol algorithm is only ten times as important as the one needed to generate a unique quasi-random number (for only 1 dimension); thus it is probable that very few gains will be obtained in this case. Solutions have to be explored to address these issues, our next focus will be given to the memory mapping optimization technique.

REFERENCES

[Antonov and Saleev 1980] I.A Antonov and V.M. Saleev, An economic method of computing LP_τ- Sequences, *USSR Comput. Maths. Math. Phys.* **19** : 252, 1980.

[Faure 1993] H. Faure, Suggestions for quasi-Monte-Carlo Users, *Lecture Notes in Pure and Applied Math*., Marcel Dekker, New York, **141** : 269-278, 1993.

[Halton 1960] J.H. Halton, On the efficiency of certain quasi-Monte Carlo sequences of points in evaluating multi-dimensional integrals, *Nummer. Math.* **2** : 84-90, 1960.

[Hammersley 1963] J.M. Hammersley, Monte Carlo methods for solving multivariate problems, *Annals of the New-York Academy of Science*, **86** : 844-874, 1960.

[Hill 2003] D. R.C. Hill, URNG: *A portable optimization technique for software applications requiring pseudo-random numbers*, Simulation Modelling Practice and Theory, **11**-7,8 : 643-654, 2003.

[Jank 2005] W. Jank: *Quasi-Monte Carlo sampling to improve the efficiency of Monte Carlo EM*, Computational Statistics & Data Analysis, **48**-4 : 685-701, 2005.

[Lehmer 1951] D.H. Lehmer, Good parameters and implementations for combined multiple recursive random number generators, *Operation Research*, **47**-1 : 159-164, 1951.

[L'Ecuyer 2003] P. L'Ecuyer, Quasi-monte carlo methods in practice: quasi-monte carlo methods for simulation, *Proceedings of the 35th conference on Winter simulation: driving innovation*, 2003, pp. 81-89

[Marsaglia 1995] G. Marsaglia, DIEHARD Battery of Tests of Randomness, *http://stat.fsu.edu/pub/diehard/*, 1995

[Matsumoto and Nishimura 1997] M. Matsumoto and T. Nishimura: Mersenne Twister: A 623-dimensionally equidistributed uniform pseudorandom number generator, *Proceedings of the 29th conference on Winter simulation*, 1997, pp. 127-134.

[Niederreiter 1992] H. Neiderreiter : "Random Number Generation and Quasi-Monte Carlo Methods" SIAM, CBMS 63, 1992, 241 pp.

[Neiderreiter, Bratley and Fox 1992] H. Neiderreiter, P. Bratley and B. L. Fox: Implementation and tests of low-discrepancy sequences, *ACM Trans. on Modeling and Computer Simulation*, **2** : 195-213, 1992

[Numerical Recipes 1992] W. H. Press, S. A. Teukolsky, W. T. Vetterling and B. P. Flannery: Numerical Recipes in C, pp. 278-285, ISBN 0-521-43108-5, 1992.

[Papageorgiou 2001] A. Papageorgiou, Fast Convergence of Quasi-Monte Carlo for a Class of Isotropic Integrals, *Mathematics of Computation*, **70**-233 : 297-306, January 2001.

[Sobol 1967] I. M. Sobol, On the distribution of points in a cube and the approximate evaluation of integrals, *USSR Computational Mathematics and Mathematical Physics*, **7**-4 : 86-112, 1967.

[Sobol 1976] I. M. Sobol, Uniformly distributed sequences with an additional uniform property, *USSR Computational Mathematics and Mathematical Physics*, **16**-5 : 236-242, 1976.

APPENDIX : FILES GENERATED BY THE *QRNGUNROLL* PROGRAM

The following paragraphs show the skeleton of the files (header and source) generated by the QRNG*Unroll* program with an array of 10 random values with a 1 dimension Sobol QRNG.

1 Header file

```
/*****************************************************************************
*                                                                            *
*                              UQRNGSob_1_10.h                               *
*                                                                            *
* Unroling method for QRNG                                                   *
*                                                                            *
*****************************************************************************/


/* Increment the pointer of the size of N doubles, N is equal to the number
   of dimensions, and return it */

#define NEXT()                      ( cur += 1 )
#define GET_NEXT_QRN_AT_DIM(d)      ( * ( cur + ( d ) ) )

float * cur;

void initUQRNG();
```

Fig. A.1: A header file generated by the QRNGUnroll *program*

2 Source file

```
/*****************************************************************************
*                                                                            *
*                                UQRNGSob_1_10.c                             *
*                                                                            *
*                                                                            *
*****************************************************************************/

#include "UQRNGSob_1_10.h"

/* Array of doubles in hexadecimal form */
float tab [] =
{
   0x1p-1,
   0x1.8p-1,
   0x1p-2,
   0x1.8p-2,
   0x1.cp-1,
   0x1.4p-1,
   0x1p-3,
   0x1.8p-3,
   0x1.6p-1,
   0x1.ep-1,
};

/* Initialization of the UQRNG*/
void initUQRNG()
{
  cur = ( float * )( tab );
}
```

Fig. A.2 : A source file generated by the QRNGUnroll *program*

Track 3

LIFE SCIENCES

A new visualization tool for Bio-Analysis: Application to wheat and rice comparative genomics

Carlos Luiz N. dos Santos
Université Blaise Pascal
ISIMA/LIMOS, UMR CNRS 6158
BP 10125
63177 Aubière - France
+33 4 73407662
carlos@isima.fr

Philippe Leroy
UMR 1095 INRA-UBP
Amélioration & Santé des Plantes
234 Avenue du Brézet
63100 Clermont-Ferrand - France
+33 4 73624337
leroy@clermont.inra.fr

ABSTRACT
Visualization methodologies are being applied to discover and represent knowledge in a form that human easily understand. The purpose is to simplify comparative genomic relationships between wheat and rice genomes in terms of genome structure evolution, gene discovery and evolution. Therefore, we started the development of a specific application using virtual reality techniques to help with bioanalysis tasks. In this application, the biologist expert can dynamically interact with the macro and micro-colinearity zones between a common wheat genome fraction and the rice genome modelled in the form of 12 pseudo-molecules.

KEYWORDS
Virtual Reality, Bioinformatics, Bioanalysis, Comparative Genomic and Internet.

1. Introduction

New techniques in molecular biology, particularly in DNA sequencing are dramatically increasing the worldwide genome databases. According to GenBank statistics [NCBI 2004], in 1982, the National Center for Biotechnology Information (NCBI) database had 606 sequences and 680,338 base pairs. In 2003, we have respectively 30,968,418 sequences and 36,553,368,485 base pairs. These data are altering and deeping the biological knowledge from all living organism processes [Berman *et al.* 2000]. However, the velocity of data growth is not always associated with the same velocity of human understanding. Most of the gathered data and their relationships are not transformed into information yet. Inside theses databases many masked information are waiting for their correct biological interpretation.

The bioanalysis area becomes a new domain of biological expertise and researches. This area, also noted hereafter as *in silico* analysis of DNA or protein sequences. This analysis deals essentially with annotation that affect our ability to rely on consistent, up-to-date and quality-ensured information about genes and genomes. In this context, the role of bioanalysis applications is mainly to help scientists to discover the relevant hidden information inside databases.

One of the major stakes of life-sciences in general, and vegetable genetics in particular, as well as on the cognitive level applied in the fields agro-food and health, is the possibility of discover and describe genes of interest, and their regulations, determining the genetic factors from characters target expression for plants improvement in term of development, food value, resistance to the biotic and abiotic stresses.

The UMR INRA-UBP "Amélioration et Santé des Plantes" from INRA at Clermont-Ferrand currently develops an international scale program around the structural and functional study in the bread wheat chromosome 3B genome (2-fold the rice genome). This project framework will generate a great number of new sequences. These very important resources return within the scientific project framework concerning the genome structure evolution within the *Poaceae* family, but an application of this knowledge about the genes of interest will also impact the baker bread quality. This project is based on comparative mapping between the genomes of bread wheat, rice and maize. One of the project goals is to seek the macro and micro-colinearity between rice and/or maize, and bread wheat genomes in order to help the stretches of Bacterial Artificial Chromosome (BAC) DNA sequences for the development of a physical map for this chromosome and the gene inference of interest from rice towards bread wheat.

Today, new visualization techniques are employed to help the biologist in his bioanalysis tasks. For us, humans, the natural world is a 3D environment. A virtual reality (VR) application takes advantage of this fact by allowing the user to walk around

the middle of the data and interact with them in the way humans interact with 3D objects every day. By presenting massive data sets from one application as interactive images, VR environments can instantly make any professional more productive when he comes to interpret his data [Santos *et al.* 2001b].

Therefore, we started the development of a specific application using VR techniques to help in bioanalysis tasks. In this application, the biologist can dynamically interact with the macro and micro-colinearity zones between a common wheat genome fraction (whole or part of a chromosome: cytogenetics, genetics and physical maps) and the rice genome modelled in the form of 12 pseudo-molecules (TIGR - The Institute for Genomic Research - http://www.tigr.org). In the following sections we present some bioanalysis and virtual reality concepts, then we expose the application developed and its current results before concluding.

2. Structural and Evolutionary Comparative Genomic and Bio-Analysis Concepts

A small number of cereals feeds most human and animal world populations, including wheat, rice, maize, sorghum and millet. Together with rice and maize, wheat is responsible for providing more than 60 % of calories and proteins needs [Gill *et al.* 2005]. All these cereals belong to the *Poaceae* family, which includes more than 10,000 species, their common ancestor originated about 55 to 75 millions years ago [Kellogg 2001].

Among agricultural crops, the bread wheat (*Triticum aesticum* L.) has the largest genome size representing 16,000 Mb (40-fold larger than the rice genome), including chromosome 3B. The wheat genome consists of seven groups of chromosomes (hexaploid form), where each group contains a set of three homologous chromosomes belonging to the A, B and D genomes [Gill *et al.* 2005]. The A genome was contributed by *Triticum urartu*, a diploid wheat ancestor, and the B genome by an unknown close relative of *Aegilops speltoides*, another diploid wheat ancestor. Finally, about 8,000 years ago, the D genome was added from a third ancestor called *Aegilops tauschii* to the AB genome tetraploid *Triticum turgidum*, giving the bread wheat has known today [Kong *et al.* 2004].

Genetic mapping remains a necessary step to identify genes of interest. This is true for all crops, but especially in the wheat, since bread making quality is still today the most important trait to be improved. Trait-directed sequencing is one of the ways available to identify these candidate genes for a giving Quantitative Trait Loci (QTL), located on a specific wheat chromosome locus for which compilation of all available data in terms of cDNA, EST (Expressed Sequence Tag), BAC, microsatellites and RFLP (Restriction Fragment length Polymorphism) markers is necessary. Moreover, one of the great value of wheat genetics is the creation of a series of lines, known as nullitetrasomic and ditelosomic [Sears 1953], which have been extremely useful in assigning markers to chromosomes and chromosome arms, respectively. Today, a higher level of resolution can be obtained by using a series of deletion lines [Endo Gill 1996]. These lines having deletions of chromosome segments (deletion bins) can be used to assign also markers, but to particular regions of chromosomes, allowing links to be made between genetic and physical maps.

First comparative genetic mapping in grasses have shown, at the macro-colinearity level, that the gene order is well conserved along the grass chromosomes, despite large differences in genome size, chromosome number, ploidy level, and content of repetitive elements. However, recent comparative studies of large stretches of BAC DNA sequences at orthologous loci, in barley, sorghum, bread wheat, maize and rice have shown numerous colinearity exceptions at the micro-colinearity level. These studies have shown that rearrangements caused by insertion/deletion of transposable elements, duplication, insertion, deletion, and inversion of genes, as well as gene movements have shaped the different grass genomes since their divergence from a common ancestor [Scherrer *et al.* 2005].

Today, the use of DNA sequence-based comparative genomics for evolutionary studies and for transferring information from model species to related large-genome species has revolutionized molecular genetics and breeding strategies for improving those crops. Comparative sequence analysis methods can be used to cross-reference genes between species map, enhance the resolution of comparative maps, study patterns of gene evolution, identify conserved regions of the genomes (colinearity), and help interspecies gene cloning [La Rota Sorrells 2004].

Rice (*Oryza sativa* L.) is commonly chosen as an excellent model within the grasses to study comparative genomic, because it has a relatively small genome among the *Poaceae* family and mostly genome compared with bread wheat. The availability of DNA sequence information for the rice genome, especially the availability of the 12 pseudo molecules, and deletion map position of a large number of wheat loci detected by EST unigenes allow to obtain a detailed picture of “orthologous” relationships between wheat and rice chromosomes.

Therefore, biological data, and DNA sequence data in particular, are accumulating at a phenomenal rate. It is obvious that the achievement of complete plant genome sequencing (*Arabidopsis*, rice) is only the beginning of structural, functional and

evolutionary studies of plant genomes. Visualization methodologies are being applied to discover and represent this knowledge in a form that human easily understands. This work has the goal to simplify comparative genomics relationships between wheat and rice genomes in terms of genome structure evolution and also gene discovery and evolution.

3. Virtual Reality Concepts (VR)

There are several synonyms that define Virtual Reality in the literature [Santos 2001a]: Synthetic Environments, Cyberspace, Artificial Reality, Simulation Technology, etc. Despite the recent developments, "Virtual Reality is not a new concept" [Balager Manguili 1991]. The oxymoron "artificial reality" was introduced by Krueger in 1983 [Krueger 1983] and Sutherland published in 1965 an IFIP congress proceedings with all the key concepts of immersion in a simulated world, as well as a complete sensory input and output, which was and still is the basis of VR research. A virtual or simulated world is created and based on three-dimensional graphs and audio elements that can be experimented in real time.

Virtual Reality techniques try to minimize the barrier between simulation and the user. In VR applications there is the notion of "freedom of ride", where the user can choose the angle or better position to observe the system, not restricting himself to just some points of pre-defined views [Hollands Mort 1994]. Beyond this point, placing a user in a simulated environment is usually far more economic than putting him in the real physical environment [Locke 1995].

Virtual reality is the generic name under which are being grouped all the means by which a user can, in real time, freely explore, examine, manipulate and interact with extremely complex information in a computerized world [Aukstakalnis Blatner 1992].

3.1. Immersive and Non-Immersive Virtual Reality

It is very important to distinguish between VR immersive applications and VR non-immersive applications. Behind this concept, there is a big discussion about what it is or what is not VR [Kirner 2002] [Carey Bell 1997].

Despite all discussions, particularly, in this application context, non-immersive VR is defined as the visualization obtained trough a window, typically the computer monitor. There are many reasons to invest in this technology since many home computers around the world are potential targets. Furthermore, the end user only needs to install a free scene viewer, web browser or viewer plug-in software to visualize almost all VR applications available on the Internet.

By Immersive application we mean an application that allows the coupling of almost all user senses, mainly the vision, audition and tactile senses. Full immersive environments are known as Caves, and other systems have less degrees of immersion. Many factors can contribute to immersion sensation as showed in figure 1a [Santos et al. 2001b] [Santos 2004].

Santos [Santos 2004] proposed a classification of immersive visualization tools: desktop system, desks systems, wall systems, room systems, and caves systems, as illustrate in figure 1.b.

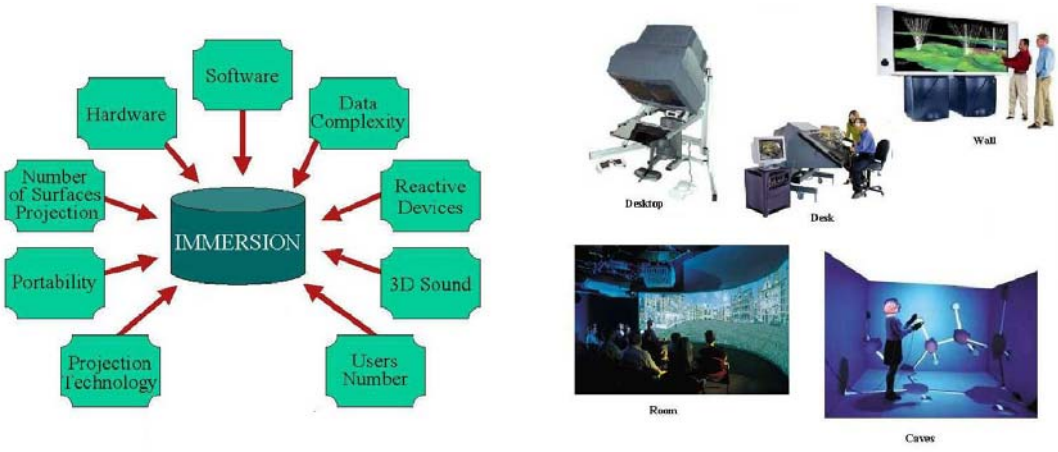

Figure 1.

a. Main Factors contributing to immersion sensation **b.** Commercial Immersive Visualization Systems.

3.2. A Non-Immersive VR Technique: the X3D/VRML Standard

The X3D/VRML is an extensible open file format standard for 3D visual effects, behavioural modelling and interaction that allows the creation of 3D scenarios, where a user can stroll, visualize objects under several angles, and yet interact with them. The VRML language was designed to describe interactive simulations of composite participants, in virtual worlds available

on the Internet and tied with World Wide Web [Fishwick Hill 1999]. A VR application designed for the Internet provides an intuitive and common interface, which facilitates interactions with 3D objects; this is one of the reasons for the recent fast acceptance and utilization of VR. Dealing with the Internet history, the Web standard and its evolution was quickly accepted since companies and universities world-wide are continually developing it [Page *et al.* 2000]. The Web is still currently the subject of much interest to both simulation researchers and simulation practitioner's.

To navigate in virtual worlds using the X3D/VRML standard, we need a scene viewer, a web browser or a viewer plug-in. Commercial, freeware and GPL-style licenses are available for all the latter mainly because a considerable number of companies and universities are involved in the X3D/VRML development and thus they created their own viewers. This diversity helps in providing creative solutions to improve the most crucial matter – the user interface; thus the user can more easily select the viewer fitting his needs.

According to Fishwick [Fishwick 1996], "…The VRML plug-ins allows one to construct 3D geometry and have it rendered in real time. A document contains an URL (Uniform Resource Locator), which points to a VRML file. The browser recognizes this particular information type and launches the VRML plug in. Then the user browses a 3D scene using whatever HCI (Human Computer Interface) devices are available…".

The X3D/VRML has a set of characteristic that turns your computer in a powerful and efficient visualization tool (among them, the most important that stands out are: cost, portability, hyperlink, usability, spread, cooperation [Santos *et al.* 2000]). Common application fields are in the following domains: medicine, computer aided design, modelling & simulation, scientific visualization, Geo-Spatial, education, entertainment and technical training [Web3D05]. In addition, users will not need any special training or previous experience to use a VRML viewer, the navigation controls helps walking through the model, flying over it. "…The quality of an interaction depends greatly on its responsiveness…" [Bryson 1994]. One of the keys to the success of visualization tools is the ease of use. Scientists whose interest is to find meaningful in data – have neither time nor patience for graphics subroutine packages, computer graphics jargon and all sort of other unnecessary details [Foley Ribarsky 1994].

In August 2001, the Web3D Consortium, the task force group that develops the X3D/VRML standard, launched the X3D open standard as a new-generation successor to VRML to bring rich and compelling 3D graphics to the Internet for a wide variety of applications and devices. The X3D is being developed under the Web3D Consortium's standardization process that provides a full and open access to the specification to interested companies and eventual submission to the International Standards Organization (ISO) for ratification to provide long-term stability for Web3D content and applications [Web3D 2005].

4. Application Development, Stages, and Strategies

The first objective of this application is to allow better biological interpretations from the study of the 3B chromosome, as illustrated in figure 2. The purpose is specially to seek the macro and micro-colinearity zones between rice and wheat genomes, in order to help the stretches of BAC DNA sequences for the development of a physical map for this chromosome. The application focus is to allow putting this entire data collection set with its features and correlations inside a VR environment, where no user skills in computer graphics are needed to manipulate them.

Today, the Internet environment is usual and quotidian to almost all biological scientists mainly due to:

a) the access centralization to updated genome databases, such as NCBI, EMBL, SWISSPROT;

b) the great number of tools and servers dedicated to sequence search, 3D homology modelling, and so on;

c) a collaborative environment among several international research groups physically distant;

d) the velocity of communication, data and information updating.

The X3D/VRML technology was chosen as a development platform for this application since:

a) the user interface (navigation, examination, etc.) is built inside available viewers;

b) there are different viewer licenses available: commercial, freeware, and GPL-style;

c) the application development is fastened since it focuses on the scientific data to visualize and not on programming;

d) it represents an evolutive Internet ISO standard (with many international research groups working, collaborating, and improving this standard, including many universities and enterprises);

e) the international support is available through many mailing lists and FAQs (Frequent Ask Questions); and

f) this standard was originally created to work fine with the new biologist environment (Internet).

This interdisciplinary collaboration project was structured and composed in several stages: the establishment of methodology work, the geometrical modelling, and the user interface modelling.

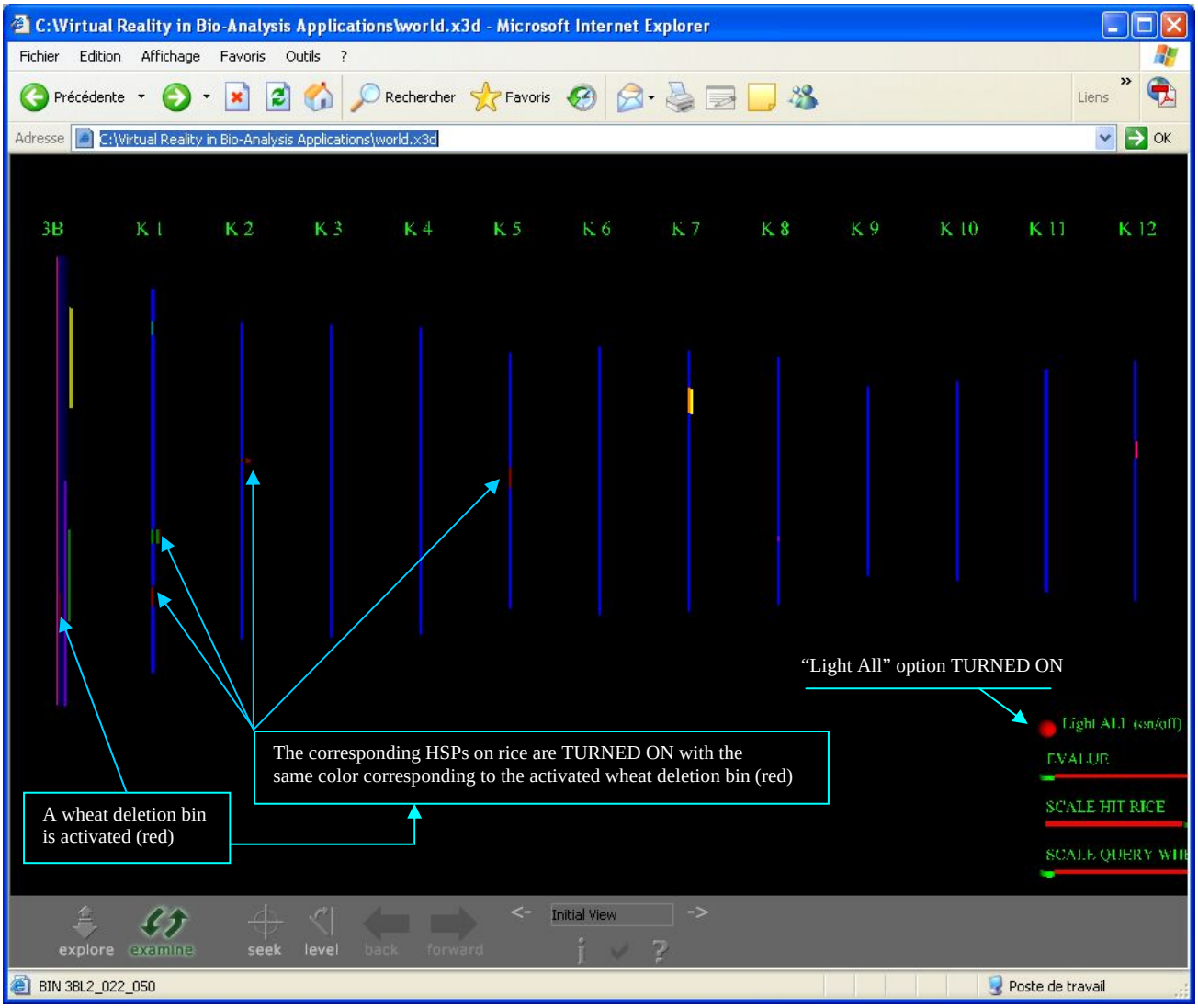

Figure 2. Application window showing all deletion bins turns on. All HSPs are visible because the "Scale Hit Rice" slider is at maximum scale.

4.1. **Interdisciplinary Collaboration**

First, biologists and computer science professionals have different methods of thinking, different languages, and different methodological ways to work. Therefore, the first basic stage was the establishment of a methodology of work. The language standardization is not an easy task to realize. So, the strategy adopted was the creation of a memory document that has been updated after each meeting, including all decisions taken, technical details as well as the reasons of our choices. This strategy has minimized several communication misunderstandings.

4.2. **Geometrical Modelling**

The second stage focused on the problem knowledge and on how to organize all information inside the input data. Two different files were used to build this application: the parameter file and the data file.

The parameter file allows the establishment of the main object structures that will represent the wheat chromosome analyzed, the deletion bin (inside the wheat chromosome structure viewed by cytogenetics), and the twelve rice pseudo-molecules (virtual chromosomes).

The data file contains all macro and micro-colinearity relationships based on similarity between genetic markers sequences (named "query" hereafter) and the rice full sequence pseudo-molecules (size alignment, pseudo-molecule coordinates, Evalue value). A query is located within a wheat bin term named hereafter "deletion bin". The similarity relationship is obtained using the BLAST (Basic Local Alignment Search Tool) algorithm. Between all algorithms available, we have chosen a BLASTn (nucleic against nucleic) algorithm using the default parameters, since we need to find true biological relationships (sequence alignments) at the DNA level.

The origin of the wheat markers sequences used for the BLASTn query analysis are molecular markers (cDNA, ESTs or genomics) assigned to a given deletion bin for a given wheat chromosome using a series of wheat deletion lines. Wheat deletion lines are specific wheat varieties, which have a peace of a break out chromosome arm.

Every query sequences (wheat genetic markers located within a deletion bin) may give a hit against the rice pseudo-molecules, that means that this specific wheat marker recognizes a specific rice pseudo-molecule. Then, for each hit, a query sequence may reveal many HSP (High-scoring Segment Pair) along the rice pseudo-molecule corresponding probably to several rice putative "genes" or relevant sequence similarity. Each HSP represent a specific DNA sequence alignment corresponding to a given Evalue or Expectation value that is the number of different alignments observed with a score equivalent or better than a given threshold expected to occur in a database search by chance.

The Evalue and its significance score work inversely. So, lower is the first, bigger is the second, and consequently greater is the HSP relevance. The main BASTn parameter for which we can define a minimum cut off is the Evalue. Therefore, we used an Evalue cut off of 10^{-1} that means that all the value above 0.1 are discarded. The values below the cut off are classified in 5 categories:

- Class A: Evalue bellow 10^{-1};
- Class B: Evalue bellow 10^{-5};
- Class C: Evalue bellow 10^{-25}
- Class D: Evalue bellow 10^{-50}; and
- Class E: Evalue bellow 10^{-100}.

The geometrical modelling stage was concluded after parsing the two input files generating all 3D elements. A scale adjusting step was needed to harmonically visualize all information, because the biological units are measured in base pairs (bp) for physical maps, percentage for cytogenetic maps, and centimorgan (cM) for genetic maps, but their proportion and graphic representation in this application are measured in meters.

4.3. **User Interface Modelling Stage**

This stage represents the most complex task developed in this application because all data correlations and its behaviours possibilities were implemented. The main features provided by the user interface are:

1. Names of deletion bin. It is possible to visualize the names of each deletion bin when the user passes the mouse cursor over it inside the wheat chromosome graphic representation, as illustrated in figure 3. This option enables the biologist to know precisely what wheat markers will be activated or deactivated. To implement this application feature, we have associated each deletion bin graphic representation to its respective name inside a hyperlink description field with a null URL.
2. Selection of a deletion bin. After selection there is a colour change inside the wheat chromosome. The corresponding HSP on rice (one or several) will be turned on with the same corresponding deletion bin colour, as illustrated in figure 2. This option enables the biologist to view similarities between the sequence of a specific wheat marker and a rice locus on the pseudo-molecules, according to the Evalue. The implementation of this feature is done this way: each selection (with a mouse click) of the deletion bin graphic representation implied a change in the colour and transparency properties of its respectively HSP. However, the sequence alignment inversions between the wheat and rice are not displayed at the graphical level.
3. Selection of all deletion bins at the same time, just by turning on the "Light All (on/off)" option. This option simplifies the complete visualization of all deletion bins as well as the corresponding HSP that will be visible with the same colour

as the deletion bins (figure 2). If a deletion bin is already turned on when this option is turned on, all deletion bins minus the last one, will be turned on, according to the Evalue.

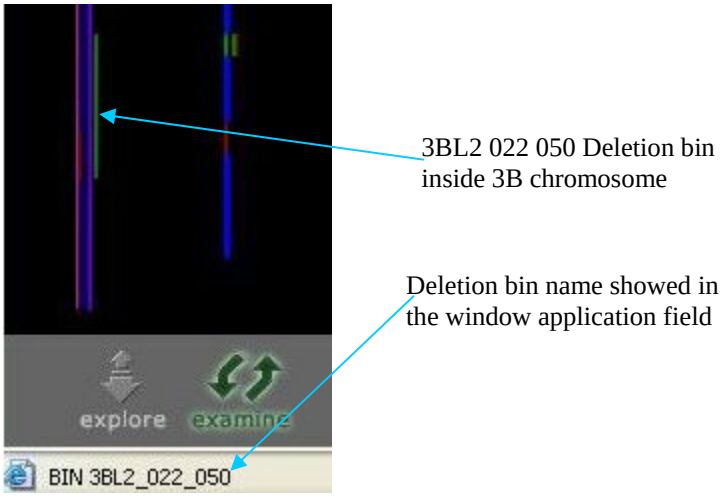

Figure 3. Window field with the name of the 3BL2 022 050 Deletion bin.

4. HSP Size. After selecting a deletion bin in the wheat 3B Chromosome, we can access to precise visual information if the user changes the position of "Scale Hit Rice" slider. At start time the HSP representation are very small in size inside the rice structure, and then it is not always visible. Therefore, the user can increase its Y size using a slider to see precisely in which rice chromosome we have the corresponding HSP.
5. Evalue Threshold. After selecting a deletion bin, we can use an "Evalue" slider. Each HSP on rice has its particular Evalue and at start position all HSP are potentially visible. If the user changes the position of this slider, the Evalue belongs to an interval (5 classes intervals are retained: A, B, C, D and E), and all HSPs that have an Evalue in the same class interval are displayed. This option enables the biologist to change very easily the threshold of each interval and then he has the opportunity to identify more or less relevant HSPs. The transparency property value of selected HSP graphic representations is used to trigger the display according the position of the "Evalue" slider.
6. HSP query name. After selecting a deletion bin, we can visualize the HSP corresponding query name when the user passes the mouse cursor over it inside the rice structure. This option enables the biologist to know with more precision the interesting target to analyse. Like for the display of deletion bin names, we implemented this application feature, by associating each HSP graphic representation to its respective name inside a hyperlink description field with a null URL.

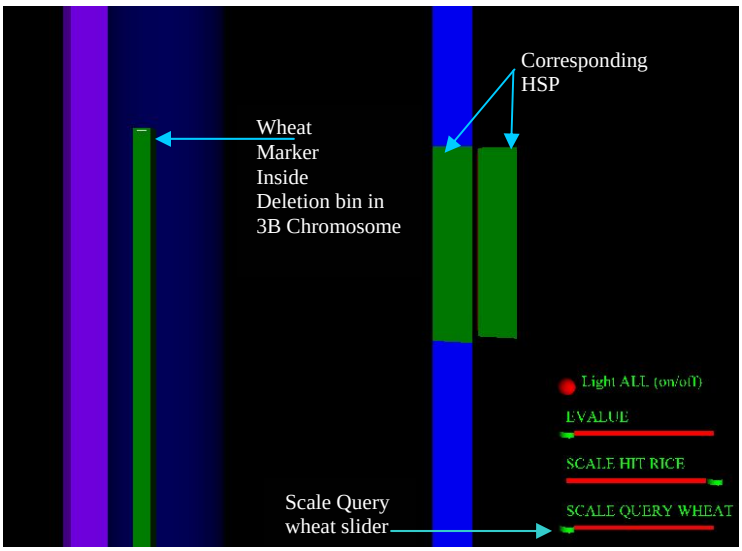

Figure 4. Selection of Wheat marker at its original size (which corresponds to a thin horizontal line).

7. Wheat marker display. After selecting a deletion bin, select a HSP and then turn on the respective wheat bin markers inside the corresponding deletion bin (see figure 4). This option enables the biologist to evaluate the starting from a zone of interest in the rice in correspondence to the specific wheat zone concerned. This application feature is achieved by changing the colour and the transparency properties of wheat bin markers on each mouse click over the HSP graphic representation.
8. Scaling on wheat marker. Changing the position of the "Scale Query wheat" slider enables to increase the wheat marker size. At start time the wheat bin markers graphic representation are a very small inside the deletion bin graphic representation (indeed they are almost invisible, see figure 4). Therefore, the user can increase the size, the Y size property of wheat bin markers is associated to the position of this slider (figure 5 shows the wheat marker with the slider at its maximum scale).

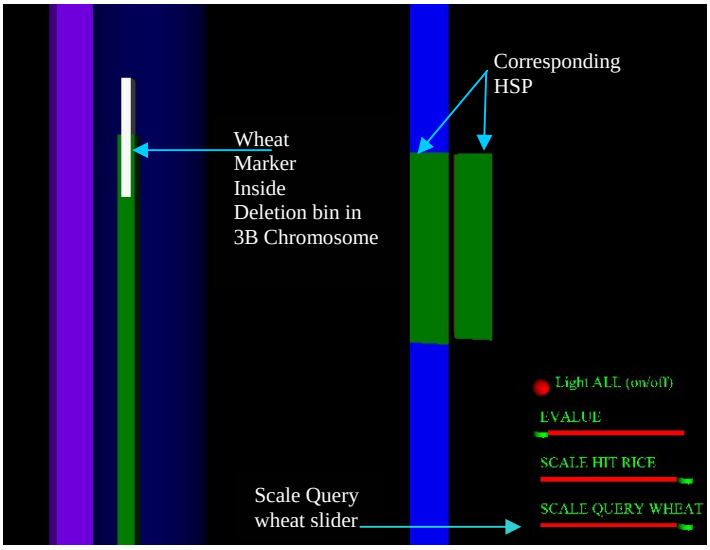

Figure 5. Selection of Wheat marker at maximum scale.

9. Wheat marker Inspector. After a HSP selection, it is possible to obtain more information about the respective wheat bin marker that has been turned on if the user touch it with mouse click. This click launches a HTML window opening inside the Web browser (figure 6). For each wheat bin marker a hyperlink is set to the corresponding ".html" file. All the corresponding files have to be generated before running the visualization tool.

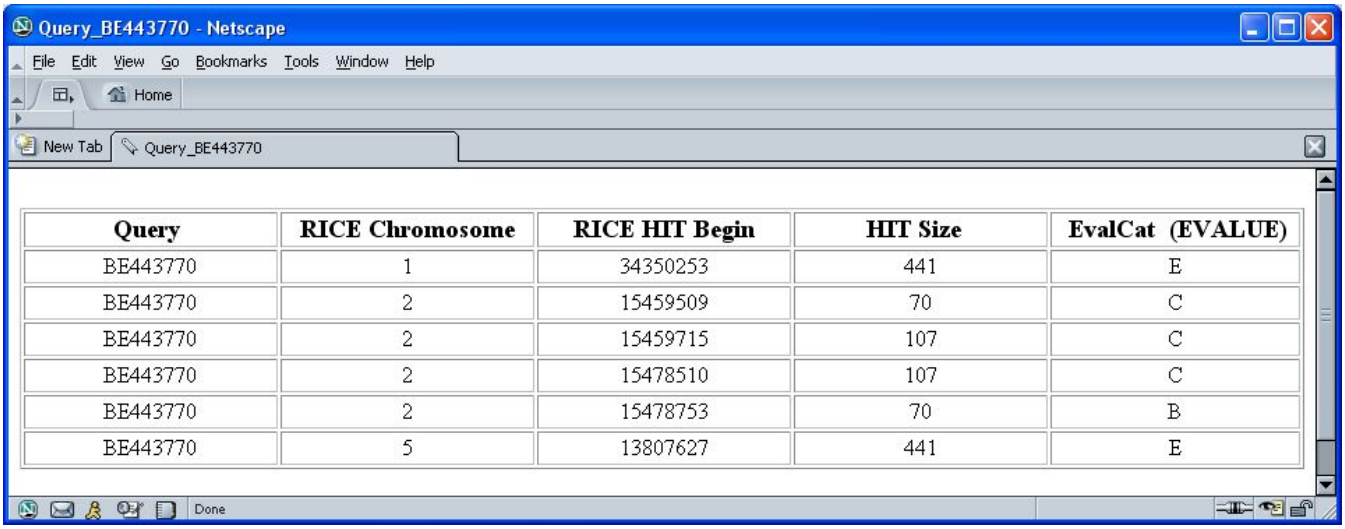

Query	RICE Chromosome	RICE HIT Begin	HIT Size	EvalCat (EVALUE)
BE443770	1	34350253	441	E
BE443770	2	15459509	70	C
BE443770	2	15459715	107	C
BE443770	2	15478510	107	C
BE443770	2	15478753	70	B
BE443770	5	13807627	441	E

Figure 6. Web page of "QUERY_BE443770" Wheat marker inside the "3BL10_050_063" deletion bin at 3B chromosome.

10. Easy access to all wheat deletion bins. All deletion bins are placed over a X3D/VRML cylinder, thus a rotation of the wheat structure enables the user to place the deletion bin of interest in front of his rice chromosome selection. VR Rotation and position sensors (vertical & horizontal) have been placed on the 3B chromosome structure to obtain this kind of graphic representation.
11. Correspondence visualisation by translation. It is possible to translate all rice chromosomes from their original position to a horizontal and vertical position just near the region of interest in the wheat graphic representation. So, the user can place HSPs and deletion bins of the same colour at the same observation level, as illustrated in figure 7. We implemented this application feature, by associating a VR position sensor (vertical & horizontal) to all rice structures.
12. Zoom. For all the features previously cited, the VR viewer enables any kind of zooms within the graphical structure domain. This option is not specific to our implementation, but it constitutes an additional and interesting feature allowing the user to concentrate on small specific regions, making all its associated information more visible, as illustrated in figures 4, 5 and 7.

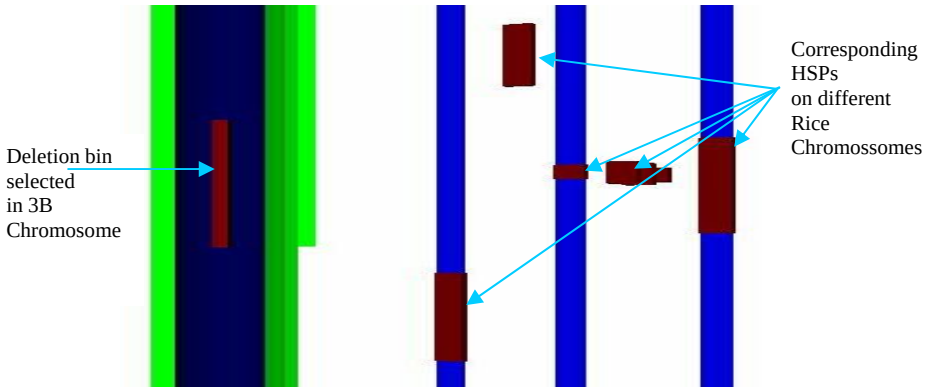

Figure 7. Selection of Deletion bin with all respective HSPs placed side-by-side after their displacement, at maximum scale and using the zoom feature.

5. Conclusion

The biological data, and DNA sequence data in particular, are accumulating at a phenomenal rate. It is obvious that the achievement of complete plant genome sequencing (*Arabidopsis*, rice) is only the beginning of structural, functional and evolutionary studies of plant genomes. Visualization methodologies are being applied to discover and represent this knowledge in a form that human easily understand. In this paper we have presented a collaborative work between a biologist and a computer scientist which purpose is to simplify comparative genomic relationships between wheat and rice genomes in terms of genome structure evolution, gene discovery and evolution. A prototype using the X3D/VRML standard has been achieved with various visualization features. The final application runs on common personal computers with a Web browser and a X3D/VRML plug-in. This application has been developed from a minimal data collection (theoretical training data set) to validate the prototype. The current release of the application is fully functional.

Our hope is that the partial application results shown above may allow better biological interpretations from massive input datasets. Indeed this visualization tool will enable the biologist to discover many masked information, with no special learning or skills. This intuitive approach of our interface mainly relies on the VR visualization engine even if we do not currently need a 3D display. After, more validation and testing, we will be able to automatically transform input databases in data compatible with our application. This will turn our prototype work in a true production environment.

ACKNOWLEDGMENTS

This work was partially supported by CNPq, a Brazilian Governmental Agency turned to Scientific and Technologic development.

REFERENCES

[NCBI 2004] Genbank Statistics. Growth of GenBank, 2004. On-line at http://www.ncbi.nlm.nih.gov/Genbank/genbankstats.html. (Current march 2005)

[Berman *et al.* 2000] Berman H. M., Bhat T. N., Bourne P. E., Feng Z., Gilliland G., Weissig H., Westbrook J. The Protein Data Bank and the challenge of structural genomics. Natural Structural & Molecular Biology Journal, November, Vol. **7**, Number 11, pp 957-959, 2000.

[Santos *et al.* 2001b] Santos CLN, Bacoccoli, G., Landau, L. A Review about the Anthropomorphic Visualization

Environments Applied to Offshore Engineering. In SCS Europe, Editor, Proceedings of The International Workshop on Harbour, Maritime & Multimodal Logistics Modeling and Simulation – (HMS), pp. 58-62. Marseille, France, 2001.

[Gill *et al.* 2005] Gill BS, Appels R, Botha-Oberholster A-M, Buell CR, Bennetzen JL, Chalhoub B, Chumley F, Dvorak J, Iwanaga M, Keller B, Li W, McCombie WR, Ogihara Y, Quétier F, Sasaki T. A workshop report on wheat genome sequencing: International Genome Research on Wheat Consortium. In: Genetics **168**:1087-1096, 2005.

[Kellogg 2001] Kellogg EA. Evolutionary history of the grasses. Plant Physiol. **125**:1198-1205, 2001.

[Kong *et al.* 2004] Kong XY, Gu YQ, You FM, Dubcovsky J, Anderson OD. Dynamics of the evolution of orthologous and paralogous portions of a complex locus region in two genomes of allopolyploid wheat. Plant Molecular Biology 54:55-59, 2004.

[Sears 1953] Sears ER. Nullisomic analysis in common wheat. Am. Natur. **87**:245-252,1953.

[Endo Gill 1996] Endo TR, Gill BS. The deletion stocks of common wheat. J. Hered. **87**:295-307, 1996.

[Scherrer *et al.* 2005] Scherrer B, Isidore E, Klein P, Kim J-s, Bellec A, Chalhoub B, Keller B, Feuillet C. Large intraspecific haplotype variability at the Rph7 locus. Results from rapid and recent divergence in the barley genome. The Plant Cell **17**:361-374, 2005.

[La Rota Sorrells 2004] La Rota M and Sorrells ME .(2004). Comparative DNA sequence analysis of mapped wheat ESTs reveals the complexity of genome relationships between rice and wheat. Funct Integr Genomics **4**:34-46.

[Santos 2001a] Santos CLN, Ferramentas de Visualização Antropomórficas através do uso de Realidade Virtual Aplicadas a Engenharia Offshore [Anthropomorphic Visualization Tools through the Use of Virtual Reality Applied to Offshore Engineeringa], Doctoral dissertation, Civil Eng. Dep., Fed. Univ. of Rio de Janeiro (COPPE/UFRJ), Rio de Janeiro, Brazil, 2001 (in Portuguese).

[Balager Manguili 1991] Balaguer F., Manguili A. Virtual Environments. New Trends in Animation and Visualization, Wiley-Interscience, New York, NY, 1991.

[Hollands Mort 1994] Hollands R. and Mort N. (1994). The Use of VR for Enhanced Visualization in Systems Simulation. First United Kingdom Virtual Reality - Special Interest Group Conference (Nottinghan, UK), 1994. On-line at http://www.crg.cs.nott.ac.uk/events/ukvrsig-1/, (Current at march 2005)

[Locke 1995] Locke J. Applying Virtual Reality, Naval Postgraduate School (Monterey, CA), 1995.

[Aukstakalnis Blatner 1992] Aukstakalnis S., Blatner D. Silicon Mirage: The Art and Science of Virtual Reality. Peatchpit Press (Berkeley,CA), 1992.

[Kirner 2002] Kirner, C. Sistemas de Realidade Virtual. Universidade Federal de São Carlos –UFSCar. Tutorial, 2002, On-line at http://www.dc.ufscar.br/~grv/tutrv/tutrv.htm (Current at march 2005)

[Carey Bell 1997] Carey, R. and Bell, G. The Annotated VRML 2.0 Reference Manual. Addison-Wesley Developer Press, 1997.

[Santos 2004] Santos CLN. Immersive Visualization Environment Tools for Collaborative Applications, Modeling and Simulation Magazine, SCS, September, Vol. **3**, N.3, pp. 11-13, 2004.

[Fishwick Hill 1999] Fishwick P., Hill D., Editors. Web-based Simulation, Special Issue of the Simulation Journal, Vol. **72**, N°3, 60 p, 1999.

[Page *et al.* 2000] Page E, Buss A, Fishwick P, Healy K, Nance R and Paul R. Web-Based Simulation: Revolution or Evolution?, ACM Transactions on Modeling and Computer Simulation. Vol. **10**, N. 1, pp. 3-17, January 2000.

[Fishwick 1996] Fishwick, P. Web-Based Simulation: Some Personal Observations, 1996 Winter Simulation Conference, December, San Diego, CA, pp. 772-779, 1996.

[Santos *et al.* 2000] Santos CLN, Cunha GG, Mello LFN, Landau L. VRML in Scientific Visualization: Porous Media Flows in Oil Reservoirs, Proceedings of the 2000 International Conference On Web-Based Modeling & Simulation. Vol. **32**, pp.75-80, San Diego, USA, 2000.

[Web3D 2005] Web3D Consortium. X3D New-Generation Open Web3D Standard, 2005. On-line at http://www.web3d.org/x3d/ (current January 2005).

[Bryson 1994] Bryson, S. Real-time Exploratory Scientific Visualization on Virtual Reality, Scientific Visualization Advances and Challenges, Published in association with IEEE Computer Society Press, Academic Press, 1994.

[Foley Ribarsky 1994] Foley J, Ribarsky W. Next-Generation Data Visualization Tools, Scientific Visualization (Academic Press Ltd. 1994) pp. 103-127, 1994.

Modelling the *in vitro* Dissolution of Soluble Binary Drug Delivery Systems using Direct Monte Carlo techniques

Ana Barat **Heather J. Ruskin** **Martin Crane**
Biocomputation Group, School of Computing, Dublin City University, Dublin 11, Ireland
+353857265902 +35317005513 +35317008974
abarat@computing.dcu.ie mcrane@computing.dcu.ie hruskin@computing.dcu.ie

ABSTRACT
Designing formulations for Drug Delivery Systems (DDS), which deliver the molecule according to a particular desired profile is an important area in pharmaceutics, requiring time-intensive experimental research. Good computer simulations of the dissolution process are desirable tools permitting the reduction of the *in vitro*, and hence *in vivo* testing required. In recent years, the direct Monte Carlo method has come to be used in simulating many complex systems such as micro-structural evolution in materials, to which the drug delivery problem bears some relation. This paper focuses on simulating a binary system consisting of a poorly soluble drug dispersed in a matrix of highly-soluble acid excipient. Experimental description and a bibliography of existing models for this particular system are also presented, thus motivating the introduction of our direct Monte Carlo model for the simulation of a DDS dissolving in an apparatus for studying the dissolution *in vitro*.

KEYWORDS
Modelling; Drug delivery systems; Dissolution; Porous layer; Design and Experiment; Multicomponent soluble compacts; Monte Carlo; Cellular Automata

1. Introduction

In vitro dissolution testing is very important in designing, developing and testing new formulations, [Siepmann & Peppas, 2001, Crane et al., 2004]. In order to achieve the appropriate concentrations of the desired drug *in vivo*, (i.e. in the target organs and tissues), during the desired period of time, the dissolution profiles *in vitro* need to satisfy certain criteria, generally established by the pharmacopoeias [Sun et al., 2003, Crane et al., 2004]. Thus the dissolution *in vitro* can be regarded as the first step toward modelling *in vivo* dissolution and absorption. The dissolution rate is measured in practise using one of a number of standard dissolution test methods outlined in international pharmacopoeias such as the European Pharmacopoeia (Ph Eur) and United States Pharmacopoeia (USP). One commonly used dissolution test apparatus is the paddle dissolution apparatus, known as Apparatus 2 [USP, 2004]. Apparatus 2 is used to reflect variations in hydrodynamic conditions in the upper gastro-intestinal tract.

However, there are a number of difficulties related to the *in vitro* dissolution testing. Very often, the relation between the formulation and process parameters of a pharmacological compact and its required *in vitro* dissolution profile is not entirely understood, due to the complexity of mass transport at dissolution, which often results in barely tractable effects like interactions and synergies. For these reasons, experimentation associated with the field of drug design is very costly and time consuming. Thus, modelling the drug release can increase the performance in the design of new products, by, on the one hand, making predictions and selecting the best candidate parameters to be experimentally tested, and, on the other hand, helping to develop scientific understanding of the complex phenomena involved in the dissolution process.

Many different modelling approaches to drug dissolution have been taken throughout the last decades, with mathematical modelling predominating [Siepmann & Peppas, 2001, Siepmann & Göpferich, 2001, Narasimhan, 2001, Costa & Lobo, 2000].

Other, less traditional alternative methods like stochastic approaches, [Chen et al., 1998], direct Monte Carlo (MC) methods, [Göpferich & Langer, 1995, Göpferich, 1997, Zygourakis & Markenscoff, 1996, Kalampokis et al., 1999, Kosmidis et al., 2003, Kosmidis & Argyrakis, 2000], artificial neural networks (ANN) and genetic algorithms (GA) [Sun et al., 2003], have recently appeared in the field of drug

dissolution. These methods, used in parallel with the traditional ones, bring complementary advantages, such as the possibility of investigating the microscopic aspects of the problem in the case of MC methods, and optimisation schemes in the case of ANN and GA.

Previous research has shown that direct MC could be a valuable tool in the field of modelling the dissolution of drug delivery systems characterised by complex internal structure, [Göpferich & Langer, 1995, Zygourakis & Markenscoff, 1996, Kosmidis et al., 2003].

Monte Carlo (MC) methods are used for solving various kinds of computational problems using random numbers (or rather pseudo-random numbers). MC is extremely important in computational physics and related applied fields, because phenomena, which are difficult to quantify, can be treated as distributions of random numbers. Direct Monte Carlo simulations applied to multiple-particle systems have been used frequently to mimic various problems from real life systems, [Chopard & Droz, 1998, Landau & Binder, 2000]. Previous to being used to simulate systems such as those involving drug dissolution and delivery, direct Monte Carlo techniques were been applied to many other kinds of systems exhibiting complex behaviour [Chopard & Droz, 1998, Landau & Binder, 2000].

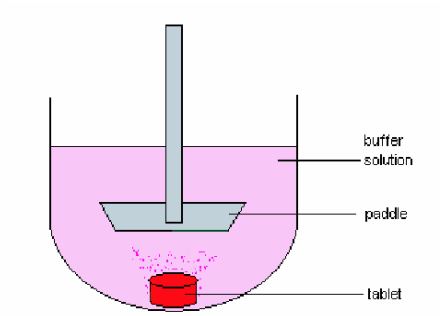

Figure 1: USP (United States Pharmacopoeia) Paddle Apparatus at 100 rpm [Mauger et al., 2003].

In this paper we explore the possibilities of MC modelling, in investigating the *in vitro* dissolution of a particular class of compacts, used as model drug delivery systems in [Healy & Corrigan, 1992, Healy & Corrigan, 1996] and exhibiting quite complex behaviour at dissolution in reactive media. Besides diffusion investigation, this model is designed to capture the particularities of the dissolution process, related to the *in vitro* environment intrinsic to a dissolution paddle apparatus.

The method consists in representing a compact (or compact cross-section in the case of 2D simulations) as a multi-particle system fitted on a grid of sites, symbolising different states of the system. The dissolution of the various particles (e.g. drug and excipient) is simulated by moving them on the grid according to a number of rules based on the situation in the neighbouring sites. Different types of such ”neighbourhoods" are considered in an effort to mimic the reality as closely as possible. The emerging macroscopic properties of the whole system are examined at the end of each simulation. Finally, the simulation results are compared to experimental data. The dissolution profiles generated by the Monte Carlo approach were found to be in accord with experimental observations on the dissolution of ibuprofen/acid excipient model drug delivery systems.

2. Multicomponent soluble compacts

In the area of modelling dissolution for different complex drug delivery systems, multicomponent soluble systems have not received enough attention despite the fact that solid dosage forms invariably contain multiple soluble components . Several theoretical approaches to describing binary systems are due to [Ramtoola & Corrigan, 1987] and references therein.

In the case of non-interacting binary systems, where the components have different solubilities (C_{S_x} and C_{S_y}) and different diffusion coefficients (D_x and D_y), at the start of the diffusion process,

the two components will tend to dissolve at rates proportional to their diffusion coefficients. Later on, only one of the components will generally remain at the solid-liquid interface. The other component will have to dissolve through the porous system formed inside the less soluble component. According to [Ramtoola & Corrigan, 1987], when steady state is reached, the limiting dissolution rate of the component which remains at the surface is given by:

$$G_x = \frac{D_x}{h} C_{S_x} \qquad (1)$$

while the dissolution rate of the receding component y is given by:

$$G_y = \frac{D_y C_{S_y}}{(h + \frac{\tau}{\varepsilon})(s_1 - s_2)} \qquad (2)$$

where h is the thickness of the diffusion film, τ is the tortuosity, referring to the complexity of the system of channels formed in 3D, ε is the porosity and $(s_1 - s_2)$ is the thickness of the porous layer formed at the solid-liquid interface. In the case where the components are ionizable, the situation is more complex, [Ramtoola & Corrigan, 1987].

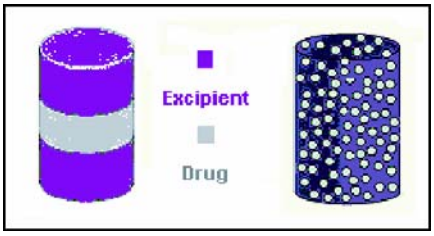

Figure 2: Layered compact versus matrix compact

[Healy & Corrigan, 1992, Healy & Corrigan, 1996] have conducted experimental and theoretical studies on the dissolution of soluble ibuprofen-acidic excipient compressed mixtures in reactive media, using model compacts. First grinding the two components into powder, mixing the products, and finally compressing them into a final compact obtained the compacts. At dissolution in reactive media, these compacts exhibit quite complex behaviour in spite of their binary composition. The drug and the excipient have dramatically different solubilities, slightly different diffusivities, and the acidic excipient has an effect on the solubility of ibuprofen at dissolution. The compact dissolves according to the following mechanism: at the dissolution of the acid excipient, the pH of the buffer decreases and this suppresses the solubility of the other component, the ibuprofen.

Direct Monte Carlo approaches are particularly attractive when simulating phenomena in complex or heterogeneous media. In this paper, we develop a model for binary systems, composed of mixed soluble components with different dissolution properties, and present a version capable of mimicking the dissolution of the compacts described in [Healy & Corrigan, 1996].

As mentioned before, one interest of this paper is to take into consideration the *in vitro* environment used for dissolution testing, since the settings of the dissolution apparatuses do affect the process of compact dissolution. A standard apparatus consists of a container filled with the dissolution medium and with the compact situated at the bottom (see Figure 1). The paddle is used to stir the buffer solution inside the apparatus, creating a stream, which curves around the obstacle presented, by the compact and producing a velocity boundary layer around it. Due to the stirring of the liquid in the apparatus, the mass transport at dissolution happens not only by simple diffusion, but by advection[1] as well, because the flow is responsible for carrying away quantities of matter proportional to the velocity. [Crane et al., 2004] studied the problem of *in vitro* radial dissolution from simple layered binary systems (with 3 to 5

[1] The term of advection refers to the transport of something from one region to another.

alternate layers, as on Figure 2). Their investigation used numerical methods in combination with a Pohlhausen profile, (Equation 3), to model the concentration boundary layer formed around the dissolving cylindrical device in the USP apparatus, where:

$$\frac{C^*}{C_{satur}} = 1 - \sin\left(\frac{\pi y}{2\delta_c}\right) \qquad (3)$$

Here, C_{satur} is the saturation concentration of a given component, C^* is the concentration at a given point y within the concentration boundary layer and δ_c is the thickness of the boundary layer at a given height of the cylindrical compact.

The results, depicting the concentration profile within the boundary layer during a short period of time, from using Finite Element techniques and those from using a semi-analytical Pohlhausen type approximation to the concentration boundary layer, agreed with experimental data and demonstrated that conditions *in vitro* had an important impact on the way in which a compact dissolves.

3. Modelling

In this investigation, we simulated the dissolution of a binary soluble system, using a 2D lattice and a Monte Carlo algorithm, as described below. Given that, in the case of the *in vitro* systems, the effect of the advection is too strong to be negligible, the model specifically takes into consideration both main mechanisms of mass transport in the system: diffusion and advection.

We define the compact and the release medium around it on a 2D lattice with each site characterised by a local state (as shown on Figure 3). The physical laws governing the dissolution dynamics are expressed in terms of rules of microscopic content on a discrete space-time structure.

We represent the two solid species by particles with different properties. In this particular case, we make the assumption that one species dissolves independently and is referred to as the excipient in the following, while the dissolution of the other species strongly depends on that of the former. We refer to this last species as the drug, to match the terminology of the experimental system we consider. Empty sites represent the solvent. The state of a site (i, j), $\psi(i, j)$, is defined by the quantity and type of the particles with which it is filled, i.e. the concentrations $C_D(i, j)$ and $C_E(i, j)$ of drug and excipient particles, respectively. Our main target is to be able to predict the dissolved quantities of either of the two species, $D_D(t)$ and $M_E(t)$, at each time step.

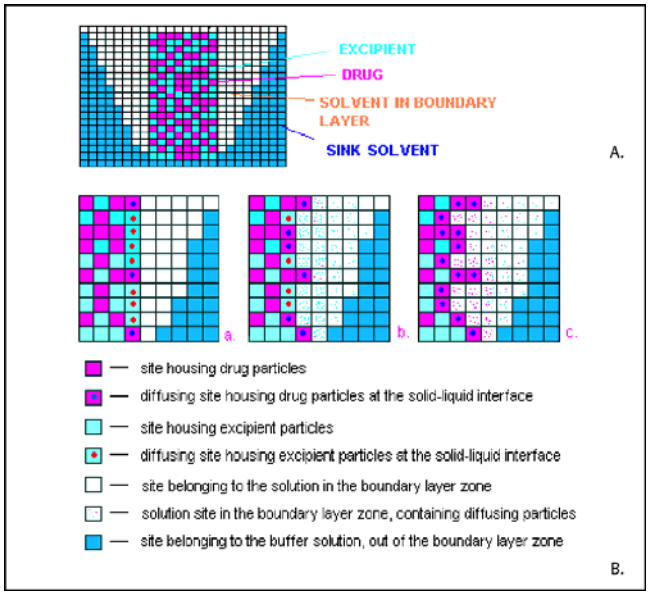

Figure 3: 2D model for a dissolving binary system. A. Schematic representation of 2D model. Real dimensions are not respected in the picture. B. Simplified model of dissolution of a drug-excipient

system, with the grid representing a cylindrical tablet in longitudinal cut. The shots show the benefits of this kind of model for simulating cases where pores are formed inside a compact by the quick dissolution of one of the components. The second component has to dissolve through these pores and this process is different from dissolution at the surface

3.1 Modelling the diffusion

Diffusion refers to the process by which molecules of different species intermingle as a result of their kinetic energy. In the model we represent the two solid species by particles. Since the components in the compact have highly different solubilities, they are expected to dissolve at different rates. In addition, the solubility of a component depends on the local concentrations [Healy & Corrigan, 1992]. We allow for more then one particle to move to an adjacent site, in order to capture the most relevant ingredients of the real system characterised by two highly different solubilities. The solubility of a given species is modelled by allowing not more than a fixed number of particles, $S = C_{MAX}$, on the sites considered as filled with solvent. The maximum allowed concentrations in the solvent, C_{MAX_D} and C_{MAX_E}, are proportional to the real solubilities. The decision to permit a batch of particles to diffuse is accepted or rejected by:

- consulting a gradient-dependent probability, p_E in the case of the excipient (Equation 4). In the following, (i, j) symbolises the current site and (i^*, j^*) -the adjacent site to which the possibility of diffusion is considered.

$$P_E = \frac{C_E(i, j) - C_E(i^*, j^*)}{C_E(i, j)} \qquad (4)$$

- consulting a probability, dependent on the excipient concentration in the neighbourhood, p_{D_0}, $p_{D_0} = f(\sum C_E(i^*, j^*))$ and a further, gradient-dependent probability, p_{D_1} (Equation 5) in the case of the drug.

$$p_{D_1} = \frac{C_D(i, j) - C_D(i^*, j^*)}{C_D(i, j)} \qquad (5)$$

- The diffusion operation itself is performed by calculating the number of particles of excipient, f_E, and those of drug, f_D, which will move to each of the adjacent sites. The number of excipient particles which hop from the site (i, j) to the site (i^*, j^*) are given by:

$$f_E = p_E * X_E \qquad (6)$$

where X_E is a variable uniformly distributed between one particle and the maximum number of particles allowed on the site (i^*, j^*). The quantity of the particles on a site is limited by the species
solubility C_{MAX}, therefore

$$X_E = U(1, C_{MAX_E}) - C_E(i^*, j^*)) \qquad (7)$$

Similarly, we compute f_D.

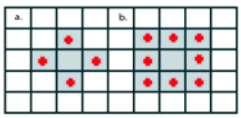

Figure 4: Examples of neighbourhoods. a. Von Neumann b. Moore

3.2 Modelling the advection

Given that the advection plays an important role in mass transport in the *in vitro* environment, and the flow in a dissolution apparatus is very complex, we choose to work with the region adjacent to the curved surface of a cylinder. Here, the advection operation can be performed using the Pohlhausen concentration profile in a discretized form, adapted for our lattice model.

In order to simulate the advection process, we consider every solution site within the boundary layer and the number of particles of drug and excipient $a_D(i, j)$ and $a_E(i, j)$ which will be carried away from it by the stream, to symbolise the mass transport property. The quantities $a_D(i, j)$ and $a_E(i, j)$ are computed considering a concentration Pohlhausen profile (Equation 3) in a discretized form. As the compact dissolves, the boundary layer recedes in the space so that the model requires re-updating of the concentration profile at all time steps.

4. Results and discussion

We average simulation results on a certain number (20) of initial configurations of DDS, because the spatial packing of the two components in the compact has some slight effect on the dissolution results.

A MC time step is thus a sequence of updating, advection and diffusion operations performed for all the sites from the lattice and corresponding to time t. The system is left to evolve during many MC iterations and samples of $M_D(t)$ and $M_E(t)$ are taken periodically, in order to plot their profiles at the end of the simulation. Two different types of neighbourhoods were considered (Figure 4), and we have found the Moore's neighbourhood is the most appropriate for our problem, because it permits for more directions of moving the particles in the 2D space, and this is evidently closer to the reality. Von Neumann's neighbourhood was found to underestimate the quantities of dissolved excipient in the cases of compacts containing low percentages of the later. This is due to isolated clusters of undissolved excipient, surrounded by slowly dissolving drug.

The suppression effect of the acid excipient is indirectly modelled by defining rules for dramatically decreasing the diffusing probabilities of the drug in the presence of local high concentrations of excipient. We have carried outsimulations with binary systems where the properties of the dependent species (drug), have been kept the same for all the experiments with different solubility of the independent and more soluble species (excipient). The excipient received a wide range of solubilities noted S_E.

Figure 5 compares the behaviour of the system for two different excipients E_1 and E_2, one with a high solubility and the other with lower solubility $S_{E1} > S_{E2}$. The properties of the dependent component, the drug, are kept constant during the two simulations and $S_{E1} > S_D, S_{E2} > S_D$. Figure 5, (a) and (c) shows the concentration profiles for, respectively, E_1 and E_2. In both cases irregular dissolution fronts are developed, but the extent of their roughness is obviously a function of the solubility of the excipient. The excipient influences the dissolution of the dependent species by filling the free space with its particles and consequently decreasing the local solubility of the drug. The higher the solubility of the excipient, the higher the capacity of a solution site to accommodate excipient particles.

For the case of E_1, it can be noticed that the excipient has strongly receded from the surface (Figure 5, (a)), and has created a porous layer, through which the poorly-soluble drug dissolves only in the region where the excipient concentrations are very low (Figure 5, (b)). The drug dissolves through the pores

created by the dissolution of E_1. For E_2 very different behaviour is exhibited. The porous layer is much thinner than in the previous case and the drug boundary has receded inward to a greater extent. ([Ramtoola & Corrigan, 1987] have mentioned this kind of behaviour in the case of binary systems).

We have plotted the fraction of the dissolved of drug and excipient against the time, comparing the dissolution profiles of drug and excipient with those obtained in the experiments. The results reproduce very well the trends and effects occurring at the dissolution of real binary compacts, containing ibuprofen and acid excipient [Healy & Corrigan, 1992]. Figure 6 shows the drug and the excipient profiles for different solubilities and for two different drug loadings. The porosity of the matrix is kept constant. Every dissolution curve is obtained by averaging the results of a particular number of simulations (20) characterised by the same initial parameters but with different initial configurations of the compact, (the 2 species are randomly distributed in the compact for each simulation). The plots show that as the solubility of the excipient increases, the dissolution of the drug is more and more suppressed. As in experiment, a positive curvature for the drug and a negative curvature for the excipient are obtained.

With highly-soluble excipients, the dissolution of the drug is very slow in the beginning, and when almost all the excipient is dissolved, the drug changes its dissolution rate, as can be seen for some of the profiles in Figure 6, (c). In Figure 6 (c), the orange ibuprofen profile corresponds to the microenvironment represented on Figure 5 (c) and the blue profile shows the case of E_2, (Figure 5 (d)).

If we take a look at Equation 2, we notice that the dissolution rate of the receding component is inversely proportional on the thickness of the porous layer formed at the surface of the compact. Even if the expression considers the thickness of the porous layer as constant in time, it is obvious it is not so in the reality, because it enlarges gradually as the acid excipient dissolves. Figure 7 shows the simulated dynamics of the thickness of the porous layer for two different acid excipients, the first more soluble then the second.

Simulations demonstrate that the thickness of the porous layer does not have a linear evolution with the time, especially for lower concentrations of acid excipients in the compact. These results can be used in order to modify Equation 2, in introducing a time dependent thickness of the porous layer.

In addition, we have studied the effects of other parameters, such as the drug loading, the excipient particle size and the porosity. Results again were in agreement with the experimental findings.
We note that suppression of the advection step from the model leads to simulation results for the drug profiles, which do not accord with experiment, hence environment-related features are important.

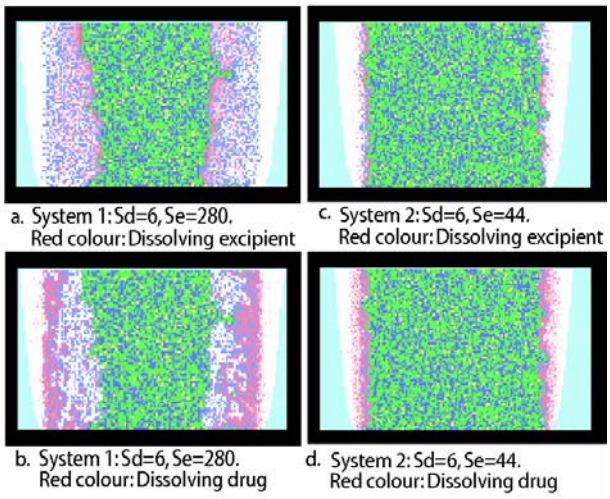

Figure 5: Colour code: green - solid excipient, blue - solid drug, yellow - pores, white - solution in theboundary layer, clear blue - sink solution, shade of red in a) and c) - the concentration of excipient in the boundary layer solution, shade of red in b) and d) - the concentration of drug in

the boundary layer solution. All figures show the state of a 130/80 sites compact after 4000 iterations a) and b) System where the excipient has a relatively high solubility S.

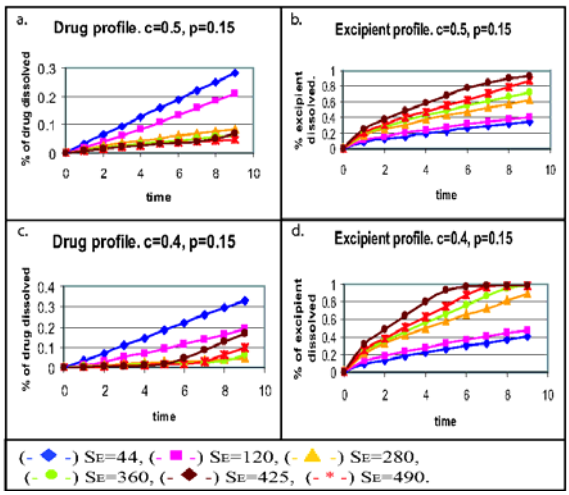

Figure 6: The effect of the solubility of the independent species on the dissolution of the dependent species

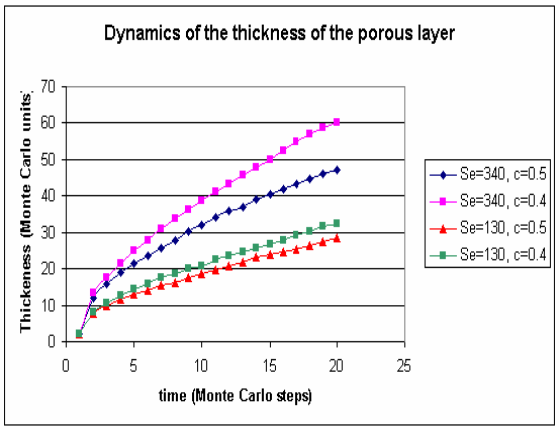

Figure 7: The evolution of the thickness of the porous layer formed during the dissolution of compacts containing different types of excipient and different concentrations of acid excipient. The process is clearly non-linear with the time.

5. Conclusions

With our simple Monte Carlo model, direct consideration is taken of aspects such as time dependent porosity and thickness of porous layer, dissolution through pores, effects of particle size and distribution of particle size, concentration dependent solubilities, receding solid-liquid interface, dissolution over long periods of time and advection due to the *in vitro* environment. Thus, essential features, necessary to reproduce the complexity observed in the real world problem of *in vitro* drug dissolution, are captured.

The model can also easily be modified to simulate multicomponent compacts, for example, they can be used to see what happens if a mixture of ibuprofen/acid excipient is compressed in an inert non-soluble matrix of ethylcellulose, (a material used in the present day in the manufacturing of controlled release systems). In this case, it is very important to examine percolation phenomena and the MC model has the advantage of permitting such type of investigations.

ACKNOWLEDGEMENTS
The authors would like to acknowledge the Irish National Institute for Cellular Biotechnology (NICB), who financially supported the present work and Dr. A.-M. Healy (School of Pharmacy, Trinity College Dublin), for access to the experimental data, used as reference in this study.

REFERENCES
[USP, 2004] United States Pharmacopoeia, 2004. Online homepage available from: http://www.usp.org/frameset.htm. Access date: 16/06/2004.
[Chen et al., 1998] Chen, X., Chen, W., Hical, A. H., Shen, B.-C., & Fan, L. T. (1998). Stochastic modeling of controlled-drug release. *Biochemical Engineering Journal*, 2: 161-177, 1998.
[Chopard & Droz, 1998] Chopard, B. & Droz, M. Cellular Automata Modelling of Physical Systems, Cambridge University Press, 1998.
[Costa & Lobo, 2000] Costa, P. & Lobo, J. M. S. Modelling and comparison of dissolution profiles. *European Journal of Pharmaceutical Sciences*, 13, 123-133: 2000.
[Crane et al., 2004] Crane, M., Crane, L., Healy, A.-M., Corrigan, O., Gallagher, K. M., & McCarthy, L. A Pohlhausen solution for the Mass Flux From a Multi-layered Compact in the USP Drug Dissolution Apparatus. *Simulation Modelling Practice and Theory (SIMPAT)*, 12: 397-411, 2004.
[Göpferich, 1997] Göpferich, A. Erosion of composite polymer matrices. *Biomaterials*, 18: 397-403, 1997.
[Göpferich & Langer, 1995] Göpferich, A. & Langer, R. Modelling monomer release from bioerodible polymers. *Journal of Controlled Release*, 33: 55-69, 1995.
[Healy & Corrigan, 1992] Healy, A.-M. & Corrigan, O. I. Predicting the dissolution rate of ibuprofen-acidic excipient compressed mixtures in reactive media. *International Journal of Pharmaceutics*, 84: 167-173, 1992.
[Healy & Corrigan, 1996] Healy, A.-M. & Corrigan, O. I. The influence of excipient particle size, solubility and acid strength on the dissolution of an acidic drug from two-component compacts. *International Journal of Pharmaceutics*, 143: 211-221, 1996.
[Kalampokis et al., 1999] Kalampokis, A., Argyrakis, P., & Macheras, P. Heterogeneous tube model for the study of small intestinal transit flow. *Pharmaceutical Research*, 16- 1: 87-91, 1999.
[Kosmidis & Argyrakis, 2000] Kosmidis, K. & Argyrakis, P. (2000). Fractal kinetics in drug release from finite fractal matrices. *Journal of Chemical Physics*, 119- 12, 2000.
[Kosmidis et al., 2003] Kosmidis, K., Rinaki, E., Argyrakis, P., & Macheras, P. Analysis of case ii drug transport with radial and axial release from cylinders. *International Journal of Pharmaceutics*, 254: 183-188, 2003.

[Landau & Binder, 2000] Landau, D. P. & Binder, K. Monte Carlo Simulations in Statistical Physics. Cambridge University Press, 2000.
[Mauger et al., 2003] Mauger, J., Ballard, J., Brockson, R., De, S., Gray, V., & Robinson, D. Intrinsic Dissolution Performance Testing of the USP Dissolution Apparatus 2 (Rotating Paddle) Using Modified Salicylic Acid Calibrator Tablets: Proof of Principle. *Dissolution Technologies*, 2003.

[Narasimhan, 2001] Narasimhan, B. (2001). Mathematical models describing polymer dissolution: consequences for drug delivery. *Advanced Drug Delivery Reviews*, 48: 195-210, 2001.
[Ramtoola & Corrigan, 1987] Ramtoola, Z. & Corrigan, O. I. Dissolution characteristics of benzoic acid and salicylic acid mixtures in reactive media. *Drug Development and Industrial Pharmacy*, 13: 9-11, 1987.
[Siepmann & Göpferich, 2001] Siepmann, J. & Göpferich, A. Mathematical modeling of bioerodible, polymeric drug delivery systems. *Advanced Drug Delivery Reviews*, 48: 229-247, 2001.
[Siepmann & Peppas, 2001] Siepmann, J. & Peppas, N. A. Modelling of drug release from delivery systems based on hydroxypropyl methylcellulose (HPMC). *Advanced Drug Delivery Reviews*, 48: 139-157, 2001.
[Sun et al., 2003] Sun, Y., Peng, Y., Chen, Y., & Shukla, A. J. Application of artificial neural networks in the design of controlled release drug delivery systems. *Advanced Drug Delivery Reviews*, Preface 55: 1201-1215, 2003.
[Zygourakis & Markenscoff, 1996] Zygourakis, K. & Markenscoff, P. A. (1996). Computer-aided design of bioerodible devices with optimal release characteristics: a cellular automata approach. *Biomaterials*, 17: 125-135, 1996.

TransCripTome, An Algorithm to Grid Automatically DNA Micro-Arrays

Gros Pierre-Emmanuel, Boyer Benoit, Boisgontier Hervé, Tucholka Alan, Férey Nicolas, Gherbi Rachid
LIMSI-CNRS, Université Paris-Sud,
BP 133, F-91403 Orsay Cedex, France
http://www.limsi.fr
E-mail: genoteam@limsi.fr
Phone: +33 1 69 85 81 64 or 66 Fax: +33 1 69 85 80 88

ABSTRACT
Thanks to the increasing number of completely sequenced genomes and EST (Expressed Sequence Tags) data accumulation, understanding of complex biological processes can benefit of global approaches. Among recent post-genomic developments, DNA microarrays represent probably the most powerful tool. The images produced by these technologies (micro-arrays, macro-arrays, DNA chips, etc.), are used both to analyze and calculate the expression of a segment of RNA or DNA [GRANJEAUD 1999, JORDAN 1998], or to compare the expression of several segments. This expression represents either instantaneous value (processing of only one image) or a profile of expression during time interval (sequence of images). In order to analyze these spots, it is necessary to be able to detect them, on the one hand in a sure way because of the sensible nature of the analysis algorithms, and on the other hand in an automatic and fast way in order to treat the huge quantity of images necessary to a biological experimentation. Quality of images increases with the technology of bio-robotics devices. We propose in this paper a tool witch implements a new algorithm based on a cooperative approach using "edge-region" segmentation

KEYWORDS
BioInformatics, Image Processing, DNA Microarray analysis, Data Acquisition

1. Introduction

Thanks to the increasing number of completely sequenced genomes and EST (Expressed Sequence Tags) data accumulation, the understanding of complex biological processes can benefit of global approaches. Among recent post-genomic developments, DNA micro-arrays represent probably the most powerful tool. Images produced by these technologies (micro-arrays, macro-arrays, DNA chips, etc.), are used both to analyze [Courcel 2001, Hastie 2001, Perou 2000, Diehn 2000] and calculate the expression of a segment of RNA or DNA [Eisen 1998], or to compare the expression of several segments.

An array is an orderly arrangement of samples. An array of experiments can make use of common assay systems such as micro-plates or standard blotting membranes, and can be created by hand or make use of robots to deposit the sample. In general, arrays are described as macro-arrays or micro-arrays, the difference being the size of sample spots. Macro-arrays contain sample spot sizes of about 300 microns or larger and can be easily imaged by existing gel and blot scanners.

The sample spot sizes in micro-array are typically less than 200 microns in diameter and these arrays usually contain thousands of spots. An experiment with a single DNA chip can provide to researchers information on thousands of genes simultaneously. The main problem of theses arrays is the difficulty to extract automatically the spots's intensity of the image. In the first image, we can see an image of four sample blocks in good experimental conditions. In Image 2, we see that the noise is the main problem to achieve a full automatic algorithm to detect [Chen 1998] spots. Here the array was scrambled by the robot and a part of the image has been destroyed:

Image 1: pretty good experimental conditions

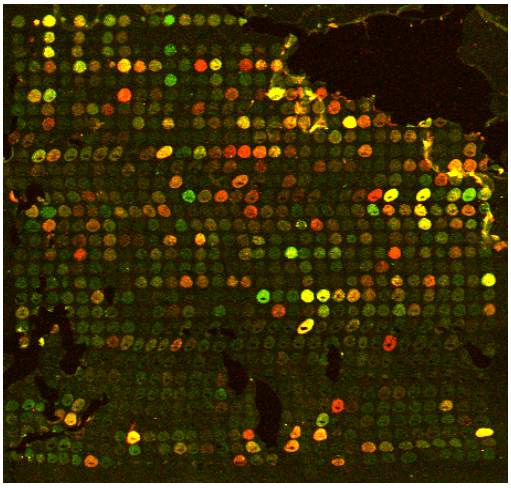

Image 2: Noisy Image

The work presented in this paper aims to lead to a fully automatic algorithm, in opposition to semi-automatic techniques, in order to speed up analyses made by biologists[Sherlock 2001], while guaranteeing a great reliability of detection. In this paper, we propose a new couple of algorithms based on a new approach using region segmentation in order to detect spot samples on images. The main idea behind our algorithm is that we need only few very well detected spots in order to find all other spots. So firstly, we will show how the algorithm manages to reveal those well-detected spots. Secondly, we will show how this detection can be use to find all the spots. In a last time, we will present some experiments with our tool.

2. Way of working

The ultimate image analysis goal is to extract automatically a quantity from every array element. The objective of our algorithm is to bring to light in a robust manner array's spots. To achieve this goal of accurately estimating the spot, the algorithm must cope with the following three major problems:

- Background noise and sometime errors like artifacts, which do not comprise gene expression information, can occur.
- Overlapping spots: Spots with high intensity or spots in low-resolution images may interfere with neighboring spots.
- Various spot shapes: Depending on the experiment type, different spot sizes and shapes are possible.

In order to achieve these aims, our algorithm works in two parts. The first one is to split the array into spot blocks. This part is important because due to the noise problem. Indeed, the noise has not an equitably repartition upon the entire array. So, we cannot use the same parameters in the spot extraction upon the whole array. By extracting firstly the block from the array, we can make a spot extraction with more locally chosen parameters. The second part consists in extracting the spots from each block. In order to achieve this aim, we are going to first extract spots with high activity trough an algorithm of region detection. Then, we are going to use these spots to reveal spots with less activity.

3. Block detection

The aim of this algorithm is to detect the sample blocks from the micro-arrays image. Indeed, we think that we can detect in an easily manner the spots after having detected the image's blocks.

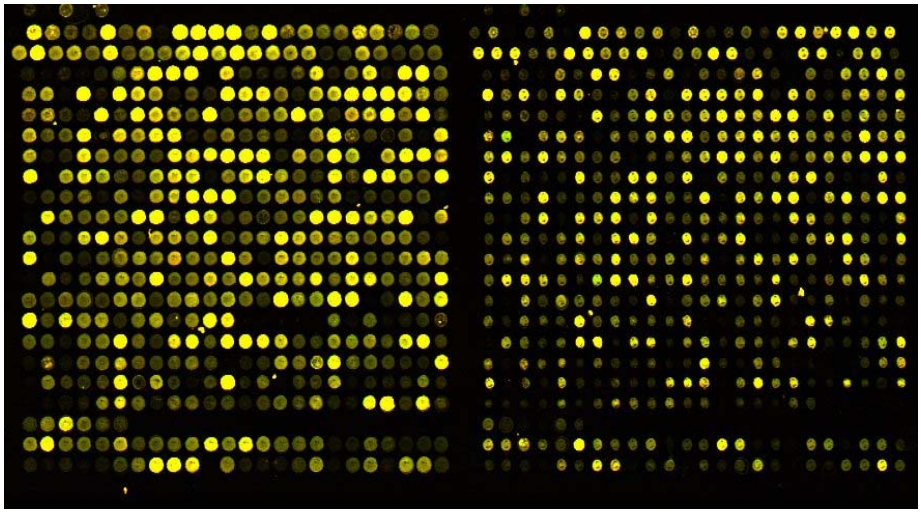

Image 3: Two blocks from a micro-array

The main problem is to make a real difference between a spot and a block. Actually, a spot and a block are both colored shape enclosed with a background color (usually dark). The main difference is that the distance between two blocks is longer than the distance between two spots. So, the main idea is to blur the images. In applying this filter, we would like to play upon the distance between the spots in order to collapse them. The hypothesis is that the blocks are not collapsed after the blur because the distance between them is higher. In order to prepare the block detection, we apply a median filter and a threshold in order to remove the Gaussian noise of the image.

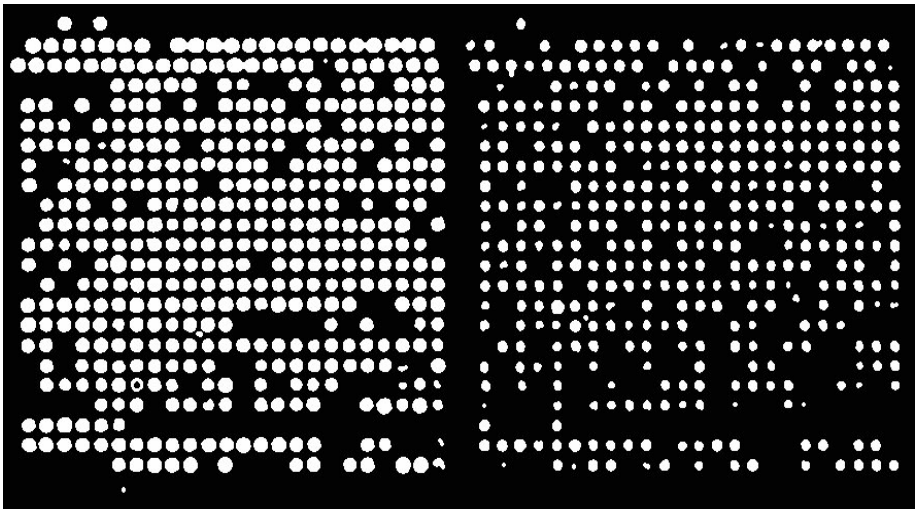

Image 4: Blocks of micro-arrays after removing the noise

After removing the Gaussian noise (*c.f.* Image 4), we are going to collapse the spots. Actually, to collapse the spots we could apply a Gaussian filter upon the image. The default of this approach is that we could collapse the blocks by applying a too large filter. So we are not going to apply this Gaussian filter directly upon the image but upon the edge of the spots. Like the edge of a spot is thin and closed, we can apply a very small Gaussian mask's size. So, we apply upon the image a Sobel filter in order to find the edge of the spot and 3x3 Gaussian filter.

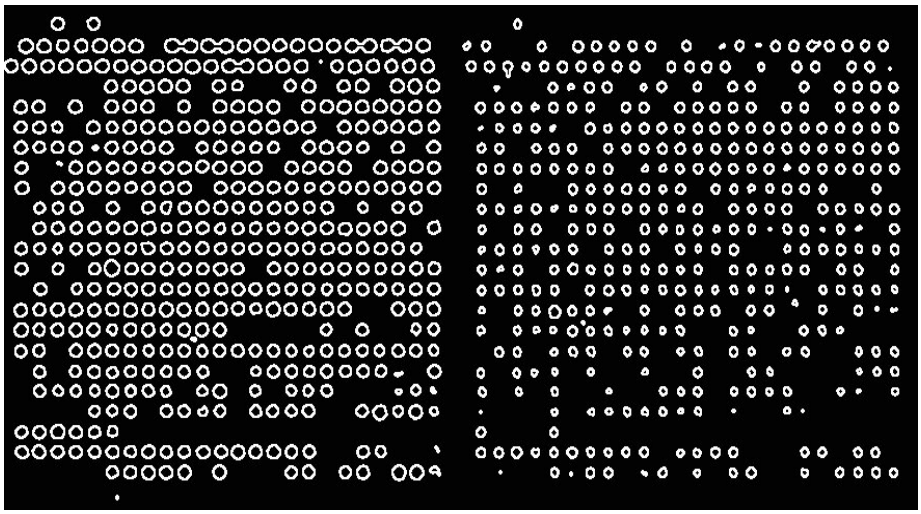

Image 5: Blocks of micro-arrays after the edge-detection filter

Image 6: Blocks of micro-arrays after the blur filter

After applying the Gaussian filter, we apply again a median filter and a threshold in order to bring the blocks to the light.

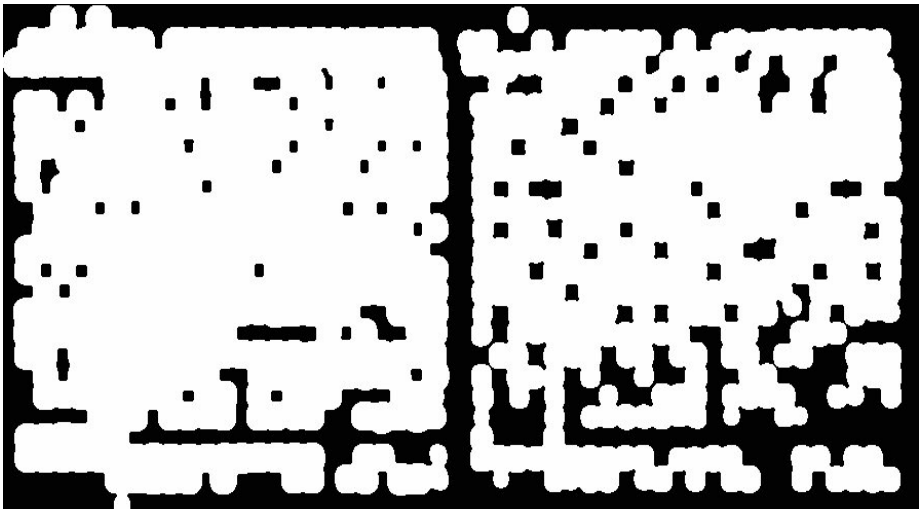

Image 7: The blocks are brought to the light

With this image, we can easily detect the image blocks in a statistic manner upon the profile of the image.

4. Spot detection

Until now we have detected the blocks from the image. We want now to detect the spots of each block in an automatic manner. The way we use is to find upon a block, spots with high activity through a region detection [Sonka 1998] algorithm. Then with these spots and statistical-tools, we are going to find spots with less activity.

4.1 Region Detection

The main goal of this algorithm part is to detect well-drawn spots, which have usually a high expression activity. In order to find easily these spots, we apply a threshold 'T' upon the original image, which set pixels to a given value if above/below a certain threshold 'p' given by the user.

After the threshold filter, we must suppress the noise of the image. An approach using a simple mean filter is not a good idea because:

- A single pixel with a very unrepresentative value can significantly affect the mean value of all the pixels in its neighborhood.
- If the filter neighborhood straddles an edge, the filter will interpolate new values for edge pixels and so will blur that edge. This may be a problem if sharp edges are required in the output. This last point prevents us to use the mean filter because this filter risks to amalgamate the spots. Another way to suppress the noise from an image is to use a median filter. Median filtering is a non-linear signal enhancement technique smoothing signals and preserving edges. We use here the median filter for almost two reasons. Firstly, unrepresentative pixels do not unduly influence the outcome of the final pixel level. Secondly, the final pixel must actually be the value of one of its neighbors, edges are preserved more faithfully. As the median filter preserves the spots' edges but do not remove enough noise, our algorithm applies a chain of a median filters. So we obtain the first image I0 of the algorithm: $\underset{0}{I} = \mathrm{T}(p, G)$ (where G is the original grayscale image). Then, we successively apply the median filter to the image: $\underset{n+1}{\mathrm{I}} = \mathrm{M}(\underset{n}{\mathrm{I}})$ (where M is the median filter). We stop the succession when:
- A white or black image is obtained. It could happen if p is to high or low. So, we apply again the algorithm to the original image G and with a higher or a lower value p.
- The difference between $\underset{n}{\mathrm{I}}$ and $\underset{n+1}{\mathrm{I}}$ is not significant.

We show here the difference between Images 8 and 9 after 15 algorithm iterations.

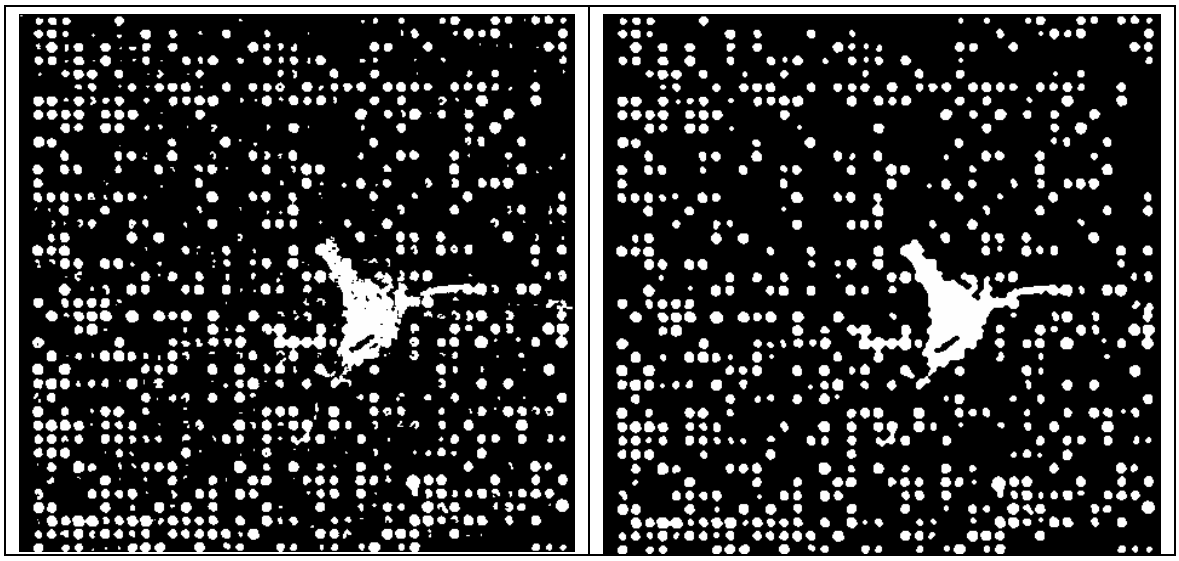

Images 8, 9: Removing the image noise with successive Median Filters

For the same kind of images, we are going to detect the grid of spots.

4.2 Grid Detection

At this processing level, spots with high activity of expression are bringing to light and we must now detect all the others. For this aim, we use the fact that spots are aligned vertically and horizontally. This idea implies two interesting points:

- If the image is oblique, we can automatically rotate the image.
- By drawing straight lines passing between the already well-detected spots we hope that all spots will be localized.

However, in the case of Image 1, one can notice that it is impossible to draw a line passing on a "dribble". Nevertheless, for major images where the “dribble” (or likely noise) concerns only a part of the image, a simple statistical processing can be performed to overcome this problem. Indeed, it is possible to compute spacing between the drawn lines keeping only the most frequently observed spacing.

In order to compute the most frequently observed spacing, we compute the sum of white and black pixels upon each axis of the “High Activity Image”. As seen in this graph, the local maximum of the graph reveals the position of grid spots.

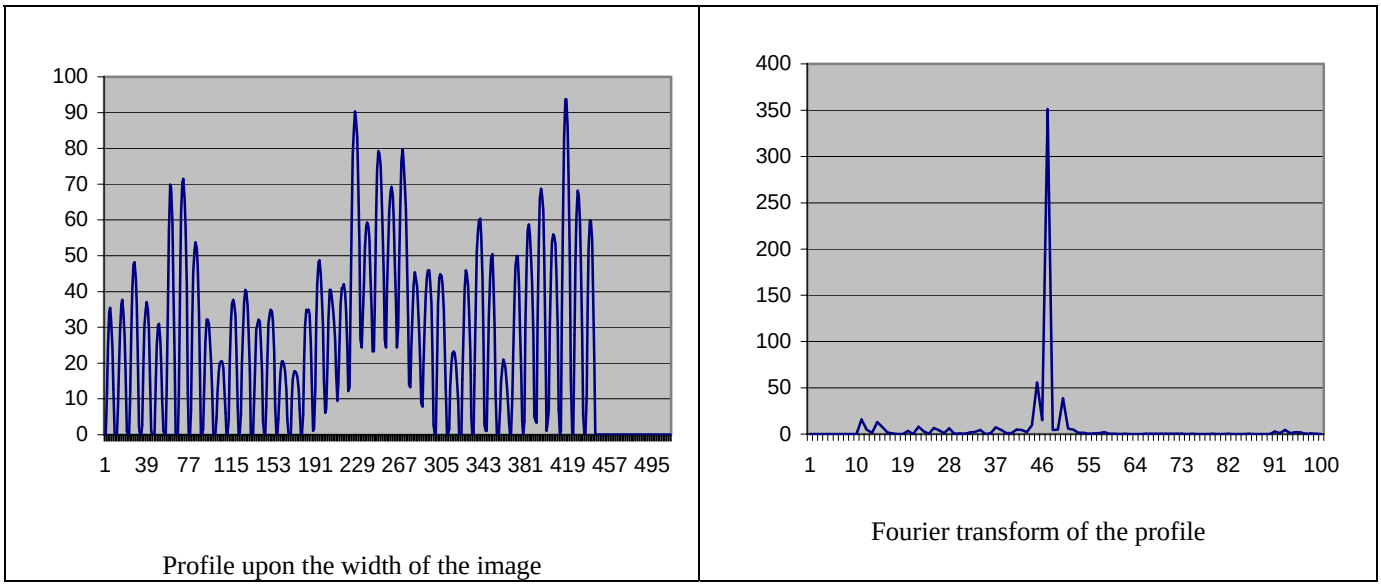

Figure 1: Image profile, and profile FFT

In order to find, the most frequent distance between two lines, we made the Fourier transformation of the graph (Figure 1). From this transformation, we take the most representative frequency and place the grid upon the spot image.

5. Experiments and Results

Here we have two tool experiments:

The first experiment is an image, which has no real noise but the spots are not aligned. Applying the tool consists in rotating first the image and then in detecting the region and finding the grid.

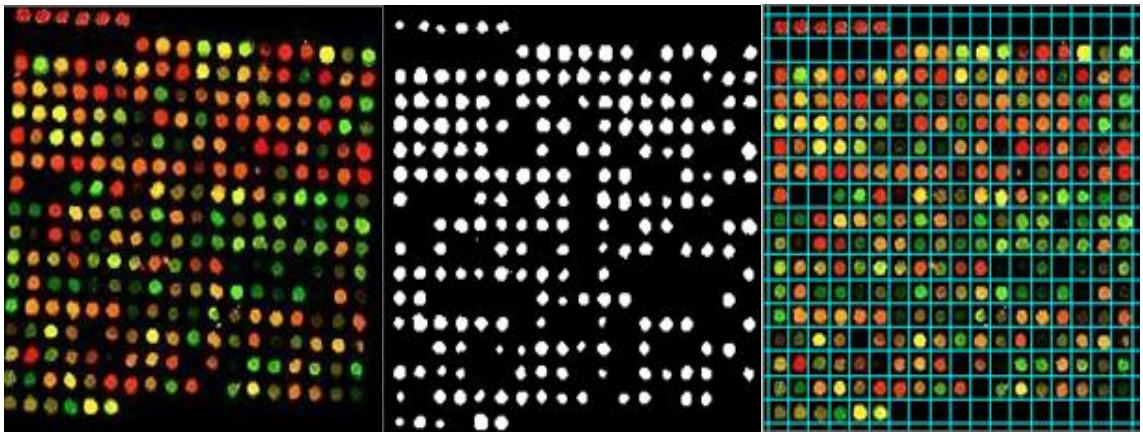

Image 10: Rotation, detection and grid finding

In the second experiment, the experiment was in part destroyed by the robot. Hence, the image has a lot of non Gaussian noise. When detecting the region, most of the well-activated spots are revealed. These few spots are in a sufficient number to reveal the grid shape.

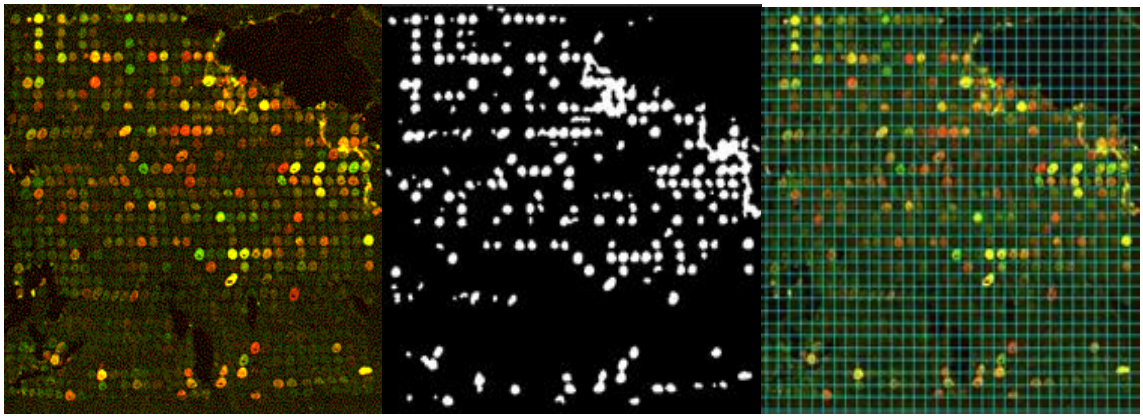

Image 11: Experiment in part destroyed by the robot

6. Conclusion

We presented a new algorithm, which is able to fully detect spots of a *Transcriptome* image. This is especially valid for spots in the neighborhood of "dribble" areas or those with low expression activity. This work is in progress. In a first step, we need be able to treat grids with variable sizes of cells. In a mid-term, it is possible to perform a snake-based [Kass 1988] or germ-based process in order to round very precisely each spot. Usually, such process must be initialized manually. This is unconceivable on *Transcriptome* images without a prior detection of the grid. Indeed, within each grid's cell, the initialization pixel (snake or germ) may be launched from the cell's centre. It will be also of great interest to combine static and dynamic information, as performed for gesture and movement processing [Collet 1998] [Braffort 1998], in order to segment and track spots along a sequence of images that represent the activity of spots at several instants.

REFERENCES

[Granjeaud 1999] Granjeaud S., Bertucci F. and Jordan B.R. (1999) Expression profiling: DNA arrays in many guises. BioEssays, 21(9):781-790.

[Jordan 1998] Jordan B.R. (1998) Large-scale expression measurement by hybridization methods: from high-density membranes to "DNA chips". J Biochem (Tokyo), 124(2), 251-8.

[Chen 1998] Chen J.J., Wu R., Yang P.C., Huang J.Y., Sher Y.P., Han M.H., Kao W.C., Lee P.J., Chiu T.F., Chang F., Chu Y.W., Wu C.W. and Peck K. (1998) Profiling expression patterns and isolating differentially expressed genes by cDNA microarray system with colorimetry detection. Genomics, 51(3), 313-24.

[Courcel 2001] Courcelle J, Khodursky A, Peter B, Brown PO, Hanawalt PC. Comparative gene expression profiles following UV exposure in wild-type and SOS-deficient Escherichia coli. Genetics. 2001 May; 158(1): 41-64.

[Hastie 2001] Hastie T, Tibshirani R, Botstein D, Brown P. Supervised harvesting of expression trees. Genome Biol. 2001 Jan 10; 2(1): RESEARCH 0003.1-0003.12.

[Sherlock 2001] Sherlock G, Hernandez-Boussard T, Kasarskis A, Binkley G, Matese JC, Dwight SS, Kaloper M, Weng S, Jin H, Ball CA, Eisen MB, Spellman PT, Brown PO, Botstein D, Cherry JM. The Stanford Microarray Database. Nucleic Acids Res. 2001 Jan 1; 29(1): 152-5.

[Perou 2000] Perou CM, Sorlie T, Eisen MB, van de Rijn M, Jeffrey SS, Rees CA, Pollack JR, Ross DT, Johnsen H, Akslen LA, Fluge O, Pergamenschikov A, Williams C, Zhu SX, Lonning PE, Borresen-Dale AL, Brown PO and Botstein D. (2000). Molecular Portraits of Human Breast Tumours. Nature 406, 747-52.

[Diehn 2000] Diehn M, Eisen MB, Botstein D and Brown PO. (2000). Large-Scale Identification of Secreted and Membrane-Associated Gene Products Using DNA Microarrays. Nat Genet 25, 58-62.

[Kass 1988] M. Kass, A. Witkin, D. Terzopoulos, « Snakes : Active Contour Models », International Journal of Computer Vision, Kluwer Academic Publishers, 1988.

[Sonka 1998] Milan Sonka, Vaclav Hlavac, and Roger Boyle, Image Processing, Analysis, and Machine Vision, book (2nd Edition) published by PWS - an Imprint of Brooks and Cole Publishing in 1998, ISBN 0-534-95393-X.

[Collet 1998] Collet C. and Gherbi R., Integration of visual perception tools for natural interaction, a Gaze capture and tracking system", in proc. of IEEE Inter. Symposium on Image Analysis and Interpretation, Tucson, USA, April 5-7, 1998, pp 91-97.

[Braffort 1998] Braffort A. and Gherbi R., Video-Tracking and Recognition of Pointing Gestures using Hidden Markov Models, in Proc. Of IEEE Inter. Conf. on Intelligent Engineering Systems, Vienna, Austria, September, 1998.

[Eisen 1998] ScanAlyze : Process fluorescent images of microarrays. Includes semi-automatic definition of grids and complex pixel and spot analyses. Written by Michael Eisen at hhp://rana.lbl.gov/EisenSoftware.htm. Eisen et al. (1998) PNAS 95:14863.

Size sample characterization for background statistical measurement in CDNA microarray image using multiple experiments

Christophe Gouinaud
LIMOS-ISIMA
Campus des Cezeaux
B.P. 10125
63173 Aubière CEDEX
+33 473 405 041
gouinaud@isima.fr

ABSTRACT
Measurements of gene expression with cDMA microarray are not error free. After image acquisition with scanner, the image processing software use background statistical measurement to reduce this kind of error. Safety of this process needs robustness statistical measurements that can be reached with a good number of sample pixel. This work describes a characterization of background measurement robustness with to scanner and to sample of blade. This improve the minimum size of sample to use for good measurements.

KEYWORDS
cDNA microarray, image processing, background, noise, statistical measurement

1. Introduction

The use of cDNA microarray technique is growing. In the beginning, these techniques provided quasi-binary measures of gene activation so it was possible to have large measurement errors in the measures of expression with no consequences because these measures were not used precisely. Now the ``spotage" technique is commonly used, the hybridation chain has been improved and the scanners are used correctly, and if of course implies that users of this technique find the need to exploit the gene expressions [Tu 2002] in a more quantitative way.

From that fact, errors committed during the treatment of image phase permitting the quantification of the gene expressions may become from unimportant to extremely damaging to the experiment results.

Most cDNA image processing software for microarray use algorithms of detection and of quantification which are based on the statistics of the first order, mean (μ), standard deviation (σ), and the coefficient of variation (σ/μ). These measures impose minimal size of the samples, especially on the high dynamic images acquired in a coherent light. In a practical point of view, this signifies that the spots and spaces that separate them must be of sufficient size so that the inevitable artifacts, such as dust, and the normal variations of the experimental process will not give statistics that do not represent the expressions [PETROV-2002].

The manufacturing blades it expensive, so the biologists have a tendency to put as many spots as possible on one blade. To this we add the fact that increasing the distance behind the spots enlargement the area to scan so generates bigger images. This extends the treatments and complicates the data storage.

We now see that there is an opposition here between the quality of the results and the easiness, see possibility, of the realizations. Therefore, we propose the experiment results, permitting to clarify the magnitude of these phenomenon for the measure of noise in the image background.

To do the tests of background noise, we used two scanners of the same model and brand but we used them in two different labs in different research sites. We also used two different kinds of blades : the new blades not having had any treatment and the hybrided blades having gone through the complete chain of production of spotage and wash.

We then did, for these two groups of blades, many acquisitions on all the surfaces of the blades by adding to the conditions of experience and by doing two series on each scanner at several days interval. Two examples of acquired images of virgin blades are presented on figures 1a and 1b.

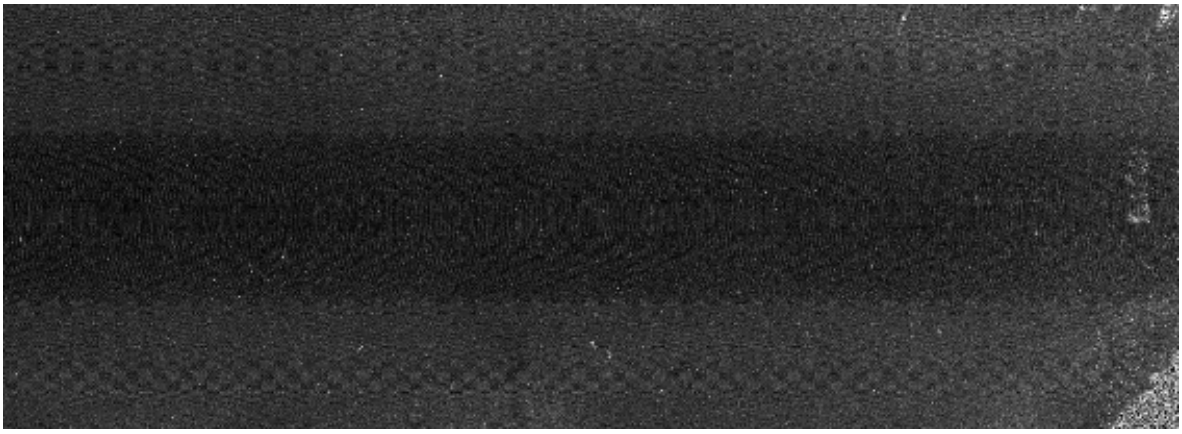

Figure 1a : Image from blade 1

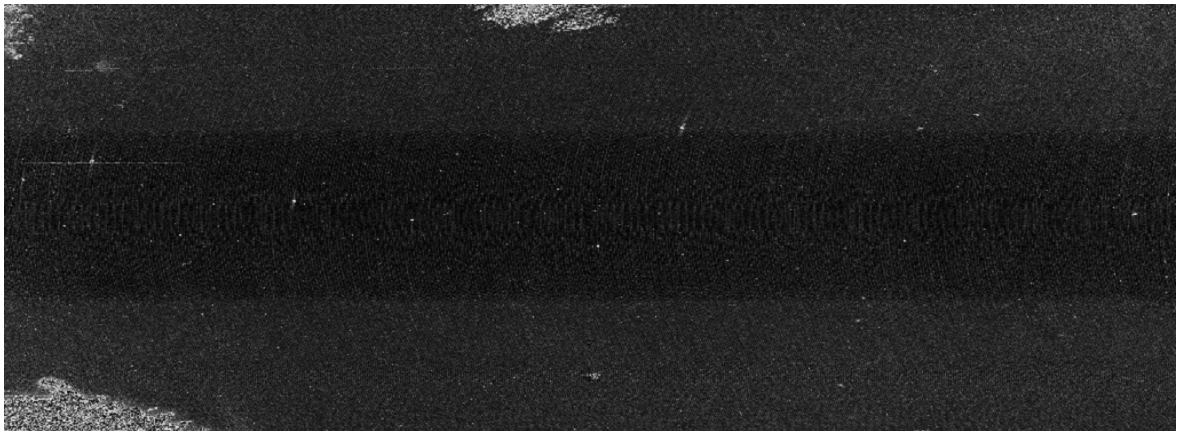

Figure 1b : Image from blade 2

All the acquisitions were done ten times so that we could estimate the variability of the noise and check our results.

The continuation of this job presents the methodology employed in the goal of getting the measure of the size of confidence intervals of the statistical measures, the results on the actual images and gives an estimation of the spaces inter-spots to observe so that we will get the correct measurements.

In this paper, an first section expose a rapid survey of background noise measurement lake consequence, a second deal with size of sample needed to obtained robust estimation of usual first order statistical measurement, and a last show guide line to choose the value of the distance behind the spots to accurate measurement.

2. Impact of error in background measurement

Source of noise are multiple when scanning a CDNA micro-array. Microarray scanners use coherent laser to illuminate blade therefore direct returning signal background look like speckle [BARA-2003]. This signal is sum with dust backscattering and other source of noise. So the distribution resulting in combination of many phenomena is unknown and obtaining a good estimation of background behind the spots is not easy. We must be careful about background noise measure quality because it modifyis the measurement of gene expression in two principal ways:

- Image segmentation for spot shape detection
- Quality of correction for gene expression

The segmentation determines which pixel is qualified to compute the gene expression and which pixel is qualified to determine the estimation of background noise intensity. We can determine two kinds of segmentation method [PAL-1993] : pure space segmentation and pure intensity based segmentation. The first class uses an ideal spot model, like circle, and the segmentation algorithm compute the size and the position that match the real spot. These operations use the background measurement and maximize the statistical contrast behind the inside and the outside of a ideal shape. In this case misestimating the background pixels values implies an important error because the size of the shape grows or decreases quickly. The second class of segmentation method uses intensity of pixel for segmentation [Bergemann-2004]. This technique use statistical measurement and threshold on pixel value to assign a class. A misestimating value of background pixel result in migrating pixel behind spot class and background class so incorrect segmentation can be small or total. Error of segmentation can be limited when we used enhanced segmentation algorithm, like quasi Markov field [GOUINAUD-2001] [DEMIRKAYA-2005], or correction technique like morphological analysis [THERNEAU-2002]. But, we notice that most segmentation techniques assume a safe measurement of background and therefore need it.

Quantification of the gene expression is the process, which deals with the intensity measurement of pixels that are identified as spots pixel. Commonly, the pixel values in a channel are computed in a mathematical function to give one value by spot. The values obtained in both channels are combined to give the gene expression. Expression used in this process currently are mean, median, mode or volume combined in a quotient expression [PETROV-2002] of the spotted pixels. There where many paper in this domain, and many authors propose many expressions but the majority of those used the local mean background value behind spots and assume that it's was a safe value [BROWN-2001][CHEN-1997][TSENG-2001].

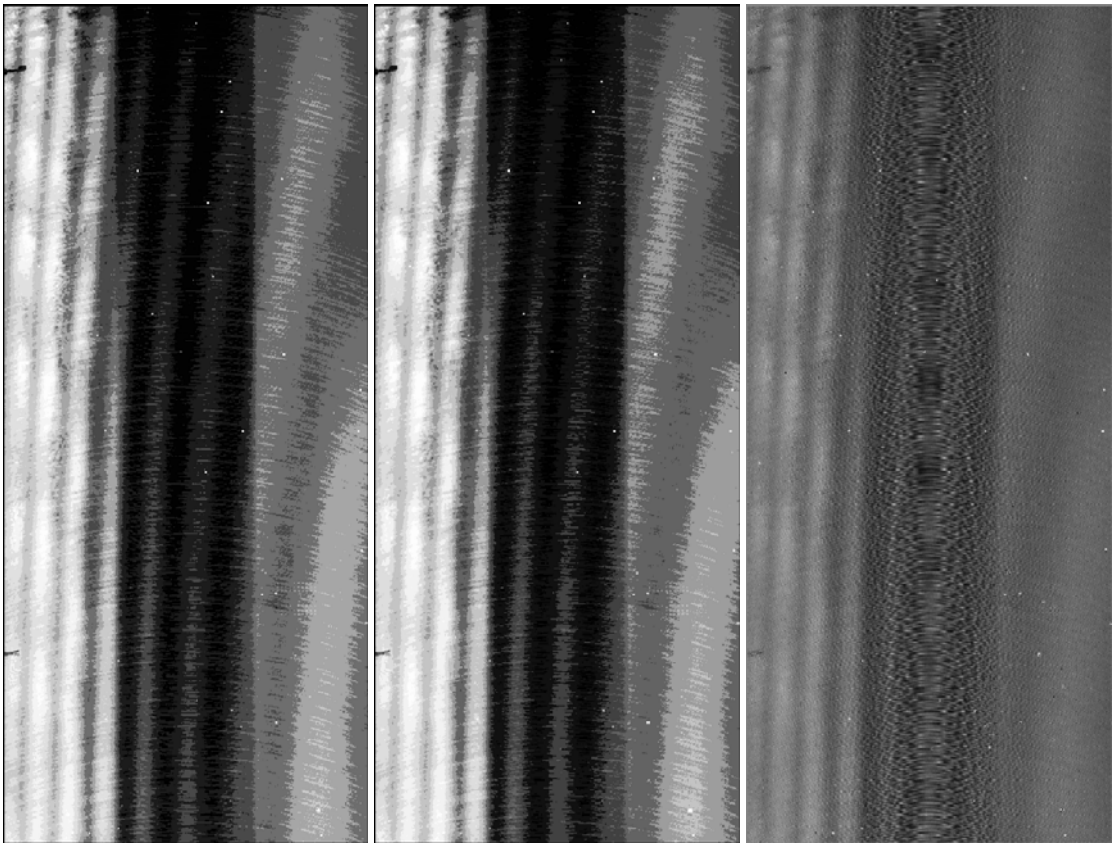

Figure 2a: 11x11 mean image Figure 2b: 12x12 mean image Figure 2c: Difference image

To shown that this assumption does not corer the general case, we do the following experiments. We scan a virgin blade with a scanner with cy3 channel at maximum resolution. That gives an image as shown on figure 1b. We compute two new images by change pixels value to mean value of there 11 by 11 neighbors for the first and 12 by 12 for the second . The result is show respectively in figure 2a and 2b. We show in figure 2c the difference between the two preceding images. When

we use micorarray image processing software the small variations of background are hidden by the brightness of fluorescents pixels, but in most cases its should be not neglected.

If the estimation of mean is robust, the two images must be the same and the difference must be a black uniform image. The mean of difference between the two mean images represent ten percent of these values. So we must conclude that this estimation of mean, respecting current used sample size, is not error free. In this images we can also see that they are not uniform. This fact shows that a simple variation of position in the images can affect the background statistical measurement. This experiments show also the effects of dusts. They generate brightness square value in the mean image so they can also modify first order statistical measurement.

An error of background measurement necessarily modifies the gene expression and may cause wrong interpretation of the biological phenomenon. This kind of error cannot be ignored because they influence all the image processing for given gene expression. That was the reason because we make the following tests to quantify background statistical variations.

3. **Estimation of the quantity of back noise**

This part is dedicated to the evaluation of the variation of the first order statistics of background noise. We choose to present here the same methodology of measurement for the results in two types of experimental conditions : the measure of two virgin blades at constant PMT gain and the measure of one group of virgin blades and one group hybrid blades with a variable PMT gain. We limit our work to study the stability of mean, standard deviation and variation coefficient because there are the most currently used measurement and their behaviors are known to be representative of first order statistical measurement [KENDAL-1952].

3.1. **Methodology**

To study the viability of the statistic measures of the first order (mean, standard deviation, variation coefficient), we do the following:

1. We select an image
2. We select one position from a poissonian process
3. We calculate the statistics at this position for a square sub image window of size t_{max} pixels by t_{max} pixels
4. Then we calculate the same statistics for a window of size t pixels by t pixels with t taking value from t_{min} to t_{max}
5. We write down if the statistic S(t) on the values of the pixels of size t . t looks like:

$$S(t_{\max}) * 0.94 < S(t) < 1.06 * S(t_{\max}) \qquad \text{(A)}$$

   where S(t) is the "statistics" value for a sample of size t^2.
6. We repeat this computation for 10000 positions in the image so we build an estimation of the probability to be in the confidence interval depending on the size of the sample.

We do the experiments on all our images by separating the results obtained on the series at constant PMT from those obtained on the series of images with a PMT variable. Of course, the measures are done on sections of the blade where there are no artifacts of the manipulations done by the operator (scratches, fingerprints ...) and no spot for blades that have be spotted and hybrided. This selection was done in image, not when scanning, because we want see there global effect and not there local action.

3.2. **Results obtained at constant PMT**

The results obtained on two different blades, acquired on the two scanners with 10 samples are presented in a chart on the figures 3, 4 and 5 for the mean, standard deviation and the coefficient of variation in Cy3 and Cy5.

Blade/Channel	1/cy3	2/cy3	3/cy3	4/cy3
Scanner 0	1089=33x33	900=30x30	1156=34x34	1089=33x33
Scanner 1	1225=35x35	1156=34x34	961=31x31	900=30x30

Figure 3 : Size of a sample required to ensure compute the means of background noise with 95 % of confidence.

Blade/Channel	1/cy3	2/cy3	3/cy3	4/cy3
Scanner 0	1444=38x38	1444=38x38	1444=38x38	1369=37x37
Scanner 1	1444=38x38	1444=38x38	1369=37x37	1369=37x37

Figure 4 : Size of a sample required for a valid computing of the standard deviation of background noise with 95 % of confidence.

Blade/Channel	1/cy3	2/cy3	3/cy3	4/cy3
Scanner 0	1369=37x37	1369=37x37	1296=36x36	1296=36x36
Scanner 1	1369=37x37	1369=37x37	1225=35x35	1296=36x36

Figure 5 : size of a sample required to ensure compute the variation coefficient of background noise with 95 % of confidence.

These show us that the stabilization of the statistics is done for samples of 1000 pixels for the mean and of the order of 1400 pixels for the coefficient of variation. This corresponds to the windows of measures of the order of 35 * 35 to 38*38 pixels which is relatively big compared to the inter spot space normally used.

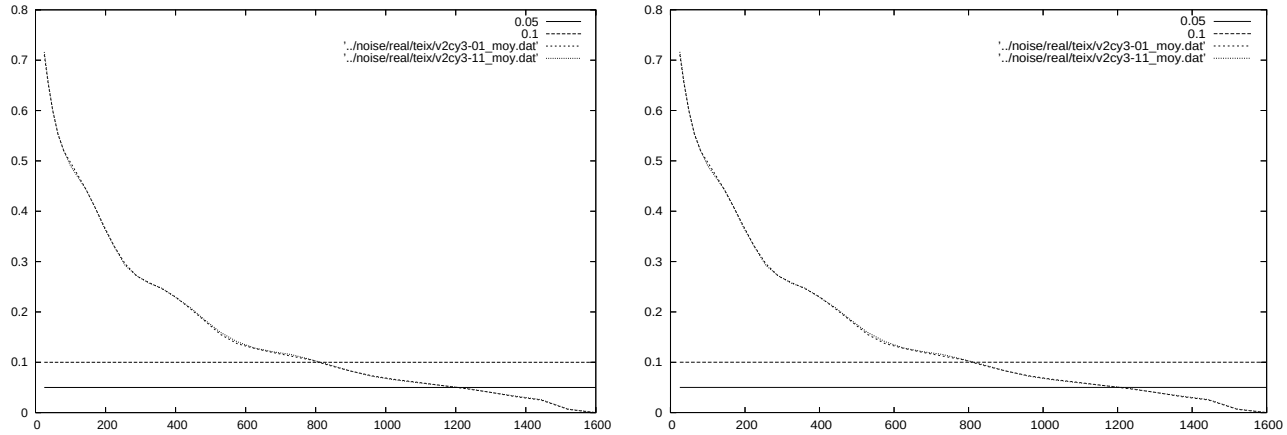

Figure 6 : Probability of mean on the left, coefficient of variation on the right value stabilization by size of sample in the Cy3 channel

To quantify the error risk put in by the obligation to hold in respect the sample sizes, we trace graphic representation of the probability to belong to the confidence interval in function of the sample size for the mean and the coefficient of variation. This gives us the curves similar to the figure 6.

On these curves, we see that the stabilization of the average around 10\% error is rapidly obtained and that, in consequence, the choice of a precise size is not too critical. The case of the coefficient of variation is much more delicate where, following the samples, we realize that the measurement variations are much more brutal which tells us that not very different samples of the measure of size could give very different measures. These brutal variations can be explained by the brutal variations of response in a vertical band that we see on certain images likes the figure 1.

3.3. **Result with a variable PMT**

The results obtained with a variable PMT on a set of virgin blades (1) and having gone through the complete process of ``hybridation'' (3) are presented on tabular of figure 8 and 9 for the mean in cy3 and in cy5 and on those of the figures 10 and 11 for the coefficient of variation.

PMT	55	60	65	70
Set 1	1024	1156	1156	1156
Set2	529	625	625	625

Figure 8: Measure of mean stabilization in the cy3 channel for a variable PMT

PMT	55	60	65	70
Set 1	1156	1225	1225	1296
Set 2	441	900	1024	1024

Figure 9: Measure of mean stabilization in the cy5 channel for a variable PMT

PMT	55	60	65	70
Set 1	1444	1444	1444	1444
Set2	1369	1369	1369	1369

Figure 10 : Measure of variation coefficient stabilization in the cy3 channel for a variable PMT

PMT	55	60	65	70
Set 1	1369	1369	1369	1369
Set2	1156	1225	1225	1225

Figure 11 : Measure of variation coefficient stabilization in the cy5 channel for a variable PMT

The results given here have been obtained in places that do not have spots. The results indicate that stabilization of the statistical measures of background noise is relatively independent for the worth of PMT, whether it is on the virgin blades or on the hybrid blades. We also noticed that the stabilization is faster on hybrid blades, which can be explained by an elimination of dust during the last procedure of cleaning. We also noticed that, in this case, the samples stay in the scales that were already fixed. The same experience done on the other scanner gave us results in the same order.

4. **Minimum size of sample**

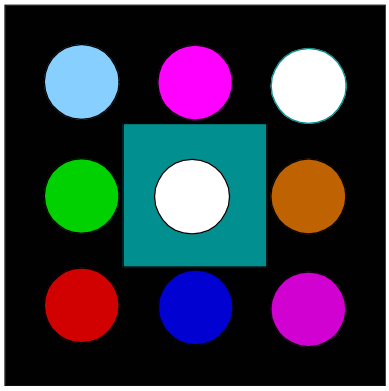

Figure 12 : Maximum background sample pixels behind spots.

The distance behind spot in microarray are define by the operator. It can be a multiple of the minimal step of the spotting robot

The maximum size of the samples that a an image processing software can use on a correctly spotted blade is equal to the number of pixels held in the biggest square centered on a spot that does not go onto the neighboring spots. This ideal surface, in grey on figure 12. This corresponds exactly to the following formula (equation B) for the spots that are supposed to be round:

$$N_{\max} = \left(\frac{2r + 2d}{P}\right)^2 - \left(\frac{\pi R}{P}\right)^2$$

(B)

Where R is the beam of spots, d is the distance between spot and the resolution of the image. The chart of figure 13 gives a look at the size of the samples in function of the different spots diameters.

D/R	5	10	15	20	25
5	321.5	586	893.5	1244	1637.5
10	821.5	1286	1793.5	2344	2937.5
15	1521.5	2186	2893.5	3644	4437.5
20	2421.5	3286	4193.5	5144	6137.5
25	3521.5	4586	5693.5	6844	8037.5

Figure 13: Number of background pixel in function interspot distance (in colums) and spot radius (in row) in pixel

We noticed that, in measurement conditions comparable to our experiments, the measures are safe with a beam of 5 for spot (diameter of 10) separated from 15 pixels. For a typical pixel size of 10 μm, this corresponds with spots of a diameter of 100 μm with their centers are distant from 350 μm. These values are at least two times superior to those noticed in the litterature. In respect to these values, It is possible to spot a square of 1x1 cm in blade with 784 samples and its permit a total of a maximum of 10976 samples for a current blade of 2x7 cm.

5. **Conclusion**

This work permits us to see that the measures can be easily filled with errors in the case of an inappropriate choice of spot size or space. It is necessary then that users of cDNA micro-array define with care the disposition of their spot on their blade while keeping in mind the disagreements stated in our paper.

It is also necessary to keep in mind that no matter the image processing software you use, if the algorithms that you use rely on statistics of the first order, the problems exposed here will be applicable. You should preferably choose a software where it is possible for simple user to change the sizes of the learn area used as well as for estimate background noise intensity as for the segmentation of spots.

We are actually continuing this work with help of theoretical approaches and with simulations with the goal to perfect a methodology pliable in an experiment framework permitting to define a confidence interval on the measures of expression or to propose a process to ameliorate the quality of measures by playing with spot positions. We will also prepare a study of the same phenomenon but dedicated to the contents of spots.

ACKNOWLEDGMENTS

I especially want to thank the Professor P. Peyret of the lab of biology of protistite of the University of Auvergne and Mme Christiane Deval of the center Theix of INRA for the charring of their material.

REFERENCES

[BARA 2003] V. Barra, C. Gouinaud, Simulation of microarray image experiments, SCSC 2003, in proceeding, pp, 2003

[BERGEMANN 2004] TL Bergemann, RJ Laws, F. Quiaoit, LP Zhao, A statistically driven approach for image segmentation and signal extraction in cDNA microarrays, Journal of Computationnal Biology,11(4), 695-713, 2004

[BROWN 2001] C. Brown, P. C. Goodwin, P. K. Sorger, Image metrics in the statistical analysis of DNA microarray data, PNAS, 98(16), 8944-8949, 2001

[CHEN 1997] Y. Chen, E. R. Dougherty, M. L. Bittner, Ratio-based decisions and the quantitative analysis of CDNA microarray images ,Journal of biomedical optics, 2(4), 364-347, 1997

[DEMIRKAYA 2005] Dermirkaya, Musa H. Asyali, M. M. Shoukri, Segmentation of Microarray cDNA Spots Using Markov Random Field Modelling, Bioinformatics, in press, 2005

[KENDAL 1952] M. G. Kendall and A. Stuart, The Advanced Theory Of Statistics, Charles Griffin and Company -Limited London and High Wycombe, 1952

[GOUINAUD 2001] C. Gouinaud, v ; Vidal , C. D'incan , An method for spot detection an qualification in microarray image, In proceeding JOBIM 2001, 197-199, 2001,

[PAL 1993] NR Pal, SK Pal, A review on image segmentation techniques. Pattern Recognition,26,1277-1294, 1993

[PETROV 2002] A. Pretrov, S. Sha, S. Draghici, and S. Shams, Microarray Image processing and quality control, Microarray Image Analysis-Nuts \& Bolts , 6, 99-130, 2002

[THERNEAU 2002] T. Therneau, R. C. Tschumper, D. Jelinek, Sharpening spots : correcting for bleedover in cDNA array image, Mathematical Biosciences, 176(1), 1-15, 2002

[TSENG 2001] G. C. Tseng, M. Oh, L? Rohlin, J. C. Liao, W. H. Wong, Issue in cDNA microarray analysis : quality filtering, channel normalization, models of variations and assessment of gene effects, Nucleic Acids Research, 29(12), 2549-2557, 2001

[TU 2002] Y. Tu* , G. Stolovitzky*, and U. Klein, Quantitative noise analysis for gene expression microarray experiments PNAS, 99-22 , 14031-14036,2002

Visual Clustering and Exploration of Splicing Sites using DNA Curvature Criteria

C. Toffano-Nioche IBP/LIMSI CNRS
N. Férey LIMSI CNRS
F. ben Hadj Ali LIMSI CNRS
J. Hérisson LIMSI CNRS
R. Gherbi LIMSI CNRS
Université Paris-Sud XI - BP 133
F-91403 Orsay
+33 (0) 1 69 85 81 64
genoteam@limsi.fr

ABSTRACT

The aim of this paper is to explore the clustering capabilities of our visual genome explorer software. *Genome3DExplorer* is a new modeling and software solution to explore textual and factual genomic data. It offers a powerful and user-centered visualization of this information within an immersive environment. The visualization is based on a graphical paradigm that automatically helps to build a graph-based representation. Based on *Genome3DExplorer*, this paper addresses a new 3D-based clustering method of spatial DNA trajectory. We applied this method to sets of 3D representations of DNA sequences focused on splicing sites from the plant *Arabidopsis thaliana*. With the aim of merging the capabilities of clustering of *Genome3DExplorer* with more classical clustering methods, we design a clustering tool based on *K-Means* algorithm. We adapted the *K-Means* algorithm to the both huge and geometrical features of our genomic data, according to the spatial shape of the DNA trajectory. By clustering genomic data via geometrical criteria, it will be possible to investigate relationships between structure and function for some of these data with the study of the clusters content.

KEYWORDS
Visual Mining, Graph-Based Visualization, Genomic Data Clustering, DNA Curvature.

1. Introduction and State of the Art

DNA is generally considered by its only primary sequence (succession of bases A, T, G, and C). A new way of studying this molecule is to increase such representation by its *in silico* spatial conformation information. One main parameter which gives the shape of naked DNA in solution is the intrinsic curvature. It is mainly caused by the deviations, which occurs by the repeating of some short patterns phased with the helix periodicity and are controlled by the energy of the base stacking. The deviations of local crystal structure geometries of B-form DNA from idealized fiber diffraction coordinates can be modeled in space by only considering three rotation angles: the *tilt* τ, the *roll* ρ and the *twist* Ω (relatively around to the Ox, Oy, and Oz axes) [Calladine 1988; Olson 1995]. Some experiments [Bolshoy 1991] demonstrated that these angles are variables according to the type of the transition between the $(n\text{-}1)^{th}$ base-pair step and the n^{th} step. An additional parameter – the translation length along the DNA axis (the *rise* h) – is also needed to model the distance between two successive base-pairs steps. Many biophysical [Bolshoy 1991; Koo 1988] and biochemical [Gorin 1995; Satchwell 1986] experiments or computations [Cacchione 1989] have led to create tables gathering all the plate rotation angles. They can be distinguished by the way they explain the curvature origin (*junction* vs. *nearest-neighbor* models, the last one being composed by non-A-tract and A-tract models).

Consequently, the modeling of DNA spatial structure of genomic sequences seems to be an interesting and complementary study. We access to this spatial representation by the way of *ADN-Viewer* [Hérisson 2001; Gherbi 2002]. *ADN-Viewer* is interactive software for the spatial modeling and visualization of naked DNA sequences at several representation levels (from gene to chromosome).

One of the main observations provided by such visualization is that two DNA sequences textually different in sense of alignment can have close spatial conformations. It thus seemed interesting to carry out studies on the relation between the intrinsic DNA curvature and some biological questions. By clustering genomic data via a spatial geometrical criterion and then study-

ing the produced clusters contents, it will be possible to investigate relationships between structure and function for some of these data.

We used *Genome3DExplorer* that allows representations in 3D of relationships between data, to represent spatial geometrical criteria of sets of DNA sequences. The genomic data sets used are intron/exon sequences focused on splicing sites (acceptors and donors) from the plant *Arabidopsis thaliana.*

The first section describes genomic data we choose and the successive transformations we apply to them. The aim is to obtain a numerical criterion that stands for intrinsic curvature of the sequences and that will be used for clustering. The two next sections detail two clustering methods we present: a *K-Means* based clustering and our visual approach with *Genome3Dexplorer*. We expose modifications we implement in order to fit algorithms to the peculiar features of our geometrical and huge data. By comparing our results *vs.* a *K-Means*-based clustering method we assume that the 3D visualization of data and its dynamic management of the space of representation could be used as a new clustering method. Our 3D-based method improves classical clustering results in term of analysis.

2. Material

This section presents genomic data and the computation applied to them: the set of genomic sequences concern some splicing sites of the dicot plant *Arabidospis thaliana*. Figure 1 shows successive processing steps we apply to the textual sequences of the splicing sites. We first compute the 3D trajectory of these sequences and their intrinsic curvature. This DNA curvature is used as criteria for the K-Means clustering and for the *Genome3DExplorer* representation. The last step concerns the visual exploration of the cluster contents.

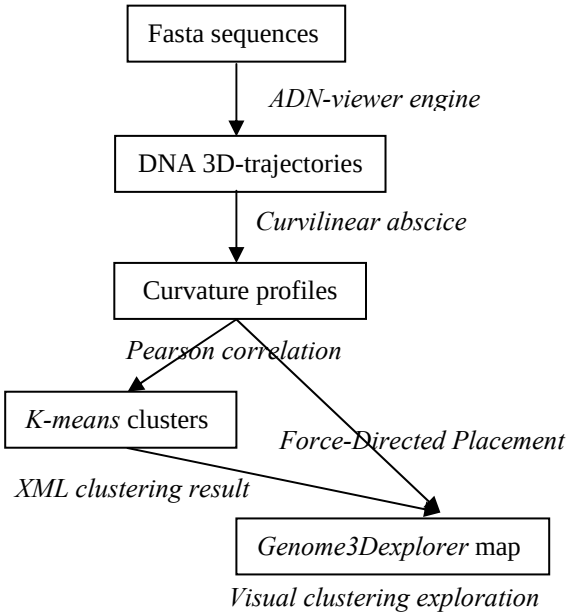

Fig. 1. Successive processing steps of the data.

2.1 **Data sets of *Arabidopsis thaliana* splicing sites**

Most of the protein-coding genes of higher eukaryotes contain sequences, named introns, which interrupt their coding region. During process that go from genomic sequence to protein, only exons are translated. So recognize exon from introns is an interesting biological problem. Many methods exist to define gene structures. They exploit experimental data at different levels, but most of them use software predictions [Hebsgaard 1996; Lukashin 1998]. And it is well-known that many errors occur in the definition of gene structures during the annotation phase of a genome [Pavy 1999; Kyrpides 1999; Cruveiller 2004]. So, more using experimental evidences and/or improving efficiency of *in silico* predictions are needed solution. With this aim, we explore the modeling of DNA spatial structure in order to address relationships between structure and function in the context of gene structures.

From the complete genome of the dicot plant *Arabidopsis thaliana* [AGI 2000], we define a data set that focus on splicing sites. We extract sequences for both donor region, at the 5' intron side (exon first, intron next), and acceptor region, at the 3'

intron side (intron first, exon next). We choose intron sequences from genes belonging to paralogous genes (a family of genes into a same organism). The family is concerned RNA-helicases (involved in nucleic acid unwinding) with DEAD-box motif into their protein sequence (D for Aspartic, E for Glutamic, A for Alanine). This family contains 56 genes in *Arabidopsis thaliana* [Boudet 2001]. Here, gene models can be the result of experimental work or generated by bioinformatics prediction software, but with a curated and experimental view [Mingam 2004].

We extract splicing site-centered sequences of 200 bp. This set of sequences contains 195 sequences of 200 bp, of both donor and acceptor splicing sites (100 and 95 sequences respectively). Number of sequences differs due to the size constraint of each splice site flanking regions.

From these sequences, we next compute three datasets of DNA trajectory and curvature in order to test different biological features (figure 2):

- On the first dataset, we attempt to sort donor sites *vs.* acceptor sites of 200 bp into 2 clusters.
- On the second one, we do to the same thing but using a smaller centered window of 100 bp.
- On the third dataset, we segment data around both acceptor and donor sites and test sorting into 4 clusters following the intron or exon type of the sequence.

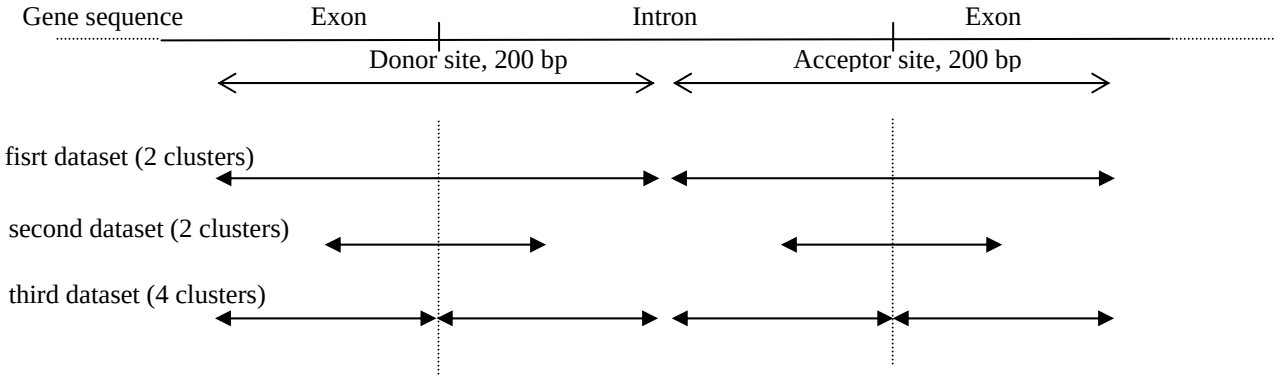

Fig.2. Sequences (thin arrows) and computed (full arrow) datasets of splicing sites.

2.2 **From DNA primary sequence to spatial trajectory**

To build the spatial structure of DNA, two kinds of input data are required: primary DNA sequence in textual format and, a spatial conformation model that offers a rotation table and a translation value. Based on gel migration decay of sequences, the [Bolshoy 1991] model gives theses components. The sketch of the used algorithm is detailed here and illustrated by the figure 3 below on an example:

(1) The first nucleotide/letter (C) of the textual sequence is read. A C-G plate centered in (0.0, 0.0, and 0.0) is placed without any geometric transformations.

(2) Then, the second nucleotide (T) is read. The second plate T-A is superimposed on the first one. The three angular values corresponding to the TA entry in the rotation table are applied. And after, the last-added plate is translated in an orthogonal way with the first one.

(3) And so on for each nucleotide of the textual sequence (A next C in figure 3).

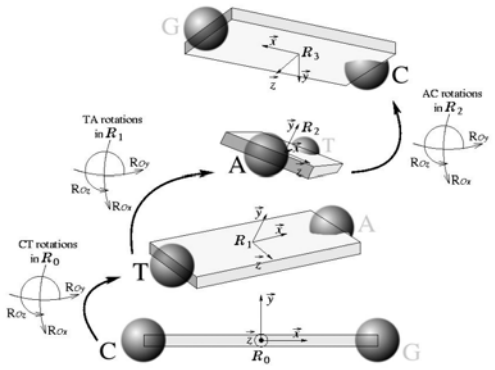

Fig. 3. The spatial structure of DNA is built recursively along the sequence.

The *ADN-Viewer* software [Hérisson 2001; Gherbi 2002] carrying out this algorithm for long DNA sequences is implemented using C++ language on a Linux-based PC computer. The graphic part is based on standard Open-GL® graphic library and the GUI one is managed using Qt toolkit (Trolltech©).

Once the DNA sequence trajectory is computed, we need to define a method that gives a numerical parameter on which based a clustering tool. We are interesting with the intrinsic curvature of DNA.

2.3 **Intrinsic curvature of DNA**

Many methods exist to compute the degree of curvature of a spatial trajectory. For our purpose, we used a method called curvilinear abscissa. For each spatial co-ordinate representing a base pair P_i, we compute its curvature degree:

$$Curve = \frac{1}{2\pi} \frac{\Delta\varphi}{\left\| \vec{v}_i \right| - \left| \vec{v}_{i-1} \right\|} \quad (1)$$

It is an approximated and normalized curvature, computed from three successive points: P_i–*granularity*, P_i, P_i+*granularity* (figure 4).

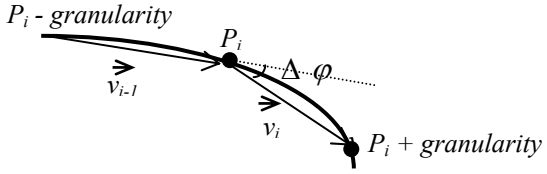

Fig. 4. Variable meanings of the curvilinear abscissa method.

This method uses two parameters, a step and a granularity. For the present study, we fix both step value and granularity value to 1bp (all the nucleotides are processed) and 40 bp, respectively. So computation of a sequence of 200 bp or 100 bp give respectively 120 or 60 values of curvilinear abscissa.

3. **3D-based clustering using generic home-made *K-Means* algorithm**

K-Means algorithm is considered as a non-hierarchical clustering method that requires fixing the maximal number of clusters. *K-Means* was first proposed by [MacQueen 1967] and it convergence properties are well-known [Bottou 1995]. *K-Means*, as described in the literature [Berkhin 2002], has to compare at each iteration all the data of the same cluster to compute the new centroid of this cluster, defining in this way new clusters at the next iteration.

The aim of *K-Means* is to minimize the intra-cluster distance and, in the same time, to maximize the inter-cluster distance:

$$Intra = \frac{1}{N} \sum_{j=1}^{N} \frac{1}{\left\| C_j \right\|} \sum_{x \in C_j} \left(x - z_j \right)^2$$

where *x* objects are data of the same cluster, N is the clusters number, and *z* represent centroids of the clusters. The criteria measurement "Inter / Intra" has to be maximizing in order to obtain the best result during clustering iterations.

To the specific study of huge genomic spatial trajectory data, we developed a generic *K-Means* algorithm able to build clus-

$$Inter = \min\left(\left(z_i - z_j\right)^2\right)$$

ters of any kind of data, with only few required modifications to be application specific. The user may provide a distance function between two data, in a C++ class that will describe the data.

In this study, the distance computed between two intrinsic curvatures is the Pearson correlation coefficient. This mathematic function returns a number between 0 and 1 depending on the likelihood of the intrinsic curvature compared. The 1 value means that they are highly correlated, while -1 value means that they are anti-correlated.

4. Visual Mining using dynamic graph paradigm

In this section, we describe how we use visualization of a huge of data in an immersive environment as a complementary analysis to classical clustering methods. We first present the description language of *Genome3DExplorer* that allows an efficient representation of genomic data. At a second time, we expose the immersive and dynamic paradigms we define to introduce dynamic into the visual graph in such way to represent the multiple binary relationships between objects in the 3D space. The resulting topology reflects the concept that objects of the same vicinity share the same features. Then, the immersive visualization within a virtual reality context gives access to the analysis and it's the meaning of our visual clustering.

4.1 Representation of huge data

In order to visualize those huge and heterogeneous data like genomic ones, *Genome3DExplorer* [Férey 2004] was developed in a virtual reality environment.

Factual genomic databases are often focused on biological objects of interest (protein, gene, *etc.*), described by a set of attributes. Attribute values can be of string type (label, genetic sequence), numerical (like co-occurrence score, alignment measurements), or symbolic type (type of interaction like positive retroaction). Moreover, these objects are compared one to another by a measurement (sequence alignment score, functional similarity).

Taking account of these characteristics, *Genome3DExplorer* uses the concept of multi-valuated objects and multi-valuated binary relationships. The characteristics of this federator description language based on XML, allow the display and storage of most of genomic data. It looks particularly well adapted to the heterogeneity and variability of the genomic data.

4.2 Graphical representation in immersive environment

We now need to transform the data representation language to a visual representation that defines a visualization paradigm. This paradigm has to be adapted as well for this genomic data and for the user's needs.

Our XML-based language describes a list of valuated objects with their binary valuated relationships. We interpreted these data as a graph, where vertices are biological objects and edges are relationships. Within a graphical framework, we developed a visualization of such data by a 3D graph. Numerical relationship values may be visualized by edge length, edge weight, edge color, or edge transparency. Each symbolic value may be represented by a predefined shape (cube or sphere for nodes, and cylinder or line for edges) or color label (red, green, blue), according to the kind of value (object or relationship value). Finally, user can visualize string values by a 3D text label within the graph representation.

Numerical relationships of the present case study can be visualized naturally by edge length. However, this implies to resolve the following problem: mapping numerical value to an edge length (distance between two vertices) adds geometrical constraints in 3D Euclidian space. In some cases, these constraints cannot be solved in a pure geometrical way. For example, figure 5 shows a graph (3 vertices and 3 edges) that can never be drawn in a Euclidian space respecting the strict distance edges constraints.

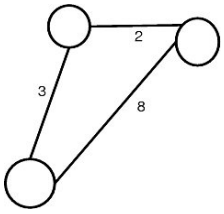

Fig. 5. Geometrical length constraints without graphic solution.

To deal with this kind of representation, *Genome3Dexplorer* uses the [Eades 1984] approach, which consists in simulating two kinds of force between graphical objects. In order to place two connected vertices respecting distance constraints, Eades proposed to apply them an attraction force. The algorithm minimizes thus the gap between an initial random Euclidian distance in the 3D graph and the desired one. Moreover, a repulsion force is applied on two close vertices, which are not in a relationship. After several iterations, this dynamic property allows the system to converge into a solution where all the distances are as closed as possible as desired edges lengths.

Within an immersive environment, *Genome3Dexplorer* takes advantage of both virtual reality environment and human perception skills in order to enhance visual interpretation of a huge amount of data. The relief assured by active stereoscopy and large screens (2 of 2x2 m2 at LIMSI-CNRS lab) increase the depth perception and helps the understanding of concepts that are not revealed on a conventional desktop environment. *Genome3Dexplorer* thus allows biologists to navigate within the 3D graph in order to explore the organization and the topology of their databank. We assume users can use their human visual capabilities to process a clustering of genomic data.

5. Results and discussion

In order to test if naked-DNA curvature may be used as discriminent criteria between intron and exon sequences, we followed an approach using both *K-Means* and visual clustering methods. We applied successively the two methods *K-Means* and our visual clustering with *Genome3DExplorer* on the three datasets of intrinsic curvature computed from genomic data described in section 2. Both methods use the same distance measurement: the Pearson correlation performed on DNA curvature profiles. So *Genome3DExplorer* uses the same correlation as *K-Means* in order to place data in the 3D space. We compute the curvature profile of the whole sequences studied using *ADN-viewer* and apply *K-Means* on the correlation of those profiles. To compare *K-means* to our visual clustering method, we visualize *K-means* results in *Genome3DExplorer* where color of node discriminates *K-Means* clusters. In figures 6, 7, and 8, node stands for splicing site sequence, while edge stands for a significant correlation curvature of the two sequences linked. Moreover, spheres and boxes represent donor sites and acceptors sites respectively. We can first validate clustering by visualization using *Genome3Dexplorer* to the *K-Means* results. Figure 6 shows that the spatial organization obtained after applying the forces paradigm gives clusters that share the same dichotomy than *K-Means* clusters.

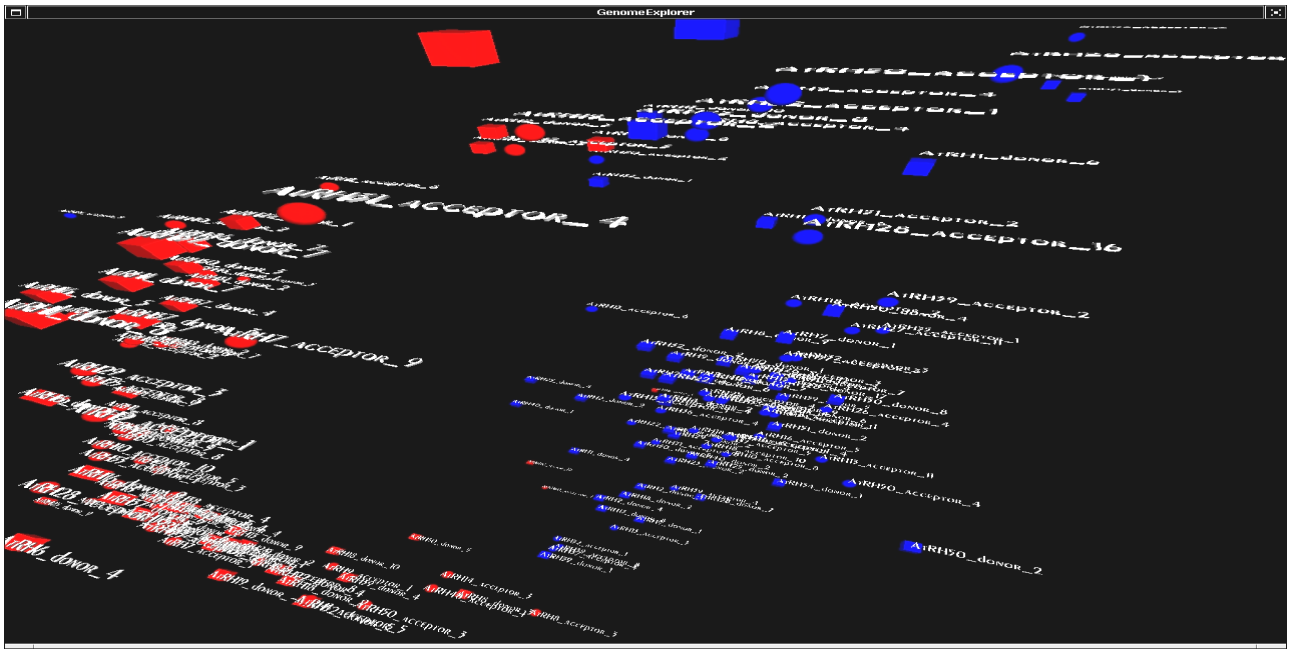

(a) first dataset

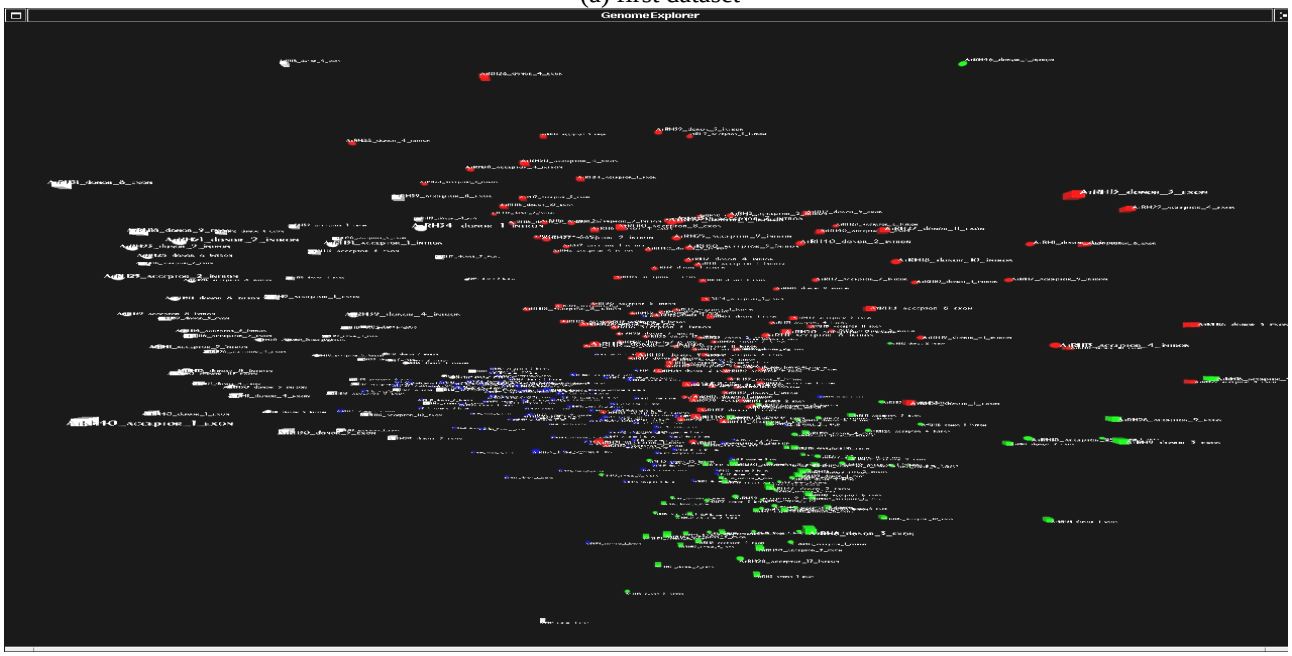

(b) third dataset

Fig. 6. For the two numbers of clusters tested, *K-Means* and *Genome3DExplorer* provide coherent results: two and four distinct visual clusters, respectively, blue/red (a) and blue/red/green/white (b). Spheres and boxes stand respectively for acceptors and donors while colors discriminate *K-means* clusters.

Genome3DExplorer implements different methods in order to increase its capabilities. One of them consists of applying a relationships threshold below which nodes are unconnected. Thus, computation and visualization concern only the connected nodes. If this method first decrease the complexity, it also allows the user to precisely explore relationships between data in a same cluster. An example is given in figure 7 where two threshold values change the extend of the visual cluster.

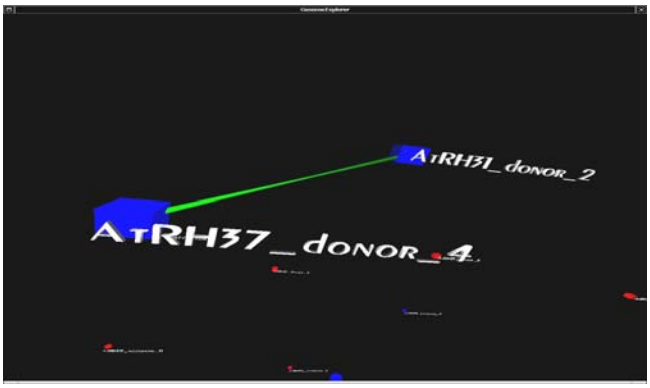

(a) second dataset, threshold of 0.025

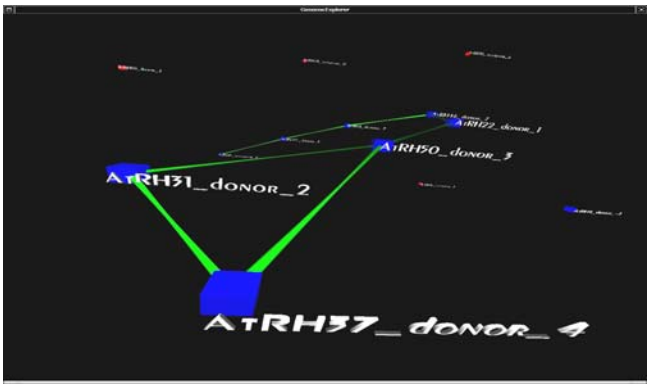

(b) second dataset, threshold of 0.04.

Fig. 7. Example of a cluster revealed by *Genome3DExplorer* threshold. Spheres and boxes stand respectively for acceptors and donors while colors discriminate *K-means* clusters. Green edges are relationships above the threshold.

Finally, *Genome3DExplorer* is able to manage a huge amount of data. Figure 8 gives three examples of this.

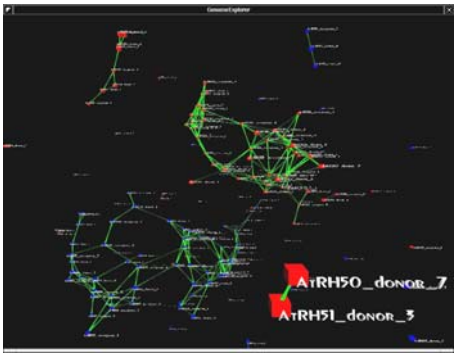

(a) second dataset, threshold of 0.05

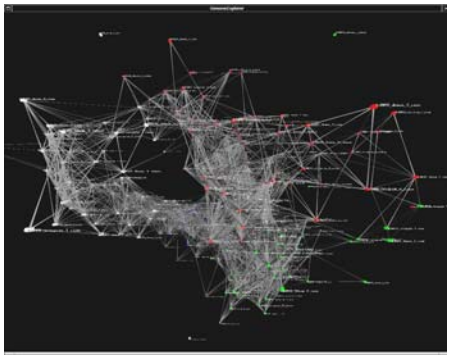

(b) third dataset, threshold of 0.15.

(c) first dataset, threshold of 0.15.

Fig. 8. Examples of visual clustering of a huge amount of data. Spheres and boxes stand respectively for acceptors and donors while colors discriminate *K-means* clusters.

5.1 Comparison of both clustering methods

When using *K-Means* and performing some statistics on the two clusters, we did not observe significant biological interpretation. The same lack of biological interpretation still stay with our visual clustering method. Taking into account on curvature, the two clustering methods do not allow us to characterize splicing regions, and many clusters contain both acceptors and donors sequences. However, we can observe using *Genome3DExplorer* several sub networks when the user fixes a threshold. These biological results have to be interpreted in future works. Indeed, figure 7 is an example of a cluster of biological interest (all the nodes are donors sites). We could assume that several splicing sites share the same spatial trajectory. Our results suggest that naked-DNA curvature is not a sufficient criterion to sort splicing sites between donor or acceptor ones.

5.2 Some biological discussions

We have compared the two clustering methods.

One the one hand, *K-Means* needs the number of clusters *a priori*. Moreover, this method does not allow knowing the relative position between elements into the same cluster (it is a black box for biological interpretation). Finally, the algorithm is sensitive to initialization phase, and output clusters are disjoined (need Fuzzy *K-Means* to obtain an overlap clustering).

On the other hand, *Genome3DExplorer* gives user a direct visual clustering. It is useful for interpretation without notion of clusters *a priori* (no problems of disjoined cluster, or cluster number…), and the visualization of whole data at the same time is possible. In this study, we can conclude that our visual clustering method allows us to visualize *K-Means* results and gives much more results than *K-Means* only. Indeed *Genome3DExplorer* takes advantage of both virtual reality environment and

human perception skills in order to enhance visual interpretation of a huge amount of data. *Genome3DExplorer* allows biologists to navigate within the 3D graph in order to explore the organization and the topology of their databank. We assume users can use their human visual capabilities to process a clustering of genomic data.

6. Conclusion and prospects

We present here a new method for DNA sequences analysis based on the predicted 3D trajectory and curvature of DNA. We use two complementary methods to analyze our datasets, *K-Means* and *Genome3DExplorer*. *K-Means* is a well known method to cluster data according to distance measurements between two data. *Genome3DExplorer* is based on a 3D dynamic graph paradigm that can be used to represent relationships between data. The genomic data used to highlight our method are intron/exon sequences from the plant *Arabidopsis thaliana*. By clustering genomic data via a spatial criterion, we investigate relationships between structure and function for some of these data. We assume that it could be done by studying the clusters contents. The immersive exploration of the 3D graph we present can be viewed as human-centered clustering methods. This is a complementary method to our generic home-made *K-Means* clustering algorithm. We show that *Genome3DExplorer* provides fine capabilities of clustering and allows the study of the clusters contents. Even the weakness of biological results presented in this paper, we highlighted our complementary clustering method based on trajectory and curvature of DNA sequences.

ACKNOWLEDGMENTS

We thank the PPF *Bioinformatique et Genomique* project of Paris-Sud University for their partial financial support.

REFERENCES

[AGI 2000] Arabidopsis Genome Initiative *Nature* **408**, 796-815, 2000.

[Berkhin 2002] Berkhin,P. Survey Of Clustering Data Mining Techniques, Technical report, Accrue Software, San Jose, CA, 2002.

[Bolshoy 1991] Bolshoy,A. McNamara,P. Harrington,R.E. Trifonov,E.N. Curved DNA without A-A: experimental estimation of all 16 DNA wedge angles. *Proc. Natl. Acad. Sci. USA,* **88**, 2312-2316, 1991.

[Bottou 1995] Bottou,L. and Bengio,Y. Convergence Properties of the K-Means Algorithms. In *Advances in Neural Information Processing Systems*, volume **7**. MIT Press, 1995.

[Boudet 2001] Boudet,N. Aubourg,S. Toffano-Nioche,C. Kreis,M. and Lecharny;A. Evolution of intron/exon structure of DEAD helicase family genes in Arabidopsis, Caenorhabditis, and Drosophila. *Genome Res*., **11**, 2101-2114, 2001.

[Cacchione 1989] Cacchione,S. De Santis,P. Foti,D.P. Palleschi,A. and Savino,M. Periodical polydeoxynucleotides and DNA curvature. *Biochemistry,* **28**, 8706-8713, 1989.

[Calladine 1988] Calladine,C.R. Drew,H.R. and McCall,M.J. The intrinsic curvature of DNA in solution. *J Mol. Biol*., **201**, 127-137, 1988.

[Cruveiller 2004] Cruveiller,S. Jabbari,K. Clay,O. and Bernardi,G. Incorrectly predicted genes in rice? *Gene,* **333**, 187-188, 2004.

[Eades 1984] Eades,P. A heuristic for graph drawing. *Congressus Nutnerantiunt*, **42**, 149–160, 1984.

[Férey 2004] Férey,N. Gros,P.E. Hérisson,J. and Gherbi,R. Exploration by visualization of numerical and textual genomic data. *Journal of Biological Physics and Chemestry*, **4**, 102-110, 2004.

[Férey 2005] Férey,N. Gros,P.E. Hérisson,J. and Gherbi,R. Immersive Exploration by Visualization of Factual and Textual Genomic Data. *Ecole de printemps: Modélisation de Systèmes Biologiques Complexes dans le Contexte de la génomique* (Montpellier 2005).

[Gherbi 2002] Gherbi,R. and Hérisson,J. Representation and Processing of Complex DNA Spatial Architecture and its Annotated Content. *Proceedings of the International Pacific Symposium on Biocomputing*, 2002.

[Gorin 1995] Gorin,A.A. Zhurkin,V.B. and Olson,W.K B-DNA twisting correlates with base-pair morphology. *J. Mol. Biol*., **247**, 34-48, 1995.

[Hebsgaard 1996] Hebsgaard,S.M. Korning,P.G. Tolstrup,N. Engelbrecht,J. Rouze,P. and Brunak,S. Splice site prediction in *Arabidopsis thaliana* pre-mRNA by combining local and global sequence information. *Nucleic Acids Res*., **24**, 3439-3452, 1996.

[Hérisson 2001] Hérisson,J. and Gherbi,R. Model-based Prediction of the 3D Trajectory of Huge DNA Sequences. *Proceeding of the IEEE BIBE*, Washington DC, 2001.

[Koo 1988] Koo,H.S. and Crothers,D.M. Calibration of DNA curvature and a unified description of sequence-directed bending. *Proc. Natl. Acad. Sci. U.S.A*., **85**, 1763-1767, 1988.

[Kyrpides 1999] Kyrpides,N.C. and Ouzounis,C.A. Whole-genome sequence annotation: 'Going wrong with confidence'. *Mol. Microbiol*., **32**, 886-887, 1999.

[Lukashin 1998] Lukashin,A.V. and Borodovsky,M. GeneMark.hmm: new solutions for gene finding. *Nucleic Acids Res*., **26**, 1107-1115, 1998.

[MacQueen 1967] MacQueen,J. Some methods for classification and analysis of multivariate observations. Pp. 281-297 in: L. M. Le Cam & J. Neyman [eds.] *Proceedings of the fifth Berkeley symposium on mathematical statistics and probability*, Vol. 1. University of California Press, Berkeley, 1967.

[Mingam 2004] Mingam,A. Toffano-Nioche,C. Brunaud,V. Boudet,N. Kreis,M. and Lecharny,A. DEAD-box RNA helicases in *Arabidopsis thaliana*: establishing a link between quantitative expression, gene structure and evolution of a family of genes. *Plant Biotechnology Journal*, **2**, 401-415, 2004.

[Olson 1995] Olson,W.K. Babcock,M.S. Gorin,A. Liu,G. Marky,N.L. Martino,J.A. Pedersen,S.C. Srinivasan,A.R. Tobias,I. and Westcott,T.P. Flexing and folding double helical DNA. *Biophys Chem*., **55**, 7-29, 1995.

[Pavy 1999] Pavy,N. Rombauts,S. Dehais,P. Mathe,C. Ramana,D.V. Leroy,P. Rouze,P. Evaluation of gene prediction software using a genomic data set: application to *Arabidopsis thaliana* sequences. *Bioinformatics,* **15**, 887-899, 1999.

[Satchwell 1986] Satchwell,S.C. Drew,H.R. and Travers,A.A. Sequence periodicities in chicken nucleosome core DNA. *J. Mol. Biol*., **191**, 659-675, 1986.

Monte Carlo tomographic reconstruction in SPECT
Impact of bootstrapping and number of generated events

Z. El Bitar[1], I. Buvat[2], V. Breton[1], D. Lazaro[2] and D. Hill[3]

[1] Laboratoire de Physique Corpusculaire, CNRS/IN2P3, Université Blaise Pascal, 24 Avenue des Landais, 63177 Aubière Cedex 1, France

[2] INSERM U678, CHU Pitié-Salpêtrière, 91 Boulevard de l'Hôpital, 75634 Paris Cedex 13, France

[3] ISIMA/LIMOS UMR 6158, Computer Science and Modeling Laboratory, Université Blaise Pascal, 24 Avenue des Landais, BP – 10125 ,63173 Aubière Cedex, France

ABSTRACT

In Single Photon Emission Computed Tomography (SPECT), 3D images usually reconstructed by performing a set of bidimensional (2D) analytical or iterative reconstructions can also be reconstructed using an iterative reconstruction algorithm involving a 3D projector. Accurate Monte Carlo (MC) simulations modeling all the physical effects that affect the imaging process can be used to estimate this projector. However, the accuracy of the projector is affected by the stochastic nature of MC simulations. In this paper, we study the accuracy of the reconstructed images with respect to the number of simulated histories used to estimate the MC projector. Furthermore, we study the impact of applying the bootstrapping technique when estimating the projector.

KEYWORDS

Single Photon Emission Computed Tomography (SPECT), Image reconstruction, Monte Carlo simulations, Bootstrapping, GATE.

1. Introduction:

Single Photon Emission Computed Tomography (SPECT) is an imaging modality appropriate for visualizing functional information about a patient's specific organ or a body system. A radio-pharmaceutical, which is a pharmaceutical labeled with a radioactive isotope, is administrated to the patient. The radiopharmaceutical is chosen as a function of the organ to be studied. For example, Iodine-131 is appropriate for thyroid imaging. In case of SPECT, the radio-pharmaceutical emits single gamma rays isotropically. Emitted gamma photons are then detected in specific directions using a rotating gamma camera. Rays detected in a given direction yield a projection. At the end of an acquisition process, a set of two-dimensional (2D) projections is available to reconstruct the three-dimensional (3D) radio-pharmaceutical distribution within the body.

In the absence of attenuation and scatter of the emitted gamma rays, each point of a projection corresponds to the sum of photons emitted by the source along a straight line (Fig. 1); the detected signal intensity is then:

$$I = \int_L f(x,y)du$$

where I is the detected signal, f(x ,y) the concentration of the radio-pharmaceutical at (x,y) and L represents the line perpendicular to the detector (the gamma camera).

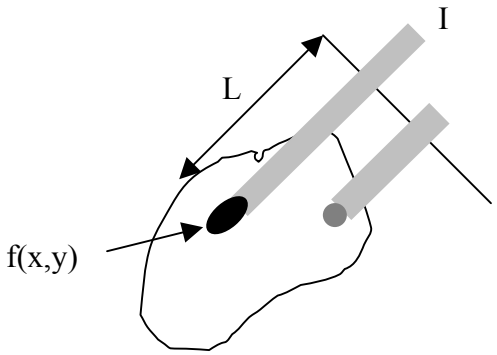

Figure 1: Detection of a projection in SPECT

The aim objective is to calculate the radio-pharmaceutical concentration f(x,y) at each point (x,y) knowing a set of projections I along different directions. This is feasible by inverting the Radon transform, thus reconstructing transaxial slices assuming that photons emitted from a transaxial slice are detected within a single line of each 2D planar projection.

A 3D radio-pharmaceutical distribution f(x,y,z) can then be reconstructed as a set of 2D reconstruction of f(x,y) radio-pharmaceutical distribution. The main problem with this approach is that signal measured in projections is affected by physical effects such as scatter, attenuation and detector response. Therefore, photons emitted from a transaxial slice may be detected not only in the projection line facing the slice but also in the neighboring slices. It has been shown that, in realistic configurations, the percentage of such photons is not negligible [Munley et al. 1991]. Furthermore, due to attenuation of the photons within the patient, not all emitted photons reach the detector. Those effects dramatically degrade the reconstructed image. When writing the reconstruction problem in its form where projections and image to be reconstructed are sampled, iterative reconstruction algorithms can be used. This makes it possible to account for most degrading physical effects affecting the projections, by considering a projector modeling these physical effects. Using iterative reconstruction, a 3D radio-pharmaceutical distribution f(x,y,z) can be reconstructed either as a set of 2D f(x,y) distributions, each f(x,y) distribution resulting from a 2D reconstruction involving a 2D projector, ignoring 3D degrading effects, or better, by a fully 3D reconstruction involving a 3D projector accounting for 3D physical effects.

Monte Carlo (MC) simulations have recently been proposed to calculate a 3D projector, in a method called F3DMC (Fully 3 Dimensions Monte Carlo) [Lazaro et al. 2004]. However, the accuracy of Monte Carlo simulations may be adversely affected by the random number generators, seeds used for these generators, number of random drawing, or correlations

between simulations. In that context, we tested the impact of the number of drawing and the value of bootstrapping to reduce variance of the projector element estimates [Cheng et al. 2001], hence hopefully improve the quality of the reconstructed images.

1 Material and Methods

1.1 Monte Carlo simulations

MC simulations were performed using the software package GATE [Jan et al. 2004]. A cylindrical water phantom including 5 rods (diameters from 4.8 to 11.1 mm) and a bony rod (diameter of 12.7 mm) (Fig 2) was considered. Rod-to-background Tc99m activity concentration ratio between any of the five smallest rods and the background was set to 4. The white rod represents the bony rod.

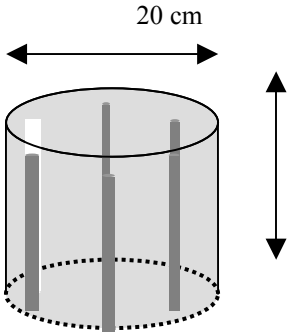

Figure 2. Simulated phantom

The simulated camera modeled an AXIS-Philips equipped with a LEHR (Low Energy High Resolution) collimator. 64 projections of 64x64 pixels (pixel dimension= 3.125mm) were simulated and photons detected in the 126-154 keV energy window were considered.

The projector needed for F3DMC was calculated by simulating a uniform activity distribution in the phantom propagation media. The 3D object to be reconstructed was sampled into 64x64x64 voxels (voxel dimension = 3.125mm), yielding a projector with at most 64^6 elements. In practice, only non-zero elements were stored. Given the projections and the projector, the 3D object was reconstructed using F3DMC, by solving the linear system using a Maximum Likelihood Estimation Method (MLEM) algorithm [Miller et al. 1985].

1.2 Image assessment

In order to assess the quality of the reconstructed images (Fig. 3. (b)), rod-to-background activity ratios were measured and compared with reference values. Reference values were obtained by considering the sampled activity distribution that was actually simulated (Fig. 3. (a))

(a) **(b)**

Figure 3: (a) Reference image; (b) Reconstructed image

1.3 Statistics used for projector estimate

An accurate projector can be obtained by generating a large number of events in MC simulations, to reduce the standard deviation of each value within the projector. Given that the maximum duration of each simulation was 24 hours, we performed 462 separate sub-simulations, supposed to be independent using the Independent Sequence (IS) technique, i.e. initializing the same generator with 'n' different seeds [Codington 1996]. The resulting projector involved in F3DMC method was calculated with 74 billion emitted photons from which 16 million photons were detected in the 126-154 keV window. Each element P_{ij} of the projector was defined as the probability that a photon emitted from a voxel i is detected in the pixel j (1)

$$Pij = \frac{Nij}{Ni}, \quad (1)$$

where Nij is the number of photons emitted from voxel i and detected in pixel j, and Ni is the number of photons emitted from voxel i.

1.4 Impact of the number of simulated events on the reconstructed image quality

The principal problem faced while using MC techniques is the long duration of simulations making it difficult to have a large number of statistical histories used in the calculation of the projector. We therefore studied the change of the activity ratio with respect to the number of generated events to determine whether it reaches a plateau, making it unnecessary to perform additional simulations.

2. A Mean Projector as a solution to reduce noise

The stochastic nature of Monte-Carlo simulations induces a statistical noise. We thought that by reconstructing images with a mean projector, probability values may be smoothed and we could reconstruct images with better homogeneity and thus with less noise. In fact, let's assume that in order to calculate the projector we perform four simulations Sim1, Sim2, Sim3 and Sim4 and that we calculate four projectors P1, P2, P3 and P4 using respectively each of these simulations. The difference in the calculation of a projector element P_{ij} performed once by appending the four sub-simulations (P_initial) and another time by calculating a mean of these four sub-simulations (P_mean) is shown in the table 1.

	P1	P2	P3	P4	P_initial	P_mean
Number of photons N_{ij} detected in the pixel j and emitted from voxel i = 1, 2, 3 and 4.	x_1	x_2	x_3	x_4	$\sum_{i=1}^{i=4} x_i$	
Number of photons emitted from voxel i	n_1	n_2	n_3	n_4	$\sum_{i=1}^{i=4} n_i$	
Projector element P_{ij}	$\frac{x_1}{n_1}$	$\frac{x_2}{n_2}$	$\frac{x_3}{n_3}$	$\frac{x_4}{n_4}$	$\frac{\sum_{i=1}^{i=4} x_i}{\sum_{i=1}^{i=4} n_i}$	$\frac{1}{4}\times\sum_{i=1}^{i=4}\frac{x_i}{n_i}$

Table 1. Calculation of projector's elements

Obviously, we can notice that except the case where $n_1 = n_2 = n_3 = n_4$, P_{ij} has different values in P_initial and P_mean. In our case, we have used the results of 460 sub-simulations in order to calculate a set of 20 projectors each one calculated from a set of 23 sub-simulations; we obtain so a set of 20 sample-projectors Pi ($i \in [1\ldots20]$).

3. Bootstrapping as an alternate issue to reduce noise

Statistically, it is known that the standard deviation is an inverse function of the number of measures. Each of the projectors Pi ($i \in [1\ldots20]$) calculated above can be considered as a sample projector.

By re-sampling, bootstrapping generates a new set of samples and increases the statistics included in the calculation of the projector estimate and thus reduces the variance of estimated parameters

[Efron et al. 1979].

Initial Projector:

Simulation1	Simulation2	Simulation3	…..	Simulation i	.....	Simulation460

Sample Projectors:

P1	P2	….	Pi	….	P20
Simulation1	Simulation24		Simulation[(i-1)x23]+1		Simulation438
Simulation2	Simulation25		…		…
….	….				
Simulation23	Simulation46		Simulation(ix23)		Simulation460

Figure 4 (a). Re-sampling projectors

P1	P2	P3	P3	P3	……..	……
P7	P9	P10	P11	P11	……..	…...
P14	P14	P15	P17	P18		
P18	P18	P18	P19	P20		

Bootstrap sample 1 (sorted by increasing i)

P7	P3	P5	P8	P6
P6	P8	P7	P5	P9
P13	P12	P13	P14	P16
P17	P11	P18	P12	P19

Bootstrap sample 100 (sorted randomly)

Figure 4 (b). Re-sampling projectors

$$\text{P\_bootstrapped} = \frac{\sum_{i=1}^{i=100} Bootstrap\_sample\_i}{20 \times 100}$$

On figure 4, we see how a sample projector Pi is computed with a set of 23 sub-simulations, whereas each bootstrap sample is a set of 20 randomly selected sample projectors (Pi). Drawings are done with replacement so we can have many identical Pi in the same bootstrap sample.

The bootstrap projector was then the mean of 100 bootstrap sample projectors. Results of relative quantitation are shown in figure 9. Reference values are plotted in the last column .We plotted relative quantitation values for each rod calculated on images reconstructed with the initial projector and the bootstrapped projector (-B refers to a bootstrapped projector). Curves obtained by the initial projector and bootstrapped projector are almost superposed.

4. Results

In order to study the change of relative quantitation with respect to the number of generated events, we calculated projectors corresponding to different statistics going from a projector calculated from 33 sub-simulations to 462 sub-simulations with a step of 33 simulations. We then reconstructed the image using each of the resulting 14 calculated projectors: P33, P66…P462. The accuracy of the reconstructed images was assessed by measuring the activity ratio in the 6 rods (Fig 5). Results were plotted for each rod (rod's diameter expressed in millimeter). We can see the improvement in accuracy with the increase of generated events. The reference to obtain is given in the last column.

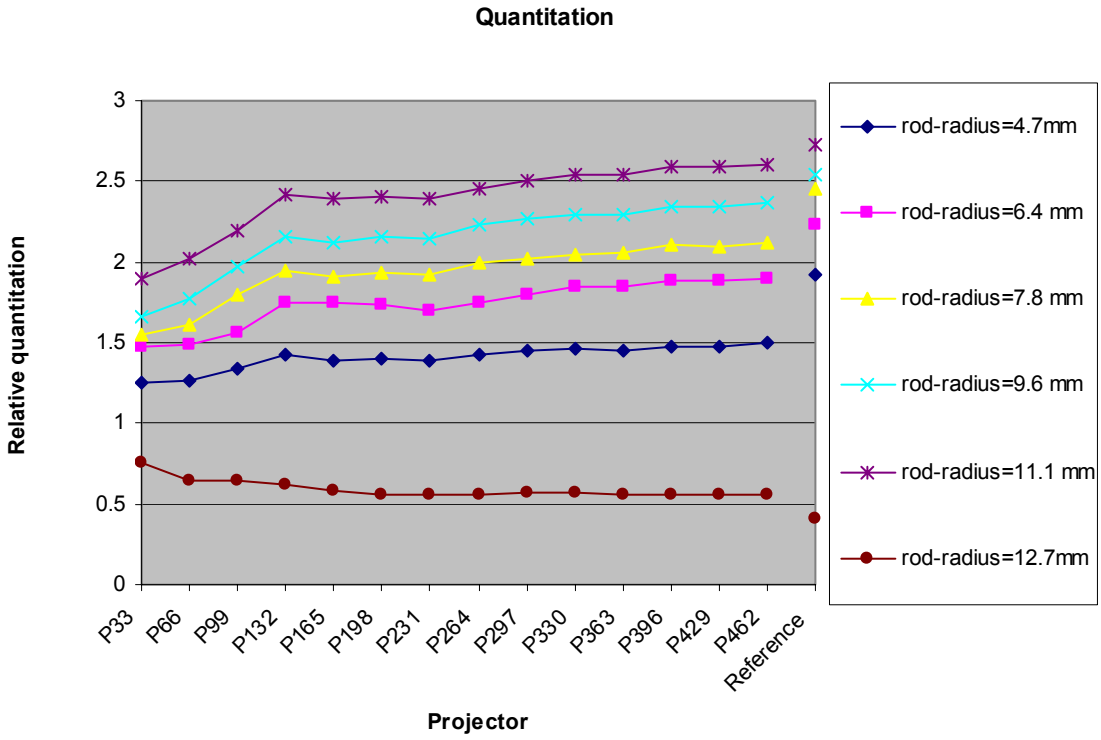

Figure 5. Relative quantitation with respect to the number of simulation output files

The mean projector used to reconstruct images was defined as the mean of 20 projectors Pi ($i \in [1..20]$), each of these 20 projectors being calculated from a set of 23 sub-simulations. Figure 6 shows the smoothing impact of the mean-projector calculation on the distribution of computed probabilities mainly in zone of high frequency. Results of quantitative ratios using the mean projector (-M refers a mean projector) are shown in Figure 7. Curves obtained by the initial projector and mean projector are almost superposed.

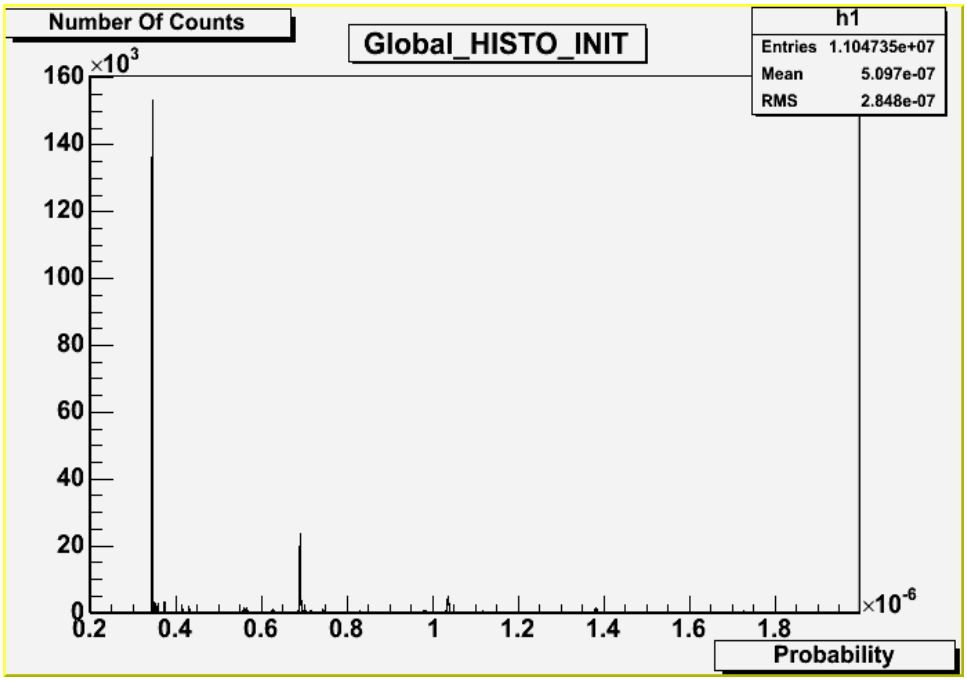
Number Of Counts
Global_HISTO_INIT
h1
Entries 1.104735e+07
Mean 5.097e-07
RMS 2.848e-07
×10^3
160
140
120
100
80
60
40
20
0
0.2
0.4
0.6
0.8
1
1.2
1.4
1.6
1.8
×10^-6
Probability

(a)

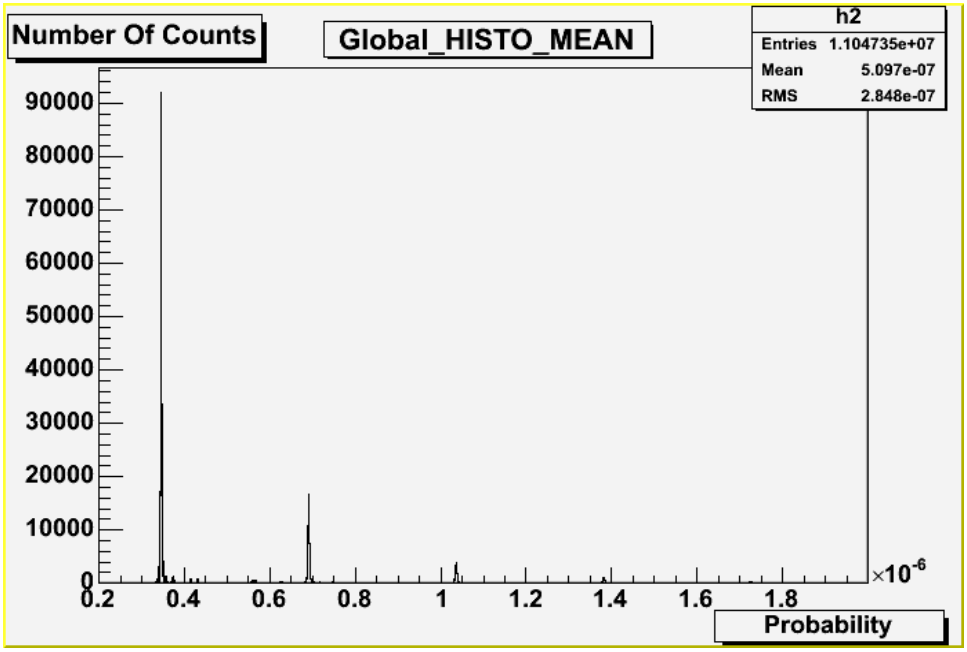
Number Of Counts
Global_HISTO_MEAN
h2
Entries 1.104735e+07
Mean 5.097e-07
RMS 2.848e-07
90000
80000
70000
60000
50000
40000
30000
20000
10000
0
0.2
0.4
0.6
0.8
1
1.2
1.4
1.6
1.8
×10^-6
Probability

(b)

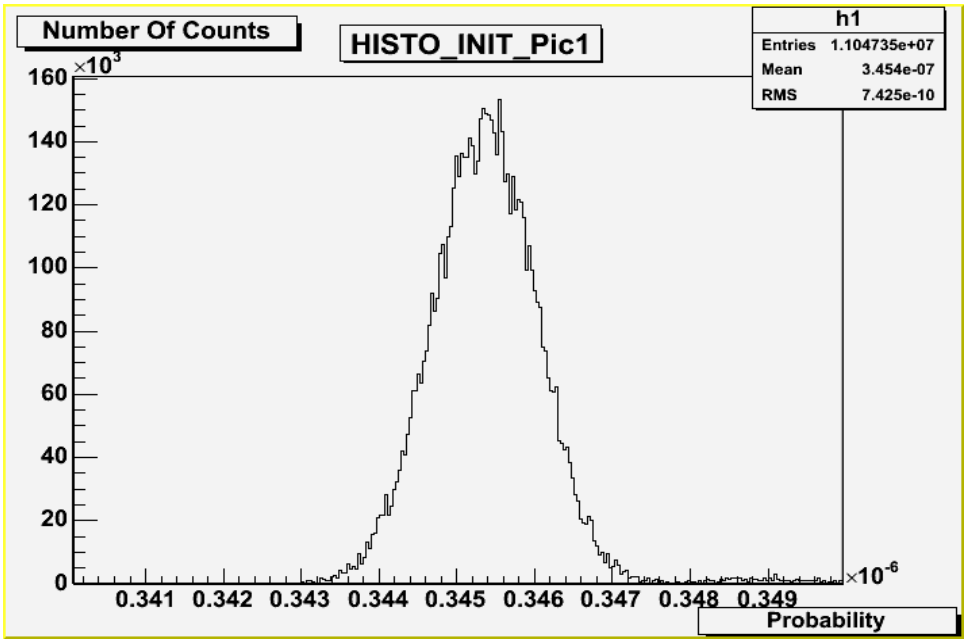

(c)

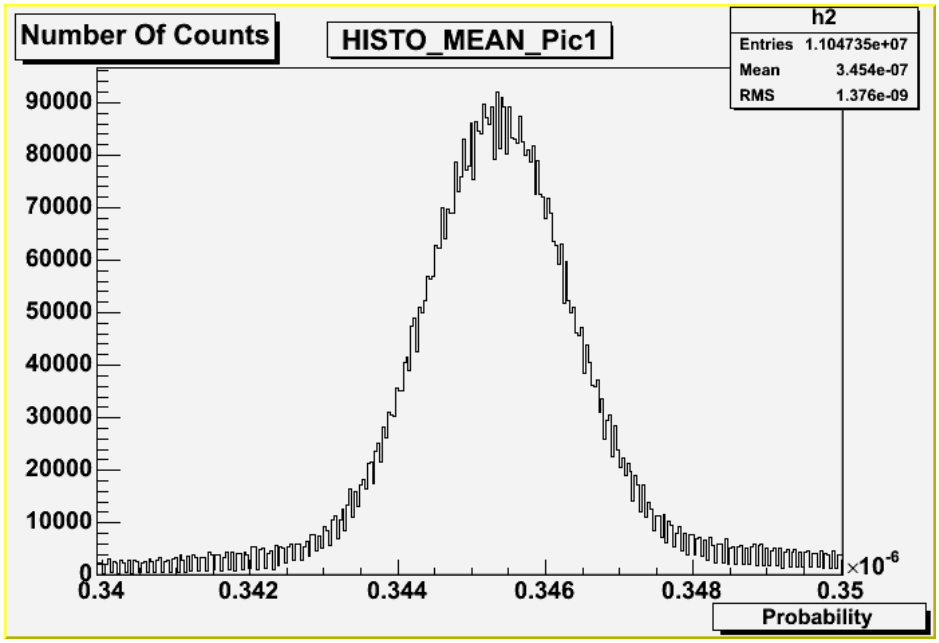

(d)

Figure 6. Probability distribution:

(a) Global view of the initial projector ; (b) Global view of the mean projector

(c) Zoom on the first peak (initial) ; (d) Zoom on the first peak (mean)

Difference between initial projector and mean projector are mainly shown in the value of the frequency of the first peak, where we have a value of 160 000 for the initial projector and 90 000 for the mean projector.

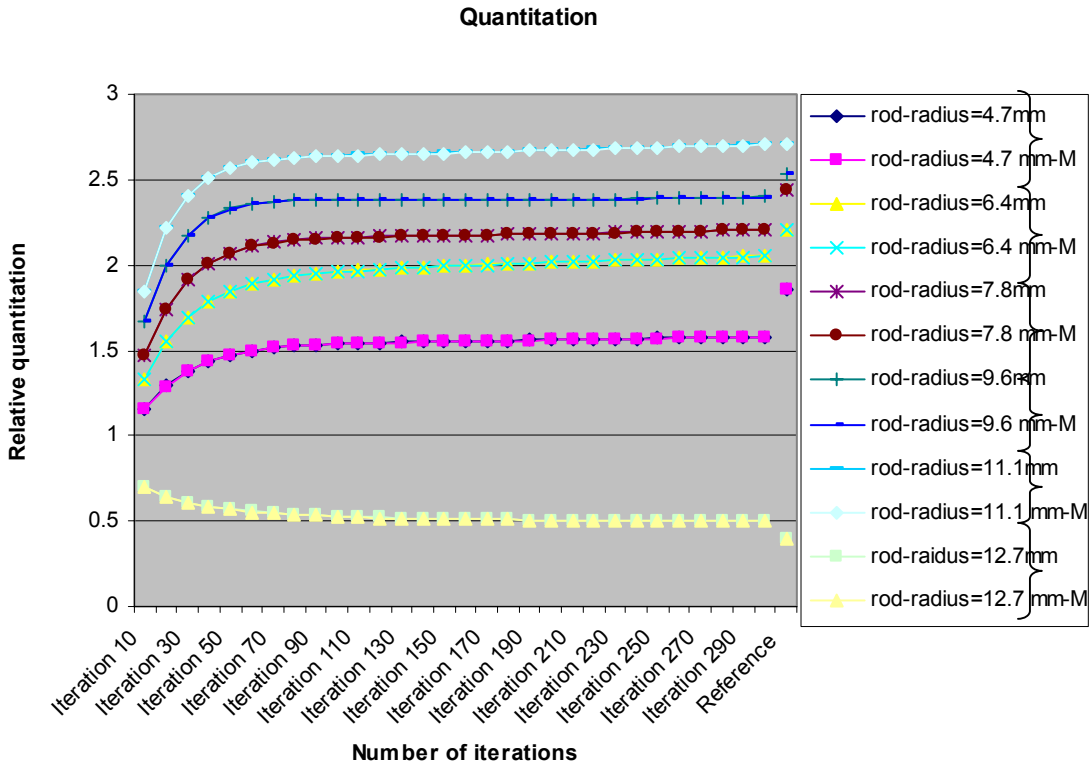

Figure 7. Comparison between convergence rates of respectively the initial projector and the mean projector

Instead of calculating the mean projector of 20 elementary projectors Pi (i going from 1 to 20 in increasing order), we drew randomly 20 projectors from the set of the 20 projectors Pi (example: P1, P2, P2, P3, P6, P6….P14, P20) (using drawing with replacement). We repeated this operation 100 times and thus obtained 100 combinations of 20 randomly selected sample projectors, each one forming a bootstrap sample [Chernick et al 1999].(Fig 4)

Figure 8 (a) shows the impact of bootstrapping in the apparition, within the probability spectrum, of new probability values; this could be explained by the fact that bootstrapped projector is obtained by dividing by 2000 the sum of the sub-projectors drawn randomly. The zoom on the zone where a pick appeared in the initial projector and the mean projector (Fig.8.b), shows that bootstrapping induces a quasi-stochastic distribution and that a set of new generated picks was involved within the bootstrapped projector.

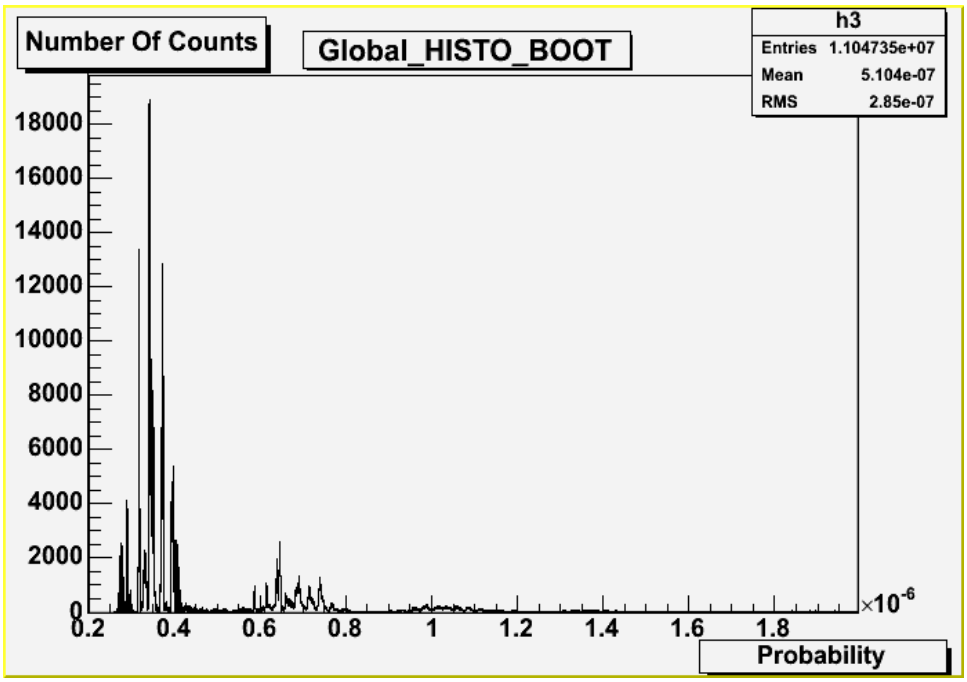

(a)

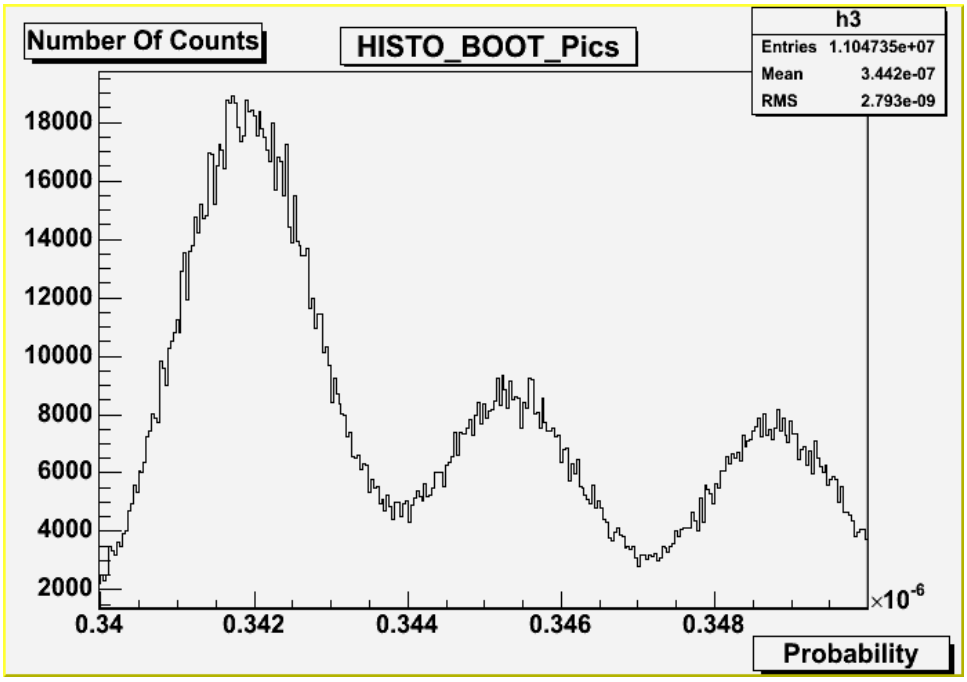

(b)

Figure 8. (a) Global spectrum of the bootstrapped projector
(b) Zoom on the zone where a pick appears in the initial projector and the mean projector

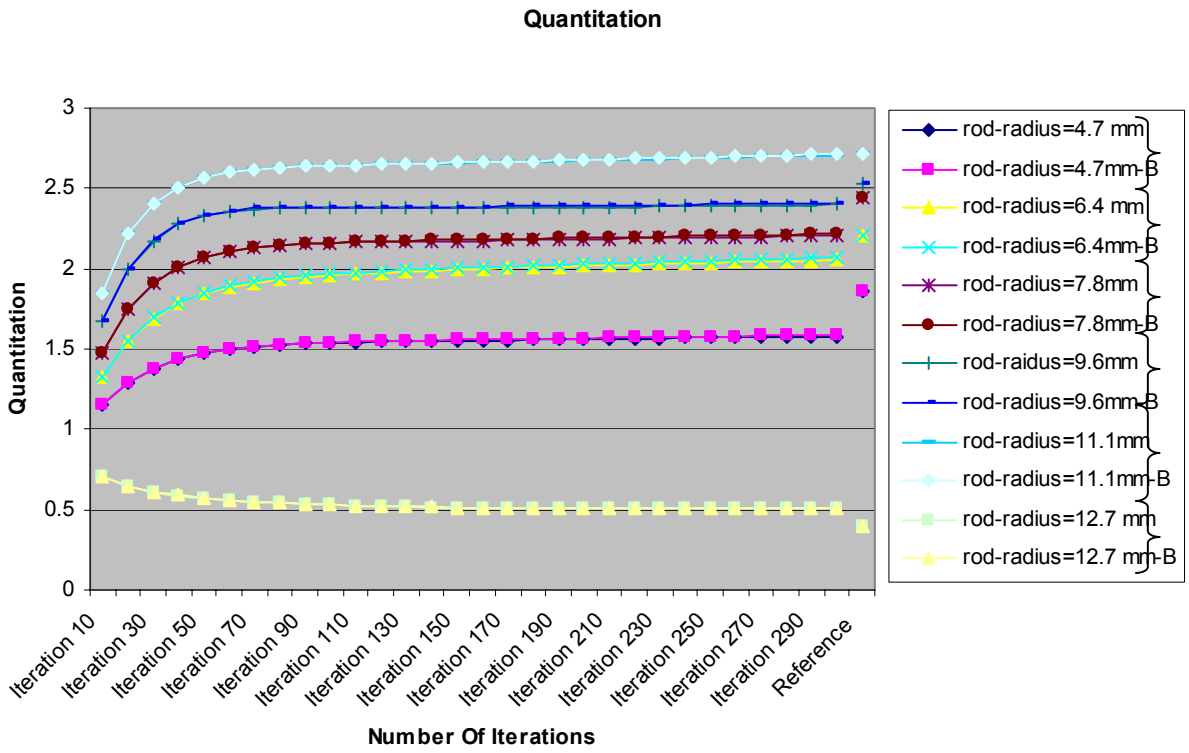

Figure 9. Comparison between convergence rates of respectively the bootstrapped projector and the initial projector

The Table 2 shown below presents critical value of probability in different projectors:

Projector	Minimal Probability	Mean Probability	Maximal Probability	Standard Deviation	Variance
Initial	3.421×10^{-7}	5.41×10^{-7}	3.01×10^{-5}	4.762×10^{-7}	2.267×10^{-13}
Mean	3.257×10^{-7}	5.41×10^{-7}	2.983×10^{-5}	4.764×10^{-7}	2.27×10^{-13}
Bootstrapped	2.606×10^{-7}	5.41×10^{-7}	3.254×10^{-5}	4.745×10^{-7}	2.251×10^{-13}

Table 2.Critical values in different projectors

We can easily notice that bootstrap technique has enlarged the interval of probability including new values lower than the minimum probability value and higher than the maximum probability value in the initial projector (i.e. in the mean projector).

5. Discussion

Results shown in figure 4 demonstrate that overall, best accuracy is obtained for the largest number of histories considered for calculating the MC projector, as expected from the stochastic nature of MC simulations. We also notice that even if P132 (calculated from 132 sub-simulations) included fewer histories than P231 (calculated from 231 sub-simulations), it tended to give better results than P231, which also reflects the stochastic nature of the calculations involved. Bias between reference values and the plateau could be explained by the fact that the number of simulated events involved in the computation of the projector is still not high enough.

Results shown in figure 4 suggest that initial projector and bootstrapped projector are nearly identical which means that combinations of initial projectors Pi in almost all cases yielded a bootstrapped projector quasi-equal to the initial projector.

The weak decrease of variance in the bootstrapped projector (Table 2) indicates that we may still not have an important statistics involved in the calculation of the projectors (P1… P20) and that we should perform more simulations. This later comment could be a first explanation of the new generated picks in the bootstrapped projector.

A second explanation could be that the projector calculated from the 460 simulations is already a kind of bootstrapped projector since the Independent Sequence technique used seeds selected in an increasing order (not randomly). Indeed the seed initialization was taken in the [1,460] interval. It is known that the IS can lead to encapsulated sub-sequences, since a random number generated in one sub-sequence can match the seed used for another sub-sequence. Some authors warn scientists who run MC experiments in parallel [Hellekalek 1998]. The problem lies in the parallelization of pseudo random numbers. As for many parallelizing techniques of Pseudo Random numbers, the main problem of those methods is the "Long-Range" correlation [De Matteis et al, 1988]. Variants of the known techniques have been developed, a notable one is the parameterization method which is a variant of the IS technique [Srinivasan et al, 1999]. It consists in parameterizing both the seed and iteration function (i.e. the function that gives the next state in the sequence). One of the main contribution of this variant is that it results in a scalable period.

A way to confirm this hypothesis is to have a simulation where we simulate a number of histories equal to the number of histories simulated within 460 separated simulations. Once this simulation is performed, we can compare the results of the quantitative ratio with those obtained by performing 460 separated simulations with independent seeds. However, we are still investigating in order to understand the spectrum of bootstrapped projector.

6. Conclusion and Perspectives

This paper is placed in the context of tomographic reconstruction in Single Photon Emission Computed Tomography (SPECT). The projector used for reconstruction is obtained by Monte Carlo Simulation. Thus we have studied the impact of

the number of generated events on the accuracy of the projector. We studied various issues in order to improve its accuracy either by computing a mean projector or by applying the bootstrap technique which has been detailed above.

Even if results were not satisfying so far, investigations are in progress to improve the accuracy of the projector. As a solution to the slowness of GATE simulations, we intend to use faster MC software named SimSet [Lewellen et al. 1998]. With this simulator, we can quickly generate a high number N of events but it relies on some analytical approximations of stochastic laws that could also be source of inaccuracy. This high number of events could then be split into 20 sub-simulations, from which bootstrapping can be implemented as described above. The fact that the variance in the bootstrapped projector hasn't decreased enough leads us to investigate two possibilities: either the number of histories is still not enough or the possibility of an eventual correlation between sub-simulations. Getting rid of possible dependencies between simulations and increasing the number of histories by using a faster simulator (SimSet), bootstrapping might still improve the quality of the projector.

REFERENCES

[Efron B, 1979], Computers and the Theory of Statistics : *Thinking the Unthinkable in SIAM Review,* **21** (4) : 460-480*, octobre* 1979.

[Cheng R.C.H, 2001], Analysis of simulation experiments by bootstrap resampling. *In proceedings of the 2001 Winter Simulation Conference*. B.A Peters, J.S.Smith, D.J.Medeiros, and M.W.Rohrer, eds

[Cheng R.C.H, 1995], Bootstrap methods for computer simulation experiments. *Proceedings of the 1995 Winter Simulation Conference,* edited by C.Alexopoulos, K.Kang, W.R.Lilegdon, and D.Goldsman.

[Chernick, M.R, 1999], *Bootstrap Methods A Pracititioner's Guide.*New York, Wiley.

[Coddington, 1996], Coddington. *Random number generators for parallel computers*. NHSE Review, 1996 Volume, Second Issue.

[De Matteis et al, 1988], De Matteis A., and Pagnutti, S. *Parallelization of random number generators and Long-Range correlations*. Numer. Math., 1988, **53** : 595-608.

[Davison,A.C and D.V. Hinkley, 1997], *Bootstrap Methods and Their Application.* Cambridge University Press.

[Friedman, L.W. and H.H. Friedman, 1995], Analyzing simulation output using the bootstrap method. *Simulation,* February 1995, **64** (2) : 95-100.

[Jan et al, 2004] GATE:a simulation toolkit for PET and SPECT *Phys.Med.Biol.***49** : 43-61

[Hellekalek 1998] Hellekalek, P. *Don't trust parallel Monte Carlo !*. Proceedings of the 12th workshop on Parallel and distributed simulation. Banff Canada. May 26 - 29, 1998, pp. 82-89.

[Lazaro D et al, 2004] Breton V. and Buvat I. Feasibility and value of fully 3D Monte Carlo reconstruction in Single Photon Emission Computed Tomography. *Nucl. Instr. and Meth. Phys. Res.* **A 527** : 195-200

[Lewellen TK et al, 1998] Harrison RL and Vannoy. The SimSET program. In: MonteCarlo calculations in nuclear medicine. Applications in diagnostic imaging. M. Ljungberg, S. E. Strand and M.A. *King editors. Bristol, Institute of physics publishing,* 1998

[Miller Mi et al, 1985] Snyder DL and Miller TR . Maximum-Likelihood reconstruction for Single-Photon Emission Computed-Tomography. *IEEE Tr.Nucl.Sci.***NS-32 :** 769-778.

[Munley M T et al, 1991] Floyd C E, Tourassi G D, Bowsher J E and Coleman R E 1991 Out-of-plane photons in SPECT *IEEE Trans.Nucl.Sci.* **38** : 776-9.

[Srinivasan et al, 1999] Srinivasan, A, Ceperley, D. and Mascagni, M. *Testing parallel random number generators*. Proceedings of the 3rd Int. Conf. on Monte Carlo and Quasi Monte Carlo Methods in Scientific Computing. J. Spanier et al. (ed.), Springer-Verlag, Berlin, 1999.

Modeling of a multimodal image aggregation process using discrete geometry

Julien Montagner
ERIM
Faculty of Medicine, BP 38
28 place Henri Dunant
63001 Clermont-Fd Cedex 1, France
+33 4 73 17 81 23
julien.montagner@u-clermont1.fr

Vincent Barra
LIMOS
Scientific complex, Les Cézeaux
63117 Aubière Cedex, France
+33 4 73 40 77 68
vincent.barra@isima.fr

Jean-Yves Boire
ERIM
Faculty of Medicine, BP 38
28 place Henri Dunant
63001 Clermont-Fd Cedex 1, France
+33 4 73 17 81 23
j-yves.boire@u-clermont1.fr

ABSTRACT
In order to help clinicians with the diagnosis of neurodegenerative diseases, we provide a synthetic functional information located in relation with anatomical structures. The final image is processed by multimodal data fusion between SPECT and MR images. We propose a new method for the management of such multiresolution data, in which a geometrical model allows an accurate correspondence of voxels from both images, while preserving at best both original pieces of information. We use this matching method to replace the interpolation step in the compulsory image registration of the data fusion process. The geometrical model is first built from registration parameters. Computational geometry algorithms, applied to this model, allow the computation of numerical values used to process the final information. The method has been applied to brain perfusion and neurotransmission SPECT images.

KEYWORDS
Medical image processing, Synthetic functional image, Multimodal data fusion, Multiresolution data, Geometrical model

1. Introduction

In the context of brain study, considering the central function and the position of this organ, medical images are the primary tool for clinical investigation. Images of this kind provide models of either anatomical structures or functional activities. Parkinsonian syndromes and Alzheimer's disease are both qualified by an abnormal death of neuronal cells, in the upper part of the brainstem in the first case [Blandini *et al.* 2000], and at least in particular regions of the cerebral cortex in the second case [Rusinek *et al.* 1991]. The major physiological consequences of this decrease in nervous cells population are: a lack of dopamine in the striatum for Parkinson's disease, involving automatic movement disorders, and a decrease in blood supply in the affected regions for Alzheimer's disease, representative of the low neuronal activity. Both neurotransmission phenomenon and brain perfusion are classically observed on single photon emission computed tomography (SPECT) images. This modality provides 3D data sets in which numerical activities may be linked with *e.g.* interneuronal exchanges or neurons blood supply, depending on the used radiotracer [Brooks 2004].

Recently, new preventive treatments appeared for neurodegenerative pathologies, such as Alzheimer or Parkinson's diseases. They require an early detection of the denervation. Despite numerous compulsory corrections applied to SPECT data during the tomographic reconstruction [Soret *et al.* 2003], the functional information they provide keep a low spatial resolution, which hinders the study of neuronal activity within small anatomical structures (figure 1). The visual information brought by the classical multimodal approach (investigation of the MR image / SPECT image couple) are thus not sufficient to draw a conclusion in the early stages of the pathology.

We propose here to provide new diagnosis elements by the synthesis of an image holding both functional and anatomical data. The anatomical part is brought by a magnetic resonance (MR) image, as in the classical multimodal approach. Nevertheless, automatic image processing makes it possible to bring out data which were not obviously visible in original images, and allows multimodal images matching by means of data fusion. In most of software applications managing multimodal medical images, the image fusion is limited to a superimposed display of *e.g.* MR and SPECT images, with different color scales (gray levels are more prevalent to display MR data). In this case, information combination concerns color models derived from numerical activities associated with image voxels.

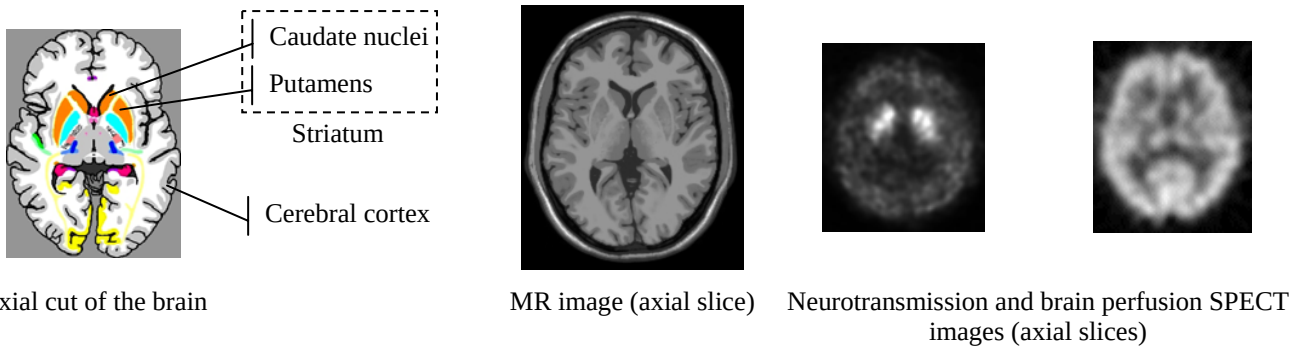

Figure 1. Schematic view, MR and SPECT images of brain structures involved in Parkinson's and Alzheimer diseases

On the contrary, we intend to compute a new information from MR and SPECT images, designed to be as close as possible to original numerical data. This fusion method was first used in the context of functional activity quantitation [Montagner *et al.* 2005]. It consists in replacing the registration step of the fusion process by the managing of spatial features (differences in orientation, position, and voxel sizes, due to differences in spatial resolution of acquisition equipments) of both images thanks to a geometrical model (tilling of the space by cubic models of the voxels). The main idea is to delay the modification of original activities until the final aggregation step of the fusion process. Original activities are then used, in combination with geometrical information extracted from the model, to compute the numerical values associated with voxels of the synthetic image (at the spatial resolution of the MR image). The idea of delaying the computations until the information quantity is sufficient, *e.g.* to take a decision or to reach the required accuracy, has previously been introduced in our work about image fusion, by the use of fuzzy logic to model the semantic part of the information [Barra Boire 2001]. Therefore, during the final step of the fusion process, the geometrical model is aggregated with the fuzzy one to generate the synthetic image.

In the following, we first place our fusion process in the general context of multimodal medical image display. The method itself is then explained, from the extraction of registration parameters to the aggregation models used to create the final image. The fuzzy information model is only briefly presented, since the real contribution of this work concerns the geometrical model. This model and the algorithm used to compute the geometrical information are thus detailed. Finally, the fusion process is applied to brain perfusion and neurotransmission SPECT images, and these results are discussed.

2. Combination of anatomical and functional information

As mentioned above, the image fusion process is not restricted to a combined display of both information sources. The general aim is to extract or emphasize diagnosis elements, not only intended to a visual perception. The application we propose in the following aims at providing a localized quantitative functional information, dedicated to the diagnosis of a given disease (*e.g.* directly showing hypoperfused gray matter). Processing a synthetic image from this new information is only one among the possible goals of the fusion process. The information we compute is a quantitative value relative to the functional activity, located in relation with the voxels of the anatomic image (the functional activity is redistributed within these voxels). The visual presentation of this information is obtained thanks to an aggregation with data of anatomical classes.

The common part of every multimodal data integration process is a preliminary registration step. During this step, at least one of the original data sets is transformed in order to give the same coordinates, on both images, to an anatomical location. As a consequence, a brain structure is finally represented by two voxel sets with similar size, position and orientation. Once the images are aligned, integration processes have different ways to display the data: using gray levels or color models, in 2D or 3D, considering high level shape models or just numerical activities. The major difference we distinguish between these processes concerns their tendency to present the information through transformed data sets or thanks to data as close to the original values as possible. The synthetic image we process from original 3D data sets is presented as a collection of 2D images called slices. Therefore, we will only make below a brief presentation of 2D rendering techniques in order to give evaluation elements for the proposed method.

2.1. Combination modes

The selective slice by slice display of two combined medical images consists in drawing, on one of the images, either an entire part of the other one (*e.g.* a square window), or geometrical features extracted from the other (*e.g.* geometrical curves, region edges, level lines [Condon 1991]). The non-selective display consists in a global mixture of both data sets. When using a SPECT image for medical diagnosis, the maximal part of the functional information should be preserved [Stokking 1998].

Display techniques for medical images are based on color models (*e.g.* variations of a hue) associated with either numerical activities or features processed from these activities. In a multimodal context, each image provides pieces of information which the other lacks. The quality of visual perception is an additional constraint. This quality depends on the image ability to emphasize relevant information (for the diagnosis) [Kundel 1990]. The interpretation of anatomical information is essentially linked to image outlines (*i.e.* strong activity gradients). In the case of a functional information, the important image features are large activity variations (within implicit anatomical structures).

2.2. **Combination of color models**

Main non-selective display modes are: arithmetical processing from numerical activities of the image (figure 2), and the association of some image features with color channels (*e.g.* RGB or HSV, possibly with an additional "alpha" channel for the management of transparency). The combined information may be confused when the multimodal data to integrate are both complex, or when they present many overlapping regions [Hill 1993]. The efficiency of color combination techniques decreases when the number of features to represent increases. In this case, it becomes necessary to use an advanced fusion strategy, as in the proposed method.

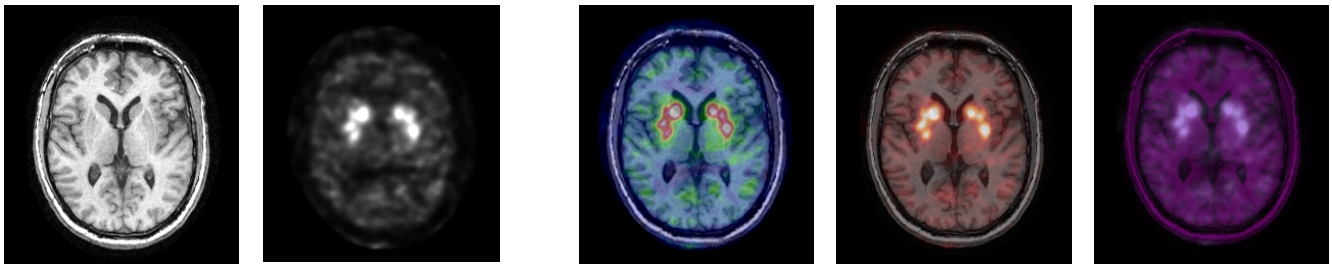

Original MR image | Registered SPECT image | MR data: gray levels SPECT data: "rainbow" palette | Combination of HSV models | Combination of RGB models

Figure 2. Non-selective combination of color models

2.3. **Synthesis of a dedicated medical information**

The image synthesis process presented in this paper belongs to the class of non-selective display methods. The redistributed functional activity may be considered as directly linked with the physical phenomenon measured in the SPECT image. The image fusion process allows reducing the complexity of the anatomical information, to emphasize the functional one. Since the anatomical information is limited to large brain tissue classes, the functional one is perceived through local activity variations within these classes.

The preliminary study about image synthesis is presented in [Colin Boire 1999]. Image fusion between MR and SPECT data comes out to process fuzzy maps for brain tissues. Each map expresses the membership $\pi_C(v)$ of a voxel v from the anatomical image to a given class C of brain tissue (cerebrospinal fluid (CSF), white matter (WM), gray matter (GM) and hypoperfused gray matter (HGM)). The final value $\mathbf{V}(v)$ associated with voxel v, in the synthetic image, is processed as

$$\mathcal{S}(v) = \frac{\pi_{GM}(v)\mu_{GM} + [\pi_{HGM}(v) + \pi_{WM}(v)]\mu_{WM} + \pi_{CSF}(v)\mu_{CSF}}{\pi_{GM}(v) + \pi_{HGM}(v) + \pi_{WM}(v) + \pi_{CSF}(v)} \quad (1)$$

where μ_C is the mean functional activity of C voxels, estimated in the registered SPECT image. The information processed by (1) is composed of activity variations between the different classes, but local variations are suppressed by the average operator. The management of spatial features in image models allows the introduction of local variations into (1).

3. **Proposed method**

Our goal is to preserve both original SPECT data and the anatomical information extracted from the MR image until the final fusion step, in which local variations of functional information are processed by proportional activity redistribution within voxels of the anatomical image. The main difficulty comes out from the difference in spatial resolution between both images. Indeed, this multiscale aspect of the data and the spatial misalignment of corresponding structures in both images involve the anatomical information and the functional information to be expressed in two different geometrical spaces (figure 3).

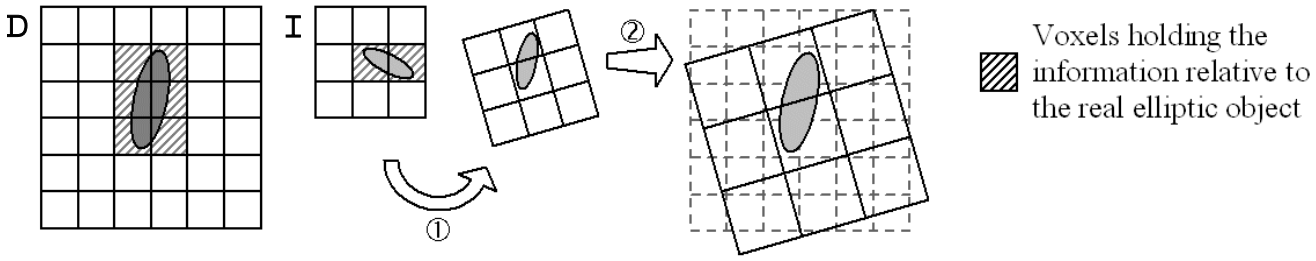

Figure 3. 2D illustration of the geometric model building according to registration step, composed of a rotation, a translation (1) and a rescaling of the data (2) between the anatomical (D) and the functional (I) images

In the proposed method, the rigid deformation resulting from the usual registration step is not applied to the data, but we use the mathematical linear function associated with this transform to generate the geometrical models of both the MR and SPECT images, based on tilings of the space by their cubic voxels (figure 4). Finally, the identification of geometrical relations between the digital grids, *i.e.* volumes of the polyhedrons resulting from the intersection of the cubic voxels in general position, allows us to manage anatomical and functional data in a common spatial context for fusion. These numerical values, injected in the fusion process, act as weights to compensate the difference in resolution between original image data. The processing of intersection volumes, and thus the model itself, are, for the moment, restricted to the case of isotropic images (*i.e.* with cubic voxels).

To our knowledge, the question of multiresolution management with preservation of both functional and anatomical original data has not been handled before. Moreover, most of the existing methods are based on the processing of the continuous information sampled in the images, and imply a compulsory resampling step [Calle 1999, Pajares DeLaCruz 2004]. To preserve the original SPECT activity and to locate it with respect to the anatomical information, we consider the discrete nature of the data, and the elementary volumes in which the continuous phenomenon has been integrated.

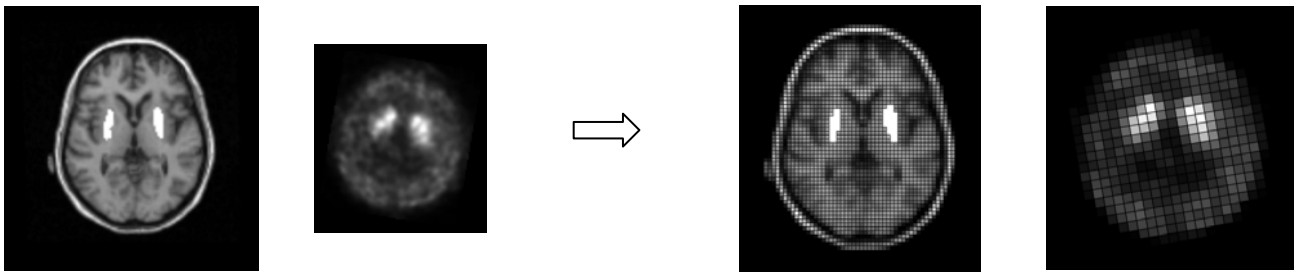

Figure 4. Alignment of the SPECT data on the MR image (with superimposed mask of the putamens), without resampling of the functional information

3.1. **Information modeling**

We assume that every anatomical structure of interest is mainly composed of pure tissue components (WM, GM and CSF). Because of partial volume effects [Wang Doddrell 2001], the numerical value associated with a MR image voxel v is a mixture of pure tissue values. Brain components are segmented in the MR image thanks to a fuzzy classification algorithm [Barra Boire 2000], fuzzy logic [Zadeh 1978] providing an adapted framework for the modeling of this tissue mixture (and for the uncertainty which qualifies medical images in general). The classification algorithm gives a set of maps, each voxel being associated with a membership degree to each tissue class (figure 5). The basic assumption is that the normalized membership of a given voxel to a tissue class may be considered as a percentage of this tissue in the basic volume element.

3.2. **Building of the geometrical model**

In the case of a brain study, rigid transforms are sufficient to match the cerebral structures on both images, since the brain is considered as a non-deformable solid [VanDenElsen *et al.* 1993]. The anatomical image being kept as spatial reference, registration parameters are processed to align SPECT data with the MR image. The 3D rigid transform is initially composed of a rotation and a translation (6 parameters). The difference in spatial resolution between acquisition systems implies a third part in the transform, based on the application of a scaling factor.

The geometrical model is based on the representation of voxels from both images by cubes. The MR image is also used as geometrical reference, and its voxels are thus arbitrarily associated with unit cubes. As a consequence of the size difference between voxels of both images, the SPECT image is associated with a tilling of the space by larger voxels in general position.

Figure 5. Fuzzy membership maps of cerebrospinal fluid, white matter and gray matter

Let **T** be the registration operator in homogenous coordinates. Since **T** changes the information expressed in a basis of $\mathbb{U}^3$ into information expressed in another basis, this matrix can be viewed as a basis change operator. **T** is the transition matrix from the basis ($\mathbf{u_i}$) associated with the MR image to the basis ($\mathbf{b_i}$) associated with the SPECT image (multiplying on the left by **T** transforms a coordinate set originally expressed in ($\mathbf{b_i}$) into coordinates expressed in the ($\mathbf{u_i}$) basis). Thus

$$\begin{pmatrix} b_{11} & b_{12} & b_{13} & p_1 \\ b_{21} & b_{22} & b_{23} & p_2 \\ b_{31} & b_{32} & b_{33} & p_3 \\ 0 & 0 & 0 & 1 \end{pmatrix} = \begin{pmatrix} u_{11} & u_{12} & u_{13} & o_1 \\ u_{21} & u_{22} & u_{23} & o_2 \\ u_{31} & u_{32} & u_{33} & o_3 \\ 0 & 0 & 0 & 1 \end{pmatrix} \mathbf{T} \tag{2}$$

where each basis is presented as an homogenous matrix, where columns 1..3 are the basis vectors ($\mathbf{b_i}$) and ($\mathbf{u_i}$), and column 4 contains the coordinates of the origin point associated with the basis: **o** (for ($\mathbf{u_i}$)) is, by definition, the origin of the canonical basis, and **p** (for ($\mathbf{b_i}$)) is the image of **o** and is possibly not null, because of the translation components in **T** (figure 6). Nevertheless, the registration transform is often built with respect to a central point (rotation and change of scale) which is not the geometrical origin (*e.g.* center of mass of SPECT data). In this case, the original transition matrix **T** has to be replaced with

$$\mathbf{M} = \mathbf{CTC}^{-1} \tag{3}$$

where **C** is the translation from the origin point $(0\ 0\ 0\ 1)^T$ to the center **c** of the **T** transform in ($\mathbf{b_i}$). The generator vectors of cubes in the general position are the images of canonical unit vectors by **M**, and other cubes of the tiling are obtained by translation of the origin voxel (based on point **p**).

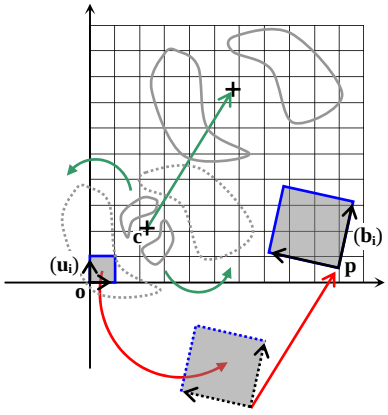

Figure 6. 2D illustration of the ($\mathbf{b_i}$) basis processing by applying the **M** transform to the {($\mathbf{u_i}$),**o**} system

3.3. **Processing of the geometrical information**

The discrete nature of MR and SPECT images makes the question of establishing their spatial relations very close to the digital coordinates change problem. The ratio between edge length of the low and large size voxels is not sufficient to disregard the committed error when rounding to integers the results of classical base changing formulas [Reveilles 2001]. In this case, one shall determine the volume of the geometrical intersection between unit volumes of the grids, in order to use this value in the compulsory interpolation step. Voxel sets of both images are modeled by cubic tilings of the space, with unit length for the MR image (preserved as spatial reference), and general position for the SPECT image. The intersection volumes between high and low size voxels are polyhedral (figure 7.a), and are computed using an efficient cube intersection

algorithm. The processing cost of a single intersection volume is lower than using a general algorithm for the intersection of convex polyhedrons, thanks to the use of analytic formulas linked with inherent cube symmetries (figure 7.b).

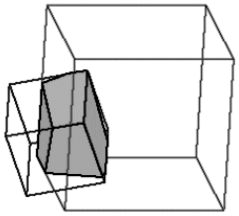

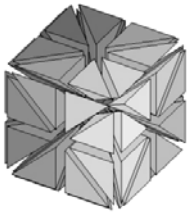

The octahedral group of cube symmetries

(a) (b)

Figure 7. Example of intersection volume processed thanks to cube symmetries

The principle is to run through the 6 faces of both cubes, processing a polygonal bound of the polyhedral volume at each iteration (at most 12 faces). Let C_1 denote the cube providing the current square face F, and C_2 the other cube (figure 8.a). The F support plan P presents a polygonal intersection I with the other voxel C_2. The I vertices depend on the normal vector **N** of the plan P and the distance from C_2 central point to P. Analytic formulas first provide vertices coordinates for a polygonal intersection I' between C_2 and a plan P', located at the same distance from the central point of C_2, and which normal vector **N'** is constrained in a predefined conic region of the space (figure 8.b). **N'** being an equivalent of **N** in the group of cube symmetries (figure 7.b), I is the image of I' by a simple linear transform. I is possibly larger than the searched polygonal face. Therefore, the final polygon is processed as the plane intersection of I with the original square face F (figure 8.c) using an adapted version of O'Rourke's general polygon intersection algorithm [ORourke 1998].

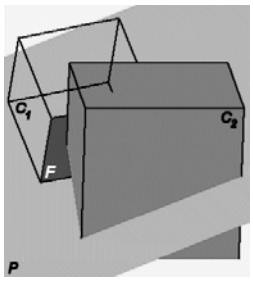

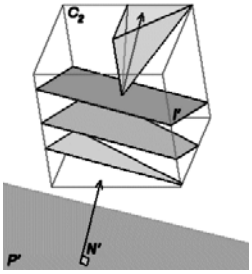

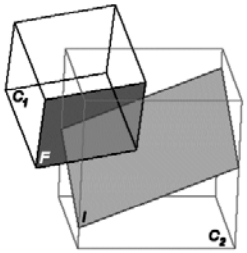

(a) (b) (c)

Figure 8. Main steps of the cube intersection algorithm (the current F is the basal face of cube C_1)

3.4. **Model combination step and image synthesis**

In the context of the image synthesis process, the digital coordinates change is carried out by using intersection volumes as weights for numerical SPECT activities. A base activity μ_C is associated with each anatomical class C (either a mean activity, or an arbitrary gray level). The anatomical information is thus preserved in the edges of these classes, and local variations of the functional activity within each class are injected, in addition to μ_C, by equation (5).

Let δ_v be the part of the activity, extracted from the original functional image **I**, associated with the voxel v in the synthetic image. This value is processed from numerical activities of voxels V from **I**, which v intersects:

$$\delta_v = \sum_{V \cap v} \rho(v, V) \mathcal{F}(V) \tag{4}$$

where $\rho(v,V) \in [0,1]$ is the intersection volume between voxels v and V. The value δ_v is thus a weighted mean activity, which belongs to the same numerical range as original functional activities. Finally, the value held by a voxel v, in the synthetic image, is

$$\mathcal{S}(v) = \frac{\sum_{C} \pi_C(v) \mu_C + \delta_v}{\sum_{C} \pi_C(v) + \sum_{V \cap v} \rho(v, V)} \tag{5}$$

4. Results and discussion

4.1. Presentation of image data

The image synthesis process has been applied to both brain perfusion SPECT ([^{99m}Tc]-ECD) and neurotransmission SPECT ([^{123}I]-FP-CIT) images (figure 9). The concerned patient was affected by a multiple system atrophy (MSA, parkinsonism plus syndrome). A unique MR data set (T_1 weight) was associated with both SPECT images, simultaneously acquired [ElFakhri *et al.* 2001]. SPECT images are thus aligned, with the same spatial resolution. Voxels from the MR image are 0.94 mm large in the slice plane. SPECT images are isotropic, with a voxel size of 2.33 mm. The slice thickness of the MR image is 1.5 mm, but the used registration process interpolates these data to cubic voxels.

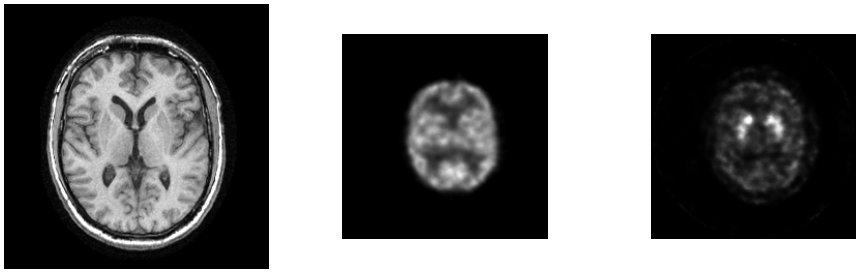

Original MR image Brain perfusion SPECT Neurotransmission SPECT

Figure 9. MR image and dual neurotransmission / brain perfusion images

4.2. Synthetic images

Among the diagnosis elements brought by the classical multimodality approach (visual assessment of the couple SPECT / MR image), we focus on functional activity peaks, activity lacks, and on the shape and position of anatomical structures. The quality of synthetic images (figure 10), in relation to these diagnosis elements, has been assessed by an expert. He answered the following questions for both the brain perfusion and the neurotransmission images:

1. Are original diagnosis elements present on final synthetic image, and are these elements clearly visible?
2. Does this image fusion process really improve the ability to locate functional activity in relation to anatomical structures?

Perfusion images refer to the activity of neurons in the whole brain. The corresponding functional activity is thus a global information, with low frequencies components. For the help in diagnosis, it has to be emphasized in the region of cerebral cortex. The concentration level of the tracer within CSF structures is null. Variations are visible in the WM and mostly in the GM (activity ratio estimated to 1/4). High activity levels in the cortical region are clearly visible, since the mean activity of this structure is already high. Nevertheless, hypoperfusion zones are mostly visible in regions with low base activity, *i.e.* white matter.

In the case of the neurotransmission image, the high activity bound in the striatum implies a decrease of visual contrast in the surrounding region. Nevertheless, deducing the shape and position of anatomical structures remains possible thanks to the outlines of close tissue classes. Indeed the functional activity presents only low variations outside the striatum (CSF in the ventricular system and GM in the cortex). Likewise, edges of the putamens and caudate nuclei can also be deduced from activity low levels within the striatum itself. The synthesis process thus emphasizes the information brought by lacks of activity.

Images presented in figure 10 were obtained by processing the voxel activities with formulas (4) and (5). The additive operator modeling information aggregation manages local variations, and the base activity associated with each tissue class, as signal deviations around a mean value. Nevertheless, this model is not unique, and other behaviors may be considered (e.g. multiplying operators). Moreover, equation (5) can be considered as incomplete, in the sense that the geometrical information don't influence the first term of the numerator (global part of the functional information). In further developments, a solution will possibly consist in processing the global part of the functional activity associated with a voxel V of the SPECT image by modifying formula (1): the membership degree $\pi_C(V)$ of voxel V to a given brain tissue class C should be written considering the memberships of voxels v (membership maps extracted from the anatomical image) intersecting V, weighed by intersection volumes $\rho(v,V)$.

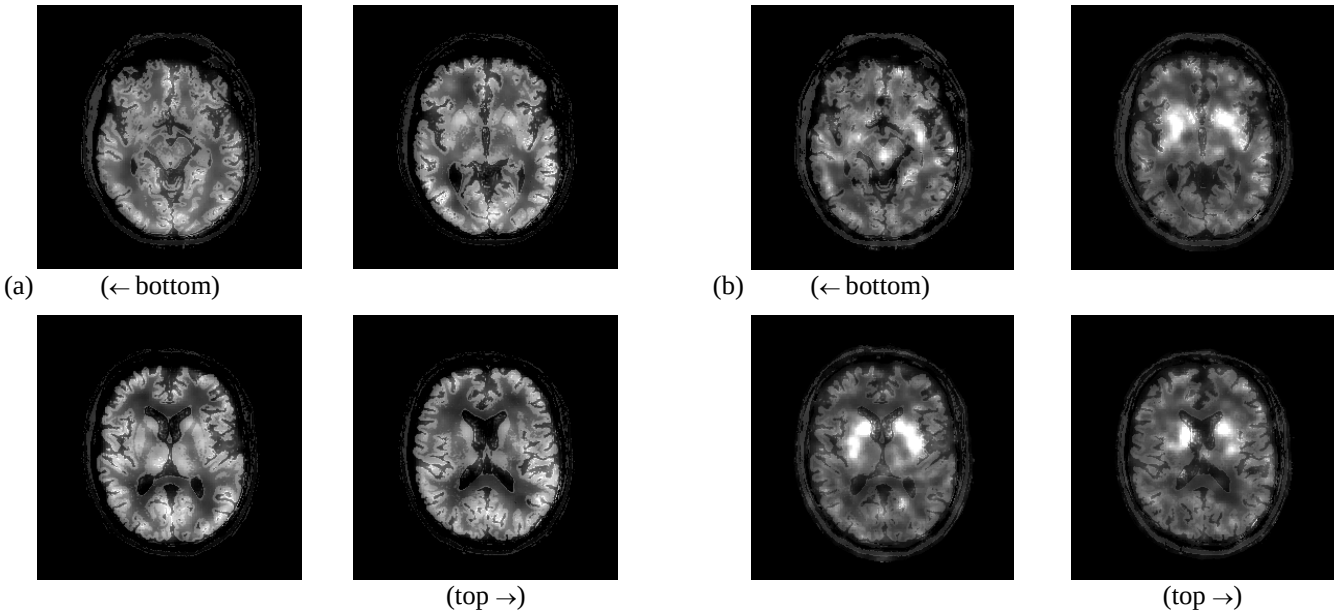

Figure 10. Axial slices of the synthetic images obtained by fusion of MR data and the brain perfusion SPECT (a) and the neurotransmission SPECT (b)

5. Conclusion

We have presented a method for the production of a new functional medical image, in which information location is improved thanks to the fusion with another reference image, delineating anatomical structures. From a clinical point of view, the produced information is fully coherent with physiological effects of the concerned pathology, and with the behavior of radiotracers used during the SPECT acquisition. The fusion of functional data with an anatomical reference provides the expected result, *i.e.* an improvement of the location of activity peaks and lacks in relation to brain anatomical structures. The clinical interest of the processed information for the differential diagnosis of parkinsonian syndromes will be assessed in the context of the FUSPARK project (French "Ministère de la Recherche").

Accuracy of the redistribution method is mainly linked with the quality of the registration step (through the transform parameters). This fusion process avoids adding an imprecision factor, linked with the location of anatomical structures, to the natural uncertainty of medical data. Moreover, the use of the geometrical model is fully coherent with the choice of fuzzy logic, since it allows delaying processing of the results until the available knowledge is sufficient.

Thanks to the introduction of the geometrical model, the fusion process may possibly generate new information sets in which local variations of the functional activity are managed. First results are promising, and require to be confirmed with a larger database. In further developments, this principle will be applied to the synthesis of new information sets holding both global and local variations of the functional activity, and designed to emphasize dedicated diagnosis elements (*e.g.* new pathological tissue classes).

ACKNOWLEDGMENTS

This work was supported by a grant from the "Réseau National Technologies pour la Santé" of the French "Ministère de la Recherche". The authors would like to thank the partners of the FUSPARK project, and specially Dr Marie-Odile HABERT ("La Pitié Salpetrière" hospital, Paris, France) for the assessment of synthetic images.

REFERENCES

[Blandini *et al.* 2000] Blandini, F., Nappi, G., Tassorelli, C., Martignoni, E. Functional changes of the basal ganglia circuitry in Parkinson's disease. *Progress in Neurobiology*, **62**: 63-88, 2000.

[Rusinek *et al.* 1991] Rusinek, H., De Leon, M.J., George, A.E., Stylopoulos, L.A., Chandra, R., Smith, G., Rand, T., Mourino, M., Kowalski, H. Alzheimer disease: measuring loss of cerebral gray matter with MR imaging. *Radiology*, **178**-1: 109-114, 1991.

[Brooks 2004] Brooks, D.J. Neuroimaging in Parkinson's disease. *NeuroRx*, **1**: 243-254, 2004.

[Soret *et al.* 2003] Soret, M., Koulibaly, P.M., Darcourt, J., Hapdey, S., Buvat, I. Quantitative accuracy of dopaminergic neurotransmission imaging with 123I SPECT. *Journal of Nuclear Medicine*, **44**: 1184-1193, 2003.

[Montagner *et al.* 2005] Montagner, J., Barra, V., Reveillès, J.P., Boire, J.Y. Multiresolution images fusion for the quantification of neuronal activity: a discrete approach. *3rd IASTED International Conference on Biomedical Engineering, Innsbruck, Austria*, 2005.

[Barra Boire 2001] Barra, V., Boire, J.Y. A general framework for the fusion of anatomical and functional medical images. *NeuroImage*, **13**: 410-424, 2001.

[Condon 1991] Condon, B.R. Multi-modality image combination: five techniques for simultaneous MR-SPECT display. *Computerized Medical Imaging and Graphics*, **15**-5: 311-318, 1991.

[Stokking 1998] Stokking, R. Integration of functional and anatomical brain images : a survey of approaches, *in* Integrated visualization of functional and anatomical brain images. *Thesis, University of Utrecht, Utrecht, Netherland*, part 3: 21-40, 1998.

[Kundel 1990] Kundel, H.L. Visual cues in the interpretation of medical images. *Journal of Clinical Neurophysiology*, **7**-4: 472-483, 1990.

[Hill 1993] Hill, D.L.G. Combination of 3D medical images from multiple modalities. *Thesis, University of London, London, England*, 1993.

[Colin Boire 1999] Colin, A., Boire, J.Y. MRI-SPECT fusion for the synthesis of high resolution 3D functional brain images: a preliminary study. *Computer Methods and Programs in Biomedicine*, **60**: 107-116, 1999.

[Calle 1999] Calle, D. Image enlargement using similarities from a pyramid and induction onto a set. *Thesis, Joseph Fourier University, Grenoble, France*, 1999. (in french)

[Pajares DeLaCruz 2004] Pajares, G., De La Cruz, J.M. A wavelet-based image fusion tutorial. *Pattern Recognition*, **37**: 1855-1872, 2004.

[Wang Doddrell 2001] Wang, D., Doddrell, D.M. A segmentation-based and partial-volume-compensated method for an accurate measurement of lateral ventricular volumes on T1-weighted magnetic resonance images. *Magnetic Resonance Imaging*, **19**: 267-272, 2001.

[Barra Boire 2000] Barra, V., Boire, J.Y. Tissue segmentation on MR images of the brain by possibilistic clustering on a 3D wavelet representation. *Journal of Magnetic Resonance Imaging*, **11**: 267-278, 2000.

[Zadeh 1978] Zadeh, L.A. Fuzzy sets as a basis for a theory of possibility. *Fuzzy Sets and Systems*, **1**: 3-28, 1978.

[VanDenElsen *et al.* 1993] Van Den Elsen, P.A., Pol, E.J.D., Viergever, M.A. Medical imaging matching - A review with classification. *IEEE Engineering in Medicine and Biology*, **12**-1: 26-39, 1993.

[Reveilles 2001] Reveilles, J.P. The geometry of the intersection of voxels spaces. *Electronic Notes in Theoretical Computer Science*, **46**, 2001.

[ORourke 1998] O'Rourke, J. Computational geometry in C., 2nd edition, *Cambridge University Press (pub.), New-York, USA*, 1998.

[ElFakhri *et al.* 2001] El Fakhri, G., Moore, S.C., Maksud, P., Aurengo, A., Foley Kijewski, M. Absolute activity quantitation in simultaneous 123I/99mTc brain SPECT. *Journal of Nuclear Medicine*, **42**-2: 300-308, 2001.

Monitoring and modeling of pupillary dynamics: Study of the autonomous nervous system

Christophe Tilmant
ERIM
Faculty of Medicine
28, place Henri Dunant BP 38
63001 Clermont-Ferrand France
(+33) 473 178 123
christophe.tilmant@u-clermont1.fr

Mathilde Charavel
Department of Reanimation
Gabriel Montpied Hospital
58, rue Montalembert BP 69
63003 Clermont-Ferrand France
(+33) 473 751 590
mcharavel@aol.com

Matthieu Ponrouch
Department of Reanimation
Gabriel Montpied Hospital
58, rue Montalembert BP 69
63003 Clermont-Ferrand France
(+33) 473 751 590
ponrouch@yahoo.fr

Guillaume Gindre
Department of Reanimation
Gabriel Montpied Hospital
58, rue Montalembert BP 69
63003 Clermont-Ferrand France
(+33) 473 751 590
ggindre@chu-clermontferrand.fr

Laurent Sarry
ERIM
Faculty of Medicine
28, place Henri Dunant BP 38
63001 Clermont-Ferrand France
(+33) 473 178 123
laurent.sarry@u-clermont1.fr

Jean-Yves Boire
ERIM
Faculty of Medicine
28, place Henri Dunant BP 38
63001 Clermont-Ferrand France
(+33) 473 178 123
j-yves.boire@u-clermont1.fr

ABSTRACT
This study deals with the analysis of pupillary dynamics. The evaluation of pupil motion provides functional information about the autonomous nervous system. A non-invasive tool has been designed to help the understanding of physiology by modeling the reflex loop of the pupil. The monitoring is made up of three parts. First, a digital camera is chosen for image acquisition because of its simple use at the patient's bed. Then a software estimates the pupillogram, i.e. the plot of the pupil area versus time, from the digital video sequence using deformable templates. And finally, the pupil light reflex is modeled by a second order linear system to compute characteristic parameters. They can be used to diagnose various affections from a statistical analysis.

KEYWORDS
Deformable template, physiological modeling, pupil light reflex, pupillogram.

1. Introduction

The humoral human system is regulated by the association of the autonomic nervous system (ANS) and the endocrine system. The integration of these two systems is done by the hypothalamus. The ANS provides involuntary control and organization of both maintenance and stress responses. The ANS has two divisions: the sympathetic nervous system (SNS) and the parasympathetic nervous system (PNS). Many but not all muscles and glands that distribute nervous impulses to larger interior organs possess a double nerve supply; in such cases the two divisions may exert opposing effects. There are several tests of the ANS: clinic (arterial blood pressure and cardiac frequency), blood biochemistry, and pupil tests. In fact, one of the interesting properties of the eye is the pupil response to light, when the pupil muscles are activated and lead to a miosis. The pupil dilation depends on the SNS and its contraction on the PNS. So the diameter and kinetics of the pupil are a consequence of the balance between these two antagonistic forces.

Pupillometry is the recording of the pupillary diameter according to time. In order to make the recording independent from the variations due to the ambient light, the reference method is based on the infra-red (IR) acquisition. Pupillometry was initially used in ophthalmology: the pupillary size is significant for the interpretation of perimetry of the visual field and electroretinography and for the preoperative assessment of a refractive surgery [Ambrosio *et al.* 2002; Duffey Leaming 2004], in neuro ophthalmology for the description of lesion of the afferent or efferent nervous ways [Loewensfeld 1993]. The modeling of pupillogram, acquired during a light stimulation, makes it possible to obtain the static and dynamic parameters driving pupil light reflex (PLR). The PLR has already been studied to detect a PNS defect [Kawasaki Kardon 2001] in various affections: alcoholism, diabetes, AIDS, Down's syndrome, depression, anxiety, drug addiction, Alzheimer diseases, schizophrenia.

In much pathology, the ANS is reached with a different prevalence. Pupillometry makes it possible to evaluate the degree of autonomic dysfunction in the migraine [Mylius *et al.* 2003]. Indeed, the final values of the pupillogram parameters are reached 48 hours after a migraine. The way the ANS is affected indicates whether the sympathetic or parasympathetic systems prevail [Bertinotti *et al.* 2002]. This evaluation is also interesting for the diabetic disease to assess the severity of the nervous attack. Other pupillogram abnormalities are observed in the Alzheimer disease.

Pupillometry is also of interest as a monitoring tool in the field of neurosurgery anesthesiology [Manley Larson 2002]. Indeed abnormalities of the different parameters of PLR are observed during the rise in intracranial pressure, the latter being either related to the effect of localized mass or a generalized oedema. They are unilateral or bilateral according to the attack mechanism [Taylor *et al.* 2003]. They last longer than intracranial hypertension. An asymmetry is found for only 1% of the subjects unharmed of all cerebral pathology. Pupillometry is used for the initial assessment of the serious brain trauma. The pupillogram was much altered for the most serious patients; it secondarily was nonreactive for patients for whom diagnosis of brain death was made afterwards.

One of the other applications of pupillometry is the monitoring of pain for conscious or deadened patients. Indeed any painful stimulation involves a pupillary dilation [Tassorelli *et al.* 1995]. Only indirect parameters enable to appreciate pain for unconscious patients, these parameters (blood pressure and rate of heartbeat) are dependent on many factors and seem modified lately in case of analgesia defect [Barvais *et al.* 2003; Onal Tuglular 1999]. The opioids, used in anesthesia for the treatment of the pain, inhibits pupillary dilation related to pain when suitably treated. Pupillometry could be therefore interesting to guide the use of analgesics in anesthesia. Moreover, when regional anesthesia is combined to a global one, monitoring of the PLR makes it possible to locate the level of the anesthetic block induced by regional anesthesia [Larson *et al.* 1993].

Many molecules modify PLR [Knaggs *et al.* 2004]. So pupillometry is used for the tracking of medicamentous drug-addiction. An evaluation of this technique was made in California and this method appeared profitable and efficient. [Richman Noriega 2002; Murillo *et al.* 2004]

Pupillometry is a non-invasive technique that seems to be promising as a tool to follow-up numerous medical problems, but it requires a more complete evaluation that will be made possible by the automated system described below. The aim of this work is to build a new tool integrating knowledge about dynamic PLR and to use image analysis, in order to track pupil motion, and physiological modeling to quantify disorders. This tool has to be easy to use at the patient's bed and to provide reproducible measures.

In section 2, the material used for this study is described. In section 3, the methodology of image analysis and physiological modeling is exposed. Finally, section 4 focuses on the results and discusses the performances and limits of this tool.

2. Materials

2.1. Video Acquisition

The choice of materials is above all justified by clinical constraints. Indeed, in order to be efficient in the clinical practice of a department of anesthesia and reanimation, image acquisition must be performed at the patient's bed (cf. figure 1b). Furthermore, the following conditions should be fulfilled:

- ✓ an initial light level as low as possible to have the most important mydriasis,
- ✓ a light edge as rapid as possible to be in the conditions of the PLR,
- ✓ and an amplitude high enough to obtain a significant modification of the pupil diameter.

Nevertheless, there is a compromise to find between the previous clinical constraints, the patient comfort (non painful light) and a good image quality in term of pupil-to-iris contrast. The selected device (cf. figure 1a) is an IR video camera equipped with two IR light emitting diodes (LED) for the acquisition, one visible light LED for the light excitation, and an opaque mask in order to isolate the patient from the external lighting. This tool is commercialized by the Synapsys society (ULMER SYNAPSYS S.A SY.VNS.VAGS/N; 58 Rue Paul Langevin 13013 Marseille, FRANCE). Its characteristics are:

- ✓ a temporal sampling of 25 fps (frames per second),
- ✓ an image size of 320*240 pixels.

It is linked to a laptop computer with an USB connection, where the data are stored. The visible light LED, that stimulates retina, emits a white light power of 200 lumens. The IR LEDs appear as two white spots in the video film. These reflections are taken into account in the image analysis method for pupil tracking.

2.2. **Acquisition Protocol**

Measurements are performed on the left eye because the PLR is symmetric, consensual and bilateral with a healthy volunteer. The presence of the opaque mask forbids the perturbation due to the presence of a consensual reflex according to the right eye. Firstly, the visible light LED is supplied with the voltage off and the mask is applied to the patient's face during two minutes, so that the eye adapts itself to the light. Secondly, the PLR is recorded when an impulsion or a step of light occurs. Afterwards, the video digital sequence is processed by the software described below.

(a) *(b)*

Figure 1: Complete view of the acquisition system (a). Portability of the system that can be used at the patient's bed using a laptop computer (b).

3. **Methods**

The analysis of the pupillary dynamics consists in two parts. The pupil is tracked for all the frames of the video sequence. Then the temporal evolution of the pupil area, called the pupillogram, is modeled by a second order linear system, parameters of which describes the pupil motion and may be used in statistical studies to detect specific diseases or phenomena affecting the ANS.

3.1. **Pupil Tracking**

The dynamic tracking for the pupillogram consists in detecting the pupil, frame per frame. Some workers have used temporal prediction by Kalman filtering for instance [Zhu *et al.* 2002] or physical properties of the eye by exploiting multiple light sources [Morimoto *et al.* 2000]. Pupil appears as a dark region compared to the light iris one. Contrast is dependent on the iris color, but is generally high enough to process the data frame per frame without using temporal information. There are many other works about pupil tracking, but they focus on eye gaze tracking for computer interaction and not on an accurate pupil size measurement.

The tracking of the pupil between successive frames is based on deformable templates [Yuille *et al.* 1992] (cf. figure 3). A deformable template model is defined by a geometrical shape (e-g circle, parabola, ellipse, line segment, etc.) defined as:

$$\begin{aligned} g : R^n \times [0;1] &\rightarrow R^2 \\ \{\mathbf{p}, s\} &\mapsto (x, y) \end{aligned}, \tag{1}$$

where $\mathbf{p}$ is a n-dimensional vector of relevant parameters, R^2 is the spatial domain, s a curvilinear parameterization of the template and (x, y) the Cartesian coordinates of a point according to s. This structure reacts to a function depending on the image gray level analogous to a potential field. Mechanical behavior (dynamics) is guided by an energy function $E(\mathbf{p})$. The optimal positioning of the template over the potential corresponds to a minimum of $E(\mathbf{p})$ which is usually found by gradient descent:

$$\gamma \frac{dp_i}{dt} - \frac{\partial E(\mathbf{p})}{\partial p_i} = 0 \tag{2}$$

where p_i is the i-th coefficient of $\mathbf{p}$ and γ the descent step.

In this section the application of elliptical template to pupil-iris boundary tracking is presented. In order to attract the template to the pupil edges, the norm of the gradient [Young Van Vliet 1995; VanVliet *et al.* 1998] is integrated along the curve to build the potential field:

$$E = -\int_g |\nabla_\sigma I|(x, y) ds \,, \tag{3}$$

where $\nabla_\sigma I$ is a smoothed version of the image gradient, obtained by convolving the image with the first derivative of a Gaussian kernel with standard deviation σ. More robust fields could be obtained by applying, for example, a region based strategy.

The prior knowledge about the elliptical shape is exploited in the energy minimizing scheme. The ellipse is determined by a set of five parameters (cf. figure 2):

$$\begin{cases} x = x_0 + l_1 \cos(\theta)\cos(\alpha) - l_2 \sin(\theta)\sin(\alpha) \\ y = y_0 + l_1 \cos(\theta)\sin(\alpha) + l_2 \sin(\theta)\cos(\alpha) \end{cases} \quad 0 \le \theta \le \pi \,, \tag{4}$$

where, (x_0,y_0) is the coordinates of the ellipse center, l_1 and l_2 are the major and minor ellipse axes, and α is the orientation angle with respect to the horizontal axis.

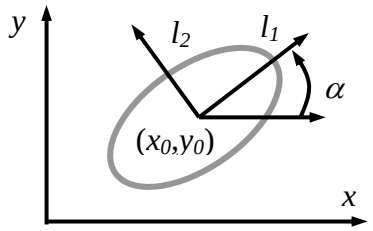

Figure 2: Parameterization of the ellipse used for the deformable template method

The advantages of this approach are:

- ✓ no need for post-processing to obtain a closed curve;
- ✓ the use of prior knowledge about the pupil geometry;
- ✓ the choice of a parameterized template constrains the model and therefore increases the robustness and speed of convergence, contrary to other active contours;
- ✓ the subpixel precision;
- ✓ and the simple estimation of the pupil area, denoted *S*, by the formula:

$$S = \pi . l_1 . l_2 \tag{5}$$

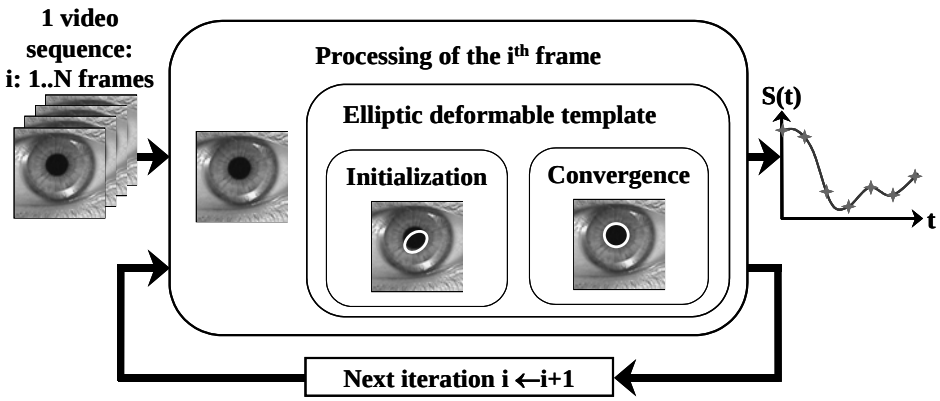

Figure 3: Summary of the method: the video film is considered frame per frame and for each one, an elliptic deformable template permit to estimate the pupil area.

3.2. **Deformable Model Initialization**

As for all methods based on active contours, initialization is crucial. Indeed, deformable template converges to the closest local minimum, so initialization acts on the final result. Therefore, a method based on thresholding and binary mathematical morphology [Matheron 1975; Serra 1982] is proposed in order to extract an initial approximation for the pupil location.

A pre-processing step is necessary because of the spots due to the reflection of the IR LEDs. These spots look like two reflection circles in the image, so a gray level mathematical morphology closing is applied by using a circular structuring

element. They are removed with hardly any change in the pupil geometry because of its smooth shape. The contrast of the pupil leads to a bimodal histogram that makes easy the determination of a global threshold by the use of the classical Otsu criterion.

The object corresponding to the pupil is extracted from the binary image by mathematical morphology operators. A binary closing is applied and all resulting connected components are labeled. The biggest one is used to initialize the ellipse parameters. Its center is given by the center of gravity and its axes are computed by identifying the surface of the object with the one of an approximating circle.

3.3. **Mathematical Modeling of Pupillar Dynamics**

There have been several models to attempt to simulate pupillary dynamics. Longtin and Milton [Longtin Milton 1988] have developed a model of the PLR using nonlinear delay-differential equations. This technique from dynamical systems theory is used to analyze complex behaviors such as the onset of oscillations under high-gain negative feedback.

In the literature [Bressloff Wood 1998; Longtin Milton 1988], pupillary control system is modeled as a linear feedback control system. The pupil contraction system can be considered as a closed-loop system with the afferent activity that acts as the amplifier and the efferent activity as the feedback (cf. figure 4a). The proposed model of the PLR, motivated by physiological knowledge and empirical observation, is the delayed step response of a second order linear system (cf. figure 4b) that can be expressed by a second order linear ordinary differential equation:

$$\frac{1}{\omega^2}\cdot\frac{d^2 s(t-\tau)}{dt^2}+\frac{2\cdot m}{\omega}\cdot\frac{ds(t-\tau)}{dt}+s(t-\tau)=K\cdot e(t) \qquad (6)$$

where $s(t)$ is the output temporal signal, $e(t)$ the excitation signal, m the damping coefficient, K the static gain, ω the natural frequency and τ the latency time. It operates essentially in the underdamped case (m<1). This modeling enables to reduce the information into a set of parameters that have a physiological meaning. In fact, the latency time is the reaction delay of the system, the natural frequency is homogeneous to the rapidity and the static gain describes the area difference between the mydriasis and the miosis.

Parameters are identified by a Marquardt-Levenberg [Marquardt 1963; Press *et al.* 1986] least-square fit of the model onto the experimental pupillogram. Indeed, the solution of second order linear ordinary differential equation (6) is not linear according to parameters, so the use of a non linear method is mandatory to solve the estimation problem.

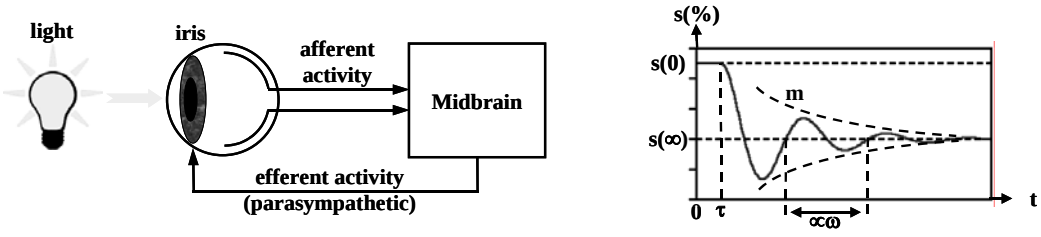

(a) *(b)*

Figure 4: Modeling of the reflex loop based on physiologic knowledge (a) by the response of second order linear system (b).

4. **Results and Discussion**

4.1. **Methodological Tests**

The sensor of the camera is a CCD matrix, so the image is embedded with an additive Gaussian noise. The precision of the measure versus signal to noise ratio (SNR) is plotted on figure 5a. The study was done with a synthetic image of a dark ellipse on a light background with noise added. The use of a deformable model enables to increase the stability of the measure because of the sub pixel precision coupled to a parametric shape that constrains the solution.

An interesting test is the validation of the model of PLR itself. Figure 5b shows the normalized average error and the standard deviation between the model and the pupillogram for 52 recordings on different people stored during a previous study done on voluntaries under morphine injection [Tilmant *et al.* 2003a]. The quadratic distance, normalized to the pupil area variation, is used as a measure of the error and is plotted against the number of samples of the pupillogram, i.e. the duration of acquisition after the light step. An optimal time of 1.13 s was found with model (6), corresponding to a minimal normalized average quadratic error of 0.07 % in area. This increase of the difference between the model and the experimental data can be explained by the adaptation of the retina sensitivity to light that causes the pupil to compensate. It permits to set the phenomena duration to modeling.

The use of more realistic physiological models is envisaged in order to analyze more accurately pupillary dynamics. For example the use of the Longtin-Milton model [Longtin Milton 1988] could be considered.

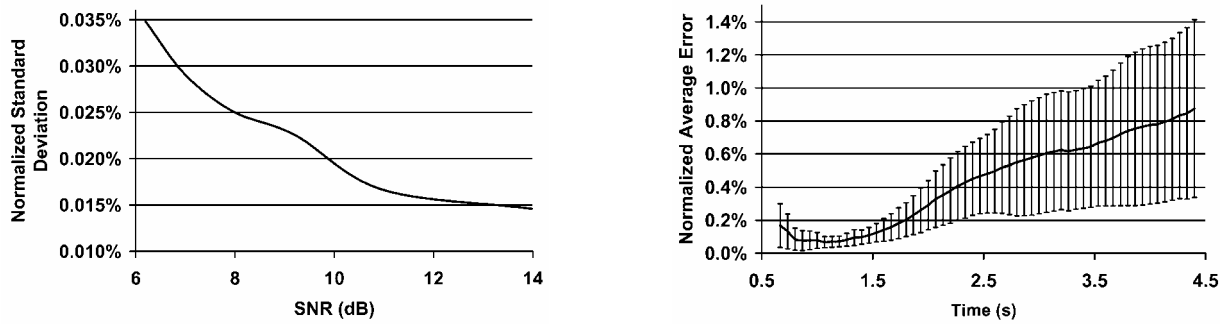

(a) *(b)*

Figure 5: Standard deviation of the measure with the signal to noise ratio (SNR)(a). Average and standard deviation of the normalized error between the dataset and the models for different numbers of temporal samples (b) [Tilmant et al. 2003a].

4.2. **Clinical applications**

The purpose of clinical work was to determine the physiological characteristics of the loop reflex of the PLR for patients in basal state and in particular situations: patients under medication (opioïds, hypnotic...), or particular neurological states: brain trauma or intracerebral hemorrhage.

The purpose of the first study, based on 95 voluntaries, was to check the influence of the color of the iris on the PLR. By using the previous modeling method, it was not discovered significant difference over the latency time: 0.190 +/- 0.03 second in the group "dark eyes" (DE) versus 0.189 +/- 0.04 second in the group "clear eyes" (CE). In the same way, no difference was found for the damping coefficient: 1.17 (DE) versus 1.2 (CE), neither for the natural frequency, nor for the maximum speed of contraction (Appendix A). The studied population comprised young adults (mean age = 36 +/- 8 years). Conversely, the study confirms that the size of the pupil in population CE is lower (0.26 % of the size of the iris), with that of population DE (0.30 % of the size of the iris); this phenomenon is described in the literature.

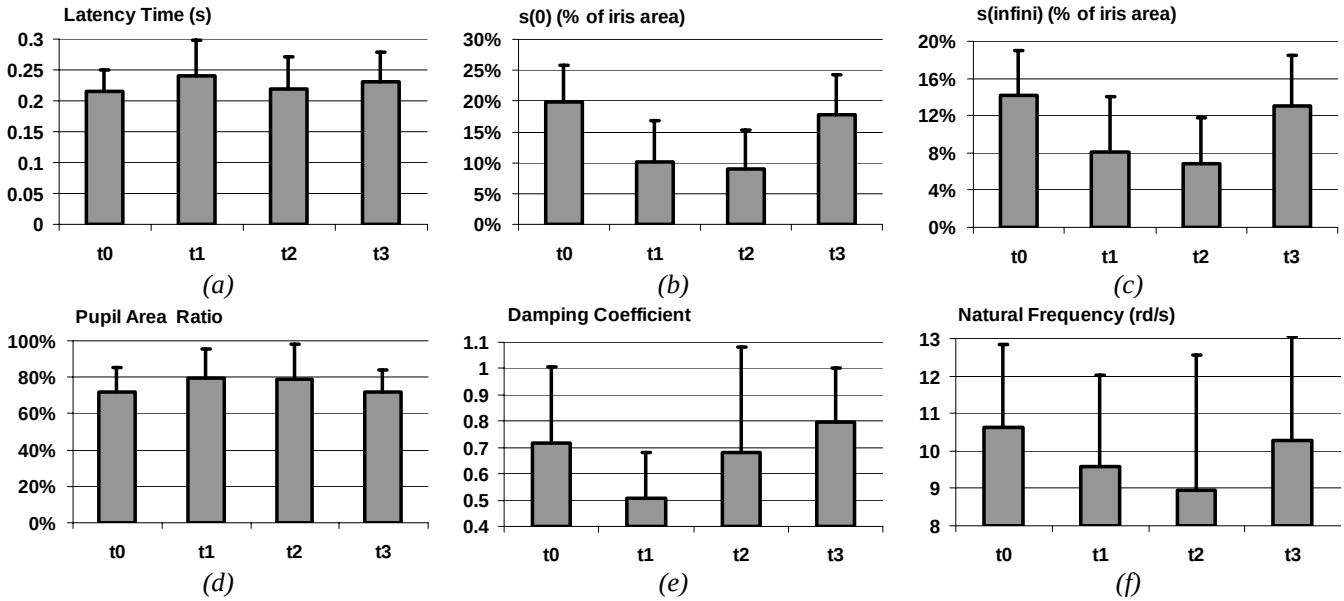

Figure 6: Values of the modeling parameters in case of electrical cardioversion. Four acquisitions were done: before the anesthesia (t0), after injection of propofol (t1), after electrical cardioversion (t2) and finally when after product elimination (t3). Latency time (a), initial pupil area (b), final pupil area (c), pupil area ratio (d), damping coefficient (e) and natural frequency (f) are given.

The second study relates to the influence of hypnotics on the loop reflex of the PLR. The studied population concerns 35 patients having to be anaesthetized without opioïds for electrical cardioversion. The hypnotic used was the propofol. The eye was filmed before anesthesia, under anesthesia (with a cerebral concentration of 3 μg/ml of propofol) before and one minute

after electrical cardioversion (so the sympathic stimulation is finished), and finally at the waking up after complete elimination of the drug.

Statistical analysis acts on each parameter of the model independently from the others. The standard level of significance used to justify a claim of a statistically significant effect is 0.05. The differences at each time are computed according to parameters estimated before anesthesia (t_0).

The latency time and the pupil area ratio do not appear to be influenced by propofol or by shock (cf. figures 6a&d). Conversely, pupil sizes (mydriasis and miosis) are decreased under anesthesia (cf. figure 6b&c). The fact that the opioids lead to a decreasing size of the pupil is a well know result, but the effects of hypnotics are not well described in the literature. The damping coefficient is decreased under anesthesia but it does not present a significant difference after the shock. Finally, the natural frequency shows a significant variation after the shock but not before. The forthcoming of this work concerns the link between these parameters and their changes with a possible defect of anesthesia (cf. figure 6).

The studies on the opioids and the head injuries are in hand.

5. Conclusions

A tool to analyze pupillary dynamics was presented. An image analysis based on deformable template followed by a mathematical modeling of the PLR was proposed. For now, a first clinical study using this tool was performed to quantify the consequences of morphine on the PLR [Tilmant *et al.* 2003b]. On the whole, these studies allow a better knowledge of physiology and pharmacological effects on the PLR that is at the junction of the neurovegetative systems.

ACKNOWLEDGMENTS

The authors want to thank the Synapsys society for the gratuitous loan of the acquisition system and are grateful to Dr. V. Fontvieille and Dr. A. Virat for valuable assistance in the clinical validation and tool conception. This study was partially supported by a grant from the Center of Clinical Pharmacology (Pr. C. Dubray), Clermont-Ferrand, France.

APPENDIX A: PARAMETERS EXTRACTED FROM THE MODEL

One interest of this modeling is the use of parameters deriving from the analytic representation of the phenomenon, giving access to physiological parameters in a less noisy and more robust way. The maximal velocity and its apparition time are two parameters usually used in the study of pupillary dynamics. They can be expressed in an analytical way for the three conditions relative to the dumping coefficient:

m>1	$t_{V\max} = \tau + \frac{1}{2\omega\sqrt{m^2-1}} \ln\left(\frac{m+\sqrt{m^2-1}}{m-\sqrt{m^2-1}}\right)$
	$v_{\max} = \left(s(0)-s(\infty)\right)\left(\frac{\omega}{2\sqrt{m^2-1}}\right)\left[\exp\left(-\omega\left(m+\sqrt{m^2-1}\right)\left(t_{V\max}-\tau\right)\right) - \exp\left(-\omega\left(m-\sqrt{m^2-1}\right)\left(t_{V\max}-\tau\right)\right)\right]$
m=1	$t_{V\max} = \tau + \frac{1}{\omega}$
	$v_{\max} = \left(s(\infty)-s(0)\right)\frac{\omega}{e}$
m<1	$t_{V\max} = \tau + \frac{1}{\omega\sqrt{1-m^2}}\left[\left(\arctan\left(\frac{2m^2-1}{2m\sqrt{1-m^2}}\right) - \arctan\left(\frac{m}{\sqrt{1-m^2}}\right)\right)\right]$
	$v_{\max} = \left(s(\infty)-s(0)\right)\omega\exp\left(-\omega m\left(t_{V\max}-\tau\right)\right)\left[\frac{m}{\sqrt{1-m^2}}\sin\left(\omega\sqrt{1-m^2}\left(t_{V\max}-\tau\right)+\arctan\left(\frac{m}{\sqrt{1-m^2}}\right)\right)\right.$ $\left. -\cos\left(\omega\sqrt{1-m^2}\left(t_{V\max}-\tau\right)+\arctan\left(\frac{m}{\sqrt{1-m^2}}\right)\right)\right]$

REFERENCES

[Ambrosio *et al.* 2002] Ambrosio, R., Schallhorn, S.C., and Wilson., S.E. The importance of pupil size in refractive surgery. *Refractive Surgery Outlook, American academy of ophtalmology*, fall 2002. (http://www.aao.org/aao/member/sig/upload/Fall-2003-Outlook.pdf)

[Duffey Leaming 2004] Duffey, R., and Leaming, D. Trends in refractive surgery in the United States. *Journal of Cataract & Refractive Surgery*, **30**-8: 1781-1785, 2004.

[Loewensfeld 1993] Loewensfeld, I.E. The pupil : Anatomy, physiology, and clinical applications. *Iowa City: Iowa State University*, 1993.

[Kawasaki Kardon 2001] Kawasaki, A., and Kardon, R. Disorders of the pupil. *Neuroophthalmology*, **14**- 1: 149-168, 2001.

[Mylius *et al.* 2003] Mylius, V., Braune, H.J., and Schepelmann, K. Dysfunction of the pupillary light reflex following migraine headache. *Clinical Autonomic Research*, **13**- 1: 16-21, 2003.

[Bertinotti *et al.* 2002] Bertinotti, L., Pietrini, U., Del Rosso, A., Casale, R., Colangelo, N., Zoppi, M., and Matucci-Cerinic, M. The use of pupillometry in joint and connective tissue diseases. *Annals of the New York Academy of Sciences*, **966**: 446-455, 2002.

[Manley Larson 2002] Manley, G.T., and Larson, M.D. Infrared pupillometry during uncal herniation. *Journal of Neurosurgical Anesthesiology*, **14**- 3: 223-228, 2002.

[Taylor *et al.* 2003] Taylor, W.R., Chen, J.W., Meltzer, H., Gennarelli, T.A., Kelbch, C., Knowlton, S., Richardson, J., Lutch, M.J., Farin, A., Hults, K.N., and Marshall, L.F. Quantitative pupillometry, a new technology: Normative data and preliminary observations in patients with acute head injury. Technical note. *Journal of Neurosurgery*, **98**- 1: 205-213, 2003.

[Tassorelli *et al.* 1995] Tassorelli, C., Micieli, G., Osipova, V., Rossi, F., and Nappi, G. Pupillary and cardiovascular responses to the cold-pressor test. *Journal of the Autonomic Nervous System*, **55**- (1-2): 45-49, 1995.

[Barvais *et al.* 2003] Barvais, L., Engelman, E., Eba, J.M., Coussaert, E., Cantraine, F., and Kenny, G. Effect site concentrations of remifentanil and pupil response to noxious stimulation. *British Journal of Anaesthesia*, **91**- 3: 347-352, 2003.

[Onal Tuglular 1999] Onal, A., and Tuglular, I. The relationship between pupil diameter and pain by the administration of morphine and antidepressant drugs in mice. *General Pharmacology*, **33**- 1: 83-89, 1999.

[Larson *et al.* 1993] Larson, M.D., Sessler, D.I., Ozaki, M., McGuire, J., and Schroeder, M. Pupillary assessment of sensory block level during combined epidural/general anesthesia. *Anesthesiology*, **79**-1: 42-48, 1993.

[Knaggs *et al.* 2004] Knaggs, R., Crighton, I., Cobby, T., Fletcher, A., and Hobbs, G. The pupillary effects of intravenous morphine, codeine, and tramadol in volunteers. *Anesthesia & Analgesia*, **99**: 108-112, 2004.

[Richman Noriega 2002] Richman, J., and Noriega, R. The sensitivity and specificity of infrared pupillometry measurements in identifying drug impairment in a country probation program. *Forensics Drug Study, Scientific Program American Academy of Optometry*, 2002. (http://www.mcjeyecheck.com/text/studies/Forensiscs Drug Study 2002.html)

[Murillo *et al.* 2004] Murillo, R., Crucilla, C., Schmittner, J., Hotchkiss, E., and Pickworth, W.B. Pupillometry in the detection of concomitant drug use in opioid-maintained patients. *Methods and Findings in Experimental and Clinical Pharmacology*, **26**- 4: 271-275, 2004.

[Zhu *et al.* 2002] Zhu, Z., Ji, Q., Fujimura, K., and Lee, K. Combining kalman filtering and mean shift for real time eye tracking under active IR illumination. *16th International Conference on Pattern Recognition (Quebec City, Canada)*, 11-15 August, 2002.

[Morimoto *et al.* 2000] Morimoto, C., Koons, D., Amir, A., and Flickner, M. Pupil detection and tracking using multiple light sources. *Image and Vision Computing, Special issue on Advances in Facial Image Analysis and Recognition Technology*,**18**- 4: 331-335, 2000.

[Yuille *et al.* 1992] Yuille, A.L., Hallinan, P.W., and Cohen, D.S. Feature extraction from faces using deformable templates. *International Journal of Computer Vision*, **8**: 99-111, 1992.

[Young Van Vliet 1995] Young, I.T., and Van Vliet, L. J. Recursive implementation of the Gaussian filter. *Signal Processing*, **44**- 2: 139-151, 1995.

[VanVliet *et al*. 1998] Van Vliet, L. J., Young, I. T., and Verbeek, P. W. Recursive Gaussian derivative filters. *14th International Conference on Pattern Recognition (Brisbane, Australia),* 16-20 August, 1998.

[Matheron 1975] Matheron, G. Random sets and integral geometry. *New-York: John Wiley & Sons,* 1975.

[Serra 1982] Serra, J. Image analysis and mathematical morphology. *London: Academic Press,* 1982.

[Longtin Milton 1988] Longtin, A., and Milton, J. Complex oscillations in the human pupil light reflex with mixed and delayed feedback. *Mathematical Biosciences,* **90**: 193-199, 1988.

[Bressloff Wood 1998] Bressloff, P.C., and Wood, C.V. Spontaneous oscillations in a nonlinear delayed-feedback shunting model of the pupil light reflex. *Physical review E,* **58**- 3:. 3597-3605, 1998.

[Marquardt 1963] Marquardt, D.W. An algorithm for least-squares estimation of nonlinear parameters. *Journal of the Society for Industrial and Applied Mathematics,* **11**- 2:431-441, 1963

[Press *et al*. 1986] Press, W.H., Flannery, B.P., Teukolsky, S.A., and Vetterling, W.T. Numerical Recipes. *Cambridge: Cambridge University Press,* 1986.

[Tilmant *et al*. 2003a] Tilmant, C., Sarry, L., Gindre, G., Boire, J.-Y. Monitoring and modeling of pupillary dynamics. *IEEE Engineering in Medicine and Biology Society 25th Annual International Conference (Cancun, Mexico),* 17-21 September 2003.

[Tilmant *et al*. 2003b] Tilmant, C., Ponrouch, M., Virat, A., Gindre, G., Dubray, C., and Schoeffler, P. Monitoring of pupillary dynamics: study of the pupil light reflex under morphine (in French). *10th Meeting of the French Society for Informatics and Monitoring in Anesthesia and Reanimation (Nantes, France),* 4-5 April 2003.

TRANSCRANIAL MAGNETIC STIMULATION : MAGNETIC FIELD COMPUTATION USING A PARAMETRICAL COIL MODEL

Sébastien Luquet
First author's affiliation
Complexe Scientifique des Cézeaux
Bâtiments ISIMA
63177 Aubière Cedex France
+33 4 73 40 76 62
sebastien.luquet@isima.fr

Vincent Barra
Advanced Research Group
Complexe Scientifique des Cézeaux
Bâtiments ISIMA
63177 Aubière Cedex France
+33 4 73 40 77 68
vincent.barra@isima.fr

Jean-Jacques Lemaire
ERIM
Faculté de Médecine
BP 38
63001 Clermont-Ferrand Cedex 1
+33 4 73 62 57 00
jjlemaire@chu-clermontferrand.fr

ABSTRACT
Transcranial Magnetic Stimulation (TMS) is a new technique for brain stimulation. TMS has several applications in medical and clinical research. However, its use is still empirical binding many stimulations to find the best coil position for stimulation. We propose to develop a simulator of transcranial magnetic stimulation which aims at computing the electromagnetic field induced in the cortex by TMS. We present in this article the first step of this tool, a parametrical coil model allowing the computation of potential magnetic field outside the head..

KEYWORDS
Transcranial Magnetic Stimulation, magnetic field computation, coil shape modelling.

1. Introduction

Transcranial Magnetic Stimulation is a new technique for brain stimulation [Ruohonen, 1998]. As another techniques like ElectroConvulsive Therapy (ECT) or the implantation of electrodes into motor cortex, TMS excites neurones. But contrary to those techniques, TMS is painless and noninvasive. Indeed, neurones are excited by electrical current induced by a rapidly changing magnetic field. This field is created by the discharge of thyristor (during about 300 μs) into a coil *i.e* a copper winding surrounded by a water-cooled system. The current circulating through the coil is about 10000 A in order to allow magnetic field to cross the skull of the patient.

- TMS has several applications in medical and clinal research :
- brain mapping [George et al,. 1999]
- psychiatry : treatment of mood disorder and schizophrenia [Davey et al,. 1997]
- treatment of epilepsy [Ziemann et al,. 1998]
- treatment of chronic pain [Lefaucheur et al, 2001]

But today, using TMS is still empirical. The clinician who wants to stimulate a specific cortex area given an expected result (phosphene, modification of vision, motor effect) will perform several stimulations, scanning over the patient's scalp to find the most important response (hot spot) [Thielscher and Kammer 2002]. The aim of our work is to avoid all those stimulations that modify the electrical activity of a wider zone of the cortex than needed. We propose to develop a transcranial magnetic stimulation simulator : according to position and orientation of the coil and to the parameters of the stimulation, the simulator will give a modelling of the stimulation effects. Result will be mapped on MRI image of the patient.

We expect to be able to compute magnetic field, eddy currents under the skull, electrical induced field etc... All those scalar or vector fields are directed by complexe laws as Maxwell equations. If we want to manage a maximum of head and brain caracteristics (skull and cortex shape, non-homogenity conductivity and permeability following biological structures [Krasteva et al, 2002], [Hédou, 1997]), we will need to use a very sophistical finite-element scheme.

Before developing such a framework, we set up a numerical tool to compute magnetic field generated by a given coil at any point of the empty-space. The aim is first to assess the magnetic field induced by the coil, then to provide a finite-element scheme boundaries conditions and finally to finite-element computation in free space.

2. Method

The distribution of magnetic field $\vec{B}$ is defined by the well-known Biot-Savart law :

$$\vec{B}(\vec{r},t) = \frac{\mu_0}{4\pi} I(t) \oint_C \frac{d\vec{l} \times (\vec{r} - \vec{r'})}{|\vec{r} - \vec{r'}|^3}$$

where μ_0 is free space permeability, *I(t)* the intensity of the current going through the coil, $\vec{r}$ the point where the magnetic field is computed $\vec{r'}$ is a vector describing the coil *i.e* the winding *C*.

Although this law was established more than 100 years ago, it is simple and allows to understand which parameters will be crucial during computation. In our care to develop simple and re-useable tools, we will consider that *I(t)* is constant and equal to its maximum. Indeed, even if TMS is time-varying we will restrict in a first step to quasi-static case as proposed in [Ruohonen, 1998] and [Krasteva et al, 2002].

In addition we will use the magnetic potential vector $\vec{A}$ formulation, where $\vec{B} = r\vec{o}t\vec{A}$. Then, the Biot and Savart law becomes :

$$\vec{A}(\vec{r},t) = \frac{\mu_0}{4\pi} I \oint_C \frac{d\vec{l}}{|\vec{r} - \vec{r'}|}$$

$\vec{A}$ thus mainly depends on winding's shape. That's why manufacturers have developed differents kinds of coils [Jalinous, 1998]:

- simple coil : a a circular winding
- 8-shaped coil : similar to two simples coils (currents circulating in opposite ways)
- double cone coil : a 8-shaped coil with an angle between the two wings of the coil.

We then propose a tool able to take into account the specificity of each winding copper shape (Fig 1). For a given contour, the user has only to define a 3D-parametrical curve and the expression of its derivative (at a long term, derivative may be computed from the other parametrical equation with a symbolic computation module). The modeling of a single-turn coil whose center is (x_0, y_0, z_0), radius *r* and axis *0z*, is for example :

$$\begin{aligned} x(t) &= x_0 + r\cos(t) \\ y(t) &= y_0 + r\sin(t) \\ z(t) &= z_0 \end{aligned} \qquad \begin{aligned} x'(t) &= -r\sin(t) \\ y'(t) &= r\cos(t) \\ z'(t) &= 0 \end{aligned}$$

where $t \in [0, 2\pi]$. To describe a n-turns coil, *t* may lie in $[0, 2\pi n]$

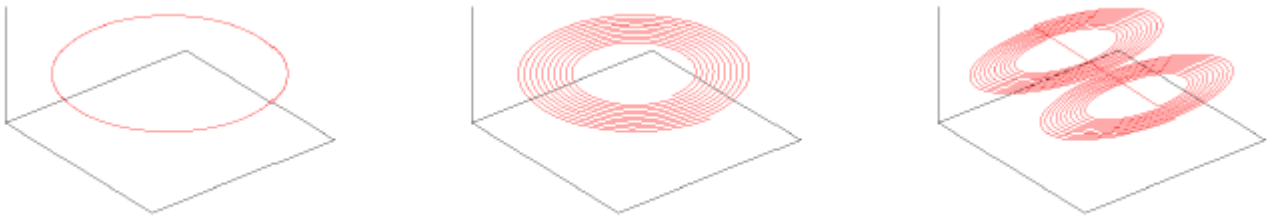

a) b) c)

Fig 1 : Circular, spiral and figure-8 shaped winding

.Every coil kind may thus be described by a parametrical model. Several particular details may also be managed; a physical n-turn coil has a specific thickness, describing how winding passes from a wing of a 8-shaped coil to the other. It might here be useful to model it with a spiral-shaped coil. In addition, some coils (see [Nadeem et al, 2003] modelling) may have covering winding. In such case, a naive modelling would be deficient.

3. Results and discussion

With those descriptions, the potential magnetic vector and by spatial derivate $(r\vec{o}t)$ the magnetic field are numerically computed at any point of the empty-space (Fig 2).

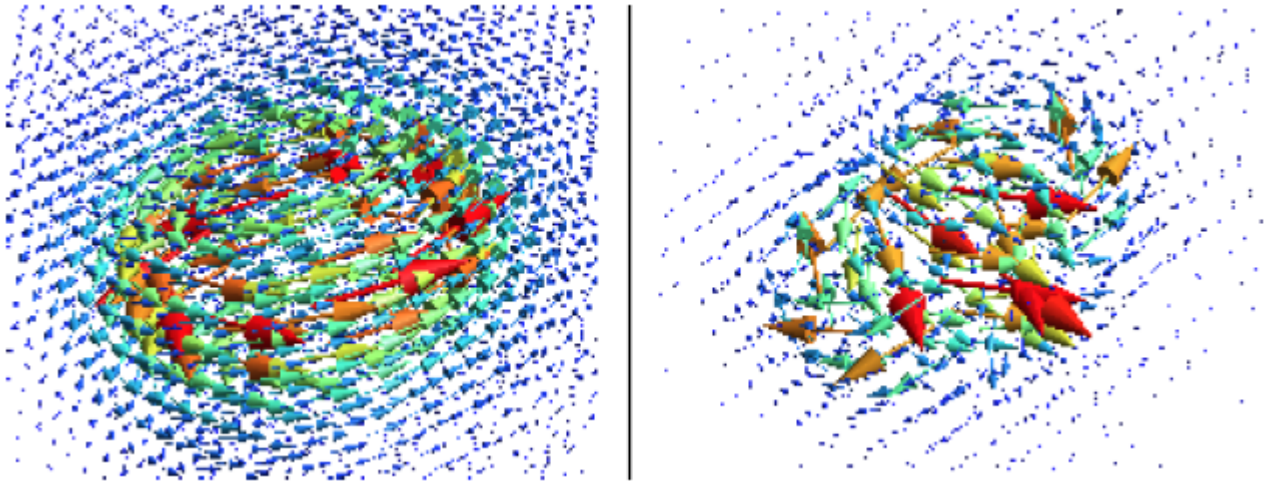

Fig 2 : Potential magnetic field computation for circular and 8-shaped coil

A 8-shaped coil is justified because $\vec{A}$ and so $\vec{B}$ are more focused. Those fields can not be computed for points nearest of the winding. Indeed, by definition field is not defined on the winding (0 division).

In a second time, $\vec{A}$ and $\vec{B}$ values could be given in a localized plane parallel to coil's one. Fig 3 shows the magnetic field modulus on plane $z = z_0$-r. Those results are typically as those obtained by [Nadeem et al, 2003]. As expected, a 8-shaped coil will produce a stronger magnetic field.

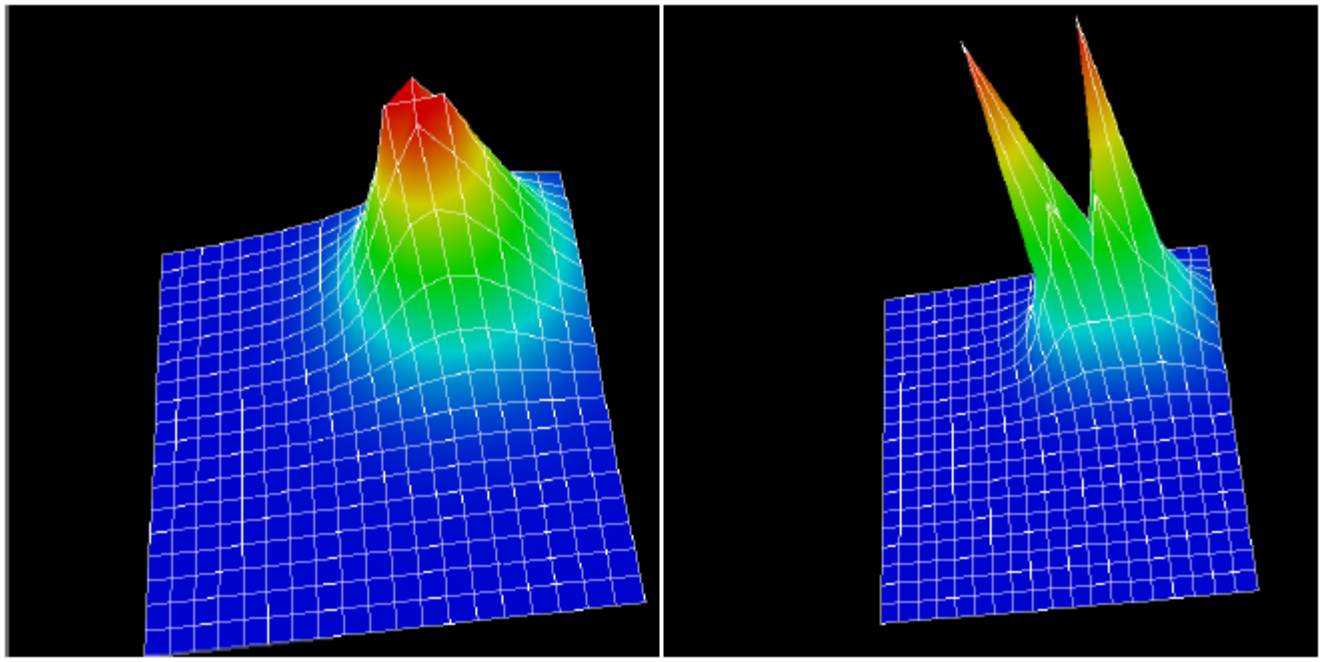

Fig 3 : Normalized magnetic field modulus on plane $z = z_0 - r$ *for circular and 8-shaped coil*

In many references like [Krasteva et al, 2002], the time varying current going through the stimulation coil is modelled as a periodic signal. In fact the discharge could have different waveformes : slope, sinusoidal pediods... Altough discharge is by definition shortly and time limited, a pragmatic way is to consider our system as an harmonic one. Under this assumption can

be deduced the electric field $\vec{E}$ generated in empty space by stimulation $\vec{E} = \frac{\partial \vec{A}}{\partial t} = i\omega \vec{A}$, where ω is the frequency of the harmonic signal (typically 10 kHz) and *i* is the complex notation. Electric field amplitude $|\vec{E}|$ is then proportional to $|\vec{A}|$ (Fig 4). 8-shaped coil has a better focusing and electric field is stronger directly under the center of the 8-shaped coil. That is why according to several authors stimulation is expected to be the strongest following coil axis. Many image-guided stimulation devices use therefore this approximation. We will try in our future work to give a better definition area of stimulation and study time effect.

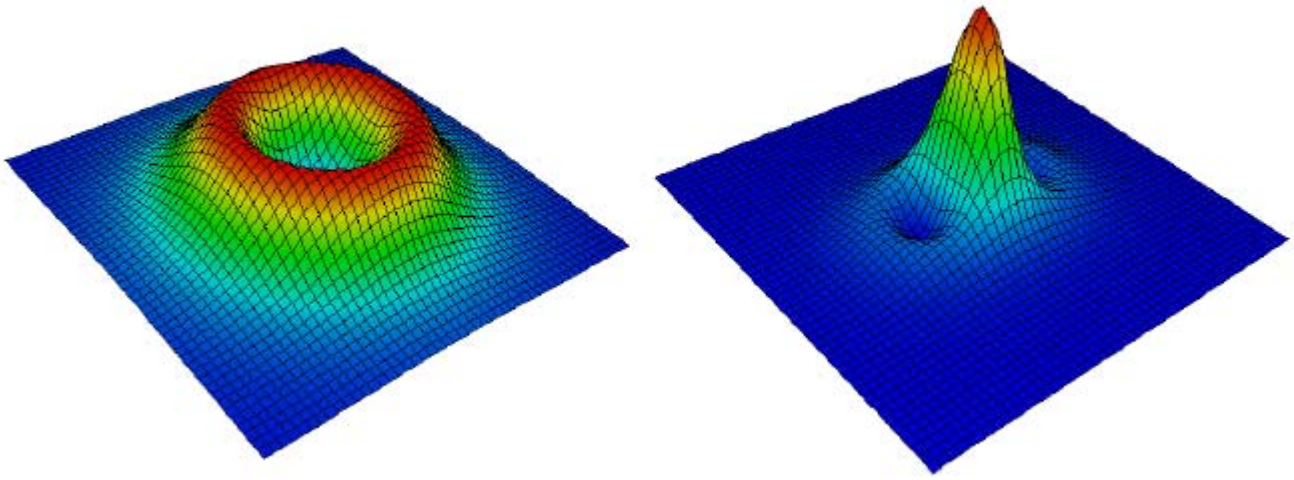

Fig : 4 Normalized electric field modulus on plane plane $z = z_0 - r$ *for circular and 8-shaped coil*

Nowadays, we restrict our image-based nagivation tools to mapping $|\vec{A}|$ on a patient's head-model generated from MRI image (Fig 5).

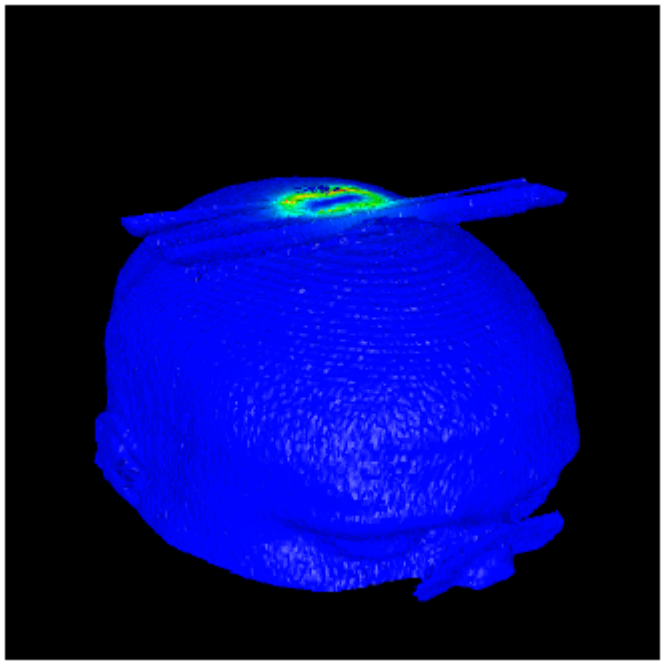

Fig 5 : Potential magnetic field mapping generated by 8-shaped coil on patient's head

4. Conclusion and future prospects

We produce a friendly and reusable tool for the computation of magnetic field generated by any coil during TMS. We now work on a finite-element based tool to compute potential magnetic vector diffusion into patient's head. This tool is based on Gmsh/GetDP http://www.geuz.org/. Our current results will be used as initial or boundary conditions.

Our first tool will be also used to numericaly validate the second one studying diffusion of $\vec{A}$ in free space. Of course it will be also validated by measurement of $\vec{A}$ with Hall-Effect sensors, and experimentation on synthetic phantom and little animals.

In another way we will set up a framework to compare magnetic fields. Indeed, numerical integration along a complex contour could be very slow whereas a simple approximation could drastically reduce computation time. The isssue is to know if variations between both fields are acceptable or not.

REFERENCES

[Davey et al, 1997] Davey, N., Puri, B., Lewis, H., Lewis, S., and Ellaway, P. Effects of antipsychotic medication on electromyographic responses to transcranial magnetic stimulation of the motor cortex in schizophrenia. *J Neurol Neurosurg Psychiatry*, 63(4):468–73, 1997.

[George et al, 1999] George, M., Lisanby, S., and Sackeim, H. Transcranial magnetic stimulation: Applications in neuropsychiatry. *Arch. Gen. Psychiatry*, 56(4):300–311, 1999.

[Hédou, 1997] Hédou, V. Méthodes numériques pour la modélisation électro-anatomique du cerveau. Mathématique et applications, Thèse de l'Université de Rennes I, 1997.

[Jalinous, 1998] Jalinous, R. Guide to magnetic stimulation. *The Magstim Company Limited, U.K* ,1998.

[Krasteva et al, 2002] Krasteva, V., Papazov, S., and Daskalov, I. Magnetic stimulation for non-homogeneous biological structures. *BioMedical Engineering OnLine*, 1(1):3, 2002.

[Lefaucheur et al, 2001] Lefaucheur, J., Drouot, X., and Nguyen, J. Interventional neurophysiology for pain control: duration of pain relief following repetitive transcranial magnetic stimulation of the motor cortex. *Neurophysiol Clin.*, 31(4):247–52, 2001.

[Nadeem et al, 2003] Nadeem, M., Thorlin, T., Gandhi, O., and Persson, M. (2003). Computation of electric and magnetic stimulation in human head using the 3-d impedance method. *IEEE Transactions on Biomedical Engineering*, 50(7):900–907, 2001.

[Ruohonen, 1998] Ruohonen, J. Transcranial magnetic stimulation: Modelling and new techniques. Doctor of technology, Helsinki University of Technology, 1998.

[Thielscher and Kammer, 2002] Thielscher, A. and Kammer, T. Linking physics with physiology in tms: A sphere field model to determine the cortical stimulation site in tms. *Neuroimage*, 17(3):1117–1130, 2002.

[Ziemann et al, 1998] Ziemann, U., Steinhoff, B., Tergau, F., and Paulus, W. Transcranial magnetic stimulation: its current role in epilepsy research. *Epilepsy Res.*, 30(1):11–30, 1998.

Index of authors

